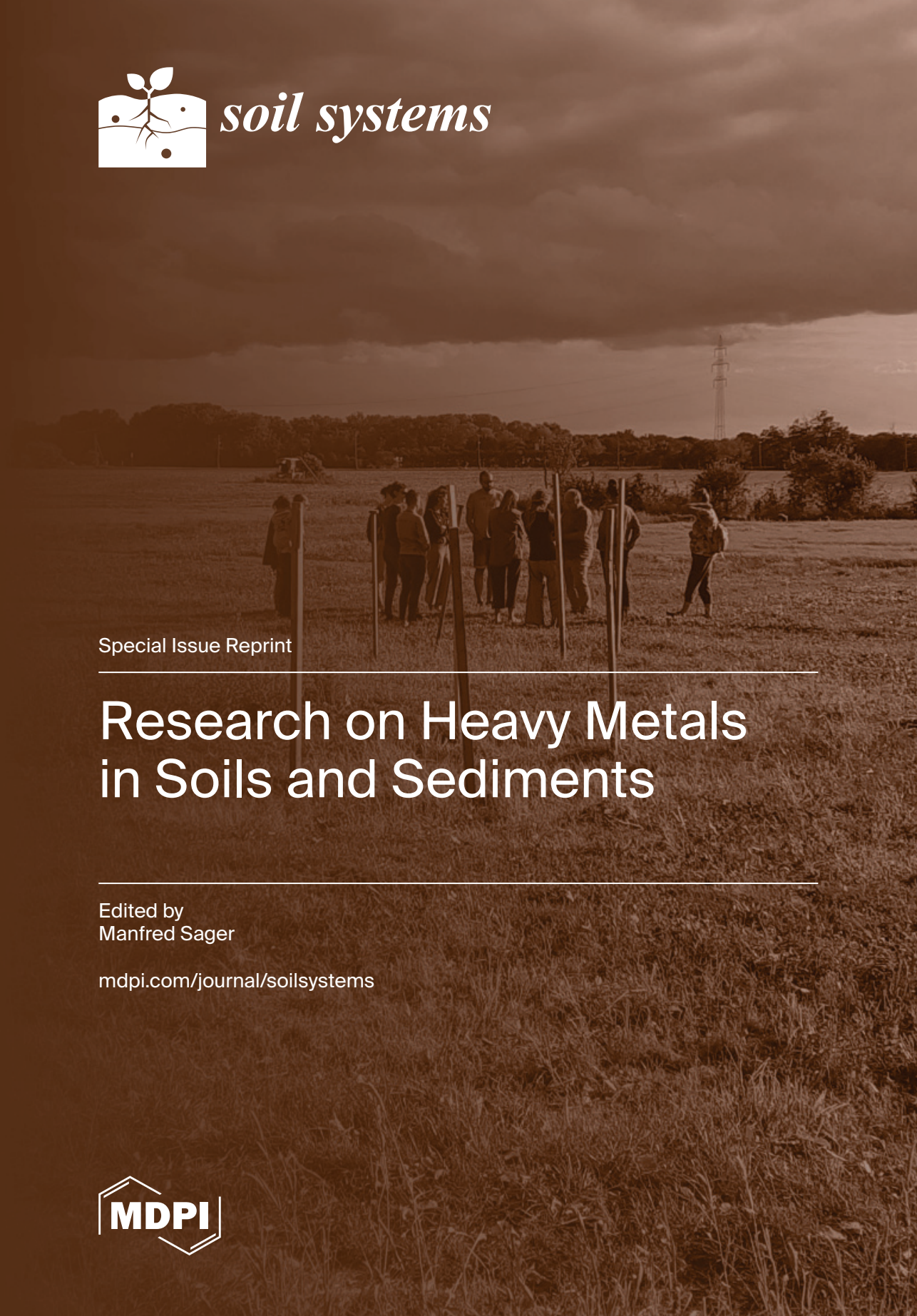

soil systems

Special Issue Reprint

Research on Heavy Metals in Soils and Sediments

Edited by
Manfred Sager

mdpi.com/journal/soilsystems

MDPI

Research on Heavy Metals in Soils and Sediments

Research on Heavy Metals in Soils and Sediments

Guest Editor

Manfred Sager

MDPI

Basel • Beijing • Wuhan • Barcelona • Belgrade • Novi Sad • Cluj • Manchester

Guest Editor
Manfred Sager
Bioforschung Austria
Vienna
Austria

Editorial Office
MDPI AG
Grosspeteranlage 5
4052 Basel, Switzerland

This is a reprint of the Special Issue, published open access by the journal *Soil Systems* (ISSN 2571-8789), freely accessible at: https://www.mdpi.com/journal/soilsystems/special_issues/NR0B2B330P.

For citation purposes, cite each article independently as indicated on the article page online and as indicated below:

Lastname, A.A.; Lastname, B.B. Article Title. *Journal Name* **Year**, *Volume Number*, Page Range.

ISBN 978-3-7258-3707-6 (Hbk)
ISBN 978-3-7258-3708-3 (PDF)
https://doi.org/10.3390/books978-3-7258-3708-3

Cover image courtesy of Manfred Sager

© 2025 by the authors. Articles in this book are Open Access and distributed under the Creative Commons Attribution (CC BY) license. The book as a whole is distributed by MDPI under the terms and conditions of the Creative Commons Attribution-NonCommercial-NoDerivs (CC BY-NC-ND) license (https://creativecommons.org/licenses/by-nc-nd/4.0/).

Contents

About the Editor . . . . . **vii**

Manfred Sager
Research on Heavy Metals in Soils and Sediments
Reprinted from: *Soil Syst.* **2025**, *9*, 9, https://doi.org/10.3390/soilsystems9010009 . . . . . **1**

Luna Araceli Pérez, Tatiana Izquierdo, Manuel Abad, Manuel Caraballo, Sebastián Ureta and Francisco Ruiz
The Past Is Never Dead: Soil Pollution from Mining in the Copiapó River Basin (Northern Chile)
Reprinted from: *Soil Syst.* **2024**, *8*, 106, https://doi.org/10.3390/soilsystems8040106 . . . . . **3**

Shatabdi Saha, Kumi Watanabe, Tomoyuki Makino, Hitoshi Kanno, Kazuhiko Kimura and Shin-Ichi Yamasaki
Verification of the Solid–Liquid Separation of Waterlogged Reduced Soil via a Centrifugal Filtration Method
Reprinted from: *Soil Syst.* **2024**, *8*, 61, https://doi.org/10.3390/soilsystems8020061 . . . . . **12**

Shamim Al Mamun, Niklas J. Lehto, Jo Cavanagh, Richard McDowell, Liv Kellermann and Brett H. Robinson
Temporal Changes in Cd Sorption and Plant Bioavailability in Compost-Amended Soils
Reprinted from: *Soil Syst.* **2023**, *7*, 107, https://doi.org/10.3390/soilsystems7040107 . . . . . **23**

Tatiana Minnikova, Sergey Kolesnikov, Anna Kuzina, Dmitry Trufanov, Ekaterina Khrapay and Anatoly Trushkov
Enzymatic Diagnostics of Soil Health of the European Part of Russia with Lead Contamination
Reprinted from: *Soil Syst.* **2024**, *8*, 76, https://doi.org/10.3390/soilsystems8030076 . . . . . **37**

Yelizaveta Chernysh, Viktoriia Chubur, Iryna Ablieieva, Polina Skvortsova, Olena Yakhnenko, Maksym Skydanenko, et al.
Soil Contamination by Heavy Metals and Radionuclides and Related Bioremediation Techniques: A Review
Reprinted from: *Soil Syst.* **2024**, *8*, 36, https://doi.org/10.3390/soilsystems8020036 . . . . . **58**

Christos Kikis, Georgios Thalassinos and Vasileios Antoniadis
Soil Phytomining: Recent Developments—A Review
Reprinted from: *Soil Syst.* **2024**, *8*, 8, https://doi.org/10.3390/soilsystems8010008 . . . . . **83**

Md Abu Raihan Chowdhury and David M. Singer
Complex Speciation and Distribution of Iron, Sulfur, and Trace Metals in Coal Mine Soils Reflect Grain- and Sub-Grain-Scale Heterogeneity during Pyrite Oxidative Dissolution
Reprinted from: *Soil Syst.* **2024**, *8*, 2, https://doi.org/10.3390/soilsystems8010002 . . . . . **117**

Maria Androudi, Vasiliki Liava, Eleni Tsaliki, Ioannis Ipsilantis and Evangelia E. Golia
Use of *Cannabis sativa* L. for Improving Cadmium-Contaminated Mediterranean Soils—Effect of Mycorrhizal Colonization on Phytoremediation Capacity
Reprinted from: *Soil Syst.* **2024**, *8*, 100, https://doi.org/10.3390/soilsystems8030100 . . . . . **135**

Zaw Min Han, Sartaj Ahmad Bhat, Shiamita Kusuma Dewi, Yongfen Wei and Fusheng Li
Adsorption of Arsenic and Cadmium on Biodegradable and Non-Biodegradable Microplastics in Soil: Comparison Based on Batch Experiment
Reprinted from: *Soil Syst.* **2024**, *8*, 116, https://doi.org/10.3390/soilsystems8040116 . . . . . **152**

Chukwudi E. Nwoko, David M. Singer, Allyson C. Tessin, Rachel Izworski and Chloe Heestand
Spatial Variability in the Speciation of Lead (Pb) and Other Metals Across Urban Lawns Is Linked to Post-Deposition Weathering Reactions
Reprinted from: *Soil Syst.* **2024**, *8*, 113, https://doi.org/10.3390/soilsystems8040113 . . . . . **167**

Matt Dodd, Abdurrazzaq Durojaiye and Julia Dupuis
Distribution and In Vitro Bioaccessibility of Potentially Toxic Metals in Soils at Select Urban Parks at Eastern Canadian Cities
Reprinted from: *Soil Syst.* **2024**, *8*, 123, https://doi.org/10.3390/soilsystems8040123 . . . . . **195**

Enilson de Barros Silva, Múcio Mágno de Melo Farnezi, Lauana Lopes dos Santos, Alexandre Chistofaro Silva, Paulo Henrique Grazziotti, Luís Reynaldo Ferracciú Alleoni, et al.
Nickel Effects on Growth and Phytolith Yield of Grasses in Contaminated Soils
Reprinted from: *Soil Syst.* **2024**, *8*, 17, https://doi.org/10.3390/soilsystems8010017 . . . . . **210**

Luis Miguel Cáceres, Francisco Ruiz, Javier Bermejo, Lucía Fernández, María Luz González-Regalado, Joaquín Rodríguez Vidal, et al.
Sediments as Sentinels of Pollution Episodes in the Middle Estuary of the Tinto River (SW Spain)
Reprinted from: *Soil Syst.* **2023**, *7*, 95, https://doi.org/10.3390/soilsystems7040095 . . . . . **222**

Jeganathan Pandiyan, Radjassegarin Arumugam, Khalid A. Al-Ghanim, Nadezhda Sachivkina, Marcello Nicoletti and Marimuthu Govindarajan
Heavy Metals in Wetland Ecosystem: Investigating Metal Contamination in Waterbirds via Primary Feathers and Its Effect on Population and Diversity
Reprinted from: *Soil Syst.* **2023**, *7*, 104, https://doi.org/10.3390/soilsystems7040104 . . . . . **231**

About the Editor

Manfred Sager

Manfred Sager was born in Vienna. He studied chemistry, specializing in inorganic analytical chemistry, and achieved the right to teach it at universities. After 8 years of geochemical analysis, he changed discipline to agricultural chemistry and food analysis. He is currently employed as a senior adviser by Bioforschung Austria to support organic farming. His general interests cover mobilities of trace elements and nutrients in soils, plant growth substrates, and sediments, as well as plant uptake.

soil systems

MDPI

Editorial

Research on Heavy Metals in Soils and Sediments

Manfred Sager

Bio Forschung Austria, 1220 Vienna, Austria; m.sager@bioforschung.at

This special edition of the journal *Soil Systems* contains 14 articles dealing with current research on cationic trace elements and semi-metals. Almost all continents have been included. Whereas As, Cd, Co, Cu, Pb and Zn have been examined quite often, the elements Hg, Tl, Mo Se and Sb and the noble metals have attracted much less attention. The everlasting questions of this topic are concerned with soil to plant transfer, accumulations in the food web, anthropogenic influences, mobilizations by weathering and fixations by remediation processes. The term "available fraction" is still controversial, as well as the sampling depth of the soils, which might lead to misinterpretations when the obtained numbers are directly compared. Unfortunately, many authors are not aware that the soil to plant transfer depends on species, timescale and climatic conditions, even on nutrient levels, and not just on the soil chemistry itself. Thus, fundamental field studies, which establish correlations between mobile fractions and plants, i.e., soil–biota uptake, should be considered. Metal levels also influence bacterial, fungal and enzymatic activities in soils.

Therefore, it is necessary to characterize test substrates using fundamental parameters, like pH, grain size, carbon and nitrogen contents, etc., to enable reasonable comparisons of data.

Whereas analytical techniques of multi-element determinations for total contents and aqua regia extracts have been established, developments to determine speciation and mobilities are still in progress. Though current research in analytical chemistry is largely focused on large biomolecules, pesticides and metabolites, some progress in the detection of surface coatings, secondary minerals and weathering products can still be seen. ICP-OES and ICP-MS are widely used techniques to determine various elements as solutions, whereas X-ray fluorescence is favored to directly target solids for total contents. Discrepancies between total contents and aqua regia mobiles still remain but are marginal for cationic trace elements like Cd, Cu, Co, Hg, Pb and Zn in many cases.

The selective and sequential leaching of soils, sediments and minerals are somehow complementary to microlocal analyses like μ-XRF (micro-X-ray fluorescence) and SEM-EDA (scanning electron microscopy electron diffraction analysis). Whereas leaching targets the mobilities of rather than the representative amounts of solids in a changing chemical environment, microlocal techniques investigate mineral phases and coatings at a small scale. Examples in this volume are details of pyrite weathering or alterations of microplastic surfaces.

A review of remediation techniques using bacterial biomass or phosphogypsum reveals that similar remediation techniques could be employed both for metal and radioactive contaminations, which emanate from the U-238 and the Th-232 decay series.

Although many sewage treatment plants and purification facilities for industrial effluents have been built, soils and sediments are still polluted by industrial effluents, mining waste, agricultural residues and urban inputs. The control and development of remediation techniques are necessary on a permanently basis. The remediation of metal-polluted sites will be surely a future challenge, through either fixation for un-soluble components,

Citation: Sager, M. Research on Heavy Metals in Soils and Sediments. *Soil Syst.* **2025**, *9*, 9. https://doi.org/10.3390/soilsystems9010009

Received: 21 January 2025
Accepted: 23 January 2025
Published: 24 January 2025

Citation: Sager, M. Research on Heavy Metals in Soils and Sediments. *Soil Syst.* **2025**, *9*, 9. https://doi.org/10.3390/soilsystems9010009

Copyright: © 2025 by the author. Licensee MDPI, Basel, Switzerland. This article is an open access article distributed under the terms and conditions of the Creative Commons Attribution (CC BY) license (https://creativecommons.org/licenses/by/4.0/).

through biosorption for bacterial biomass, or through transfer to hyperaccumulator plants, which was discussed in two reviews.

Conflicts of Interest: The author declares no conflicts of interest.

List of Contributions:

1. Cáceres, L.; Ruiz, F.; Bermejo, J.; Fernández, L.; González-Regalado, M.; Vidal, J.; Abad, M.; Izquierdo, T.; Toscano, A.; Gómez, P.; Romero, V. Sediments as Sentinels of Pollution Episodes in the Middle Estuary of the Tinto River (SW Spain). *Soil Syst.* **2023**, *7*, 95. https://doi.org/10.3390/soilsystems7040095.
2. Pandiyan, J.; Arumugam, R.; Al-Ghanim, K.; Sachivkina, N.; Nicoletti, M.; Govindarajan, M. Heavy Metals in Wetland Ecosystem: Investigating Metal Contamination in Waterbirds via Primary Feathers and Its Effect on Population and Diversity. *Soil Syst.* **2023**, *7*, 104. https://doi.org/10.3390/soilsystems7040104.
3. Al Mamun, S.; Lehto, N.; Cavanagh, J.; McDowell, R.; Kellermann, L.; Robinson, B. Temporal Changes in Cd Sorption and Plant Bioavailability in Compost-Amended Soils. *Soil Syst.* **2023**, *7*, 107. https://doi.org/10.3390/soilsystems7040107.
4. Chowdhury, M.; Singer, D. Complex Speciation and Distribution of Iron, Sulfur, and Trace Metals in Coal Mine Soils Reflect Grain- and Sub-Grain-Scale Heterogeneity during Pyrite Oxidative Dissolution. *Soil Syst.* **2024**, *8*, 2. https://doi.org/10.3390/soilsystems8010002.
5. Kikis, C.; Thalassinos, G.; Antoniadis, V. Soil Phytomining: Recent Developments—A Review. *Soil Syst.* **2024**, *8*, 8. https://doi.org/10.3390/soilsystems8010008.
6. Silva, E.; Farnezi, M.; Santos, L.; Silva, A.; Grazziotti, P.; Alleoni, L.; Horák-Terra, I.; Nascimento, S.; Uane, B. Nickel Effects on Growth and Phytolith Yield of Grasses in Contaminated Soils. *Soil Syst.* **2024**, *8*, 17. https://doi.org/10.3390/soilsystems8010017.
7. Chernysh, Y.; Chubur, V.; Ablieieva, I.; Skvortsova, P.; Yakhnenko, O.; Skydanenko, M.; Plyatsuk, L.; Roubík, H. Soil Contamination by Heavy Metals and Radionuclides and Related Bioremediation Techniques: A Review. *Soil Syst.* **2024**, *8*, 36. https://doi.org/10.3390/soilsystems8020036.
8. Saha, S.; Watanabe, K.; Makino, T.; Kanno, H.; Kimura, K.; Yamasaki, S. Verification of the Solid–Liquid Separation of Waterlogged Reduced Soil via a Centrifugal Filtration Method. *Soil Syst.* **2024**, *8*, 61. https://doi.org/10.3390/soilsystems8020061.
9. Minnikova, T.; Kolesnikov, S.; Kuzina, A.; Trufanov, D.; Khrapay, E.; Trushkov, A. Enzymatic Diagnostics of Soil Health of the European Part of Russia with Lead Contamination. *Soil Syst.* **2024**, *8*, 76. https://doi.org/10.3390/soilsystems8030076.
10. Androudi, M.; Liava, V.; Tsaliki, E.; Ipsilantis, I.; Golia, E. Use of Cannabis sativa L. for Improving Cadmium-Contaminated Mediterranean Soils—Effect of Mycorrhizal Colonization on Phytoremediation Capacity. *Soil Syst.* **2024**, *8*, 100. https://doi.org/10.3390/soilsystems8030100.
11. Pérez, L.; Izquierdo, T.; Abad, M.; Caraballo, M.; Ureta, S.; Ruiz, F. The Past Is Never Dead: Soil Pollution from Mining in the Copiapó River Basin (Northern Chile). *Soil Syst.* **2024**, *8*, 106. https://doi.org/10.3390/soilsystems8040106.
12. Nwoko, C.; Singer, D.; Tessin, A.; Izworski, R.; Heestand, C. Spatial Variability in the Speciation of Lead (Pb) and Other Metals Across Urban Lawns Is Linked to Post-Deposition Weathering Reactions. *Soil Syst.* **2024**, *8*, 113. https://doi.org/10.3390/soilsystems8040113.
13. Han, Z.; Bhat, S.; Dewi, S.; Wei, Y.; Li, F. Adsorption of Arsenic and Cadmium on Biodegradable and Non-Biodegradable Microplastics in Soil: Comparison Based on Batch Experiment. *Soil Syst.* **2024**, *8*, 116; https://doi.org/10.3390/soilsystems8040116.
14. Dodd, M.; Durojaiye, A.; Dupuis, J. Distribution and In Vitro Bioaccessibility of Potentially Toxic Metals in Soils at Select Urban Parks at Eastern Canadian Cities. *Soil Syst.* **2024**, *8*, 123. https://doi.org/10.3390/soilsystems8040123.

Disclaimer/Publisher's Note: The statements, opinions and data contained in all publications are solely those of the individual author(s) and contributor(s) and not of MDPI and/or the editor(s). MDPI and/or the editor(s) disclaim responsibility for any injury to people or property resulting from any ideas, methods, instructions or products referred to in the content.

soil systems

MDPI

Communication

The Past Is Never Dead: Soil Pollution from Mining in the Copiapó River Basin (Northern Chile)

Luna Araceli Pérez [1], Tatiana Izquierdo [2], Manuel Abad [2], Manuel Caraballo [3], Sebastián Ureta [4] and Francisco Ruiz [5,*]

[1] Unidad de Peligros Geológicos y Ordenamiento Territorial, Dirección Regional Magallanes, Servicio Nacional de Geología y Minería, Punta Arenas 6200000, Chile; luna.perez@sernageomin.cl
[2] Departamento de Biología y Geología, Física y Química Inorgánica, Universidad Rey Juan Carlos, 28933 Móstoles, Spain; tatiana.izquierdo@urjc.es (T.I.); manuel.abad@urjc.es (M.A.)
[3] Departamento de Ingeniería Minera, Mecánica, Energética y de la Construcción, Universidad de Huelva, 21071 Huelva, Spain; mcaraballo@dimme.uhu.es
[4] College & Instituto para el Desarrollo Sustentable, Pontificia Universidad Católica de Chile, Macul 7821093, Chile; sureta@uc.cl
[5] Departamento de Ciencias de la Tierra, Universidad de Huelva, 21071 Huelva, Spain
* Correspondence: ruizmu@uhu.es

Abstract: This short paper analyses the concentrations of two major components (Fe, S) and eight trace elements (As, Au, Co, Cu, Hg, Ni, Mn, Zn) in soils and tailings from Tierra Amarilla (northern Chile) using ICP-Ms analysis. The levels of As, Au, Cu, Fe and S are very high and come from polymetallic sulphides from nearby mines, together with minor contributions of Co, Ni and Mn. Hg has its origin in the extreme seasonal flows of the Copiapó River, which erodes the dumps of old precious metal mines. These high concentrations require further analysis of possible metal immobilisation techniques, bioavailability or analysis in cultivated plants.

Keywords: pollution; soils; tailings; Tierra Amarilla; northern Chile

Citation: Pérez, L.A.; Izquierdo, T.; Abad, M.; Caraballo, M.; Ureta, S.; Ruiz, F. The Past Is Never Dead: Soil Pollution from Mining in the Copiapó River Basin (Northern Chile). *Soil Syst.* **2024**, *8*, 106. https://doi.org/10.3390/soilsystems8040106

Academic Editor: Manfred Sager

Received: 9 August 2024
Revised: 4 October 2024
Accepted: 8 October 2024
Published: 11 October 2024

Copyright: © 2024 by the authors. Licensee MDPI, Basel, Switzerland. This article is an open access article distributed under the terms and conditions of the Creative Commons Attribution (CC BY) license (https://creativecommons.org/licenses/by/4.0/).

1. Introduction

'The past is never dead. It's not even past', said the Nobel Prize in literature 1949 winner William Faulkner. This reflection is particularly applicable to certain regions of our planet whose current environmental scenario is a direct consequence of past actions, especially in mining regions. Waste dumps and slag heaps of past centuries have changed the original landscapes and caused heavy contamination of both soils and sediments [1,2]. Their removal by river currents, rainfall or agriculture can cause a redistribution of heavy metals and a new affectation of current environments, with notable consequences on the environment or on the food chain [3,4]. This is particularly dangerous in the case of some elements such as Hg, which is potentially poisonous to humans [5,6].

The Chilean Iron Belt is one of the most important mineralogenetic provinces in South America, as it encompasses the world's largest copper ore deposits, which have been exploited since pre-Hispanic times [7,8]. Copper is extracted from more than 40 ore deposits, as well as smaller but significant amounts of Ag, Au, Fe, Hg or Zn, among other ores [9,10]. This has caused significant environmental deterioration and the contamination of soils and sediments near the waste dumps or the redistribution of pollutants through rivers or occasional rainfall [11,12].

This communication analyses the geochemical content of soils and mining tailings located in the Copiapó river basin, around the town of Tierra Amarilla (northern Chile). Correlation analysis is applied to determine chemical associations and the possible sources of the detected elements.

2. Materials and Methods

2.1. Study Area

The Copiapó river flows through the region of Atacama (northern Chile) (Figure 1A,B) and its basin covers some 18,400 km^2. This area is characterised by a semi-arid climate and the presence of deserts, with an annual rainfall of less than 20 mm [13]. However, this river suffers periodic flooding episodes, as can be seen from historical information [14–16]. These floods can inundate areas subject to intense degradation due to heavy extensive mining activities in this region [17].

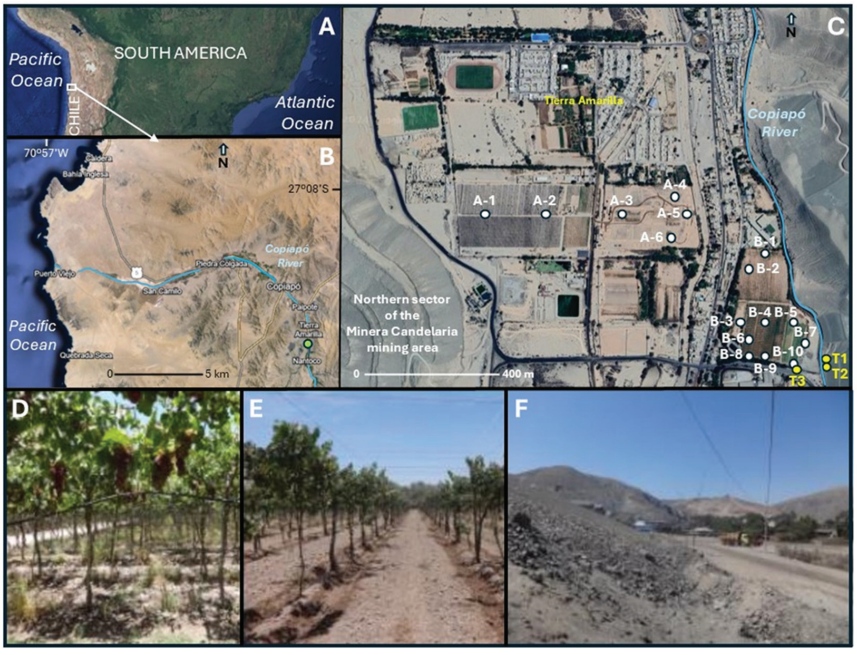

Figure 1. (**A**,**B**): location of Tierra Amarilla (northern Chile); (**C**): location of soil samples (white) and tailing samples (yellow). (**D**): partial view from sample A-1; (**E**): partial view from sample B-4; (**F**): partial view of tailings T1–T2. (**A**,**B**): courtesy of Google Earth.

Wastes from mining operations are very abundant in the basin of this river, with very high Cu contents in most cases [18,19]. In addition, some of them come from the cyanidation and amalgamation of precious metals such as Ag or Au [20] and are in close proximity to this river. This location can lead to a result in the partial redistribution of Hg-contaminated tailings due to periodic fluvial action and the presence of alluvial sediments with high Hg contents in the catchment, as already established for other metals such as Cr, Ni, Pb or Fe [21].

This paper analyses the geochemical content of soils and mining waste adjacent to two mining areas located in Tierra Amarilla (northern Chile) (Figure 1A,B). Minera Candelaria is a large open-pit and underground Cu and Au mine, while Minera Carola is an underground copper mine (Figure 1C).

2.2. Chemical Analysis, Geoaccumulation Index and Statistical Procedures

Sixteen soil samples were taken from two agricultural plots located near the mines of Minera Candelaria (A-1 to A-6) and Minera Carola (B-1 to B-10), as well as three samples from mine waste near Minera Carola (T1 to T3) (Figure 1C). The samples were manually pulverised in an agate mortar at the sedimentology laboratory of the Geology Department

of the University of Chile. They were then placed in polypropylene jars. An ICP-MS analysis of 0.5 g of each sampling point was performed via acid digestion with aqua regia (method AQ250) at ACME Analytical Laboratories S.A. (Bureau Veritas Mineral Laboratories Chile). The concentrations of major components (Fe and S, in %) and trace elements (As, Co, Cu, Mn, Ni and Zn in ppm; Au and Hg in ppb) were obtained. The quality control report (number SAN18000095.1) includes a check with three reference materials (STD DS11, STD OREAS45EA and BLK). The geoaccumulation index I_{geo} [22] was applied to the eight minor elements, based on the equation

$I_{geo} = \log_2 C_n / 1.5 B_n$ where C_n is the concentration of an element in a sample and B_n is the average concentration of that element in the earth's crust. Factor 1.5 is used to reflect the possible fluctuation of the element in the background value as well as minimal anthropogenic influences or inputs. In this paper, samples were classified as unpolluted ($I_{geo} < 0$), very low polluted ($0 < I_{geo} < 1$), low polluted ($1 < I_{geo} < 2$), moderately polluted ($2 < I_{geo} < 3$), highly polluted ($3 < I_{geo} < 4$), very highly polluted ($4 < I_{geo} < 5$) and extremely polluted ($I_{geo} > 5$). This index is also used in conjunction with the enrichment factor (EF) to assess the degree of soil contamination [23].

Linear correlation analysis has been used to test the relationship between the ten elements analysed, as well as to differentiate possible associations between them and different sources of origin, in coordination with their raw values. Positive correlations denote that one variable increases when the other also increases and negative correlations mean that one variable tends to increase when the other decreases. Values closer to 0 indicate an absence of correlation.

3. Results and Discussion

3.1. Chemistry

The results of the chemical analyses clearly differentiate mining waste from agricultural plots (Table 1). Tailings have the highest concentrations of As (93.7–163.2 ppm), Au (up to 1881.7 ppb), Co (74.1–197.5 ppm), Cu (3279–5658 ppm), Fe (11.53–15.7%), Mn (1016–1804 ppm), Ni (46.1–120.2 ppm) and S (1.6–4.5%), while their Hg levels (576–746 ppb) are lower or similar on average than those of agricultural soils (>1500 ppb in most samples). Average Zn contents remain in similar ranges in both groups (tailings: 146.2–186.7 ppm; soils: 99.2–226.8 ppm). Although mineralogical studies of these dumps have not been carried out, this chemical composition points to the presence of high percentages of polymetallic Fe and Cu sulphides with significant Au contents, e.g., the ores mined at Mina Carola [24].

The geochemical content of the soils is markedly different between the northwest area, close to Minera Candelaria (Zone 1-Z1-: samples A-1 to A-6), and the southeastern sector, close to the Minera Carola tailings (Zone 2 -Z2-: samples B-1 to B-10). The former parcel includes most of the lowest values of Cu (<450 ppm in most samples), As (21.7–28.5 ppm), Au (8.1–33.5 ppb), Co (13.2–15.1 ppm in most samples) and Ni (17.4–25.8 ppm in most samples), while the Hg values increase significantly from the vicinity of Mina Candelaria (337–861 ppb) towards the Copiapó River (>5000 ppb in most samples near the river). The absence of high Hg contents near Mina Candelaria (e.g., sample A-1) as well as in the Mina Carola tailings dumps (T1 to T3) would indicate that high levels of Hg in both zones are coming from the Copiapó river. Historically, this region is subject to major hydrometeorological events that cause the Copiapó River to overflow [17] and the erosion of tailings from old Ag, Au and Cu mines, with the consequent contamination of the surrounding floodplain with these metals [17,25].

Table 1. Geochemical analysis of soils (A-1 to A-6 close to Minera Candelaria; B-1 to B-10 close to Minera Carola tailings) and tailings (T1 to T3 near Minera Carola).

SAMPLE	As (ppm)	Au (ppb)	Co (ppm)	Cu (ppm)	Fe (%)	Hg (ppb)	Mn (ppm)	Ni (ppm)	S (%)	Zn (ppm)
A-1	23.7	74.4	14.6	447	3.33	337	688	44.4	0.1	147.4
A-2	28.5	8.1	15.1	333	3.71	861	760	18	0.34	144.3
A-3	58.9	33.5	21.1	408	3.34	5480	946	25.8	0.21	173
A-4	92.2	12.5	14.7	535	3.03	8570	768	22.5	0.28	151.3
A-5	21.7	8.9	13.2	187	3.02	660	633	17.4	0.21	99.2
A-6	69.9	21.2	14.1	287	2.98	6077	761	21.7	0.66	189.4
B-1	59.1	25.5	18.7	658	3.49	2668	990	27.1	0.21	205.7
B-2	47.9	21.9	15.9	676	3.06	1545	799	23.7	0.22	146.2
B-3	52	26.3	16.7	731	3.16	3172	781	22.3	0.26	169.6
B-4	56.4	30	18.3	858	3.47	2749	972	26.7	0.22	188.6
B-5	48.8	16.6	17	473	3.39	889	990	21.2	0.11	159.2
B-6	75.5	48.2	16.7	720	3.16	3220	839	22.3	0.18	166.9
B-7	90	105.5	25	1447	4.14	3007	1205	25.2	0.27	226.8
B-8	67.5	36.5	17.3	571	3.19	4681	846	22.6	0.15	164.9
B-9	79.6	55.3	20.2	896	3.6	6848	1005	29.5	0.13	213.8
B-10	101.4	116	18.2	739	3.22	6017	941	23.3	0.11	205.5
T1	93.7	99.3	74.1	3279	11.53	746	1214	47.1	1.6	125
T2	159.8	1881.7	87.2	5658	12.55	576	1804	46.7	1.65	186.7
T3	163.2	318.4	197.5	4725	15.7	618	1016	120.2	4.5	131.6

Z2 shows higher average values than Z1, especially in As (Z1: 49.1 ppm; Z2: 67.8 ppm), Au (Z1: 26.4 ppb; 48.2 ppb), Cu (Z1: 366 ppm; 777 ppm), Mn (Z1: 759.3 ppm; Z2: 936.8 ppm) and, to a lesser extent, Zn (Z1: 150.8 ppm; Z2: 184.7 ppm). These differences are even more pronounced if only the samples closest to the tailings of Minera Carola are taken into account (Figure 1: samples B-7, B-9 and B-10), where the soils that are most contaminated in terms of As (up to 101.4 ppm), Au (up to 116 pp), Cu (up to 1447 ppm), Mn (up to 1205 ppm) or Zn (up to 226.8 ppm) are found. Consequently, the pollution of the Z2 soils would come from the adjoining Mina Carola tailings dumps. This direct relationship between the chemical compositions of mine dumps and adjacent soils has been repeatedly observed in various mining regions of Chile [26,27].

3.2. Geoaccumulation Index

Most of the soil samples are highly to extremely polluted by As (Figure 2A; $2.78 < I_{geo} < 5.77$), while Z2 shows moderate to very high I_{geo} values for Cu (Figure 2D; $2.81 < I_{geo} < 4.42$), clearly higher than Z1 ($1.47 < I_{geo} < 2.98$). Z2 is also heavily contaminated by Au (Figure 2B) and Hg (Figure 2E), especially at its southeastern end. Some samples of Z1 are also heavily contaminated by this metal (e.g., A-4 or A-6). These high values contrast with the very low to low Zn contamination (Figure 2H; $0.02 < I_{geo} < 1.22$) or the negative values of Igeo for Co (Figure 2C), Mn (Figure 2F) or Ni (Figure 2G). These values are similar to those deduced in other polluted soils in Chile, although this index depends on the background considered [11]. The mine tailings from Mina Carola are heavily to extremely polluted by As ($4.97 < I_{geo} < 5.76$), Au ($3.92 < I_{geo} < 7.97$) and Cu ($5.6 < I_{geo} < 6.39$). Also noteworthy is their low to moderate Co contamination ($1.1 < I_{geo} < 2.52$) and the negative I_{geo} values for Hg in these tailings dumps.

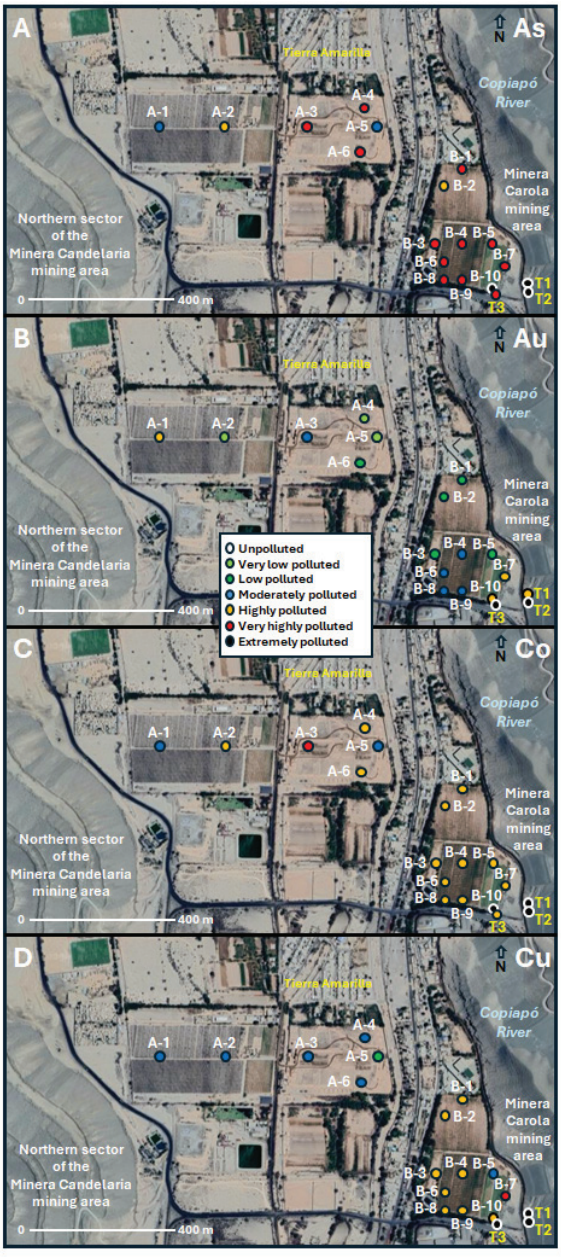

Figure 2. *Cont*.

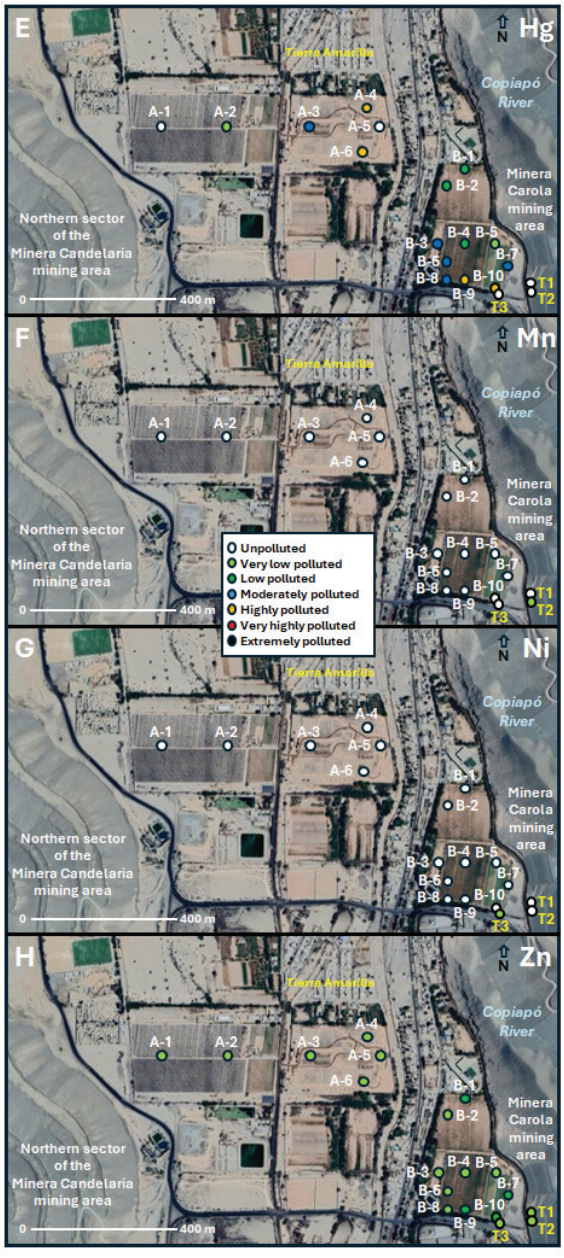

Figure 2. Geoaccumulation index. (**A**): As; (**B**): Au; (**C**): Co; (**D**): Cu; (**E**): Hg; (**F**): Mn; (**G**): Ni; (**H**): Zn.

3.3. Correlation Analysis

The bivariate analysis reveals a strong positive and significant correlation between As, Au, Co, Cu, Fe, Mn, Ni and S (Table 2; r > 0.6 in most cases; $p < 0.01$). Hg and Zn show negative correlations with most of these elements, which contrasts with a positive and significant correlation between these two elements. The first group would be mainly contributed to by nearby mining facilities and a statistically significant correlation between some of these elements is frequent in soils close to ore deposits due to weathering [28,29].

Nevertheless, Hg would come from the erosion of former small precious metal mines by seasonal flows of the Copiapó river upstream. These small mines are numerous in this region [30].

Table 2. Correlation coefficient matrix. Bold: r > 0.6; $p < 0.01$.

	As	Au	Co	Cu	Fe	Hg	Mn	Ni	S	Zn
As	1									
Au	**0.65**	1								
Co	**0.77**	0.44	1							
Cu	**0.85**	**0.79**	**0.86**	1						
Fe	**0.79**	**0.61**	**0.94**	**0.96**	1					
Hg	0.06	−0.28	−0.37	−0.41	−0.45	1				
Mn	**0.71**	**0.82**	0.46	**0.81**	**0.65**	−0.24	1			
Ni	**0.66**	0.31	**0.96**	**0.75**	**0.86**	−0.36	0.32	1		
S	**0.73**	0.38	**0.98**	**0.8**	**0.91**	−0.33	0.36	**0.94**	1	
Zn	0.22	0.13	−0.24	−0.05	−0.23	0.44	0.37	−0.23	−0.3	1

3.4. Considerations for Future Research

The obtained levels of heavy metals, such as Cu or Hg, require further analysis in the following lines of research: (i) possibilities for the partial immobilisation of these metals in soils; (ii) an analysis of their bioavailability in the plants that grow on them, with the application of the free ion activity model (FIAM) or the correlation between labile metals in soils, determined using simple or sequential extraction methods, and their accumulation in plants; or (iii) a study of metal concentrations in roots, stems and fruits of cultivated plants, in order to prevent possible subsequent negative effects on human health [31,32].

4. Conclusions

The main findings of this research are as follows:

(i) The studied soils of Tierra Amarilla are highly to extremely polluted by As, Au, Cu, Fe and S from nearby mining operations, mainly from the Mina Carola mine;
(ii) Hg also shows moderate to high levels and geoaccumulation rates in most of the soils analysed, while the waste dumps are not contaminated;
(iii) The contents of this metal would come from the erosion of old tailings of precious metal mines, which used it in their production processes;
(iv) These high concentrations require further analysis to investigate the relationship between these soils and the plants grown in them.

Author Contributions: Conceptualisation: all authors; methodology, all authors.; software; L.A.P. and F.R.; validation, T.I. and M.A.; formal analysis, all authors; investigation, L.A.P.; resources, all authors; data curation, all authors; writing—original draft preparation, L.A.P. and F.R.; writing—review and editing, T.I., M.A.; visualisation, L.A.P., T.I.; supervision, F.R.; project administration, L.A.P.; funding acquisition, all authors; research and first manuscript, M.C., S.U. All authors have read and agreed to the published version of the manuscript.

Funding: This research was funded by Junta de Andalucía (RNM-238 and RNM-283).

Institutional Review Board Statement: Not applicable.

Informed Consent Statement: Not applicable.

Data Availability Statement: Data are available upon request.

Acknowledgments: The authors acknowledge ANID (Agencia Nacional de Investigación) for its financial support through grant FONDECYT (Fondo Nacional de Desarrollo Científico y Tecnológico) 11160405 (COPIFLOOD project), Universidad Rey Juan Carlos for its financial support through the IMPULSO project VARHIDRO (M2994) and Junta de Andalucía (group RNM-238). This study is a contribution to the Research Center in Historical, Cultural and Natural Heritage (CIPHCN) of the University of Huelva.

Conflicts of Interest: The authors declare no conflicts of interest.

References

1. Benvenuti, M.; Mascaro, I.; Corsini, F.; Lattanzi, P.; Parrini, P.; Tanelli, G. Mine waste dumps and heavy metal pollution in abandoned mining district of Boccheggiano (Southern Tuscany, Italy). *Environ. Earth Sci.* **1997**, *30*, 238–243. [CrossRef]
2. García-Guinea, J.; Correcher, V.; Recio-Vázquez, L.; Crespo-Feo, E.; González-Martín, R.; Tormo, L. Influence of accumulation of heaps of steel slag on the environment: Determination of heavy metals content in the soils. *An. Acad. Bras. Ciênc.* **2010**, *82*, 267–277. [CrossRef] [PubMed]
3. Omatola, M.; Mpode, V.; Oluranti, O. Heavy metal pollution from gold mines: Environmental effects and bacterial strategies for resistance. *Int. J. Environ. Res. Public Health* **2016**, *13*, 1047. [CrossRef] [PubMed]
4. Cáceres, L.M.; Ruiz, F.; Bermejo, J.; Fernández, L.; González-Regalado, M.L.; Rodríguez Vidal, J.; Abad, M.; Izquierdo, T.; Toscano, A.; Gómez, P.; et al. Sediments as sentinels of pollution episodes in the middle estuary of the Tinto River (SW Spain). *Soil Syst.* **2024**, *7*, 95. [CrossRef]
5. Li, R.; Wu, H.; Ding, J.; Fu, W.; Gan, L.; Li, Y. Mercury pollution in vegetables, grains and soils from areas surrounding coal-fired power plants. *Sci. Rep.* **2017**, *7*, 46545. [CrossRef]
6. Al-Zahra, F. Mercury Pollution: Dangers and Treatment. In *Marine Pollution-Recent Developments*; Mancuso, M., Abbas, M.H.H., Bottari, T., Abdelhafez, A.A., Eds.; IntechOpen: Rijeka, Croatia, 2023; Chapter 10. [CrossRef]
7. Figueroa, V.; Salazar, D.; Salinas, H.; Núñez-Regueiro, P.; Manríquez, G. Pre-hispanic mining ergology of northern Chile: An archaeological perspective. *Chungara Rev. Antropol. Chil.* **2013**, *45*, 61–81. [CrossRef]
8. Pederson, L. *La Industria Minera del Norte Chico, Chile: Desde la Conquista a 1963*; RIL Editores: Santiago, Chile, 2008.
9. Maksaev, V.; Zentilli, M. Chilean strata-bound Cu-(Ag) Deposits: An overview. In *Hydrothermal Iron Oxide Copper-Gold & Related Deposits: A Global Perspective*; Porter, T., Ed.; PGC Publishing: Adelaide, Australia, 2002; pp. 185–205.
10. Heuser, G.; Arancibia, G.; Veloso, E.E.; Cembrano, J.; Oliveira, P.F.; Nehler, M.; Bracke, R. The evolution of the Dominga Fe-Cu deposit (northern Chile): Insights from mineral textures and micro-CT analysis. *Ore Geol. Rev.* **2020**, *119*, 103316. [CrossRef]
11. Ministerio de Ambiente de Chile. *Informe del Estado del Medioambiente*; Ministerio del Medio Ambiente, Gobierno de Chile: Santiago, Chile, 2016; p. 557. Available online: https://bibliotecadigital.infor.cl/handle/20.500.12220/21354 (accessed on 5 May 2024).
12. Garcia, D.; Tapia, J.; Aguilera, J.; Vega, C.; Zúñiga, P.; Lavin, P.; Rojas, L.; Valdés, J. Contamination of urban soils in a historical mining town of northern Chile. *Environ. Earth Sci.* **2024**, *83*, 182. [CrossRef]
13. CADE-IDEPE. *Cuenca del río Cipiapó. Diagnóstico y Clasificación de los Cursos y Cuerpos de Agua Según Objetivos de Calidad*; Gobierno de Chile, Ministerio de Obras Públicas, Dirección General de Aguas: Santiago, Chile, 2004; p. 122.
14. Simón, I. Desbordamientos del río Copiapó, Chile, e inundaciones urbanas: 1833–1929. *Agua Territ.* **2023**, *22*, 43–60. [CrossRef]
15. Izquierdo, T.; Abad, M.; Gómez, Y.; Gallardo, D.; Rodríguez-Vidal, J. The March 2015 catastrophic flood event and its impacts in the city of Copiapó (southern Atacama Desert). An integrated analysis to mitigate future mudflow derived damages. *J. S. Am. Earth Sci.* **2021**, *105*, 102975. [CrossRef]
16. Izquierdo, T.; Rivera, A.; Galeano, A.; Gallardo, D.; Salas, V.; Aparicio, O.; Buylaert, J.P.; Ruiz, F.; Abad, M. Historical catastrophic floods at the southern edge of the Atacama Desert: A multi-archive reconstruction of the Copiapó river extreme events. *Global Planet. Chang.* **2024**, *236*, 104411. [CrossRef]
17. Aguilar, G.; Valdés, A.; Cabré, A.; Galdames, F. Flash floods controlling Cu, Pb, As and Hg variations in fluvial sediments of a river impacted by metal mining in the Atacama Desert. *J. S. Am. Earth Sci.* **2021**, *109*, 103290. [CrossRef]
18. Higueras, P.; Oyarzún, R.; Oyarzún, J.; Maturana, H.; Lillo, J.; Morata, D. Environmental assessment of copper-gold-mercury mining in the Andacollo and Punitaqui districts, northern Chile. *Appl. Geochem.* **2004**, *19*, 1855–1864. [CrossRef]
19. Espinoza, F. Influencia de los Factores Naturales y Antropogénicos en la Geoquímica de Sedimentos Fluviales de las Cuencas Vítor y San José de Azapa; XV Región de Arica y Parinacota, Chile. Tesis de Licenciatura, Universidad de Chile, Santiago, Chile, 2013; p. 137.
20. CEDEUS. *Contaminación por Metales en Suelos de Copiapó: Diagnóstico y Propuestas Públicas*; Cedeus, Reporte Técnico: Santiago, Chile, 2022; p. 37.
21. Cortés, I.; Ríoz, J.; Gaete, L.; Tchernitchin, A.N. Metales pesados en muestras ambientales de la Región de Atacama. Situación postaluviones. In Proceedings of the Actas XIV Congreso Geológico Chileno, La Serena, Chile, 4–8 October 2015; pp. 302–305.
22. Müller, G. Index of geoaccumulation in sediments of the Rhine River. *Geojournal* **1969**, *2*, 108–118.
23. Arooj, S.; Naz, S.; Qaisar, A.; Satti, S.; Razzaq, A.; Alhidary, I.; Tufarelli, V. Estimation of Heavy Metals Enrichment and Geo-Accumulation Associated with Habitat Quality from Selected Wildlife Parks. *Soil Sedim. Contam. Int. J.* **2024**, 1–18. [CrossRef]

24. Rabbia, O.M.; Frutos, J.; Pop, N.; Isache, C.; Sanhueza, V.; Edelstein, O. Características isotópicas de la mineralización de Cu)-Fe) de Mina Carola, distrito minero Punta del Cobre, norte de Chile. In Proceedings of the Actas XIII Congreso Geológico Argentino y III Congreso de Exploración de Hicrocarburos, Buenos Aires, Argentina, 13–18 October 1996; pp. 241–253.
25. Izquierdo, T.; Bonnail, E.; Abad, M.; Dias, M.I.; Prudencio, M.I.; Marques, R.; Rodríguez Vidal, J.; Ruiz, F. Pollution and potential risk assessment of flood sediments in the urban area of the mining Copiapó basin (Atacama Desert). *J. S. Am. Earth Sci.* **2020**, *103*, 102714. [CrossRef]
26. Lam Esquenazi, E.; Norambuena, B.K.; Montofré, I.; Gálvez, M. Evaluation of soil intervention values in mine tailings in northern Chile. *PeerJ* **2018**, *6*, e5879. [CrossRef]
27. Espinoza, S.E.; Quiroz, I.A.; Magni, C.R.; Yáñez, M.A.; Martínez, E.E. Long-Term effects of copper mine tailings on surrounding soils and sclerophyllous vegetation in central Chile. *Water Air Soil Pollut.* **2022**, *233*, 288. [CrossRef]
28. Roca-Perez, L.; Boluda, R.; Rodríguez-Martín, J.A.; Ramos-Miras, J.; Tume, P.; Roca, N.; Bech, J. Potentially harmful elements pollute soil and vegetation around the Atrevida mine (Tarragona, NE Spain). *Environ. Geochem. Health* **2023**, *45*, 9215–9230. [CrossRef]
29. Cheng, C.; Xu, Z.1; Feng, S.; Wang, L. Distribution, ecological risk and Source analysis of heavy metals in farmland soil around Chating copper ore in Xuancheng region of southern China. *Pol. J. Environ. Stud.* **2023**, *32*, 1581–1594. [CrossRef]
30. Cabello, J. Gold deposits in Chile. *Andean Geol.* **2021**, *48*, 1–23. [CrossRef]
31. Peijnenburg, W.; Jager, T. Monitoring approaches to assess bioaccessibility and bioavailability of metals: Matrix issues. *Ecotoxic. Environ. Saf.* **2003**, *56*, 63–77. [CrossRef] [PubMed]
32. Verdejo, J.; Ginocchio, R.; Sauvé, S.; Salgado, E.; Neaman, A. Thresholds of copper phytotoxicity in field-collected agricultural soils exposed to copper mining activities in Chile. *Ecotoxic. Environ. Saf.* **2015**, *122*, 171–177. [CrossRef] [PubMed]

Disclaimer/Publisher's Note: The statements, opinions and data contained in all publications are solely those of the individual author(s) and contributor(s) and not of MDPI and/or the editor(s). MDPI and/or the editor(s) disclaim responsibility for any injury to people or property resulting from any ideas, methods, instructions or products referred to in the content.

soil systems

MDPI

Article

Verification of the Solid–Liquid Separation of Waterlogged Reduced Soil via a Centrifugal Filtration Method

Shatabdi Saha [1], Kumi Watanabe [2], Tomoyuki Makino [1,*], Hitoshi Kanno [1], Kazuhiko Kimura [3] and Shin-Ichi Yamasaki [4]

[1] Graduate School of Agricultural Science, Tohoku University, Sendai 980-8572, Japan; shatabdisaha.esrm@gmail.com (S.S.); hitoshi.kanno.a2@tohoku.ac.jp (H.K.)
[2] Graduate School of Life Sciences, Tohoku University, Sendai 980-8577, Japan; kumi.watanabe.r4@dc.tohoku.ac.jp
[3] School of Food, Agriculture and Environmental Sciences, Miyagi University, Sendai 981-3298, Japan; kimurakz@myu.ac.jp
[4] Graduate School of Environmental Studies, Tohoku University, Sendai 980-8579, Japan; ikasamay@plum.ocn.ne.jp
* Correspondence: tomoyuki.makino.d6@tohoku.ac.jp; Tel.: +81-022-757-4099

Abstract: The efficient separation of solid and liquid phases of soil under reductive conditions is of the utmost importance to study soil chemistry and to predict the mobility and bioavailability of nutrients and toxic contaminants in waterlogged reduced soils (WRSs). However, there is no established method for efficiently separating the solid and liquid phases of WRS within a short time while maintaining its reductive conditions. This study aimed to verify the applicability of a simple centrifugal filtration method (CFM) for the efficient separation of solid and liquid phases of a WRS and examine the CFM-extracted soil solution to confirm that the reductive condition was maintained during the solid–liquid separation process. Incubation experiments were performed under reductive conditions with or without ethanol/molasses used as additional organic material (OM), while the soil solution was collected by both a suction method and CFM at different centrifugation speeds (700, 2760, and 11,000 rpm) and times (1–7 min). The results showed that the soil pH increased with time while the Eh decreased, indicating that its reducing state was enhanced during the incubation experiments. The addition of OM promoted the reductive conditions in the first days of the experiments. Centrifugation speed, rather than time, was found to be the key to extract the maximum amount of soil solution, while a higher centrifugation speed (11,000 rpm), which represents the permanent wilting point, was found to be most effective for extracting the maximum amount of soil solution. The results exhibited no significant difference in solute (As, Fe(II), and Mn) concentrations when varying amounts of CFM-extracted soil solution were measured. The statistical analysis also indicated no significant ($p > 0.05$) difference between the solute concentrations in the CFM-extracted soil solution and the solute concentrations in the soil solution extracted by the suction method, confirming that the reductive condition was maintained during solid–liquid separation by CFM. This study suggests that CFM operating at a higher centrifugation speed could potentially be employed as a simple and highly effective technique to efficiently separate the solid and liquid phases of WRS (sandy clay loam) within a short time while maintaining its reductive conditions.

Keywords: soil properties; soil solution; suction method; soil redox potential; solute concentrations; reductive conditions

Citation: Saha, S.; Watanabe, K.; Makino, T.; Kanno, H.; Kimura, K.; Yamasaki, S.-I. Verification of the Solid–Liquid Separation of Waterlogged Reduced Soil via a Centrifugal Filtration Method. *Soil Syst.* **2024**, *8*, 61. https://doi.org/10.3390/soilsystems8020061

Academic Editor: Girish Choppala

Received: 29 April 2024
Revised: 18 May 2024
Accepted: 28 May 2024
Published: 30 May 2024

Copyright: © 2024 by the authors. Licensee MDPI, Basel, Switzerland. This article is an open access article distributed under the terms and conditions of the Creative Commons Attribution (CC BY) license (https://creativecommons.org/licenses/by/4.0/).

1. Introduction

The extraction and study of soil solutions is the basis for understanding pedogenic processes, the fate and transport of solutes, nutrient cycling, equilibrium and kinetic factors, and the bioavailability and leaching of toxic contaminants under both natural and engineered conditions [1,2]. Thus, the efficient separation of solid (soil) and liquid

(soil solution) phases from the soil matrix is of paramount importance. Various in situ (field-based) and ex situ (laboratory-based) methods have been established to collect soil solutions, either with or without the separation of the solid–liquid phases of the soil matrix, under aerobic/upland conditions. For example, Elkhatib et al. reported that centrifugation is a rapid, reliable, and cost-effective method for soil solution collection and subsequent chemical characterization [3]. Dahlgren found that high-speed centrifugation was the simplest method that resulted in higher solute concentrations compared to column equilibrium or immiscible displacement techniques when the soil was sufficiently moist and investigated them to study pH-sensitive solutes such as trace metals [1]. Similar results were also reported by Geibe et al. when the authors compared the centrifugation drainage method with suction and zero-tension lysimeters [2]. Fraters et al. also observed constant concentrations of solutes with an increasing amount of soil solution when using the centrifugation drainage method [4].

On the other hand, the suction method has also been widely used to extract soil solutions, even from flooded lowland soils or waterlogged reduced soils (WRSs), which have been found to be associated with several problems resulting from soil macropore inhomogeneities and the spatial variability of the investigated soil properties [5]. Although studies reported that the pressure (or squeezing) method can be used to separate the water from sediment samples under a N_2 supply, this method requires several hours for such solid–liquid separation [6,7]. However, to the best of our knowledge, there is no established method for collecting soil solutions by efficiently separating the solid and liquid phases of WRS within a short time while maintaining its reductive (anaerobic) conditions.

Under waterlogged reduced conditions, significant changes occur in soil physicochemical properties, behavior and transport of essential nutrients, and toxic contaminants [8]. Among the major changes that occur are the alteration of soil pH, the lowering of the soil redox potential (Eh), the reduction of Fe(III) to Fe(II) and Mn(IV) to Mn(II), the reduction of nitrate (NO_3^-) and sulphate (SO_4^{2-}), an increase in the concentration and availability of P, Ca, Mg, Mo, and Si, and a decrease in the concentration and availability of Zn and Cu [8]. The reduction of As(V) to As(III) also occurs as a result of the reduction of Fe(III), Mn(IV), and SO_4^{2-} [9]. Therefore, the study of subsurface chemistry under waterlogged reducing conditions is of the utmost importance for a better understanding of the behavior of soil nutrients and trace metals in WRS, which is still scarce in the literature. Moreover, since rice (*Oryza sativa* L.), a staple food for about 3 billion people worldwide [10], is predominantly grown under lowland/waterlogged conditions where toxic metals (e.g., As, Cd, Cu, Pb and Zn) are the main contaminants of concern [8,11]. Acquiring in-depth knowledge on the dynamics of these toxic metals in soil solutions and solid phases under waterlogged conditions is of great importance for developing effective strategies to address and tackle the problem of toxic metal pollution in paddy soils.

Therefore, considering the advantages of the centrifugation method, including its ease of use, effectiveness, applicability to almost all soil types, and the benefit of reusing the separated soil for further studies [4], this study aimed to verify the applicability of a centrifugal filtration method (CFM) for the efficient separation of solid and liquid phases of WRS while maintaining its reductive conditions. Specifically, this research investigated soil pH, Eh, and solute (As, Fe(II), and Mn) concentrations in the soil solution extracted by CFM at different centrifugation speeds and times, while maintaining its reductive conditions, and compared these results with those obtained by the suction method.

2. Materials and Methods

2.1. Soil

Soil samples were collected from the plough layer (Ap horizon, at a depth of 0–15 cm) of a paddy field. Samples were collected from five different points in the field and then mixed properly to form a composite sample. The collected soil sample was then air dried at 25 °C, passed through a 2 mm stainless steel sieve, and stored at −4 °C until used for analysis and incubation experiments. Since the main purpose of our study was to compare

the results obtained by suction method and CFM, air-dried and disaggregated soil was used in this study to start the incubation experiments, as this soil sample has uniform soil physicochemical properties.

2.2. Analysis of Soil Physicochemical Properties

The particle size distribution (% sand, silt, and clay) of the soil was determined using the pipette method [12]. Soil pH was analyzed using a digital pH meter (LAQUAtwin-pH-33, HORIBA Scientific, Kyoto, Japan) at a ratio of soil to either water or 1 mol/L KCl of 1:2.5 [13], while electrical conductivity (EC) was measured using a digital EC meter (D-52, HORIBA Scientific, Kyoto, Japan) in a soil–water suspension of 1:5 [14]. Total carbon (TC) and nitrogen (TN) contents were analyzed by the dry combustion method (Sumigraph NC-900, Shimadzu, Kyoto, Japan) [13]. The C/N ratio was calculated by dividing TC by TN. Exchangeable cations (Mg^{2+}, Ca^{2+}, K^+, and Na^+) extracted by ammonium acetate were determined by an inductively coupled plasma optical emission spectrometer (ICP-OES; 5110, Agilent Technologies, Santa Clara, CA, USA) [13]. The cation exchange capacity (CEC) of the soil was determined by displacement with NH_4OAc, while the base saturation percentage (BSP) was measured and expressed as the percentage of total soil CEC contributed to by Mg^{2+}, Ca^{2+}, K^+, and Na^+ [15]. The available phosphate (P_2O_5) was extracted and determined using Olsen's extractant (0.5 M $NaHCO_3$ at pH 8.5) and method [16]. Acid ammonium oxalate-extractable Fe (Fe_o), Al (Al_o), and Si (Si_o) were extracted according to the methods described by McKeague and Day [17]. Sodium pyrophosphate-extractable Fe (Fe_p) and Al (Al_p) were extracted by the methods as described by Schuppli et al. [18], while dithionite-citrate-bicarbonate (DCB)-extractable Fe (Fe_d) and Al (Al_d) were extracted according to the methods described by Mehra and Jackson [19]. The concentration of metals in the extracts was determined by ICP-OES (5110, Agilent Technologies, Santa Clara, CA, USA) [20]. The concentration of 1 M HCl-extractable As was measured by inductively coupled plasma mass spectrometry (ICP-MS; ELAN® DRC-e, PerkinElmer, Waltham, MA, USA). The DRC-e mode can effectively suppress the formation of a 40Ar + 35Cl complex. The blank samples were also measured with the same dilution ratio (100 times dilution) and the intensity of the blank samples was very low.

2.3. Incubation Experiments

Incubation experiments were carried out under flooded conditions to create a reducing environment, with or without additional organic materials (OMs). In this study, ethanol and molasses (a sugar-rich by-product of sugar extraction from sugarcane) were used as additional OM to enhance the reductive conditions in the soil [21]. For each treatment, 600 g of soil sample (oven-dried basis) was thoroughly mixed with ultra-pure water (w/v = 1/2, using a hand mixer fitted with an agitator blade, at 1180 rpm for 2 min), 0.5% ethanol, or 0.3% molasses. Each mixture was then placed in a 2 L glass beaker, and two silver chloride reference electrodes (LAQUA Electrode, HORIBA Scientific, Kyoto, Japan) and two soil solution samplers (DIK-300A, Daiki Rika Kogyo Co., Ltd., Saitama, Japan) were installed below the soil surface in each beaker. Thus, a total of 3 glass beakers were used to represent 3 different treatments, and the beakers were finally incubated for 18 days at 30 °C in an incubator (LH-220SP, Nippon Medical & Chemical Instruments Co., Ltd., Osaka, Japan). The reference electrodes were used to regularly monitor the Eh using a digital multimeter (LAQUAact-pH/ORP Meter-D-72, HORIBA Scientific, Kyoto, Japan), whereas the soil solution samplers (SSSs) were used to extract soil solutions (known as the suction method). The extracted soil solution samples were preserved using 10% HNO_3 or 1.19 M acetate solution for chemical analysis. The incubation experiments were conducted in duplicate.

2.4. Solid–Liquid Separation by CFM

For solid–liquid separation under reductive conditions, the surface water, electrodes, and SSSs were first removed from the incubated beakers at the end of the incubation experiments. The beakers were then quickly taken into a glove box (AS-800S, AS ONE

Corporation, Osaka, Japan) and a thin layer (~1 cm) of the surface of the wet soil was removed under a continuous supply of N_2 while maintaining 0.1–1% O_2, indicated by an oximeter to prevent oxidation of the sample. The remaining wet soil was collected and centrifuged (CR20G, Hitachi Co., Ltd., Tokyo, Japan) at different centrifugation speeds (700, 2760, and 11,000 rpm) and times (1–7 min), with 90 g of soil taken for each centrifugation. Three different centrifugation speeds were considered to represent different centrifugation conditions, i.e., 700 rpm indicated the field water, 2760 rpm indicated the relatively mobile and plant-available water, and 11,000 rpm indicated the permanent wilting point [4]. The solid (soil) and liquid (soil solution) fractions were then collected separately in the glove box under reducing conditions. Finally, the soil solution samples extracted by the above-mentioned CFM were preserved similarly, as carried out for the soil solution samples extracted by the suction method (discussed in Section 2.3) prior to chemical analysis, while the soil samples were stored at 4 °C. A schematic diagram of the CFM is shown in Figure 1.

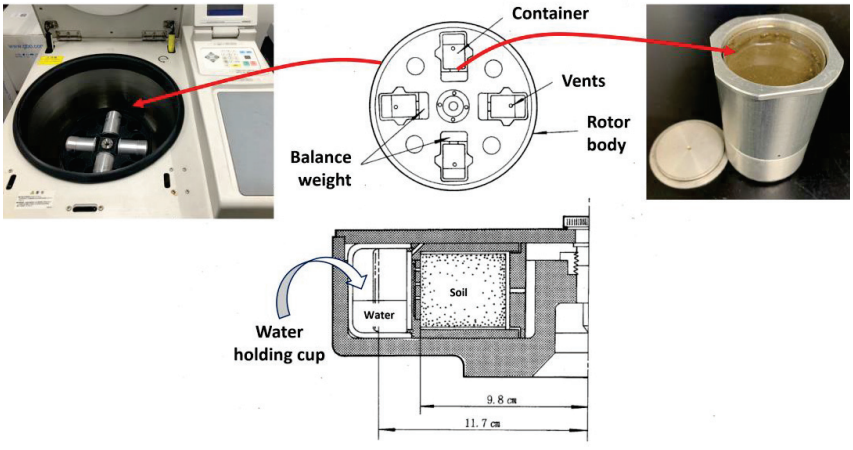

Figure 1. Schematic diagram of the centrifugal filtration method (CFM).

2.5. Analysis of Soil Solution

Soil solution samples extracted by the suction method and/or CFM were analyzed for their pH and As, Fe(II), and Mn concentrations. The pH was determined using a digital pH meter (LAQUAtwin-pH-33, HORIBA Scientific, Kyoto, Japan). The concentration of total As was measured by ICP-MS (ELAN® DRC-e, PerkinElmer, Waltham, MA, USA), whereas the concentration of total Mn was quantified by ICP-OES (5110, Agilent Technologies, Santa Clara, CA, USA). The concentration of Fe(II) was determined using a UV spectrophotometer (V-630, JASCO Corporation, Tokyo, Japan). For this, 1 M sodium acetate and 0.2% o-phenanthroline were added during the dilution of the preserved soil solution. To allow o-phenanthroline to fully react with Fe(II), the solution was then kept in an incubator at 30 °C for 30 min. The concentration was then determined from the absorbance at 510 nm.

2.6. Statistical Analysis

Statistical analyses including a correlation coefficient analysis (CCA) were performed using BellCurve for Excel (Version: 3.21), Social Survey Research Information Co., Ltd. (Shinjuku, Tokyo, Japan). As the normal distribution of the sample could not be confirmed, a non-parametric analysis, Kruskal–Wallis's test, was performed to detect whether there was any statistically significant ($p < 0.05$) difference among the solute concentrations in the soil solution extracted by the suction method and CFM at different centrifugation speeds.

3. Results

3.1. Soil Properties

The physicochemical properties of the collected soil sample are shown in Table 1. The soil shows a relatively high sand content, and the soil texture is sandy clay loam (SCL). The soil was classified as Epiaquepts (soil type) based on the United States Department of Agriculture (USDA) Soil Taxonomy system.

Table 1. Physicochemical properties of soil sample.

Parameters	Extraction Methods	Values
Sand	-	67.1%
Silt	-	17.6%
Clay	-	15.3%
pH	H_2O	5.27
	KCl	4.01
EC	-	0.04 dS/m
TC	-	15 g/kg
TN	-	1.35 g/kg
C/N	-	11.1
Mg^{2+}	-	0.71 $cmol_c$/kg
Ca^{2+}	-	4.41 $cmol_c$/kg
K^+	-	0.23 $cmol_c$/kg
Na^+	-	0.13 $cmol_c$/kg
CEC	-	10.4 $cmol_c$/kg
BSP	-	52.7%
Available phosphate	-	92.8 mg P_2O_5/kg
Fe_o	Acid ammonium oxalate	2.31 g/kg
Al_o		1.68 g/kg
Si_o		0.476 g/kg
Fe_p	Sodium pyrophosphate	1.73 g/kg
Al_p		0.846 g/kg
Fe_d	DCB	3.96 g/kg
Al_d		1.19 g/kg
As	HCl	2.03 mg/kg

3.2. Changes in Soil pH and Eh during Incubation Experiments

Soil pH was found to increase with time during the incubation experiments, whereas the highest pH (~6.0) was observed in soil treated with just water followed by OM (~5.4), i.e., ethanol and molasses (Figure 2). The lower pH in the soil treated with OM can be partiality explained by the low pH of the OM itself. On the other hand, a decrease in soil Eh (water: +212 to −397 mV; ethanol: +187.5 to −323.5 mV; molasses: +261.5 to −358 mV) was observed with incubation time (day 0 to 18). Noticeably, a sharp decline in soil Eh was observed within the first 3 days of incubation, especially for the samples treated with ethanol and molasses, while a comparatively slower decrease in Eh was observed when just water was added (Figure 2). The decrease in Eh was relatively faster until day 5, although no significant difference was found among the treatments from day 5 to 18.

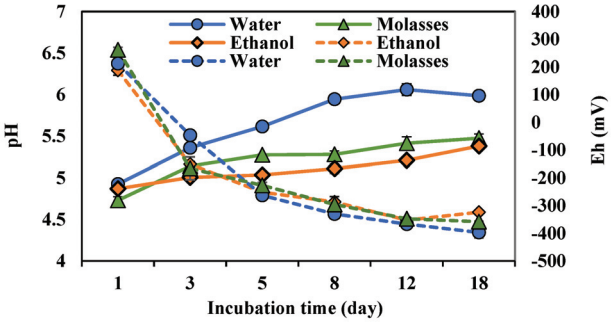

Figure 2. Changes in soil pH (indicated by solid lines) and Eh (indicated by dotted lines), during the incubation experiments, under different treatments.

3.3. Behavior of Solutes (Metals) during Incubation Experiments

With the increasing soil pH and decreasing soil Eh, the solute (As, Fe(II), and Mn) concentrations in the soil solution (extracted by the suction method) increased sharply, regardless of the treatments applied, compared to adding just water (Figure 3). Interestingly, the addition of OM significantly increased the metal concentrations in the soil solution compared to the no-material treatment (water). The results showed that the addition of ethanol increased As, Fe(II), and Mn concentrations by 71, 106, and 118%, respectively, whereas the addition of molasses increased these corresponding concentrations by 43, 83, and 70%, respectively (Figure 3).

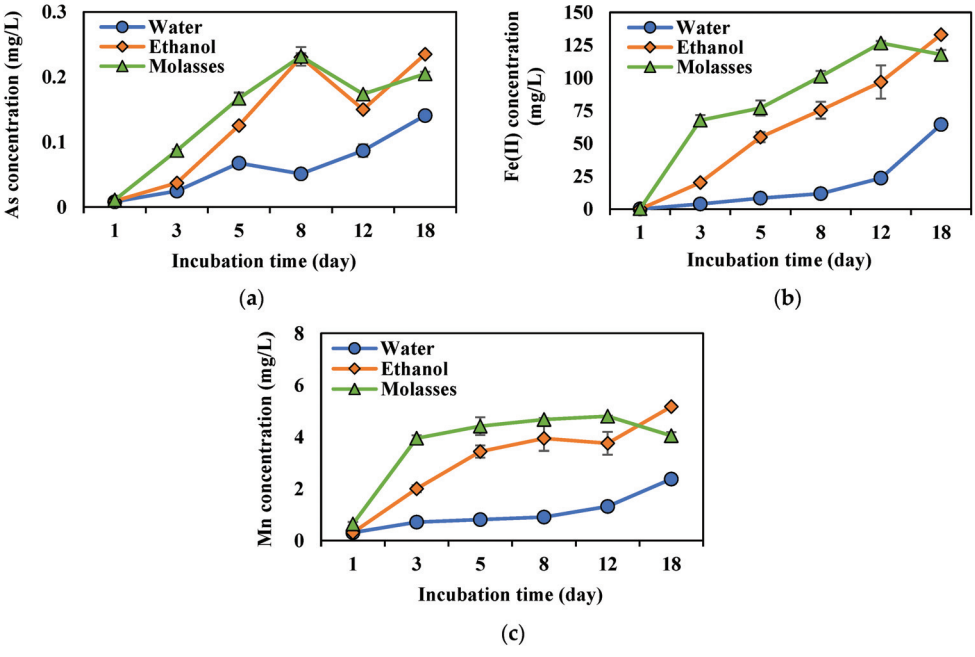

Figure 3. Behavior of (**a**) As, (**b**) Fe(II), and (**c**) Mn in the soil, during incubation experiments, under different treatments.

The increased metal concentrations with the increasing soil pH and decreasing Eh, especially under OM treatments, indicated that the behavior and chemistry of As, Fe(II), and Mn are closely interrelated and influenced by similar edaphic factors. The CCA also exhibited very strong positive correlations between As, Fe(II), and Mn (r = 0.902–0.951) (Table 2).

Table 2. Correlation matrix showing the interrelationships between the studied solutes (As, Fe(II), and Mn) in the soil solution.

	As	Fe(II)	Mn
As	-	-	-
Fe(II)	0.914	-	-
Mn	0.902	0.951	-

3.4. Effects of Centrifugation Time and Speed on Soil Solution Extraction

For our study, a shorter centrifugation time was crucial to avoid the unintentional oxidation of soil samples, while the extraction of the maximum amount of soil solution was another important consideration. Therefore, a preliminary experiment was performed

using random wet soil samples to evaluate whether centrifugation time has any significant effect on the amount of soil solution extracted. The results revealed that centrifugation for more than 1 min resulted in no significant ($p > 0.05$) increase in the amount of extracted soil solution, which was true for all three centrifugation speeds. While centrifugation for only 1 min extracted 3.045, 10.855, and 18.35 g of soil solution at 700, 2760, and 11,000 rpm, respectively, the centrifugation, when continued for 7 min, extracted a cumulative of only 4.925, 13.895, and 20.3 g of soil solution at those corresponding centrifugation speeds (Figure 4).

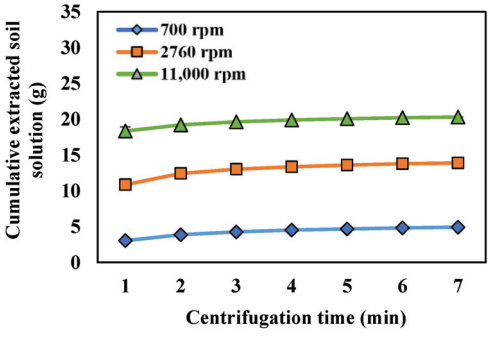

Figure 4. Preliminary experiment showing the effect of centrifugation time on the amount of soil solution extracted.

Once the preliminary experiment confirmed that a longer centrifugation has no significant effect on the amount of soil solution extracted (Figure 4), a shorter centrifugation time (i.e., 1 min) was used for the soil solution extraction, by CFM, from incubated soil samples at three different centrifugation speeds. The results revealed that a higher centrifugation speed resulted in a higher amount of soil solution extracted (Figure 5), as was also found during the preliminary experiment (Figure 4). Centrifugation at 11,000 rpm for 1 min resulted in a 5- and 1.4-times higher amount of soil solution compared to that obtained by centrifugation for 1 min at 700 and 2760 rpm, respectively (Figure 5).

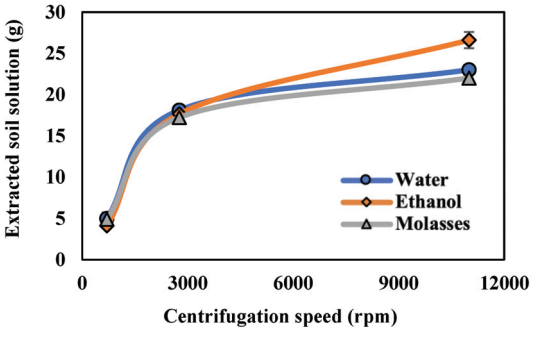

Figure 5. Amount of soil solution extracted by CFM at three centrifugation speeds for 1 min.

3.5. Solute Concentrations in CFM-Extracted Soil Solutions

The results exhibited no significant difference in solute (As, Fe(II), and Mn) concentrations when the varying amounts of soil solution extracted by CFM at different centrifugation speeds were measured (Figure 6). The relationship between the solute concentrations and amount of CFM-extracted soil solution was found to be identical to that observed in the soil solution extracted by the suction method (Figure 3), while significantly higher solute concentrations were measured in the OM-treated samples compared to the samples treated with just water (Figure 6). Moreover, Kruskal–Wallis's test revealed that there was no

significant ($p > 0.05$) difference between the solute concentrations detected in soil solutions extracted by CFM at different centrifugation speeds and the solute concentrations extracted by the suction method (Table 3).

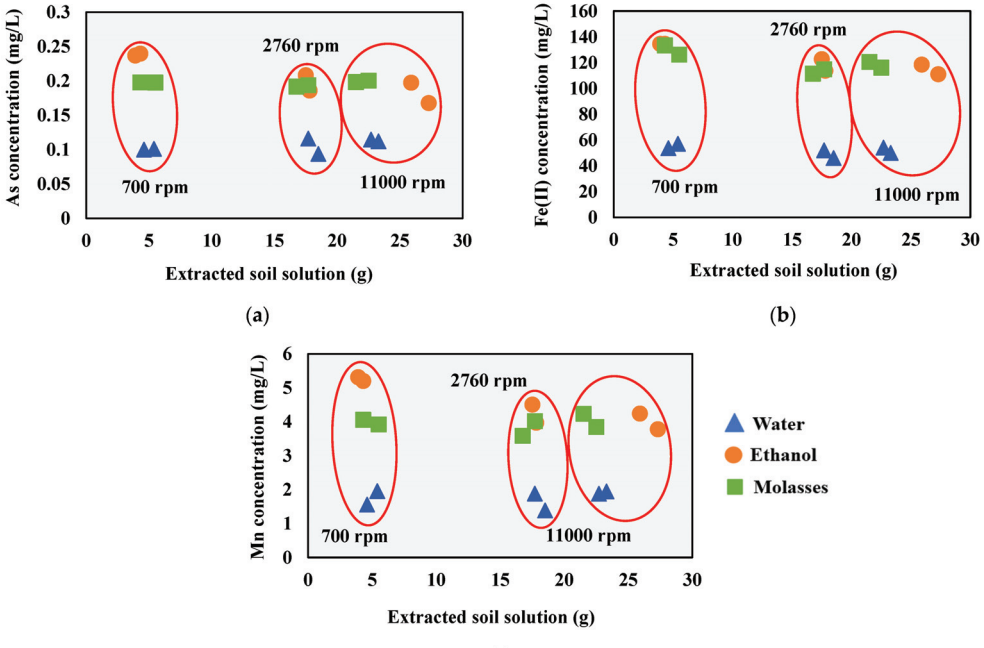

Figure 6. Relationship between solute ((**a**): As, (**b**): Fe(II), and (**c**): Mn) concentrations and amount of soil solution extracted by CFM at different centrifugation speeds under various treatments.

Table 3. Comparison between the solute concentrations in the CFM-extracted soil solutions and the solute concentrations in the soil solution extracted by the suction method, under different treatments.

Treatments	Extraction Method	Solute Concentrations (mg/L)		
		As	Fe(II)	Mn
Water	CFM-700 rpm	0.101 ± 0.001 a	55.369 ± 2.480 a	1.753 ± 0.280 a
	CFM-2760 rpm	0.105 ± 0.016 a	49.012 ± 4.185 a	1.630 ± 0.351 a
	CFM-11,000 rpm	0.113 ± 0.002 a	52.081 ± 2.945 a	1.907 ± 0.045 a
	Suction method	0.142 ± 0.002 a	64.466 ± 1.705 a	2.381 ± 0.110 a
	Test value	$\chi^2 = 4.667$	$\chi^2 = 5.500$	$\chi^2 = 4.500$
	p value	0.198	0.139	0.212
Ethanol	CFM-700 rpm	0.238 ± 0.002 a	134.610 ± 0.000 a	5.258 ± 0.079 a
	CFM-2760 rpm	0.197 ± 0.016 a	118.280 ± 6.355 a	4.239 ± 0.378 a
	CFM-11,000 rpm	0.183 ± 0.021 a	114.773 ± 5.270 a	4.010 ± 0.326 a
	Suction method	0.238 ± 0.000 a	132.966 ± 1.240 a	5.180 ± 0.023 a
	Test value	$\chi^2 = 5.500$	$\chi^2 = 6.241$	$\chi^2 = 6.167$
	p value	0.139	0.101	0.104
Molasses	CFM-700 rpm	0.198 ± 0.000 a	129.843 ± 5.037 a	3.989 ± 0.098 a
	CFM-2760 rpm	0.193 ± 0.001 a	113.183 ± 2.402 a	3.800 ± 0.305 a
	CFM-11,000 rpm	0.199 ± 0.001 a	118.389 ± 3.100 a	4.038 ± 0.274 a
	Suction method	0.207 ± 0.003 a	117.841 ± 3.565 a	4.052 ± 0.140 a
	Test value	$\chi^2 = 6.667$	$\chi^2 = 6.167$	$\chi^2 = 1.167$
	p value	0.083	0.104	0.761

Note: the lowercase letter (a) indicates that there is no significant ($p > 0.05$) difference between the solute concentrations in soil solutions extracted by the CFM and suction method.

4. Discussion

Soil pH and Eh were found to increase and decrease, respectively, with time during the incubation experiments (Figure 2). Similar results were also reported by Kashem and Singh, who studied the effects of OM's application on soil pH and Eh in metal-contaminated soils under flooded conditions using a growth chamber experiment [22]. Under waterlogged conditions, soils usually have an Eh of <+350 mV [23,24]. Depending on the Eh, soil conditions can also be categorized as moderately reduced soils (+100 to +400 mV), reduced soils (−100 to +100 mV), and highly reduced soils (−100 to −300 mV) [23]. On the other hand, soil pH and Eh are known to be negatively correlated [23,25], as a decrease in Eh is accompanied by an increase in pH as a result of reduction reactions, which consume H^+ [22,26]. Thus, the increase and decrease in soil pH and Eh, respectively, with time clearly demonstrated that the soil's reductive condition was maintained and essentially promoted over time during the incubation experiments. Since the application of OM promotes soil reductive conditions by accelerating anaerobic microbial activities [21], the addition of ethanol or molasses promoted the soil's reductive conditions, as indicated by a sharp decrease in soil Eh for the first 3 days until day 5 (Figure 2), although the OM did not show any significant effect in later days (day 5 to 18).

Such an increase in the concentrations of As, Fe(II), and Mn during the incubation can be explained by two mechanisms occurring under waterlogged reductive conditions: (i) the reduction of oxyhydroxides of Fe and Mn, which results in the release of sorbed As into the liquid phase, and (ii) the reduction of As(V) sorbed on the solid phase (mineral surfaces) to As(III), which thereby remains available in the solution phase [27–29]. Moreover, significantly higher solute concentrations in the OM-amended samples supported the idea that the addition of OM substantially enhances the reduction of As, Fe, and Mn under reduction conditions essentially through promoting microbial activity [21,30–32].

Under centrifugation for more than 1 min, no significant increase in the volume of the soil solution observed (Figure 4), which implied that centrifugation for 1 min is enough to extract most of the soil solution by CFM when the soil texture is sandy clay loam (Table 1). However, longer centrifugation times are probably needed to collect a sufficient volume of soil solution from clayey soils because of their higher soil matric potential [3]. Nevertheless, the results demonstrated that centrifugation speed, and not centrifugation time, is the predominant factor for extracting the maximum amount of soil solution (Figures 5 and 6), which was found to be in line with the results of Fraters et al. [4]. The major effect of centrifugation speed and the lesser effect of centrifugation time on soil solution extraction can be attributed to the level of compaction, which occurs during centrifugation, with an increase in dry bulk density and a reduction in soil pore size, and is essentially dependent on centrifugation speed [4]. The faster and stronger compaction of soil at a higher centrifugation speed (11,000 rpm) possibly decreased the soil pore size and increased the flow of water [33,34], which thereby resulted in a higher volume of soil solution.

The results demonstrated that there will be no significant difference in solute (As, Fe(II), and Mn) concentrations even though varying amounts of soil solution are extracted by CFM at different centrifugation speeds (700, 2760, and 11,000 rpm). Additionally, the As, Fe(II), and Mn concentrations in the CFM-extracted soil solution showed identical chemical behavior for each tested treatment (Figure 6), which was also in line with the results observed for the solute concentrations in the soil solution extracted by the suction method (Figure 3). The changing of soil reductive conditions to oxidation conditions results in a decrease in the concentrations and availability of As, Fe, and Mn in the soil solution [8,27]. Interestingly, no significant difference was observed between the solute (As, Fe(II), and Mn) concentrations in the CFM-extracted soil solution and the corresponding solute concentrations in the soil solution extracted by the suction method (Table 3), confirming that the reductive conditions were maintained during the extraction of soil solution by CFM. All these results suggested that a CFM operating at a higher centrifugation speed (11,000 rpm) could potentially be employed as an effective method for the efficient separa-

tion of solid and liquid phases of WRS within a short time period while maintaining its reductive conditions, maximizing the amount of soil solution extracted and not affecting its solute concentrations.

5. Conclusions

Although various established methods are available for the separation of the solid–liquid phases of upland soils, there is no established method in the literature for effectively separating the solid and liquid phases of WRS while maintaining its reductive conditions. This study verified that the solid and liquid phases of WRS can be efficiently separated by CFM while maintaining its reductive conditions. The results demonstrated that a higher centrifugation speed (11,000 rpm), representing the permanent wilting point, would be the most effective for the efficient separation of solid–liquid phases while extracting most of the soil solution within a short time (i.e., 1 min). Moreover, our findings on the solute concentrations in the extracted soil solution confirmed that the application of CFM would greatly help us to quickly separate and study the chemistry of solid and liquid phases of WRS. However, further research is needed to verify the effectiveness of CFM on other soil types, as well as to widely apply this simple solid–liquid separation method for a better understanding of the chemical behavior and dynamics of the solutes in soil solutions under reductive conditions.

Author Contributions: Conceptualization, T.M.; methodology, S.S., K.W., T.M. and S.-I.Y.; software, S.S. and T.M.; validation, T.M.; formal analysis, S.S. and K.W.; investigation, S.S. and K.W.; resources, T.M., H.K., K.K. and S.-I.Y.; data curation, S.S. and T.M.; writing—original draft preparation, S.S.; writing—review and editing, T.M.; visualization, S.S.; supervision, T.M.; project administration, T.M.; funding acquisition, T.M. All authors have read and agreed to the published version of the manuscript.

Funding: This work was supported by the Project of Integrated Compost Science (PICS), Tohoku University (Ministry of Education, Culture, Sports, Science and Technology).

Institutional Review Board Statement: Not applicable.

Informed Consent Statement: Not applicable.

Data Availability Statement: The data presented in this study are available on request from the corresponding author.

Acknowledgments: The authors are grateful to the anonymous reviewers for providing their valuable comments and suggestions on how to improve the manuscript.

Conflicts of Interest: The authors declare no conflicts of interest.

References

1. Dahlgren, R.A. Comparison of soil solution extraction procedures: Effect on solute chemistry. *Commun. Soil Sci. Plant Anal*. **1993**, *24*, 1783–1794. [CrossRef]
2. Geibe, C.E.; Danielsson, R.; van Hees, P.A.W.; Lundström, U.S. Comparison of soil solution chemistry samples by centrifugation, two types of suction lysimeters and zero-tension lysimeters. *Appl. Geochem.* **2006**, *21*, 2096–2111. [CrossRef]
3. Elkhatib, E.A.; Hern, J.L.; Staley, T.E. A rapid centrifugation method for obtaining soil solution. *Soil Sci. Soc. Am. J.* **1987**, *51*, 578–583. [CrossRef]
4. Fraters, D.; Boom, G.J.F.L.; Boumans, L.J.M.; de Weerd, H.; Wolters, M. Extraction of soil solution by drainage centrifugation-effects of centrifugal force and time of centrifugation on soil moisture recovery and solute concentrations in soil moisture of loess subsoils. *Environ. Monit. Assess.* **2017**, *189*, 83. [CrossRef] [PubMed]
5. Grossmann, J.; Udluft, P. The extraction of soil water by the suction-cup method: A review. *Eur. J. Soil Sci.* **1991**, *42*, 83–93. [CrossRef]
6. Presley, B.J.; Brooks, R.R.; Kappel, H.M. A simple squeezer for removal of interstitial water from ocean sediments. *J. Mar. Sci.* **1967**, *25*, 355–357.
7. Moore, J.N.; Ficklin, W.H.; Johns, C. Partitioning of arsenic and metals in reducing sulfidic sediments. *Environ. Sci. Technol*. **1988**, *22*, 432–437. [CrossRef]
8. Fageria, N.K.; Carvalho, G.D.; Santos, A.B.; Ferreira, E.P.B.; Knupp, A.M. Chemistry of lowland rice soils and nutrient availability. *Commun. Soil Sci. Plant Anal*. **2011**, *42*, 1913–1933. [CrossRef]

9. Burton, E.D.; Johnston, S.G.; Kocar, B.D. Arsenic mobility during flooding of contaminated soil: The effect of microbial sulfate reduction. *Environ. Sci. Technol.* **2014**, *48*, 13660–13667. [CrossRef] [PubMed]
10. Hussain, M.M.; Bibi, I.; Niazi, N.K.; Shahid, M.; Iqbal, J.; Shakoor, M.B.; Ahmad, A.; Shah, N.S.; Bhattacharya, P.; Mao, K.; et al. Arsenic biogeochemical cycling in paddy soil-rice system: Interaction with various factors, amendments and mineral nutrients. *Sci. Total Environ.* **2021**, *773*, 145040. [CrossRef]
11. Kwon, J.C.; Nejad, Z.D.; Jung, M.C. Arsenic and heavy metals in paddy soil and polished rice contaminated by mining activities in Korea. *Catena* **2017**, *148*, 92–100. [CrossRef]
12. Gee, G.W.; Bauder, J.W. Particle-size analysis. In *Methods of Soil Analysis: Part 1 Physical and Mineralogical Methods*, 2nd ed.; Arnold, K., Ed.; Soil Science Society of America: Madison, WI, USA, 1986; pp. 383–411.
13. Makino, T.; Sugahara, K.; Sakurai, Y.; Takano, H.; Kamiya, T.; Sasaki, K.; Itou, T.; Sekiya, N. Remediation of cadmium contamination in paddy soils by washing with chemicals: Selection of washing chemicals. *Environ. Pollut.* **2006**, *144*, 2–10. [CrossRef] [PubMed]
14. He, Y.; DeSutter, T.; Prunty, L.; Hopkins, D.; Jia, X.; Wysocki, D.A. Evaluation of 1:5 soil to water extract electrical conductivity methods. *Geoderma* **2012**, *185–186*, 12–17. [CrossRef]
15. Summer, M.E.; Miller, W.P. Cation exchange capacity and exchange coefficients. In *Methods of Soil Analysis: Part 3 Chemical Methods*; Sparks, D.L., Ed.; Soil Science Society of America: Madison, WI, USA, 1996; pp. 1201–1229.
16. Olsen, S.R.; Cole, C.V.; Watanabe, F.S.; Dean, L.A. *Estimation of Available Phosphorus in Soils by Extraction with Sodium Bicarbonate*; USDA Circular 939; US Government Printing Office: Washington, DC, USA, 1954.
17. McKeague, J.A.; Day, J.H. Dithionite- and oxalate-extractable Fe and Al as aids in differentiating various classes of soils. *Can. J. Soil. Sci.* **1966**, *46*, 13–22. [CrossRef]
18. Schuppli, P.A.; Ross, G.J.; McKeague, J.A. The effective removal of suspended materials from pyrophosphate extracts of soils from tropical and temperate regions. *Soil Sci. Soc. Am. J.* **1983**, *47*, 1026–1032. [CrossRef]
19. Mehra, O.P.; Jackson, M.L. Iron oxide removal from soils and clays by a dithionite-citrate system buffered with sodium bicarbonate. *Clays Clay Miner.* **1960**, *7*, 317–327.
20. Suda, A.; Makino, T.; Higashi, T. An improved selective extraction method for Mn oxides and occluded metals with emphasis on applicability to Andisols. *Soil Sci. Plant Nutr.* **2013**, *59*, 840–851. [CrossRef]
21. Reddy, K.R.; Feijtel, T.C.; Patrick, W.H. Effect of soil redox conditions on microbial oxidation of organic matter. In *The Role of Organic Matter in Modern Agriculture*; Chen, Y., Avnimelech, Y., Eds.; Springer: Dordrecht, The Netherlands, 1986; Volume 25, pp. 117–156.
22. Kashem, M.A.; Singh, B.R. Metal availability in contaminated soils: I. Effects of flooding and organic matter on changes in Eh, pH and solubility of Cd, Ni and Zn. *Nutr. Cycling Agroecosyst.* **2001**, *61*, 247–255. [CrossRef]
23. Husson, O. Redox potential (Eh) and pH as drivers of soil/plant/microorganisms systems: A transdisciplinary overview pointing to integrative opportunities for agronomy. *Plant Soil* **2013**, *362*, 389–417. [CrossRef]
24. Pezeshki, S.R. Wetland plant responses to soil flooding. *Environ. Exp. Bot.* **2001**, *46*, 299–312. [CrossRef]
25. Bohrerova, Z.; Stralkova, R.; Podesvova, J.; Bohrer, G.; Pokorny, E. The relationship between redox potential and nitrification under different sequences of crop rotations. *Soil Till. Res.* **2004**, *77*, 25–33. [CrossRef]
26. Narteh, L.T.; Sahrawat, K.L. Influence of flooding on electrochemical and chemical properties of West African soils. *Geoderma* **1999**, *87*, 179–207. [CrossRef]
27. Caporale, A.G.; Violante, A. Chemical processes affecting the mobility of heavy metals and metalloids in soil environments. *Curr. Pollution Rep.* **2016**, *2*, 15–27. [CrossRef]
28. Bose, P.; Sharma, A. Role of iron in controlling speciation and mobilization of arsenic in subsurface environment. *Water Res.* **2002**, *36*, 4916–4926. [CrossRef] [PubMed]
29. Xu, X.; Chen, C.; Wang, P.; Kretzschmar, R.; Zhao, F.-J. Control of arsenic mobilization in paddy soils by manganese and iron oxides. *Environ. Pollut.* **2017**, *231*, 37–47. [CrossRef] [PubMed]
30. Wang, S.; Mulligan, C.N. Effect of natural organic matter on arsenic release from soils and sediments into groundwater. *Environ. Geochem. Health* **2006**, *28*, 197–214. [CrossRef]
31. Lindsay, W.L. Iron oxide solubilization by organic matter and its effect on iron availability. *Plant Soil* **1991**, *130*, 27–34. [CrossRef]
32. Khoshru, B.; Mitra, D.; Nosratabad, A.F.; Reyhanitabar, A.; Mandal, L.; Farda, B.; Djebaili, R.; Pellegrini, M.; Guerra-Sierra, B.E.; Senapati, A.; et al. Enhancing manganese availability for plants through microbial potential: A sustainable approach for improving soil health and food security. *Bacteria* **2023**, *2*, 129–141. [CrossRef]
33. Jones, D.L.; Edwards, A.C. Effect of moisture content and preparation technique on the composition of soil solution obtained by centrifugation. *Commun. Soil Sci. Plant Anal.* **1993**, *24*, 171–186. [CrossRef]
34. Amer, A.M. Water flow and conductivity into capillary and non-capillary pores of soils. *J. Soil Sci. Plant Nutr.* **2012**, *12*, 99–112. [CrossRef]

Disclaimer/Publisher's Note: The statements, opinions and data contained in all publications are solely those of the individual author(s) and contributor(s) and not of MDPI and/or the editor(s). MDPI and/or the editor(s) disclaim responsibility for any injury to people or property resulting from any ideas, methods, instructions or products referred to in the content.

soil systems

MDPI

Article

Temporal Changes in Cd Sorption and Plant Bioavailability in Compost-Amended Soils

Shamim Al Mamun [1,2], Niklas J. Lehto [2], Jo Cavanagh [3], Richard McDowell [2,4], Liv Kellermann [2] and Brett H. Robinson [5,*]

[1] Department of Environmental Science and Resource Management, Mawlana Bhashani Science and Technology University, Tangail 1902, Bangladesh; shamimal.mamun@canterbury.ac.nz
[2] Department of Soil Science, Faculty of Agricultural and Life Sciences, Lincoln University, Lincoln 7647, New Zealand; richard.mcdowell@agresearch.co.nz (R.M.); liv.kellermann@bfh.ch (L.K.)
[3] Landcare Research, Lincoln 7640, New Zealand; cavanaghj@landcareresearch.co.nz
[4] AgResearch, Lincoln Science Centre, Private Bag 4749, Christchurch 8140, New Zealand
[5] School of Physical and Chemical Sciences, University of Canterbury, 20 Kirkwood Ave, Ilam, Christchurch 8041, New Zealand
* Correspondence: brett.robinson@canterbury.ac.nz

Abstract: The application of Cd-contaminated phosphate fertiliser has enriched concentrations of this non-essential element in many agricultural soils. Consequently, concentrations of the metal in some agricultural products exceed the Maximum Limit in foods. Composts can reduce the transfer of Cd from soil to plants; however, it is unclear how long this beneficial effect endures. We aimed to determine temporal changes of phytoavailable Cd in two market garden soils (an Allophanic Orthic Granular Soil and a Recent Silt Loam). Soils were amended with either municipal green waste compost or sawdust and animal waste compost at a rate of 2.5% *w*/*w* under three incubation regimes: at 19 °C, at 30 °C, and at 30 °C with additional N added as urea at 0.6 g urea/kg soil added over 1 year. Each replicate was sampled after 1, 5, 9, 13, 21, 31, and 49 weeks, and phytoavailable Cd was estimated through 0.05 M $Ca(NO_3)_2$ extraction. Seed potato (*Solanum tuberosum*), 'Nadine' variety, was grown in the Pukekohe Allophanic Orthic Granular Soil, freshly amended with municipal compost and the same soil aged for one year. The concentration of Cd in all samples was analysed using an ICP-OES (Inductively Coupled Plasma-Optical Emission Spectrometer). The C concentration in the soil—compost mixtures decreased over the year, with the greatest decreases occurring in the soils incubated at 30 °C with added N. Unexpectedly, the concentration of $Ca(NO_3)_2$-extractable Cd in the compost-amended soils did not increase over time and in some cases even decreased. This was confirmed through a pot experiment, which showed the Cd concentration in potato was reduced by 50% in both the freshly amended soil and the amended soil aged for one year. Cadmium immobilisation in soils might be due to both the sorption of Cd by organic matter and the occlusion of sorbed Cd by oxy-hydroxides of iron and aluminium. Over 49 weeks, soluble Cd does not increase as organic matter oxidises. The application of municipal compost to soil will reduce both plant Cd solubility and plant Cd uptake for at least one year in the soils tested.

Keywords: $Ca(NO_3)_2$-extractable Cd; incubation; potato; organic amendment

Citation: Al Mamun, S.; Lehto, N.J.; Cavanagh, J.; McDowell, R.; Kellermann, L.; Robinson, B.H. Temporal Changes in Cd Sorption and Plant Bioavailability in Compost-Amended Soils. *Soil Syst.* **2023**, *7*, 107. https://doi.org/10.3390/soilsystems7040107

Academic Editor: Adriano Sofo

Received: 6 October 2023
Revised: 20 November 2023
Accepted: 27 November 2023
Published: 29 November 2023

Copyright: © 2023 by the authors. Licensee MDPI, Basel, Switzerland. This article is an open access article distributed under the terms and conditions of the Creative Commons Attribution (CC BY) license (https://creativecommons.org/licenses/by/4.0/).

1. Introduction

Cadmium (Cd) is a non-essential trace element that is present at elevated concentrations in many agricultural soils [1,2]. It occurs naturally as a contaminant in all phosphate rocks. Rock phosphate originating from igneous rocks contains Cd concentrations of 0.7–30 mg/kg P [3], whereas rock phosphate refined from sedimentary rocks may contain Cd concentrations >556 mg/kg P [4] and accounts for between 85 and 90% of world P production [3]. The use of Cd-containing phosphate fertiliser to sustain agricultural produc-

tivity has resulted in an enrichment of Cd in agricultural soils worldwide [2,5,6]. Elevated Cd in soil is a key driver of increased Cd concentration in plant tissue and foodstuffs [7–13].

Most Cd in soil is bound to the solid phase, with relatively low concentrations present in soil solution [14]. Soil K_d (sorbed/solution Cd quotient) values for silt loam soils range from 50 to 200 and from pH 5 to 6.5 [15,16]. Nevertheless, soil-borne Cd is readily taken up by plants [17] and then transferred to animals and humans through plant consumption [18,19]. Exceedances of food safety standards have been reported in vegetables worldwide [10,20–22]. The availability of soil Cd for uptake by plants (i.e., phytoavailability) largely depends on the amount of metal that exists as a soluble species, which is a function of the total concentration as well as physicochemical and biological properties of the soils [2].

Some 55–90% of Cd in soil solution is present as free metal ion Cd^{2+} [23]. Cadmium may occur as cationic species, $CdCl^+$, $CdOH^+$, $CdHCO_3{}^+$, and $CdHS^+$; and as anionic species, $CdCl_3{}^-$, $Cd(OH)_3$, $Cd(OH)_4{}^{2-}$, and $Cd(HS)_4{}^{2-}$ [2]. It also forms complexes with organic ligands, such as low-molecular-weight organic acids, fulvates, and humates [2]. The most phytoavailable species in soil solution are Cd^{2+} and $CdCl^+$ [24]. Phytoavailability of soluble Cd is also affected by plant nutrients (especially Ca, Zn, and Cl^-), as well as pH, ionic strength, and aeration [25]. Most studies report reduced plant uptake at high soil pH, presumably due to increased K_D values [26,27]. However, some studies have shown an increase in plant Cd uptake at high pH, despite reduced Cd concentrations in soil solution. The drivers underlying these effects are complex and difficult to disentangle: Zn deficiency at high soil pH may result in an increase in the expression of Zn transporter proteins that can facilitate Cd uptake [28]. Increased Cd solubility at higher Ca^{2+} ion concentrations following liming may also play a role [1,29]. Increased activity of $CdCl^+$ species activity in saline soils has also been associated with elevated Cd concentrations in wheat (*Triticum aestivum* cv. Halberd) and Swiss chard (*Beta vulgaris* cv. Foodhook Giant) [13,30].

The addition of organic matter to soil as carbonaceous amendments can reduce Cd uptake by plants [1,31–35] through binding Cd into less phytoavailable solid phase species [16,34,36]. Following the application of 2–5% compost, Al Mamun et al. [37] reported a reduction in Cd concentration in potato tubers (*Solanum tuberosum*) by 29–66%, depending on the compost. Compost made from mixtures of food waste, lawn clippings, tree prunings, sawdust, and animal offal effectively reduced Cd solubility in batch sorption experiments, which was associated with significantly decreased Cd uptake by *Allium cepa* L., *Spinacia oleracea* L., and *Lactuca sativa* L. of up to 60% [15]. Shuman et al. [38] reported that the larger surface area of humified organic matter removes Cd from soil solution making it less available to *Zea mays* L. Inorganic components in compost, particularly Fe and Al (oxyhydr)oxides, may further reduce Cd solubility and thence plant uptake [39].

The organic matter in the compost can be degraded by soil microorganisms, so it may be expected that the abundance and nature of functional group ligands that bind Cd in soils would change over time. However, there is a lacuna of information on the rate of change of the Cd-binding capacity of composts over time following their addition to soil. Karaca [40] showed that soils amended with mushroom compost and grape mark (added at rates of 2%, 4%, and 8%) retained their ability to bind Cd, even after incubation at 25 °C for six months. Similarly, Lee et al. [34] showed in a greenhouse study that the reduction in DTPA-extractable Cd resulting from hog manure application persisted for at least six months.

It was hypothesised that the bound Cd in composts will be released into soil solution as the compost decomposes and that its phytoavailability will, therefore, increase. Depending on environmental conditions, compost manufacturers recommend that compost be added annually to triennially to maintain the soil's organic matter content [41]. Therefore, most Cd that is bound to the compost is likely to be released over this timeframe. To test this hypothesis, this research sought to fulfil two objectives. The first objective was to determine the temporal changes in $Ca(NO_3)_2$-extractable Cd in two soils amended with composts of different provenances under contrasting incubation regimes over one year. The second

objective was to compare the transfer of Cd from a soil to potatoes grown in a pot trial using freshly amended compost and the same soil a year later.

2. Materials and Methods

2.1. Soil Sample Collection

Two distinct soils were collected from market gardens in New Zealand: an Allophanic Orthic Granular Soil from Pukekohe (37°13′18.92″ S 174°52′5.94″ E) and a Recent Silt Loam from Levin (40°38′17.49″ S 175°14′23.61″ E) in the North Island of New Zealand. Henceforth, these soils will be referred to as 'Pukekohe soil' and 'Levin soil', respectively. Soils were collected from within the plough layer (top 0.25 m) and were dried, ground, sieved (7 mm mesh), and their chemical properties determined (Tables 1 and 2). Cadmium concentrations in the Pukekohe and Levin soils were 1.45 mg/kg and 0.47 mg/kg, respectively, at the time of collection. One year before the experiment, a subset of the Pukekohe soil was amended with municipal compost (2.5% *w*/*w*, as reported by Al Mamun et al. [37]), and another subset of the Pukekohe soil and a subset of the Levin soil were spiked with Cd (as the sulphate salt) to increase their Cd concentrations by ca. 1 mg/kg. All soils were left to incubate in pots in a greenhouse where they were watered occasionally. Following spiking, Cd concentrations in the Pukekohe and Levin soils had increased to 2.08 (±0.09) mg/kg and 0.99 (±0.05) mg/kg, respectively.

Table 1. Chemical properties and elemental concentrations (mg/kg unless otherwise indicated) of the materials used in the experiments. Values in brackets represent the standard error of the mean (n = 3).

Properties	Municipal Compost (Living Earth Compost)	Sawdust Compost (Parkhouse Compost)	Pukekohe Soil	Levin Soil
pH (H_2O)	7.4	7.0	6.0	6.5
CEC ($cmol_c/kg$)	45 (<1)	47 (<1)	22 *	15 *
C (%)	21	21	2.1 *	1.2 *
N (%)	2.3	1.6	0.23 *	0.13
P	4178 (37)	5159 (227)	3414 (26)	2247 (20)
S	2644 (27)	3610 (70)	491 (6)	296 (1)
Ca=	24,903 (588)	37,416 (1456)	4147 (117)	7008 (99)
Mg	4177 (16)	2186 (34)	2400 (95)	2873 (43)
K	14,938 (33)	5412 (67)	1951 (59)	2242 (54)
B (mg/kg)	20 *	<1	33 (0)	9 (0)
Cd	0.70 (0.10)	0.45 (0.10)	1.45 (0.03)	0.47 (0.01)
Cu	59 (1)	25 (1)	65 (1)	20 (0.2)
Zn	310 (11)	34 (2)	173 (1)	67 (1)
Cr	28 (1)	37 (1)	40 (2)	15 (0.3)
Ni	9.3 (1)	5.2 (0.1)	25 (1)	7.4 (0.5)
Fe	12,472 (261)	8218 (2030)	44,606 (96)	22,729 (1527)
Al	9534 (164)	8126 (147)	93,008 (476)	32,412 (1188)

* data from Hill Laboratories, New Zealand.

Table 2. Extractable [0.05 M $Ca(NO_3)_2$] concentrations (mg/kg) of selected elements from the Pukekohe and Levin soils. Values in brackets represent the standard error of the mean (n = 5).

Element	Pukekohe Soil	Levin Soil
Cd	0.011 (0.003)	0.008 (0.002)
Cu	0.13 (0.02)	0.12 (0.01)
Zn	0.38 (0.06)	0.18 (0.02)
Ni	0.090 (0.012)	0.014 (0.002)
Fe	0.65 (0.20)	0.51 (0.04)
Al	0.82 (0.20)	0.49 (0.04)

2.2. Collection of Composts

We collected municipal compost from Living Earth Ltd. (Christchurch, New Zealand). The source materials for this compost were mainly lawn clippings, tree prunings, and food waste. Hereafter, this compost will be referred to as MC (Municipal Compost). The second compost, manufactured from sawdust and animal residues (manure and carcasses), was obtained from Parkhouse Garden Supplies (Christchurch, New Zealand). Hereafter, this compost will be referred to as SC (Sawdust Compost). Table 1 shows the chemical properties of the composts.

2.3. Incubation Experiment

The two composts were mixed into separate subsets of the spiked soils at a rate of 2.5% *w*/*w* (Table 3). This corresponds to a rate of 50 t/ha (assuming a plough depth of 15 cm and bulk density 1.3 gm/cm^3), after Horrocks et al. [42]. Each soil had a control where no compost was applied. For each soil and soil–compost mixture, three incubation regimes were imposed under dark conditions. These sought to simulate a typical soil temperature (T-19, incubation at 19 °C) that might be encountered in temperate regions, as well as extreme cases intended to maximise microbially driven soil C turnover using incubations at 30 °C with and without N added as urea (T-30+N and T-30, respectively). Each treatment was replicated thrice.

Table 3. Summary of experimental design.

Soil—Compost Mixture	Treatments (*n* = 3)
Levin soil control (no compost)	T-19, T-30, T-30+N
Levin soil + 2.5% municipal compost	T-19, T-30, T-30+N
Levin soil + 2.5% sawdust compost	T-19, T-30, T-30+N
Pukekohe soil control (no compost)	T-19, T-30, T-30+N
Pukekohe soil + 2.5% municipal compost	T-19, T-30, T-30+N
Pukekohe soil + 2.5% sawdust compost	T-19, T-30, T-30+N
T-19 = Incubated at 19 °C T-30 = Incubated at 30 °C, T-30+N = Incubated at 30 °C with added Urea-N.	

The experiment started on 11th March 2014. Analytical-grade urea (N_2H_4CO LabServ^{TM}, Biolab Aust. Ltd., Hindmarsh, Australia) was applied in T-30+N experimental units in three separate applications on weeks 1, 5, and 13 as a source of N for microorganisms to enhance the microbial activity in soils. A total of 413 mg of urea (dissolved in 10 mL of water) was added to the N treatments, which was equivalent to an N addition rate of 200 kg/ha.

The soils and soil–compost mixtures were mixed twice a week, and their moisture content was maintained at 25% through compensating for lost weight with deionized water. Each replicate was sampled after 1, 5, 9, 13, 21, 31, and 49 weeks, where 40 g of soil was collected from each box. The change in organic matter (soil or soil with compost) was

determined through measuring total C. We did not determine CO_2 emissions from the soils. The samples were dried in an oven at 70 °C until a constant weight was obtained (<5 days) and sieved (2 mm nylon mesh) for chemical characterisation (see Section 2.5).

2.4. Pot Trial

Al Mamun et al. [37] measured Cd uptake by potatoes from a Pukekohe soil, freshly amended with MC. Subsets of unamended and MC-amended soils (rate of 2.5% *w/w*) left-over from the work of Al Mamun et al. [37] a year prior (and now 'aged') were transferred into 5 kg plastic pots. Each treatment was replicated thrice. The pots were placed in a randomised block design in the Plant Growth Unit at Lincoln University. Seed potato (*Solanum tuberosum;* var: 'Nadine') was obtained from Morton and Smith DWE, Christchurch, New Zealand. Seed potatoes were sprouted in moist trays covered with black polythene. After one week, the plants were transferred to individual pots and grown for nine weeks, during which the pots were watered regularly while maintaining the moisture content below the soils' maximum water holding capacity to avoid excessive drainage. The tubers had formed by the end of the growth period and the shoots were showing signs of chlorosis, at which point the tubers were gently removed from the soil to avoid scratching (and, hence, soil contamination). They were then washed thrice with tap water, dried using paper towels, and weighed to get the fresh weight of the potato tubers. The tubers were then washed thrice with reverse osmosis water and thrice with deionized water. The peel (1–2 mm thickness) was separated with a clean stainless peeler. The peeled tubers were divided into quarters, placed in paper bags, and dried in an oven at 70 °C until a constant weight was obtained. The dry weights were recorded, after which the tubers were ground using a Retsch ZM200 grinder (Düsseldorf, Germany) and stored in sealed plastic vials.

2.5. Chemical Analyses

Soil pH was measured at a soil–water ratio of 1:2.5 [43] using a SevenEasy^{TM} pH sensor (Mettler Toledo, Hamilton, New Zealand). Total C (forthwith C_T) and N concentrations were analysed in soil and compost samples using an Elementar Vario Max CN elemental analyser (Elementar $^{®TM}$, Langenselbold, Germany). Cation exchange capacity of the original materials was measured using the 0.01 M silver thiourea (AgTU) method [43]. Samples (0.70 g of dry soil with 35 mL of 0.01 M AgTU in a 50 mL vial) were placed on an end-over-end shaker for 16 h, followed by centrifuging for 10 min at 2000 rpm. The supernatant was filtered through a Whatman no. 40 filter and analysed for silver (Ag) using the ICP-OES.

Cadmium extractable through 0.05 M $Ca(NO_3)_2$ was used to provide a general estimate of Cd phytoavailability [44,45]. Briefly, 5 g of soil was mixed with 30 mL of 0.05 M $Ca(NO_3)_2$ and agitated using a vortex mixer for 3 min, shaken on an end-over-end shaker for 2 h, and centrifuged at 3000 rpm for 10 min. The supernatant was filtered through a Whatman no. 52 filter paper into 30 mL vials and analysed using ICP-OES (Inductively Coupled Plasma-Optical Emission Spectrometer), Varian 720, Palo Alto, CA, USA.

Pseudo-total elemental analyses of soil and plant samples were carried out using microwave digestion in 8 mL of Aristar^{TM} nitric acid (± 69%), after which the digest was diluted with milliQ water to a volume of 25 mL and filtered using Whatman no. 52 filter paper [46]. The concentrations of B, Ca, Cd, Co, Cr, Cu, Fe, K, Mg, Mo, Mn, Na, P, S, and Zn were determined using ICP-OES (Varian 720, Palo Alto, CA, USA).

The Certified Reference materials (soil and plant material, International Soil analytical Exchange—ISE 921 and International Plant analytical Exchange IPE 100, Wageningen University, Wageningen, The Netherlands) were analysed to confirm recovery of elements in the digests.

2.6. Statistical Analysis

Data were analysed using Minitab® 17 (Minitab Inc., State College, PA, USA) and Microsoft Excel 2013. Data were tested for normality, and log-normally distributed data

were log transformed prior to analysis. Significant differences were assessed using Analysis of Variance (ANOVA) with a post-hoc Fisher's test. Correlation analyses were used to determine significant temporal trends in extractable elements. The level of significance for both tests was set at 0.05.

3. Results

3.1. Changes in Total Carbon Concentration with Time

The addition of municipal compost and sawdust compost at 2.5% *w/w* initially increased C_T in the soils by 0.65% and 0.75%, respectively. However, by week 49, C_T in soil and soil–compost mixtures had significantly decreased in all treatments (control, municipal compost, and sawdust compost) in both soils (Figure 1A–F). In general, the magnitude of decrease followed the order T-19 < T-30 < T-30+N, indicating that the organic matter degradation was more rapid at higher temperatures and with added N. While the differences in C_T between T-30 and T-30+N soils were generally not significant throughout the incubation (Pukekohe soil + MC after 21 weeks was the exception), the difference was significant between the T-19 soil and the other two treatments in most soils after 13 weeks. Some treatments had a small but significant increase in C_T during weeks 5–13 (Figure 1, Table S1).

3.2. Effect of Composts on Extractable Cadmium and Other Elements

The $Ca(NO_3)_2$-extractable Cd concentrations in both the treatments and the controls decreased overall during the 49 week incubation. The reduction was greater in the two compost-amended soils than in the control soils (Figure 2). However, within that time $Ca(NO_3)_2$-extractable Cd concentrations increased significantly between weeks 2 and 10, before decreasing to achieve a net reduction. At the end of the incubation, the extractable Cd concentration in the compost treatments had decreased to between 23 and 89% of the control soils, with the greatest reduction in both soils generally achieved in the warmer incubations (Figure 2).

In contrast to Cd, the composts had little effect on the $Ca(NO_3)_2$-extractable Cu, Mg, Mn, and P, while there were significant increases in $Ca(NO_3)_2$-extractable K, Na, and S (Tables S3 and S5–S10). Both composts increased the $Ca(NO_3)_2$-extractable Zn in the Levin soil but not the Pukekohe soil (Table S11). Regarding the temporal changes in $Ca(NO_3)_2$-extractable elements, the concentrations of Cu, K, Mn, Na, P, S, and Zn followed a similar pattern to Cd in that they either remained unchanged or significantly decreased during the experimental period. In contrast, concentrations of Fe significantly increased (Table S4). Aluminium mostly remained unchanged or significantly increased in the Pukekohe soil (Table S2). Magnesium remained unchanged throughout the experiment (Table S6). The urea application to the soils and soil–compost mixtures decreased the pH of soils by ca. 0.4 pH units (Table S1).

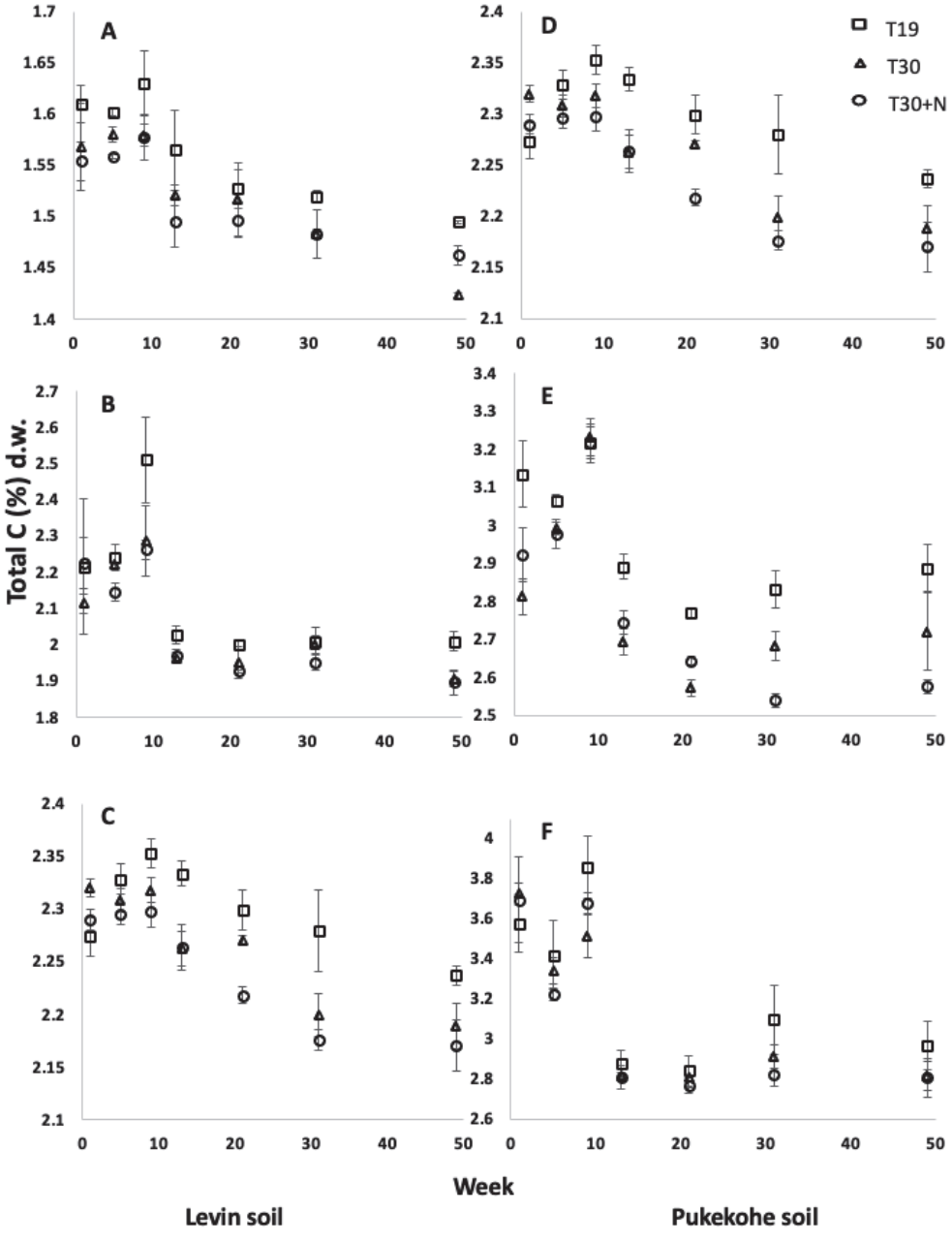

Figure 1. Changes of total C (C_T) in soils with time in treatments T-19, T-30, and T-30+N ((**A**) Levin soil control, (**B**) Levin soil+MC, (**C**) Levin soil+SC, (**D**) Pukekohe soil control, (**E**) Pukekohe soil+MC, (**F**) Pukekohe soil+SC). Error bars represent the standard error of the mean (n = 3).

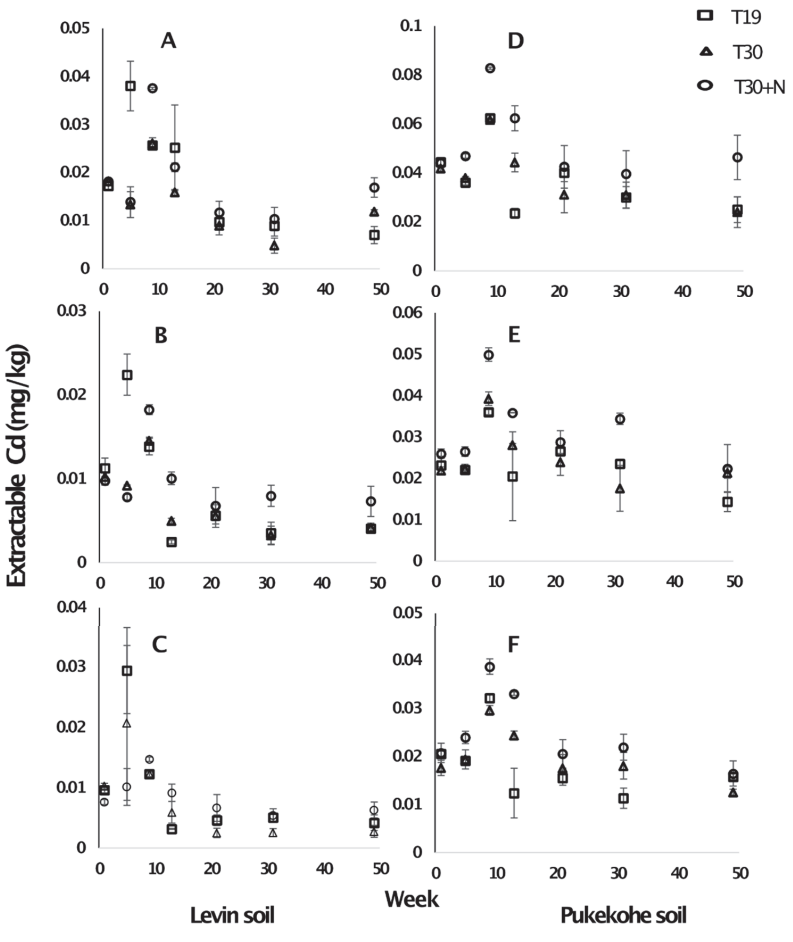

Figure 2. Changes in $Ca(NO_3)_2$-Extractable Cd with time in treatments T-19, T-30, and T-30+N ((**A**) Levin soil control, (**B**) Levin soil+MC, (**C**) Levin soil+SC, (**D**) Pukekohe soil control, (**E**) Pukekohe soil+MC, (**F**) Pukekohe soil+SC). Error bars represent the standard error of the mean (n = 3).

3.3. Accumulation of Cd and Other Elements by Potato Grown in Incubated Soils

Cadmium uptake by the potatoes grown in both of the MC-amended soils (freshly amended and aged soil) was about half of the control soils (Table 4). The concentration of Cd in the peeled potato tubers ranged from 0.011 to 0.044 mg/kg dry weight (d.w.), equivalent to 0.002–0.008 mg/kg fresh weight, which is well below the Maximum Limit of 0.1 mg/kg F.W. stated in the Food Standards of Australia and New Zealand (FSANZ) standard 1.4.1 and EU legislation (EU 1881/2006). Comparing the freshly amended soil with aged soil, there was a significant decrease in Cd in both the controls and the compost-amended soil. This decrease mirrors the results of the $Ca(NO_3)_2$ extractions. Unlike the extractions, there was no significant increase in Fe uptake into the potato tuber.

Table 4. Mean elemental concentrations (mg/kg DW) in the peeled tubers grown in a freshly amended compost-treated soil [37] and an "aged" soil that had been amended with compost for 1 year, and total C and $Ca(NO_3)_2$-extractable Cd concentrations in Pukekohe soils. The different letters (A–D) show where differences between means are significant.

Treatments	Freshly-Amended Soil [#]		Soils Aged for 1 Year	
Parameters	**Control**	**Municipal Compost**	**Control**	**Municipal Compost**
Cd	0.040 (0.003) ^{A}	0.020 (0.011) ^{B}	0.020 (0.001) ^{B}	0.011 (0.001) ^{C}
B	7.40 (0.04) ^{A}	7.33 (0.3) ^{A}	5 (0.5) ^{B}	6 (0.2) ^{B}
Ca	419 (65) ^{A}	289 (15) ^{B}	247 (11) ^{B}	357 (40) ^{AB}
Cu	6.1 (0.3)	6.4 (0.4)	5.7 (0.5)	5.5 (0.1)
Fe	23 (2) ^{A}	21 (0.2) ^{AB}	19 (1) ^{AB}	18 (1) ^{B}
K	20811 (424) ^{A}	21565 (705) ^{A}	21833 (408) ^{A}	20256 (544) ^{B}
Mg	1268 (72) ^{B}	1253 (39) ^{B}	1465 (46) ^{A}	1244 (103) ^{B}
Mn	6.7 (0.7) ^{A}	6.7 (0.2) ^{A}	6.2 (0.3) ^{A}	4.8 (0.4) ^{B}
Mo	0.6 (0.05) ^{B}	1.4 (0.2) ^{A}	0.8 (0.2) ^{B}	1.5 (0.1) ^{A}
Na	87 (16) ^{B}	153 (1) ^{A}	75 (8) ^{B}	163 (19) ^{A}
P	3356 (179) ^{AB}	3245 (60) ^{B}	3521 (106) ^{A}	3351 (26) ^{AB}
S	1248 (71) ^{BC}	1214 (37) ^{B}	1606 (68) ^{A}	1336 (84) ^{BC}
Zn	20 (2)	19 (1)	17 (0.3)	16 (0.5)
Extractable Cd in soil	0.011 (0.003) ^{A}	0.002 (0.000) ^{B}	<0.001	<0.001
Total C in soil (%)	2.29 (0.02) ^{C}	3.0 (0.01) ^{A}	2.0 (0.01) ^{D}	2.4 (0.01) ^{B}

[#] Data from Al Mamun et al. [37].

4. Discussion

The overall decrease in the total carbon concentration of all the soils and soil–compost mixtures shows the mineralization of organic matter (either from the compost or the original soil) by microorganisms, and is consistent with other compost-amended soil incubation studies that have used measurements of CO_2 production to show this [47,48]. The greater decrease at higher temperatures with added N was expected due to the increased microbial activity under these conditions [49,50]. The brief and small increase in C_T in all treatments between weeks 5 and 10 was most likely due to the rapid mineralization of oxygen-rich, low-molecular-weight moieties such as carbohydrates that are easily consumed by soil microorganisms [51], thus briefly increasing the C concentration, particularly in the compost-amended soils.

We did not measure the change in CEC in our soils. Other authors have reported a general reduction in the soils' organic matter results in a decrease of the soils' CEC [52], which would lead to a concomitant increase in cation solubility. Nevertheless, the decomposition of composts has also been reported to produce humic substances with a higher CEC [53,54], which would be consistent with our finding that the solubility of Cd and other elements either remained unchanged or even decreased in the compost-treated soils. The elements whose $Ca(NO_3)_2$-extractable concentrations decreased commonly exist as both cations (Cd, Cu, K, Na, and Zn) and oxyanions (P and S) in aerobic soils [55]. Therefore, changes in the charges of functional groups in the organic matter over time is unlikely to have had a significant impact on the solubility of those elements. The Cd results are consistent with previous studies where EDTA and DTPA-extractable Cd in compost-amended soils were lower than in corresponding control soils up to 6 months after application [40]. In a phytoremediation/phytostabilisation operation on heavily contaminated soils, compost addition led to an improvement in biodiversity after five years [56]. The lack of consistent differences in the $Ca(NO_3)_2$-extractable Cd across the different temperature and nitrogen addition treatments (T-19, T-30, and T-30+N) indicates that the aforementioned breakdown of labile organic materials did not affect the sorption of Cd to these significantly. Increased formation of strong organo-Cd associations in the ageing compost [57] may also have contributed to the metal immobilisation.

The significant increases in $Ca(NO_3)_2$-extractable Fe and Al concentrations suggest that the decreases in the extractable concentrations of most elements could have been partly an artefact of the experimental conditions. The regular mechanical disturbance of the moist soils will have disrupted soil aggregates [55,58,59] that would have maintained high surface areas of reactive surfaces for binding elements and high concentrations of colloidal Fe and Al [60]. These colloids may have occluded sorbed elements and thus reduced their solubility. This may have also occurred with colloidal organic matter liberated from aggregates whose re-attachment and coating of reactive surfaces would have further reduced the solubility of elements sorbed onto those surfaces. This process is a well-recognised mechanism for stabilising organic matter in soils [61–63].

In the field, mechanical disturbance of aggregates may occur following repeated ploughing. Previous studies on the role of ploughing on the solubility and phytoavailability of elements in soil have shown contradicting results. Lavado et al. [60] observed in a field trial that DTPA-extractable Cd concentrations did not change due to mechanical disturbance. In contrast, EDTA-extractable Cd was shown to have decreased due to mechanical disturbance for soils treated under laboratory conditions [55], which agreed with the reports of reduced Cd uptake in field-grown plants where the soils had not been subject to mechanical disturbance when compared to plants grown on mechanically disturbed soils.

The Cd concentrations in the potatoes grown here are generally below the previously reported range of concentrations (0.040–0.113 mg/kg D.W.) across different field-grown potato varieties grown in the Pukekohe region [64]. In the aged soils, the concentrations were less than 18% of the same varietal ("Nadine") grown in the field [64]. These differences may be partly due to fresh fertiliser (including Cd) inputs to the field soils during the growing season; however, differences in Cd uptake by that variety between different regions has also been recognised as having an influence, with significantly greater uptake at lower latitudes [64]. The cooler air temperature during the growth in the austral winter may also have reduced Cd uptake in the pot trial, when compared to the field-grown potatoes that are grown mainly in the summer [65]. The reduced uptake of Cd into potato tubers in the aged compost-amended soils reflected the low extractable concentrations of the metal in the same soils. These results suggest that MC can significantly reduce phytoavailability of Cd both in soils that have been freshly amended and one year later, after the reactive organic matter fractions in the compost have been mineralized. This agrees with the results from a previous pot trial that showed a significant reduction in the Cd concentration in the grain, leaf, and stem of wheat plants six months after compost addition [36]. The fact that these effects persist for up to a year, despite a gradual loss of C from soils, suggest that natural soil processes and mechanical disturbance may be converting compost into forms that either directly bind Cd to them, rendering Cd sorbed onto mineral fractions inert, or both. Potentially, leaching losses from the pots may have contributed to the reduction in Cd uptake by potatoes. However, other authors have shown that Cd leaching is negligible. For example, Gray et al. [66] reported leaching losses of 0.27–0.86 g/ha/yr from New Zealand soils, representing < 0.05% of the total Cd loading of the soil (assuming an average concentration of 0.89 mg/kg [67], a depth of 0.15 m, and a density of 1.5 g/cm^3).

5. Conclusions

The addition of composts to soil reduces the $Ca(NO_3)_2$-extractable Cd concentrations compared to the control. While incubation with mechanical disturbance and the addition of urea resulted in a significant decrease in the soil carbon concentrations, there was no corresponding increase in $Ca(NO_3)_2$-extractable Cd, and the plant uptake of Cd remained either unchanged or decreased over a one-year incubation period. The lack of increase in $Ca(NO_3)_2$-extractable Cd may be partly due to the experimental conditions, which included regular mechanical disturbance, potentially occluding Cd and other elements attached to the surfaces of soil colloids. Future work should identify the formation of mineral-associated organic carbon in the compost-amended soil and elucidate the fraction

of organic matter that binds Cd in these compost-amended soils. Furthermore, field trials could confirm the longevity of compost-bound Cd in agricultural soils.

Supplementary Materials: The following supporting information can be downloaded at: https://www.mdpi.com/article/10.3390/soilsystems7040107/s1, Table S1: pH over time (week) in Levin soil and Pukekohe with and without composts. SE is the standard error of the mean (n = 3); Table S2: Extractable Al (mg/kg) over time (week) in Levin soil and Pukekohe with and without composts. SE is the standard error of the mean (n = 3); Table S3: Extractable Cu (mg/kg) over time (week) in Levin soil and Pukekohe with and without composts. SE is the standard error of the mean (n = 3); Table S4: Extractable Fe (mg/kg) over time (week) in Levin soil and Pukekohe with and without composts. SE is the standard error of the mean (n = 3); Table S5: Extractable K (mg/kg) over time (week) in Levin soil and Pukekohe with and without composts. SE is the standard error of the mean (n = 3); Table S6: Extractable Mg (mg/kg) over time (week) in Levin soil and Pukekohe with and without composts. SE is the standard error of the mean (n = 3); Table S7: Extractable Mn (mg/kg) over time (week) in Levin soil and Pukekohe with and without composts. SE is the standard error of the mean (n = 3); Table S8: Extractable Na (mg/kg) over time (week) in Levin soil and Pukekohe with and without composts. SE is the standard error of the mean (n = 3); Table S9: Extractable P (mg/kg) over time (week) in Levin soil and Pukekohe with and without composts. SE is the standard error of the mean (n = 3); Table S10: Extractable S (mg/kg) over time (week) in Levin soil and Pukekohe with and without composts. SE is the standard error of the mean (n = 3); Table S11: Extractable Zn (mg/kg) over time (week) in Levin soil and Pukekohe with and without composts. SE is the standard error of the mean (n = 3); Table S12: Fisher's post hoc test of the data used in Figure 1 (A–F). Values with the same capital letters in the rows are not significantly different. Values with the same lower-case letters in the columns are not significantly different. The "*" indicates no significant difference; Table S13: Fisher's post hoc test of the data used in Figure 2 (A–F). Values with the same capital letters in the rows are not significantly different. Values with the same lower-case letters in the columns are not significantly different. The "*" indicates no significant difference.

Author Contributions: Conceptualisation, B.H.R. and N.J.L.; methodology, S.A.M.; formal analysis, B.H.R., N.J.L., S.A.M., J.C., L.K. and R.M.; data curation, B.H.R.; writing original draft preparation, S.A.M.; writing review and editing, B.H.R., N.J.L., S.A.M., J.C., L.K. and R.M.; supervision, B.H.R., N.J.L. and J.C. All authors have read and agreed to the published version of the manuscript.

Funding: This work was funded, in part, by Environmental Science and Research, the Fertiliser Association of NZ, and by the Ministry of Business Innovation and Employment's Our Land and Water National Science Challenge (contract C10X1507).

Institutional Review Board Statement: Not applicable.

Informed Consent Statement: Not applicable.

Data Availability Statement: The data used in this study are included in the Supplementary Information and will be made available on https://www.kiwiscience.com/journal-articles.html.

Acknowledgments: The lead author gratefully acknowledges the receipt of a New Zealand Aid PhD scholarship. We are grateful for the help of Lynne Clucas for the chemical analysis of the samples.

Conflicts of Interest: The authors declare no conflict of interest.

References

1. Bolan, N.S.; Adriano, D.C.; Duraisamy, P.; Mani, A. Immobilization and Phytoavailability of Cadmium in Variable Charge Soils. III. Effect of Biosolid Compost Addition. *Plant Soil* **2003**, *256*, 231–241. [CrossRef]
2. Kabata-Pendias, A.; Mukherjee, A.B. *Trace Elements from Soil to Human*; Springer Science & Business Media: Berlin/Heidelberg, Germany, 2007; ISBN 9783540327134.
3. Oosterhuis, F.H.; Brouwer, F.M.; Wijnants, H.J. A Possible EU Wide Charge on Cadmium in Phosphate Fertilisers: Economic and Environmental Implications. *IVM Rep.* **2000**. Available online: https://research.vu.nl/ws/portalfiles/portal/1646586/E-00-02+Cadmiumheffing+rapport.pdf (accessed on 19 November 2023).
4. Mar, S.S.; Okazaki, M. Investigation of Cd Contents in Several Phosphate Rocks Used for the Production of Fertilizer. *Microchem. J.* **2012**, *104*, 17–21. [CrossRef]
5. Hooda, P. *Trace Elements in Soils*; John Wiley & Sons: New York, NY, USA, 2010; ISBN 9781444319484.

6. Bergen, B.; Verbeeck, M.; Smolders, E. Trace Metal Accumulation in Agricultural Soils from Mineral Phosphate Fertiliser Applications in European Long-term Field Trials. *Eur. J. Soil Sci.* **2022**, *73*, 13167. [CrossRef]
7. Dziubanek, G.; Piekut, A.; Rusin, M.; Baranowska, R.; Hajok, I. Contamination of Food Crops Grown on Soils with Elevated Heavy Metals Content. *Ecotoxicol. Environ. Saf.* **2015**, *118*, 183–189. [CrossRef] [PubMed]
8. Fekete, S.G.; Bersényi, A.; Kádár, I.; Glávits, R.; Koncz, J.; Zöldág, L. Study of Soil-Plant (potato and Beetroot)-Animal Cycle of Nutritive and Hazardous Minerals in a Rabbit Model. *Acta Vet. Hung.* **2001**, *49*, 301–310. [PubMed]
9. Maclean, A.J. Cadmium in different plant species and its availability in soils as influenced by organic matter and additions of lime, P, Cd and Zn. *Can. J. Soil Sci.* **1976**, *56*, 129–138. [CrossRef]
10. McLaughlin, M.J.; Maier, N.A.; Rayment, G.E.; Sparrow, L.A.; Berg, G.; McKay, A.; Milham, P.; Merry, R.H.; Smart, M.K. Cadmium in Australian Potato Tubers and Soils. *J. Environ. Qual.* **1997**, *26*, 1644–1649. [CrossRef]
11. Pérez, A.L.; Anderson, K.A. DGT Estimates Cadmium Accumulation in Wheat and Potato from Phosphate Fertilizer Applications. *Sci. Total Environ.* **2009**, *407*, 5096–5103. [CrossRef]
12. Rai, S.; Gupta, S.; Mittal, P.C. Dietary Intakes and Health Risk of Toxic and Essential Heavy Metals through the Food Chain in Agricultural, Industrial, and Coal Mining Areas of Northern India. *Hum. Ecol. Risk Assess. Int. J.* **2015**, *21*, 913–933. [CrossRef]
13. Weggler-Beaton, K.; McLaughlin, M.J.; Graham, R.D. Salinity Increases Cadmium Uptake by Wheat and Swiss Chard from Soil Amended with Biosolids. *Soil Res.* **2000**, *38*, 37–46. [CrossRef]
14. Christensen, T.H.; Haung, P.M. Solid Phase Cadmium and the Reactions of Aqueous Cadmium with Soil Surfaces. In *Cadmium in Soils and Plants*; McLaughlin, M.J., Singh, B.R., Eds.; Springer Netherlands: Dordrecht, The Netherlands, 1999; pp. 65–96, ISBN 9789401144735.
15. Al Mamun, S.; Chanson, G.; Muliadi; Benyas, E.; Aktar, M.; Lehto, N.; McDowell, R.; Cavanagh, J.; Kellermann, L.; Clucas, L.; et al. Municipal Composts Reduce the Transfer of Cd from Soil to Vegetables. *Environ. Pollut.* **2016**, *213*, 8–15. [CrossRef] [PubMed]
16. Simmler, M.; Ciadamidaro, L.; Schulin, R.; Madejón, P.; Reiser, R.; Clucas, L.; Weber, P.; Robinson, B. Lignite Reduces the Solubility and Plant Uptake of Cadmium in Pasturelands. *Environ. Sci. Technol.* **2013**, *47*, 4497–4504. [CrossRef] [PubMed]
17. Nan, Z.; Li, J.; Zhang, J.; Cheng, G. Cadmium and Zinc Interactions and Their Transfer in Soil-Crop System under Actual Field Conditions. *Sci. Total Environ.* **2002**, *285*, 187–195. [CrossRef] [PubMed]
18. Alloway, B.J.; Jackson, A.P.; Morgan, H. The Accumulation of Cadmium by Vegetables Grown on Soils Contaminated from a Variety of Sources. *Sci. Total Environ.* **1990**, *91*, 223–236. [CrossRef] [PubMed]
19. Food Safety Authority, E. Cadmium Dietary Exposure in the European Population. *Efsa J.* **2012**, *10*, 2551. [CrossRef]
20. Kim, N. *Cadmium Accumulation in Waikato Soils*; Environment Waikato Regional Council: North Island, New Zealand, 2008.
21. Zheng, N.; Wang, Q.; Zheng, D. Health Risk of Hg, Pb, Cd, Zn, and Cu to the Inhabitants around Huludao Zinc Plant in China via Consumption of Vegetables. *Sci. Total Environ.* **2007**, *383*, 81–89. [CrossRef] [PubMed]
22. Zhuang, P.; McBride, M.B.; Xia, H.; Li, N.; Li, Z. Health Risk from Heavy Metals via Consumption of Food Crops in the Vicinity of Dabaoshan Mine, South China. *Sci. Total Environ.* **2009**, *407*, 1551–1561. [CrossRef] [PubMed]
23. Taylor, M.D.; Percival, H.J. Cadmium in Soil Solutions from a Transect of Soils Away from a Fertiliser Bin. *Environ. Pollut.* **2001**, *113*, 35–40. [CrossRef]
24. Sposito, G.; Page, A.L. Cycling of Metal Ions in the Soil Environment. *Met. Ions Biol. Syst.* **1984**, *18*, 287–332.
25. McLaughlin, M.J.; Palmer, L.T.; Tiller, K.G.; Beech, T.A.; Smart, M.K. Increased Soil Salinity Causes Elevated Cadmium Concentrations in Field-Grown Potato Tubers. *J. Environ. Qual.* **1994**, *23*, 1013–1018. [CrossRef]
26. Loganathan, P.; Hedley, M.J.; Grace, N.D.; Lee, J.; Cronin, S.J.; Bolan, N.S.; Zanders, J.M. Fertiliser Contaminants in New Zealand Grazed Pasture with Special Reference to Cadmium and Fluorine—A Review. *Soil Res.* **2003**, *41*, 501. [CrossRef]
27. McLaughlin, M.J.; Tiller, K.G.; Naidu, R.; Stevens, D.P. The Behaviour and Environmental Impact of Contaminants in Fertilizers. *Soil Res.* **1996**, *34*, 1–54. [CrossRef]
28. Smolders, E.; McLaughlin, M.J. Effect of Cl on Cd Uptake by Swiss Chard in Nutrient Solutions. *Plant Soil* **1996**, *179*, 57–64. [CrossRef]
29. Temminghoff, E.J.M.; Zee, S.E.A.T.M.; Haan, F.A.M. Speciation and Calcium Competition Effects on Cadmium Sorption by Sandy Soil at Various pHs. *Eur. J. Soil Sci.* **1995**, *46*, 649–655. [CrossRef]
30. Ghallab, A.; Usman, A.R.A. Effect of Sodium Chloride-Induced Salinity on Phyto-Availability and Speciation of Cd in Soil Solution. *Water Air Soil Pollut.* **2007**, *185*, 43–51. [CrossRef]
31. Basta, N.T.; Gradwohl, R.; Snethen, K.L.; Schroder, J.L. Chemical Immobilization of Lead, Zinc, and Cadmium in Smelter-Contaminated Soils Using Biosolids and Rock Phosphate. *J. Environ. Qual.* **2001**, *30*, 1222–1230. [CrossRef] [PubMed]
32. Bjerre, G.K.; Schierup, H.-H. Uptake of Six Heavy Metals by Oat as Influenced by Soil Type and Additions of Cadmium, Lead, Zinc and Copper. *Plant Soil* **1985**, *88*, 57–69. [CrossRef]
33. Chen, Z.S.; Lee, G.J.; Liu, J.C. The Effects of Chemical Remediation Treatments on the Extractability and Speciation of Cadmium and Lead in Contaminated Soils. *Chemosphere* **2000**, *41*, 235–242. [CrossRef]
34. Lee, T.-M.; Lai, H.-Y.; Chen, Z.-S. Effect of Chemical Amendments on the Concentration of Cadmium and Lead in Long-Term Contaminated Soils. *Chemosphere* **2004**, *57*, 1459–1471. [CrossRef]
35. Li, Z.; Ryan, J.A.; Chen, J.L.; Al-Abed, S.R. Adsorption of Cadmium on Biosolids-Amended Soils. *J. Environ. Qual.* **2001**, *30*, 903–911. [CrossRef]

36. Vaca-Paulín, R.; Esteller-Alberich, M.V.; Lugo-de la Fuente, J.; Zavaleta-Mancera, H.A. Effect of Sewage Sludge or Compost on the Sorption and Distribution of Copper and Cadmium in Soil. *Waste Manag.* **2006**, *26*, 71–81. [CrossRef] [PubMed]
37. Al Mamun, S.; Lehto, N.J.; Cavanagh, J.; McDowell, R.; Aktar, M.; Benyas, E.; Robinson, B.H. Effects of Lime and Organic Amendments Derived from Varied Source Materials on Cadmium Uptake by Potato. *J. Environ. Qual.* **2017**, *46*, 836–844. [CrossRef] [PubMed]
38. Shuman, L.M.; Dudka, S.; Das, K. Cadmium Forms and Plant Availability in Compost-Amended Soil. *Commun. Soil Sci. Plant Anal.* **2002**, *33*, 737–748. [CrossRef]
39. Tapia, Y.; Cala, V.; Eymar, E.; Frutos, I.; Gárate, A.; Masaguer, A. Chemical Characterization and Evaluation of Composts as Organic Amendments for Immobilizing Cadmium. *Bioresour. Technol.* **2010**, *101*, 5437–5443. [CrossRef] [PubMed]
40. Karaca, A. Effect of Organic Wastes on the Extractability of Cadmium, Copper, Nickel, and Zinc in Soil. *Geoderma* **2004**, *122*, 297–303. [CrossRef]
41. Ouattara, K.; Ouattara, B.; Nyberg, G.; Sédogo, M.P.; Malmer, A. Ploughing Frequency and Compost Application Effects on Soil Infiltrability in a Cotton–maize (Gossypium hirsutum–Zea Mays L.) Rotation System on a Ferric Luvisol and a Ferric Lixisol in Burkina Faso. *Soil Tillage Res.* **2007**, *95*, 288–297. [CrossRef]
42. Horrocks, A.; Curtin, D.; Tregurtha, C.; Meenken, E. Municipal Compost as a Nutrient Source for Organic Crop Production in New Zealand. *Agronomy* **2016**, *6*, 35. [CrossRef]
43. Blakemore, L.C.; Searle, P.L.; Daly, B.K. *Methods for Chemical Analysis of Soils; NZ Soil Bureau*; Department of Scientific and Industrial Research: Lower Hutt, New Zealand, 1987.
44. Black, A.; Mclaren, R.G.; Reichman, S.M.; Speir, T.W.; Condron, L.M. Examining the Integrity of Soil Metal Bioavailability Assays in the Presence of Organic Amendments to Metal-Spiked Soils. *Soil Use Manag.* **2012**, *28*, 89–100. [CrossRef]
45. Gray, C.W.; Mclaren, R.G.; Roberts, A.H.C.; Condron, L.M. Effect of Soil pH on Cadmium Phytoavailability in Some New Zealand Soils. *N. Z. J. Crop Hortic. Sci.* **1999**, *27*, 169–179. [CrossRef]
46. Gray, C.W.; McLaren, R.G.; Roberts, A.H.C.; Condron, L.M. Cadmium Phytoavailability in Some New Zealand Soils. *Soil Res.* **1999**, *37*, 461–478. [CrossRef]
47. Lim, S.-S.; Lee, K.-S.; Lee, S.-I.; Lee, D.-S.; Kwak, J.-H.; Hao, X.; Ro, H.-M.; Choi, W.-J. Carbon Mineralization and Retention of Livestock Manure Composts with Different Substrate Qualities in Three Soils. *J. Soils Sediments* **2012**, *12*, 312–322. [CrossRef]
48. Shah, A.; Lamers, M.; Streck, T. N_2O and CO_2 Emissions from South German Arable Soil after Amendment of Manures and Composts. *Environ. Earth Sci.* **2016**, *75*, 427. [CrossRef]
49. Kuzyakov, Y.; Friedel, J.K.; Stahr, K. Review of Mechanisms and Quantification of Priming Effects. *Soil Biol. Biochem.* **2000**, *32*, 1485–1498. [CrossRef]
50. Hamer, U.; Potthast, K.; Makeschin, F. Urea Fertilisation Affected Soil Organic Matter Dynamics and Microbial Community Structure in Pasture Soils of Southern Ecuador. *Appl. Soil Ecol.* **2009**, *43*, 226–233. [CrossRef]
51. Leifeld, J.; Siebert, S.; Kögel-Knabner, I. Changes in the Chemical Composition of Soil Organic Matter after Application of Compost. *Eur. J. Soil Sci.* **2002**, *53*, 299–309. [CrossRef]
52. Helling, C.S.; Chesters, G.; Corey, R.B. Contribution of Organic Matter and Clay to Soil Cation-Exchange Capacity as Affected by the pH of the Saturating Solution 1. *Soil Sci. Soc. Am. J.* **1964**, *28*, 517–520. [CrossRef]
53. Harada, Y.; Inoko, A. The Measurement of the Cation-Exchange Capacity of Composts for the Estimation of the Degree of Maturity. *Soil Sci. Plant Nutr.* **1980**, *26*, 127–134. [CrossRef]
54. Muller, J.F. Some Observations on Base Exchange in Organic Materials. *Soil Sci.* **1933**, *35*, 229–237. [CrossRef]
55. Brady, N.C.; Weil, R. *Nature and Properties of Soils, the: Pearson New International Edition*; Pearson Higher Ed: Hoboken, NJ, USA, 2013.
56. Bouwman, L.A.; Vangronsveld, J. Rehabilitation of the Nematode Fauna in a Phytostabilized, Heavily Zinc-Contaminated, Sandy Soil. *J. Soils Sediments* **2004**, *4*, 17–23. [CrossRef]
57. Kleber, M.; Sollins, P.; Sutton, R. A Conceptual Model of Organo-Mineral Interactions in Soils: Self-Assembly of Organic Molecular Fragments into Zonal Structures on Mineral Surfaces. *Biogeochemistry* **2007**, *85*, 9–24. [CrossRef]
58. Bissonnais, Y. Aggregate Stability and Assessment of Soil Crustability and Erodibility: I. Theory and Methodology. *Eur. J. Soil Sci.* **1996**, *47*, 425–437. [CrossRef]
59. Watts, C.W.; Dexter, A.R.; Dumitru, E.; Arvidsson, J. An Assessment of the Vulnerability of Soil Structure to Destabilisation during Tillage. Part I. A Laboratory Test. *Soil Tillage Res.* **1996**, *37*, 161–174. [CrossRef]
60. Lavado, R.S.; Porcelli, C.A.; Alvarez, R. Concentration and Distribution of Extractable Elements in a Soil as Affected by Tillage Systems and Fertilization. *Sci. Total Environ.* **1999**, *232*, 185–191. [CrossRef]
61. Baldock, J.A.; Skjemstad, J.O. Role of the Soil Matrix and Minerals in Protecting Natural Organic Materials against Biological Attack. *Org. Geochem.* **2000**, *31*, 697–710. [CrossRef]
62. Deng, Y.; Dixon, J.B. Soil Organic Matter and Organic-Mineral Interactions. In *Soil Mineralogy with Environmental Applications*; SSSA Book Series; Soil Science Society of America: Madison, WI, USA, 2002; pp. 69–107, ISBN 9780891188919.
63. Huang, P.-M.; Wang, M.-K.; Chiu, C.-Y. Soil Mineral–organic Matter–microbe Interactions: Impacts on Biogeochemical Processes and Biodiversity in Soils. *Pedobiologia* **2005**, *49*, 609–635. [CrossRef]
64. Gray, C.W.; Yi, Z.; Lehto, N.J.; Robinson, B.H. Effect of Cultivar Type and Soil Properties on Cadmium Concentrations in Potatoes. *N. Z. J.* **2019**, *47*, 182–197. [CrossRef]

65. Yi, Z.; Lehto, N.J.; Robinson, B.H.; Cavanagh, J.-A.E. Environmental and Edaphic Factors Affecting Soil Cadmium Uptake by Spinach, Potatoes, Onion and Wheat. *Sci. Total Environ.* **2020**, *713*, 136694. [CrossRef]
66. Gray, C.W.; McLaren, R.G.; Roberts, A.H.C. Cadmium Leaching from Some New Zealand Pasture Soils. *Eur. J. Soil Sci.* **2003**, *54*, 159–166. [CrossRef]
67. Reiser, R.; Simmler, M.; Portmann, D.; Clucas, L.; Schulin, R.; Robinson, B. Cadmium Concentrations in New Zealand Pastures: Relationships to Soil and Climate Variables. *J. Environ. Qual.* **2014**, *43*, 917–925. [CrossRef]

Disclaimer/Publisher's Note: The statements, opinions and data contained in all publications are solely those of the individual author(s) and contributor(s) and not of MDPI and/or the editor(s). MDPI and/or the editor(s) disclaim responsibility for any injury to people or property resulting from any ideas, methods, instructions or products referred to in the content.

soil systems

MDPI

Article

Enzymatic Diagnostics of Soil Health of the European Part of Russia with Lead Contamination

Tatiana Minnikova [1,*], Sergey Kolesnikov [1], Anna Kuzina [1], Dmitry Trufanov [1], Ekaterina Khrapay [1] and Anatoly Trushkov [2]

[1] Academy of Biology and Biotechnology by D.I. Ivanovsky, Southern Federal University, Rostov-on-Don 344090, Russia; kolesnikov1970@list.ru (S.K.); nyuta_1990@mail.ru (A.K.); dtrufanov@sfedu.ru (D.T.); katerinap1996@mail.ru (E.K.)

[2] Azov-Black Sea Branch, The Federal State Budgetary Scientific Branch, All-Russian Research Institute of Fishing and Oceanography, Rostov-on-Don 344002, Russia; trushkov_tolik@mail.ru

* Correspondence: loko261008@yandex.ru; Tel.: +7-988-539-0134

Abstract: Lead (Pb) is one of the most common environmental pollutants. Lead has an acute toxic effect on soil biotas and the enzymatic system of soils. The objective of this study is to carry out enzymatic diagnostics of soil health in the European part of Russia after Pb contamination. As a part of the simulation experiment, Pb (at maximum permissible concentrations (MPCs) of 1, 10, and 100) was used to contaminate 12 types of soils in the south and center of the European part of Russia, which differed in their physical and chemical properties. To assess soil health, the activity of oxidoreductases (catalase, dehydrogenases, and cysteine reductase) and hydrolases (invertase, urease, and phosphatase) was studied. Most enzymes were inhibited with increased Pb dosage. The most sensitive soils to Pb contamination, assessed by enzyme activity, are soils of semi-deserts and dry steppes. Cysteine reductase is considered the most sensitive enzyme to Pb contamination. The most informative indicators for Pb contamination were phosphatase, cysteine reductase, and invertase. The P (phosphatase) cycle and the redox enzyme (catalase) also have instability in Pb-contaminated soils. The C (invertase and dehydrogenases) and N (urease) cycles do not change significantly when contaminated with lead. The results of this study can be used for the diagnostics of the condition of soils in different natural areas after Pb contamination.

Keywords: soil; oxidoreductases; hydrolases; steppes; saline soils; meadow soils; dry steppes; geometric mean; integral indicator of enzymatic activity

Citation: Minnikova, T.; Kolesnikov, S.; Kuzina, A.; Trufanov, D.; Khrapay, E.; Trushkov, A. Enzymatic Diagnostics of Soil Health of the European Part of Russia with Lead Contamination. *Soil Syst.* **2024**, *8*, 76. https://doi.org/10.3390/soilsystems8030076

Academic Editor: Manfred Sager

Received: 23 April 2024
Revised: 2 July 2024
Accepted: 3 July 2024
Published: 5 July 2024

Copyright: © 2024 by the authors. Licensee MDPI, Basel, Switzerland. This article is an open access article distributed under the terms and conditions of the Creative Commons Attribution (CC BY) license (https://creativecommons.org/licenses/by/4.0/).

1. Introduction

Lead (Pb) is a priority pollutant found in soils due to the use of leaded fuel, the burning of coal in furnaces of thermal power plants, and the operation of plants for processing metal ore containing Pb [1]. Soil pollution leads to the accumulation of Pb in plant organs, which entails the migration of heavy metal into the body of animals and ultimately humans [2–5]. Lead contamination of soils is mainly due to atmospheric emissions rather than discharges [6,7]. Soil contamination with Pb also occurs in landfills with local soil contamination with equipment and consumables containing Pb: batteries, cells, lead-sheathed cables, etc. [8,9]. The main sources of soil contamination with Pb are transport (which uses leaded gasoline) and mining enterprises [10,11]. Lands with an alkaline pH as well as a high content of organic matter, Fe hydroxides, carbonates, and clay deposits contribute to the fixation of Pb in the soil and the toxic effect on living organisms of the environment [12].

To assess the ecological state of soils in case of soil contamination with heavy metals and oil, the activity of soil enzymes is often used as one of the sensitive and informative indicators of soil health [13–17]. This is since enzymes are involved in the biogeochemical cycles of carbon (C), nitrogen (N), phosphorus (P), oxygen (O), sulfur (S), and other elements

in the soil. The enzymatic activity serves as an indicator of many anthropogenic processes occurring in the soil, including those associated with biogeochemical cycles of C, N, P, S, and other cycles [18–22]. When soils are polluted with heavy metals and petroleum hydrocarbons, as well as when soil cultivation technology changes, the activity of soil enzymes changes [14,17,23–25]. The enzymatic activity of soils, especially the activity of dehydrogenases and arylsulfatase, was significantly inhibited in the case of contamination with Cd, Pb, Cu, Ni, V, and Cr [26]. The least sensitive enzymatic activities to heavy metal contamination are the activity of β-glucosidase and protease. It is interesting and relevant to develop soil health scales for indicators of enzymatic activity in the case of heavy metal contamination, using the example of lead. Lead, as one of the most common and toxic heavy metals, causes oxidative stress, disrupts disulfide bonds in the proteins of soil microorganisms, reduces the vital activity of nitrifying and ammonifying bacteria, reduces the availability of phosphorus to plants, and has other negative effects [2,27].

Soil contamination with Pb affects the enzymatic activity of soils and plants [28–30]. According to Zhou (2014), low concentrations of Pb (less than 500 mg/kg) can stimulate the activity of soil enzymes, whereas concentrations of Pb greater than 500 mg/kg inhibit the activity of soil enzymes (urease and invertase) [31]. The effect of Cd(II), Cu(II), and Pb(II) at different doses and with different incubation periods has been studied for arylsulfatase, the β-activity of glucosidase, acid phosphatase, protease, and urease in uncontaminated brown forest soil (Argentina) [32]. It was found that the studied metals inhibited the activity of arylsulfatase, acid phosphatase, protease, and urease. The effect on the activity of β-glucosidase was insignificant or absent altogether. The toxicity of various metals, estimated by the percentage of inhibition of enzymatic activity, was in the following sequence: Cd ≅ Cu > Pb. It was concluded that protease turned out to be the enzyme most sensitive to soil contamination with Cd, Cu, and Pb. The activity of peroxidase and polyphenol oxidase in chernozem, alluvial, and urban soils contaminated with Pb and Cd was evaluated 3, 90, 180, and 360 days after the start of the experiment [33]. It was found that Pb and Cd increased the activity of peroxidase in soils, while polyphenol oxidase did not change. Considering the problem of soil contamination with lead, attempts have been made to reduce the metal content and restore the ecological state of the soil after contamination. Therefore, it is of real interest to study the enzymatic activity characterizing the biogeochemical cycles of C, N, P, O, and S in 12 types of soils in different climatic zones of the European part of Russia.

This study's aim is to carry out enzymatic diagnostics on the soil health of the European part of Russia in the case of lead contamination.

2. Materials and Methods

Object of study. Twelve types of soils in southern and central part of Russia were analyzed (Table 1). These soils represent 5 types of ecosystems: meadow soils, saline and brackish soils, soils of dry steppes and semi-deserts, soils of steppes, and soils of broad-leaved forests and forest steppes. These soils differ in the following physical, chemical, and biological properties: pH, organic matter content, cation exchange capacity, and granulometric composition (clay, sand, and silt content).

The pollutant. Lead was investigated as a pollutant, as one of the priority environmental toxicants. The main sources of Pb in the soils of the European part of Russia are road transport, coal burning, processing of ores containing heavy metals, etc. The background Pb content in soils was analyzed using a Spectroscan MAX-GVM analyzer. The absence of Pb in soils or its trace content was found. Lead oxide (PbO_2) was added to the soil in terms of Pb atoms in concentrations of 1, 10, and 100 MPC (1 MPC = 100 mg/kg).

Experimental design. Contamination of 12 different types of Pb soils was carried out according to a single scheme (Figure 1). Lead was added to the purified and sifted soil in concentrations of 1, 10, and 100 MPC. For the experimental model, soils were selected at a distance from roads and processing plants. Therefore, controls for each soil were considered to be free from contamination with heavy metals, including Pb. The soil was thoroughly mixed to simulate Pb soil contamination and moistened (40% of the soil mass). The incubation period for soil contaminated with Pb lasted 30 days.

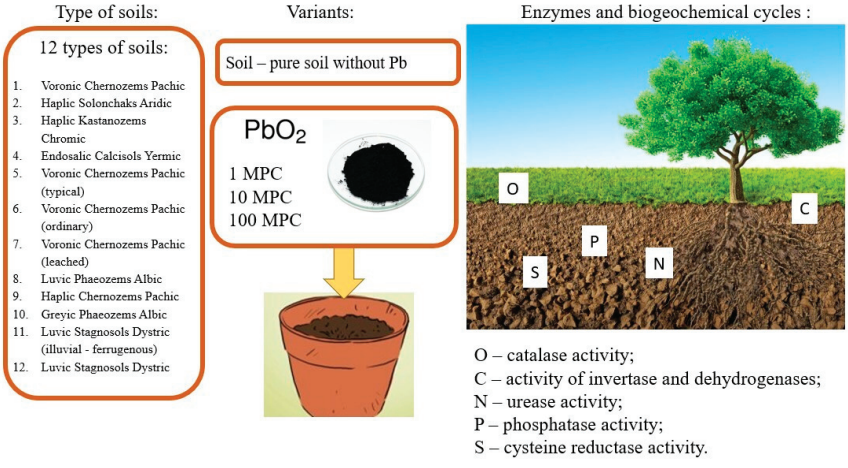

Figure 1. Scheme of the model experiment.

During experiment, soil samples were kept at a constant of temperature, humidity, and illumination in the climate growth chamber (Binder KBW240-230V (BINDER GmbH, Tuttlingen, Germany)).

Physical and chemical properties of soils. To assess the physical and chemical state of soils, the following soil properties were determined according to standard methods [34,35]: granulometric composition in terms of silt, sand, and clay (%), organic matter content (%), pH, and cation exchange capacity (mg × eq/100 g of soil). The granulometric composition of the soil was determined by the method of Kaczynski. The content of clay (<0.002 mm), silt (0.05–0.002 mm), and sand (>0.05 mm) was estimated using the soil texture triangle (in %). The content of total organic matter was determined by acid oxidation of potassium dichromate with a spectrophotometric termination (in %). The reaction of the soil medium (pH) was measured using an electrode potentiometer in distilled water in a ratio of 1 part soil to 2.5 parts water (w/v). The capacity of cation exchange in soils was determined by acid–base titration (in mg × eq/100 g of soil).

Methods for determining enzymatic activity. To diagnose the ecological state and health of soils, changes in enzymes of the oxidoreductase (catalase, dehydrogenases, and cysteine reductase) and hydrolase (invertase, urease, and phosphatase) classes were analyzed according to F.Kh. Khaziev (2005) [36]. Each enzyme characterizes a part of the cycle of a certain element necessary for the optimal functioning of the ecosystem. Methods for the determination of enzymes are presented in Table 2. Analyses to determine enzymatic activity were performed 3–4 times in duplicate.

Table 1. Characteristics of sampling sites and soil properties.

No	Type of Soil (WRB, 2022)	Place of Selection	Coordinates	Soil Granulometric Composition, %			C_{org}, %	pH	CEC, mg × eq/100 g Soil
				Clay	Sand	Silt			
			Soils of meadow						
1.	Voronic Chernozems Pachic (VCP)	Stavropol Territory, Kochubeevsky district, st. Barsukovskaya	44°47′43.93″ N 41°51′3.70″ E	22	38	40	3.59	8.2	23.0
2.	Haplic Solonchaks Aridic (HSA)	Saline and alkaline soils, Republic of Kalmykia, Yashkul district, Utta village	46°18′33.96″ N 45°51′34.98″ E	14	79	14	1.75	7.4	21.7
			Soils of dry steppes and semi-deserts						
3.	Haplic Kastanozems Chromic (HKC)	Rostov region, Remontnensky district, Privolny village	46°42′41.92″ N 43°17′49.24″ E	11	5	84	0.51	8.1	28.5
4.	Endosalic Calcisols Yermic (ECY)	Republic of Kalmykia, Yashkul district, Khulkhuta village	46°12′4.89″ N 45°25′32.07″ E	14	72	14	0.30	8.0	21.7
			Soils of steppe						
5.	Voronic Chernozems Pachic (typical) (VCP(typ.))	Voronezh region, Kashira district, Mosalskoe village	51°22′15.40″ N 39°32′50.20″ E	43	28	29	8.87	7.6	54.5
6.	Voronic Chernozems Pachic (ordinary) (VCP(ord.))	Voronezh region, Bogucharsky district, Filonovo village	50° 3′5.41″ N 40°25′59.22″ E	30	29	41	6.26	7.8	51.2
7.	Voronic Chernozems Pachic (leached) (VCP(leach))	Tula region, Volovsky district, Zapovednoe village	53°25′57.89″ N 38°10′11.54″ E	30	39	31	7.79	7.4	49.5
8.	Luvic Phaeozems Albic (LPA)	Tula region, Venevsky district, Ulyanovka village	54°23′54.78″ N 54°23′54.78″ E	31	38	31	6.00	7.3	31.7
9.	Haplic Chernozems Pachic (HCP)	Rostov region, Millerovsky district, st. Malchevskaya	49°1′59.58″ N 40°27′27.81″ E	42	37	21	3.47	7.2	47.7
10.	Greyic Phaeozems Albic (GPA)	Moscow region, Kashira urban district, Zlobino village	54°44′1.19″ N 38°5′41.17″ E	18	60	22	5.35	7.4	17.4
			Soils of broad-leaved forests and forest-steppes						
11.	Luvic Stagnosols Dystric (illuvial-ferrugenous) (LSD(ill.-ferr.))	Moscow region, Stupinsky district, Tutykhino village	54°52′38.14″ N 37°59′47.60″ E	1	95	4	2.41	5.4	9.1
12.	Luvic Stagnosols Dystric (LSD)	Moscow region, Domodedovo urban district, village of the Podmoskovye sanatorium	55°21′42.48″ N 37°46′32.05″ E	16	64	20	6.70	5.2	13.4

Table 2. Methods for determining the activity of soil enzymes.

No	Enzyme	Method
	Class of oxidoreductases	
1.	Catalase activity (H_2O_2:H_2O_2-oxidoreductase, EC 1.11.1.6.)	By the volume of oxygen released during the decomposition of hydrogen peroxide (according to A.Sh. Galstyan), ml O_2 in 1 g of soil per 1 min
2.	Activity of dehydrogenases (substrate: NAD (P)-oxidoreductase, EC 1.1.1)	For the reduction of tetrazolium salts into formazan (according to A.Sh. Galstyan, modified by F.Kh. Khaziev), mg triphenylformazan in 1 g of soil in 24 h
3.	Cysteine reductase activity (cysteine NAD(P)-oxidoreductase EC 1.8.1)	The method is based on the oxidation of sulfur of the sulfhydryl group of cysteine into the sulfide group of cystine with a colorimetric end (according to A.Sh. Galstyan, A.D. Antonyan (1981), mg of formazan per 10 g in 2 h
	Class of hydrolases	
4.	Activity of β-fructofuranosidase (invertase, sucrase, EC 3.2.1.26)	According to the amount of glucose during the hydrolysis of sucrose, colorimetrically using Felling's reagent (according to F.Kh. Khaziev (2005)), mg of glucose in 1 g of soil in 24 h
5.	Urease activity (urea-amidohydrolase, EC 3.5.1.5.)	According to the amount of ammonia formed with Nessler's reagent during the hydrolysis of urea (according to F.Kh. Khaziev (2005)), mg NH_3 per g of soil per 24 h
6.	Phosphatase activity (phosphohydrolase of orthophosphoric acid monoesters. EC 3.1.3.1-2)	According to the change in the content of nitrophenols with the formation of organic phosphorus and mineral substrates (according to Tabatabai and Dick (2002)), μg of p-nitrophenol in 1 g of soil per 1 h

According to the average values of the activity of all soil enzymes (catalase, dehydrogenase, cysteine reductase, invertase, phosphatase, and urease), the integrated index of enzymatic activity (IIEA) was calculated according to Equation (1) [37]:

$$\text{IIEA} = \frac{A_1}{A_{1\ \text{contr}}} \times 100\% \quad (1)$$

where A_1, A_2…, and A_n are the relative scores for each of the indicators of enzymatic activity in %; and $A_{1\ \text{contr}}$—control value.

The geometric mean of enzymatic activity (GMea) was calculated using Equations (2) and (3) [38] as follows:

$$A_1 = \frac{A_{op}}{A_{\ \text{contr}}} \times 100\% \quad (2)$$

where A_1, A_2…, and A_n are the relative scores for each of the indicators of enzymatic activity in %; and A_{op}—absolute value of enzyme activity.

The final GMea calculation is presented in Equation (3) as follows:

$$\text{GMea} = \sqrt[n]{A_1 + A_2 + \cdots + A_n} \quad (3)$$

where A_1, A_2…, and A_n are the relative scores for each of the indicators of enzymatic activity in %.

The complex nature of the GMea indicator makes it possible to evaluate the response of enzymes of different classes (oxidoreductases and hydrolases), which reflects the totality of the processes of restoration or degradation occurring in the soil. This indicator, along with IIEA, can be used to diagnose soil health under various types of anthropogenic stress, including pollution with heavy metals, petroleum hydrocarbons, etc. [24,25,39,40].

Statistical analysis of the obtained data was carried out using the Statistica 12.0 software package. The mean values and variance were determined, and the reliability of various samples was established using variance analysis (Student's *t*-test). An analysis of variance (ANOVA) was calculated on the activity of soil enzymes for different soil types.

3. Results

Catalase activity. The change in the activity of catalase, as an enzyme involved in the decomposition of hydrogen peroxide, which is toxic to microorganisms, to oxygen and hydrogen after soil contamination with Pb, is shown in Figure 2. Lead contamination of VCP, HSA, ECY, GPA, and HCP reduced the enzymatic activity only at an MPC of 100 by 15, 10, 17, 16, and 13% compared to the control.

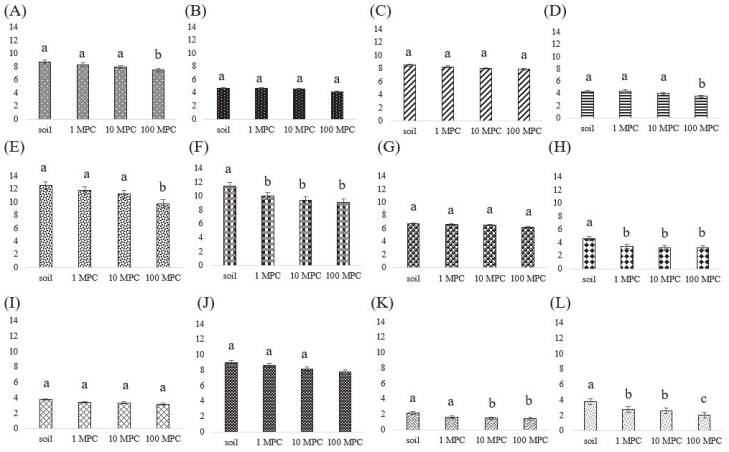

Figure 2. Change in catalase activity in soils contaminated with lead, ml O_2/1 g/1 min: (**A**) Voronic Chernozems Pachic; (**B**) Haplic Solonchaks Aridic; (**C**) Haplic Kastanozems Chromic; (**D**) Endosalic Calcisols Yermic; (**E**) Voronic Chernozems Pachic (typical); (**F**) Voronic Chernozems Pachic (ordinary); (**G**) Voronic Chernozems Pachic (leached); (**H**) Luvic Phaeozems Albic; (**I**) Greyic Phaeozems Albic; (**J**) Haplic Chernozems Pachic; (**K**) Luvic Stagnosols Dystric (illuvial ferrugenous); (**L**) Luvic Stagnosols Dystric. Note: The different lowercase letters per column indicate significant differences ($p < 0.05$) among different ages that based on one-way ANOVA: (a)—does not differ significantly from the control; (b)—significant difference from control ($p < 0.05$); (c)—significant difference from control ($p < 0.01$).

In the VCP (typ.) soils, a decrease in catalase activity was observed at MPCs of 10 and 100 of Pb of 11 and 23% compared to the control. The inhibition of enzymatic activity at the minimum dose (1 MPC) with a proportional decrease in activity and an increase in the Pb dose was observed in the VCP (ord.) (13–21%), LPA (26–31%), LSD (ill.-ferr.) (25–33%), and LSD soils (28–47%). In the HKC and VCP (leach) soils, there was no significant difference in catalase activity with an increase in the Pb dose.

Among the studied soils, the VCP (typ.) (9.8–12.6 mL O_2/1 g/1 min) and VCP (ord.) (9.1–11.4 mL O_2/1 g/1 min) soils had the highest enzymatic activity, even after the Pb contamination. The least catalase activity was observed in the HSA (4.2–4.7 mL O_2/1 g/1 min),

ECY (3.6–4.3 mL O_2/1 g/1 min), GPA (3.2–3.8 mL O_2/1 g/1 min), LSD (ill.-ferr.) (1.4–2.2 mL O_2/1 g/1min), and LSD (2.0–3.8 mL O_2/1 g/1 min) soils.

All soils with the lowest catalase activity have a light and medium loamy granulometric composition, a low cation exchange capacity, and an lower content of organic matter. This leads to a decrease in the rate of decomposition of hydrogen peroxide, which is toxic to the microbiota, and as a result, underestimated values of enzyme activity. Nitrogen in the soil stimulates catalase, and phosphorus can inhibit enzyme activity. According to Galstyan, in the presence of a high concentration of phosphorus in soil (for example, in soils with a high phosphorus content or the introduction of phosphorus fertilizers), a decrease in catalase activity is due to the blocking of the prosthetic group of the catalase enzyme by phosphoric acid anions [41].

Dehydrogenases activity. The carbon cycle in soils is one of the most important in the life of microorganisms, plants, animals, and humans. In the soil, the activity of dehydrogenases (Figure 3) and invertase (Figure 4) is directly involved in the biogeochemical carbon cycle.

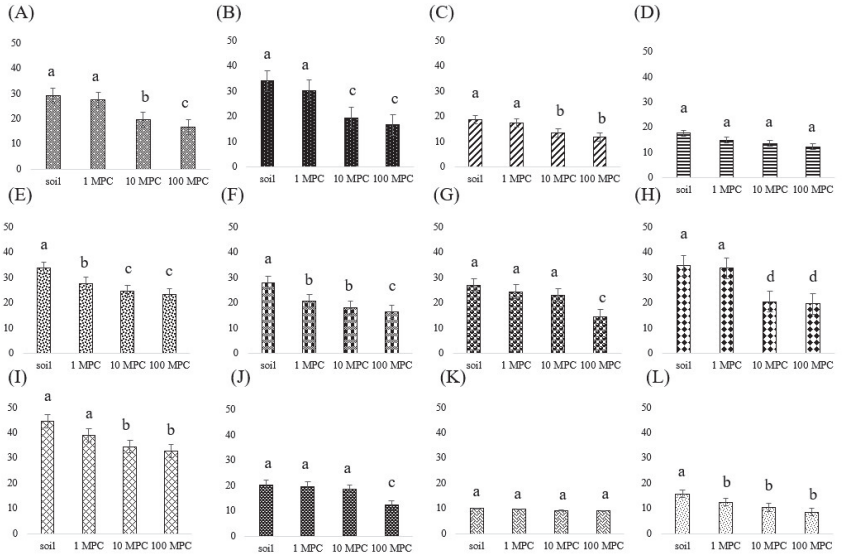

Figure 3. Change in the activity of dehydrogenases in soils contaminated with lead, mg TPF/1 g/24 h: (**A**) Voronic Chernozems Pachic; (**B**) Haplic Solonchaks Aridic; (**C**) Haplic Kastanozems Chromic; (**D**) Endosalic Calcisols Yermic; (**E**) Voronic Chernozems Pachic (typical); (**F**) Voronic Chernozems Pachic (ordinary); (**G**) Voronic Chernozems Pachic (leached); (**H**) Luvic Phaeozems Albic; (**I**) Greyic Phaeozems Albic; (**J**) Haplic Chernozems Pachic; (**K**) Luvic Stagnosols Dystric (illuvial ferrugenous); (**L**) Luvic Stagnosols Dystric. Note: The different lowercase letters per column indicate significant differences ($p < 0.05$) among different ages that based on one-way ANOVA: (a)—does not differ significantly from the control; (b)—significant difference from control ($p < 0.05$); (c)—significant difference from control ($p < 0.01$): (d)—significant difference from control ($p < 0.0075$).

The most resistant soil to Pb pollution in terms of dehydrogenase activity is LSD (ill-ferr.) soil, the activity of which is reduced only at an MPC of 100 of Pb by 10% compared to the control group. The activity of dehydrogenases in the case of contamination with MPCs of 10 and 100 of Pb decreased in the VCP (33–43%), HKC (29–37%), LPA (42–44%), and HCP (10–40%) soils. In other types of soils, even with the minimum dose of Pb (1 MPC), a decrease in dehydrogenase activity was found, which increased by the following percentages with increasing concentrations: HSA (11–52%), ECY (17–31%), VCP (typ.) (18–31%), VCP (ord.) (26–42%), VCP (leach) (10–47%), GPA (13–27%), and LSD (22–46%).

The highest activity of dehydrogenases, despite the Pb contamination, was found in the HSA (16.6–34.0 mg TPF/1 g/24 h), VCP (typ.) (23.3–33.8 mg TPF/1 g/24 h), LPA (19.6–34.7 mg TPF/1 g/24 h), and GPA (32.9–44.6 mg TPF/1 g/24 h) soils. The lowest enzymatic activity was found in the LSD (ill.-ferr.) (9.1–10.0 mg TPF/1 g/24 h) and LSD (8.6–15.8 mg TPF/1 g/24 h) soils.

The activity of dehydrogenases in soil is closely related to the catalysis of redox reactions by the dehydrogenation of organic substances in soil [23,42]. When Pb contaminates the soil, the oxidation of organic compounds in the soil is disrupted, and as a result, the activity of dehydrogenases decreases [2]. Therefore, there is no sharp decrease in the activity of dehydrogenases. A significant decrease in the activity of this enzyme is observed in soils contaminated with petroleum hydrocarbons [43].

Invertase activity. The invertase activity after the Pb contamination at an MPC of 100 decreased only in the VCP and HCP soils by 42 and 25% (Figure 4).

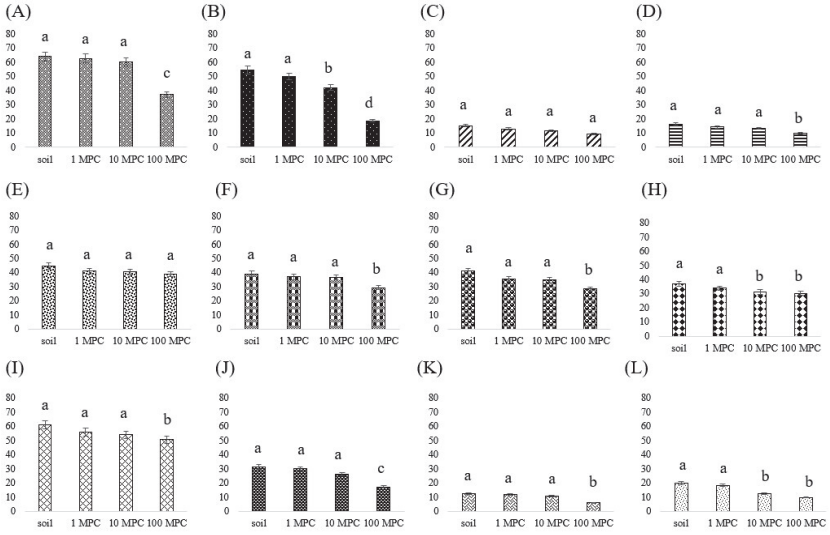

Figure 4. Change in invertase activity in soils contaminated with lead, mg glucose/1 g/24 h: (**A**) Voronic Chernozems Pachic; (**B**) Haplic Solonchaks Aridic; (**C**) Haplic Kastanozems Chromic; (**D**) Endosalic Calcisols Yermic; (**E**) Voronic Chernozems Pachic (typical); (**F**) Voronic Chernozems Pachic (ordinary); (**G**) Voronic Chernozems Pachic (leached); (**H**) Luvic Phaeozems Albic; (**I**) Greyic Phaeozems Albic; (**J**) Haplic Chernozems Pachic; (**K**) Luvic Stagnosols Dystric (illuvial ferrugenous); (**L**) Luvic Stagnosols Dystric. Note: The different lowercase letters per column indicate significant differences ($p < 0.05$) among different ages that based on one-way ANOVA: (a)—does not differ significantly from the control; (b)—significant difference from control ($p < 0.05$); (c)—significant difference from control ($p < 0.01$): (d)—significant difference from control ($p < 0.0075$).

When the doses were increased to MPCs of 10 and 100, the toxic effect of Pb was exerted on the HSA (23–66%), VCP (typ.) (10–13%), LPA (16–18%), GPA (12–18%), LSD (ill.-ferr.) (15–51%), and LSD (47–51%) soils. Starting with the minimum dose (1 MPC) and increasing to an MPC of 100, a decrease in the enzymatic activity compared to that of the control was found in the HKC (15–40%), ECY (13–39%), and VCP (leach) (14–39%) soils. The highest invertase activity in the case of Pb contamination was found in the VCP (37.3–64.1 mg glucose/1 g/24 h), HSA (18.8–54.6 mg glucose/1 g/24 h), and GPA soils (50.8–61.4 mg glucose/1 g/24 h). The lowest enzymatic activity was found in the HKC (9.3–15.3 mg glucose/1 g/24 h), ECY (10.2–16.5 mg glucose/1 g/24 h), and LSD (ill.-ferr.) (6.2–12.6 mg glucose/1 g/24 h) soils.

The activity of invertase in the soil is characterized by the quantitative accounting of reducing sugars according to Bertrand and by changes in the optical properties of a sucrose solution. The activity of this enzyme is closely related to the humus content in the soil [41,43–45]. All soils with the lowest invertase activity have a low humus content, ranging from 0.5% (HKC) to 2.41 (LSD ill.-ferr.).

Cysteine reductase activity. An indicator of the biogeochemical cycle of sulfur in soil with Pb contamination is the activity of soil cysteine reductase (Figure 5). The inhibition of enzymatic activity relative to that of the control at Pb MPCs 10 and 100 was found in the VCP (typ.) (83–98%), GPA (28–87%), and LSD (ill.-ferr.) (18–94%) soils.

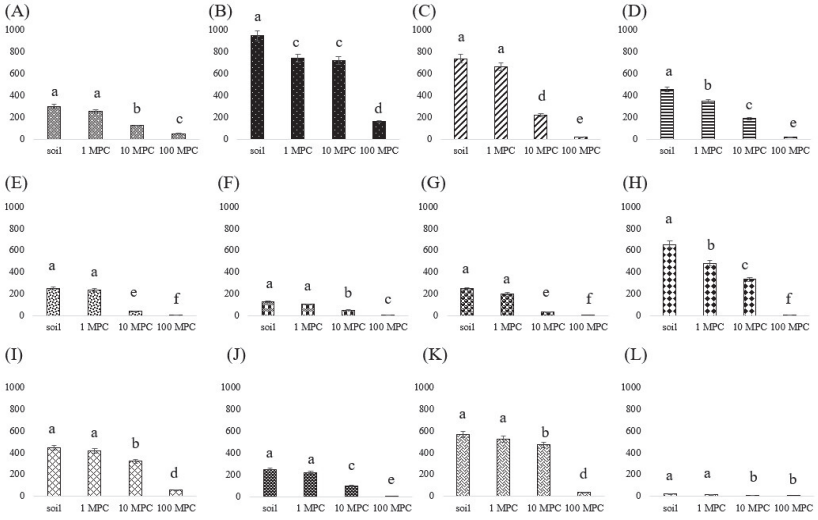

Figure 5. Change in the activity of cysteine reductase in soils contaminated with lead, mg formazan/10 g/2 h: (**A**) Voronic Chernozems Pachic; (**B**) Haplic Solonchaks Aridic; (**C**) Haplic Kastanozems Chromic; (**D**) Endosalic Calcisols Yermic; (**E**) Voronic Chernozems Pachic (typical); (**F**) Voronic Chernozems Pachic (ordinary); (**G**) Voronic Chernozems Pachic (leached); (**H**) Luvic Phaeozems Albic; (**I**) Greyic Phaeozems Albic; (**J**) Haplic Chernozems Pachic; (**K**) Luvic Stagnosols Dystric (illuvial ferrugenous); (**L**) Luvic Stagnosols Dystric. Note: The different lowercase letters per column indicate significant differences ($p < 0.05$) among different ages that based on one-way ANOVA: (a)—does not differ significantly from the control; (b)—significant difference from control ($p < 0.05$); (c)—significant difference from control ($p < 0.01$); (d)—significant difference from control ($p < 0.0075$); (e)—significant difference from control ($p < 0.005$); (f)—significant difference from control ($p < 0.0025$).

After applying Pb at a minimum dose (1 MPC) and with its increase to 100 MPC, a decrease in cysteine reductase activity was found compared to that of the control group in the VCP (16–84%), HSA (22–83%), HKC (11–98%), ECY (24–97%), VCP (ord.) (20–95%), VCP (leach) (19–98%), LPA (26–99%), HCP (12–100%), and LSD (19–99%) soils.

The highest activity of cysteine reductase, despite the Pb soil contamination, was found in the HSA (162.2–946.0 mg of formazan/10 g/2 h), HKC (17.5–738.1 mg of formazan/10 g/2 h), LPA (10.7–654.6 mg of formazan/10 g/2 h), and LSD (ill.-ferr.) soils (37.5–569.6 mg of formazan/10 g/2 h). The lowest activity of cysteine reductase was found in the VCP (ord.) (6.8–131.0 mg formazan/10 g/2 h) and LSD soils (0.4–21.2 mg formazan/10 g/2 h).

Cysteine reductase, as an enzyme that oxidizes sulfur from the sulfhydryl group of cysteine to the disulfide group of cystine, is very sensitive to Pb contamination, as it is to any heavy metal. However, the activity of this enzyme is also related to the chemical composition of each soil type. The highest activity of this enzyme corresponds to slightly acidic (HSA, HKC, and LPA) or very acidic soils (LSD ill.-ferr.). In addition, the organic

matter content in these soils is low. It is likely that the high activity of cysteine reductase is due to sulfur-containing compounds released into the soil solution. The availability of sulfur to plants allows for access to nitrogen, phosphorus, and other elements [46,47]. Sulfur is mainly contained in the soil in the form of organic compounds (70–90%) and is closely related to the availability of humus in soils [48]. In light and medium loamy soils, the humus content is reduced, sulfur is easily washed out, and the activity of cysteine reductase is high.

Phosphatase activity. The phosphorus cycle in the soil is involved in the formation of humic substances and the provision of nutrients to microorganisms, plants, and animals. In the soil, the phosphorus cycle is also influenced by the activity of phosphatase. According to Figure 6, the activity of this enzyme is more resistant to Pb contamination. The introduction of Pb at any dosage into the VCP (leach), VCP (typ.), and LSD soils did not have a significant effect on the enzymatic activity.

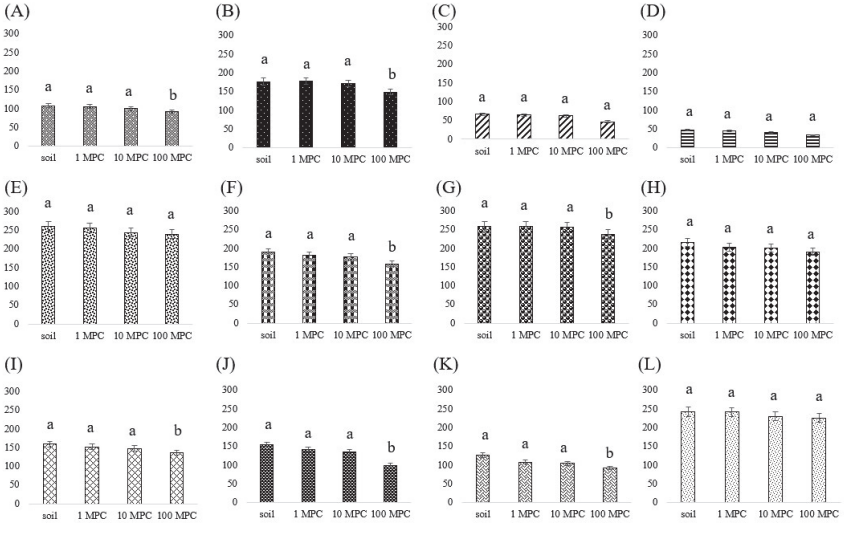

Figure 6. Change in phosphatase activity in soils contaminated with lead, μg of p-nitrophenol in 1 g of soil per 1 h: (**A**) Voronic Chernozems Pachic; (**B**) Haplic Solonchaks Aridic; (**C**) Haplic Kastanozems Chromic; (**D**) Endosalic Calcisols Yermic; (**E**) Voronic Chernozems Pachic (typical); (**F**) Voronic Chernozems Pachic (ordinary); (**G**) Voronic Chernozems Pachic (leached); (**H**) Luvic Phaeozems Albic; (**I**) Greyic Phaeozems Albic; (**J**) Haplic Chernozems Pachic; (**K**) Luvic Stagnosols Dystric (illuvial ferrugenous); (**L**) Luvic Stagnosols Dystric. Note: The different lowercase letters per column indicate significant differences ($p < 0.05$) among different ages that based on one-way ANOVA: (a)—does not differ significantly from the control; (b)—significant difference from control ($p < 0.05$).

At the maximum concentration of Pb (100 MPC), the inhibition of enzymatic activity was found in the VCP (15%), HSA (17%), HKC (30%), VCP (ord.) (17%), LPA (12%), GPA (15%), and LSD (ill.-ferr.) soils (28%).

The highest phosphatase activity, despite the Pb contamination, was found in the VCP (ord.) (240–260 μg of p-nitrophenol in 1 g of soil per 1 h) and VCP (leach) (238–259 μg of p-nitrophenol in 1 g of soil per 1 h) soils. The lowest phosphatase activity was found in the HKC (47.1–67.1 μg of p-nitrophenol in 1 g of soil per 1 h) and ECY soils (33.8–47.2 μg of p-nitrophenol in 1 g of soil per 1 h).

Soil phosphatases hydrolyze organic phosphorus compounds in the soil and release free phosphate ions for plant nutrition [36].

Urease activity. The nitrogen cycle and the phosphorus cycle in the soil are of crucial importance for the formation of humic substances in the soil. Urease is directly involved in the formation of alkaline hydrolyzable nitrogen in the soil (Figure 7).

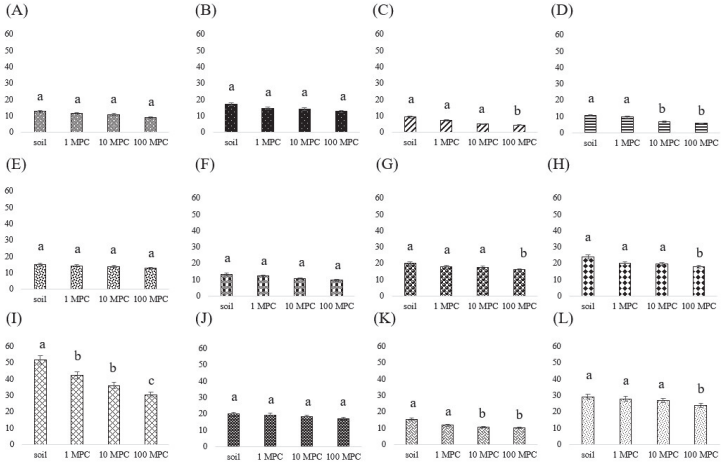

Figure 7. Change in urease activity in soils contaminated with lead, mg NH_3 per g of soil over 24 h: (**A**) Voronic Chernozems Pachic; (**B**) Haplic Solonchaks Aridic; (**C**) Haplic Kastanozems Chromic; (**D**) Endosalic Calcisols Yermic; (**E**) Voronic Chernozems Pachic (typical); (**F**) Voronic Chernozems Pachic (ordinary); (**G**) Voronic Chernozems Pachic (leached); (**H**) Luvic Phaeozems Albic; (**I**) Greyic Phaeozems Albic; (**J**) Haplic Chernozems Pachic; (**K**) Luvic Stagnosols Dystric (illuvial ferrugenous); (**L**) Luvic Stagnosols Dystric. Note: The different lowercase letters per column indicate significant differences ($p < 0.05$) among different ages that based on one-way ANOVA: (a)—does not differ significantly from the control; (b)—significant difference from control ($p < 0.05$); (c)—significant difference from control ($p < 0.01$).

Among the studied soils, the VCP (typ.), HCP, and LSD soils had the greatest resistance to Pb contamination: at the maximum dose of Pb (100 MPC), the inhibition of enzymatic activity was 15, 14, and 18% compared to the control. The urease activity in the VCP (ord.) soil decreased at MPCs of 10 and 100 by 20 and 28% compared to the control. Regardless of the Pb concentration in the soil, a decrease in the urease activity was found in the VCP (10–30%), HSA (15–28%), HKC (20–52%), ECY (10–46%), VCP (leach) (10–20%), LPA (17–25%), GPA (19–42%), and LSD (ill.-ferr.) soils (24–35%).

The highest urease activity, despite the Pb contamination, was found in the GPA (30.5–51.7 mg of NH_3 per g of soil in 24 h) and LSD (24.1–29.2 mg NH_3 per g of soil in 24 h) soils. These soils (GPA and LSD) are forest soils in broad-leaved and mixed forests. These types of soils contain a lot of organic matter, including ammonifying and nitrifying bacteria, which cause high urease activity [49,50]. The lowest urease activity was found in the HKC (4.5–9.3 mg NH_3 per g of soil in 24 h) and ECY soils (5.8–10.6 mg NH_3 per g of soil in 24 h).

Urease activity is closely related to the processes of ammonification, the nitrification of nitrogen in soil, and the content of organic matter [51]. Carbon functions are closely involved in the regulation of the mineralization and immobilization cycle of nitrogen [52,53]. In soils with a high content of organic matter (GPA and LSD soils), the maximum value of urease was established, and with a low content of organic matter (HKC and ECY soils), the lowest enzymatic activity was observed (Table 1). Earlier, Vasbieva (2019) confirmed that prolonged cultivation of soil leads to a decrease in the content of organic matter, as well as the content of total nitrogen and its non-hydrolyzable, difficult-to-hydrolyze, and easily hydrolyzable fractions, which can be replenished only after the application of organic fertilizers [54].

The change in the integral index of soil enzymatic activity (IIEA). The data obtained in determining the activity of each enzyme were used to calculate the integral index of soil enzymatic activity (IIEA) by enzyme classes (Figure 8). The maximum value of the IIEA generalized by the activity of all enzymes was found in the VCP, VCP (typ.), VCP (leach), and HCP soils, and the lowest value was found in the HKC and LSD soils.

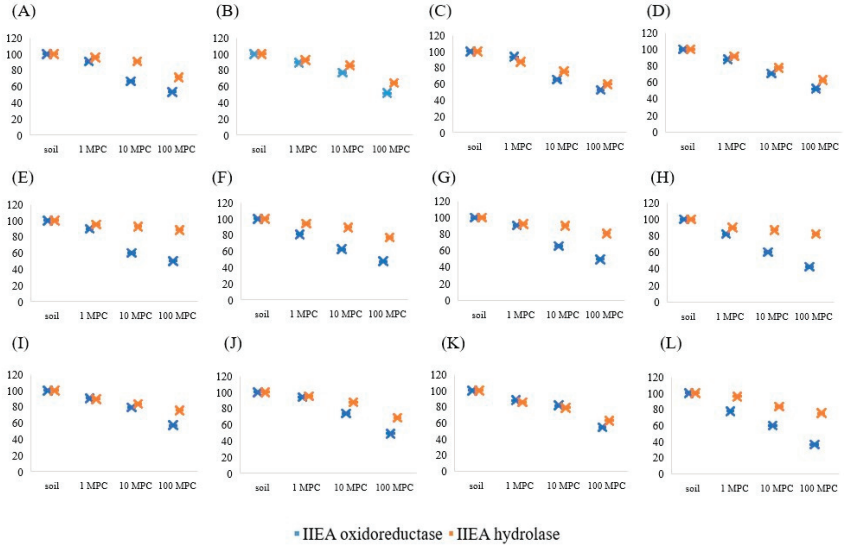

Figure 8. Change in the integral indicator of enzymatic activity of soils contaminated with lead: (**A**) Voronic Chernozems Pachic; (**B**) Haplic Solonchaks Aridic; (**C**) Haplic Kastanozems Chromic; (**D**) Endosalic Calcisols Yermic; (**E**) Voronic Chernozems Pachic (typical); (**F**) Voronic Chernozems Pachic (ordinary); (**G**) Voronic Chernozems Pachic (leached); (**H**) Luvic Phaeozems Albic; (**I**) Greyic Phaeozems Albic; (**J**) Haplic Chernozems Pachic; (**K**) Luvic Stagnosols Dystric (illuvial ferrugenous); (**L**) Luvic Stagnosols Dystric.

The integral indicator of the soil enzymatic activity of oxidoreductases was less than the IIEA of hydrolases in all soils. The greatest difference between the classes of enzymatic activity was found in the VCP (typ.) (26%), VCP (ord.) (23%), LPA (25%), and LSD soils (27%). In arid soils (HSA, ECY, HKC, and HCP) under the conditions of a lack of precipitation and a light granulometric composition, as well as in the LSD (ill.-ferr.) soil from the Moscow region (a zone of broad-leaved forests), differences between the IISEAs of oxidoreductases and hydrolases could not be established.

The geometric mean of enzymatic activity. Figure 9 shows the values of the geometric mean (GME) enzymes of the oxidoreductase and hydrolase classes of the soils contaminated with Pb. It was found that Pb soil pollution most simulated GME oxidoreductases in comparison with GME hydrolases in soils of dry steppes and semi-deserts (HSA, HKC, and ECY soils), as well as in soils of meadows (VCP), steppes (LPA, HCP, GPA), and broad-leaved forests (LSD ill.-ferr.).

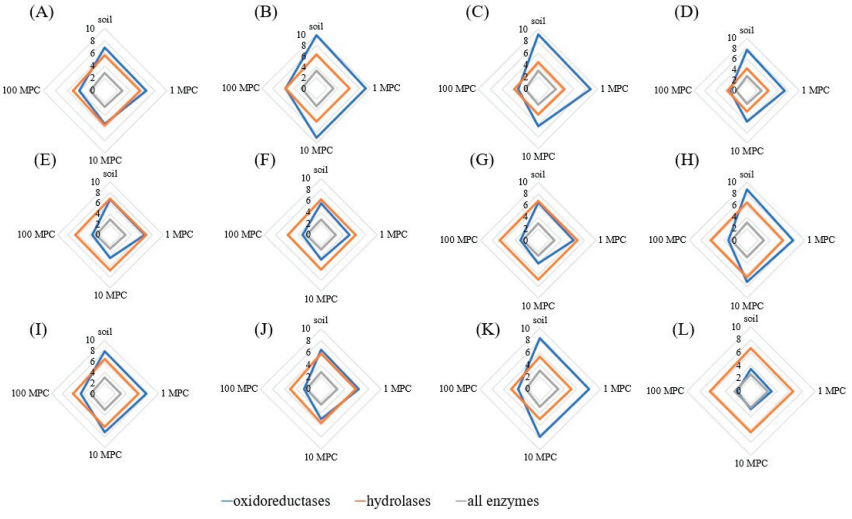

Figure 9. Change in geometric mean of enzymes (GME) of the oxidoreductase and hydrolase classes in lead-contaminated soils: (**A**) Voronic Chernozems Pachic; (**B**) Haplic Solonchaks Aridic; (**C**) Haplic Kastanozems Chromic; (**D**) Endosalic Calcisols Yermic; (**E**) Voronic Chernozems Pachic (typical); (**F**) Voronic Chernozems Pachic (ordinary); (**G**) Voronic Chernozems Pachic (leached); (**H**) Luvic Phaeozems Albic; (**I**) Greyic Phaeozems Albic; (**J**) Haplic Chernozems Pachic; (**K**) Luvic Stagnosols Dystric (illuvial ferrugenous); (**L**) Luvic Stagnosols Dystric.

The GME value calculated from the activity of all enzymes for all soils varied in the range of 2.1–3.3. At the same time, the maximum GME value calculated from the activity of all enzymes was found in the HSA (2.7–3.3) and LPA (2.5–3.1) soils. The lowest GME value was found in the ECY (2.1–2.9), VCP (ord.) (2.5–2.7), HCP (2.3–2.8), and LSD soils (2.5–2.6). The GME value calculated from the activity of all enzymes and the GME value of hydrolases were the same in the LSD soil. The predominance of the GME of oxidoreductases is mainly characteristic of soils of the arid zone with a light or medium loamy granulometric composition (except for the VCP (leach) and HCP soils). The amount of precipitation in the region also influences the enzymatic activity of each class [55]. In the soils of the central part of Russia with a large amount of precipitation in the region, a heavy granulometric composition and, as a result, a greater amount of soil moisture, the GME of hydrolases are greater than the GME of oxidoreductases for the VCP (typ.), VCP (ord.), and LSD soils.

It was found that the enzymatic activity of soils was closely related not only to the type of anthropogenic impact but also to the amount of productive moisture in the soil [24]. The index of the GME of oxidoreductases in the VCP (ord.) soil with sunflowers decreased by 16% in the summer compared to the spring, and that of the GME of hydrolases decreased by 60%. The values of the mean geometric enzymatic activity (GMea) of oxidoreductases and hydrolases of oil-contaminated chernozem were stimulated relative to a control with a minimum dose of biochar, sodium humate, nitroammophos, and Baikal EM-1 [14].

Sensitivity and informativeness of biological indicators. The sensitivity of biological indicators for each type of soil was assessed for Pb contamination in Table 3. The enzymes are ranked from “1” to “6”, where “1” is the most sensitive and “6” is the least sensitive enzyme for a given soil type.

Table 3. Ranking of enzymes by sensitivity to soil contamination with Pb.

Type of Soil	DEH	INV	URE	CAT	CYST	PHOS
VCP	2	4	3	5	1	6
HSA	2	3	4	6	1	5
HKC	3	5	2	6	1	4
ECY	4	4	2	5	1	6
VCP(typ.)	2	4	5	3	1	6
VCP(ord.)	2	5	3	4	1	6
VCP(leach)	2	3	4	5	1	6
LPA	3	5	4	3	1	6
HCP	4	2	6	5	1	3
GPA	3	4	2	5	1	6
LSD(ill.-ferr.)	6	4	3	3	1	5
LSD	3	4	5	3	1	6

Note: DEH—dehydrogenases activity (mg TPF per 10 g per 24 h), INV—invertase activity (mg glucose per 1 g per 24 h), URE—urease activity (mg NH_3 per g soil per 24 h), CAT—catalase activity (mL O_2 in 1 g of soil in 1 min), CYST—cysteine reductase activity (mg formazan per 10 g in 2 h), PHOS—phosphatase activity (μg p-nitrophenol in 1 g of soil in 1 h).

The most sensitive enzyme to Pb contamination for all types of soils, without exception, was cysteine reductase. The least sensitive enzymes were phosphatase (in eight out of the twelve soil types) and catalase (in two out of the twelve soil types).

The informativeness of each indicator for each type of soil was assessed by the close relationship between the Pb content and the change in the biological indicator. The series of informative biological indicators for each type of soil are presented below in Table 4. Enzymes are ranked from "1" to "6", where "1" is the most informative and "6" is the least informative enzyme for a given soil type.

Table 4. Ranking of enzymes according to informativeness in case of soil contamination with Pb.

Type of Soil	DEH	INV	URE	CAT	CYST	PHOS
VCP	6	1	3	4	5	2
HSA	5	3	4	2	3	1
HKC	4	2	6	5	3	1
ECY	5	2	4	1	3	1
VCP(typ.)	6	5	2	1	4	3
VCP(ord.)	6	1	4	5	3	2
VCP(leach)	3	4	5	2	6	1
LPA	4	3	4	5	1	2
HCP	6	3	4	5	1	2
GPA	1	2	3	5	4	2
LSD(ill.-ferr.)	4	2	5	5	1	3
LSD	5	3	1	5	2	4

Note: DEH—dehydrogenases activity (mg TPF per 10 g per 24 h), INV—invertase activity (mg glucose per 1 g per 24 h), URE—urease activity (mg NH_3 per g soil per 24 h), CAT—catalase activity (mL O_2 in 1 g of soil in 1 min), CYST—cysteine reductase activity (mg formazan per 10 g in 2 h), PHOS—phosphatase activity (μg p-nitrophenol in 1 g of soil in 1 h).

The most informative indicators for Pb contamination were phosphatase (in three out of the twelve soils), cysteine reductase (in three out of the twelve soils), and invertase (in two out of the twelve soils). The least informative indicators were dehydrogenases (in seven out of the twelve soils) and catalase (in three out of the twelve soils).

As can be seen from the above series, the most sensitive and informative enzyme was cysteine reductase only for four out of the twelve soils (HCP, LPA, LSD (ill.-ferr.), and LSD soils). For the other soils, other enzymes were the most informative. The sensitivity of enzymes to contamination with various heavy metals depends on the concentration and chemical form of the metal (oxide, nitrate, or sulfide) [56,57].

When the VCP (ord.) soil was contaminated with oxides and nitrates of Ag, Bi, Te, and Tl, it was found that oxidoreductases showed a greater sensitivity to Ag, Bi, Te, and Tl than hydrolases [25]. Among the oxidoreductases, the greatest sensitivity was found in ferrireductase, and the greatest informativeness was found for peroxidase. Among the enzymes of the hydrolase class, invertase was the most sensitive and informative enzyme.

Thus, the S (cysteine reductase) cycle in soils contaminated with Pb is the most vulnerable. The P (phosphatase) cycle and the redox enzyme (catalase) also have instability in Pb-contaminated soils. The C (invertase and dehydrogenase) and N (urease) cycles do not change significantly when contaminated with heavy metals.

According to the data obtained above, Table 5 was compiled, which shows the state of the enzymatic soil system (from very high to very low activity) of the following different climatic zones with Pb contamination: meadow soils, brackish soils, dry steppes, true steppes, and forest soils.

The activity of dehydrogenases had similar values (30–35 mg of TPF in 10 g in 24 h) in all climatic zones except dry steppes. The catalase activity was also the lowest in the brackish and forest soils. For arid soils, the low activity of oxidoreductases is associated with their physical and chemical properties and the amount of precipitation, while for forest soils, the most important effect on the activity of soil enzymes is exerted by a light and sandy loam granulometric composition. The lowest values of another oxidoreductase, cysteine reductase, were found in the meadow soils (280 mg of formazan per 10 g in 2 h) and dry steppes (250 mg of formazan per 10 g in 2 h), which is associated with the sulfur cycle in these soils [48,58]. The urease activity was the lowest in the meadow soils (12 mg of NH_3 per g of soil in 24 h), saline soils (15 mg of NH_3 per g of soil in 24 h), and dry steppes (10 mg of NH_3 per g of soil in 24 h). The activity of this enzyme is closely related to the carbon content in the soil, expressed in terms of the humus content. In these soils, the humus content, according to Table 1, varies from 0.3 to 3.6%. In contrast, the activity of another hydrolase, invertase, was the highest in the meadow soils (50 mg of glucose in 1 g/24 h) and the lowest in the soils of the dry steppes and semi-deserts (15 mg of glucose in 1 g/24 h). The phosphatase activity was the highest in the soils of the true steppes (250 μg of p-nitrophenol in 1 g of soil per 1 h) and the lowest in the soils of the dry steppes and semi-deserts (65 μg of p-nitrophenol in 1 g of soil per 1 h).

Earlier, scales for assessing the activity of soil enzymes were proposed by Zvyagintsev (1978), Gaponyuk, and Malakhov (1985) [59,60]. However, there is no information on which types of soils and which climatic zones these scales of activity of soil enzymes were developed for. Such scales are actively used for comparative assessments of the ecological state of soil under various types and factors of anthropogenic impacts [61–64].

Thus, for the first time, the values of the enzymatic activity of soils of different climatic zones were ranked on a scale of assessment from very strong to very poor. Subarid and arid soils, including saline brackish soils and dry steppes, are characterized by high values of enzymes of the S cycle and low values of enzymes of the C, N, P, and O cycles. In subhumid and humid soils, including those of meadows, forests, and true steppes, high values of enzymes of the C, N, P, and O cycles and low values of enzymes of the S cycle are characteristic. Such differences in enzyme values characterizing the C, N, P, O, and S cycles are associated with soil formation factors and the fertilizers applied to the soil [65–71]. In humid areas, soils accumulate organic matter, compounds of silicon, iron, manganese, and phosphorus, and in arid areas, they accumulate lime, gypsum, and water-soluble salts.

Table 5. A scale for assessing the ecological state of the fermentative system of soils in different climatic zones when contaminated with lead.

Enzyme Activity	Element/Enzyme Cycle					
	Carbone (C)		Nitrogen (N)	Oxygen (O)	Sulfur (S)	Phosphorus (P)
	DEH	INV	URE	CAT	CYST	PHOS
Meadow soils						
very strong	>30	>50	>12	>8	>280	>110
strong	19–30	35–50	8–12	5–8	180–250	80–110
weak	15–19	20–35	6–8	2–5	40–180	60–80
very weak	<15	<20	<6	<2	<40	<60
Saline and alkaline soils						
very strong	>30	>45	>15	>4	>600	>160
strong	20–30	25–45	12–15	2–4	350–600	130–160
weak	10–20	15–25	8–12	1–2	120–350	110–130
very weak	<10	<15	<8	<1	<120	<110
Dry steppes and semi-deserts						
very strong	>18	>15	>10	>8	>500	>65
strong	15–18	12–15	8–10	5–8	200–500	50–65
weak	11–15	9–12	4–8	3–5	50–200	30–50
very weak	<11	<9	<4	<3	<50	<30
Real steppes						
very strong	>35	>40	>20	>12	>250	>250
strong	25–35	25–40	18–20	10–12	120–250	150–250
weak	15–25	18–25	12–18	6–10	20–120	100–150
very weak	<15	<18	<12	<6	<20	<100
Soils of broad-leaved forests and forest-steppes						
very strong	>25	>45	>30	>5	>400	>230
strong	18–25	25–45	20–30	2–5	150–400	150–230
weak	9–18	15–25	12–20	1–2	25–150	90–150
very weak	<9	<15	<12	<1	<25	<90

Note: DEH—dehydrogenases activity (mg TPF per 10 g per 24 h), INV—invertase activity (mg glucose per 1 g per 24 h), URE—urease activity (mg NH_3 per g soil per 24 h), CAT—catalase activity (mL O_2 in 1 g of soil in 1 min), CYST—cysteine reductase activity (mg formazan per 10 g in 2 h), PHOS —phosphatase activity (μg p-nitrophenol in 1 g of soil in 1 h).

4. Discussion

The reduction and solubility of PbO_2 in different types of soils vary depending on their physicochemical properties and the biological and enzyme activity of soil [72]. Lead from fertilizers (e.g., composts and organic amendments) has a toxic effect on the morphological, physiological, and biochemical functions of plants: it changes the permeability of cell membranes, reacts with the active groups of various enzymes involved in plant metabolism, and reacts with phosphate groups of ADP or ATP, as well as replaces essential Ca ions [73,74].

Non-controlled organic amendments may be a source of Pb, whereas mineral phosphate is usually clean. Lead from atmospheric deposition has a less-pronounced toxic effect on soil biotas because its path in the soil begins from above and not from the inside, as in the case of fertilizers. Among all the studied enzymes of different biogeochemical cycles of soils in different natural zones, it was the activity of cysteine reductase that was the most sensitive to Pb contamination. Soil contamination with Pb has been found to inhibit cysteine reductase activity by 40–78%. When Pb contaminates the soil, hydrophobins containing eight cysteine residues form disulfide bridges [75]. Disulfide bonds in proteins (−S−S−) are formed between thiol groups of cysteine residues during the oxidation process. Soil contamination with Pb causes soil oxidation [76–78]. Among the 12 soils, the greatest inhibition of cysteine reductase was found for the VCP (leach) soil. Previously, the resistance of the VCP (leach) soil to Pb and oil pollution was studied in the direction of soil bioremediation [79]. At the end of the bioremediation experiment, the enzymatic activity of the oily soil decreased, and the presence of Pb slightly increased the catalase and invertase activity in the first half of the experiment. With joint contamination, the activity of catalase and urease is noticeably suppressed. When Pb acetate contaminates VCP (leach) soil, it has been established that invertase and cellulase are inhibited [80]. The least sensitive enzymes to Pb contamination are catalase (HSA, HKC, ECY, and HCP soils), phosphatase (VCP, VCP (typ.), VCP (ord.), VCP (leach), LPA, GPA, and LSD soils), and dehydrogenases (LSD ill.-ferr.). These enzymes are also indicators of the ecological state and health of the soil in the case of Cd and Hg pollution, soil erosion, different types of land use, etc. [21,81–83]. A direct relationship has been established between the concentration of copper and the degree of a decrease in enzyme activity in VCP (leach) soil in the following order of descending sensitivity: catalase > urease > invertase > protease [84]. When VCP (leach) soil is contaminated with Cd, Pb, and Cu, the activity of catalase and urease increases, and the activity of protease and invertase decreases [85]. Simulation experiments on soil contamination with Zn, Pb, Cd, Cr, and Ni show enzymatic activity to be an indicator of the level of degradation and the course of ecosystem restoration [86].

According to the change in enzymatic activity, a number of soils (from the least sensitive to the most sensitive) were compiled for their resistance to Pb pollution in the following order: VCP (typ.) > GPA = HCP > ECY = VCP > HSA > VCP (leach) > VCP (ord.) = LSD ill.-ferr. > LPA > HKC > LSD soils. It was found that the most resistant to Pb pollution were the VCP (typ.), GPA, and HCP soils, and the least stable were the LSD, HKC, and LPA soils. The least resistant soils to Pb contamination are the soils of the arid zone with a light granulometric composition and the forest soils with medium loamy and heavy loamy granulometric compositions.

In the alkaline reaction of the soil environment, the level of metal retention is significantly higher than that in acidic soils [87]. Accordingly, LSD soils (pH = 5.2–5.4) are more unstable and subject to significant contamination with Pb and other heavy metals [88,89]. According to Ivanov et al., in addition to pH, the processes of Pb fixation in sedentary compounds were more strongly influenced by an increased humus content and light granulometric composition of cultivated LSD soils [90]. One of the most recent sources of Pb in soils worldwide is shooting ranges [91]. It was found that the coexistence of Pb and Ca in combination with different ratios with P suggested mechanisms for the exchange of Pb^{2+} for Ca^{2+}, which led to the stabilization of Pb in orthophosphates. There is a decrease in the mobility and leachability of Pb in the studied soil, which means that the toxicity is reduced. With an increase in the levels of contamination of VCP (leach), GPA, and HKC soils with Cd, Zn, and Pb, a gradual decrease in the intensity of soil respiration was noted, especially when the soils were contaminated with Cd compounds and in the case of polyelement contamination [92]. It was found that due to inoculation by bacteria of the *Pseudomonas* genus, the content and ratio of forms of heavy metal compounds in the soils of the experiment changed: the content of mobile and organic-related Cd compounds increased, and the content of Cu, Ni, Pb, and Zn associated with organic matter and iron compounds increased [93].

5. Conclusions

Soil pollution with Pb in different climatic zones has a significant impact on the enzymatic system of soils. It was found that the most resistant to Pb pollution were the VCP (typ.), GPA, and HCP soils, and the least stable were the LSD, HKC, and LPA soils. Cysteine reductase is considered the most sensitive enzyme to Pb contamination. Cysteine reductase is the most informative and sensitive enzyme for the HCP, LSD (ill.-ferr.), and LSD soils. For the other soils, the most informative enzymes were phosphatase and catalase. In arid soils, such as the HSA, ECY, HKC, and HCP soils, when there is a lack of precipitation or the soils have a light granulometric composition, as well as in LSD (ill.-ferr.) (zone of broad-leaved forests) soils, differences between the IISEAs of oxidoreductases and hydrolases have not been established. In soils with a large amount of precipitation in the region, a heavy granulometric composition, and, as a result, a greater amount of soil moisture, GME hydrolases are greater than GME oxidoreductases, such as in VCP (typ.), VCP (ord.), and LSD soils. The S (cysteine reductase) cycle in soils contaminated with Pb is the most vulnerable. The P (phosphatase) cycle and the redox enzyme (catalase) also have instability in Pb-contaminated soils. The C (invertase, dehydrogenase) and N (urease) cycles do not change significantly when contaminated with Pb. The results of this study can be used to assess the ecological state and health of soils with Pb pollution.

Author Contributions: Conceptualization, T.M., S.K. and A.K.; methodology, S.K.; software, T.M.; formal analysis, A.K.; investigation, A.K., T.M. and S.K.; resources, T.M.; data curation, T.M.; writing—original draft preparation, D.T., E.K., T.M. and A.T.; writing—review and editing, A.K., E.K., A.T. and T.M.; visualization, T.M.; supervision, T.M.; project administration, S.K. and T.M.; funding acquisition, T.M. and S.K. All authors have read and agreed to the published version of the manuscript.

Funding: This research was funded by financial support from the project of the Strategic Academic Leadership Program of the Southern Federal University ("Priority 2030") (No. SP-12-23-01), the Ministry of Science and Higher Education of the Russian Federation, the Soil Health Laboratory of the Southern Federal University (agreement No. 075- 15-2022-1122), of the Ministry of Science and Higher Education of Russia on the Young Scientist Laboratory within the framework of the Interregional Scientific and Educational Center of the South of Russia (FENW-2024-0001).

Institutional Review Board Statement: Not applicable.

Informed Consent Statement: Not applicable.

Data Availability Statement: Data are contained within the article.

Conflicts of Interest: The authors declare no conflicts of interest.

References

1. Ladonin, D.V. Lead Isotopic Composition in Soils of the Impact Zone of the Cherepovets Steel Mill. *Moscow Univ. Soil Sci. Bull.* **2022**, *77*, 253–257. [CrossRef]
2. Titov, A.F.; Kaznina, N.M.; Karapetyan, T.A.; Dorshakova, N.V. Effect of lead on living organisms. *J. Gen. Biol.* **2020**, *81*, 147–160. [CrossRef]
3. Zubarev, V.A.; Mishchuk, S.N. Changes in the concentrations of heavy metals in soils in the south of the Middle Amur Lowland during long-term agricultural use. *News Tomsk. Polytech. Univ. Georesources Eng.* **2019**, *330*, 18–26.
4. Voloshin, E.I.; Polosina, V.A.; Burina, M.V. The influence of chemicalization agents on the content of heavy metals, fluorine in soils and the quality of plant products in JSC Iskra and the agricultural firm Uchumskaya in the Uzhur region of Central Siberia. *Bull. Krasn. State Agrar. Univ.* **2020**, *8*, 18–26.
5. Pobilat, A.E.; Kirichuk, A.A.; Baranova, O.V. Monitoring the content of heavy metals in agricultural crops in the South of Central Siberia. *Probl. Reg. Ecol.* **2023**, *6*, 56–62. [CrossRef]
6. He, Z.L.; Yang, X.E.; Stoffella, P.J. Trace elements in agroecosystems and impacts on the environment. *J. Trace Elem. Med. Biol.* **2005**, *19*, 125–140. [CrossRef]
7. Gómez, V.; Molina-Roco, M.; Chichipe, E.; Morales Rojas, E. Trace Elements in Fertilizers Used in Peru. *OnLine J. Biol. Sci.* **2023**, *23*, 225. [CrossRef]
8. Ivanova, Y.S.; Gorbachev, V.N. Soil contamination with heavy metals under the influence of unauthorized landfills (medical and environmental aspect). *Ulyanovsk. J. Med. Biol.* **2012**, *1*, 119–124.

9. Makarov, O.A.; Strokov, A.S.; Tsvetnov, E.V.; Abdulkhanova, D.R.; Krasilnikova, V.S.; Shcherbakova, L.S. Assessment of damage from soil degradation and lands of the constituent entities of the Russian Federation. *Agriculture* **2020**, *6*, 3–6. [CrossRef]
10. Kushwaha, A.; Hans, N.; Kumar, S.; Rani, R. A critical review on speciation, mobilization andtoxicity of lead in soil-microbe-plant system and bioremediation strategies. *Ecotoxicol. Environ. Saf.* **2018**, *147*, 1035–1045. [CrossRef]
11. Ouabo, R.E.; Ogundiran, M.B.; Sangodoyin, A.Y.; Babalola, B.A. Ecological risk and human health implications of heavy metals contamination of surface soil in Ewaste recycling sites in Douala, Cameroun. *J. Health Pollut.* **2019**, *9*, 190310. [CrossRef] [PubMed]
12. Baenguev, B.A.; Belogolova, G.A.; Chuparina, E.V.; Prosekin, S.N.; Dolgikh, P.G.; Pastukhov, M.V. Distribution of lead content and forms of its compounds in technogenic soil of Svirsk (Southern Baikal region). *News Tomsk. Polytech. Univ. Georesource Eng.* **2022**, *333*, 205–214. [CrossRef]
13. Minnikova, T.; Kolesnikov, S.; Evstegneeva, N.; Timoshenko, A.; Tsepina, N. Estimation of the Enzymatic Activity of Haplic Chernozem under Contamination with Oxides and Nitrates of Ag, Bi, Te and Tl. *Agronomy* **2022**, *12*, 2183. [CrossRef]
14. Minnikova, T.V.; Ruseva, A.S.; Kolesnikov, S.I. Assessment of enzymatic activity of oil-contaminated chernozem after bioremediation. *News Timiryazev Agric. Acad.* **2022**, *5*, 5–20. [CrossRef]
15. Goswami, O.; Rouff, A.A. Soil Lead Concentration and Speciation in Community Farms of Newark, New Jersey, USA. *Soil Syst.* **2021**, *5*, 2. [CrossRef]
16. Obrycki, J.F.; Perez-Guzman, L. The Utility and Futility of Soil Health Assessment. In *Soil Health Series*; American Society of Agronomy: Madison, WI, USA, 2021. [CrossRef]
17. Minnikova, T.; Kolesnikov, S.; Revina, S.; Ruseva, A.; Gaivoronsky, V. Enzymatic Assessment of the State of Oil-Contaminated Soils in the South of Russia after Bioremediation. *Toxics* **2023**, *11*, 355. [CrossRef] [PubMed]
18. Utobo, E.B.; Tewari, L. Soil enzymes as bioindicators of soil ecosystem status. *Appl. Ecol. Environ. Res.* **2014**, *13*, 147–169. [CrossRef]
19. Acosta-Martínez, V.; Perez-Guzman, L.; Johnson, J.M.F. Simultaneous determination of β-glucosidase, β-glucosaminidase, acid phosphomonoesterase, and arylsulfatase activities in a soil sample for a biogeochemical cycling index. *Appl. Soil Ecol.* **2019**, *142*, 72–80. [CrossRef]
20. Acosta-Martinez, V.; Cotton, J.; Slaughter, L.C.; Ghimire, R.; Roper, W. Soil Health Assessment to Evaluate Conservation Practices in SemiArid Cotton Systems at Producer Site Scale. *Soil Syst.* **2023**, *7*, 72. [CrossRef]
21. Revina, S.; Minnikova, T.; Ruseva, A.; Kolesnikov, S.; Kutasova, A. Catalase activity as a diagnostic indicator of the health of oil-contaminated soils after remediation. *Environ. Monit. Assess.* **2024**, *196*, 449. [CrossRef]
22. Reinersmann, T.; Herre, M.; Marschner, B.; Heinze, S. Soil Enzyme Activity Response to Substrate and Nutrient Additions on Undisturbed Forest Subsoil Samples. *Soil Syst.* **2023**, *7*, 57. [CrossRef]
23. Polyak, Y.M.; Sukharevich, V.I. Soil enzymes and soil pollution: Biodegradation, bioremediation, bioindication. *Agrochemistry* **2020**, *3*, 83–93. [CrossRef]
24. Mokrikov, G.; Minnikova, T.; Kazeev, K.; Kolesnikov, S. Use of soil enzyme activity in assessing the effect of No-Till in the South of Russia. *Agron. Res.* **2021**, *19*, 171–184. [CrossRef]
25. Minnikova, T.V.; Kolesnikov, S.I.; Evstegneeva, N.A.; Timoshenko, A.N.; Tsepina, N.I.; Kazeev, K.S. Assessment of enzymatic activity of haplic chernozem soils contaminated with Ag, Bi, Te, and Tl. *Eurasian Soil Sci.* **2024**, *57*, 395–408. [CrossRef]
26. Papa, S.; Alvarez-Romero, M. Biological Activities in Artificially Heavy-Metal-Contaminated Growing Substrates. *Soil Syst.* **2023**, *7*, 111. [CrossRef]
27. Sevak, P.I.; Pushkar, B.K.; Kapadne, P.N. Lead pollution and bacterial bioremediation: A review. *Environ. Chem. Lett.* **2021**, *19*, 4463–4488. [CrossRef]
28. Chen, F.; Zhang, S.; Chen, Z.; Zhang, Y.; Cao, B. Phytoremediation of Toxic Lead from Contaminated Soil Using Neyraudia reynaudiana: Soil of Xuzhou as a Case Study. *Agronomy* **2024**, *14*, 118. [CrossRef]
29. Marzadori, C.; Ciavatta, C.; Montecchio, D.; Gessa, C. Effects of lead pollution on different soil enzyme activities. *Biol. Fertil. Soils* **1996**, *22*, 53–58. [CrossRef]
30. Zeng, L.S.; Liao, M.; Chen, C.L.; Huang, C.Y. Effects of lead contamination on soil enzymatic activities, microbial biomass, and rice physiological indices in soil-lead-rice (*Oryza sativa* L.) system. *Ecotoxicol. Environ. Saf.* **2007**, *67*, 67–74. [CrossRef]
31. Zhou, F.; Wang, J.; Yang, N.; Zhang, Q.; Zou, P. Effects of Lead and Water Stress on Soil Enzyme Activities from Two Plant Species. *Nat. Environ. Pollut. Technol.* **2014**, *13*, 31–36.
32. Effron, D.; de la Horra, A.M.; Defrieri, R.L.; Fontanive, V.; Palma, R.M. Effect of Cadmium, Copper, and Lead on Different Enzyme Activities in a Native Forest Soil. *Commun. Soil Sci. Plant Anal.* **2004**, *35*, 1309–1321. [CrossRef]
33. Novoselova, E.I.; Volkova, O.O.; Turyanova, R.R. Enzymatic transformation of organic residues in soils contaminated with heavy metals. *Ecol. Urban Areas* **2019**, *1*, 75–81. [CrossRef]
34. Prokopchuk, V.F.; Chernositova, T.N.; Naumenko, A.V.; Khairulina, T.P. Methods for studying the composition, properties and regimes of soils: Workshop. In *Blagoveshchensk: Far Eastern State Publishing House*; Agrarian University: Yerevan, Armenia, 2018; 31p.
35. Semendyaeva, N.V.; Marmulev, A.N.; Dobrotvorskaya, N.I. Methods for studying soils and soil cover: Textbook. In *Novosibirsk State Agrarian University, SibNIIZIKh—Novosibirsk*; Publishing House of NGAU: Novosibirsk, Novosibirsk Region, Russia, 2011; p. 202.
36. Khaziev, F.K. *Methods of Soil Enzymology*; Nauka, M., Ed.; Wiley: Moscow, Russia, 2005; 252p.
37. Kolesnikov, S.I.; Kazeev, K.S.; Akimenko, Y.V. Development of regional standards for pollutants in the soil using biological parameters. *Environ. Monit. Assess.* **2019**, *191*, 544–550. [CrossRef]

38. Garcia-Ruiz, R.; Ochoa, V.; Hinojosa, M.B.; Carreira, J.A. Suitability of enzyme activities for the monitoring of soil quality improvement in organic agricultural systems. *Soil Biol. Biochem.* **2008**, *40*, 2137–2145. [CrossRef]
39. Gao, Y.; Wang, J.; Xu, J.; Kong, X.; Zhao, L.; Zeng, D.H. Assessing the quality of oil contaminated saline soil using two composite indices. *Ecol. Indic.* **2013**, *24*, 105–112. [CrossRef]
40. Galstyan, A.S. *Enzymatic Activity of Soils in Armenia*; Hayastan: Yerevan, Armenia, 1974; 275p.
41. Khaziev, F.K. Functional role of enzymes in soil processes. *Bull. Acad. Sci. Repub. Bashkortostan* **2015**, *20*, 14–24.
42. Wyszkowska, J.; Wyszkowski, M. Activity of soil dehydrogenases, urease, and acid and alkaline phosphatases in soil polluted with petroleum. *J. Toxicol. Environ. Health* **2010**, *73*, 1202–1210. [CrossRef]
43. Belousova, E.N.; Belousov, A.A. The influence of soil protection technologies on the content of mobile organic matter and the enzymatic activity of the soil. *Agrochemistry* **2022**, *5*, 30–37. [CrossRef]
44. Lapa, V.V.; Mikhailovskaya, N.A.; Barashenko, T.B.; Pogirnitskaya, T.V.; Dyusova, S.V. Biochemical and microbiological indicators for assessing the influence of anthropogenic load on soil fertility. *Soil Sci. Agrochem.* **2014**, *2*, 28–42.
45. Marcinkeviciene, A.; Boguzas, V.; Balnyte, S.; Pupaliene, R.; Velicka, R. Influence of crop rotation, intermediate crops, and organic fertilizers on the soil enzymatic activity and humus content in organic farming systems. *Eurasian Soil Sci.* **2013**, *46*, 198–203. [CrossRef]
46. Merkusheva, M.G.; Ubugunov, L.L.; Boloneva, L.N.; Lavrentieva, I.N. Sulfur in rain-fed and irrigated chestnut soils and assessment of the use of increasing doses of sulfur fertilizers (against the background of NPK) for potatoes. *Agrochemistry* **2023**, *3*, 20–28. [CrossRef]
47. Chevychelov, A.V.; Levshakov, L.V.; Lazarev, V.I. The influence of fertilizers containing sulfur on the yield and grain quality of spring wheat in the conditions of the Kursk region. *Int. J. Agric.* **2019**, *4*, 54–57. [CrossRef]
48. Aristarkhov, A.N. Sulfur in Russian agroecosystems: Monitoring the content in soils and the effectiveness of its use. *Int. Agric. J.* **2016**, *5*, 39–47.
49. Błońska, E.; Lasota, J.; Gruba, P. Effect of temperate forest tree species on soil dehydrogenase and urease activities in relation to other properties of soil derived from loess and glaciofluvial sand. *Ecol. Res.* **2016**, *31*, 655–664. [CrossRef]
50. Pajares, S.; Bohannan, B.J.M. Ecology of Nitrogen Fixing, Nitrifying, and Denitrifying Microorganisms in Tropical Forest Soils. *Front. Microbiol.* **2016**, *7*, 1045–1052. [CrossRef] [PubMed]
51. Naimi, O.I. Patterns of profile distribution of urease in ordinary chernozem in agrocenosis. *Int. J. Humanit. Nat. Sci.* **2019**, *8*, 12–14. [CrossRef]
52. Nieder, R.; Benbi, D.K. *Carbon and Nitrogen in the Terrestrial Environment*; Springer: Dordrecht, The Netherlands, 2008; 430p.
53. Semenov, V.M. Functions of carbon in the mineralization-immobilization turnover of nitrogen in soil. *Agrochemistry* **2020**, *6*, 78–96. [CrossRef]
54. Vasbieva, M.T. Effect of long-term application of organic and mineral fertilizers on the organic carbon content and nitrogen regime of soddy-podzolic soil. *Eurasian Soil Sci.* **2019**, *52*, 1422–1428. [CrossRef]
55. Mokrikov, G.V.; Minnikova, T.V.; Kazeev, K.S.; Kolesnikov, S.I. The influence of productive moisture reserves and the amount of precipitation on yields under the condition of direct sowing of agricultural crops in the Rostov region. *Samara Sci. Bull.* **2019**, *8*, 69–75. [CrossRef]
56. Karaca, A.; Cetin, S.C.; Turgay, O.C.; Kizilkaya, R. Effects of Heavy Metals on Soil Enzyme Activities. In *Soil Heavy Metals. Soil Biology*; Springer: Berlin/Heidelberg, Germany, 2010; Volume 19. [CrossRef]
57. Hong, Y.K.; Kim, J.W.; Lee, S.P.; Yang, J.E.; Kim, S.C. Heavy metal remediation in soil with chemical amendments and its impact on activity of antioxidant enzymes in Lettuce (*Lactuca sativa*) and soil enzymes. *Appl. Biol. Chem.* **2020**, *63*, 42. [CrossRef]
58. Cherkasov, E.A.; Lobachev, D.A.; Zakharova, D.A. Content of mobile sulfur in soils of agricultural lands in the Ulyanovsk region. *Bull. Ulyanovsk. State Agric. Acad.* **2018**, *1*, 54–59. [CrossRef]
59. Zvyagintsev, D.G. Biological activity of soils and scales for assessing some of its indicators. *Eurasian Soil Sci.* **1978**, *6*, 48–54.
60. Gaponyuk, E.I.; Malakhov, S.V. Complex system of indicators of soils environmental monitoring. In Proceedings of the 4th All-Union Conference Gidrometeoizdat, Moscow, Russia, 14–16 May 1985; pp. 3–10.
61. Tovstik, E.V.; Olkova, A.S. Assessment of the influence of factors of abiotic nature on the enzymatic activity of soil. *Ecobiotech* **2021**, *4*, 128–134. [CrossRef]
62. Piletskaya, O.A.; Yachnaya, D.A. The influence of storage times and methods on changes in the activity of enzymes in the chernozem-like soil of the Zeya-Bureya Plain. *Bull. Soil Inst.* **2022**, *112*, 48–72. [CrossRef]
63. Tsandekova, O.L.; Ufimtsev, V.I. Activity of soil hydrolytic enzymes in the phytogenic field of *Acer negundo* L. in conditions of disturbed floodplain communities. *News Samara Sci. Cent. Russ. Acad. Sci.* **2018**, *20*, 92–96. [CrossRef]
64. Tsandekova, O.L.; Ufimtsev, V.I. Enzymatic activity of soil under ash-leaved maple plantations in floodplain forest biogeocenoses. *Lesovedenie* **2021**, *4*, 437–445. [CrossRef]
65. Litvinovich, A. Degradation of well-cultivated soils in humid and arid regions. In *Lap Lambert*; Academic Publishing: Cambridge, MA, USA, 2011; 279p, ISBN 978-3-8454-2837-6.
66. Semenkov, I.N.; Sharapova, A.V.; Lednev, S.A.; Koroleva, T.V. Fractional composition of metal and sulfur compounds in the upper layer of soil in zones affected by a coal mine waste heap (Central Russian forest-steppe). *Arid. Ecosyst.* **2023**, *29*, 118–127.
67. Kulikova, A.K.; Dozorov, A.V.; Cherkasov, E.A.; Zakharova, D.A.; Smyvalov, V.S. Sulfur content in soils of the Ulyanovsk region, the yield of spring wheat and the balance of nutrients in leached chernozem when using sulfur-containing fertilizers. *Int. J. Agric.* **2019**, *3*, 50–54. [CrossRef]

68. Prudnikova, E.Y.; Savin, I.Y.; Lebedeva, M.P.; Volkov, D.S.; Rogova, O.B.; Varlamov, E.B.; Abrosimov, K.N. Transformation of the surface layer in the arable soil horizon under the impact of atmospheric precipitation. *Eurasian Soil Sci.* **2021**, *54*, 1770–1781. [CrossRef]
69. Sorokin, A.S.; Kust, G.S.; Abrosimov, K.N.; Lebedeva, M.P. Composition and structure of aggregates from compacted soil horizons in the southern steppe zone of European Russia. *Eurasian Soil Sci.* **2016**, *49*, 326–337. [CrossRef]
70. Mikkelsen, R.; Norton, R. Sulfur in soils and sulfur-containing fertilizers. *Int. Inst. Plant Nutr.* **2014**, *3*, 6–9.
71. Yudin, S.A.; Plotnikova, O.O.; Belobrov, V.P.; Lebedeva, M.P.; Abrosimov, K.N.; Ermolaev, N.R. Quantitative charactristics of the microstructure of typical chernozems using different agricultural technologies. Eurasian Soil Science. *Eurasian Soil Sci.* **2023**, *6*, 774–786. [CrossRef]
72. Lin, Y.-P.; Valentine, R.L. Reduction of Lead Oxide (PbO_2) and Release of Pb(II) in Mixtures of Natural Organic Matter, Free Chlorine and Monochloramine. *Environ. Sci. Technol.* **2009**, *43*, 3872–3877. [CrossRef] [PubMed]
73. Pourrut, B.; Shahid, M.; Dumat, C.; Winterton, P.; Pinelli, E. Lead uptake, toxicity, and detoxification in plants. *Rev. Environ. Contam. Toxicol.* **2011**, *213*, 113–136. [CrossRef] [PubMed]
74. Hassan, S.H.; Chafik, Y.; Lebrun, M.; Sferra, G.; Bourgerie, S.; Scippa, G.; Morabito, D.; Trupiano, D. Lead Toxicity and Tolerance in Plants: Insights from Omics Studies. In *Heavy Metal Toxicity and Tolerance in Plants: A Biological, Omics, and Genetic Engineering Approach*; Wiley: Hoboken, NJ, USA, 2023. [CrossRef]
75. Popov, A.I.; Konoplina, L.Y.; Komolkina, N.A.; Prilepa, S.V.; Sazanova, E.V.; Kholostov, G.D. Component composition of soil organic matter. *Sci. Herit.* **2021**, *65*, 11–19. [CrossRef]
76. Wuana, R.A.; Okieimen, F.E. Heavy Metals in Contaminated Soils: A Review of Sources, Chemistry, Risks and Best Available Strategies for Remediation. *Int. Sch. Res. Not.* **2011**, 402647. [CrossRef]
77. Darma, A.; Ibrahim, S.; Sani, A.; Zandi, P.; Yang, J. Appraisal of lead (Pb) contamination and potential exposure risk associated with agricultural soils and some cultivated plants in gold mines. *Environ. Syst. Res.* **2022**, *11*, 14. [CrossRef]
78. Mosina, L.V.; Dovletyarova, E.A.; Efremova, S.Y.; Norvosuren, Z. Ecological danger of soil pollution with heavy metals (using the example of lead). *News Penza State Pedagog. Univ.* **2012**, *29*, 383–386.
79. Rafikova, G.F.; Kuzina, E.V.; Korshunova, T.Y. The influence of bioremediation on the biological activity of leached chernozem contaminated with oil and lead. *Eurasian Soil Sci.* **2022**, *3*, 354–369. [CrossRef]
80. Ananyeva, Y.S.; Shpis, T.E. The influence of lead contamination on the biological properties of leached chernozem. *Bull. Altai State Agrar. Univ.* **2010**, *72*, 29–32.
81. Yeboah, J.O.; Shi, G.; Shi, W. Effect of Heavy Metal Contamination on Soil Enzymes Activities. *J. Geosci. Environ. Prot.* **2021**, *9*, 135–154. [CrossRef]
82. Zheng, L.; Li, Y.; Shang, W.; Dong, X.; Tang, Q.; Cheng, H. The inhibitory effect of cadmium and/or mercury on soil enzyme activity, basal respiration, and microbial community structure in coal mine-affected agricultural soil. *Ann. Microbiol.* **2019**, *69*, 849–859. [CrossRef]
83. Donkova, R.; Deribeeva, D.; Nedyalkova, K. Enzyme activity of Chromic Luvisols under different degree of erosion and land use. *Eurasian J. Soil Sci.* **2017**, *6*, 37–43. [CrossRef]
84. Korotchenko, I.S.; Kirienko, N.N. Enzymatic activity of leached chernozem contaminated with copper. *Bull. Krasn. State Agrar. Univ.* **2014**, *3*, 103–109.
85. Korotchenko, I.S. Phytotoxicity and Enzymatic activity of leached chernozem due to contamination with heavy metals. *Bull. Krasn. State Agrar. Univ.* **2011**, *5*, 109–115.
86. Ciarkowska, K. Enzyme Activities in Soils Contaminated with Heavy Metals in Varying Degrees. In *Heavy Metal Contamination of Soils. Soil Biology*; Sherameti, I., Varma, A., Eds.; Springer: Cham, Switzerland, 2015; Volume 44. [CrossRef]
87. Golia, E.E.; Kantzou, O.D.; Chartodiplomenou, M.A.; Papadimou, S.G.; Tsiropoulos, N.G. Study of Potentially Toxic Metal Adsorption in a Polluted Acid and Alkaline Soil: Influence of Soil Properties and Levels of Metal Concentration. *Soil Syst.* **2023**, *7*, 16. [CrossRef]
88. Vitkovskaya, S.E.; Yakovlev, O.N.; Shavrina, K.F. The influence of increasing doses of dolomite flour on the acid-base properties of sod-podzolic soil. *Agrochemistry* **2016**, *7*, 3–11.
89. Vitkovskaya, S.E.; Shavrina, K.F. Dynamics of acidity of sod-podzolic soil depending on the dose of lime ameliorant. *Agrophysics* **2021**, *1*, 1–6. [CrossRef]
90. Ivanov, A.I.; Sukhanov, P.A.; Ivanova, Z.A.; Yakovleva, T.I. Agroecological significance of the cultivation of sandy soddy-podzolic soils with Pb and Cd contamination. *Agrochemistry* **2019**, *4*, 70–78. [CrossRef]
91. Porfido, C.; Gattullo, C.E.; Allegretta, I.; Fiorentino, N.; Terzano, R.; Fagnano, M.; Spagnuolo, M. Investigating Lead Bioavailability in a Former Shooting Range by Soil Microanalyses and Earthworms Tests. *Soil Syst.* **2022**, *6*, 25. [CrossRef]
92. Plekhanova, I.O.; Zolotareva, O.A. Assessment and regulation of the ecological state of soils contaminated with heavy metals. *Agrochemistry* **2021**, *7*, 83–94.
93. Plekhanova, I.O.; Kulikov, V.O.; Shabaev, V.P. Influence of rhizosphere bacteria on the fractional composition of heavy metal compounds in the soil-plant system. *Eurasian Soil Sci.* **2022**, *9*, 1179–1186.

Disclaimer/Publisher's Note: The statements, opinions and data contained in all publications are solely those of the individual author(s) and contributor(s) and not of MDPI and/or the editor(s). MDPI and/or the editor(s) disclaim responsibility for any injury to people or property resulting from any ideas, methods, instructions or products referred to in the content.

soil systems

MDPI

Review

Soil Contamination by Heavy Metals and Radionuclides and Related Bioremediation Techniques: A Review

Yelizaveta Chernysh [1,2,*], Viktoriia Chubur [1,2], Iryna Ablieieva [1,3], Polina Skvortsova [1], Olena Yakhnenko [1], Maksym Skydanenko [1], Leonid Plyatsuk [1] and Hynek Roubík [2,*]

[1] Departament of Ecology and Environmental Protection Technologies, Sumy State University, Kharkivska st. 116, 40007 Sumy, Ukraine; chuburv@ftz.czu.cz (V.C.); i.ableyeva@ecolog.sumdu.edu.ua (I.A.); p.skvortsova@aspd.sumdu.edu.ua (P.S.); o.jakhnenko@ecolog.sumdu.edu.ua (O.Y.); m.skydanenko@pohnp.sumdu.edu.ua (M.S.); l.plyacuk@ecolog.sumdu.edu.ua (L.P.)
[2] Department of Sustainable Technologies, Faculty of Tropical AgriSciences, Czech University of Life Sciences Prague, Kamýcká 129, 16500 Prague, Czech Republic
[3] Department of Thematic Studies, Faculty of Arts and Sciences, Linköping University, SE-581 83 Linköping, Sweden
* Correspondence: e.chernish@ssu.edu.ua (Y.C.); roubik@ftz.czu.cz (H.R.)

Abstract: The migration of heavy metals and radionuclides is interrelated, and this study focusses on the interaction and complex influence of various toxicants. The rehabilitation of radioactively contaminated territories has a complex character and is based on scientifically supported measures to restore industrial, economic, and sociopsychological relations. We aim for the achievement of pre-emergency levels of hygienic norms of radioactive contamination of output products. This, in its sum, allows for further economic activity in these territories without restrictions on the basis of natural actions of autoremediation. Biosorption technologies based on bacterial biomass remain a promising direction for the remediation of soils contaminated with radionuclides and heavy metals that help immobilise and consolidate contaminants. A comprehensive understanding of the biosorption capacity of various preparations allows for the selection of more effective techniques for the elimination of contaminants, as well as the overcoming of differences between laboratory results and industrial use. Observation and monitoring make it possible to evaluate the migration process of heavy metals and radionuclides and identify regions with a disturbed balance of harmful substances. The promising direction of the soil application of phosphogypsum, a by-product of the chemical industry, in bioremediation processes is considered.

Keywords: toxicants; remediation; biosorption technologies; phosphogypsum

Citation: Chernysh, Y.; Chubur, V.; Ablieieva, I.; Skvortsova, P.; Yakhnenko, O.; Skydanenko, M.; Plyatsuk, L.; Roubík, H. Soil Contamination by Heavy Metals and Radionuclides and Related Bioremediation Techniques: A Review. *Soil Syst.* **2024**, *8*, 36. https://doi.org/10.3390/soilsystems8020036

Academic Editor: Manfred Sager

Received: 15 February 2024
Revised: 15 March 2024
Accepted: 18 March 2024
Published: 22 March 2024

Copyright: © 2024 by the authors. Licensee MDPI, Basel, Switzerland. This article is an open access article distributed under the terms and conditions of the Creative Commons Attribution (CC BY) license (https://creativecommons.org/licenses/by/4.0/).

1. Introduction

The pollution of soils by toxicants of different natures and origins is a current issue, as it disrupts the homeostasis of ecosystems. The soil is the starting point of the food chain, where all nutrients accumulate. Therefore, one of the most dangerous types of pollution associated with radioactive contamination and heavy metal contamination requires significant efforts in soil remediation [1,2].

An analysis of radioactive contamination of the territory of Europe with cesium-137 shows that about 35% of radionuclide fallout after the Chernobyl radiation accident on the European continent is located in the territory of Belarus. The contamination of Belarusian territory with cesium-137 with a density greater than 37 kBq/m^2 amounted to 23% of the entire country's area; for Ukraine, ~5%. In Ukraine, more than 3.5 million hectares of forest land is radioactively contaminated by accidental emissions from the Chornobyl nuclear power plant. A complex set of factors determines the current radiation situation in radioactively contaminated forests, in particular, the density of radioactive soil contamination, the

composition of radionuclides, the physical and agrochemical properties of soils, etc., which determine the intensity of the biological circulation of radionuclides in ecosystems [3].

In research by Morooka et al. [4], areas affected by nuclear power plant (NPP) disasters are presented. Thus, 31 radioactive particles from surface soils were detected in an area 3.9 km northwest of the Fukushima-1 NPP. $^{134+137}$Cs had the highest activity ever recorded for Fukushima-1 NPP (6.1×10^5 and 2.5×10^6 Bq per particle after decay correction until March 2011). Taking into account their large size (120 μm), the impact of these particles on human health will be minimal, including radiation during static skin contact [4].

The polluting of soils with heavy metals and radionuclides can be natural or anthropogenic. Furthermore, different heavy metals have a specific accumulation rate and bioavailability based on the physical and chemical properties of soils; therefore, they have a different biomagnification rate, impact on human health, and ecological risk level [5]. In this regard, it is important to identify the main sources, fate, and specific features in the distribution of heavy metals and radionuclides in soils.

A complex interplay of biogeochemical processes, affected by factors such as pH, clay content, and redox potential, controls the transport and chemical stability of metallic contaminants in soil and sediment deposits. The transfer of heavy metals from the soil to plants depends on quantity factors, intensity factors, and reaction kinetics. These factors represent indicators of the overall quantity of potentially available elements, the activity and ionic ratios of elements in the soil solution, and the rate of transition of elements from the solid phase to the liquid phase and within the roots of the plant. Physical clay (particles < 0.01 mm) and silt particles (particles < 0.001 mm), which have a higher absorption capacity compared to larger fractions, have the greatest impact on the radionuclide mobility in soils. The addition of a silt fraction from chernozem or sod–podzolic soils to sand reduces the accumulation of Sr in oats and wheat by 1.5–2 times, and this effect is more significant for ^{137}Cs. The transfer of ^{90}Sr from soil to plants is four times higher on sandy soils compared to loamy soils. Similarly, the transfer rates for ^{137}Cs and ^{60}Co are 100 times and 40 times higher, respectively, on sandy soils [6]. According to the sorption efficiency of these isotopes, the soil is arranged in the following order: sod–podzolic soils (Albeluvisols), grey soils (Calcisols), yellow soils, red soils (Ferralsols, Alisols, and Acrisols), chestnut soils (Kastanozems), and black soils (Chernozem). Substantial transfer of radiocaesium to plants in sandy and sandy loam soils with a low content of clay minerals and organic matter has been reported [7]. However, within the same soil group, the nature of the uptake of ^{137}Cs into plants may vary depending on the absorption capacity of the soil, the content of macro and microelements, and the pH of the soil solution. The sorption of ^{137}Cs in the soil depends on the clay mineral content of the soil and K-saturation.

This effect of fine soil fractions is associated with a stronger fixation of radionuclides in them, which, in turn, is due to a larger specific surface of clay and silt particles and changes in the chemical properties of the soil: the content of exchangeable cations and organic matter, as well as the absorption capacity, increases [6]. In general, the effect of soil properties on the biological rate of radionuclides can be described as follows: the transfer of radionuclides to plants increases with a decrease in the content of clay, silt, organic matter, and the absorption capacity in the soil [8,9].

Adsorbed radionuclides are more strongly retained by organic mineral complexes than when sorbed in minerals of a different nature [10,11].

Summarising several studies, two soil management directions can be outlined:

1. Incorporating soil amendments can effectively fixate toxicants [12,13].
2. Supplying the soil with deficient nutrients is a method that helps plants resist heavy metal stress [14,15].

The type of soil should be taken into account for its effective treatment. For example, on loamy soils, the use of almost all types of fertilisers will increase yields and reduce the level of radioactive substances in plant products. On poorly mineralised and hydromorphic soils, the absorption of some radioactive substances can sometimes increase with the application of mineral fertilisers. Research on new fertiliser compositions (also biosolids)

based on a combination of organic and mineral components of sustainable raw materials to increase the stability of soil–plant systems remains relevant [16,17]. Furthermore, resistance of the soil–plant system to radionuclides and heavy metals refers to the ability of the system to limit the mobility of chemical pollutants due to the inherent buffering properties of the soil, thus controlling the transition of the latter to the aerial part of the plant [18].

The migration of heavy metals and radionuclides is interrelated, and this study focusses on the interaction and complex influence of various toxicants. Therefore, this research aimed to review the problems of the rehabilitation of contaminated ecosystems and the areas of application of bioremediation processes for this purpose. According to the goal, the task was set as follows:

1. Review of the state of ecosystems contaminated with heavy metals and radionuclides.
2. Identification of the advantages and disadvantages of using biosorption technologies for the joint fixation of heavy metals and radionuclides.
3. Substantiation of the possibility of using phosphogypsum for soil bioremediation.

2. Methodological Approach

To implement the objectives of the review, taking into account the analysis of the general scheme of the pollution cycle to structure the impact and means of reducing it, a bibliometric analysis was used using data from the Scopus and Web of Science databases. For the systematisation of data and their management, Mendeley software (Elsevier, Amsterdam, The Netherlands) was used.

Therefore, the methodological approach to the literature analysis consists of the following steps described in the flowchart in Figure 1.

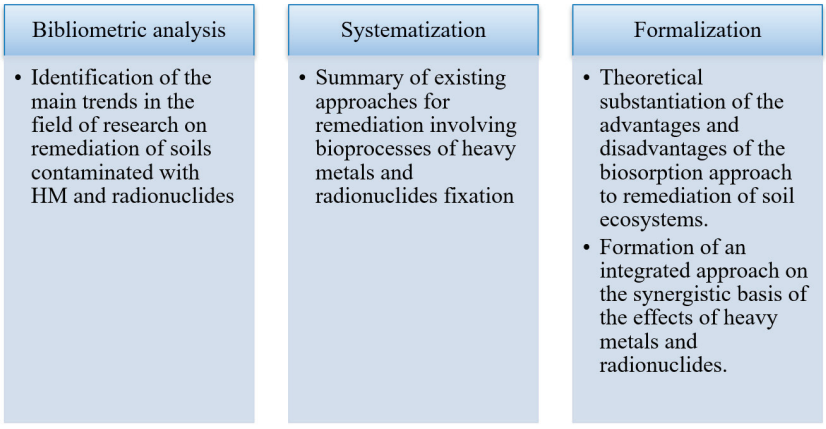

Figure 1. The methodological approach to the implementation of the topic review rehabilitation of contaminated ecosystems and the areas of application of bioremediation processes.

To validate the approach of using phosphogypsum in bioremediation, a comparative analysis of the elemental composition of phosphogypsum of various origins and locations was conducted in different regions of the world. This analysis was based on the results of research on Ukrainian phosphogypsum, as well as previous studies by other authors in different countries and regions around the world. This allowed for the synthesis of existing information on the subject and provided a rationale for recommending the genesis of suitable phosphogypsum for use in bioremediation processes. The main stages of the analysis are illustrated in Figure 2.

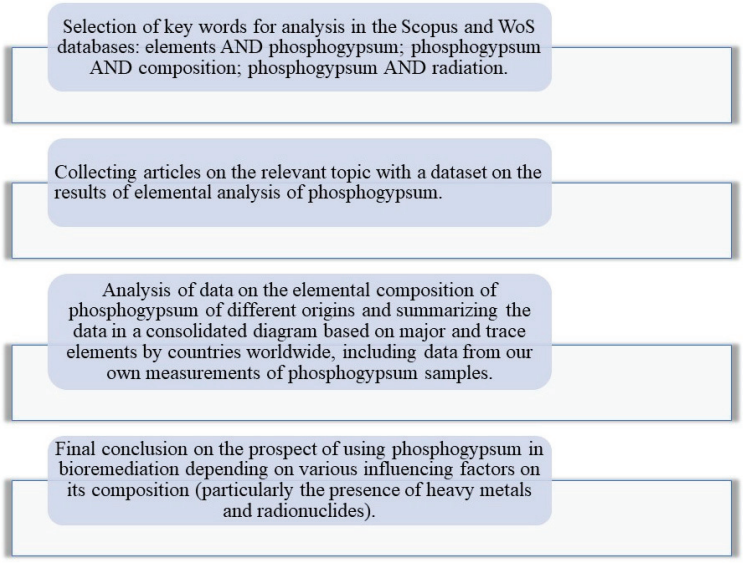

Figure 2. The methodological approach for the comparative review of phosphogypsum.

The ICP-OES method was used to analyse the elemental composition of phosphogypsum. The measurement protocol is shown in Table 1.

Table 1. Protocol to analyse the elemental composition of phosphogypsum.

Step	Description
1 Drying	Over-drying at 40 °C for 24 h
2 Milling	Fraction size smaller than 1 mm
3 Digestion	Ethos 1 (MLS GmbH, Leutkirch im Allgäu, Germany) microwave-assisted wet digestion system for 35 min at 210 °C
4 Measurement	Inductively coupled plasma-atomic emission spectrometry (ICP-OES, Agilent 720, Agilent Technologies Inc., Santa Clara, CA, USA)

3. Review of the State of Ecosystems Contaminated with Heavy Metals and Radionuclides

3.1. Sources of Radionuclides and Heavy Metals in the Ecosystem

Soil is a complex mixture and a non-renewable natural resource, as it can only be restored on a geological timescale. Heavy metals, unlike biological compounds, are rarely biodegradable and therefore accumulate in the environment. Heavy metals in the soil have a toxicological effect on soil microorganisms, leading to a decrease in abundance and activity [8,19]. The relatively long half-life of radionuclides contributes to their long-term presence in the environment, leading to various health complications, such as cancer [20].

Table 2 shows that the mentioned metals have a common anthropogenic source. These activities have led to increased concentrations of heavy metals in the soil, contributing significantly to their occurrence in the environment [21,22].

Table 2. Main sources of some heavy metals in soils.

HM	Sources	Effects on Soil	References
Cd	Non-ferrous metal extraction, production of phosphate fertilisers, burning of fossil fuels, waste incineration, tannery industry, electroplating, and battery disposal.	The disruption of metabolic functions hinders enzyme activities, reducing the availability of N and S in the soil for crops.	[20,21,23–25]
Pb	Emissions from power generation, metallurgy, mechanical engineering, metalworking, electrical engineering, chemistry and petrochemistry, woodworking and pulp and paper industries, food industry, and construction-material production, as well as automotive transport.	Organisms' metabolic abnormalities affect soil enzymes and interrupt nutrient balance, reducing soil productivity.	[19,21,23,26–28]
Zn	Emissions from non-ferrous metallurgy, waste incineration plants, coal combustion, and tyre wear.	Phytotoxic effects on soil fertility, diminishing microbial biomass N; and lacking essential soil macronutrients, such as phosphorus.	[9,21,26,29,30]
Cu	Emissions of non-ferrous metallurgy enterprises; combustion of leaded gasoline, municipal incinerators, and copper mining residue.	Limited amounts of soil N and S hinder crop production. Inhibit β-glycosidase more than cellulose. Diminish microbial biomass N.	[21,26,27,31,32]
Hg	Emissions from non-ferrous metallurgy, fossil fuel burning, steel production, metal smelting.	Disruption of metabolic function in organisms.	[21,26,33,34]
As	Burning of fuel, emissions from power generation, production of construction materials, pharmaceutical and textile industry. As used in herbicides, insecticides, and desiccants.	Disruption of metabolic function in organisms.	[21,22,26,27]
Cr	Emissions from ferrous and non-ferrous metallurgy (alloying additives, alloys, and refractories) and mechanical engineering (electroplating).	Disruption of metabolic function in organisms.	[21,26,35,36]
Ni	Emissions from non-ferrous metallurgy, burning of fuel, waste incineration, and chemical industries.	Disruption of metabolic function in organisms.	[21,26,37–39]

The application of mineral fertilisers contributes to the increase in these elements (Cd, Pb, etc.) in the soil. Cu, Cr, As, Hg, Mn, Pb, or Zn enter the soil, along with other toxic chemicals, such as pesticides. The application of a wide variety of biosolids, such as livestock manure, composts, and sewage sludge, to the soil unintentionally leads to the accumulation of heavy metals such as As, Cd, Cr, Cu, Pb, Hg, Ni, Se, Mo, Zn, Tl, Sb, etc., in the soil [40,41]. The extensive mining and smelting of Pb and Zn ore have resulted in soil contamination that poses a risk to human and ecological health [42].

3.2. Monitoring of Radionuclides and Heavy Metals in Ecosystems and Impact on Humans: Ukraine CASE Study

Monitoring radioactive substances and heavy metals in the environment is essential since pollutants can accumulate and migrate in the elements of the trophic chain. Soil is an indicator of the ecological state of the environment. Proper organisation of background monitoring of contaminated areas allows for an effective assessment of the state of environmental objects, development of methods for biological soil remediation, and prediction of the future state of the biological environment. Therefore, the authors investigated [43] the migration and accumulation of heavy metals and radionuclides in the most significant protected areas of the Transcarpathian region and identified the main possible factors that affect the environmental monitoring process. As stated in Savchuk et al. [44], years after the Chernobyl disaster, the environmental situation in the Polesie zone of Ukraine remains difficult, as confirmed by the increased content of heavy metals in feed, milk, beef, and

pork. The highest concentration of Pb was detected in coarse feed and sunflower cake and meal (2462 mg/kg and 1639 mg/kg); 41.9% and 60.0% of samples of these types of feed, respectively, had exceeded the maximum allowed concentrations of Cd.

The study revealed that coal mining in Jiangxi Province, China, causes radioactive uranium contamination and heavy metal contamination with zinc and cadmium in the soil, and the proposed in situ leaching method can be used to remediate contaminated soils, but with attention paid to the potential environmental risks to the soil [45]. The study by Mohuba et al. [46], conducted in the Thyspunt area of South Africa's Eastern Cape province, a potential site for a nuclear power plant, revealed elevated levels of radionuclides, including 238U, 235U, 234U, 226Ra, 232Th, and 210Pb, mainly in rock formations of shale and quartzite due to the natural geochemistry of these rocks. This indicates the potential health risks associated with the ingestion of groundwater commonly used in the area. The study by Baghdady et al. [47] in the Bahariya Oasis of Egypt, located near large iron mines, identified elevated levels of Ba, Cr, Cu, Fe, and V in cultivated soils and Al, Cr, Cu, and V in uncultivated soils, exceeding acceptable limits, with the highest concentrations recorded in the northern oases near iron mines, while the highest values of activity concentrations, i.e., 40 K, were recorded in uncultivated soils rich in evaporites. The study by Mitrovic et al. [48] observed a significant decrease in soil 137Cs activity levels over a ten-year study period (2007–2017) in Palilula, Belgrade, with values declining from 16 Bq/kg to 3.9 Bq/kg; and in Surcin, Belgrade, from 18 Bq/kg to 12 Bq/kg. The study also identified variations in soil heavy metal concentrations and attributed the primary source of radionuclides and heavy metals to the widespread use of mineral phosphate fertilisers in agricultural fields.

In the context of the analysis performed, it is possible to define the main aspects of the effectiveness of soil-monitoring implementation [49]:

- Availability of sufficient areas that are subject to minimal anthropogenic impact (for example, biosphere reserves, nature reserves, and national nature parks);
- Selection of background monitoring criteria that would take into account the prevalence of individual substances in nature, their migration in the natural environment, and the presence of potential sources of their anthropogenic intake;
- Selection of effective methods for monitoring the state parameters of environmental objects.

The impact of the Chornobyl accident is not limited to the exclusion zone. Studies were carried out in different regions of Ukraine and protected areas to establish the migration processes of radionuclides and heavy metals and the possible relationships between them. The determination of the heavy metal content in soils in the Carpathian Mountains region and bottom sediments and the absolute activity of gamma-active nuclides was measured by Symkanych et al. [43]. Based on the data obtained, a map of the distribution of the total gross content of heavy metals and radionuclides was formed, which allowed for the evaluation of the migration process and the identification of regions with a disturbed balance of harmful substances.

According to the data of Lee et al. [50], the monitoring of radioactive pollutants, mainly lying at a depth of 15 cm of the soil surface layer, can be carried out using several radiochemical analytical methods: plasma or laser spectrometry; and scintillation or semiconductor spectrometry. Plasma or laser spectrometry can effectively detect vertical variations in surface contamination only at a depth of about 10 cm because of its minimal penetration depth. Therefore, mobile scintillator spectrometry was proposed to comprehensively characterise the radioactive contamination of decommissioned nuclear facilities. In the study by Lee et al. [50], a mobile in situ scanning system, consisting of a gamma-ray spectrometer, was developed and tested for application in nuclear decommissioning sites. The results demonstrated its potential as an integrated performance-assessment tool for in situ monitoring at nuclear decommissioning sites.

Minimising the pollution of agricultural products is the main direction of the state in ensuring environmental safety and public health, as radionuclides enter the human body

during the consumption of contaminated products. This relationship characterises the trophic chain: radioactive fallout–soil–agricultural plants–farm animals–humans [51].

It is possible to form three main migration flows of radionuclides that fell on the territory of Ukraine (Figure 3) [50–52].

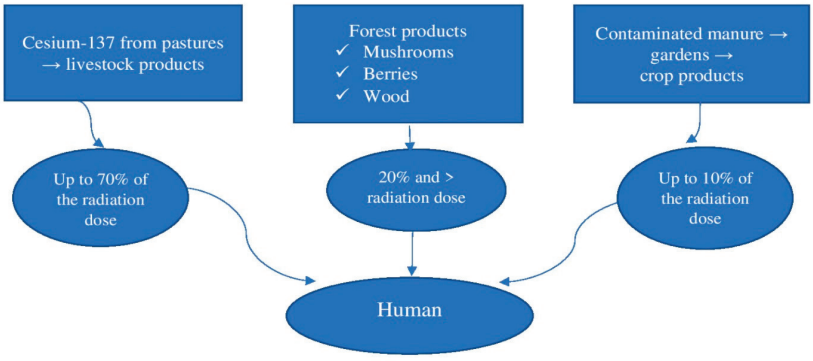

Figure 3. Radionuclide migration flows through the trophic chain to the human body.

The set of measures that prevents the entry of radionuclides into agricultural products includes the following [7,53]:

- Natural autorehabilitation (radioactive decay, and fixation and redistribution of radionuclides in the soil);
- Strengthening of biogeochemical barriers to fix radionuclides in soils, reducing the risk of radiation contamination of food;
- Strengthening the radioecological monitoring of soils and agricultural products, radiological control, and compliance with recommendations for agricultural production.

The restoration of radioactive soils is carried out using methods based on such strategies as dry separation, soil washing, flotation separation, thermal desorption, electrokinetic remediation, phytoremediation, etc. The main factors that help to select soil-cleaning methods effectively include soil type, particle size, percentage of fine particles, and radionuclide characteristics [54].

The characteristics and composition of radioactive particles depend on the source of release, and emission scenarios affect the properties of these particles, which is directly essential for the transfer to the environment. Radioactive particles in the bio-environment can come in a variety of physical and chemical forms, ranging from low-molecular-weight particles, colloids, or nanoparticles to pseudocolloids, particles, and fragments. Therefore, information on the types of radionuclides that transform over time is important for assessing the state of contaminated areas and irradiated organisms [55,56]. Radioactive particles can also carry a certain amount of radioactivity and be point sources of radiological danger [57].

For the sorption of radionuclides and heavy metals, various matrices can be used. Basic rock-forming minerals (framework aluminosilicates) are better suited for immobilisation of radionuclides of alkaline and alkaline-earth element groups, as well as halogens, and the use of accessory minerals (phosphates, titanates, and titanium zirconate). As reviewed in our previous studies [14], matrix materials such as phosphates, zirconolites, and sphenes can be recommended for use. In more detail, it is worth dwelling on biosorption methods of ecosystem remediation, which are of increasing interest in applied technologies of radionuclide and heavy metal fixation.

4. Biotechnologies for Integrated Fixation of Heavy Metals and Radionuclides: Identification of Advantages and Disadvantages

4.1. Soil Bioremediation Methods

The soil rehabilitation process of microbes is carried out using mechanisms such as bioprecipitation, biosorption, bioaccumulation, bio-assimilation, bio-extraction, biodegradation, and biotransformation [58–63]. Some methods for fixing heavy metals and radionuclides are shown in Figure 4. In situ remediation, which involves treating the contaminated site directly in place, can be further subdivided into intrinsic bioremediation and engineered bioremediation. Intrinsic bioremediation occurs naturally without human intervention, while engineered bioremediation involves manipulating the environment to accelerate the degradation of the contaminant [64].

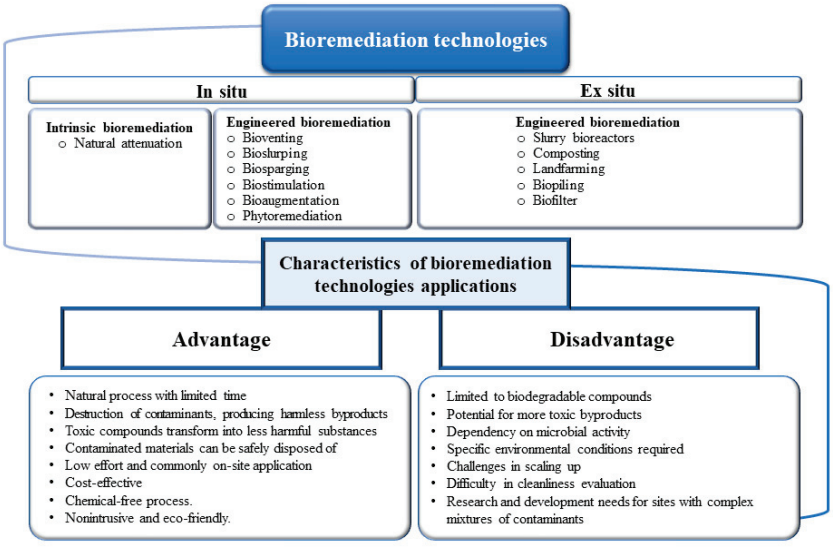

Figure 4. Generalisation of remediation methods.

The connection between engineered bioremediation methods and physical and chemical treatment methods is to complement each other. Therefore, stage-by-stage soil remediation is needed, including physical, chemical, and biological treatment methods. Physical and chemical methods can precede biological methods and serve as a preliminary stage. Groudeva et al. [59] investigated the dissolution and removal of contaminants from soil using Na_2CO_3 and $NaHCO_3$ solutions, linked to the activity of heterotrophic and basophilic chemo-lithotrophic microorganisms. This activity was intensified by the corresponding changes in environmental factors, such as water, oxygen, and nutrient levels. Furthermore, dissolved-impurities soil leachates were efficiently treated using a nearby natural wetland ecosystem [59].

In the context of mechanical and physicochemical soil remediation methods, the contaminated soil fraction is excavated and then transported to a designated disposal site, where it is stored and treated, incurring additional space requirements and transportation costs [60]. This approach has the disadvantage that it essentially relocates contamination to another location, necessitating ongoing monitoring of the previously contaminated soil and the surrounding environment. Furthermore, during the removal and transport of contaminated soil, there is a risk of spreading contaminated soil and dust particles.

Chemical or physicochemical remediation can be used as a standalone method (when heavy metal concentrations are less than 100 mg/L), but it is more advisable to use it as a preliminary step before biological remediation. The latter approach allows for the

removal of heavy metals from an environment with concentrations significantly lower, but exceeding background levels due to pollution [61].

The chemical and physicochemical methods in the separate application require soil treatment with certain reagents and subsequent leaching with an organic or inorganic solvent, which can lead to deterioration of soil properties, creating an additional factor of destruction of natural soil properties, excluding the possibility of their further use [45].

There are many factors to consider when using physicochemical methods, e.g., pH, temperature, time, nature of the desorbing agent, etc., making the physicochemical method not always suitable, effective, or economically feasible [32]. For example, ion exchange, as a chemical treatment method, can be used to remove various types of metals from the soil but requires the replacement of ion exchange materials and can be expensive [56,63,65].

Compared to organic contaminants, heavy metals and radionuclides in soil cannot be destroyed but must either be converted into a stable form or removed. For this purpose, it is appropriate to use chemical methods to clean soils contaminated with heavy metals and radionuclides, which allow the reaction mixture to be applied directly to the contaminated area, while the topsoil that is being cleaned does not have a significant impact on the functioning of the ecosystem in general [66].

One such approach for the purification of heavy metal-contaminated chernozem soils involves the incorporation of a residual mixture of organic and mineral compost. In this scenario, pollutants are not extracted from the soil; instead, they are temporarily transformed into less readily available forms for plants over a specific duration, typically 4–5 years. However, this method itself does not provide a solution to the problem of removing pollutants from soils but can be combined with biological methods to achieve a positive effect.

The biological soil remediation of heavy metals and radionuclides is achieved through biotransformation. Microorganisms, such as bacteria, fungi, and microscopic algae that reside in the soil, are effective biotic entities that are capable of efficiently absorbing or transforming heavy metal and radionuclide compounds [67].

Heavy metals that penetrate living cells exhibit their toxic effects primarily in the form of ions. However, if heavy metals and radionuclides are transformed into bound forms through various means, they lose their toxic properties [68]. Consequently, heavy metals deposited in the cell wall in a crystalline or poorly soluble compound form become non-toxic to microorganisms but are eventually removed from the environment as a result of biological remediation.

The mechanisms through which microorganisms interact most frequently with heavy metals include biosorption (the sorption of metals on cell surfaces through physicochemical mechanisms), bioleaching (the mobilisation of heavy metals through the excretion of organic acids or methylation), biomineralization (the immobilisation of heavy metals through the formation of insoluble sulphides or polymeric complexes), bioaccumulation (intracellular accumulation), and enzyme transformation catalysis (oxidation-reduction reactions) (Figure 4) [69,70].

Biological methods of soil remediation offer partial solutions to challenges in this field. From an economic point of view, they provide benefits by avoiding the need for significant one-time investments. The associated costs can be spread over several years. These methods also eliminate the requirement for mandatory soil excavation and can be applied to larger areas. Furthermore, they avoid the introduction of specific harmful chemical mixtures, solutions, or reagents into the soil, thus preventing secondary pollution [71,72]. The general disadvantages of biological methods are their delayed effectiveness; long duration; and dependence on climatic conditions, including the rate of development of bioremediation organisms and biotransformations carried out by microorganisms in climatic conditions with variable temperature and humidity throughout the year [73,74].

Table 3 presents a classification of soil bioremediation methods. The approach chosen may vary depending on the concentration and type of target metals. It is also essential to consider an ecosystem-based approach within the context of interconnectedness because

the soil environment interacts with water resources and the atmosphere, influenced by the biochemical activities of organisms in the natural components of the ecosystem [75–77].

Table 3. Classification of soil bioremediation methods.

Method	Brief Definition	Process Features Considering Their Limitations	References
Biomineralisation	Deposition of heavy metals as insoluble compounds. It includes two primary methods: microbiological carbonate precipitation and enzymatic carbonate precipitation.	It is considered an environmentally friendly bioremediation method that is not less effective than chemical methods. However, limitations related to microorganism strains, pollutant concentrations, and soil properties must be taken into account. Further research on soils treated with biomineralization, the solidification and stabilisation (S/S) of toxicants, is necessary to understand the patterns of strength change in polluted soils treated with biomineralization. Additionally, it is important to investigate changes in the rate of heavy metal fixation and the mechanical properties of contaminated soil.	[77–83]
Biosorption	This is a physicochemical and metabolically independent process that relies on various mechanisms, including absorption, adsorption, ion exchange, surface complexation, and precipitation.	Advantages include low cost and significantly higher efficiency in removing metals from diluted solutions. Heavy metal adsorption and removal can be performed using biomass, which can generate income for businesses that do not use biomass, such as organic waste. Various environmental parameters, such as temperature, metal type and concentration, metal oxidation state, microbe type, metal removal method, and biosorbent concentration, can influence the ability of microorganisms to bind metals. This may have a negative impact on biosorption efficiency.	[84–92]
Bioprecipitation	In the process of bioprecipitation, the formed metabolites react with metals present in the groundwater, resulting in the precipitation of metals, i.e., the transformation of metals from the aqueous phase to the solid phase.	Bioprecipitation is more effective in treating wastewater than soils; however, the profitability of recycling or selling recovered metals can vary depending on the investments in infrastructure of the investments in infrastructure of a company. It is recommended to use it in conjunction with other biological methods.	[78,93–98]
Bioaccumulation	Active uptake of heavy metals into cells involves the binding of toxic metals or chemical compounds inside the cellular structure.	This method not only is cost-effective but also helps minimise the environmental impact of pollution. Metal bioaccumulation is particularly useful as an impact indicator, as metals are not metabolised. Metal ions initially attach to the cell surface and are later transported into the cell. This process can lead to a temporary reduction in metal ion concentration. However, it can be utilised to synthesise metal-rich nanoparticles, provided that the processing is performed in specialised bioreactors rather than in situ.	[85,99–105]
Biotransformation	Breakdown of heavy metal compounds into less toxic forms or their conversion into less toxic forms (associated with biodegradation).	Photoautotrophic microbes are capable of biotransforming heavy metals into relatively biologically inaccessible and insoluble metal sulphides. By characterising the role of sulphur assimilation pathways in the biotransformation of heavy metals, we can develop more effective processes for heavy metal bioremediation. The use of additional sulphate nutrition can enhance the rate of biotransformation in aerobic microbes.	[78,85,106–111]

Bioremediation-based processes can be considered a promising area based on the transformation of heavy metals and radionuclides into a less dangerous state and, at the same time, provide sustainable restoration of the environment. Thus, as part of the study of transformations of metals such as Pb, Zn, and Cd by Thakare et al., a number of regularities were identified. Metals cannot be decomposed by microorganisms involved in contaminated soil rehabilitation, but they can be changed from one oxidised form to another, allowing them to become fixed in insoluble form and be removed from biogeochemical cycles of migration in the environment [112].

Heavy-metal ions and radionuclides can usually be adsorbed by functional groups such as carbonyl, carboxyl, sulfhydryl, phosphate, sulphate, amino, and hydroxyl groups on the bacterial surface. The ability of bacteria to absorb heavy-metal ions generally varies from 1 mg/g to 500 mg/g [113]. Extracellular polymer substances consisting of proteins, lipids, nucleic acids, and complex carbohydrates play an important role in the adsorption of heavy-metal ions. These substances on the surface of the bacterial cell can prevent heavy metal toxicity and penetration into the inner cell region [112]. When studying the effect of metals on soil biological properties, it is feasible to use a set of methods, such as microbial biomass, C and N mineralisation, respiration, and enzyme activity, that will allow for a complete evaluation of this interaction [114].

In general, the following types of microorganisms are used in the bioremediation methodology [78]: *Bacillus* sp., *Lysinibacillus* sp., *Rhodococcus* sp., *Ascomycota*, *Basidiomycota*, *Perenniporia subtephropora*, *Daldinia starbaeckii*, *Phanerochaete concrescens*, etc.

4.2. Biosorption Technologies and Their Aspects of Realisation

Today, biosorption has been accepted as an environmentally friendly alternative green technology for the removal of various human-made pollutants, with the help of microbes such as bacteria, fungi, algae, and yeast. Pollutants are substances that do not decompose, are relatively unyielding, are insoluble in water, are impervious to microbial cells, and are harmful to lower and higher classes of living organisms. Desorbing eluents can be used to remove adsorbed pollutants, and biosorbent regeneration can be carried out by chemical, thermal, or electrochemical methods [115].

Fundamental to understanding the biosorption process is knowledge of the mechanism of the process. Based on cellular metabolism, biosorption mechanisms can be classified into independent and dependent mechanisms. Based on the location of biosorption, the following are distinguished [116–121]: (i) intracellular accumulation, (ii) extracellular accumulation and deposition, and (iii) cell surface sorption and deposition. The mechanisms belonging to the first two groups depend on metabolism and are caused by the processes of complexation, precipitation, and ion exchange; and the last group of mechanisms are also adsorption (physical and chemisorption).

The process of adsorption involves the attraction of other dissolved particles to the surface of a solid substance (adsorbent), primarily through adhesion, electrostatic attraction, and ion exchange. The adsorbent "fixes" all contaminants in its structure and thus purifies the sample [116].

An integrated approach is necessary for the restoration, regeneration, revegetation, and management of areas with a high level of anthropogenic loads, such as areas contaminated with heavy metals and radionuclides. Methods can be applied effectively for soil restoration, including some green activities, such as phytoremediation, and an appropriate soil cleanup process can be established. The enhancement of phytoremediation takes place through organic additives, namely agricultural waste and pretreated sewage sludge, biochar, humic substances, plant extracts, exudates, etc. [117].

At the same time, the commercialisation of biosorption technologies is hindered by technical problems associated with the operation and regeneration of native biosorbents. This problem is partially solved by immobilising microorganisms in a solid inert carrier, such as biochar, zeolites, and vermiculite, or by including them in an alginate gel. In this case, it becomes possible to apply a dynamic sorption process, the so-called "column

variant" [118–121]. However, the sorption capacity of the biosorbent decreases significantly in comparison to static biosorption. Furthermore, there are still problems with biosorbent regeneration and replacement in the event of complete depletion.

The key advantages and disadvantages of biosorption technologies are shown in Figure 5. Biosorption is well suited for use in large areas of contaminated soil where other remediation methods are not economically feasible or difficult to implement practically and where soil productivity can be restored over long periods of time. It can be combined with other technologies, such as phytoremediation, for the final closure of the site with vegetation. In emergency situations or military action that involves the release of high concentrations of pollutants into the ecosystem, it is initially necessary to use physicochemical methods to quickly stop vertical and horizontal migration into natural components. Biosorption technology has some limitations that should be considered before choosing it for the remediation of areas contaminated with heavy metals and radionuclides: the prolonged duration of territorial restoration and the fixation and transformation of pollutants into less toxic forms have a long-term positive effect, but there is a potential risk of contamination through the food chain.

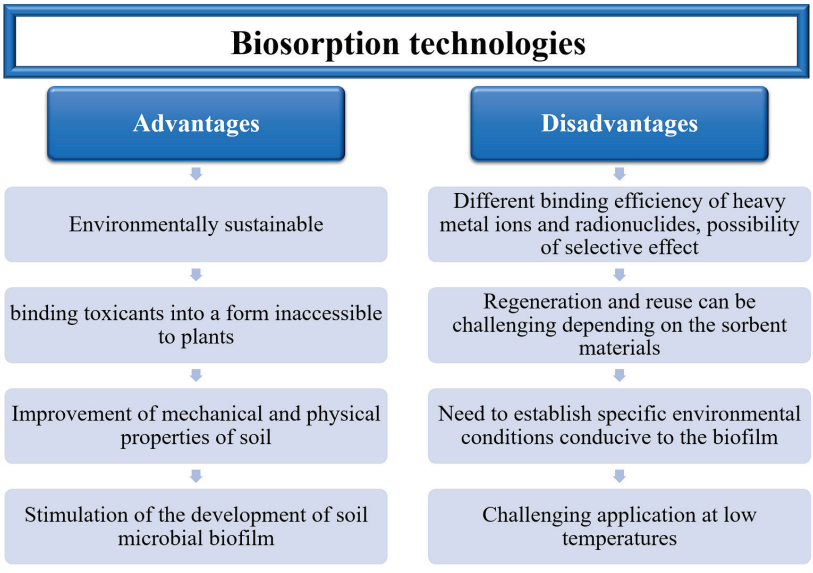

Figure 5. Characteristics of biosorption technologies.

A biostimulation approach is used to improve biosorption processes. It includes stimulating the growth of microorganisms in a contaminated soil area to introduce pH-correcting substances, nutrients, surfactants, and oxygen [122], which requires further research.

However, it should be noted that there is a lack of information on the synergistic or inhibitory effect on the sorption processes of metal ions in multicomponent solutions with different ionic strengths, effective methods of immobilisation of microorganisms for the implementation of flow biosorption processes, selectivity and ways to increase it in the concentration of heavy metals, etc. This indicates the need to create a research algorithm for the study of biosorption processes using microorganisms.

Thus, to date, the following directions are relevant [60,123–128]:

- Studies of microorganisms of different physiological groups (including the use of genetically modified strains) on the ability to sorb and transform soluble forms of heavy metals and radioactive elements into insoluble ones;

- Bacterial reduction processes of technetium, chromium, and uranium when used as final electron acceptors in bacterial energy metabolism for the purpose of their detoxification in systems with neutral, acidic, and alkaline pH values;
- Determining the products of bacterial transformation of radionuclides and heavy metals formed under different conditions;
- Possibilities of reducing the toxic effects of heavy metals and radionuclides on soil microorganisms;
- Development of nanobioremediation technology.

5. Possibility of Using Phosphogypsum for Soil Bioremediation

The use of phosphogypsum is associated with challenges that have gained increasing importance [129], as shown in Figure 6. Furthermore, it should be noted that phosphogypsum may be contaminated with radionuclides [130]. According to EPA data, phosphogypsum contains significant quantities of uranium and its decay products, such as radium-226, attributed to its presence in phosphate ores. The concentration of uranium in phosphate ores identified in the United States varies within the range of 0.26 to 3.7 Bq/g (7 to 100 pCi/g) [131]. However, various raw materials are used in different countries and regions globally; consequently, not all phosphogypsum exhibits elevated levels of radioactivity [129,132].

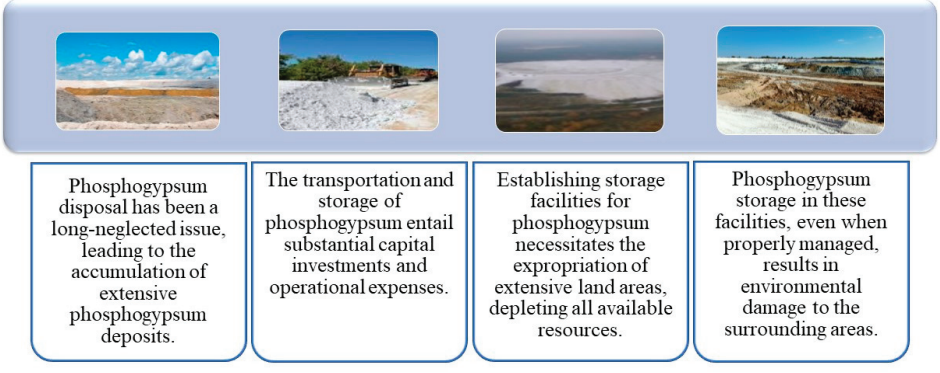

Figure 6. Accumulation of phosphogypsum in the environment.

In order to address the development of environmentally friendly technologies for the use of phosphogypsum within the context of the bionics concept that integrates biological methods and structures for engineering solutions and technological approaches, it is necessary to improve the technical solutions and technologies for phosphogypsum utilisation in potential soil applications. A crucial element involves precise control over the composition of the soil solution through in situ synthesis of essential compounds directly within the soil. Given the present issue of soil degradation, there is a pressing need to actively explore novel soil management strategies. Furthermore, the effective resolution of this problem requires the availability of suitable design tools [18].

We emphasise the use of phosphogypsum, which does not have significant radioactive contamination, in bioprocesses. Therefore, Figure 7 shows the main elements of phosphogypsum that positively affect soil properties [133,134]. Furthermore, phosphogypsum has an impact on the growth of microorganisms, which has been confirmed by several studies [135–139]. Through the regulation of soil moisture, it is possible to significantly reduce the leaching of unproductive substances and address issues related to the hydromorphic regime of the soil, including the degradation of organic matter and the reduction of sulphate to sulphides. Moisture control also enhances the protective effect of the geochemical

barrier "soil–rhizosphere", effectively retaining harmful compounds within soil solution, particularly for Pb, Cd, and Sr [140].

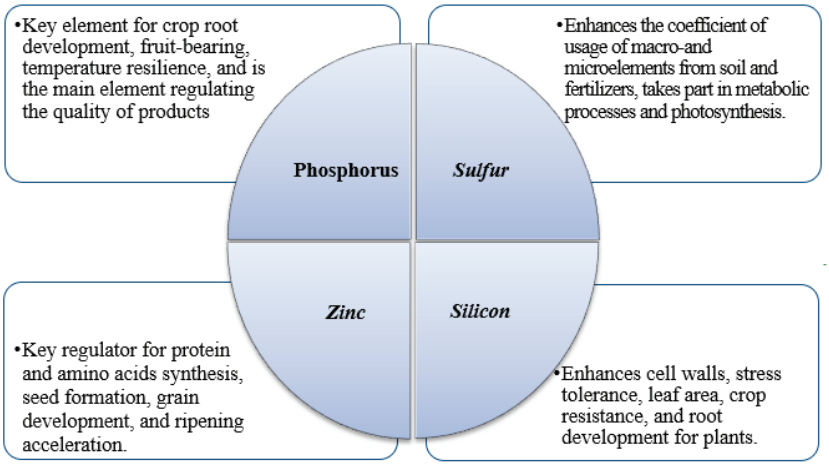

Figure 7. Beneficial elements in the composition of phosphogypsum (case study: phosphogypsum dump in Sumy region, Ukraine).

Figure 8 shows the distribution of countries according to their publication activity in the phosphogypsum research documented in the Scopus database. Distribution of countries by publication activity in the field of phosphogypsum research according to the Scopus database.

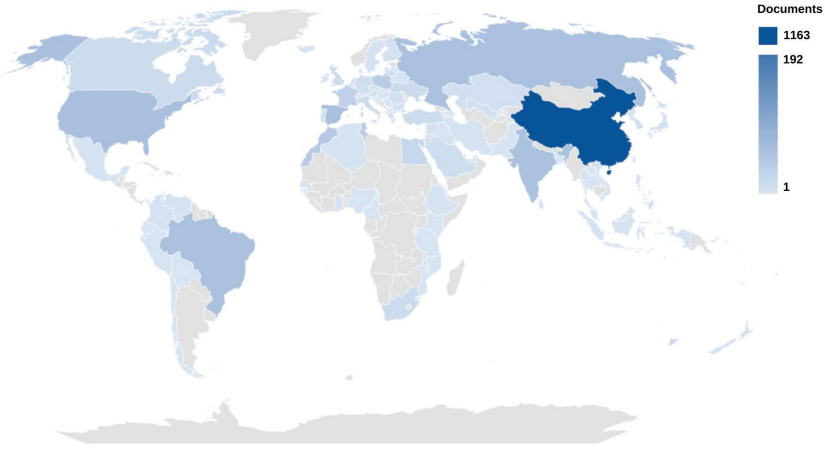

Figure 8. Distribution of countries by publication activity in the field of phosphogypsum research according to the Scopus database.

Tables 4 and 5 show a comparative analysis of the concentrations of elements in phosphogypsum from different countries.

Table 4 shows that the main components of calcium and sulphur oxides fluctuate in significant intervals in phosphogypsum samples from different regions of the world, with calcium in the range of 17.7–45.9 wt% and sulphur in the range of 17–51.4 wt%, respectively. At the same time, components such as iron, potassium, aluminium, magnesium, and manganese also have a significant difference in the amount of content in phosphogypsum

from different locations of generation in the world. This is due to the technological process of production, but the special influence on changes in the content of trace elements is influenced by the raw materials used (phosphates and apatites).

In terms of the content of radionuclide isotopes, the data vary significantly depending on the region of phosphogypsum deposition. A review of previous studies [130,141,142] showed that radioactivity varies according to the type of phosphate ore and is mainly caused by the decay series U-238 and Th-232. Since U-235 is not as common in nature as U-238, the radiation of this decay series is not considered a threat [143]. However, the information about harmful impurities in phosphogypsum related to its environmental impact is not yet fully understood, which requires scientific evaluation in the future and the expansion of research in this area [144].

Therefore, it is worth concluding that Ukrainian phosphogypsum (in particular, from the Sumy region, since its samples were studied) is the most environmentally acceptable for bioremediation processes (Tables 4 and 5):

- Heavy metals (e.g., As, Pb, and Cr) have lower concentrations in phosphogypsum from the Sumy region than in phosphogypsum from China, Spain, the USA, and Brazil;
- Some rare earth elements (such as La, Ce, Pr, and Y) are represented in phosphogypsum from the Sumy region (Ukraine) and less represented in phosphogypsum from other regions of the world.

However, this conclusion requires several further studies on the testing of Sumy phosphogypsum on different types of soil in bioremediation practice.

Table 4. Concentrations of major elements in phosphogypsum.

wt.%	Ukraine [a]	China [b]	United States [c]	Spain [d]	Brazil [e]	India [f]	Morocco [g]	Poland [h]	Tunisia [i]	France [j]	Greece [k]
CaO	22.9–31.4	31.6–43.3	22.7–39.4	17.7–32.6	31–36	30.9–38.9	32.2–35	29.6–42.7	30.7–37.2	31.3–33.4	34.30
SO_3	29.8–36	34–49	22.9–51.9	30.7–46	44.5	44.2–52.9	17–45.1	42.1–56.5	37.5–47	n.m.	41.50
SiO_2	13.1–24.7	3.6–15.3	3.2–51.3	n.m.	0.8	0.5–4.3	0.3–9.7	0.4–1.8	1.0–3.8	0.6–1.5	n.m.
Al_2O_3	0.96–2.52	0.08–2.59	0.069–1.14	n.m.	0.11–0.2	0.1–0.77	0.13–0.77	0.18–1.7	0.04–0.11	0.11–0.31	n.m.
P_2O_5	0.63–0.79	0.68–1.82	0.5–3.8	0.49–1.18	0.07–1.29	0.82–1.04	0.59–1.62	1.5	0.8–1.69	0.36–0.69	n.m.
Fe_2O_3	0.41–0.94	0.05–1.95	0,13–1.15	n.m.	0.25–0.77	0.1–0.56	0.15–0.83	0.06–0.20	0.03–0.13	n.m.	0.84
K_2O	0.1–0.32	0.17–0.33	0.02–0.9	0.02	0.04	0.03	0.05–0.4	n.m.	0.01–0.03	n.m.	n.m.
TiO_2	0.05–0.17	0.04–0.27	0.03–0.46	n.m.	0.18–0.52	0.02–0.05	0.01–0.03	n.m.	n.m.	n.m.	n.m.
Na_2O	0.02–0.07	0.05	0.11–1.42	0.02	0.02–0.09	0.03–0.11	0.14–0.55	n.m.	0.05–0.29	0.02–0.19	n.m.
MnO	0.01	0.08–0.18	0.06–0.07	n.m.	0.004–0.017	n.m.	0.01	n.m.	n.m.	0.0002–0.0004	n.m.
MgO	0.01	0.01–0.23	0.03–0.13	n.m.	0.02–0.76	0.02–0.56	0.21–0.54	n.m.	0.01–0.07	n.m.	0.13

[a] Ukraine (author's results); [b] China [145–149]; [c] United States [150–152]; [d] Spain [153,154]; [e] Brazil [155–157]; [f] India [158–160]; [g] Morocco [161–165]; [h] Poland [166–170]; [i] Tunisia [171–174]; [j] France [175]; [k] Greece [176,177]; n.m., not measured.

The selective removal of Na^+ and Cl^- from soil, without affecting other macroelement ions, is an integral aspect of the scientific and technical field known as biogeosystem engineering. Biogeosystem engineering deals with engineering solutions and technologies, unprecedented in nature, aimed at managing the cycling of biogeochemical substances in gaseous, liquid, and solid phases. Its primary focus is the ecologically safe use of substances in soils, the improvement of resources and food products, and the solution of the production and environmental challenges in the noosphere through a unified technological cycle based on the principle of natural consistency. In the context of ensuring a quality environment for healthy living, the issue of phosphogypsum involves considering methods for its neutralisation as a more environmentally friendly alternative to the disposal in storage facilities [18,178]. However, for the reclamation of saline soils, neutralising phosphogypsum should be avoided, as its residual acids enhance the solubility of calcium compounds in the soil, promoting sodium displacement by calcium. Therefore, the supply of phosphogypsum to consumers in reusable containers for soil application appears to be a rational solution.

Mixing phosphogypsum with ash from a power plant appears promising for optimising the use of by-products [179]. The lower the coal quality, the higher the CaO content in the ash, leading to a higher level of phosphogypsum neutralisation. Simultaneously, both materials can be recirculated in the soil.

Table 5. Concentrations of trace elements in phosphogypsum.

ppm	Ukraine [a]	China [b]	United States [c]	Spain [d]	Brazil [e]	India [f]	Morocco [g]	Poland [h]	Tunisia [i]	France [j]	Greece [k]
Cu	3.6–7.0	27.6	2.5–35.1	2.5–11	6.3–9	n.m.	1.5–2.9	3.39	6–9.6	5.4–17.5	13
As	<4.96	7.15	0.77–20.1	0.6–8.56	n.m.	n.m.	1.84–1.94	8.05	1	n.m.	0.61–17
Pb	4.6–4.7	28.15	2.06–11.4	1.99–10.8	7.2–31	0.07	0.17–1.7	10.4	0.9	1.68–4.57	11
Zn	3.2–19.7	37.5	1.19–32.1	1.92–13.1	4.4–85.1	n.m.	3–28	n.m.	9–137	n.m.	12–123
Cr	4.6–11.9	37	1.69–20.2	3.59–20.3	11.1–14.7	2.73	5.85–11	5.9	6–13	n.m.	15.8–153
Ni	1.4–1.7	16.6	0.21–17.79	0.87–2.67	5.4–11	14.48	1.2–300	3.6	0.94–4.1	n.m.	21
Cd	1.19–6.36	0.48	0.28–10.8	1.39–2.83	<0.1	n.m.	0.8–7.38	1.7	8–17.7	1.2–2.1	0.98–6.67
V	1.6–2.2	27.5	0.38–10.7	2.9–12.8	6.9–9.2	n.m.	1.94–5	n.m.	2–3	1.43–3.91	n.m.
Ga	0.49–0.78	n.m.	n.m.	n.m.	9–10.4	n.m.	n.m.	n.m.	0.87	n.m.	n.m.
Sr	981	n.m.	1.05–899	360–596	4884.9–6179.1	n.m.	530–778	n.m.	n.m.	813.2–1275	172–470
Ba	20.5–27.2	215	30.3–88.9	37	767.1–6104	n.m.	23–63.3	n.m.	10	92.36–215.6	38.3–331
Y	197.2–148.8	74	43.36	106–142	90–105.3	n.m.	127	n.m.	53.2	34.65–100.7	n.m.
La	195.3–137.1	36.5–46	36.38	n.m.	921.1–1969	n.m.	60.7	40	46.3	12.96–43.35	24.9–30.5
Ce	282.1–200	30.6–32	63.84	19.5–81.2	2109.1–3547	n.m.	39	53	74.4	6.53–18.72	19.2–60.7
Pr	46.7–33.4	5	5.01	n.m.	256.1–276.2	n.m.	11	8	n.m.	1.9–6.9	n.m.
Eu	0.98	n.m.	1.4	n.m.	23.7–25.9	n.m.	2.48	2	n.m.	0.49–1.7	0.85–1.08
Cs	0.38	n.m.	n.m.	n.m.	<0.1	n.m.	n.m.	n.m.	0.05	n.m.	0.09–4.82
Th	3.3–5.8	n.m.	n.m.	1.1	67.2–81	n.m.	3.04–3.27	n.m.	0.74	0.22–1.39	0.59–10.1

[a] Ukraine (author's results); [b] China [145–149]; [c] United States [150–152]; [d] Spain [153,154]; [e] Brazil [155–157]; [f] India [158–160]; [g] Morocco [161–165]; [h] Poland [166–170]; [i] Tunisia [171–174]; [j] France [175]; [k] Greece [176,177]; n.m., not measured.

In our previous study, Chernysh et al. [18], the introduction of phosphogypsum into the process of anaerobic fermentation of sustainable feedstock (sewage sludge, etc.) leads to the introduction of additional macroanalogues into the organo-mineral structure of digestate. It should be noted that the introduction of phosphorus and calcium compounds contained in phosphogypsum intensified the process of fixation of heavy metals and radionuclides in the sludge. As a result, calcium and potassium hydrogen phosphate compounds, which have the ability to adsorb radionuclides, were found in the mineral composition of the digestate [18].

The factors that influence the migration of radionuclides into the ecosystem and the impact of the organo-mineral complex on the fixation of heavy metals and radionuclides in soils are described in Figure 9.

Thus, the uptake of radionuclides by plants and their accumulation by chemicals in crop fields are largely dependent on the amount of their chemical analogues in the environment. An increase in the exchange capacity usually leads to an increase in the adsorption strength of radionuclide traces. Therefore, the accumulation of 137Cs by plants in most cases is inversely proportional to the absorption capacity of the soil and the amount of exchangeable K in it, and for 90Sr [3]. The uptake of 90Sr and 137Cs by plants decreases with an increase in the content of calcium and potassium in the soil or growing medium [18].

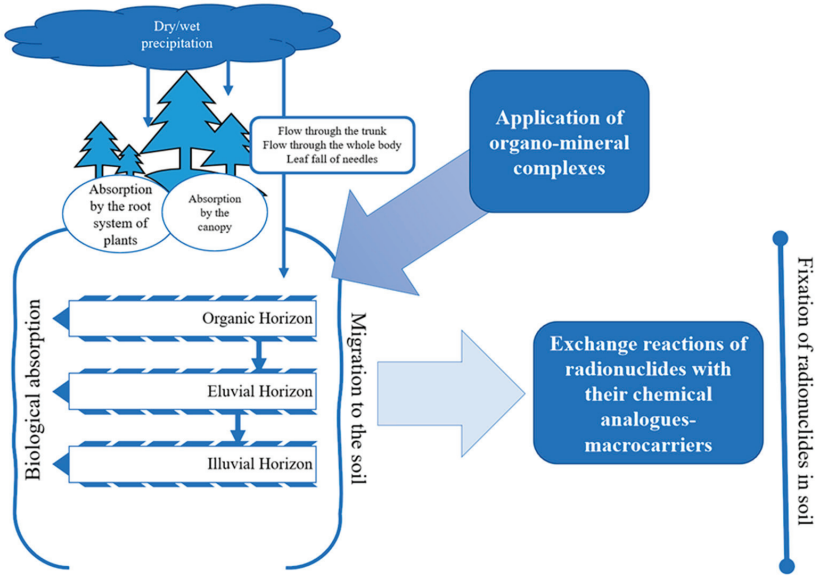

Figure 9. Influence of the organic–mineral complex on the fixation of heavy metals and radionuclides in soils.

6. Conclusions

A review of studies of heavy metal content was conducted in radioactively contaminated areas. In particular, the sources of heavy metals and radionuclides in the soil and their impact on ecosystem services with inclusion in food chains were identified. This article discusses the important issue that is the remediation of soils contaminated with heavy metals and radionuclides, especially if these toxicants are present simultaneously in contaminated areas. Therefore, remediation methods should take into account the specificity of both of them.

The advantages and disadvantages of immobilising heavy metals and radionuclides are identified using biosorption methods. Technical problems associated with the use and regeneration of local biosorbents have hindered the commercialisation of biosorption technologies. The immobilisation of biomass on solid inert carriers (e.g., biochar, zeolite, and vermiculite) can partially solve this problem. However, the issue of regeneration and replacement of the biosorbent in case of its complete exhaustion arises. In addition, the directions for the use of phosphogypsum as a sorption carrier for soil bioremediation were determined. It is necessary to take into account the neutralisation of phosphogypsum in this field as a promising one, which requires further research within the framework of the development of the biogeosystem approach. It should be noted that the post-war restoration of the contaminated territories of Ukraine is a complex and strategic task within the framework of the global issue of food security.

Author Contributions: Conceptualisation, Y.C.; validation, H.R.; formal analysis, P.S., V.C. and M.S.; investigation, V.C. and P.S.; writing—original draft preparation, Y.C.; writing—review and editing, I.A., V.C., P.S., O.Y., L.P. and H.R.; visualization, I.A., P.S. and V.C.; funding acquisition, Y.C. and H.R.; supervision, H.R. All authors have read and agreed to the published version of the manuscript.

Funding: This project, "Phosphogypsum as a mineral resource for bioprocesses", received funding through the MSCA4Ukraine project, which is funded by the European Union (Y.Ch.). This research project was carried out as planned research projects of the Department of Ecology and Environmental Protection Technologies of Sumy State University, related to the topics "Assessment of the technogenic load of the region with changes in industrial infrastructure" according to the scientific and technical

programme of the Ministry of Education and Science of Ukraine (state registration no 0121U114478). Finally, we would like to acknowledge Technology Agency of the Czech Republic (Grant Number TH79020003; support for this project is offered under the coordination of the ERA-MIN3 action, which received funding from the European Union under the Horizon 2020 Programme (European Commission Grant Agreement No. 101003575).

Institutional Review Board Statement: Not applicable.

Informed Consent Statement: Not applicable.

Data Availability Statement: The data sets generated during and/or analysed during the current study are available from the corresponding author on request.

Conflicts of Interest: The authors declare that they have no competing interests.

References

1. Zhang, J.; Chen, Q.; Tian, L.; Shi, K.; Wu, M. Environmental-Friendly Remediation Technology and Its Application in Heavy Metal Polluted Soil. *Mater. Rep.* **2023**, *37*, 21030018-11.
2. Bhaduri, D.; Sihi, D.; Bhowmik, A.; Verma, B.C.; Munda, S.; Dari, B. A Review on Effective Soil Health Bio-Indicators for Ecosystem Restoration and Sustainability. *Front. Microbiol.* **2022**, *13*, 938481. [CrossRef] [PubMed]
3. Chornobyl Radiation Ecological Biosphere Reserve. History of Creation. Available online: https://zapovidnyk.org.ua/index.php?fn=istor (accessed on 22 January 2023).
4. Morooka, K.; Kurihara, E.; Takehara, M.; Takami, R.; Fueda, K.; Horie, K.; Takehara, M.; Yamasaki, S.; Ohnuki, T.; Grambow, B.; et al. New Highly Radioactive Particles Derived from Fukushima Daiichi Reactor Unit 1: Properties and Environmental Impacts. *Sci. Total Environ.* **2021**, *773*, 145639. [CrossRef] [PubMed]
5. Akbay, C.; Aytop, H.; Dikici, H. Evaluation of Radioactive and Heavy Metal Pollution in Agricultural Soil Surrounding the Lignite-Fired Thermal Power Plant Using Pollution Indices. *Int. J. Environ. Health Res.* **2023**, *33*, 1490–1501. [CrossRef] [PubMed]
6. Melnychuk, A.O.; Tarariko, M.Y. Eco-Energy and Economic Efficiency of Alternative Fertilization Systems on Radioactively Contaminated Soils of Polissya of Ukraine. *Agroecol. J. Sci. Theor.* **2015**, *1*, 121–125. [CrossRef]
7. Bulyhin, S.Y.; Vitvitskyi, S.V.; Bulanyi, O.V.; Tonkha, O.L. *Monitoring of Quality of Soils*; Publishing House of the National University of Life and Environmental Sciences of Ukraine: Kyiv, Ukraine, 2019; 421p.
8. Feng, G.; Yong, J.; Liu, Q.; Chen, H.; Mao, P. Response of Soil Microbial Communities to Natural Radionuclides along Specific-Activity Gradients. *Ecotoxicol. Environ. Saf.* **2022**, *246*, 114156. [CrossRef] [PubMed]
9. Horvath, M.; Heltai, G.; Várhegyi, A.; Mbokazi, L.A. Study on the Possible Relationship between Physico-Chemical Properties of the Covering Soil and the Mobility of Radionuclides and Potentially Toxic Elements in a Recultivated Spoil Bank. *Minerals* **2022**, *12*, 1534. [CrossRef]
10. Dinis, M.D.L.; Fiúza, A.; Góis, J.; de Carvalho, J.S.; Meira Castro, A.C. Assessment of Natural Radioactivity, Heavy Metals, and Particulate Matter in Air and Soil around a Coal-Fired Power Plant—An Integrated Approach. *Atmosphere* **2021**, *12*, 1433. [CrossRef]
11. Kim, J.H.; Anwer, H.; Kim, Y.S.; Park, J.-W. Decontamination of Radioactive Cesium-Contaminated Soil/Concrete with Washing and Washing Supernatant—Critical Review. *Chemosphere* **2021**, *280*, 130419. [CrossRef]
12. Yang, L.; Fan, L.; Huang, B.; Xin, J. Efficiency and mechanisms of fermented horse manure, vermicompost, bamboo biochar, and fly ash on Cd accumulation in rice. *Environ. Sci. Pollut. Res. Int.* **2020**, *27*, 27859–27869. [CrossRef]
13. Yin, A.; Shen, C.; Huang, Y.; Yue, M.; Huang, B.; Xin, J. Reduction of Cd accumulation in Se-biofortified rice by using fermented manure and fly ash. *Environ. Sci. Pollut. Res. Int.* **2020**, *27*, 39391–39401. [CrossRef]
14. Shen, C.; Fu, H.; Huang, B.; Liao, Q.; Huang, Y.; Wang, Y.; Wang, Y.; Xin, J. Physiological and molecular mechanisms of boron in alleviating cadmium toxicity in Capsicum annuum. *Sci. Total Environ.* **2023**, *903*, 166264. [CrossRef]
15. Huang, B.; Liao, Q.; Fu, H.; Ye, Z.; Mao, Y.; Luo, J.; Wang, Y.; Yuan, H.; Xin, J. Effect of potassium intake on cadmium transporters and root cell wall biosynthesis in sweet potato. *Ecotoxicol. Environm. Saf.* **2023**, *250*, 114501. [CrossRef]
16. Selim, H.M. (Ed.) *Phosphate in Soils*; CRC Press: Boca Raton, FL, USA, 2018.
17. Pozzebon, E.A.; Seifert, L. Emerging Environmental Health Risks Associated with the Land Application of Biosolids: A Scoping Review. *Environ. Health* **2023**, *22*, 57. [CrossRef]
18. Chernysh, Y.; Balintova, M.; Shtepa, V.; Skvortsova, P.; Skydanenko, M.; Fukui, M. Integration of Processes of Radionuclide-Contaminated Territories Decontamination in the Framework of Their Ecological-Socio-Economic Rehabilitation. *Ecol. Eng. Environ. Technol.* **2022**, *23*, 110–124. [CrossRef]
19. Awasthi, G.; Nagar, V.; Mandzhieva, S.; Minkina, T.; Sankhla, M.S.; Pandit, P.P.; Aseri, V.; Awasthi, K.K.; Rajput, V.D.; Bauer, T.; et al. Sustainable Amelioration of Heavy Metals in Soil Ecosystem: Existing Developments to Emerging Trends. *Minerals* **2022**, *12*, 1. [CrossRef]
20. Basu, S.; Banerjee, P.; Banerjee, S.; Ghosh, B.; Bhattacharjee, A.; Roy, D.; Singh, P.; Kumar, A.A. Bioremediation Strategies to Overcome Heavy Metals and Radionuclides from the Environment. In *Development in Wastewater Treatment Research and Processes*; Elsevier: Amsterdam, The Netherlands, 2022; pp. 287–302. [CrossRef]

21. Bakshi, S.; Banik, C.; He, Z. The Impact of Heavy Metal Contamination on Soil Health. In *Managing Soil Health for Sustainable Agriculture*; Reicosky, D., Ed.; Burleigh Dodds Science Publishing: Cambridge, UK, 2018; Volume 2, pp. 1–36.
22. Nyiramigisha, P.; Komariah, A.; Sajidan, M. Harmful Impacts of Heavy Metal Contamination in the Soil and Crops Grown Around Dumpsites. *Rev. Agric. Sci.* **2021**, *9*, 271–282. [CrossRef] [PubMed]
23. Somani, M.; Datta, M.; Gupta, S.K.; Sreekrishnan, T.R.; Ramana, G.V. Comprehensive Assessment of the Leachate Quality and Its Pollution Potential from Six Municipal Waste Dumpsites of India. *Bioresour. Technol. Rep.* **2019**, *6*, 198–206. [CrossRef]
24. Ramelli, G.P.; Taddeo, I.; Herrmann, U.; Weber, P. Toxicological Profile for Cadmium: U.S. Department of Health and Human Services Public Health Service Agency for Toxic Substances and Disease Registry. *Eur. J. Paediatr. Neurol.* **2012**, *13*, 105–180. [CrossRef]
25. Rezapour, S.; Samadi, A.; Kalavrouziotis, I.K.; Ghaemian, N. Impact of the Uncontrolled Leakage of Leachate from a Municipal Solid Waste Landfill on Soil in a Cultivated-Calcareous Environment. *Waste Manag.* **2018**, *82*, 51–61. [CrossRef] [PubMed]
26. Khan, A.; Khan, S.; Khan, M.A.; Qamar, Z.; Waqas, M. The Uptake and Bioaccumulation of Heavy Metals by Food Plants, Their Effects on Plants Nutrients, and Associated Health Risk: A Review. *Environ. Sci. Pollut. Res.* **2015**, *22*, 13772–13799. [CrossRef] [PubMed]
27. Rashid, A.; Ayub, M.; Ullah, Z.; Ali, A.; Sardar, T.; Iqbal, J.; Gao, X.; Bundschuh, J.; Li, C.; Khattak, S.A.; et al. Groundwater Quality, Health Risk Assessment, and Source Distribution of Heavy Metals Contamination around Chromite Mines: Application of GIS, Sustainable Groundwater Management, Geostatistics, PCAMLR, and PMF Receptor Model. *Int. J. Environ. Res. Public Health* **2023**, *20*, 2113. [CrossRef] [PubMed]
28. Raheem, A.; Sikarwar, V.S.; He, J.; Dastyar, W.; Dionysiou, D.D.; Wang, W.; Zhao, M. Opportunities and Challenges in Sustainable Treatment and Resource Reuse of Sewage Sludge: A Review. *Chem. Eng. J.* **2018**, *337*, 616–641. [CrossRef]
29. Beschkov, V. Control of Pollution in the Non-Ferrous Metals Industry. In: Control of Pollution in the Non-ferrous Metals Industry. Available online: http://www.eolss.net/sample-chapters/c09/e4-14-04-05.pdf (accessed on 19 January 2023).
30. Pan, X.; Zhang, S.; Zhong, Q.; Gong, G.; Wang, G.; Guo, X.; Xu, X. Effects of soil chemical properties and fractions of Pb, Cd, and Zn on bacterial and fungal communities. *Sci. Total Environ.* **2020**, *715*, 136904. [CrossRef] [PubMed]
31. Zhang, J.; Sun, X.; Deng, J.; Li, G.; Li, Z.; Jiang, J.; Wu, Q.; Duan, L. Emission characteristics of heavy metals from a typical copper smelting plant. *J. Hazard. Mater.* **2021**, *424*, 127311. [CrossRef] [PubMed]
32. Fekiacova, Z.; Cornu, S.; Pichat, S. Tracing contamination sources in soils with Cu and Zn isotopic ratios. *Sci. Total Environ.* **2015**, *517*, 96–105. [CrossRef]
33. Müller, A.K.; Westergaard, K.; Christensen, S.; Sørensen, S.J. The effect of long-term mercury pollution on the soil microbial community. *FEMS Microbiol. Ecol.* **2001**, *36*, 11–19. [CrossRef]
34. Pacyna, J.M.; Sundseth, K.; Pacyna, E.G. Sources and Fluxes of Harmful Metals. In *Environmental Determinants of Human Health. Molecular and Integrative Toxicology*; Pacyna, J., Pacyna, E., Eds.; Springer: Cham, Switzerland, 2016. [CrossRef]
35. Environment Agency. Ferrous and Non-Ferrous Metals: Pollution Inventory Reporting. Available online: https://www.gov.uk/government/publications/pollution-inventory-reporting-guidance-notes/ferrous-and-non-ferrous-metals-pollution-inventory-reporting (accessed on 20 December 2023).
36. Qi, M.; Wu, Y.; Zhang, S.; Li, G.; An, T. Pollution Profiles, Source Identification and Health Risk Assessment of Heavy Metals in Soil near a Non-Ferrous Metal Smelting Plant. *Int. J. Environ. Res. Public. Health* **2023**, *20*, 1004. [CrossRef]
37. Non-Ferryytrrous Metals—AR4 WGIII Chapter 7: Industry. IPCC—Intergovernmental Panel on Climate Change. Available online: https://archive.ipcc.ch/publications_and_data/ar4/wg3/en/ch7s7-4-2.html (accessed on 20 December 2023).
38. United Nations Environment Programme. UNEP Global Mercury Partnership Study Report on Mercury from Non-Ferrous Metals Mining and Smelting. 2021. Available online: https://www.unep.org/globalmercurypartnership/resources/report/mercury-non-ferrous-metals-mining-and-smelting (accessed on 21 December 2023).
39. Emission Control for Non-Ferrous Industry. GEA Engineering for a Better World. Available online: https://www.gea.com/en/chemical/emission-control/non-ferrous.jsp (accessed on 20 December 2023).
40. Basta, N.T.; Ryan, J.A.; Chaney, R.L. Trace Element Chemistry in Residual-Treated Soil: Key Concepts and Metal Bioavailability. *J. Environ. Qual.* **2005**, *34*, 49–63. [CrossRef]
41. Rosen, V.; Chen, Y. Effects of Compost Application on Soil Vulnerability to Heavy Metal Pollution. *Environ. Sci. Pollut. Res.* **2018**, *25*, 35221–35231. [CrossRef]
42. Raymond, A.W.; Felix, E.O. Heavy Metals in Contaminated Soils: A Review of Sources, Chemistry, Risks, and Best Available Strategies for Remediation. *Int. Sch. Res. Netw. ISRN Ecol.* **2012**, *2011*, 402647. [CrossRef]
43. Symkanych, O.I.; Sukharev, S.M.; Delehan-Kokayko, S.V.; Maslyuk, V.T.; Svatyuk, A.N.I. Distribution of Heavy Metals and Radionuclides in the Protected Areas of Transcarpathia. Uzhhorod University Scientific Herald. *Series Physics* **2015**, *3*, 145–152.
44. Savchuk, I.M.; Romanchuk, L.D.; Yashchuk, I.V.; Kovalyova, S.P.; Bondarchuk, L.V. Monitoring of Heavy Metals in Fodder and Animal Husbandry Products of the Polissia Zone of Ukraine. *Sci. Horiz.* **2022**, *25*, 45–54. [CrossRef]
45. Yang, Z.; Zhang, W.; Wu, W.; Ma, Z.; Li, H.; Zhang, L. Study on Remediation Effect of Radioactive-Heavy Metal Contaminated Soil in Stone Coal Mines by Chemical Elution. *Coal Sci. Technol.* **2022**, *50*, 261–266.
46. Mohuba, S.C.; Abiye, T.A.; Demlie, M.B.; Nhleko, S. Natural Radioactivity and Metal Concentration in the Thyspunt Area, Eastern Cape Province, South Africa. *Environ. Monit. Assess.* **2022**, *194*, 112. [CrossRef]

47. Baghdady, A.; Awad, S.; Gad, A. Assessment of Metal Contamination and Natural Radiation Hazards in Different Soil Types Near Iron Ore Mines, Bahariya Oasis, Egypt. *Arab. J. Geosci.* **2018**, *11*, 506. [CrossRef]
48. Mitrovic, B.; Vranjes, B.; Kostic, O.; Perovic, V.; Mitrovic, M.; Pavlovic, P. Radionuclides and Heavy Metals in Soil, Vegetables, and Medicinal Plants in Suburban Areas of the Cities of Belgrade and Pancevo, Serbia. *Nucl. Technol. Radiat. Prot.* **2019**, *34*, 278–284. [CrossRef]
49. Cuenca, R.H.; Hagimoto, Y.; Moghaddam, M. Three-and-a-half Decades of Progress in Monitoring Soils and Soil Hydraulic Properties. *Procedia Environ. Sci.* **2013**, *19*, 384–393. [CrossRef]
50. Lee, C.; Park, S.-W.; Kim, A.H.R. Development of Mobile Scanning System for Effective In-Situ Spatial Prediction of Radioactive Contamination at Decommissioning Sites. *Nucl. Instrum. Methods Phys. Res.* **2020**, *966*, 163833. [CrossRef]
51. Bida, P.I.; Rudko, O.M.; Malimon, S.S.; Kushniruk, A.O.M. Introduction of Drainage and Sorption Systems on Radioactively Contaminated Peat Soils of Polissya of Ukraine. *Environ. Sci.* **2020**, *5*, 36–40. [CrossRef]
52. Chobotko, H.M.; Landin, V.P.; Yaskovets, I.I.; Raichuk, L.A.; Shvydenko, I.K. Radiologically Critical Ecosystems and Their Role in the Formation of Contamination of Agricultural Products. *Ahroekolohichnyi Zhurnal* **2018**, *4*, 29–35. [CrossRef]
53. Kovalyova, S.P.; Mozharivska, I.A. Heavy Metal Concentration in Soils while Growing Energy Crops in the Radioactively Contaminated Territory. *Sci. Horiz.* **2020**, *3*, 121–126. [CrossRef]
54. Yoon, I.-H.; Park, C.W.; Kim, I.; Yang, H.-M.; Kim, S.-M.; Kim, J.-H. Characteristic and Remediation of Radioactive Soil in Nuclear Facility Sites: A Critical Review. *Environ. Sci. Pollut. Res.* **2021**, *28*, 67990–68005. [CrossRef] [PubMed]
55. Lysenko, L.; Mishchuk, N.; Kovalchuk, V. Basic Principles and Problems in Decontamination of Natural Disperse Systems. *Electrokinet. Treat. Soils. Adv. Colloid. Interface Sci.* **2022**, *310*, 102798. [CrossRef] [PubMed]
56. Impens, N.R.E.N.; Jensen, K.A.; Skipperud, L.; Gompel, A.V.; Vanhoudt, N. In-Depth Understanding of Local. Soil. Chemistry Reveals That Addition of Ca May Counteract the Mobilisation of 226Ra and Other Pollutants before Wetland Creation on the Grote Nete River Banks. *Sci. Total Environ.* **2022**, *823*, 153703. [CrossRef] [PubMed]
57. Salbu, B.; Lind, O.C. Analytical Techniques for Characterizing Radioactive Particles Deposited in the Environment. *J. Environ. Radioact.* **2020**, *211*, 106078. [CrossRef] [PubMed]
58. Arora, V.; Khosla, A.B. Conventional and Contemporary Techniques for Removal of Heavy Metals from Soil. In *Biodegradation Technology of Organic and Inorganic Pollutants*, 2nd ed.; Mendes, K.F., Sousa, R.N., Mielke, K.C., Eds.; IntechOpen: Rijeka, Croatia, 2021; Volume 3, pp. 154–196. [CrossRef]
59. Groudeva, V.I.; Doycheva, A.; Krumova, K.; Groudev, S.N. Bioremediation In Situ of an Alkaline Soil Polluted with Heavy Metals. *Adv. Mater. Res.* **2007**, *20–21*, 287–290. [CrossRef]
60. Marcon, L.; Oliveras, J.; Puntes, V.F. In Situ Nanoremediation of Soils and Groundwaters from the Nanoparticle's Standpoint: A Review. *Sci. Total Environ.* **2021**, *791*, 148324. [CrossRef] [PubMed]
61. Bhatt, J.; Desai, S.; Wagh, N.S.; Lakkakula, J. New Bioremediation Technologies to Remove Heavy Metals and Radionuclides. In *Industrial Wastewater Reuse*; Springer Nature Singapore: Singapore, 2023; pp. 267–316.
62. Zhang, H.; Chen, Y.; Liu, S.X.; Jachimowicz, A.E.; Li, A. Big Data Research on Agricultural Soil Contamination by Zeolite Application. *J. Elem.* **2022**, *27*, 265–287. [CrossRef]
63. Kornilovich, B.; Mishchuk, N.; Abbruzzese, K.; Pshinko, G.; Klishchenko, R. Enhanced Electrokinetic Remediation of Metals-Contaminated Clay. *Colloids Surf. A Physicochem. Eng. Asp.* **2005**, *265*, 114–123. [CrossRef]
64. Megharaj, M.; Venkateswarlu, K.; Naidu, R. Bioremediation. In *Encyclopedia of Toxicology*; Elsevier: Amsterdam, The Netherlands, 2014; pp. 485–489. [CrossRef]
65. Nadaf, M.; Jadav, K.D.; Gingine, V. *Decontamination of Soil by Electro Kinetic Treatment*; Lecture Notes in Civil Engineering; Springer: Singapore, 2021; pp. 91–103. [CrossRef]
66. Olodovskii, P. Theory of the Effect of Inhibition of the Transfer of Radionuclides and Heavy Metals from Soil to Plants by an Ameliorant. V. Calculation of the Binding Energy of Exchange Ions in Disperse Systems with Low pH. *J. Eng. Phys. Thermophys.* **2001**, *74*, 243–249. [CrossRef]
67. Sethi, S. Holistic Approach to Remediate Heavy Metals and Radionuclides. In *Industrial Wastewater Reuse*; Springer Nature: Singapore, 2023; pp. 113–132. [CrossRef]
68. Chandra, D.; General, T.; Nisha; Chandra, S. Microorganisms: An Asset for Decontamination of Soil. In *Smart Bioremediation Technologies*; Academic Press: Cambridge, MA, USA, 2019; pp. 319–345.
69. Gadd, G.M. Heavy Metal Pollutants: Environmental and Biotechnological Aspects. In *Reference Module in Life Sciences*; Elsevier: Amsterdam, The Netherlands, 2019.
70. Mishra, M.; Mohan, D. Bioremediation of Contaminated Soils: An Overview. In *Adaptive Soil Management: From Theory to Practices*; Springer: Singapore, 2017; pp. 323–337.
71. Singh, B.S.M.; Singh, D.; Dhal, N.K. Enhanced Phytoremediation Strategy for Sustainable Management of Heavy Metals and Radionuclides. *Case Stud. Chem. Environ. Eng.* **2022**, *5*, 100176. [CrossRef]
72. Devedee, A.K.; Sahoo, M.; Choudhary, K.; Singh, M.; Ghanshyam. Bioremediation of Soil: An Overview. In *Microbes and Microbial Biotechnology for Green Remediation*; Elsevier: Amsterdam, The Netherlands, 2022; pp. 13–27.
73. Phian, S.; Nagar, S.; Kaur, J.; Rawat, C.D. Emerging Issues and Challenges for Microbes-Assisted Remediation. In *Microbes and Microbial Biotechnology for Green Remediation*; Elsevier: Amsterdam, The Netherlands, 2022; pp. 47–89.

74. Xing, Y.; Tan, S.; Liu, S.; Xu, S.; Wan, W.; Huang, Q.; Chen, W. Effective Immobilization of Heavy Metals via Reactive Barrier by Rhizosphere Bacteria and Their Biofilms. *Environ. Res.* **2022**, *207*, 112080. [CrossRef]
75. Chen, P.; Liu, Y.; Sun, G.-X. Evaluation of Water Management on Arsenic Methylation and Volatilization in Arsenic-Contaminated Soils Strengthened by Bioaugmentation and Biostimulation. *J. Environ. Sci.* **2024**, *137*, 515–526. [CrossRef]
76. Khalid, M.; Liu, X.; ur Rahman, S.; Rehman, A.; Zhao, C.; Li, X.; Yucheng, B.; Hui, N. Responses of Microbial Communities in Rhizocompartments of King Grass to Phytoremediation of Cadmium-Contaminated Soil. *Sci. Total Environ.* **2023**, *904*, 167226. [CrossRef] [PubMed]
77. Li, S.; Wu, X.; Xie, J. Biomineralization Technology for Solidification/Stabilization of Heavy Metals in Ecosystem: Status and Perspective. *Front. Ecol. Evol.* **2023**, *11*, 1189356. [CrossRef]
78. Mendoza-Burguete, Y.; de la Luz Pérez-Rea, M.; Ledesma-García, J.; Campos-Guillén, J.; Ramos-López, M.A.; Guzmán, C.; Rodríguez-Morales, J.A. Global Situation of Bioremediation of Leachate-Contaminated Soils by Treatment with Microorganisms: A Systematic Review. *Microorganisms* **2023**, *11*, 857. [CrossRef] [PubMed]
79. Lai, H.-J.; Ding, X.-Z.; Cui, M.-J.; Zheng, J.-J.; Chen, Z.-B.; Pei, J.-L.; Zhang, J.-W. Mechanisms and Influencing Factors of Biomineralization Based Heavy Metal Remediation: A Review. *Biogeotechnics* **2023**, *1*, 100039. [CrossRef]
80. Li, M.; Cheng, X.; Guo, H. Heavy metal removal by biomineralization of urease producing bacteria isolated from soil. *Int. Biodeterior. Biodegrad.* **2013**, *76*, 81–85. [CrossRef]
81. Lopez-Fernandez, M.; Jroundi, F.; Ruiz-Fresneda, M.A.; Merroun, M.L. Microbial interaction with and tolerance of radionuclides: Underlying mechanisms and biotechnological applications. *Microb. Biotechnol.* **2020**, *14*, 810–828. [CrossRef] [PubMed]
82. Zhang, W.; Zhang, H.; Xu, R.; Qin, H.; Liu, H.; Zhao, K. Heavy metal bioremediation using microbially induced carbonate precipitation: Key factors and enhancement strategies. *Front. Microbiol.* **2023**, *14*, 1116970. [CrossRef]
83. Renshaw, J.; Mackay, R.; Macaskie, L. Immobilization of Metals and Radionuclides by Microbial Biomineralization Processes. Available online: https://www.birmingham.ac.uk/Documents/college-les/gees/biomineralizationprocesses.pdf (accessed on 21 December 2023).
84. Priya, A.K.; Gnanasekaran, L.; Dutta, K.; Rajendran, S.; Balakrishnan, D.; Soto-Moscoso, M. Biosorption of Heavy Metals by Microorganisms: Evaluation of Different Underlying Mechanisms. *Chemosphere* **2022**, *307*, 135957. [CrossRef]
85. Vasconcellos, S.; Paganotti, A.; Vital, V.G.; Santos Lima, L.M.; Paiva, G.M.S.; de Lima, L.F.; Moreira, E.; Sousa, L.O.; Guerini, G.G.; Santos, V.T.; et al. Biotransformation of Metal-Rich Effluents and Potential Recycle Applications. In *Bioremediation for Global Environmental Conservation*; IntechOpen: Rijeka, Croatia, 2023. [CrossRef]
86. White, C.; Wilkinson, S.C.; Gadd, G.M. The role of microorganisms in biosorption of toxic metals and radionuclides. *Int. Biodeterior. Biodegrad.* **1995**, *35*, 17–40. [CrossRef]
87. Gavrilescu, M. Removal of heavy metals from the environment by biosorption. *Eng. Life Sci.* **2004**, *4*, 219–232. [CrossRef]
88. Das, N. Remediation of Radionuclide Pollutants through Biosorption—An Overview. *Clean. Soil. Air Water* **2012**, *40*, 16–23. [CrossRef]
89. Kotrba, P. Microbial Biosorption of Metals—General Introduction. In *Microbial Biosorption of Metals*; Kotrba, P., Mackova, M., Macek, T., Eds.; Springer: Dordrecht, The Netherlands, 2011. [CrossRef]
90. Zabochnicka-Świątek, M.; Krzywonos, M. Potentials of Biosorption and Bioaccumulation Processes for Heavy Metal Removal. *Pol. J. Environ. Studies.* **2014**, *23*, 551–561.
91. Mathew, A.T.; Saravanakumar, M.P. Removal of Bisphenol A and Methylene Blue by α -MnO_2 Nanorods: Impact of Ultrasonication, Mechanism, Isotherm, and Kinetic Models. *J. Hazard. Toxic Radioact. Waste* **2021**, *25*, 04021005. [CrossRef]
92. Fomina, M.; Gadd, G.M. Biosorption: Current perspectives on concept, definition and application. *Bioresour. Technol.* **2014**, *160*, 3–14. [CrossRef] [PubMed]
93. Janyasuthwiong, S.; Rene, E.R. Bioprecipitation—A Promising Technique for Heavy Metal Removal and Recovery from Contaminated Wastewater Streams. *MOJ Civil. Eng.* **2017**, *2*, 191–193. [CrossRef]
94. Kim, Y.; Kwon, S.; Roh, Y. Effect of Divalent Cations (Cu, Zn, Pb, Cd, and Sr) on Microbially Induced Calcium Carbonate Precipitation and Mineralogical Properties. *Front. Microbiol.* **2021**, *12*, 646748. [CrossRef]
95. Pande, V.; Pandey, S.C.; Sati, D.; Bhatt, P.; Samant, M. Microbial Interventions in Bioremediation of Heavy Metal Contaminants in Agroecosystem. *Front. Microbiol.* **2022**, *13*, 824084. [CrossRef] [PubMed]
96. Xu, Q.; Wu, B.; Chai, X. In Situ Remediation Technology for Heavy Metal Contaminated Sediment: A Review. *Int. J. Environ. Res. Public Health* **2022**, *19*, 16767. [CrossRef] [PubMed]
97. Mugwar, A. Bioprecipitation of Heavy Metals and Radionuclides with Calcium Carbonate in Aqueous Solutions and Particulate Media. Cardiff University. 2015. Available online: https://www.semanticscholar.org/paper/Bioprecipitation-of-heavy-metals-andradionuclides-Mugwar/a0070cd67b0c051e674db74c8257ad955d79c308 (accessed on 21 December 2023).
98. Kumari, D.; Qian, X.Y.; Pan, X.; Achal, V.; Li, Q.; Gadd, G.M. Microbially-induced Carbonate Precipitation for Immobilization of Toxic Metals. *Adv. Appl. Microbiol.* **2016**, *94*, 79–108. [CrossRef] [PubMed]
99. Nnaji, N.D.; Onyeaka, H.; Miri, T.; Ugwa, C. Bioaccumulation for Heavy Metal Removal: A Review. *SN Appl. Sci.* **2023**, *5*, 125. [CrossRef]
100. Rahmat, M.A.; Ismail, A.F.; Rodzi, N.D.; Aziman, E.S.; Idris, W.M.R.; Lihan, T. Assessment of natural radionuclides and heavy metals contamination to the environment: Case study of Malaysian unregulated tin-tailing processing industry. *Nucl. Eng. Technol.* **2022**, *54*, 2230–2243. [CrossRef]

101. Zalewska, T.; Saniewski, M. Bioaccumulation of gamma emitting radionuclides in red algae from the Baltic Sea under laboratory conditions. *Oceanologia* **2011**, *53*, 631–650. [CrossRef]
102. Abdelkarim, M.S.; Imam, N. Radiation hazards and extremophiles bioaccumulation of radionuclides from hypersaline lakes and hot springs. *Int. J. Environ. Sci. Technol.* **2023**, *21*, 3021–3036. [CrossRef]
103. Borghei, S.M.; Arjmandi, R.; Moogouei, R. Bioaccumulation of Radionuclide Metals in Plants: A Case Study of Cesium. In *Radionuclide Contamination and Remediation Through Plants*; Springer International Publishing: Cham, Switzerland, 2014; pp. 177–195. [CrossRef]
104. Srisuksawad, K.; Prasertchiewchan, N. Experimental Studies on the Bioaccumulation of Selected Heavy Metals and Radionuclides in the Blood Cockle Anadara granosa of the Bang Pakong Estuary. *Environ. Bioindic.* **2007**, *2*, 253–263. [CrossRef]
105. Tykva, R. Sources of Environmental Radionuclides and Recent Results in Analyses of Bioaccumulation. *A review. Nukleonika* **2004**, *49*. Available online: https://bibliotekanauki.pl/articles/147281 (accessed on 22 December 2023).
106. Diaz-Bone, R.; Van de Wiele, T. Biotransformation of metal(loid)s by intestinal microorganisms. *Pure Appl. Chemistry.* **2010**, *82*, 409–427. [CrossRef]
107. Jabbar, T.; Wallner, G. Biotransformation of Radionuclides: Trends and Challenges. In *Radionuclides in the Environment*; Walther, C., Gupta, D., Eds.; Springer: Cham, Switzerland, 2015. [CrossRef]
108. Lloyd, J.R.; Lovley, D.R. Microbial detoxification of metals and radionuclides. *Curr. Opin. Biotechnol.* **2001**, *12*, 248–253. [CrossRef] [PubMed]
109. Francis, A. Microbial Transformations of Radionuclides and Environmental Restoration through Bioremediation. Symposium on "Emerging Trends in Separation Science and Technology" SESTEC 2006 Bhabha Atomic Research Center (BARC), Trombay, Mumbai. Brookhaven National Laboratory. 2006, pp. 1–15. Available online: https://citeseerx.ist.psu.edu/document?repid=rep1&type=pdf&doi=fdce929bc2c9995a1567fc17853c0b6b443cd3c8 (accessed on 22 December 2023).
110. Mani, D.; Kumar, C. Biotechnological advances in bioremediation of heavy metals contaminated ecosystems: An overview with special reference to phytoremediation. *Int. J. Environ. Sci. Technol.* **2014**, *11*, 843–872. [CrossRef]
111. Gadd, G.M. Geomicrobiology of Metal and Mineral Transformations in the Environment. Extremophiles. Encyclopedia of Life Support Systems. Available online: https://www.eolss.net/sample-chapters/c03/E6-38-18.pdf (accessed on 22 December 2023).
112. Thakare, M.; Sarma, H.; Datar, S.; Roy, A.; Pawar, P.; Gupta, K.; Pandit, S.; Prasad, R. Understanding the Holistic Approach to Plant-Microbe Remediation Technologies for Removing Heavy Metals and Radionuclides from Soil. *Curr. Res. Biotechnol.* **2021**, *3*, 84–98. [CrossRef]
113. Harher, Y.K.; Voitsekhovych, O.V. *Twenty-Five Years since the Chornobyl Disaster. Security of the Future*; National Report of Ukraine; KIM: Kyiv, Ukraine, 2011; pp. 39–42.
114. Chibuike, G.U.; Obiora, S.C. Heavy Metal Polluted Soils: Effect on Plants and Bioremediation Methods. *Appl. Environ. Soil. Sci.* **2014**, 752708. [CrossRef]
115. Yaashikaa, P.R.; Senthil Kumar, P.; Saravanan, A.; Vo, D.-V.N. Advances in Biosorbents for Removal of Environmental Pollutants: A Review on Pretreatment, Removal Mechanism, and Future Outlook. *J. Hazard. Mater.* **2021**, *420*, 126596. [CrossRef]
116. Kumar, M.; Seth, A.; Singh, A.K.; Rajput, M.S.; Sikandar, A.M. Remediation Strategies for Heavy Metals Contaminated Ecosystem: A Review. *J. Environ. Sustain.* **2021**, *12*, 100155. [CrossRef]
117. Priyadarshanee, M.; Das, S. Biosorption and Removal of Toxic Heavy Metals by Metal Tolerating Bacteria for Bioremediation of Metal Contamination: A Comprehensive Review. *J. Environ. Chem. Eng.* **2021**, *9*, 104686. [CrossRef]
118. Han, J.; Zhang, J.; Meng, J.; Cai, Y.; Cheng, M.; Wu, S.; Li, Z. Characterization of Modified Rice Straw Biochar in Immobilizing Bacillus subtilis 168 and Evaluation on Its Role as a Novel Agent for Zearalenone-Removal Delivery. *J. Hazard. Mater.* **2023**, *453*, 131424. [CrossRef]
119. Li, M.; Yao, J.; Sunahara, G.; Hawari, J.; Duran, R.; Liu, J.; Liu, B.; Cao, Y.; Pang, W.; Li, H.; et al. Novel Microbial Consortia Facilitate Metalliferous Immobilization in Non-Ferrous Metal(loid)s Contaminated Smelter Soil: Efficiency and Mechanisms. *Environ. Pollut.* **2022**, *313*, 120042. [CrossRef]
120. Zhang, Y.; Majeed, Z.; Tian, M.; Xie, Y.; Zheng, K.; Luo, Z.; Li, C.; Zhao, C. Application of Hydrogen-Bonded Organic Frameworks in Environmental Remediation. *Separations* **2023**, *10*, 196. [CrossRef]
121. Qi, X.; Xiao, S.; Chen, X.; Ali, I.; Gou, J.; Wang, D.; Zhu, B.; Zhu, W.; Shang, R.; Han, M. Biochar-Based Microbial Agent Reduces U and Cd Accumulation in Vegetables and Improves Rhizosphere Microecology. *J. Hazard. Mater.* **2022**, *436*, 129147. [CrossRef]
122. Oziegbe, O.; Oluduro, A.O.; Oziegbe, E.J.; Ahuekwe, E.F.; Olorunsola, S.J. Assessment of Heavy Metal Bioremediation Potential of Bacterial Isolates from Landfill Soils. *Saudi J. Biol. Sci.* **2021**, *28*, 3948–3956. [CrossRef]
123. Maqsood, Q.; Sumrin, A.; Waseem, R.; Hussain, M.; Imtiaz, M.; Hussain, N. Bioengineered Microbial Strains for Detoxification of Toxic Environmental Pollutants. *Environ. Res.* **2023**, *227*, 115665. [CrossRef]
124. Salah-Tazdaït, R.; Tazdaït, D. *Phyto and Microbial Remediation of Heavy Metals and Radionuclides in the Environment*; Routledge: London, UK, 2022.
125. Singha, S.; Chatterjee, S. Soil Pollution by Industrial Effluents, Solid Wastes, and Reclamation Strategies by Microorganisms. In *Microbes and Microbial Biotechnology for Green Remediation*; Springer International Publishing: Cham, Switzerland, 2022; pp. 471–488.
126. Chen, Z.; Li, Q.; Yang, Y.; Sun, J.; Li, G.; Liu, X.; Shu, S.; Li, X.; Liao, H. Uranium Removal from a Radioactive Contaminated Soil by Defined Bioleaching Bacteria. *J. Radioanal. Nucl. Chem.* **2022**, *331*, 439–449. [CrossRef]

127. Bryukhanov, A.L.; Khijniak, T.V. The Application of Sulfate-Reducing Bacteria in the Bioremediation of Heavy Metals and Metalloids. *Appl. Biochem. Microbiol.* **2022**, *58* (Suppl. S1), S1–S15. [CrossRef]
128. Aslam, F.; Mazhar, S. Nano-Bioremediation of Heavy Metals from Environment Using a Green Synthesis Approach. *Int. J. Adv. Appl. Sci.* **2023**, *12*, 7. [CrossRef]
129. Bilal, E.; Bellefqih, H.; Bourgier, V.; Mazouz, H.; Dumitraş, D.-G.; Bard, F.; Laborde, M.; Caspar, J.P.; Guilhot, B.; Iatan, E.-L.; et al. Phosphogypsum Circular Economy Considerations: A Critical Review from More than 65 Storage Sites Worldwide. *J. Clean. Prod.* **2023**, *414*, 137561. [CrossRef]
130. Diwa, R.R.; Tabora, E.U.; Palattao, B.L.; Haneklaus, N.H.; Vargas, E.P.; Reyes, R.Y.; Ramirez, J.D. Evaluating radiation risks and resource opportunities associated with phosphogypsum in the Philippines. *J. Radioanal. Nucl. Chem.* **2022**, *331*, 967–974. [CrossRef]
131. TENORM: Fertilizer and Fertilizer Production Wastes. U.S. Environmental Protection Agency. Available online: https://www.epa.gov/radiation/tenorm-fertilizer-and-fertilizer-production-wastes (accessed on 22 December 2023).
132. Plyatsuk, L.; Balintova, M.; Chernysh, Y.; Demcak, S.; Holub, M.; Yakhnenko, E. Influence of Phosphogypsum Dump on the Soil Ecosystem in the Sumy region (Ukraine). *Appl. Sci.* **2019**, *9*, 5559. [CrossRef]
133. Mahmoud, E.; Ghoneim, A.M.; Seleem, M.; Zuhair, R.; El-Refaey, A.; Khalafallah, N. Phosphogypsum and Poultry Manure Enhance Diversity of Soil Fauna, Soil Fertility, and Barley (*Hordeum aestivum* L.) Grown in Calcareous Soils. *Sci. Rep.* **2023**, *13*, 9944. [CrossRef] [PubMed]
134. Qi, J.; Zhu, H.; Zhou, P.; Wang, X.; Wang, Z.; Yang, S.; Yang, D.; Li, B. Application of Phosphogypsum in Soilization: A Review. *Int. J. Environ. Sci. Technol.* **2023**, *20*, 10449–10464. [CrossRef]
135. Li, C.; Dong, Y.; Yi, Y.; Tian, J.; Xuan, C.; Wang, Y.; Wen, Y.; Cao, J. Effects of Phosphogypsum on Enzyme Activity and Microbial Community in Acid Soil. *Sci. Rep.* **2023**, *13*, 6189. [CrossRef] [PubMed]
136. Ben Mefteh, A.; Bouket, L.; Daoud, A.; Luptakova, L.; Alenezi, F.N.; Gharsallah, N.; Belbahri, L. Metagenomic Insights and Genomic Analysis of Phosphogypsum and Its Associated Plant Endophytic Microbiomes Reveals Valuable Actors for Waste Bioremediation. *Microorganisms* **2019**, *7*, 382. [CrossRef]
137. Lei, L.; Gu, J.; Wang, X.; Song, Z.; Wang, J.; Yu, J.; Hu, T.; Dai, X.; Xie, J.; Zhao, W. Microbial Succession and Molecular Ecological Networks Response to the Addition of Superphosphate and Phosphogypsum during Swine Manure Composting. *J. Environ. Manag.* **2021**, *279*, 111560. [CrossRef] [PubMed]
138. Trifi, H.; Najjari, A.; Achouak, W.; Barakat, M.; Ghedira, K.; Mrad, F.; Saidi, M.; Sghaier, H. Metataxonomics of Tunisian Phosphogypsum Based on Five Bioinformatics Pipelines: Insights for Bioremediation. *Genomics* **2020**, *112*, 981–989. [CrossRef]
139. Chernysh, Y.; Hasegawa, K. *Improvement of the Model System to Develop Eco-Friendly Bio-Utilization of Phosphogypsum*; Lecture Notes in Mechanical Engineering; Springer: Cham, Switzerland, 2020; pp. 357–366.
140. Ulianchuk-Martyniuk, O.V.; Michuta, O.R.; Ivanchuk, N.V. Finite Element Analysis of the Diffusion Model of the Bioclogging of the Geobarrier. *Eurasian J. Math. Comput. Appl.* **2021**, *9*, 100–111. [CrossRef]
141. Yimer, A.M.; Assen, A.H.; Mghaimimi, I.E.L.; Lakbita, O.; Adil, K.; Belmabkhout, Y. Unlocking the potential of phosphogypsum waste: Unified synthesis of functional metal-organic frameworks and zeolite via a sustainable valorization route. *Chem. Eng. J.* **2024**, *479*, 147902. [CrossRef]
142. Ait Brahim, J.; Merroune, A.; Mazouz, H.; Beniazza, R. Recovery of rare earth elements and sulfuric acid solution from phosphate byproducts via hydrofluoric acid conversion. *J. Ind. Eng. Chem.* **2023**, *127*, 446–453. [CrossRef]
143. Akfas, F.; Elghali, A.; Aboulaich, A.; Munoz, M.; Benzaazoua, M.; Bodinier, J.-L. Exploring the potential reuse of phosphogypsum: A waste or a resource? *Sci. Total Environ.* **2024**, *908*, 168196. [CrossRef]
144. Wei, Z.; Deng, Z. Research hotspots and trends of comprehensive utilization of phosphogypsum: Bibliometric analysis. *J. Environ. Radioact.* **2022**, *242*, 106778. [CrossRef]
145. Wang, J.; Dong, F.; Wang, Z.; Yang, F.; Du, M.; Fu, K.; Wang, Z. A novel method for purification of phosphogypsum. *Physicochem. Probl. Miner. Process.* **2020**, *56*, 975–983. [CrossRef]
146. Zou, C.; Shi, Z.; Yang, Y.; Zhang, J.; Hou, Y.; Zhang, N. The Characteristics, Enrichment, and Migration Mechanism of Cadmium in Phosphate Rock and Phosphogypsum of the Qingping Phosphate Deposit, Southwest China. *Minerals* **2023**, *13*, 107. [CrossRef]
147. Guan, Q.; Sui, Y.; Liu, C.; Wang, Y.; Zeng, C.; Yu, W.; Gao, Z.; Zang, Z.; Chi, R.-A. Characterization and Leaching Kinetics of Rare Earth Elements from Phosphogypsum in Hydrochloric Acid. *Minerals* **2022**, *12*, 703. [CrossRef]
148. Zhou, B.; Zhu, H.; Xu, S.; Du, G.; Shi, S.; Liu, M.; Xing, F.; Ren, J. Effect of phosphogypsum on the properties of magnesium phosphate cement paste with low magnesium-to-phosphate ratio. *Sci. Total Environ.* **2021**, *798*, 149262. [CrossRef] [PubMed]
149. Wu, F.; Liu, S.; Qu, G.; Chen, B.; Zhao, C.; Liu, L.; Li, J.; Ren, Y. Highly targeted solidification behavior of hazardous components in phosphogypsum. *Chem. Eng. J. Adv.* **2022**, *9*, 100227. [CrossRef]
150. Weiksnar, K.D.; Clavier, K.A.; Robey, N.M.; Townsend, T.G. Changes in trace metal concentrations throughout the phosphogypsum lifecycle. *Sci. Total Environ.* **2022**, *851*, 158163. [CrossRef]
151. Liang, H.; Zhang, P.; Jin, Z.; DePaoli, D. Rare earths recovery and gypsum upgrade from Florida phosphogypsum. *Miner. Metall. Process.* **2017**, *34*, 201–206. [CrossRef]
152. Al-Thyabat, S.; Zhang, P. REE extraction from phosphoric acid, phosphoric acid sludge, and phosphogypsum. *Miner. Process. Extr. Metall.* **2015**, *124*, 143–150. [CrossRef]

153. Romero-Hermida, M.I.; Flores-Alés, V.; Hurtado-Bermúdez, S.J.; Santos, A.; Esquivias, L. Environmental Impact of Phosphogypsum-Derived Building Materials. *Int. J. Environ. Res. Public Health* **2020**, *17*, 4248. [CrossRef]
154. Pérez-López, R.; Nieto, J.M.; López-Coto, I.; Aguado, J.L.; Bolívar, J.P.; Santisteban, M. Dynamics of contaminants in phosphogypsum of the fertilizer industry of Huelva (SW Spain): From phosphate rock ore to the environment. *Appl. Geochem.* **2010**, *25*, 705–715. [CrossRef]
155. Costa, R.P.; de Medeiros, M.H.G.; Rodriguez Martinez, E.D.; Quarcioni, V.A.; Suzuki, S.; Kirchheim, A.P. Effect of soluble phosphate, fluoride, and pH in Brazilian phosphogypsum used as setting retarder on Portland cement hydration. *Case Stud. Constr. Mater.* **2022**, *17*, e01413. [CrossRef]
156. Calado, B.; Tassinari, C. Geochemistry of the upper estuarine sediments of the Santos estuary: Provenance and anthropogenic pollution. *J. Geol. Surv. Braz.* **2020**, *3*, 189–209. [CrossRef]
157. Lütke, S.F.; Oliveira, M.L.S.; Silva, L.F.O.; Cadaval, T.R.S.; Dotto, G.L. Nanominerals assemblages and hazardous elements assessment in phosphogypsum from an abandoned phosphate fertilizer industry. *Chemosphere* **2020**, *256*, 127138. [CrossRef] [PubMed]
158. Shah, J.; Puthiyaveetil Othayoth, S.; Pania, R.; Parikh, S.; Vaishnav, P. Efficient Recovery of Trapped Phosphorus from Waste Phosphogypsum of a Phosphoric Acid Plant. *Chem. Sci. Rev. Lett.* **2022**, *11*, 340–348. [CrossRef]
159. Raut, S.P.; Patil, U.S.; Madurwar, M.V. Utilization of phosphogypsum and rice husk to develop sustainable bricks. *Mater. Today Proc.* **2022**, *60*, 595–601. [CrossRef]
160. Muthukumar, P.; Shewale, M.; Asalkar, S.; Shinde, N.; Korke, P.; Anitha, M.; Gobinath, R.; Anuradha, R. Experimental study on lightweight panel using phosphogypsum. *Mater. Today Proc.* **2022**, *49*, 1852–1856. [CrossRef]
161. Yassine, I.; Joudi, M.; Hafdi, H.; Hatimi, B.; Mouldar, J.; Bensemlali, M.; Nasrellah, H.; El Mahammedi, M.A.; Bakasse, M. Synthesis of Brushite from Phosphogypsum Industrial Waste. *Biointerface Res. Appl. Chem.* **2021**, *12*, 6580–6588. [CrossRef]
162. Ennaciri, Y.; Bettach, M.; El Alaoui-Belghiti, H. Recovery of nano-calcium fluoride and ammonium bisulphate from phosphogypsum waste. *Int. J. Environ. Stud.* **2020**, *77*, 297–306. [CrossRef]
163. Arhouni, F.E.; Hakkar, M.; Ouakkas, S.; Haneklaus, N.; Boukhair, A.; Nourreddine, A.; Benjelloun, M. Evaluation of the physicochemical, heavy metal and radiological contamination from phosphogypsum discharges of the phosphoric acid production unit on the coast of El Jadida Province in Morocco. *J. Radioanal. Nucl. Chem.* **2023**, *332*, 4019–4028. [CrossRef]
164. Akfas, F.; Elghali, A.; Bodinier, J.-L.; Parat, F.; Muñoz, M. Geochemical and mineralogical characterization of phosphogypsum and leaching tests for the prediction of the mobility of trace elements. *Environ. Sci. Pollut. Res.* **2023**, *30*, 43778–43794. [CrossRef]
165. Abouloifa, W.; Belbsir, H.; Ettaki, M.; Mounir, S.H.; El-Hami, K. Moroccan Phosphogypsum: Complete Physico-Chemical Characterization and Rheological Study of Phosphogypsum-Slurry. *Chem. Afr.* **2023**, *6*, 1605–1618. [CrossRef]
166. Szajerski, P.; Bogobowicz, A.; Bem, H.; Gasiorowski, A. Quantitative evaluation and leaching behavior of cobalt immobilized in sulfur polymer concrete composites based on lignite fly ash, slag and phosphogypsum. *J. Clean. Prod.* **2019**, *222*, 90–102. [CrossRef]
167. Grabas, K.; Pawełczyk, A.; Stręk, W.; Szełęg, E.; Stręk, S. Study on the Properties of Waste Apatite Phosphogypsum as a Raw Material of Prospective Applications. *Waste Biomass Valor.* **2019**, *10*, 3143–3155. [CrossRef]
168. Gijbels, K.; Nguyen, H.; Kinnunen, P.; Samyn, P.; Schroeyers, W.; Pontikes, Y.; Schreurs, S.; Illikainen, M. Radiological and leaching assessment of an ettringite-based mortar from ladle slag and phosphogypsum. *Cem. Concr. Res.* **2020**, *128*, 105954. [CrossRef]
169. Myka, A.; Łyszczek, R.; Zdunek, A.; Rusek, P. Thermal analysis of materials based on calcium sulphate derived from various sources. *J. Therm. Anal. Calorim.* **2022**, *147*, 9923–9934. [CrossRef]
170. The Possibility of Obtaining Rare Earth Elements from Potential Sources in Poland. Warszawa: Institute of Nuclear Chemistry and Technology. 2019. Available online: http://www.ichtj.waw.pl/ichtj/publ/annual/anrep18.pdf#page=47 (accessed on 29 December 2023).
171. El Zrelli, R.; Rabaoui, L.; Daghbouj, N.; Abda, H.; Castet, S.; Josse, C.; van Beek, P.; Souhaut, M.; Michel, S.; Bejaoui, N.; et al. Characterization of phosphate rock and phosphogypsum from Gabes phosphate fertilizer factories (SE Tunisia): High mining potential and implications for environmental protection. *Environ. Sci. Pollut. Res.* **2018**, *25*, 14690–14702. [CrossRef]
172. Antar, K.; Jemal, M. A thermogravimetric study into the effects of additives and water vapor on the reduction of gypsum and Tunisian phosphogypsum with graphite or coke in a nitrogen atmosphere. *J. Therm. Anal. Calorim.* **2018**, *132*, 113–125. [CrossRef]
173. Jalali, J.; Magdich, S.; Jarboui, R.; Loungou, M.; Ammar, E. Phosphogypsum biotransformation by aerobic bacterial flora and isolated Trichoderma asperellum from Tunisian storage piles. *J. Hazard. Mater.* **2016**, *308*, 362–373. [CrossRef]
174. Moalla, R.; Gargouri, M.; Khmiri, F.; Kamoun, L.; Zairi, M. Phosphogypsum purification for plaster production: A process optimization using full factorial design. *Environ. Eng. Res.* **2017**, *23*, 36–45. [CrossRef]
175. Bisone, S.; Gautier, M.; Chatain, V.; Blanc, D. Spatial distribution and leaching behavior of pollutants from phosphogypsum stocked in a gypstack: Geochemical characterization and modeling. *J. Environ. Manag.* **2017**, *193*, 567–575. [CrossRef]
176. Gaidajis, G.; Anagnostopoulos, A.; Garidi, A.; Mylona, E.; Zevgolis, I.E. Laboratory evaluation of phosphogypsum for alternative uses. *Environ. Geotech.* **2018**, *5*, 310–323. [CrossRef]
177. Noli, F.; Sidirelli, M.; Tsamos, P. Dispersion of radionuclides and heavy metals from phosphogypsum stacks in soil and plants at Northwestern Greece. *J. Radioanal. Nucl. Chem.* **2023**, *332*, 4213–4221. [CrossRef]

178. Kalinitchenko, V.P.; Glinushkin, A.P.; Minkina, T.M.; Mandzhieva, S.S.; Sushkova, S.N.; Sukovatov, V.A.; Il'ina, L.P.; Makarenkov, D.A. Chemical Soil-Biological Engineering Theoretical Foundations, Technical Means, and Technology for Safe Intrasoil Waste Recycling and Long-Term Higher Soil Productivity. *ACS Omega* **2020**, *5*, 17553–17564. [CrossRef] [PubMed]
179. Yusupov, U.; Kasimov, I.; Mukhamedgaliev, B. Contemporary Generation Additives for Modification of Cements and Other Knitting Building Materials. *Int. J. Sci. Technol. Res.* **2020**, *9*, 1191–1192.

Disclaimer/Publisher's Note: The statements, opinions and data contained in all publications are solely those of the individual author(s) and contributor(s) and not of MDPI and/or the editor(s). MDPI and/or the editor(s) disclaim responsibility for any injury to people or property resulting from any ideas, methods, instructions or products referred to in the content.

soil systems

MDPI

Review

Soil Phytomining: Recent Developments—A Review

Christos Kikis, Georgios Thalassinos and Vasileios Antoniadis *

Department of Agriculture, Crop Production and Rural Environment, University of Thessaly, Fytokou Street, 38446 Volos, Greece; chkikis@uth.gr (C.K.); thalassinosgeorgios@hotmail.gr (G.T.)
* Correspondence: antoniadis@uth.gr

Abstract: Phytomining (PM) is defined as the process of using plants capable of bio-extracting metals from soil in order to explore them economically. This relatively new, innovative method has been gathering significant attention in both the academic and commercial domains. Conventional mining methods are often economically unviable when applied to lean ores, and they can lead to secondary pollution in soil—a situation that applies to all excavated metals. On the other hand, PM is an environmentally friendly and economically viable solution that addresses the growing demands for metal resources, while simultaneously contributing to energy production by harnessing biomass energy. This comprehensive review presents the current PM techniques, challenges, and the hyperaccumulator plant species that may be used for the extraction of the main targeted elements in the process. Typically, the targeted metals are those of economic value, which can later be deposited or sold to various industries. This review also analyzes the factors influencing the economic viability of PM and proposes potential enhancements. Undeniably, PM offers the opportunity for economically sustainable exploration of metal-rich soils, but its full commercial viability remains constrained under current conditions as scientists are actively searching for the identification and utilization of new hyperaccumulator plant species in different locations worldwide, while creating new relationships and business avenues within the mining industry. Overall, this review highlights the current status of PM technology and the plants used, emphasizing the need for further research to enhance its commercial implementation and its potential to assist the mining industry. We conclude that PM, although a relatively new and unexplored concept, may provide economic and environmental benefits to soil end-users and managers who must cultivate on metal-contaminated soils as PM may turn yield shortages (of specific commercial crops) to benefits if high-yield hyperaccumulators are cultivated for industrial valorization of their high metal-content biomass.

Keywords: hyperaccumulators; metal-rich soils; biomass energy; environmental sustainability; economics of agromining

Citation: Kikis, C.; Thalassinos, G.; Antoniadis, V. Soil Phytomining: Recent Developments—A Review. *Soil Syst.* **2024**, *8*, 8. https://doi.org/10.3390/soilsystems8010008

Academic Editor: Manfred Sager

Received: 16 November 2023
Revised: 14 December 2023
Accepted: 4 January 2024
Published: 8 January 2024

Copyright: © 2024 by the authors. Licensee MDPI, Basel, Switzerland. This article is an open access article distributed under the terms and conditions of the Creative Commons Attribution (CC BY) license (https://creativecommons.org/licenses/by/4.0/).

1. Introduction

Phytoremediation is the process of remediating (or cleaning up) a soil elevated with pollutants with the use of plants ("phyto"). Many endemic plants, also known as metallophytes, can be found to be naturally grown in soils with elevated metal concentrations [1]. These unique plant species, also called "hyperaccumulators", have portrayed natural tolerance to the presence of metals in soil or an enhanced ability for their accumulation. These plants might be genotypes that have evolved such tolerant characteristics due to their establishment in metalliferous areas for centuries or millennia [2]. The accumulation of metals in plants occurs in their root system or in the aerial biomass like stems, leaves, and flowers. According to Soleymanifar et al. [3], a plant capable of concentrating a metal significantly higher than a "regular" plant in its tissues when grown in the same area is characterized as a hyperaccumulator. Hyperaccumulators have the potential of absorbing metals from soil via their root system and translocating them into their aerial parts [4]. In this way, a contaminated soil may be phytoextracted. Thus, phytoextraction is the process of using hyperaccumulator plants to absorb potentially toxic elements from soil with the aim of

remediating the soil. A variation in phytoextraction is phytomining (PM). Phytomining is the process under which plants are used to extract ("mine") valuable inorganic elements from soil in a natural or in an induced manner for the specific purpose of financial gain after valorizing the produced biomass. The difference between PM and phytoextraction is the valorization of the plant biomass; in the former case, it is solely dedicated to being used for recovering the metals for use in the metallurgical industry. In the latter, it can have any uses except from that—pharmaceutical, aromatic, energy, biochar, etc. Conventional mining is only performed in ore deposits where metal contents are highly enriched (i.e., soil concentrations are well above the maximum legal regulation limits). Nevertheless, these kinds of deposits are being depleted because of increased population and emerging needs, as well as rapid industrial and economic advancement [5]. Even though traditional mining methods are successful, they cannot recover all of the valuable metals. After the completion of the mining process, there is still about 3% to 10% of metals left in the soil [5]. These areas are characterized as "degraded" due to the fact that they contain lower concentrations of metals and minerals than what would be economically explorable [6]. Usually, such ore bodies are related to soils formed on ultramafic and serpentine parent materials. During the cool-down of ultramafic magma, minerals such as olivine and pyroxene, rich in magnesium (Mg) and iron (Fe), have a higher melting point and therefore crystallize at higher temperatures, leading to their dominance, along with some elements like nickel (Ni) and chromium (Cr), in ultramafic rocks. These types of soils are rich in various metals such as Mg, Fe, Ni, Cr, manganese (Mn), cobalt (Co), and titanium (Ti) [7,8].

In order to facilitate the phytoaccumulation, metals can be dissolved from the ore by applying strong acids or with the technique of electrorefining, in which metal ions gain electrons and form soil metal deposits at the electrode's surface [9]. In this way, metals in soil may become more phytoavailable, and thus their uptake to hyperaccumulator plants may be increased and, in turn, PM may occur. Hence, instead of going through the usual procedures of soil excavation for mining, the extractions are performed with the use of hyperaccumulator plants.

The concept of metal accumulation in plants and PM was first introduced by Jaffré et al. [10]. To date, scientists also refer to the process as "agromining" [11], in order to encompass the entire agricultural system of ore–soil–plants. The whole process offers the opportunity to extract metals from sites where conventional mining methods are not economically viable. The environmental effect of the method is minimal due to the balance action of the plants opposing soil erosion caused by excavation [12]. This method offers a sustainable way to remediate or restore soil, while simultaneously recovering valuable metals from soil [13]. Conventional methods used to remediate and decontaminate polluted sites often result in secondary pollution, aggravating the environmental challenges. The presence of plants minimizes the spread of metals and reduces the risk of wind and water soil erosion. Moreover, in large-scale PM applications, there is the possibility to harness the energy stored within the harvested plant biomass [3].

The bioaccumulation factor (BAF) and translocation factor (TF) are used to determine the efficiency of metal uptake from soil to plant and metal translocation within the plant, respectively [14]. The BAF is an index obtained by dividing the concentration of a metal in the aerial parts of a plant by its concentration in the surrounding soil. This factor provides insights into the ability of the plant to absorb and accumulate metals from the soil. On the other hand, TF is the ratio of metal concentration in the aerial plant parts to that in the roots. Higher TF values indicate a greater ability to efficiently translocate metals from the roots to the above-ground parts of a plant [14]. To be classified as a hyperaccumulator, a plant must have both BAF and TF values exceeding 1.0, signifying a great ability to absorb metals from soil and translocate them upwards in the aerial parts [15]. These indicators can be influenced by the effect of metal concentration in the plant. Therefore, biomass production and metal availability in the soil or substrate must be taken into consideration.

The aim of this review was (a) to provide a comprehensive overview on the current PM status, including challenges associated with the method, (b) to analyze the economic

viability of PM as an eco-friendly alternative to conventional mining, and (c) to discuss PM technology and the plants used, highlighting the importance of further research and development to enhance large scale implementation. We see this contribution as a highly necessary input so that essential knowledge and technological and scientific advancements may be updated and the community of scientists, interested stakeholders, and other soil end-users may benefit from the elucidation of mechanisms, processes, and practical considerations.

2. Elements Involved in Phytomining

2.1. Phytomining Elements

The elements of interest in the PM process are Ni, Co, cadmium (Cd), zinc (Zn), selenium (Se), Mn, thallium (Tl), and the noble metals (NMs). However, the majority of research efforts have focused on advancing the PM process of Ni [16]. For each metal, there is an established threshold that needs to be satisfied in order for a plant to be acknowledged as a hyperaccumulator. The selection of the limits is not entirely random but instead an indicator of a unique form of plant response, suggesting the presence of an unusual behavior. For instance, Sheoran et al. [5] suggested a limit of 1000 mg kg^{-1} of dry plant weight (DW) for Ni, after tests conducted on *Homalium* and *Hybanthus* plants in different areas. Similarly, Baker and Brooks [17] set the limit to 10,000 mg kg^{-1} DW for Mn and Zn after reporting high Zn concentrations in *Thlaspi calaminare* and *Viola calaminaria* leaves. Generally, over 700 plant species have been identified for their PM capabilities, most of which are Ni hyperaccumulators. The established limits for most of the elements that demonstrate an interest for being phytomined are shown in Table 1. When selecting plants for metal extraction, certain characteristics are important; these include three important features: high biomass yield, high Ni concentration in shoots (>1%), and fast growth [18]. The reason is that the phytoextracted amount of any given metal is equal to the concentration times biomass yield. All discussion is based on results obtained from field experiments, unless otherwise stated per particular case.

Table 1. Minimum threshold concentration of a metal in plants so that the species may be regarded as a hyperaccumulator. The accumulation refers to vegetative parts which can be harvested, most likely aerial biomass.

Element	Hyperaccumulation Threshold (mg kg^{-1})	Number of Hyperaccumulator Plant Species	Reference
Ag	1	-	Sheoran et al. [5]
Au	1	-	Sheoran et al. [5]
Cd	100	24	Van der Ent et al. [18]
Co	300	29	Krämer et al. [19]
Mn	10,000	22	Baker and Brooks [17]
Ni	1000	532	Soleymanifar et al. [3]
Se	100	20	Reeves [20]
Tl	100	1	Sheoran et al. [5]
Zn	3000	24	Van der Ent et al. [18]

The hyperaccumulation threshold was originally established as a metal concentration in plant shoots 10 to 100 times higher when compared to measurements in the shoots of "normal" plants under similar conditions. It was redefined by Van der Ent et al. [18], who suggested that the initial concentrations should be at least 10 times higher than the measurements obtained in plants on metalliferous soils, and 100 to 1000 times higher in plants grown on regular soils (non-metal-enriched). Typically, most of the hyperaccumulating plant species are endemic to metalliferous soils. Since the root system of these plants is

not usually collected during harvest, it is also mandatory for hyperaccumulators to exhibit BAF and TF values over 1, indicating that metals can be relocated in the upper part of the plant and recovered through combustion [14].

2.1.1. Nickel

As already mentioned, soils developed on ultramafic materials are expected to contain large amounts of Ni; hence, they are considered prime cases for Ni PM. Even though Ni in soil can be retained by Fe and Mn oxides, Ni hyperaccumulators can still accumulate a sufficient amount of the metal until the depletion of the source. According to Nkrumah et al. [16], 15–50 years are required before all easily accessible Ni is depleted. In addition, the physical properties of the soil are very important when it comes to PM. Well-drained soils are optimum for the cultivation of Ni hyperaccumulators, while soils that do not drain well may lead to decreased amount of plant biomass that is produced and, therefore, to a decreased amount of Ni that is extracted. For successful and economically viable Ni PM, soils should have an optimum content of moisture to maximize the amount of Ni absorbed by hyperaccumulator plants [21]. In the future, plant breeding techniques can make PM operations more profitable. Table 2 shows the main Ni hyperaccumulator plants that have great potential in Ni extraction from soils. Most of the plants that can hyperaccumulate Ni are species from approximately 40 different families, with the most important representatives being the Brassicaceae, Euphorbiaceae, Phyllanthaceae, Salicaceae, Buxaceae, and Rubiaceae family groups. Most of them are endemic plants found in soils derived from ultramafic rocks. The first report for Ni hyperaccumulation was made by Minguzzi and Vergnano [22], but the work was not widely recognized. Jaffré et al. [10] were the first to establish the term "phytomining" after noticing the accumulation of Ni in *Sebertia accuminata*, an endemic tree in forests of New Caledonia. Chaney et al. [23] were the first to conduct a field experiment for PM in the US Bureau mines in Reno, Nevada, where a Ni hyperaccumulator *Streptanthus polygaloides* was found to have bioaccumulated 10,000 mg kg^{-1} DW in serpentine soils containing 3500 mg kg^{-1} Ni. The second field trial was a two-year research study conducted by Robinson et al. [24], who extracted up to 8000 mg kg^{-1} DW Ni and had 110,000 mg kg^{-1} Ni in ash in *Alyssum bertolonii*. They also planted *Berkheya coddii,* which accumulated a total of 5500 mg kg^{-1} DW. It was also reported that *B. coddii* was a very good candidate for Ni extraction due to its high biomass yield, perennial life cycle, and tolerance to abiotic stress [24].

Numerous research studies have reported elevated concentrations of Ni in plant tissues when grown in these types of soils. All Ni PM research has focused on plants that can accumulate amounts more than 1% (i.e., 10,000 mg kg^{-1}) in their leaves and the harvested biomass, after collecting small plant samples (1 cm^2 or less) from serpentine soils in California. Indeed, Reeves et al. [25] found that *Streptanthus polygaloides* was able to accumulate Ni up to 1.5%, which led Mohsin et al. [26] to mention this plant as a good option for PM. Cole [27] reported the uptake of 5000 mg kg^{-1} Ni in the dried leaves of *Hybanthus floribundus* in lateritic soils in Western Australia, where background levels were approximately 500 mg kg^{-1} in the surface soil. In another study, Li et al. [7] reported a concentration of up to 22,000 mg kg^{-1} that was absorbed by *Alyssum murale* and *Alussum corsicum* plants (Brassicaceae), grown in Ni-contaminated soils in a 120-day greenhouse experiment. In addition, plants were fertilized and the pH was adjusted. Recently, Alyssum hyperaccumulators have received wide interest regarding their phytoextraction potential [16]. Durand et al. [28] conducted a 7-month pot experiment using *Odontarrhena chalcidica* (syn. *Alyssum murale*) spiked with Ni sulfate. They reported increased metal availability as well as BAF and TF values.

Table 2. Ni hyperaccumulation plant species. The accumulation of the elements refers to vegetative plant parts which can be harvested and valorized for the contained metal.

Plant Species	Family	Ni Concentration (mg kg^{-1})/Biomass Yield (t ha^{-1})	Experimental Conditions—Country	Reference
Alyssum baldaccii	Brassicaceae	1430–17,670	Ex situ; plant analysis; serpentine soils; Mediterranean climate; Mt. Smolikas, Greece	Bani et al. [29]
Alyssum bertolonii	Brassicaceae	4653–13,102/7–9	Hydroponics experiment; contained 400 mL Hoagland solution; plants spiked with $NiSO_4$; Italy	Galardi et al. [30]
Alyssum bertolonii	Brassicaceae	800/9	2-year field experiment; applied various amounts of NPK fertilizer; Mediterranean climate; Murlo, Italy	Robinson et al. [24]
Alyssum chalcidicum	Brassicaceae	1700	Ex situ; plant analysis; ultramafic rocks and hot springs; pseudo-total Ni concentration 1560 mg kg^{-1} soil; Mediterranean climate; Euboea Island, Greece	Kanellopoulos and Argyraki [31]
Alyssum euboeum	Brassicaceae	26–4550	Ex situ; plant analysis; serpentine soils; Mediterranean climate; Turkey	Bani et al. [29]
Alyssum heldreichii	Brassicaceae	11,800	Ex situ; plant analysis; serpentine soils; pseud-total Ni concentrations 1160 mg kg^{-1} soil; Mediterranean climate; Katara pass, Greece	Bani et al. [29]
Alyssum lesbiacum	Brassicaceae	2900–22,400/4.2–10	Hydroponics experiment; applied nutrient solution; solution spiked with 0–250 μmol L^{-1} $NiSO_4$; Greece	Adamidis et al. [32]
Alyssum markgrafii	Brassicaceae	<3–19,100	Ex situ; plant analysis; serpentine soils; pseudo-total Ni concentration in soil 1670 mg kg^{-1}; Mediterranean climate; Gjegjan; Albania	Bani et al. [29]
Alyssum murale	Brassicaceae	7–34,690/10.2–20	5-year field experiment; pseudo-total Ni concentration in soil 3180 mg kg^{-1}; fertilized with 100 kg ha^{-1} N; Mediterranean climate; Pojska, Albania	Bani et al. [29]
Berkeya coddii	Asteraceae	40–5800	Pot experiment in glasshouses; plants spiked with 4−1000 mg Ni kg^{-1} potting mix; New Zealand	Keeling et al. [33]
Brackenridgea palustris	Melastomataceae	1440/6.74	Ex situ; plant analysis; ultramafic rocks; pseudo- total Ni concentration—7051–10,521 mg kg^{-1}; Tropical climate; Sulawesi, Indonesia	Van der Ent et al. [34]
Cloezia artensis	Myrtaceae	35–1729	Field experiment; extractable Ni concentrations in soil—35–208 mg kg^{-1}; Semi-Tropical climate; New Caledonia	Becquer et al. [35]
Codia spatulata	Cunoniaceae	27–1420/6.5	Field experiment around mine sites; Semi-Tropical climate; New Caledonia	Jaffré et al. [36]

Table 2. *Cont.*

Plant Species	Family	Ni Concentration (mg kg^{-1})/Biomass Yield (t ha^{-1})	Experimental Conditions—Country	Reference
Dichapetalum gelonioides	Dichapetalaceae	3160	Ex situ; plant analysis; ultramafic rocks; pseudo-total Ni concentrations—7051–10,251 mg kg^{-1} soil; Tropical climate; Sulawesi, Indonesia	Van der Ent et al. [34]
Geissois Pruinosa	Cunoniaceae	3000–15,106/38.5	Field experiment around mine sites; Semi-tropical climate; New Caledonia	Jaffré et al. [36]
Knema matanensis	Myristicaceae	2500–5000	Ex situ; plant analysis; ultramafic rocks; pseudo total Ni concentrations—7051–10,251 mg kg^{-1} soil; Tropical climate; Sulawesi, Indonesia	Van der Ent et al. [34]
Miscanthus floridulus	Poaceae	667–778	Ex situ; plant analysis; uranium tailings with background Ni concentration 11.5 mg kg^{-1} soil; Tropical climate; South China	Li et al. [37]
Myristica laurifolia	Myristicaceae	1100	Ex situ; plant analysis; ultramafic rocks; pseudo-total Ni concentrations—7051–10,251 mg kg^{-1}; Tropical climate; Sulawesi, Indonesia	Van der Ent et al. [34]
Peripterygia marginata	Araliaceae	23–1800	Field experiment around mine sites; Semi-Tropical climate; New Caledonia	Jaffré et al. [36]
Phyllanthus discolor	Phyllanthaceae	13,670–31,490	Ex situ; plant analysis; ultramafic rocks; Tropical climate; Cuba	Berazain et al. [38]
Phyllanthus orbicularis	Phyllanthaceae	4140–10,950	Ex situ; plant analysis; ultramafic rocks; Tropical climate; Cuba	Berazain et al. [38]
Phyllanthus xpallidus	Phyllanthaceae	15,390–60,170	Ex situ; plant analysis; ultramafic rocks; Tropical climate; Cuba	Berazain et al. [38]
Phyllantus insulae	Phyllanthaceae	34,330–38,720	Ex situ analysis; ultramafic rocks; pseudo-total Ni concentrations—7051–10,251 mg kg^{-1}; Tropical climate; Sulawesi, Indonesia	Van der Ent et al. [34]
Planchonella oxyhedra	Sapotaceae	19,600/10	Ex situ; plant analysis; ultramafic rocks; pseudo-total Ni concentrations—7051–10,251 mg kg^{-1} soil; Tropical climate; Sulawesi, Indonesia	Van der Ent et al. [34]
Planchonella oxyhedra	Sapotaceae	24,100–27,500/30–40	Ex situ; plant analysis; ultramafic rocks; Tropical climate; Halmahera Island, Indonesia	Hamdan et al. [39]
Rinorea bengalensis	Violaceae	20,000–25,100/30–40	Ex situ; plant analysis sampling; ultramafic rocks; Tropical climate; Halmahera Island, Indonesia	Hamdan et al. [39]
Sarcotheca celebica	Oxalidaceae	700–1000	Ex situ; plant analysis; ultramafic rocks; pseudo-total Ni concentrations—7051–10,251 mg kg^{-1} soil; Tropical climate; Sulawesi, Indonesia	Van der Ent et al. [34]

Table 2. *Cont.*

Plant Species	Family	Ni Concentration (mg kg^{-1})/Biomass Yield (t ha^{-1})	Experimental Conditions—Country	Reference
Streptanthus polygaloides	Brassicaceae	4000/21.4	Ex situ; plant analysis; serpentine soil; California, USA	Davis and Boyd [40]
Thlaspi apterum	Brassicaceae	16,600–21,500	Ex situ; plant analysis; serpentine soils; pseudo-total Ni concentrations 2858 mg kg^{-1} soil; Mediterranean climate; Fotinovo, Bulgaria	Bani et al. [29]
Thlaspi ochroleucum	Brassicaceae	3400	Ex situ; plant analysis; serpentine soils; pseudo-total Ni concentrations 2770 mg kg^{-1} soil; Mediterranean climate; Kardzali, Bulgaria	Bani et al. [29]
Thlaspi tymphaeum	Brassicaceae	7000	Ex situ; plant analysis; serpentine soils; pseudo-total Ni concentrations 2340 mg kg^{-1} soil; Mediterranean climate; Malakasi, Greece	Bani et al. [29]
Trichospermum kjelbergii	Malvaceae	3770	Ex situ; plant analysis; ultramafic rocks; pseudo-total Ni concentrations—7051–10,251 mg kg^{-1} soil; Tropical climate; Sulawesi, Indonesia	Van der Ent et al. [34]

2.1.2. Cobalt

The standard for plants to be classified as Co hyperaccumulators was set at 1000 mg kg^{-1} by Baker and Brooks [17] until Krämer [19] revised it to 300 mg kg^{-1}, reporting that the former accumulation of Co is rare. Normal amounts of Co in plants are well below 0.1 mg kg^{-1}. Even in soils characterized with elevated amounts of Co, such as those deriving from ultramafic rocks, the amount of Co in plants rarely surpasses 20 mg kg^{-1}. It seems that the presence of Ni in such soils interferes with Co accumulation. For instance, as mentioned before, *Berkheya coddii* is also a Ni hyperaccumulator. The presence of Co can inhibit the absorption of Ni when these metals are both present in the medium, leading to PM limitations. Keeling et al. [33] reported that Co can be absorbed by *B. coddii* plants with or without the presence of Ni in the growing medium (50% peat and 50% pumice). On the other hand, increased Co concentrations in soil from 125 up to 1000 mg kg^{-1} significantly decreased the harvested biomass due to plant toxicity, although the plant's BAF was not affected. In trials where only Ni (at 1000 mg kg^{-1}) or only Co (at 4–1000 mg kg^{-1}) were present in soil, the crop yielded approximately 14.5 kg ha^{-1} (when for Ni) and 12.6 kg ha^{-1} (for Co). On the other hand, when Co and Ni were both present in soil (with concentrations of Ni = 500 and Co = 500 mg kg^{-1}), the metal yield significantly dropped to 0.9 kg of Ni ha^{-1} and 3.9 kg of Co ha^{-1}, and this indicates that PM may be limited due to interference of each other's absorption by the plant. Similar to this, Rue et al. [41] suggested that *B. coddii* could be utilized in areas with high concentrations of Co but low Ni after testing the plant in pot experiments. Specifically, they found that the Co concentration reached 1980 mg kg^{-1} when treated with 10 mg kg^{-1} Ni (as $Ni(NO_3)_2{\cdot}6H_2O$) and 100 mg kg^{-1} Co (as $Co(NO_3)_2{\cdot}6H_20$), while total biomass can reach up to 22 t ha^{-1}, which could yield 16.3 t Co ha^{-1}. Similar findings were reported by Parks [42], who noticed the competitive role between Ni and Co accumulation in *Rinorea bengalensis*. However, *R. bengalensis* was found to be tolerant to Ni and managed to accumulate a concentration of 1200 mg Co kg^{-1} when grown on ultramafic rocks. Both Ni and Co were added as $Ni(NO_3)_2{\cdot}6H_2O$ and $Co(NO_3)_2{\cdot}6H_20$ at 750 mg kg^{-1}, respectively. An exceptional ability for Co PM was shown after collecting leaf samples of *Nyssa sylvatica* var. *biflora* and var. *sylvatica* (Nyssaceae) grown on ultramafic rocks in New Caledonia, which were found to accumulate up to 845 mg Co kg^{-1} [43]. The same was

reported for the well-known Ni hyperaccumulator *Alyssum murale*, which accumulated 1320 mg Co kg^{-1} DW when grown in sandy loam soils (<2 mg Co kg^{-1} dry soil) spiked with 59.8 mg (1 mmol) Co kg^{-1} dry soil [44].

The addition of elemental zero-valent sulfur in soil can help increase the amount of metal that plants can absorb. According to Robinson et al. [45], sulfur content in soil at a rate of 5000 mg kg^{-1} increased the amount of Co that was absorbed by *Berkheya coddii* plants to 299 mg kg^{-1} DW, 5 times greater than the control treatment (56 mg kg^{-1} DW). Hence, this is especially beneficial in soils that do contain some amount of metals but not enough for the plants to take up the maximum quantity they need. In addition, sulfur is a cost–benefit additive, compared to EDTA, ethylenediaminetetraacetic acid, a synthetic molecule frequently used to increase metal mobility and soil, for enhancing the growth of metal-rich plants in soils with low metal concentrations. Overall, plant species that have demonstrated Co hyperaccumulation are shown in Table 3.

Table 3. List of all Co hyperaccumulators. Concentrations in plants refer to leaves unless otherwise stated.

Plant Species	Family	Co (mg kg^{-1} DW)/Biomass Yield (t ha^{-1})	Experimental Conditions—Country	References
Acalypha cupricola	Euphorbiaceae	207–904	Ex situ; plant analysis; samples from Co/Cu mine sites; Equatorial climate; Katanga, Congo	Faucon et al. [46]
Aeollanthus subacaulis	Lamiaceae	0–1900	Pot experiment (200 g sterilized soil); soil containing 10,000 mg Co kg^{-1} as nitrate; Congo	Morisson et al. [47]
Alectra sessiliflora	Orobanchaceae	21–866	Ex situ; plant analysis; samples collected from Co/Cu mine sites; Equatorial climate; Katanga, Congo	Faucon et al. [46]
Alyssum corsicum	Brassicaceae	1080 (shoot)/4.2–10	Field experiment in various soil types; 150 kg N ha^{-1}, 100 kg P ha^{-1}, and 75 kg K ha^{-1} were applied; Beltsville, USA	Malik et al. [44]
Alyssum heldreichii	Brassicaceae	1000	Pot experiment; plants spiked with different concentrations of metals; New Zealand	Homer et al. [48]
Alyssum murale	Brassicaceae	2070 (shoot)/10.2–20	Field experiment in various soil types; 150 kg N ha^{-1}, 100 kg P ha^{-1}, and 75 kg K ha^{-1} were applied; Beltsville, USA	Malik et al. [44]
Alyssum pintodasilvae	Brassicaceae	1000	Pot experiment; plants spiked with different concentrations of metals; New Zealand	Homer et al. [48]
Alyssum tenium	Brassicaceae	1000	Pot experiment; plants spiked with different concentrations of metals; New Zealand	Homer et al. [48]
Alyssum troodii	Brassicaceae	10–2325	Pot experiment; plants spiked with different concentrations of metals; Cyprus	Lange et al. [49]
Anisopappus chinensis	Asteraceae	3–1300	Ex situ; leaf analysis; Equatorial climate; Congo	Lange et al. [49]
Aporosa chalarocarpa	Phyllanthaceae	468	Ex situ; leaf analysis; samples collected from ultramafic rocks; Tropical climate; Sabah, Malaysia	Lange et al. [49]

Table 3. *Cont.*

Plant Species	Family	Co (mg kg^{-1} DW)/Biomass Yield (t ha^{-1})	Experimental Conditions—Country	References
Berkeya coddii	Asteraceae	40–2116/4.96–9.30	Experiment in controlled climate glasshouses; plants spiked with 4–500 mg Co kg^{-1}; New Zealand	Keeling et al. [33] Rue et al. [41]
Buchnera henriquesii	Orobanchaceae	404–930	Ex situ; plant analysis; plant samples collected from Co/Cu mine sites; Equatorial climate; Katanga, Congo	Faucon et al. [46]
Celosia trigyna L.	Amaranthaceae	75–501/9.5	Ex situ; plant analysis; plant samples collected from Co/Cu mine sites; Equatorial climate; Katanga, Congo	Olawuyi et al. [50]
Crepidorhopalon perennis	Linderniaceae	61–1105/0.32	Ex situ; plant analysis; plant samples collected from Co/Cu mine sites; Equatorial climate; Katanga, Congo	Faucon et al. [46]
Crepidorhopalon tenuis	Linderniaceae	8–605/0.16–0.32	Ex situ; plant analysis; plant samples collected from Co/Cu mine sites; Equatorial climate; Katanga, Congo	Faucon et al. [46]
Lemna minor L.	Araceae	5000	Pre-cultivated under laboratory conditions; fertilized with Hoagland solution; plants spiked with 0–200 µM $CoCl_2 \cdot 6H_2O$; Nanjing, China	Hu et al. [51]
Glochidion cf. *sericeum*	Phyllanthaceae	442–1310	Ex situ; leaf analysis; leaf samples collected from ultramafic rocks; Tropical climate; Sabah, Malaysia	Lange et al. [49]
Haumaniastrum katangense	Lamiaceae	864	Ex situ; leaf analysis; leaf samples collected from Cu/Co-Zn/Cu mine sites; background Co levels 1.2–85 mg kg^{-1}; Congo	Van der Ent et al. [52]
Haumaniastrum robertii	Lamiaceae	6160/20	Ex situ; leaf analysis; leaf samples collected from Cu/Co-Zn/Cu mine sites; background Co levels 1.2–85 mg kg^{-1}; Congo	Lange et al. [49]
Hibiscus rhodanthus	Malvaceae	42–274/0.054–1.6	Ex situ; plant analysis; Sub-tropical climate; Nyika Plateu, Zambia and Mozambique	Medwecka [53]
Nyssa sylvatica var. biflora	Nyssaceae	0–438/6	Ex situ; plant analysis; plant samples from granite derivatives; available Co content in soil—2.5%; Inabu-cho, Japan	Memon and Yatazawa [54]
Nyssa sylvatica var. sylvatica	Nyssaceae	800/6	Ex situ; plant analysis; South Carolina, USA	Busbee et al. [55]
Rinorea bengalensis	Violaceae	0.5–1200/30–40	Ex situ; leaf analysis; ultramafic rocks; Tropical climate; Halmahera Island, Indonesia	Hamdan et al. [39]

Table 3. *Cont.*

Plant Species	Family	Co (mg kg^{-1} DW)/Biomass Yield (t ha^{-1})	Experimental Conditions—Country	References
Rinorea javanica	Violaceae	3–670/30–40	Ex situ; leaf analysis; leaf samples collected from ultramafic rocks; Tropical climate; Halmahera Island, Indonesia	Hamdan et al. [39]
Triumfetta welwitschii	Malvaceae	162–1971	Ex situ; plant analysis; plant samples collected from Co/Cu mine sites; Equatorial climate; Katanga, Congo	Faucon et al. [46]
Vernoniastrum latifolium	Asteraceae	82–549	Ex situ; plant analysis; Equatorial climate; Congo	Lange et al. [49]
Vigna dolomitica	Fabaceae	241–540	Ex situ; plant analysis; Equatorial climate; Congo	Lange et al. [49]

2.1.3. Cadmium

Higher concentrations of cadmium (Cd), ranging from 10 to 200 mg kg^{-1}, can be found in soils that have been exposed to waste materials due to Zn mining. In addition, such elevated Cd levels may also arise in soils that have received industrial waste or phosphate fertilizers enriched with Cd [7]. Natural levels of Cd in plants are usually less than 0.1 mg kg^{-1}, but in Cd-contaminated soils these levels can exceed 20 mg kg^{-1}. The cadmium established threshold in plants is defined as having a concentration of higher than 100 mg kg^{-1}, as proposed by Van der Ent et al. [18]. However, in certain Zn-Pb mines, Noccaea species, such as *N. caerulescens* and *N. praecox*, have been found to contain Cd concentrations exceeding 100 mg kg^{-1}, or even higher than 1000 mg kg^{-1}. Shoots of *N. caerulescens* can easily contain over 2000 mg Cd kg^{-1}, even when grown on contaminated soils, and over 20,000 mg kg^{-1} when tested in nutrient solutions [56]. Other plants like *Impatiens walleriana*, *Pteris vittata*, *Sedum alfredii*, and *Thlaspi caerulescens* are capable of removing from soil 1168, 6434, 922.6, and 7400 mg kg^{-1} of Cd, respectively [57]. Specifically, Nedelkoska et al. [58] treated the roots of *T. caerulescens* with a H^+-ATPase inhibitor and measured a concentration of 62,800 mg Cd kg^{-1} DW (6.3%) in the hair roots of the plant, which was grown in nutrient medium amended with a Cd concentration of 3710 ppm. On the other hand, there are significant variations among sites and within these plants [59]. Similar findings have been reported for *Arabidopsis halleri* by Bert et al. [60] and *Viola baoshanensis* by Deng et al. [61]. Specifically, *A. halleri* has been reported for its great ability to grow in different environments and its capability to store high amounts of Cd, especially when grown in polluted soils. According to Claire-Lise and Nathalie [62], *A. halleri* was able to accumulate up to 157 mg kg^{-1} leaf dry weight when treated with 5 μM Cd or more. Also, it has been used as a plant model on metal tolerance and accumulation for identifying the genes involved. However, it has not been further tested due to the fact that it produces low biomass. Nevertheless, it was noted that for a plant to be considered as a Cd hyperaccumulator, it needs to be naturally grown in an area and sustain itself without human intervention [18]. The list of Cd hyperaccumulating species are shown in Table 4.

2.1.4. Zinc

As for Zn, it was found that *Thlaspi alpestre* var. *calaminare* (nowadays classified as *Noccaea caerulescens*) contained a minimum of 1% Zn in the dry leaf biomass [89]. Rascio [90] observed another Zn hyperaccumulator, *Thlaspi rotundifolium* ssp. *Cepaeifolium*, while Reeves and Brooks [91] proved that the Thlaspi genus consists of many Zn hyperaccumulators, with accumulated concentrations surpassing 1000 mg kg^{-1} after experiments in mine tailings in Northern Italy. Baker et al. [92] showed that *T. caerulescens*, when

grown in nutrient-rich soils, could accumulate high concentrations of Zn, Cd, Co, Mn, and Ni. There were even instances where Zn accumulation reached the threshold of 10,000 mg kg^{-1} [17] or surpassed it, which was initially considered as the established limit to characterize a plant as a Zn hyperaccumulator. Furthermore, Brown et al. [93] added 10,000 μM Zn and 200 μM Cd in a nutrient solution and caused an accumulation of 33,600 mg Zn kg^{-1} in *T. caerulescens*. Also *A. halleri,* after being tested in a hydroponics experiment treated with 1 μM and 1000 μM Zn, managed to accumulate Zn in the shoots 300 mg kg^{-1} and 32,000 mg kg^{-1}, respectively [94]. Also, in a hydroponics experiment conducted in China using *Potentilla griffithii*, it was shown that the plant was able to accumulate up to 11,400 mg Zn kg^{-1} leaf dry weight after being treated with 160 mg Zn L^{-1} [95]. However, the threshold of 10,000 mg kg^{-1} was later revised to 3000 mg kg^{-1} by Van der Ent et al. [18]. Also, Grimm [96] reported an accumulation of up to 11,700 mg kg^{-1} in stems of *Brassica juncea*, when the soil concentration of Zn was only 330 mg kg^{-1}. The list of all Zn hyperaccumulator plant species is shown in Table 5.

Table 4. List of Cd hyperaccumulating plant species.

Plant Species	Family	Achieved Concentration (mg kg^{-1})/Biomass Yield (t ha^{-1})	Experimental Conditions—Country	References
Arabidopsis halleri	Brassicaceae	117.2	Pot experiment; nutrient solution applied as fertilizer; plants exposed to 0–100 μM $CdSO_4$; Blankerode, Germany	Zhao et al. [63]
Arabis paniculata	Brassicaceae	457	Hydroponics experiment; Hoagland solution applied as fertilizer; plants spiked with 0–267 μM $CdCl_2 \cdot 2.5H_2O$; Yunnan Province, China	Tang et al. [64]
Bidens pilosa	Asteraceae	400.7/5–6.7	Field experiment with total Cd concentration in soil 19.63 mg kg-1; $(NH_4)_2SO_4$ and $Ca(NO_3)_2$ were added at 200 mg kg^{-1} as fertilizers; Shaanxi, China	Dai et al. [65]
Centela asiatica	Apiaceae	105	Field and laboratory experiment; field pseudo-total Cd concentration—124–1000 mg kg^{-1}, plants were spiked at levels 0–5 mg L^{-1} in lab; South China	Liu et al. [66]
Viola baoshanensis	Cyperaceae	1168	Field survey and greenhouse experiment; nutrient solution was applied as fertilizer; plants spiked with 0–30 mg L^{-1}; Humid sub-tropical climate; Hunan Province, China	Liu et al. [67]
Elodea canadensis	Hydrocharitaceae	300	Hydroponics experiment; plants exposed to 0–0.5 μM $CdCl_2$; Stockholm, Sweden	Ali et al. [57] Nyquist and Greger [68]
Helianthus annus	Helianthoideae	230/4.5	Pot experiment; background total Cd concentration in soil—30 mg kg^{-1}; pot spiked with 0–500 mg Cd L^{-1} solution; Tropical climate; Korea	Lee et al. [69]

Table 4. *Cont.*

Plant Species	Family	Achieved Concentration (mg kg^{-1})/Biomass Yield (t ha^{-1})	Experimental Conditions—Country	References
Impatiens walleriana	Balsaminaceae	1168	Pot experiment; containing total Cd—0.61 mg kg^{-1}; soil spiked with 20, 40, and 80 mg $Cd(NO_3)$ kg^{-1}; China	Wei et al. [70]
Ipomoea aquatica	Convolvulaceae	138/7–30	Hydroponics experiment; nutrient solution containing 1 M of HNO_3, H_3PO_4, and H_2SO_4 was added; Beijing, China	Wang et al. [71]
Lonicera japonica	Caprifoliaceae	470.25/2.1–3.8	Hydroponics experiment; plant samples were collected from uncontaminated site; Hoagland solution was applied as fertilizer; plants were spiked with 0–50 mg $CdCl_2 \cdot 2.5H_2O$ L^{-1}; China	Liu et al. [72]
Siegesbeckia orientalis L.	Asteraceae	192.92–6762	Field experiment and pot experiment; total Cd concentration 28.44 and 150 mg kg^{-1} in soil and pots respectively; Huidong, China	Zhang et al. [73]
Panicum virgatum	Poaceae	280/18	Field experiment; N-fertilization ranged from 0–240 kg ha^{-1}; Mediterranean climate; Thessaly, Greece	Giannoulis et al. [74]
Phytolacca americana	Phytolaccaceae	42–637.7/0.53	Field experiment and hydroponic experiment; pseudo-total concentration in soil 1–1000 mg kg^{-1}, plants spiked with 0–100 μM $CdCl_2$; Hoagland solution applied as fertilizer; China	Liu et al. [66]
Potentilla griffithi	Rosaceae	174	Field experiment; contaminated soil contained a total of 331 mg Cd kg^{-1}; Monsoon climate; Lanping, China	Hu et al. [51]
Populus nigra	Salicaceae	96.8/82	Hydroponics experiment; plant cuttings were exposed to 0–20 μM $CdSO_4$; Rome, Italy	Marmiroli et al. [75] Stolarski et al. [76]
Picris divaricata	Asteraceae	1343	Pot experiment with contaminated soil; total Cd amount in soil—15 mg kg^{-1}; Monsoon climate; Lanping, China	Tang et al. [77]
Raphanus sativus	Brassicaceae	326.75/33–42	Hydroponics experiment; 400 μmol L^{-1} $CaCl_2$ was added; Korea, and Jiangxi, China	Kim and Hong [78] Chen et al. [79]
Ricinus communis	Euphorbiaceae	288/2–2.6	Ex situ; plant analysis; plant sampling from Cd contaminated sites; Cd concentration on soil—2.8 mg kg^{-1}; Subtropical climate; Zhejiang, China	Koutroubas et al. [80] Huang et al. [81]
Salix viminalis	Salicaceae	200/12	Hydroponics experiment; plant material spiked at 0, 10, 50, 200 μM $CdCl_2$; Birmensdorf, Switzerland	Stolarski et al. [76] Vollenweider et al. [82]

Table 4. *Cont.*

Plant Species	Family	Achieved Concentration (mg kg^{-1})/Biomass Yield (t ha^{-1})	Experimental Conditions—Country	References
Sedum alfredii	Crassulaceae	6500–9000	Greenhouse experiment in pots; nutrient solution was applied; plants were treated with 12.5–800 μmol Cd L^{-1}; Quzhou, China	Yang et al. [83]
Solanum nigrum L.	Solanaceae	307–3163	Pot experiment; soil in pots spiked with various Cd concentrations (as $CdCl_2$) up to 80 mg kg^{-1}; Daegu, Korea	Khan et al. [84]
Tagetes patula	Asteraceae	324/26.8	Pot experiment; containing total Cd—0.61 mg kg^{-1}; soil spiked with 20, 40, and 80 mg $Cd(NO_3)$ kg^{-1}; China	Marotti et al. [85] Wei et al. [70]
Thlaspi caerulescens	Brassicaceae	380–7400/1.6	Pot experiment containing contaminated soil—total Cd 20.3 mg kg^{-1}; fertilized with 13 mg N, 33 mg P, and 41 mg K kg^{-1} soil; Northern France	Martínez et al. [86]; Perronnet et al. [87]
Wolffia globosa	Araceae	500/0.08	Hydroponics experiment in greenhouse; Hoagland solution applied as fertilizer; solution spiked at 0–100 μM $Cd(NO_3)$; China	Xie et al. [88]

Table 5. Zn hyperaccumulating plant species.

Plant Species	Family	Achieved Concentrations (%) (Aerial Parts Are Specified)/Biomass Yield (t ha^{-1})	Experimental Conditions—Country	References
Anthyllis vulneraria	Fabaceae	>1% (leaf)/0.1–0.4	Ex situ; plant analysis; plant samples were assisted by symbiotic bacteria; spiked with 0–35 mM $ZnSO_4$; Saint-Laurent-Le-Minier, France	Grison et al. [97]
Arabidopsis helleri	Brassicaceaa	>1% (leaf)	Pot experiment; nutrient solution applied as fertilizer; plants exposed to 0–100 μM $ZnSO_4$; Blankerode, Germany	Zhao et al. [94] Peer et al. [98]
Arabis paniculata	Brassicaceae	>2% (leaf)	Hydroponics experiment; Hoagland solution applied as fertilizer; plants spiked with 0–2447 μM $ZnSO_4 \cdot 7H_2O$; Yunnan Provinence, China	Reeves et al. [99]; Tang et al. [64]

Table 5. *Cont.*

Plant Species	Family	Achieved Concentrations (%) (Aerial Parts Are Specified)/Biomass Yield (t ha^{-1})	Experimental Conditions—Country	References
Corydalis davidii	Papaveraceae	>1% (leaf)	Field study and hydroponics experiment; total Zn in soil—9847 mg kg^{-1}; plants spiked with 50–400 mg $Zn(NO_3)_2$ L^{-1} in hydroponic experiment; Sub-tropical climate; Magu, China	Balafrej et al. [100]; Lin et al. [101]
Haumaniastrum katangense	Lamiaceae	1.98% (shoot)/20	Field study, in situ leaf samples; Zair	Balafrej et al. [100]
Noccaea alpestre	Brassicaceaa	>1% (leaf)	Ex situ; plant analysis; total Zn in soil 1900–35,000 mg kg^{-1}; Derbyshire, England	Shimwell and Laurie [102]
Noccaea brachypetalum	Brassicaceaa	2% (shoot)	Field study, in situ leaf samples; Paris, France	Reeves and Brooks [103]
Noccaea bulbosum Spruner	Brassicaceaa	1.05% (shoot)	Field study, in situ leaf samples; Mediterranean climate; Athens, Greece	Reeves and Brooks [103]
Noccaea caerulescens	Brassicaceaa	2.73% (leaf)/1.6	Field study, in situ leaf samples; Temperate climate; Belgium	Martínez et al. [85] Reeves and Brooks [103]
Noccaea calaminare	Brassicaceaa	3.96% (leaf)	Field study, in situ leaf samples; Temperate climate; München, Germany	Reeves et al. [99] Reeves and Brooks [103]
Noccaea cepaeifolium	Brassicaceaa	2.10% (shoot)	Field study; total Zn concentration in soil—17,300 mg kg^{-1}; Mediterranean climate; Northern Italy	Reeves and Brooks [103]
Noccaea eburneosa	Brassicaceaa	1.05% (shoot)	Field study, in situ leaf samples; Temperate climate; Zurich, Switzerland	Balafrej et al. [100] Reeves and Brooks [103]
Noccaea limosellifolium	Brassicaceaa	1.10% (shoot)	Field study, in situ leaf samples; Paris, France	Reeves and Brooks [103]
Noccaea praecox	Brassicaceaa	2.10% (leaf)	Field study, in situ leaf samples; Mediterranean climate; Bulgaria	Reeves and Books [103]
Noccaea stenopterum	Brassicaceaa	1.60% (leaf)	Field study, in situ leaf samples; Temperate climate; Spain	Reeves and Brooks [103]
Sedum alfredii	Crassulaceae	0.45–1.9% (shoot)	Field survey and greenhouse experiment; plants exposed to 5–320 mg Zn L^{-1} (as $ZnSO_4 \cdot 7H_2O$); Sub-tropical humid climate; Zhejiang Province, China	Yang et al. [104]
Pieris divaricata	Ericaceae	>6% (shoot)	Pot experiment with contaminated soil; total Zn amount in soil—352 mg kg^{-1}; Sub-tropical climate; Lanping, China	Balafrej et al. [100]

Table 5. *Cont.*

Plant Species	Family	Achieved Concentrations (%) (Aerial Parts Are Specified)/Biomass Yield (t ha^{-1})	Experimental Conditions—Country	References
Potentilla griffithii	Rosaceae	>2.2% (leaf)	Field survey and hydroponics experiment; Hoagland solution was added as fertilizer; plants spiked with $ZnSO_4 \cdot 7H_2O$ at 20–320 mg L^{-1}; Yunnan Province; China	Reeves et al. [99] Qiu et al. [105]
Sedum plumbizincicola	Crassulaceae	0.45–1.9% (shoot)	Field survey and greenhouse experiment; plants exposed to 5–320 mg Zn L^{-1} (as $ZnSO_4 \cdot 7H_2O$); Sub-tropical humid climate; Zhejiang Province, China	Reeves et al. [99] Yang et al. [104]
Viola baoshanensis	Violaceae	>0.9%	Field survey and greenhouse experiment; modified Hoagland solution was applied as fertilizer; plants spiked with 0–130 mg $ZnSO_4 \cdot 7H_2O$ L^{-1}; Humid sub-tropical climate; Hunan Province, China	Balafrej et al. [100]; Wu et al. [106]

2.1.5. Manganese

Manganese is a major trace nutrient with an expected concentration in plants grown in normal soil of ca. 40–50 mg kg^{-1} and usual soil pseudo-total concentrations ca. 500–600 mg kg^{-1}. However, in Mn-rich soils, Mn hyperaccumulator plants may accumulate 2 or even 3 orders of magnitude higher Mn concentrations. Research conducted by Jaffré [36,106] reported that 98 out of 450 of the plant species growing on soils developed on ultramafic rocks in New Caledonia with background Mn concentrations of 1000–5000 mg kg^{-1} had average Mn concentrations above 1000 mg kg^{-1}, while six species among them surpassed even 10,000 mg kg^{-1}. Based on these findings, Baker and Brooks [17] decided to establish a threshold of 10,000 mg kg^{-1} to define Mn hyperaccumulation. To date, there are 22 species that are known as Mn hyperaccumulators and these are listed in Table 6. In fact, due to exceptionally high levels of Mn, in some cases reaching a concentration of 2–5% of plant DW, the ash of these plants can contain as much as 10–25% Mn.

Table 6. List of Mn hyperaccumulator species.

Plant Species	Family	Achieved Concentration (mg kg^{-1})/Biomass Yield (t ha^{-1})	Experimental Conditions—Country	Reference
Alyxia poyaensis	Apocynaceae	1.4%	Ex situ; plant analysis; Semi-tropical climate; New Caledonia	Losfeld et al. [107]
Beaupreopsis paniculata	Urticaceae	1.2%	Ex situ; plant analysis; Semi-tropical climate; New Caledonia	Jaffré [108]
Chengiopanax sciadophylloides	Araliaceae	2.4%	7-month field trial; exchangeable Mn in soil—931 mg kg^{-1}; Mie, Japan	Mizuno et al. [109]

Table 6. *Cont.*

Plant Species	Family	Achieved Concentration (mg kg^{-1})/Biomass Yield (t ha^{-1})	Experimental Conditions—Country	Reference
Denhamia cunninghamii	Sapindaceae	2.5%	Ex situ; plant analysis; Queensland, Australia	Fernando et al. [110]; Fernando et al. [111]
Denhamia silvestris	Sapindaceae	1.2%	Pot experiment; medium spiked with soluble Mn^{2+} at 0, 250, 500, and 1000 mg kg^{-1}; Queensland, Australia	Abubakari et al. [112]
Denhamia fournieri	Sapindaceae	2.0%	Ex situ; plant analysis; Semi-tropical climate; New Caledonia	Fernando et al. [110];
Celosia argentea	Sapindaceae	3.3%	Field survey and hydroponics experiment; Hoagland solution applied as fertilizer; plants exposed to 2.5–600 mg Mn L^{-1}; Guangxi Province, China	Jaffré [36] Liu et al. [113]
Garcinia amplexicaulis	Clusiaceae	1.2%/280	Ex situ; plant analysis; Semi-tropical climate; New Caledonia	Jaffré [36]
Gossia bamagensis	Myrtaceae	4.0%	Ex situ; leaf analysis; Queensland, Australia	Fernando et al. [110]; Fernando et al. [111]
Gossia bidwillii	Myrtaceae	1.9% (leaf), 2.6% (bark)	Ex situ; plant analysis; Sub-tropical climate; Brisbane, Australia	Losfeld et al. [107]; Bidwell et al. [114]
Gossia clusioides	Myrtaceae	1.0%	Ex situ; plant analysis; Semi-tropical climate; New Caledonia	Jaffré [36]
Gossia diversifolia	Myrtaceae	1.8%	Ex situ; plant analysis; Semi-tropical climate; New Caledonia	Losfeld et al. [107]
Gossia fragrantissima	Myrtaceae	3.5%	Ex situ; leaf analysis; Queensland, Australia	Fernando et al. [110] Fernando et al. [111]
Gossia gonoclada	Myrtaceae	1.5%	Ex situ; leaf analysis; Queensland, Australia	Fernando et al. [110]; Fernando et al. [111]
Gossia lucida	Myrtaceae	1.5%	Ex situ; leaf analysis; Queensland, Australia	Fernando et al. [110] Fernando et al. [111]
Gossia sankowskiorum	Myrtaceae	3.0%	Ex situ; leaf analysis; Queensland, Australia	Fernando et al. [110] Fernado et al. [111]
Gossia shepherdii	Myrtaceae	1.5%	Ex situ; leaf analysis; Queensland, Australia	Fernando et al. [110] Fernado et al. [111]
Phytolacca americama	Proteaceae	1.1%	Ex situ; analysis; Semi-tropical climate; New Caledonia	Jaffré [108]

Table 6. *Cont.*

Plant Species	Family	Achieved Concentration (mg kg^{-1})/Biomass Yield (t ha^{-1})	Experimental Conditions—Country	Reference
Phytolacca acinosa	Phytolaccaceae	1.9%	Field survey and hydroponics experiment; Hoagland's nutrient solution was applied; plants were exposed to 0–15,000 µmol Mn L^{-1} (as $MnCl_2 \cdot 4H_2O$); Hunan Province, China	Xue et al. [115]
Polygonum pubescens	Polygonaceae	1.6%	Field survey and hydroponics experiment; Hoagland solution applied; Plants exposed to 0–20 mmol Mn L^{-1} (as $MnCl_2 \cdot 4H_2O$); China	Deng et al. [116]
Polygonum lapathifolium	Araliaceae	1.4%	Field survey and hydroponics experiment; Hoagland solution was applied; plants exposed to 0–16 mmol Mn L^{-1} (as $MnCl_2 \cdot 4H_2O$); Guangxi Province, China	Liu et al. [117]
Schima superba	Typhaceae	1.2%	Pot experiment; Hoagland solution was added as a fertilizer; *S. superba* saplings were exposed to 0–200 mmol L^{-1} $MnCl_2 \cdot 4H_2O$; China	Yang et al. [118]
Virotia neurophylla	Typhaceae	5.5%	Ex situ; plant analysis; Semi-tropical climate; New Caledonia	Jaffré [108]

2.1.6. Selenium

Selenium (Se) levels in soil are often lower than 2 mg kg^{-1}, but they can increase to a few hundreds of mg kg^{-1}. The selenium concentration in plants dry biomass is typically lower than 0.1 mg kg^{-1} and may even be as low as 0.01 mg kg^{-1}. Nonetheless, it was discovered that legumes belonging to the Astragalus genus were able to accumulate Se to elevated concentrations, locally exceeding 1000 mg kg^{-1} in the USA in Se-rich soils [119]. Table 7 shows the 20 hyperaccumulators for Se. Due to the typically low levels of Se in plant tissues, Reeves [20] argued that a limit of 100 mg kg^{-1} should be considered for identifying Se hyperaccumulators. To date, utilizing Se hyperaccumulators for the economic extraction of Se has not been suggested. However, there are potential uses of these plant species in phytoremediation for cleaning up contaminated soils in crops harvested for stock feed and Se biofortification [120].

2.1.7. Thallium

Thallium is a precious metal high in demand but comparatively rare in nature. Although it is very toxic and difficult to find in the environment, natural, along with anthropogenic, origins can introduce significant amounts of Tl in soil. Several plant species are capable of extracting Tl from soils, making them useful for reclaiming it. Specifically, according to Leblanc et al. [130], there was an unexpected accumulation of Tl in *Iberis intermedia* and *Biscutella laevigata* in Pb/Zn mines in France. Moreover, for *I. intermedia*, an uptake of 4000 mg of Tl kg^{-1} was reported and over 14,000 mg kg^{-1} DW for *B. laevigata*, where the background concentration of Tl was 10 mg kg^{-1} in mine tailings. The presence of Tl in soil at levels that make Tl PM feasible is a possibility. However, there are only a

few sites where this could be realistically implemented due to the limited availability of suitable soil conditions.

Table 7. List of Se hyperaccumulator species.

Plant Species	Family	Achieved Concentration (mg kg^{-1})/Biomass Yield (t ha^{-1})	Experimental Conditions—Country	Reference
Asparagus bisculateus	Asparagaceae	0.88%/12.3	Ex situ; plant analysis; Canada	Reeves [121] Moon [122]
Asparagus patersonii	Asparagaceae	0.25%/12.3	Ex situ; plant analysis; USA	Reeves [121] Moon [122]
Asparagus pectinatus	Asparagaceae	0.51%	Ex situ; plant analysis; USA	Reeves [121]
Asparagus racemosus	Asparagaceae	1.5%	Ex situ; plant analysis; USA	Reeves [121]
Atriplex canescens	Amaranthaceae	0.17%/34.75	Ex situ; plant and soil analysis; Arid climate; Algeria	Nadaf et al. [123]; Nedjimi [124]
Castilleja chromosa	Orobanchaceae	0.18%	Ex situ; plant analysis; USA	Reeves [121];
Cardamine violifolia	Brassicaceae	0.48%	Ex situ; plant analysis; Korea and Yutangba, China	Ma et al. [125] Huang et al. [126]
Lecythis ollaria	Lecythidaceae	1.8%	Ex situ leaf analysis; Venezuela	Reeves [121]
Machaeranthera gabriulscula	Asteraceae	0.18%	Ex situ leaf analysis; USA	Reeves [121]
Machaeranthera parryi	Asteraceae	0.53%	Ex situ; leaf analysis; USA	Reeves [121]
Machaeranthera ramosa	Asteraceae	0.13%	Ex situ; leaf analysis; USA	Reeves [121]
Machaeranthera venusta	Asteraceae	0.34%	Ex situ; leaf analysis; Colorado, USA	Reeves [121]
Neptunia amplexicaulis	Fabaceae	0.11%/43.3	Pot experiment; soil spiked with 0, 5, and 30 mg Se kg^{-1} (as Na_2SeO_4 or $CaSeO_3$); Queensland, Australia	O'Donohue et al. [127]; Irish et al. [128]
Stanleya bipinnata	Brassicaceae	0.23%	Ex situ; leaf analysis; USA	Reeves [121]
Stanleya pinnata	Brassicaceae	0.11%	Climate controlled experiment; Hoagland solution applied as fertilizer; plants exposed to 0–80 µM N_2SeO_4; Colorado, USA	Harris et al. [129]

2.1.8. Noble Metals

Recently, NMs are being examined for their PM potential. This category constitutes metals such as gold (Au) and silver (Ag), as well as a sub-group of platinum metals including iridium (Ir), osmium (Os), palladium (Pd), platinum (Pt), rhodium (Rh), and ruthenium (Ru) [15]. These metals find extensive use across different industries and are often referred to as precious metals, obtaining significant attention due to their economic value. Interestingly, while the demand for NMs increases, their primary ore sources are gradually depleted. Hence, alternative methods of extraction, like PM, are being explored. Recent research and development on the extraction and accumulation of these metals in plants has shed light on the PM pathway for recovering these metals, although real-time implementation remains limited [131]. It should be noted that NMs can not be absorbed by plants from the metallic state as plants are capable of absorbing only the soluble species of any inorganic element found in the soil solution.

Gold

Across the world, considerable quantities of Au deposits can be found in natural enriched soils and mine tailings. Mohan [132] mentioned that PM of Au is a cost-effective way to extract Au from mine tailings and low-grade ores. Conventional mining removes the most Au from ores, leaving behind a significant portion of Au that cannot be extracted due to economic disadvantages. Since 1988, the hyperaccumulation limit of Au has been set to be higher than 1 mg kg^{-1} DW, based on the normal concentrations of Au in plants, which are usually around 0.01 mg kg^{-1}. However, Au must be in the soluble form before absorption can take place. This can be achieved by adding several types of lixiviants (e.g., NaCN, SCN^-, $S_2O_3^{-2}$) depending on the properties of the substrate. In low-pH sulphate containing substrates, thiocyanate can solubilize Au.

It is reported that conifers growing in areas with Au ores in Canada could accumulate up to 0.02 mg of Au kg^{-1}, while the background levels in plants are 100 times lower [133]. Also, in an experiment where *Brassica juncea* was planted in pots containing 5 mg Au kg^{-1} in artificial substrate, Anderson et al. [134] concluded that the application of 160 mg of ammonium thyocanate kg^{-1} of dry substrate weight achieved an accumulation of 57 mg Au kg^{-1}. Wilson et al. [135] also referred to research where *B. juncea* was able to absorb 63 mg Au kg^{-1} DW after soil was treated with sodium cyanide. The plants were grown on an oxidized ore pile containing 0.6 mg Au kg^{-1}. They concluded that an economically viable option for Au extraction that could yield 1 kg of Au ha^{-1} would require a total harvested biomass of 10,000 kg ha^{-1} containing 100 mg kg^{-1}. Furthermore, Msuya et al. [136] mentioned that carrots (*Daucus carota*) accumulated 0.779 mg ha^{-1} of Au when ammonium thiocyanate was added and 1.45 mg ha^{-1} when thiosulphate was added, while the concentration of Au in the growing substance was 3.8 mg kg^{-1}. Lamb et al. [137] performed a study where they used cyanide and thiocyanate to test the accumulation of Au in *Berkheya coddii*, *Brassica juncea*, and *Cichorium intybus*. They found that the leaves of *B. juncea* and *C. intybus* in soils spiked with cyanide had the highest Au accumulation at a rate of 326 mg kg^{-1} (*B. juncea*) and 164 mg kg^{-1} (*C. intybus*). Another study conducted by Vural and Safari [138] evaluated the potential of *Helichrysum arenarium* for Au accumulation; they reported TF and BAF values of 2.04 and 0.59, respectively. They concluded that enhancing the availability of Au in soil by adding chelators like NaCN, SCN^-, and thiosulfates can lead to the usage of *Helichrysum arenarium* in the PM process.

Silver

To date, there are no reports about the hyperaccumulation of Ag by plants. Even though the Ag concentration in plants can be up to 1 mg kg^{-1}, some plants such *as Lupinus angustifolius* can reach up to 126 mg kg^{-1} by induced accumulation [5]. Harris and Bali [139] were the first to propose the uptake of Ag nanoparticles by plants. They conducted research in which they observed an accumulation of significant amounts of Ag in *Brassica juncea* and *Medicago sativa* plants. Specifically, *B. juncea* absorbed up to 12.4% of its weight in Ag when exposed to 1000 mg L^{-1} of $AgNO_3$ for 72 h, while *M. sativa* accumulated up to 13.6% of its weight in Ag when exposed to a solution containing 10,000 mg L^{-1} $AgNO_3$ for 24 h. Silver nanoparticles that were stored inside the plant's tissues had a size of 50 nm. In addition, the application of EDTA was not helpful in enhancing the absorption of Ag. EDTA had a rather negative effect as it caused toxicity to plants and this decreased the amount of Ag that would otherwise be capable for extraction. They concluded that plants could be used to produce large quantities of metallic nanoparticles.

Palladium

Out of all the platinum group metals, Pd has gathered significant attention due to its high abundance compared to others. The first report for Pd accumulation in plants was made by Fuchs and Rose [140], who measured a concentration of 285 μg kg^{-1} in ash from *Pinus flexilis*. In addition, Kothny [141] reported an accumulation of 400 μg kg^{-1} of Pd in the ash of *Quercus chrysolepsis*, while the background level was 140 μg kg^{-1}. The hyperaccumulator

Berkeya coddii was investigated for its ability to absorb Pd by Nemutandani et al. [142] from a contaminated site with 70 μg kg^{-1} Pd. It was found that *B. coddii* was able to extract 180 μg kg^{-1} in roots and 710 μg kg^{-1} in leaves. The plant demonstrated a notable ability to accumulate and translocate Pd, with BAF and TF values reaching 10.1 and 3.9, respectively.

There have been no officially defined Pd hyperaccumulators; it is anticipated that the threshold for all NMs would be approximately 1 mg kg^{-1}, assuming their normal low concentration in plants. On the other hand, Pd, like Au, has limited solubility in soil. Hence, soil amendments are often used in order to increase Pd solubility and improve the accumulation in plants. For instance, KCN has been utilized to increase the absorption of Pd by plants. Walton [143] used KCN at a rate of 10 g L^{-1} to enhance Pd accumulation in *B. coddii* when cultivated in mine tailings containing 315 μg kg^{-1}. They reported that plants had accumulated Pd to levels as high as 7677 μg Pd kg^{-1}. In addition, Aquan [144] conducted an experiment utilizing gossan rock as a substrate, containing 205.5 μg Pd kg^{-1}. They assessed the Pd accumulation in *Cannabis sativa* and found that the average Pd concentration was 30,336 μg kg^{-1} in the aboveground part of the plant, reaching as high as 62,420 μg kg^{-1} when KCN was applied. Another study conducted by Harumain et al. [145] managed to trigger the hyperaccumulation of Pd in *Salix purpurea* and *Miscanthus* through the use of KCN. They employed a synthetic ore with a Pd concentration of 50–100 mg kg^{-1} as growth medium. As a result, the leaves of *S. purpurea* and *Miscanthus* were found to contain 820 and 505 mg kg^{-1}, respectively. Overall, the idea of phytomining Pd is relatively new. The effectiveness of using plants to extract this valuable element has only been minimally demonstrated so far.

Platinum

While the potential of plants to accumulate Pt in its tissues was mentioned by Fuchs and Rose [140], it is noteworthy that numerous studies on Pt PM have emerged recently. Nemutandani et al. [142] revealed that *B. coddii* grown in Pt-polluted areas with concentrations of 0.04 mg kg^{-1} soil achieved an uptake of 0.22 mg kg^{-1} in leaves and 0.18 mg kg^{-1} in roots. The plant exhibited BAF (5.5) and TF (1.2) values greater than 1.0, highlighting its ability to accumulate and translocate Pt. A study conducted by Kovacs et al. [146] reported the identification of plants from contaminated brownfield land with a Pt concentration of 3.06 mg kg^{-1}. Also, Diehl and Gagnon [147] found concentrations of 14.6 mg kg^{-1} in *Daucus carota* collected from an area near a heavy-traffic motorway. White mustard, *Sinapis alba*, was also reported to show great ability in accumulating Pt by Kińska and Kowalska [148]. They found an impressive accumulation of 5973 mg kg^{-1} dry root weight, while the concentration of Pt in the nutrient solution was 1.0 mg L^{-1}. Despite numerous reports on Pt in plants, it is worth mentioning that experiments aimed at Pt PM have not been conducted.

Rhodium

Generally, studies regarding the occurrence of Rh in plant tissues are very limited due to its scarce presence. A study conducted by Diehl and Gagnon [147] reported a Rh concentration of 0.7 mg kg^{-1} in *Daucus carota* that was collected from four different areas near heavy-traffic roads. Bonanno [149] found that the Rh concentration in *Phragmites australis*, collected from an extremely urbanized riverside area, ranged from 1.11 to 1.13 mg kg^{-1}. Generally, it is worth noting that Rh has the highest solubility among the platinum group elements [15]. This suggests that Rh has great potential use in PM applications.

2.2. Factors Influencing Metal Availability and Behavior in Soil

2.2.1. pH

Soil activity plays a crucial role in how easily certain nutrients can dissolve in the soil solution and be taken up by the plants. As a result, soil pH affects the ability of plants to absorb essential nutrients and other elements from soil. For instance, Punjari [150] reported that when the pH of soil drops below 6.5 and 5.3, the amount of soluble Cd and Zn increases.

Likewise, the solubility of Cu and Pb increases at pH levels below 4.5 and 3.5, respectively. On the other hand, at this low pH level, the mobility of As ions decreases. This is related to the fact that As is present in the soil solution as oxyanion, either in its trivalent (arsenite; $As^{III}O_3^{3-}$) or its pentavalent species (arsenate; $As^{V}O_4^{3-}$). The same is the case with any other contaminant anions (such as hexavalent chromium; $Cr^{VI}O_4^{2-}$)—their availability is proportional to soil pH. The significance of pH in determining metal solubility and availability can be indicated by the fact that the pH in the root zone of certain plants is often up to 2 units lower than the surrounding soil pH due to the release of organic acids [151]. The amount of metal extraction is directly related to the concentration of the metal in soil and pH of the extracting agent.

There are various ways to reduce soil pH. This can be achieved by using different substances, including fertilizers containing ammonia, acids, and zero-valent sulfur, as amendments. However, there are limitations as to how much the pH can be lowered because most plant species can only thrive within a specific pH range. Usually, the lowest pH that many plants can tolerate is c. 4.5 [5]. Hence, while it is possible to adjust the pH utilizing soil amendments, it is important to carefully consider the range that allows plants to grow without adverse effects. On the other hand, acidic pH values can be corrected with the application of "liming" materials, which are mainly phases with abundant inorganic carbonate phases, i.e., CO_3^{2-} and HCO_3^-, such as marble dust (either calcitic or dolomitic), as well as their derivative, caustic calcium oxide. Robinson et al. [45] studied the effects of different substances, namely $MgCO_3$, $CaCO_3$ (both alkalinity-bearing materials), and sulfur (an acidifying material), on the uptake of Ni and Co by *Berkeya coddii*. When $MgCO_3$ was added to the soil, it increased the soil pH from 6.9 to 8.7 which led to reduced uptake of Ni and Co by *B. coddii*. On the other hand, the application of sulfur resulted in a decrease in soil pH from 6.9 to 5.5, which increased the plant's uptake of both metals. In addition, the application of Ca salts made plants tolerant to Ni [8]. The authors concluded that the addition of acidifying materials, like sulfur, can help extract more metals from soil by making them more available to plants. The shoot Ni concentration increased in Alyssum sp. at pH levels ranging from 5 to 7, with maximum concentrations being obtained at a pH of 6.5 [152]. The same relationship between cationic metal species and soil pH (which is inversely proportional—the former increases when the latter decreases and vice versa) has repeatedly been confirmed in experimental studies [36,110]. This was also found by Zhong et al. [153] in soil samples collected from heavy metal-contaminated soils in China; they reported a significant availability in soil for Ni, Zn, Cu, Cd, and Cr at pH levels lower than 4.5. They also concluded that soil pH is the most important factor concerning metal availability in soil. Specifically, pH was reported to affect all physicochemical and biological processes in soil, which in turn affect the behavior and the way metals interact with other substances. Since acidic pH tends to decrease metal sorption in soil, metal availability increases due to increased metal concentration in soil solution.

2.2.2. Fertilizers

In order to successfully implement the technique of PM, the availability of metals in soil needs to be ensured. Besides optimizing soil pH levels to guarantee metal absorption, adding fertilizers to achieve high-yielding phytoextraction crops is another factor that needs to be mentioned. Fertilizers containing NH_4-N can reduce soil pH due to the fact that NH_4^+ in aerated soils is readily oxidized within weeks to NO_3^-, a process yielding 2 mols of H^+ per mol of nitrified N. This enhances further the availability of metals in soil, as well as providing optimal conditions for the growth of these certain plant species [154]. In fact, hyperaccumulators grown in soils derived from ultramafic rocks exhibit a noticeable positive response to the application of fertilizers. For instance, in Vertisols in Albania, there was a 10-fold increase in the yield of *A. murale* after applying inorganic fertilizers [23].

Sheoran et al. [5] highlighted that the application of fertilizers significantly increased the maximum annual growth of *Alyssum bertolonii* compared to the non-fertilized treatment, which resulted in higher biomass yields. Specifically, the application of NPK fertilizers

achieved an overall increase of 308%. Thus, fertilization can greatly affect the phytoextraction process, to remove metals from soil, making it more effective. The same work reported that Ni levels were increased in the leaves of *Berkeya coddii* from 2500 mg kg^{-1} to 4200 mg kg^{-1}. Similar results were reported by Bennett et al. [155], where the application of NPK fertilizers doubled the annual biomass production of *Alyssum bertolonii*, *Streptanthus polygalonoides,* and *Thlaspi caerulescens,* without reducing the concentration of Ni in their shoots. In another study, the application of 100 kg P ha^{-1} in serpentine soils led to an improved yield in *Alyssum murale* plants [7]. Overall, high N fertilization promotes higher accumulation of Ni, Cd, and Zn. Sheoran et al. [156] used *Salix* on contaminated soil containing low levels of Cd (1.9–2.4 mg kg^{-1}) and showed that the application of $(NH_4)_2SO_4$ at 100 mg N kg^{-1} significantly increased the Cd and Zn plant concentrations to 4.5 for Cd and 400 mg kg^{-1} for Zn. Similar results were reported by Schmidt [157], who noticed a significant increase in Cd in *Lolium perenne* after adding $(NH_4)_2SO_4$ as fertilizer. In that same work, in soils with low concentrations of Zn and Ni, the application of this fertilizer also significantly increased the crop metal concentrations without any loss of total yield. The same was agreed by Babau et al. [158], who tested *Robinia pseudoacacia* for its ability to absorb Pb, Cd, and Cu with and without the presence of NPK fertilizer. We conclude based on the above-reviewed literature that the addition of nutrients to soil (mostly N) increases the ability of plants to absorb metals and thus it is likely to increase the phytomining effectiveness of hyperaccumulators; hence, fertilizers are considered a critical factor for the success of commercial PM processes.

2.2.3. Chelates

In hyperaccumulators, the number of metals these plants can remove from soil depends on biomass production and the concentration of the metals within their tissues; thus, often their extraction ability is limited [159]. In order to increase the extraction of metals, chelates can be a possible option for higher growth rates. Chelates are capable of extracting various metals from soil. They have the ability to bind metals and form water-soluble organometallic complexes. Once they are formed, they can introduce metals into the soil solution by removing them from the surfaces they were attached to [160]. Some of the most used chelating agents are EDTA (ethylenediaminetetraacetic acid), CA (citric acid), DTPA (diethylenetriaminepentaacetic acid), NTA (nitrolenetriaceticacid), EDDS (ethylenediaminedisuccinicacid), and thiosolutions like thiocyanates. The former two agents are the most widely utilized [10,161]. Specifically, Robinson et al. [162] used EDTA and CA on *B. coddii* in order to phytomine Ni. Interestingly, they found that even though soluble Ni increased in the rhizosphere, the Ni concentration in the shoots decreased. They concluded that competition between EDTA, CA, and the plant's own excretes resulted in trapping Ni in the root system of the plant. However, Meers et al. [163] reported an increase in Ni uptake in sunflowers which was 1.8 to 2.8 times greater by adding 1.6 mmol kg^{-1} EDTA and EDDS. Another study conducted by Blaylock et al. [164] where EDTA was applied in heavy metal-contaminated soils showed an enhanced accumulation of Pb, Cd, Cu, and Zn in *Brassica juncea* shoots. Nevertheless, they concluded that chelators like EDTA may pose an environmental risk due to the fact that they can not be easily degradable by soil microbes, resulting in groundwater pollution. Additionally, Wang et al. [165] reported results from a field experiment where soil-applied EDTA and EDTA−ethyl lactate were found to enhance Cd extraction by 20 and 29%, respectively, in Salix. Gold has also been found to accumulate in plants like *Brassica juncea*, *Zea mays*, *Daucus carota*, and *Cichorium* spp. by adding chelate agents like thiosolutions.

3. Metal Accumulation in Plants and Their Subsequent Recovery

3.1. Mechanisms of Metal Accumulation in Plants

The process of metal hyperaccumulation in plants, and thus phytomining, consists of several different stages that plants go through. Making the soil in the immediate vicinity of the plant's roots more acidic and releasing organic compounds is one of the

plant's strategies to absorb metals from soil. The acidification of soil can occur due to the secretion of hydrogen ions (H^+), which can help in dissolving metals and making them available for absorption. This process is carried out by essential enzymes like the H^+ pumps, such as the plasma-membrane H^+ ATPases [164]. Additionally, roots excrete organic acids, such as malonic and oxalic, as well as enzymes and metal-chelating molecules, like phytosiderophores. These substances have the ability to enhance the absorption of metals from soil by binding them and thus assist their phytomining [166]. The movement of metals inside the plant cells can have two potential pathways, which are the apoplastic flow and the symplast transport. Metals can enter the root apoplast, which is the space between cells in the root. Even though solutes are capable of moving upwards through the plant using this pathway, the more effective way is through the plant's vascular system, the xylem [5]. Moreover, to enter the xylem, where long-distance transport occurs, metals have to go through the Casparian strip, which is a waxy layer of cells that surrounds the xylem and is impermeable to solutes. Thus, metals must cross membranes aided by pumps or channels in the endodermal cells. After crossing the Casparian strip or membranes, the movement of metals within the xylem is called "symplast transport". Symplast transport is more regulated than apoplastic flow because the movement of metals is controlled by the properties of the cell membranes and the presence of specialized transport proteins or channels that facilitate their movement [164]. Generally, plants have the ability to manage heavy metals, avoid toxicity, and store them safely [167]. Different oxidation levels of heavy metals have varying characteristics during absorption, conveyance, and detoxing within the plant. After being translocated to shoot cells, metals can be stored in specific cellular locations such as in the apoplast, epidermis cells, the mesophyll, and cell walls, where they will not disrupt any cellular processes. This is achieved by sequestering metals away from cellular processes that could otherwise be harmed. The trapping of the metals often takes place in plant vacuoles [168].

3.2. Metal Recovery

To recover the metals accumulated in plants, various metal extraction technologies are employed. However, before extraction can be undertaken, the plant biomass needs to be reduced to a manageable quantity so that any plant-borne metals may be concentrated in the remaining material. This is crucial for reduction in the transportation costs, as well as the size of machinery used for metal extraction. Biomass reduction can occur in various ways, including composting, compaction, and thermal conversion.

According to Hu and Gholizadeh [169], the thermal conversion methods of combustion and ashing are considered to be the most practical for concentrating metals. In fact, these processes involve high temperatures, ranging from 350 to 1000 °C, that lead to fast reaction times and effective biomass volume reduction. During combustion, the polluted biomass turns into gas and energy is released as heat. Metals cannot easily escape as gases during the process, resulting in the formation of ash containing high concentrations of valuable metals. On the other hand, unwanted emissions of C and N oxides are issues that need to be considered. However, the overall approach is considered to be a neutral C-releasing activity in terms of greenhouse gas emissions due to the fact that C can be captured and be stored via oxy-fuel combustion [15].

Ashing is the same process as combustion but takes place at lower temperatures (300–550 °C) and is commonly used in laboratory environments for analytical purposes. For instance, Zhang et al. [170] found that the best conditions of biomass combustion for Ni recovery were ashing at 550 °C for a duration of 3 h. By doing this, they were able to obtain high quality ash reaching 20% of the weight of Ni. However, according to Dastyar et al. [171], in order to recover good quality ash, it is important to understand the behavior of metal dynamics during thermal conversion. Specifically, metal behavior is influenced by various factors, including the type of plant biomass, the equipment that is being used, and combustion conditions like temperature, pressure, and duration. For example, Hazotte et al. [172] compared metal concentrations in three Ni hyperaccumulators

(*Odontarrhena chalcidica*, *Leptoplax emarginata*, and *Berkheya coddii*), along with biomass volume reduction in two different temperatures (550 and 900 °C) and standard pressure. They reported that the Ni concentration at 900 °C was higher compared to that at 550 °C in all three hyperaccumulator plant tissues. In addition, they reported that at 550 °C, over 95% of the organic material was broken down and 99% of C was eliminated from all plant species. They concluded that combustion is an effective method for the degradation of plant biomass, while achieving high concentrations of metals with no notable loss up to 900 °C. In another study conducted by Kovacs et al. [147], Au could not be detected in the woody biomass. Nevertheless, after the combustion of plant material, Au could be detected in the residual solid, where it exhibited a considerable concentration of 4.10 mg kg^{-1}. Nevertheless, despite findings regarding the importance of biomass combustion and ashing, there is rather limited information in the literature regarding enrichment in the solid residues with valuable phytomined metals.

After biomass combustion or ashing are finished, a metal-rich ash is obtained. However, it may still contain impurities that need to be further processed in order to isolate the target metal. This can be achieved by employing pyrometallurgical, hydrometallurgical, and bio-metallurgical methods. Pyrometallurgy refers mainly to the traditional process of smelting, but it can contain other methods too, such as incineration, chlorination, and volatilization [15]. Pyrometallurgy involves the use of high temperatures to separate the metals from other materials. However, the environmental effects of this method, like the release toxic fumes, and the expensive equipment, are some limitations of this approach. Hydrometallurgy involves the use of leaching agents in order to extract and separate the metals. Metals within the solution are separated and isolated by utilizing various techniques, including ion capture, liquid separation, ion exchange, and electrochemical reduction. Compared to pyrometallurgy, hydrometallurgy is easier to use, offers great metal selection, is efficient in recovering metals, and less expensive in terms of equipment. Interestingly, most of the studies examine the use of both methods for isolating metals. For instance, Lamb et al. [137] managed to isolate Au from woody plant material after ashing the biomass and using 2 M HCl as a leaching agent. The solution was separated by adding methyl isobutyl ketone, followed by the addition of sodium borohydrate. This resulted in the formation of a black deposit which was heated at 800 °C, which led to the formation of pure Au.

During the last decade, a new approach called bio-metallurgy has become popular for recovering metals. It consists of two main parts: "bioleaching" and "biosorprtion". Bioleaching refers to the use of microorganisms, like bacteria, fungi, and algae, to interact with metals through oxidation-reduction reactions. Bioleaching has been considered to be an eco-friendly and economically viable option. However, it is not efficient enough for metal recovery and it takes a lot of time to be completed, which leads to restricted use and means it is only used for laboratory-scale operations [173]. On the other hand, biosorprtion utilizes microbes, fungi, yeasts, algae, and waste products, which are used to collect metals. These organisms act like "magnets" by entrapping metals through physical and chemical interactions between metals and the surface of these microbes. Generally, biosorption has emerged as a cost-effective and environmentally friendly technique compared to traditional methods, especially for aquatic media [174]. Processes are shown in Figure 1.

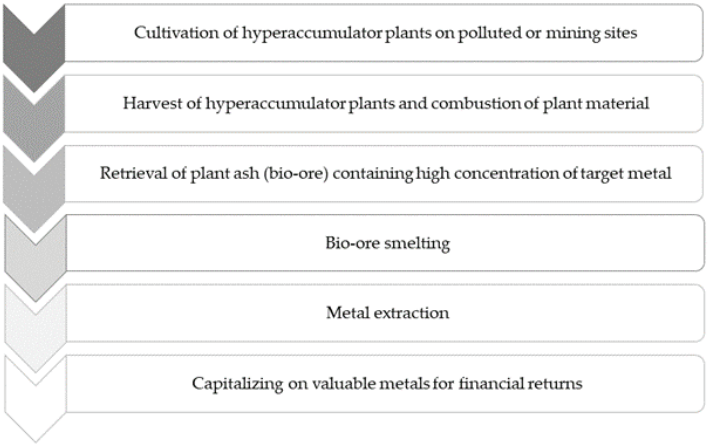

Figure 1. Main stages in the phytomining process for metal extraction.

4. Financial Considerations of Phytomining

The economic success of PM relies on several factors, such as (i) the metal content in soil and plants, (ii) the amount of biomass production, and (iii) the amount of retrieved (or phytomined) metal that can be recovered during the combustion of the produced biomass which can then be captured and sold. However, the most imperative factor for PM is the revenue generation, which depends on the market demands and the world price of the metal being extracted through plants [10,174]. Metal prices can vary from USD 0.75 kg^{-1} for Fe ores to USD 61,375 kg^{-1} for Au [175]. As a result, metals with high prices offer better economic prospects. Precious metals can be very costly and their price keeps rising consistently (Figure 2); thus, there must be a sufficient amount of these metals in the harvested biomass in order for the PM process to be profitable. The economic proposed concentration of precious metals is shown in Table 8.

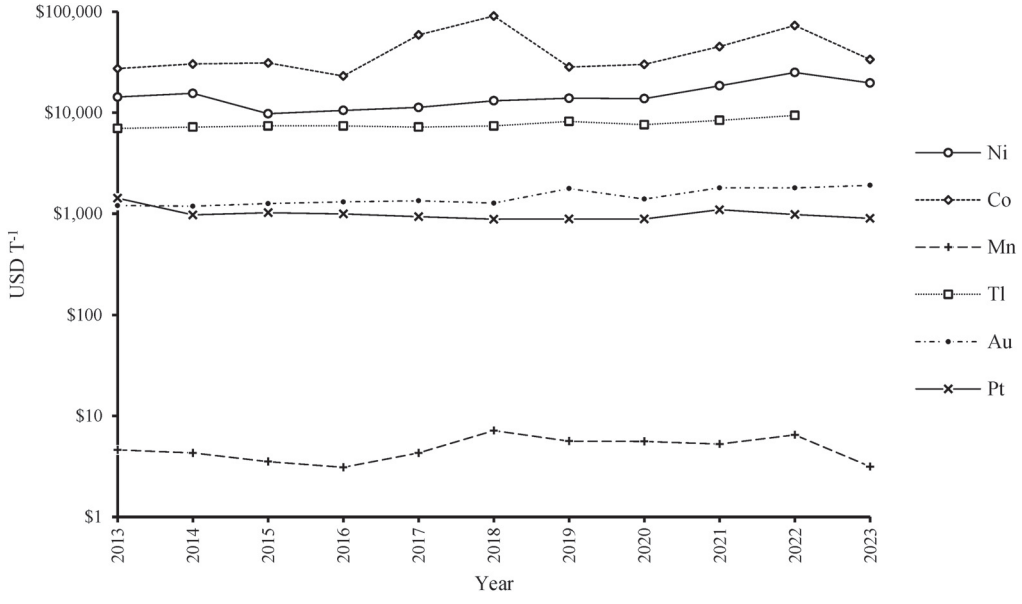

Figure 2. Metal price trends of the last decade.

Table 8. Economically viable concentrations of precious metals in the harvested biomass that are necessary to make the phytomining process profitable.

Element	Natural Occurrence in the Earth's Crust (mg kg^{-1})	Economically Viable Plant Metal Concentration (mg kg^{-1})	Economic Proposed Concentration in Biomass (mg kg^{-1})	Reference
Au	0.0040	6	0.06–0.6	Lee et al. [176]
Ag	0.0750	1000	10–100	Lee et al. [176]
Pd	0.0150	5–15	0.05–1.5	Lee et al. [176]
Pt	0.0050	4	0.04–0.4	Dinh et al. [15]
Rh	0.0010	5–15	0.05–1.5	Dinh et al. [15]

Manganese is an example of an element where even though its price is low, USD 6.5 t^{-1}, there are certain plants that can accumulate large quantities of it. Macadamia plants have been reported to accumulate high concentrations of Mn in their tissues; therefore, they can be a feasible and profitable option. However, metal prices often undergo cycles of fluctuations—PM may be viable, if technically possible, even while current market prices happen to be low. There is always the capability of combusting the biomass which contains the extracted metal to recover the economic value; metals can be extracted from plants and the remaining material can be burned to generate energy. After combustion, the ash could be stored until the world price of the extracted metals improves [10,174]. Moreover, companies do not only make profit just from the PM process but also from harnessing the biomass for energy production. Additionally, they may be utilizing the resulting ash as a source of C and potash. Furthermore, they may be deriving advantages from the sale of CO_2 credits [57].

As mentioned earlier, during the first field experiment for extracting Ni, *Streptanthus polygaloides* yielded a total dry biomass of 10,000 kg ha^{-1} containing 10,000 mg kg^{-1} Ni. It is reported that a net profit of USD 513 ha^{-1} could be achieved with a price of USD 7.65 kg^{-1} at that time. In addition, a net return of USD 131 ha^{-1} could be achieved due to energy yield during the combustion of the biomass, leading to a gross return of USD 765 ha^{-1}. Considering Ni current prices, of approximately USD 20 kg^{-1}, such yields and Ni uptake could achieve a gross profit of USD 1341 ha^{-1}. Anderson et al. [177] utilized the Tl hyperaccumulator *I. intermedia* and extracted 8 kg ha^{-1} of Tl in a total of 10,000 kg ha^{-1} dry biomass, which was worth a total of USD 2400. This means that a crop with 10,000 kg ha^{-1} of biomass would need to accumulate at least 170 mg kg^{-1} Tl, which is achievable by *I. intermedia*. On the other hand, as previously stated, *B. laevigata* produces lower biomass (4000 kg ha^{-1}), which means that an average of 425 mg Tl kg^{-1} is required—it was found that 39% of the plants surpassed this threshold in that work. Selling biomass for power generation could also add a profitable amount to the farmer's income.

In addition, Nkrumah et al. [178] suggested the use of both an intensive and extensive Ni production system. Moreover, both approaches were found to be profitable. Extensive systems are those where the only costs are herbicides, fertilizers, and any management practices, while an intensive production system requires additional labor and equipment costs. They even made a hypothetical scenario where they calculated the economic potential of Ni PM, comparing the two approaches. Specifically, they (a) considered an average market price of USD 18 over a 5-year period from 2010 to 2015, (b) estimated the amount of Ni that plants can produce in the two systems, which was leveled at 200 kg ha^{-1} for the intensive system and 110 kg ha^{-1} for the extensive, (c) calculated the cost of the production in 2016, which was approximately USD 1074 ha^{-1} $year^{-1}$ and USD 600 ha^{-1} $year^{-1}$ for the intensive and the extensive systems, respectively, and (d) included in that about 20% of the value of Ni that would cover expenses and costs associated with metal recovery from plants. Assuming these factors, they calculated the gross values of an annual PM crop, which was found to be USD 3600 ha^{-1} $year^{-1}$ for the intensive system and USD 1980 ha^{-1} $year^{-1}$

for the extensive system. After accounting the costs that were mentioned before, they measured a net value of USD 1806 ha^{-1} $year^{-1}$ for the intensive system and a net value of USD 980 ha^{-1} $year^{-1}$ for the extensive system. In addition, other sources for enhancing profit could be harnessing energy from combustion or selling carbon credits for reducing gas emissions.

Lee et al. [176] mentioned the remarkable metal-accumulating abilities of *Haumaniastrum robertii* and *Aeolanthus biformifolius*. Specifically, *H. robertii* is capable of accumulating up to 1% of its dry biomass as Co, while *A. biformifolius* can accumulate up to 1% of its dry biomass as Cu. As a result, commercial use of *H. robertii* can lead to a harvest of 200 kg Co per 20 t of dry biomass per year. Assuming 100% Co recovery and a current Co market price per ton of USD 33,618, this could potentially result in USD 6723 of income ha^{-1} per year. Similarly, *A. biformifolius* has the potential to yield 200 kg of Cu from 20 t of dry biomass ha^{-1} per year. Assuming 100% Cu recovery and a current market price of USD 7963 for Cu, this could lead to a gross income of USD 1592 ha^{-1} per year.

As the process of PM continues over time, the ore deposits eventually get depleted, making it less economically viable to obtain them. Nevertheless, compared to the conventional mining methods, the time when it will no longer be cost effective to mine these metals through PM is much higher. This is because PM is a cost–benefit method. Moreover, plants used in the PM process can have a multifaceted application until the soil where they are planted is ready for food production once again. Ongoing research towards a better understanding of the mechanisms involved in the PM process, along with other improvements, is expected to extend the economic viability of mined metals through PM.

5. Conclusions and Need for Future Research

While PM holds significant potential, it faces certain limitations, such as the selection of specific plants for certain metals, along with any challenges presented by the formation of the metal compounds in soil. However, PM leverages the natural ability of the plants to accumulate large amounts of valuable metals. It can not only create income for growers but it also provides mineral supplementation and biofuel resources. We indicated that generated income is not improbable; e.g., significant earnings are possible if a yield of 10 t ha^{-1} of the hyperaccumulator is combined with an average Ni concentration of 1000 mg kg^{-1}. Specifically, economic viability depends on factors like metal content in soil, BAF and TF values of the selected plant species, biomass yields, and metal prices. On the other hand, extensive research remains necessary so that the capabilities and limitations of the PM process may be fully understood. While the majority of the studies have been conducted at the laboratory scale and in a controlled environment for short periods, the true potential of PM awaits investigation at the commercial scale under field conditions for longer periods of time. In addition, interdisciplinary research efforts that combine expertise in different fields of science, such as soil science, plant biology, genetics, and soil chemistry, as well as knowledge of farming practices, are essential for unlocking PM's full potential. Moreover, it is essential to acknowledge that most of the conducted experiments have taken place in developed countries, leaving a knowledge gap for developing nations. We conclude that PM, although a relatively new and unexplored concept, may provide economic and environmental benefits to soil end-users and managers who must cultivate on metal-contaminated soils as PM may turn yield shortages (of specific commercial crops) into benefits if high-yield hyperaccumulators are cultivated for industrial valorization of their high-metal-content biomass. The future of PM should be approached with a balanced perspective, realizing that it may represent a shift in our resource extraction. Phytomining could be the transformative concept whose time has come, provided that we continue to invest in comprehensive research, innovation, and sustainable practices.

Author Contributions: Conceptualization V.A.; writing—original draft preparation, C.K.; review and editing, V.A. and G.T.; visualization, C.K. and G.T.; supervision, V.A. All authors have read and agreed to the published version of the manuscript.

Funding: This research received no external funding.

Institutional Review Board Statement: Not applicable.

Informed Consent Statement: Not applicable.

Data Availability Statement: No new data were created or analyzed in this study. Data sharing is not applicable to this article.

Conflicts of Interest: The authors declare no conflicts of interest.

References

1. Aziz, I.; Mujeeb, A. Halophytes for phytoremediation of hazardous metal (loid) s: A terse review on metal tolerance, bio-indication and hyperaccumulation. *J. Hazard. Mat.* **2022**, *424*, 127309. [CrossRef] [PubMed]
2. Reeves, R.D.; van Der Ent, A.; Echevarria, G.; Isnard, S.; Baker, A.J. Global distribution and ecology of hyperaccumulator plants. In *Agromining: Farming for Metals*, 2nd ed.; van der Ent, A., Baker, A.J., Echevarria, G., Simonnot, M.O., Eds.; Springer: Cham, Switzerland, 2021; pp. 133–154. [CrossRef]
3. Soleymanifar, S.; Ehsanpour, A.A.; Ghasemi, R.; Schat, H. The effect of L-histidine on nickel translocation and the activities of antioxidant enzymes in hyperaccumulator (*Odontarrhena inflata*) and non-accumulator (*Aurinia saxatilis*) plants. *Plant Soil* **2023**, *491*, 1–18. [CrossRef]
4. Siyar, R.; Doulati Ardejani, F.; Norouzi, P.; Maghsoudy, S.; Yavarzadeh, M.; Taherdangkoo, R.; Butscher, C. Phytoremediation potential of native hyperaccumulator plants growing on heavy metal-contaminated soil of Khatunabad copper smelter and refinery, Iran. *Water* **2022**, *14*, 3597. [CrossRef]
5. Sheoran, V.; Sheoran, A.S.; Poonia, P. Phytomining: A review. *Miner. Eng.* **2009**, *22*, 1007–1019. [CrossRef]
6. Akinbile, B.J.; Makhubela, B.C.; Ambushe, A.A. Phytomining of valuable metals: Status and prospective-a review. *Int. J. Environ. Anal. Chem.* **2023**, *103*, 39133933. [CrossRef]
7. Li, Y.M.; Chaney, R.L.; Brewer, E.P.; Angle, J.S.; Nelkin, J. Phytoextraction of nickel and cobalt by hyperaccumulator Alyssum species grown on nickel-contaminated soils. *Environ. Sci. Technol.* **2003**, *37*, 1463–1468. [CrossRef]
8. Chaney, R.L.; Chen, K.Y.; Li, Y.M.; Angle, J.S.; Baker, A.J. Effects of calcium on nickel tolerance and accumulation in Alyssum species and cabbage grown in nutrient solution. *Plant Soil* **2008**, *311*, 131–140. [CrossRef]
9. Rai, V.; Liu, D.; Xia, D.; Jayaraman, Y.; Gabriel, J.C.P. Electrochemical approaches for the recovery of metals from electronic waste: A critical review. *Recycling* **2021**, *6*, 53. [CrossRef]
10. Jaffré, T.; Brooks, R.R.; Lee, J.; Reeves, R.D. *Sebertia acuminata*: A hyperaccumulator of nickel from New Caledonia. *Science* **1976**, *193*, 579–580. [CrossRef]
11. Xie, C.; Xiao, Y.; He, C.; Liu, W.S.; Tang, Y.T.; Wang, S.; Qiu, R.L. Selective recovery of rare earth elements and value-added chemicals from the *Dicranopteris linearis* bio-ore produced by agromining using green fractionation. *J. Hazard. Mater.* **2023**, *443*, 130253. [CrossRef]
12. Robinson, B.; Fernández, J.E.; Madejón, P.; Marañón, T.; Murillo, J.M.; Green, S.; Clothier, B. Phytoextraction: An assessment of biogeochemical and economic viability. *Plant Soil.* **2003**, *249*, 117–125. [CrossRef]
13. Subašić, M.; Šamec, D.; Selović, A.; Karalija, E. Phytoremediation of cadmium polluted soils: Current status and approaches for enhancing. *Soil Syst.* **2022**, *6*, 3. [CrossRef]
14. Islam, M.D.; Hasan, M.M.; Rahaman, A.; Haque, P.; Islam, M.S.; Rahman, M.M. Translocation and bioaccumulation of trace metals from industrial effluent to locally grown vegetables and assessment of human health risk in Bangladesh. *SN Appl. Sci.* **2020**, *2*, 1315. [CrossRef]
15. Dinh, T.; Dobo, Z.; Kovacs, H. Phytomining of noble metals—A review. *Chemosphere* **2022**, *286*, 131805. [CrossRef] [PubMed]
16. Nkrumah, P.N.; Chaney, R.L.; Morel, J.L. Agronomy of 'metal crops' used in agromining. In *Agromining: Farming for Metals*; Metal Resources Reviews; van der Ent, A., Baker, A.J., Echevarria, G., Simonnot, M.O., Eds.; Springer: Cham, Switzerland, 2021; pp. 23–46. [CrossRef]
17. Baker, A.J.; Brooks, R. Terrestrial higher plants which hyperaccumulate metallic elements. A review of their distribution, ecology and phytochemistry. *Biorecovery* **1989**, *1*, 81–126.
18. Van der Ent, A.; Baker, A.J.M.; Reeves, R.D.; Pollard, A.J.; Schat, H. Hyperaccumulators of metal and metalloid trace elements: Facts and fiction. *Plant Soil* **2013**, *362*, 319–334. [CrossRef]
19. Krämer, U. Metal hyperaccumulation in plants. *Annu. Rev. Plant Biol.* **2010**, *61*, 517–534. [CrossRef] [PubMed]
20. Reeves, R.D. Hyperaccumulation of trace elements by plants. In *Phytoremediat. Of Metal-Contaminated Soils*; Morel, J.L., Echevarria, G., Goncharova, N., Eds.; Springer: New York, NY, USA, 2006; pp. 1–25.
21. Mustafa, A.; Zulfiqar, U.; Mumtaz, M.Z.; Radziemska, M.; Haider, F.U.; Holatko, J.; Brtnicky, M. Nickel (Ni) phytotoxicity and detoxification mechanisms: A review. *Chemosphere* **2023**, *328*, 138574. [CrossRef]
22. Minguzzi, C.; Vergnano, O. Il contenuto di nichel nelle ceneri di *Alyssum Bertolonii*. *Atti. Soc. Tosc. Sci. Nat.* **1948**, *55*, 49–74.
23. Chaney, R.L.; Angle, J.S.; Baker, A.J.M.; Li, J.M. Method for Phytomining of Nickel, Cobalt, and Other Metal from Soil. U.S. Patent 5,711,784, 31 August 1999.

24. Robinson, B.H.; Chiarucci, A.; Brooks, R.R.; Petit, D.; Kirkman, J.H.; Gregg, P.E.H.; Dominicis, V. The nickel hyperaccumulator plant *Alyssum bertolonii* as a potential agent for phytoremediation and phytomining of nickel. *J. Geochem. Explor.* **1997**, *59*, 75–86. [CrossRef]
25. Reeves, R.D.; Brooks, R.R.; Macfarlane, R.M. Nickel uptake by Californian Streptanthus and Caulanthus with particular reference to the hyperaccumulator *S. polygaloides* Gray (Brassicaceae). *Am. J. Bot.* **1981**, *68*, 708–712. [CrossRef]
26. Mohsin, M.; Nawrot, N.; Wojciechowska, E.; Kuittinen, S.; Szczepanska, K.; Dembska, G.; Pappinen, A. Cadmium Accumulation by *Phragmites australis* and *Iris pseudacorus* from Stormwater in Floating Treatment Wetlands Microcosms: Insights into Plant Tolerance and Utility for Phytoremediation. *J. Environ. Manag.* **2023**, *331*, 117339. [CrossRef] [PubMed]
27. Cole, M.M. Geobotanical and biogeochemical investigations in the sclerophyllous woodland and shrub associations of the Eastern Goldfield Area of Western Australia, with particular reference to the role of *Hybanthus floribundus* (Lindl.) F. Muell. As a nickel indicator and accumulator plant. *J. Appl. Ecol.* **1973**, *10*, 269–320. [CrossRef]
28. Durand, A.; Goux, X.; Lopez, S.; Leglize, P.; Benizri, E. Soil nickel contamination levels entail changes in the bacterial communities associated to the rhizosphere and endosphere of *Odontarrhena chalcidica*. *Plant Soil* **2023**, *493*, 17–43. [CrossRef]
29. Bani, A.; Echevarria, G.; Sulçe, S.; Morel, J.L. Improving the agronomy of *Alyssum murale* for extensive phytomining: A five-year field study. *Int. J. Phytoremediat.* **2015**, *17*, 117–127. [CrossRef]
30. Galardi, F.; Corrales, I.; Mengoni, A.; Pucci, S.; Barletti, L.; Barzanti, R.; Gonnelli, C. Intra-specific differences in nickel tolerance and accumulation in the Ni-hyperaccumulator *Alyssum bertolonii*. *Environ. Exp. Bot.* **2007**, *60*, 377–384. [CrossRef]
31. Kanellopoulos, C.; Argyraki, A. Soil baseline geochemistry and plant response in areas of complex geology. Application to NW Euboea, Greece. *Geochemistry* **2013**, *73*, 519–532. [CrossRef]
32. Adamidis, G.C.; Aloupi, M.; Kazakou, E.; Dimitrakopoulos, P.G. Intra-specific variation in Ni tolerance, accumulation and translocation patterns in the Ni-hyperaccumulator *Alyssum lesbiacum*. *Chemosphere* **2014**, *95*, 496–502. [CrossRef]
33. Keeling, S.M.; Stewart, R.B.; Anderson, C.W.N.; Robinson, B.H. Nickel and cobalt phytoextraction by the hyperaccumulator *Berkheya coddii*: Implications for polymetallic phytomining and phytoremediation. *Int. J. Phytoremediat.* **2003**, *5*, 235–244. [CrossRef]
34. Van der Ent, A.; Baker, A.J.M.; Van Balgooy, M.M.J.; Tjoa, A. Ultramafic nickel laterites in Indonesia (Sulawesi, Halmahera): Mining, nickel hyperaccumulators and opportunities for phytomining. *J. Geochem. Explor.* **2013**, *128*, 72–79. [CrossRef]
35. Becquer, T.; Rigault, F.; Jaffré, T. Nickel bioavailability assessed by ion exchange resin in the field. *Commun. Soil Sci. Plant Anal.* **2002**, *33*, 439–450. [CrossRef]
36. Jaffré, T.; Pillon, Y.; Thomine, S.; Merlot, S. The metal hyperaccumulators from New Caledonia can broaden our understanding of nickel accumulation in plants. *Front. Plant. Sci.* **2013**, *4*, 279. [CrossRef]
37. Li, G.Y.; Hu, N.; Ding, D.X.; Zheng, J.F.; Liu, Y.L.; Wang, Y.D.; Nie, X.Q. Screening of plant species for phytoremediation of uranium, thorium, barium, nickel, strontium and lead contaminated soils from a uranium mill tailings repository in South China. *Bull. Environ. Contam. Toxicol.* **2011**, *86*, 646–652. [CrossRef]
38. Berazaín, R.; de la Fuente, V.; Rufo, L.; Rodríguez, N.; Amils, R.; Díez, G.B.; Asensi, A. Nickel localization in tissues of different hyperaccumulator species of Euphorbiaceae from ultramafic areas of Cuba. *Plant Soil* **2007**, *293*, 99–106. [CrossRef]
39. Hamdan, A.M.; Bijaksana, S.; Tjoa, A.; Dahrin, D.; Kirana, K.H. Magnetic characterizations of nickel hyperaccumulating plants (*Planchonella oxyhedra* and *Rinorea bengalensis*) from Halmahera, Indonesia. *Int. J. Phytoremediat.* **2019**, *21*, 364–371. [CrossRef] [PubMed]
40. Davis, M.A.; Boyd, R.S. Dynamics of Ni-based defence and organic defences in the Ni hyperaccumulator, *Streptanthus polygaloides* (Brassicaceae). *New Phytol.* **2000**, *146*, 211–217. [CrossRef]
41. Rue, M.; Paul, A.L.; Echevarria, G.; van Der Ent, A.; Simonnot, M.O.; Morel, J.L. Uptake, translocation and accumulation of nickel and cobalt in *Berkheya coddii*, a 'metal crop'from South Africa. *Metallomics* **2020**, *12*, 1278–1289. [CrossRef]
42. Parks, S. Cobalt hyperaccumulation in *Rinorea* cf. *bengalensis* (Violaceae) from Sabah: Accumulation potential and tissue and cellular-level distribution of cobalt. *Plant Soil* **2020**, *455*, 289–303. [CrossRef]
43. Jaffré, T. Plant mineral nutrition on ultramafic rocks of New Caledonia. *Bot. Lett.* **2023**, *170*, 375–411. [CrossRef]
44. Malik, M.; Chaney, R.L.; Brewer, E.P.; Li, Y.M.; Angle, J.S. Phytoextraction of soil cobalt using hyperaccumulator plants. *Int. J. Phytoremediat.* **2000**, *2*, 319–329. [CrossRef]
45. Robinson, B.H.; Brooks, R.R.; Clothier, B.E. Soil amendments affecting nickel and cobalt uptake by *Berkheya coddii*: Potential use for phytomining and phytoremediation. *Ann. Bot.* **1999**, *84*, 689–694. [CrossRef]
46. Faucon, M.P.; Shutcha, M.N.; Meerts, P. Revisiting copper and cobalt concentrations in supposed hyperaccumulators from SC Africa: Influence of washing and metal concentrations in soil. *Plant Soil* **2007**, *301*, 29–36. [CrossRef]
47. Morrison, R.S.; Brooks, R.R.; Reeves, R.D.; Malaisse, F. Copper and cobalt uptake by metallophytes from Zaïre. *Plant Soil* **1979**, *53* 535–539. [CrossRef]
48. Homer, F.A.; Morrison, R.S.; Brooks, R.R.; Clemens, J.; Reeves, R.D. Comparative studies of nickel, cobalt, and copper uptake by some nickel hyperaccumulators of the genus Alyssum. *Plant Soil* **1991**, *138*, 195–205. [CrossRef]
49. Lange, B.; van Der Ent, A.; Baker, A.J.M.; Echevarria, G.; Mahy, G.; Malaisse, F.; Faucon, M.P. Copper and cobalt accumulation in plants: A critical assessment of the current state of knowledge. *New Phytol.* **2017**, *213*, 537–551. [CrossRef]
50. Olawuyi, O.J.; Bamigbegbin, B.J.; Bello, O.B. Genetic variation of morphological and yield characters of *Celosia argentea* L. germplasm. *J. Bas. Appl. Res. Int.* **2016**, *13*, 160–169.
51. Hu, D.; Cheng, M.; Hu, K.; Zhang, W.; Yang, Y.; Xu, Q. Evaluation of cobalt hyperaccumulation and tolerance potential of the duckweed (*Lemna minor* L.). *Ecotoxicol. Environ. Saf.* **2019**, *179*, 79–87. [CrossRef]

52. Van Der Ent, A.; Malaisse, F.; Erskine, P.D.; Mesjasz-Przybyłowicz, J.; Przybyłowicz, W.J.; Barnabas, A.D.; Harris, H.H. Abnormal concentrations of Cu–Co in *Haumaniastrum katangense*, *Haumaniastrum robertii* and *Aeolanthus biformifolius*: Contamination or hyperaccumulation? *Metallomics* **2019**, *11*, 586–596. [CrossRef]
53. Medwecka-Kornaś, A. *Hibiskus rhodanthus* (Malvaceae): An interesting plant species in Southeastern Africa. *Pol. Bot. J.* **2013**, *58*, 325–335. [CrossRef]
54. Memon, A.R.; Itô, S.; Yatazawa, M. Taxonomic characteristics in accumulating cobalt and nickel in the temperate forest vegetation of central Japan. *Soil Sci. Plant Nutr.* **1980**, *26*, 271–280. [CrossRef]
55. Busbee, W.S.; Conner, W.H.; Allen, D.M.; Lanham, J.D. Composition and aboveground productivity of three seasonally flooded depressional forested wetlands in coastal South Carolina. *South. Nat.* **2003**, *2*, 335–346. [CrossRef]
56. Küpper, H.; Leitenmaier, B. Cadmium-accumulating plants. *Met. Ions Life Sci.* **2012**, *11*, 373–393. [CrossRef]
57. Ali, A.; Guo, D.; Mahar, A.; Ping, W.; Wahid, F.; Shen, F.; Zhang, Z. Phytoextraction and the economic perspective of phytomining of heavy metals. *Solid Earth Discuss.* **2017**, *6*, 1–40. [CrossRef]
58. Nedelkoska, T.V.; Doran, P.M. Hyperaccumulation of cadmium by hairy roots of *Thlaspi caerulescens*. *Biotechnol. Bioeng.* **2000**, *67*, 607–615. [CrossRef]
59. Schwartz, C.; Sirguey, C.; Peronny, S.; Reeves, R.D.; Bourgaud, F.; Morel, J.L. Testing of outstanding individuals of *Thlaspi caerulescens* for cadmium phytoextraction. *Int. J. Phytoremediat.* **2006**, *8*, 339–357. [CrossRef] [PubMed]
60. Bert, V.; Bonnin, I.; Saumitou, L.P.; De Laguérie, P.; Petit, D. Do *Arabidopsis halleri* from nonmetallicolous populations accumulate zinc and cadmium more effectively than those from metallicolous populations? *New Phytol.* **2002**, *155*, 47–57. [CrossRef] [PubMed]
61. Deng, D.M.; Deng, J.C.; Li, J.T.; Zhang, J.; Hu, M.; Lin, Z.; Liao, B. Accumulation of zinc, cadmium, and lead in four populations of *Sedum alfredii* growing on lead/zinc mine spoils. *J. Integr. Plant Biol.* **2008**, *50*, 691–698. [CrossRef]
62. Claire-Lise, M.; Nathalie, V. The use of the model species *Arabidopsis halleri* towards phytoextraction of cadmium polluted soils. *New Biotechnol.* **2012**, *30*, 9–14. [CrossRef]
63. Zhao, F.J.; Jiang, R.F.; Dunham, S.J.; McGrath, S.P. Cadmium uptake, translocation and tolerance in the hyperaccumulator *Arabidopsis halleri*. *New Phytol.* **2006**, *172*, 646–654. [CrossRef]
64. Tang, Y.T.; Qiu, R.L.; Zeng, X.W.; Ying, R.R.; Yu, F.M.; Zhou, X.Y. Lead, zinc, cadmium hyperaccumulation and growth stimulation in *Arabis ommercial* Franch. *Environ. Exp. Bot.* **2009**, *66*, 126–134. [CrossRef]
65. Dai, H.; Wei, S.; Skuza, L. Effects of different soil pH and nitrogen fertilizers on *Bidens ommer L*. Cd accumulation. *Environ. Sci. Pollut. Res.* **2020**, *27*, 9403–9409. [CrossRef]
66. Liu, X.; Peng, K.; Wang, A.; Lian, C.; Shen, Z. Cadmium accumulation and distribution in populations of *Phytolacca americana* L. and the role of transpiration. *Chemosphere* **2010**, *78*, 1136–1141. [CrossRef] [PubMed]
67. Liu, W.; Shu, W.; Lan, C. *Viola baoshanensis*, a plant that hyperaccumulates cadmium. *Chin. Sci. Bull.* **2004**, *49*, 29–32. [CrossRef]
68. Nyquist, J.; Greger, M. Response of two wetland plant species to Cd exposure at low and neutral pH. *Environ. Exp. Bot.* **2009**, *65*, 417–424. [CrossRef]
69. Lee, K.K.; Cho, H.S.; Moon, Y.C.; Ban, S.J.; Kim, J.Y. Cadmium and lead uptake capacity of energy crops and distribution of metals within the plant structures. *KSCE J. Civ. Eng.* **2013**, *17*, 44–50. [CrossRef]
70. Wei, J.L.; Lai, H.Y.; Chen, Z.S. Chelator effects on bioconcentration and translocation of cadmium by hyperaccumulators, *Tagetes patula* and *Impatiens walleriana*. *Ecotoxicol. Environ. Saf.* **2012**, *84*, 173–178. [CrossRef] [PubMed]
71. Wang, L.; Chen, X.; Guo, W.; Li, Y.; Yan, H.; Xue, X. Yield and Nutritional Quality of Water Spinach (*Ipomoea aquatica*) as Influenced by Hydroponic Nutrient Solutions with Different pH Adjustments. *Int. J. Agric. Biol.* **2017**, *19*, 635. [CrossRef]
72. Liu, Z.; He, X.; Chen, W.; Yuan, F.; Yan, K.; Tao, D. Accumulation and tolerance characteristics of cadmium in a potential hyperaccumulator—*Lonicera japonica* Thunb. *J. Hazard. Mat.* **2009**, *169*, 170–175. [CrossRef]
73. Zhang, S.; Lin, H.; Deng, L.; Gong, G.; Jia, Y.; Xu, X.; Chen, H. Cadmium tolerance and accumulation characteristics of *Siegesbeckia orientalis* L. *Ecol. Eng.* **2013**, *51*, 133–139. [CrossRef]
74. Giannoulis, K.D.; Karyotis, T.; Sakellariou-Makrantonaki, M.; Bastiaans, L.; Struik, P.C.; Danalatos, N.G. *Switchgrass* biomass partitioning and growth characteristics under different management practices. *NJAS Wagening. J. Life Sci.* **2016**, *78*, 61–67. [CrossRef]
75. Marmiroli, M.; Imperiale, D.; Maestri, E.; Marmiroli, N. The response of *Populus spp*. to cadmium stress: Chemical, morphological and proteomics study. *Chemosphere* **2013**, *93*, 1333–1344. [CrossRef] [PubMed]
76. Stolarski, M.J.; Warmiński, K.; Krzyżaniak, M. Energy value of yield and biomass quality of poplar grown in two consecutive 4-year harvest rotations in the north-east of Poland. *Energies* **2020**, *13*, 1495. [CrossRef]
77. Tang, Y.; Qiu, R.; Zeng, X.; Fang, X.; Yu, F.; Zhou, X.; Wu, Y. Zn and Cd hyperaccumulating characteristics of Picris divaricata Vant. *Int. J. Environ. Pollut.* **2009**, *38*, 26–38. [CrossRef]
78. Kim, T.Y.; Hong, J.H. Nickel Tolerance and the Complexing Role of Histidine in *Raphanus sativus*. *J. Environ. Sci. Int.* **2004**, *13*, 711–719. [CrossRef]
79. Chen, Y.X.; Lin, Q.; Luo, Y.M.; He, Y.F.; Zhen, S.J.; Yu, Y.L.; Wong, M.H. The role of citric acid on the phytoremediation of heavy metal contaminated soil. *Chemosphere* **2003**, *50*, 807–811. [CrossRef] [PubMed]
80. Koutroubas, S.D.; Papakosta, D.K.; Doitsinis, A. Adaptation and yielding ability of castor plant (*Ricinus communis* L.) genotypes in a Mediterranean climate. *Eur. J. Agron.* **1999**, *11*, 227–237. [CrossRef]
81. Huang, H.; Yu, N.; Wang, L.; Gupta, D.K.; He, Z.; Wang, K.; Yang, X.E. The phytoremediation potential of bioenergy crop *Ricinus communis* for DDTs and cadmium co-contaminated soil. *Bioresour. Technol.* **2011**, *102*, 11034–11038. [CrossRef]

82. Vollenweider, P.; Cosio, C.; Günthardt-Goerg, M.S.; Keller, C. Localization and effects of cadmium in leaves of a cadmium-tolerant willow (*Salix viminalis* L.): Part II Microlocalization and cellular effects of cadmium. *Environ. Exp. Bot.* **2006**, *58*, 25–40. [CrossRef]
83. Yang, X.E.; Long, X.X.; Ye, H.B.; He, Z.L.; Calvert, D.V.; Stoffella, P.J. Cadmium tolerance and hyperaccumulation in a new Zn-hyperaccumulating plant species (*Sedum alfredii Hance*). *Plant Soil* **2004**, *259*, 181–189. [CrossRef]
84. Khan, A.R.; Ullah, I.; Khan, A.L.; Hong, S.J.; Waqas, M.; Park, G.S.; Shin, J.H. Phytostabilization and physicochemical responses of Korean ecotype *Solanum nigrum* L. to cadmium contamination. *Water Air Soil Pollut.* **2014**, *225*, 1–11. [CrossRef]
85. Marotti, M.; Piccaglia, R.; Biavati, B.; Marotti, I. Characterization and yield evaluation of essential oils from different Tagetes species. *J. Essent. Oil Res.* **2004**, *16*, 440–444. [CrossRef]
86. Martínez, M.; Bernal, P.; Almela, C.; Vélez, D.; García-Agustín, P.; Serrano, R.; Navarro-Aviñó, J. An engineered plant that accumulates higher levels of heavy metals than *Thlaspi caerulescens*, with yields of 100 times more biomass in mine soils. *Chemosphere* **2006**, *64*, 478–485. [CrossRef] [PubMed]
87. Perronnet, K.; Schwartz, C.; Morel, J.L. Distribution of cadmium and zinc in the hyperaccumulator *Thlaspi caerulescens* grown on multicontaminated soil. *Plant Soil* **2003**, *249*, 19–25. [CrossRef]
88. Xie, W.Y.; Huang, Q.; Li, G.; Rensing, C.; Zhu, Y.G. Cadmium accumulation in the rootless macrophyte *Wolffia ommerc* and its potential for phytoremediation. *Int. J. Phytoremediat.* **2013**, *15*, 385–397. [CrossRef] [PubMed]
89. Oladoye, P.O.; Olowe, O.M.; Asemoloye, M.D. Phytoremediation technology and food security impacts of heavy metal contaminated soils: A review of literature. *Chemosphere* **2022**, *288*, 132555. [CrossRef] [PubMed]
90. Rascio, N. Metal accumulation by some plants growing on zinc-mine deposits. *Oikos* **1977**, *29*, 250–253. [CrossRef]
91. Reeves, R.D.; Brooks, R.R. Hyperaccumulation of lead and zinc by two metallophytes from mining areas of Central Europe. *Environ. Pollut. Ser. A Ecol. Biol.* **1983**, *31*, 277–285. [CrossRef]
92. Baker, A.J.M.; Reeves, R.D.; Hajar, A.S.M. Heavy metal accumulation and tolerance in British populations of the metallophyte *Thlaspi caerulescens* J. & C. Presl (Brassicaceae). *New Phytol.* **1994**, *127*, 61–68. [CrossRef]
93. Brown, S.L.; Chaney, R.L.; Angle, J.S.; Baker, A.J.M. Zinc and cadmium uptake by hyperaccumulator *Thlaspi caerulescens* grown in nutrient solution. *Soil Sci. Soc. Am. J.* **1995**, *59*, 125–133. [CrossRef]
94. Zhao, F.J.; Lombi, E.; Breedon, T.M.S.P. Zinc hyperaccumulation and cellular distribution in *Arabidopsis halleri*. *Plant Cell Environ.* **2000**, *23*, 507–514. [CrossRef]
95. Hu, P.J.; Qiu, R.L.; Senthilkumar, P.; Jiang, D.; Chen, Z.W.; Tang, Y.T.; Liu, F.J. Tolerance, accumulation and distribution of zinc and cadmium in hyperaccumulator *Potentilla griffithii*. *Environ. Exp. Bot.* **2009**, *66*, 317–325. [CrossRef]
96. Grimm, M. Feasibility of *Brassica juncea* as a Hyperaccumulator in Phytomining of Cu and Zn. In Proceedings of the EGU General Assembly Conference Abstracts, Vienna, Austria, 23–27 May 2022. [CrossRef]
97. Grison, C.M.; Mazel, M.; Sellini, A.; Escande, V.; Biton, J.; Grison, C. The leguminous species *Anthyllis vulneraria* as a Zn-hyperaccumulator and eco-Zn catalyst resources. *Environ. Sci. Pollut. Res.* **2015**, *22*, 5667–5676. [CrossRef]
98. Peer, W.A.; Mahmoudian, M.; Freeman, J.L.; Lahner, B.; Richards, E.L.; Reeves, R.D.; Salt, D.E. Assessment of plants from the Brassicaceae family as genetic models for the study of nickel and zinc hyperaccumulation. *New Phytol.* **2006**, *172*, 248–260. [CrossRef]
99. Reeves, R.D.; Baker, A.J.; Jaffré, T.; Erskine, P.D.; Echevarria, G.; van Der Ent, A. A global database for plants that hyperaccumulate metal and metalloid trace elements. *New Phytol.* **2018**, *218*, 407–411. [CrossRef]
100. Balafrej, H.; Bogusz, D.; Triqui, Z.E.A.; Guedira, A.; Bendaou, N.; Smouni, A.; Fahr, M. Zinc hyperaccumulation in plants: A review. *Plants* **2020**, *9*, 562. [CrossRef] [PubMed]
101. Lin, W.; Xiao, T.; Wu, Y.; Ao, Z.; Ning, Z. Hyperaccumulation of zinc by *Corydalis davidii* in Zn-polluted soils. *Chemosphere* **2012**, *86*, 837–842. [CrossRef] [PubMed]
102. Shimwell, D.W.; Laurie, A.E. Lead and zinc contamination of vegetation in the Southern Pennines. *Environ. Pollut.* **1972**, *3*, 291–301. [CrossRef]
103. Reeves, R.D.; Brooks, R.R. European species of *Thlaspi* L. (Cruciferae) as indicators of nickel and zinc. *J. Geochem. Explor.* **1983**, *18*, 275–283. [CrossRef]
104. Yang, X.E.; Long, X.; Ni, W.; Fu, C. *Sedum alfredii* H: A new Zn hyperaccumulating plant first found in China. *Chin. Sci. Bull.* **2002**, *47*, 1634–1637. [CrossRef]
105. Qiu, R.; Fang, X.; Tang, Y.; Du, S.; Zeng, X.; Brewer, E. Zinc hyperaccumulation and uptake by *Potentilla griffithii* Hook. *Int. J. Phytoremediat.* **2006**, *8*, 299–310. [CrossRef]
106. Wu, C.; Liao, B.; Wang, S.L.; Zhang, J.; Li, J.T. Pb and Zn accumulation in a Cd-hyperaccumulator (*Viola baoshanensis*). *Int. J. Phytoremediat.* **2010**, *12*, 574–585. [CrossRef] [PubMed]
107. Losfeld, G.; L'huillier, L.; Fogliani, B.; Coy, S.M.; Grison, C.; Jaffré, T. Leaf-age and soil-plant relationships: Key factors for reporting trace-elements hyperaccumulation by plants and design applications. *Environ. Sci. Pollut. Res.* **2015**, *22*, 5620–5632. [CrossRef] [PubMed]
108. Jaffré, T. Accumulation Du Manganèse Par Les Proteacées de Nouvelle-Calédonie. *Acad. Sci.* **1979**, *289*, 425–428.
109. Mizuno, T.; Asahina, R.; Hosono, A.; Tanaka, A.; Senoo, K.; Obata, H. Age-dependent manganese hyperaccumulation in *Chengiopanax sciadophylloides* (Araliaceae). *J. Plant Nutr.* **2008**, *31*, 1811–1819. [CrossRef]
110. Fernando, D.R.; Marshall, A.; Baker, A.J.; Mizuno, T. Microbeam methodologies as powerful tools in manganese hyperaccumulation research: Present status and future directions. *Front. Plant Sci.* **2013**, *4*, 319. [CrossRef]

111. Fernando, D.R.; Guymer, G.; Reeves, R.D.; Woodrow, I.E.; Baker, A.J.; Batianoff, G.N. Foliar Mn accumulation in eastern Australian herbarium specimens: Prospecting for 'new'Mn hyperaccumulators and potential applications in taxonomy. *Ann. Bot.* **2009**, *103*, 931–939. [CrossRef]
112. Abubakari, F.; Nkrumah, P.N.; Erskine, P.D.; Brown, G.K.; Fernando, D.R.; Echevarria, G.; van Der Ent, A. Manganese (hyper) accumulation within *Australian denhamia* (Celastraceae): An assessment of the trait and manganese accumulation under controlled conditions. *Plant Soil* **2021**, *463*, 205–223. [CrossRef]
113. Liu, J.; Shang, W.; Zhang, X.; Zhu, Y.; Yu, K. Mn accumulation and tolerance in *Celosia argentea* Linn: A new Mn-hyperaccumulating plant species. *J. Hazard. Mater.* **2014**, *267*, 136–141. [CrossRef]
114. Bidwell, S.D.; Woodrow, I.E.; Batianoff, G.N.; Sommer-Knudsen, J. Hyperaccumulation of manganese in the rainforest tree *Austromyrtus bidwillii* (Myrtaceae) from Queensland, Australia. *Funct. Plant Biol.* **2002**, *29*, 899–905. [CrossRef]
115. Xue, S.G.; Chen, Y.X.; Reeves, R.D.; Baker, A.J.; Lin, Q.; Fernando, D.R. Manganese uptake and accumulation by the hyperaccumulator plant *Phytolacca ommerc* Roxb. (Phytolaccaceae). *Environ. Pollut.* **2004**, *131*, 393–399. [CrossRef]
116. Deng, H.; Li, M.; Chen, Y.; Luo, Y.; Yu, F. A new discovered manganese hyperaccumulator-*Polygonum pubescens* Blume. *Fresenius Environ. Bull.* **2010**, *19*, 94–99.
117. Liu, K.; Yu, F.; Chen, M.; Zhou, Z.; Chen, C.; Li, M.S.; Zhu, J. A newly found manganese hyperaccumulator—*Polygonum lapathifolium* Linn. *Int. J. Phytoremediat.* **2016**, *18*, 348–353. [CrossRef]
118. Yang, S.X.; Deng, H.; Li, M.S. Manganese uptake and accumulation in a woody hyperaccumulator, *Schima superba*. *Plant Soil Environ.* **2008**, *54*, 441–446. [CrossRef]
119. White, P.J. Selenium accumulation by plants. *Ann. Bot.* **2016**, *117*, 217–235. [CrossRef] [PubMed]
120. Parker, D.R.; Feist, L.J.; Varvel, T.W.; Thomason, D.N.; Zhang, Y. Selenium phytoremediation potential of *Stanleya pinnata*. *Plant Soil* **2003**, *249*, 157–165. [CrossRef]
121. Reeves, R.D. Metal-Accumulating Plants. In *Phytoremediat. Of Toxic Metals: Using Plants to Clean Up the Environment*; Ensley, B.D., Ed.; John Wiley & Son: London, UK, 2000; pp. 193–229.
122. Moon, D.M. Yield potential of *Asparagus officinalis* L. *N. Z. J. Exp. Agric.* **1976**, *4*, 435–438. [CrossRef]
123. Nadaf, S.K.; Al-Khamisi, S.A.; AI-Lawati, A.H.; Ibrahim, Y.M.; EI-Hag, M.G. Productivity of saltbush (Atriplex) species under saline soil and water conditions in Oman. *J. Agric. Mar. Sci.* **1999**, *4*, 41–46. [CrossRef]
124. Nedjimi, B. Measurement of selenium in two Algerian chenopods (*Atriplex canescens* (Pursh.) Nutt. And *Suaeda ommercia* (Linn.) Forssk). *Measurement* **2018**, *129*, 256–259. [CrossRef]
125. Ma, Y.; Yin, J.; Wang, J.; Liu, X.; He, J.; Zhang, R.; Wu, M. Selenium speciation and volatile flavor compound profiles in the edible flowers, stems, and leaves of selenium-hyperaccumulating vegetable *Cardamine violifolia*. *Food Chem.* **2023**, *427*, 136710. [CrossRef]
126. Huang, C.; Ying, H.; Yang, X.; Gao, Y.; Li, T.; Wu, B.; Wang, L. The *Cardamine enshiensis* genome reveals whole genome duplication and insight into selenium hyperaccumulation and tolerance. *Cell Discov.* **2021**, *7*, 62. [CrossRef]
127. O'Donohue, B.; Hiti-Bandaralage, J.; Gleeson, M.; O'Brien, C.; Harvey, M.A.; van der Ent, A.; Hayward, A. Tissue culture tools for selenium hyperaccumulator *Neptunia amplexicaulis* for development in phytoextraction. *Nat. Prod. Bioprosp.* **2022**, *12*, 28. [CrossRef]
128. Pinto Irish, K.; Harvey, M.A.; Erskine, P.D.; van der Ent, A. Root foraging and selenium uptake in the Australian hyperaccumulator *Neptunia amplexicaulis* and non-accumulator Neptunia gracilis. *Plant Soil* **2021**, *462*, 219–233. [CrossRef]
129. Harris, J.; Schneberg, K.A.; Pilon-Smits, E.A. Sulfur–selenium–molybdenum interactions distinguish selenium hyperaccumulator *Stanleya pinnata* from non-hyperaccumulator *Brassica juncea* (Brassicaceae). *Planta* **2014**, *239*, 479–491. [CrossRef]
130. Leblanc, M.; Petit, D.; Deram, A.; Robinson, B.H.; Brooks, R.R. The phytomining and environmental significance of hyperaccumulation of thallium by *Iberis intermedia* from southern France. *Econ. Geol.* **1999**, *94*, 109–113. [CrossRef]
131. Sinha, R.; Singh, A.K.; Bauddh, K.; Sharma, T.R.; Sharma, P. Phytomining: A sustainable approach for recovery and extraction of valuable metals. In *Phytorestoration of Abandoned Mining and Oil Drilling Sites*; Bauddh, K., Korstad, J., Sharma, P., Eds.; Elsevier: Amsterdam, The Netherlands, 2021; pp. 487–506. [CrossRef]
132. Mohan, B.S. Phytomining of gold. *Curr. Sci.* **2005**, *88*, 1021–1022.
133. Corzo, R.A.; Chaney, R.L.; Baker, A.J.; Edraki, M.; Erskine, P.D.; Echevarria, G.; van der Ent, A. Phytoextraction of high value elements and contaminants from mining and mineral wastes: Opportunities and limitations. *Plant Soil* **2020**, *449*, 11–37. [CrossRef]
134. Anderson, C.W.; Brooks, R.R.; Stewart, R.B.; Simcock, R. Harvesting a crop of gold in plants. *Nature* **1998**, *395*, 553–554. [CrossRef]
135. Wilson, C.V.; Anderson, C.W.; Rodriguez, L.M. Gold phytomining. A review of the relevance of this technology to mineral extraction in the 21st century. *J. Environ. Manag.* **2012**, *111*, 249–257. [CrossRef]
136. Msuya, F.A.; Brooks, R.R.; Anderson, C.W. Chemically-induced uptake of gold by root crops: Its significance for phytomining. *Gold Bull.* **2000**, *33*, 134–137. [CrossRef]
137. Lamb, A.E.; Anderson, C.W.N.; Haverkamp, R.G. The extraction of gold from plants and its application to phytomining. *Chem. N. Z.* **2001**, *65*, 31–33.
138. Vural, A.; Safari, S. Phytoremediation ability of *Helichrysum arenarium* plant for Au and Ag: Case study at Demirören village (Gümüşhane, Turkey). *Gold Bull.* **2022**, *55*, 129–136. [CrossRef]
139. Harris, A.T.; Bali, R. On the formation and extent of uptake of silver nanoparticles by live plants. *J. Nanopart. Res.* **2008**, *10*, 691–695. [CrossRef]
140. Fuchs, W.A.; Rose, A.W. The geochemical behavior of platinum and palladium in the weathering cycle in the Stillwater Complex, Montana. *Econ. Geol.* **1974**, *69*, 332–346. [CrossRef]

141. Kothny, E.L. Palladium in plant ash. *Plant Soil* **1979**, *53*, 547–550. [CrossRef]
142. Nemutandani, T.; Dutertre, D.; Chimuka, L.; Cukrowska, E.; Tutu, H. The potential of *Berkheya coddii* for phytoextraction of nickel, platinum, and palladium contaminated sites. *Toxicol. Environ. Chem.* **2006**, *88*, 175–185. [CrossRef]
143. Walton, D. The Phytoextraction of Gold and Palladium from Mine Tailings. Ph.D. Thesis, Massey University, Wellington, New Zealand, 2002.
144. Aquan, H.M. Phytoextraction of Palladium and Gold from Broken Hill Gossan. Ph.D. Thesis, Massey University, Manawatū, New Zealand, 2015.
145. Harumain, Z.A.S.; Parker, H.L.; Austin, M.J.; McElroy, M.C.; Andrea, M.G.; Robert, M.C.; WN, A.C.; Luca, C.; Graedel, T.E.; Rylott, E.L.; et al. Toward Financially Viable Phytoextraction and Production of Plant-Based Palladium Catalysts. *Environ. Sci. Technol.* **2017**, *51*, 2992–3000. [CrossRef]
146. Kovacs, H.; Dobo, Z.; Koos, T.; Gyimesi, A.; Nagy, G. Influence of the flue gas temperature on the behavior of metals during biomass combustion. *Energy Fuels* **2018**, *32*, 7851–7856. [CrossRef]
147. Diehl, D.B.; Gagnon, Z.E. Interactions between essential nutrients with platinum group metals in submerged aquatic and emergent plants. *Water Air Soil Pollut.* **2007**, *184*, 255–267. [CrossRef]
148. Kińska, K.; Kowalska, J. Comparison of platinum, rhodium, and palladium bioaccumulation by *Sinapis alba* and their influence on phytochelatin synthesis in plant tissues. *Pol. J. Environ. Stud.* **2019**, *28*, 1735–1740. [CrossRef]
149. Bonanno, G. Trace element accumulation and distribution in the organs of *Phragmites australis* (common reed) and biomonitoring applications. *Ecotoxicol. Environ. Saf.* **2011**, *74*, 1057–1064. [CrossRef]
150. Pujari, G.N. Phytomining of Low Grade Ore. *SGAT Bull.* **2018**, *19*, 15–22.
151. Custos, J.M.; Moyne, C.; Sterckeman, T. How root nutrient uptake affects rhizosphere pH: A modelling study. *Geoderma* **2020**, *369*, 114314. [CrossRef]
152. Chaney, R.L.; Angle, J.S.; Broadhurst, C.L.; Peters, C.A.; Tappero, R.V.; Sparks, D.L. Improved understanding of hyperaccumulation yields commercial phytoextraction and phytomining technologies. *J. Environ. Qual.* **2007**, *36*, 1429–1443. [CrossRef]
153. Zhong, X.; Chen, Z.; Li, Y.; Ding, K.; Liu, W.; Liu, Y.; Qiu, R. Factors influencing heavy metal availability and risk assessment of soils at typical metal mines in Eastern China. *J. Hazard. Mater.* **2020**, *400*, 123289. [CrossRef] [PubMed]
154. Yan, A.; Wang, Y.; Tan, S.N.; Mohd Yusof, M.L.; Ghosh, S.; Chen, Z. Phytoremediation: A promising approach for revegetation of heavy metal-polluted land. *Front. Plant Sci.* **2020**, *11*, 359. [CrossRef] [PubMed]
155. Bennett, F.A.; Tyler, E.K.; Brooks, R.R.; Gregg, P.E.H.; Stewart, R.B. Fertilisation of hyperaccumulators to enhance their potential for phytoremediation and phytomining. In *Plants That Hyperaccumulate Heavy Metals*; Brooks, R.R., Ed.; CAB International: New York, NY, USA, 1998; pp. 249–259.
156. Sheoran, V.; Sheoran, A.S.; Poonia, P. Factors affecting phytoextraction: A review. *Pedosphere* **2016**, *26*, 148–166. [CrossRef]
157. Schmidt, U. Enhancing phytoextraction: The effect of chemical soil manipulation on mobility, plant accumulation, and leaching of heavy metals. *J. Environ. Qual.* **2003**, *32*, 1939–1954. [CrossRef]
158. Băbău, A.M.C.; Micle, V.; Damian, G.E.; Sur, I.M. Sustainable ecological restoration of sterile dumps using *Robinia pseudoacacia*. *Sustainbility* **2021**, *13*, 14021. [CrossRef]
159. Ebbs, S.D.; Lasat, M.M.; Brady, D.J.; Cornish, J.; Gordon, R.; Kochian, L.V. Phytoextraction of Cadmium and Zinc from a Contaminated Soil. *J. Environ. Qual.* **1997**, *26*, 1424–1430. [CrossRef]
160. Barona, A.; Aranguiz, I.; Elıas, A. Metal associations in soils before and after EDTA extractive decontamination: Implications for the effectiveness of further clean-up procedures. *Environ. Pollut.* **2001**, *113*, 79–85. [CrossRef]
161. Evangelou, M.W.; Ebel, M.; Schaeffer, A. Chelate assisted phytoextraction of heavy metals from soil. Effect, mechanism, toxicity, and fate of chelating agents. *Chemosphere* **2007**, *68*, 989–1003. [CrossRef]
162. Robinson, B.H.; Brooks, R.R.; Howes, A.W.; Kirkman, J.H.; Gregg, P.E.H. The potential of the high-biomass nickel hyperaccumulator *Berkheya coddii* for phytoremediation and phytomining. *J. Geochem. Explor.* **1997**, *60*, 115–126. [CrossRef]
163. Meers, E.; Ruttens, A.; Hopgood, M.J.; Samson, D.; Tack, F.M.G. Comparison of EDTA and EDDS as potential soil amendments for enhanced phytoextraction of heavy metals. *Chemosphere* **2005**, *58*, 1011–1022. [CrossRef] [PubMed]
164. Blaylock, M.J.; Salt, D.E.; Dushenkov, S.; Zakharova, O.; Gussman, C.; Kapulnik, Y.; Raskin, I. Enhanced accumulation of Pb in Indian mustard by soil-applied chelating agents. *Environ. Sci. Technol.* **1997**, *31*, 860–865. [CrossRef]
165. Wang, L.; Hou, D.; Shen, Z.; Zhu, J.; Jia, X.; Ok, Y.S.; Rinklebe, J. Field trials of phytomining and phytoremediation: A critical review of influencing factors and effects of additives. Crit. Rev. *Environ. Sci. Technol.* **2020**, *50*, 2724–2774. [CrossRef]
166. Rascio, N.; Navari-Izzo, F. Heavy metal hyperaccumulating plants: How and why do they do it? And what makes them so interesting? *Plant Sci.* **2011**, *180*, 169–181. [CrossRef] [PubMed]
167. Gendre, D.; Czernic, P.; Conéjéro, G.; Pianelli, K.; Briat, J.F.; Lebrun, M.; Mari, S. TcYSL3, a member of the YSL gene family from the hyper-accumulator *Thlaspi caerulescens*, encodes a nicotianamine-Ni/Fe transporter. *Plant J.* **2007**, *49*, 1–15. [CrossRef]
168. Baruah, S.; Bora, M.S.; Sharma, P.; Deb, P.; Sarma, K.P. Understanding of the distribution, translocation, bioaccumulation, and ultrastructural changes of *Monochoria hastata* plant exposed to cadmium. *Water Air Soil Pollut.* **2017**, *228*, 1–21. [CrossRef]
169. Hu, X.; Gholizadeh, M. Biomass pyrolysis: A review of the process development and challenges from initial researches up to the ommercialization stage. *J. Energy Chem.* **2019**, *39*, 109–143. [CrossRef]
170. Zhang, X.; Houzelot, V.; Bani, A.; Morel, J.L.; Echevarria, G.; Simonnot, M.O. Selection and combustion of Ni-hyperaccumulators for the phytomining process. *Int. J. Phytoremediat.* **2014**, *16*, 1058–1072. [CrossRef]

171. Dastyar, W.; Raheem, A.; He, J.; Zhao, M. Biofuel production using thermochemical conversion of heavy metal-contaminated biomass (HMCB) harvested from phytoextraction process. *J. Chem. Eng.* **2019**, *358*, 759–785. [CrossRef]
172. Hazotte, C.; Laubie, B.; Pacault, S.; Dufaud, O.; Simonnot, M.O. Evaluation of the performance of nickel hyperaccumulator plants as combustion fuel. *Biomass Bioenergy* **2020**, *140*, 105671. [CrossRef]
173. Soundararajan, R.K.V.; Varjani, S.; Chandrasekaran, R.; Kandasamy, D. Recovery of Gold and Other Precious Metals by Biosorption. In *Sustainable Resource Management*; Guo, W., Ngo, H.H., Surampalli, R.Y., Zhang, T.C., Eds.; John Wiley & Sons: Weinheim, Germany, 2021; Volume 2, pp. 463–488. [CrossRef]
174. Won, S.W.; Kotte, P.; Wei, W.; Lim, A.; Yun, Y.S. Biosorbents for recovery of precious metals. *Bioresour. Technol.* **2014**, *160*, 203–212. [CrossRef] [PubMed]
175. U.S. Department of the Interior. *Mineral Commodity Summaries. U.S. Geological Survey 2003*; U.S. Department of the Interior: Reston, VA, USA, 2003; p. 210. [CrossRef]
176. Lee, J.; Kaunda, R.B.; Sinkala, T.; Workman, C.F.; Bazilian, M.D.; Clough, G. Phytoremediation and phytoextraction in Sub-Saharan Africa: Addressing economic and social challenges. *Ecotoxicol. Environ. Saf.* **2021**, *226*, 112864. [CrossRef]
177. Anderson, C.W.N.; Brooks, R.R.; Chiarucci, A.; LaCoste, C.J.; Leblanc, M.; Robinson, B.H.; Stewart, R.B. Phytomining for nickel, thallium and gold. *J. Geochem. Explor.* **1999**, *67*, 407–415. [CrossRef]
178. Nkrumah, P.N.; Baker, A.J.; Chaney, R.L.; Erskine, P.D.; Echevarria, G.; Morel, J.L.; van der Ent, A. Current status and challenges in developing nickel phytomining: An agronomic perspective. *Plant Soil* **2016**, *406*, 55–69. [CrossRef]

Disclaimer/Publisher's Note: The statements, opinions and data contained in all publications are solely those of the individual author(s) and contributor(s) and not of MDPI and/or the editor(s). MDPI and/or the editor(s) disclaim responsibility for any injury to people or property resulting from any ideas, methods, instructions or products referred to in the content.

soil systems

MDPI

Article

Complex Speciation and Distribution of Iron, Sulfur, and Trace Metals in Coal Mine Soils Reflect Grain- and Sub-Grain-Scale Heterogeneity during Pyrite Oxidative Dissolution

Md Abu Raihan Chowdhury and David M. Singer *

Department of Earth Sciences, Kent State University, Kent, OH 44242, USA; mchowdh7@kent.edu
* Correspondence: dsinger4@kent.edu

Abstract: Historical coal mining practices have caused various soil and water hazards, particularly through the dumping of mine waste. The primary environmental risk associated with this waste is the leaching of toxic metals from dumps of spoil or refuse into the subsurface soil or into nearby water resources. The extent of metal release is controlled via the oxidative dissolution of pyrite and potential re-sequestration through secondary Fe oxides. The characterization of the dominant Fe-bearing phase and the distribution of trace metals associated with these phases was determined via electron microscopy, synchrotron-based X-ray micro-fluorescence (μ-XRF) element and redox mapping from shallow mine soils from an impacted watershed in Appalachian Ohio. The dominant Fe-bearing phases were: (1) unweathered to partially weathered pyrite; (2) pseudomorphic replacement of pyrite with Fe(III) oxides; (3) fine-grained Fe oxide surface coatings; and (4) discrete Fe(III) oxide grains. Thicker secondary coatings and larger particles were sulfate rich, whereas smaller grains and thinner coatings were sulfate poor. The discrete Fe oxide grains exhibited the highest concentrations of Cr, Mn, Ni, and Cu, and sub-grain-scale concentration trends (Mn > Cr > Ni > Cu) were consistent with bulk soil properties. Predicting future metal transport requires an understanding of metal speciation and distribution from the sub-grain scale to the pedon scale.

Keywords: coal mine soil; Fe oxides; trace metal sequestration; synchrotron-based redox mapping

Citation: Chowdhury, M.A.R.; Singer, D.M. Complex Speciation and Distribution of Iron, Sulfur, and Trace Metals in Coal Mine Soils Reflect Grain- and Sub-Grain-Scale Heterogeneity during Pyrite Oxidative Dissolution. *Soil Syst.* **2024**, *8*, 2. https://doi.org/10.3390/soilsystems8010002

Academic Editor: Manfred Sager

Received: 4 October 2023
Revised: 18 December 2023
Accepted: 20 December 2023
Published: 22 December 2023

Copyright: © 2023 by the authors. Licensee MDPI, Basel, Switzerland. This article is an open access article distributed under the terms and conditions of the Creative Commons Attribution (CC BY) license (https://creativecommons.org/licenses/by/4.0/).

1. Introduction

Historical coal mining practices have caused various soil, water, and air hazards to the environment and humans [1–3]. Coal mining drastically and negatively affects surface environments, particularly through the dumping of mine waste (i.e., mine spoil) [4]. It has been estimated that in Ohio alone, there are approximately 36 billion tons of known coal mine spoil spread over 600 km^2 [5]. Further, depending on local geology and surface mining practices, approximately a half ton of waste is produced for every ton of mined coal [6]. Further, it has been estimated that there are 32,000 km^2 of land in the U.S. that have been impacted by coal mining, and only 685 km^2 of those mines (~2%) have been reclaimed [7,8]. One of the primary environmental risks associated with this waste is the leaching of toxic metal(loid)s from dumps of spoil or refuse into the subsurface soil or into nearby water resources [1]. These elements (e.g., Cr, Mn, Cu, and Ni) are typically bound primarily within pyrite (FeS_2) and other sulfides that form during coal deposition and later diagenetic processes [9]. As the unreclaimed mine spoil weathers, the oxidative dissolution of pyrite present in the waste and mine soils can leach acidity and toxic elements, resulting in local water quality impairment [10]. Chromium and Ni are toxic and produce mutagenic, carcinogenic, and genotoxic effects; Cu can cause significant toxicological effects, and there is growing concern regarding the impact of Mn on human health and ecosystems [11,12]. It is therefore critical to fully assess the potential for metal transport from these systems.

The extent of toxic element leaching from coal mine waste is controlled using a complex set of hydrogeochemical conditions following the oxidative dissolution of pyrite.

At low pH and high concentrations of Fe and trace metals (Mn, Cu, and Ni) released from pyrite, dissolution can occur in the aqueous phase and be transported with pore water downgradient [13]. As the released acidity is consumed through further weathering reactions and pore water pH is buffered, the deposition of secondary Fe(III)-bearing phases is thermodynamically favored [14,15]. These phases can include a wide range of Fe(III)-(oxy)hydroxides and (oxy)hyroxysulfates, referred to hereafter as "Fe-oxides". The common phases include jarosite ($KFe_3(SO_4)_2(OH)_6$), schwertmannite ($Fe_8O_8(OH)_{8-2x}(SO_4)_x$ with $1 \leq x \leq 1.75$), ferrihydrite (approximately $5Fe_2O_3 \cdot 9H_2O$), goethite (FeOOH), and hematite (Fe_2O_3), with varying texture and morphology based on the combined effects of pore water composition, rainwater infiltration, and mine soil porosity and permeability [16–18]. Further, local micro-zones may also control the formation and transition between phases through the changes in pH, Eh, and pore connectivity [19–21].

In this study, we examined the dominant Fe-bearing phases that formed following oxidative pyrite dissolution in soils developing on historic mine spoils to explore the range of weathering outcomes. The formation and transformations of secondary Fe oxides can impact pore water composition by re-sequestering trace metals released from pyrite weathering [22–24]; however, the efficacy of secondary uptake is controlled by Fe oxide composition, grain size and texture, and local pore water conditions. It was hypothesized that fine-grained secondary Fe oxides with a high surface would dominate metal re-sequestration. This work also aimed to gauge the potential future release of toxic elements, as predicting future metal transport requires an understanding of metal speciation and distribution from the sub-grain scale to the pedon scale. In the current study, electron microscopy and synchrotron-based X-ray micro-fluorescence (μ-XRF) element and redox mapping were used to determine: (1) the texture, morphology, and composition of the dominant Fe-bearing phase in these soils; and (2) the distribution of trace metals associated with these phases. Trends in metal enrichment in secondary Fe oxides were also compared to trends in bulk metal concentrations in the parent coal shale and the mine soils.

2. Materials and Methods

2.1. Site Description

The study site HR-25, sub-watershed #25 of Huff Run watershed, contains an abandoned underground mine area located near Mineral City, Ohio (Figure 1). This area experienced extensive coal mining operations from 1890 to 1946 [25]. After 1946, the site was abandoned, leaving all mine spoils and underground mine tunnels unreclaimed. The oxidation of pyrite present in the coal and sedimentary formation led to a massive acid mine drainage (AMD) generation, which severely impacted the surface and groundwater condition in HR-25 [25]. To date, remediation projects installed at the site since 1996 have cost USD 590,000, which has curbed the AMD release from the site and significantly improved the surface water. However, despite the success in improving the surface water quality, abandoned mine waste and spoils continue to leach non-point sources (e.g., mine spoils) and have the potential to continually release toxic elements over a time period of approximately decades, resulting in ongoing negative impacts on the local ecosystem. Previous studies have focused on abandoned spoils adjacent to the current study sites [26–29], and these previous projects provide further information about the history, climate, and remediation activities of the Huff Run Watershed and sub-watershed 25.

2.2. Soil Sample Collection, Thin-Section Preparation, and Grain-Scale Characterization

Shallow soil samples (0–10 cm) were collected in 2016 from two locations within HR-25; these soils have been extensively studied to determine the relationship between bulk mineralogy, geochemistry, and pore water composition [29], the relationship between trace metal transport and the presence of secondary mineral surface coatings [26], and the importance of colloid transport of trace metals [29,30]. Site 1 is located at the bottom of a mine spoil heap adjacent to a tributary (known as the HR-25 tributary); site 2 is located at the bottom of another mine spoil heap further uphill of site 1 (Figure 1). Site 1 has a shallow

slope with sparse grass and a few trees, whereas site 2 has a steeper slope and minimal vegetation. Site 1 had a thin (<2 cm) organic layer, while site 2 did not exhibit an organic layer. These mine soils have been reported to exhibit a loam-type texture [27] with pore water pH values of approximately 5.5 [28].

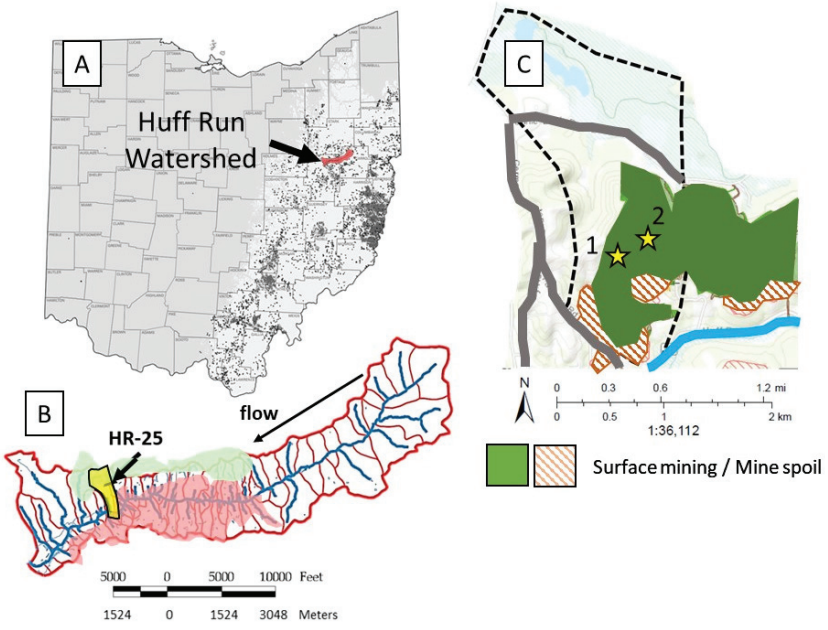

Figure 1. (**A**) Location of the Huff Run Watershed (in red), with Ohio coal counties shown in light gray and known abandoned coal mines in dark gray [31]; (**B**) a watershed map [32] showing the location of sub-watershed HR-25 (in yellow), stream flow direction, and portions of the watershed impacted by historic surface mines and abandoned mine spoils (pink) and areas that still have active permits (green); (**C**) Map of sub-watershed HR-25 (the dashed outline), which includes the spatial extent of known surface area affected by coal surface mining (green) and mine spoil emplacement (hatched orange), the Huff Run stream (blue line) and roads (gray lines). The stars represent sampling sites 1 and 2. The coal mining data were obtained from: https://gis.ohiodnr.gov (accessed on 7 December 2014).

2.3. Characterization of Fe, S, and Trace Metal Speciation and Distribution

A subset of these soils was air-dried and passed through a 1-mm sieve following field sampling, embedded in epoxy (EPO-TEK 301-2FL) and polished using kerosene instead of water to prevent redox changes from occurring during thin-section preparation. The samples were cut to ~30 μm thick and mounted onto high-purity quartz glass slides (Spectrum Petrographics, Inc., Vancouver, WA, USA). The grain size, texture, morphology, and composition of soil minerals were determined using a Hitachi Benchtop TM3030 scanning electron microscope (SEM) equipped with energy-dispersive spectroscopy (EDS; Quantax70), operated at 15 keV voltage, with a spot size of 10 nm, and a detector-to-sample working distance typically of 10 mm. Micro-XRF analyses were performed at beamline 13-ID-E at the Advanced Photon Source [33]. The synchrotron beam size for μ-XRF was 2 μm × 2 μm, focused using a Pt-coated Kirkpatrick–Baez (K–B) focusing optical system (XRadia, Zeiss Microscopy, Pleasanton, CA, USA). A four-element Si vortex detector (SSD, Hitachi, Tokyo, Japan) was used for X-ray fluorescence data collection. Monochromatic X-rays were selected using a water-cooled Si(111) (ϕ = 90) double-crystal monochromator. Multiple maps were collected near the S–K edge (E_0 = 2474 eV) (for S) and the Fe–K edge

(E_0 = 7112 eV) (for Fe) and at 13 keV for other elements (Si, P, S, K, Ca, Ti, V, Cr, Mn, Fe, Ni, Cu, and Zn). Data were collected at a 2 μm pixel size and 50 ms dwell time per point, and fluorescent maps were analyzed using the Larch v.0.9.55 software package [34]. The measured intensity of the incident energy of the X-ray beam (I0) was used to normalize the fluorescent counts of each energy map across each line, and the change in I0 was less than 1%. Sulfur oxidation state speciation maps were constructed based on maps that were collected across the S–K edge (2471 eV, 2473 eV, 2478 eV, 2482 eV, and 2490 eV) to produce maps of the distribution of the operationally defined oxidation states, reduced ("S_{red}", which ranges from S(-II) to S(0)) and oxidized ("S_{ox}", which ranges from S(0) to S(VI)); Fe oxidation state speciation maps were constructed based on maps that were collected across the Fe–K edge (7123 eV, 7127 eV, and 7136 eV) to produce maps of Fe(II) and Fe(III) [5,24,35]. Based on the experimental setup, the distributions of Cr, Mn, Cu, and Ni were determined with maximum I0-normalized values of each element in the maps collected at 7136 eV of 7×10^{-4}, 3.7×10^{-3}, 9×10^{-4}, and 2×10^{-4}, respectively. Using these values as proxies for concentration results in relative concentration values (Mn > Cr > Ni > Cu) that are consistent with trace element compositions determined via the bulk XRF of soils collected from the same site [25], justifying the use of intensity counts as a proxy for concentration at the grain scale. Box-and-whisker plots were therefore created by separating regions of each map based on the dominant type of Fe-bearing phase, described below, to determine their relative trace metal content as a function of Fe speciation. For each type of Fe-bearing phase, four separate regions from each map of a representative grain or aggregate of grains were used to extract I0-normalized counts, which were then compiled for the box-and-whisker plots. The Fe-bearing phases of concern (pyrite and Fe oxides) were in either extremely low abundance or not detectable in the other lithologies that comprise the mine spoil. The other Fe-bearing phases (e.g., clays and organic matter) were in low abundance and were not the focus of this study.

3. Results

Based on the SEM–EDS and μ-XRF analyses, four categories of the dominant Fe-bearing phases were described based on their composition, morphology, and Fe and S redox state distributions: (1) unweathered to partially weathered pyrite; (2) pseudomorphic replacement of pyrite with Fe(III)-bearing phases, which were typically hollow; (3) fine-grained Fe(III) oxide surface coatings often co-localized in aggregates with clays, covering primary silicate grains; and (4) discrete Fe(III) oxide grains. Other Fe-bearing phases, such as clays and organic matter, were observed as minor constituents and were not the focus of this work. The distribution of Fe and S redox states and the association of trace metals with each of the four types of Fe-bearing phases are discussed below. The four types of Fe phases were observed in samples from sites 1 and 2, and the text below does not differentiate the results between the two sites; representative SEM–EDS and μ-XRF analyses from both sites are highlighted in the figures.

3.1. Unweathered to Partially Weathered Pyrite

The SEM–EDS analyses of the soil samples showed the presence of grains with their morphologies and compositions consistent with unweathered to partially weathered pyrite in the soils forming on mine spoils (Figure 2). These Fe–S-rich phases were commonly present in relatively larger aggregates of Fe–O-rich grains (likely secondary Fe oxides) and/or clay minerals (Figure 2). The pyritic Fe–S-rich grains themselves were typically 2–10 μm (Figure 2A,C), and pyritic grains greater than ~10 μm were less commonly observed. The Fe–O-rich aggregates were usually larger in size (~200 μm, Figure 2A) compared to the clay-rich aggregates (35–40 μm at their widest dimension, Figure 2C). The relatively smaller framboids of pyrite were present in a loosely packed aggregate and showed physical signs of oxidative weathering, resulting in an uneven framboidal/euhedral morphology (Figure 2B). Pyritic grains that were smaller and/or embedded in thinner aggregates exhibited depleted Fe and S concentrations, based on the EDS analyses, compared to

larger, unweathered pyritic grains in thicker aggregates. The larger grains also tended to exhibit euhedral shapes with sharp contact boundaries (Figure 2C).

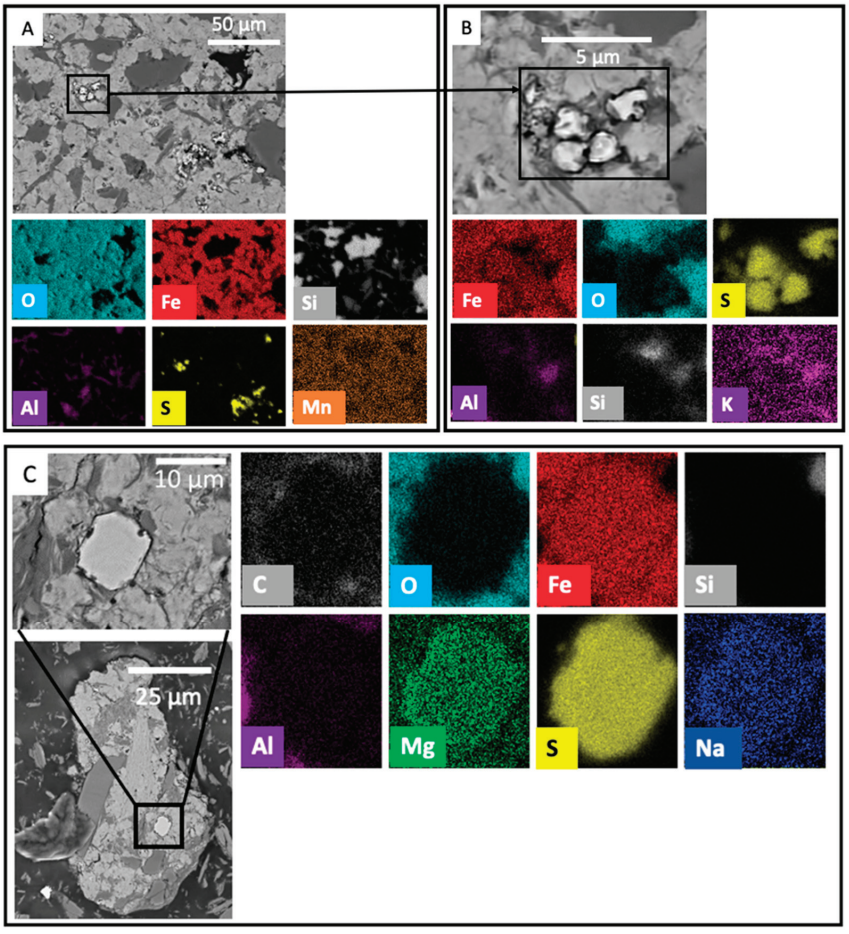

Figure 2. Representative SEM backscattered electron images and EDS elemental maps of grains consistent with the composition and morphology of framboidal pyrite, showing evidence of dissolution pits and weathering features for sites 1 (**A**,**B**) and 2 (**C**). The black box in (**A**) indicates the field of view in (**B**); the black box in (**B**) indicates the EDS map regions. The black box in (**C**) indicates the EDS map region of a grain with its morphology and composition consistent with a euhedral grain of pyrite that is protected from dissolution from a complex matrix of grains dominated by grains consistent with phyllosilicate composition and textures.

The presence of unweathered and partially weathered pyritic grains was confirmed by the µ-XRF analyses, which indicated the presence of Fe(II)-S_{red}-dominated grains that were approximately 5 µm in diameter (Figure 3). The presence of partially weathered pyrite grains was not observed in the µ-XRF analyses, likely because the spatial distribution of the chemical features associated with these grains is lower than the spatial resolution of the µ-XRF analyses. However, grains characteristic of weathering products that were Fe(III) rich and S poor were typically aggregated around the pyritic grains and were approximately 10–20 µm in diameter (Figure 3, left column). A number of pyritic grains lacked surface coatings at the resolution of the µ-XRF analyses (Figure 3, right column) and

were not present in the aggregates with Fe oxides or clays; however, it is possible that these grains were liberated from soil aggregates during sample collection and preparation. The concentrations of Cr, Mn, Ni, and Cu, based on I0-normalized μ-XRF counts, associated with pyritic grains were typically low (Figure 3) and were the lowest of the four types of Fe-bearing phases in the soils based (Figure 4). However, the concentrations of these metals in all four types of Fe-bearing phases, including pyrite, were higher compared to the total sample concentration (Figure 4).

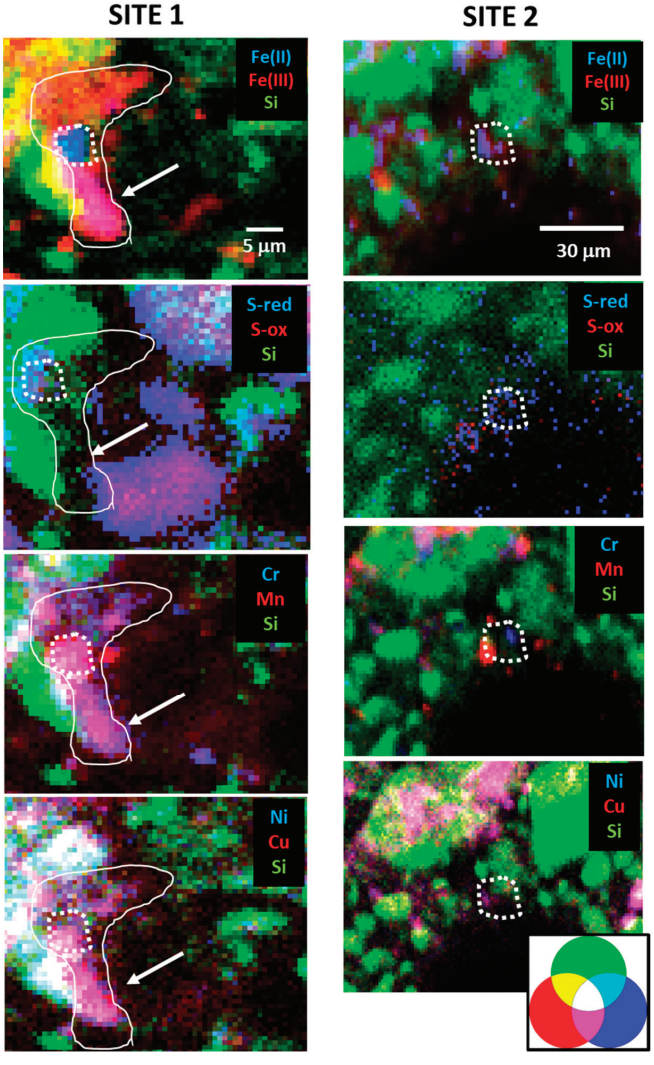

Figure 3. Representative μ-XRF images for unweathered pyrite (regions in white-dashed lines) and weathered products (regions in a solid white line and highlighted by the white arrow), including redox maps (for Fe and S) and elemental maps (for Si, Cr, Mn, Ni, and Cu) for the samples from site 1 (**left column**) and site 2 (**right column**). The Fe and S maps are shown as two-component images (Fe(II) and Fe(III); S_{red} and S_{ox}) plus Si for orientation relative to the other maps. The color key is shown at the bottom right.

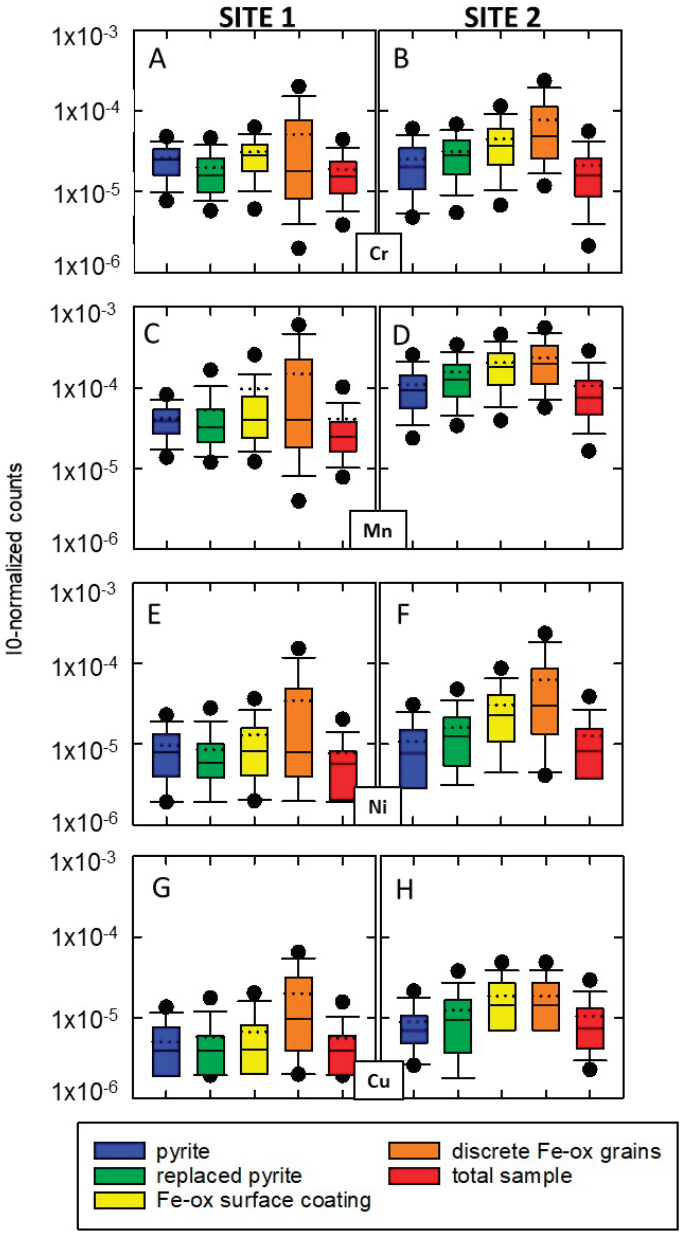

Figure 4. Box-and-whisker plots showing I0-normalized m-XRF counts as a proxy for the concentrations of Cr (**A**,**B**), Mn (**C**,**D**), Ni (**E**,**F**), and Cu (**G**,**H**) in the samples from sites 1 (**left**) and 2 (**right**) as a function of the type of Fe-bearing host phases: pyrite (blue), pseudomorphic replacement of pyrite with Fe oxides (green), Fe oxide surface coatings (yellow), and larger discrete grains of Fe oxides (orange). The range of total metal counts for the m-XRF maps is shown in red. Median values are shown as black-dashed lines, and the black circles represent the 5th and 95th percentile of outliers.

3.2. Partial to Complete Pseudomorphic Replacement of Pyrite

Thin, hexagonal to semi-circular Fe–O-rich rinds were observed in cross-sections around cavities that are consistent with the formation of partial to complete pseudomorphic replacement of primary framboidal pyrite with Fe oxides. The Fe–O-rich layer varies from less than 1 μm (Figure 5A) to approximately 20 μm (Figure 5B). The pre-existing pyrite grains varied from approximately 1 μm (Figure 5A) to 100 μm (Figure 5B). Unweathered pyrite framboids were often observed within aggregates with fully weathered and pseudomorphically replaced pyrite framboids (replaced with Fe oxide, Figure 5B). In several cases, Fe–S-rich cores were observed covered in S-depleted rims (Figure 5B).

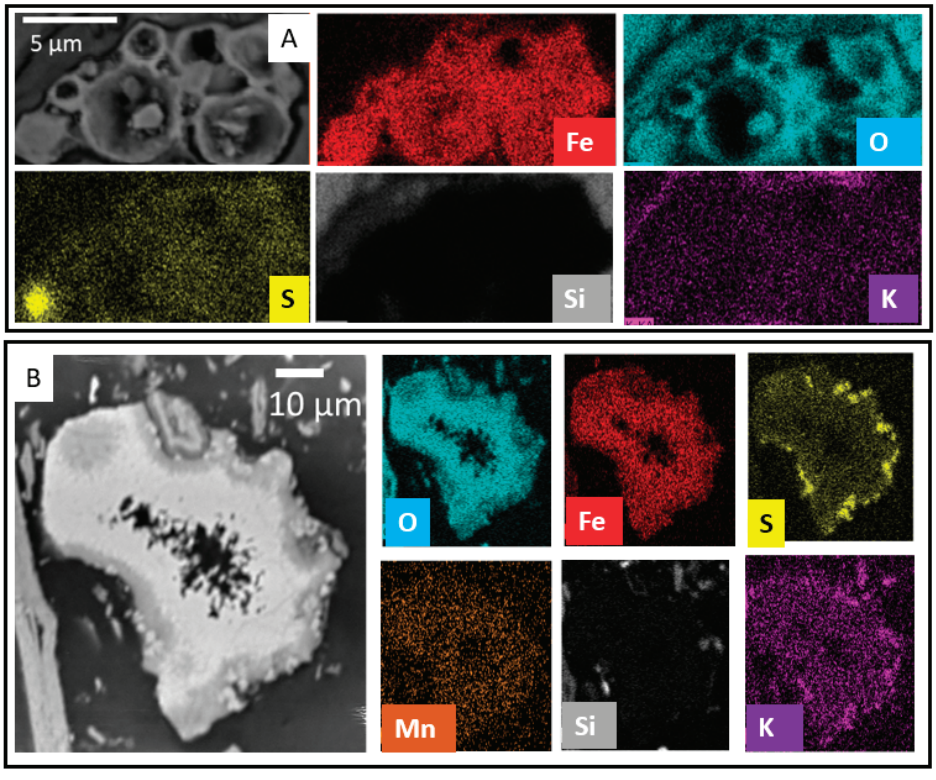

Figure 5. Representative SEM backscattered electron images and EDS elemental maps of Fe oxide pseudomorphically replacing framboidal pyrite with one possible unweathered pyrite remaining (in the top panel, lower left corner) and around the particle rims in the lower panel for site 1 (**A**) and site 2 (**B**).

The pseudomorphic replacement features observed via the SEM–EDS analyses were not detected via the μ-XRF analyses and were likely below the detection limit of the μ-XRF spatial resolution. However, pyritic cores (dominated by Fe(II) and S_{red}) with oxidized rims (dominated by Fe(III) with little S) were observed (Figure 6). The trace metal loading of the pseudomorphically replaced pyrite was typically low and dominated by Mn (Figures 5 and 6) and were higher in thicker replacement features (from ~10 to 15 μm) compared to thinner ones (<1 μm) (Figure 3). In general, the concentrations of Cr, Mn, Ni, and Cu were higher in the replacement features compared to unweathered pyrite but lower than in Fe oxide surface coatings or discrete Fe oxide grains (Figure 4).

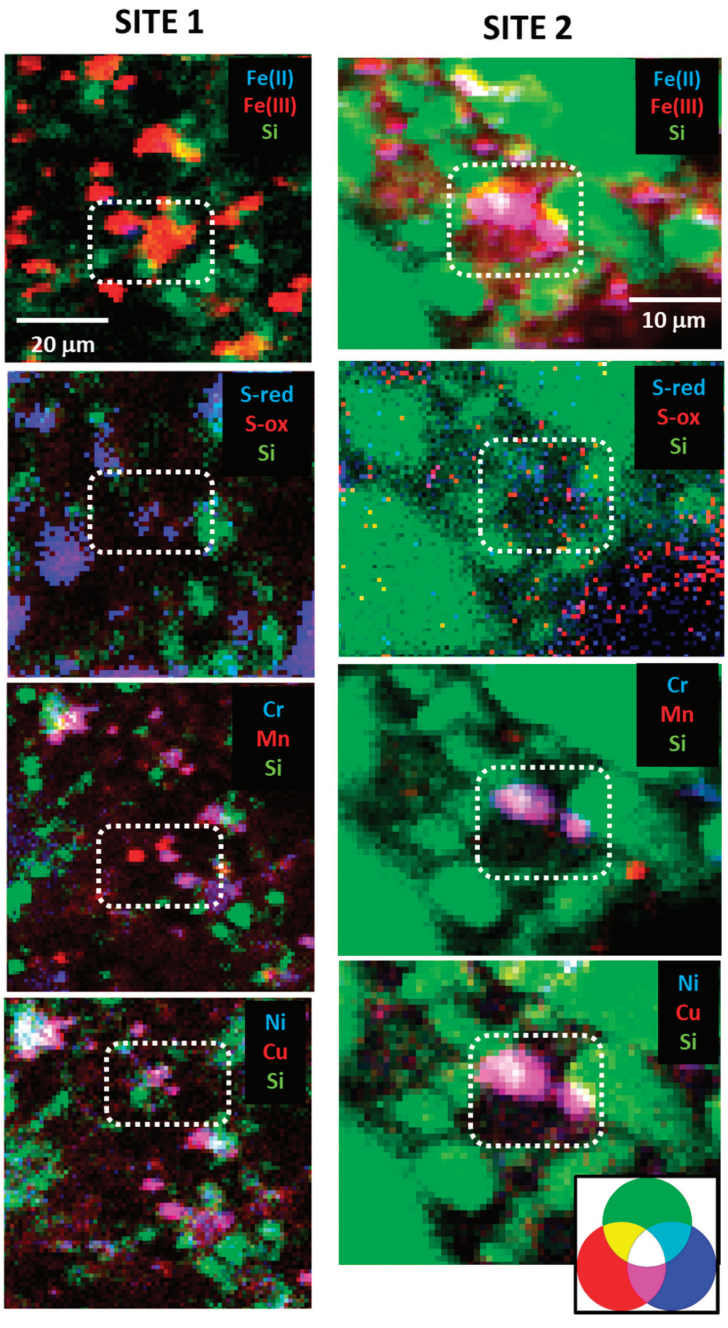

Figure 6. Representative µ-XRF images for pyrite replaced with Fe oxides (regions in white-dashed lines); structures observed in the SEM–EDS analyses were not able to be observed at the resolution of the µ-XRF analyses; however, pyritic cores with oxidized rims were observed. The images include redox maps (for Fe and S) and elemental maps (for Si, Cr, Mn, Ni, and Cu) for the samples from site 1 (**left column**) and site 2 (**right column**). The Fe and S maps are shown as two-component images (Fe(II) and Fe(III); S_{red} and S_{ox}) plus Si for orientation relative to the other maps. The color key is shown at the bottom right.

3.3. Fe Oxide Secondary Mineral Surface Coatings

Fine-grained aggregates of Fe oxides were observed as secondary mineral surface coatings (MSCs) on larger Si–O-rich grains that were likely quartz (Figure 7). The composition of the Fe MSCs were both Fe–O-rich (Figure 7A) and Fe–O–S-rich (Figure 7B), the latter of which was likely composed of Fe(III)-(oxy)hydroxides-sulfates. The MSCs typically contained aggregates of Fe-rich grains with Si–Al–O-rich grains, likely clay minerals. The MSCs were heterogeneous with respect to their thickness and coverage of the underlying grain and ranged in thickness from less than 5 μm (Figure 7A) to thicker, more physically complex aggregates that were up to 15–20 μm in thickness (Figure 7B). The thinner MSCs also tended be dominantly Fe–O-rich, whereas the thicker ones were Fe–O–S-rich.

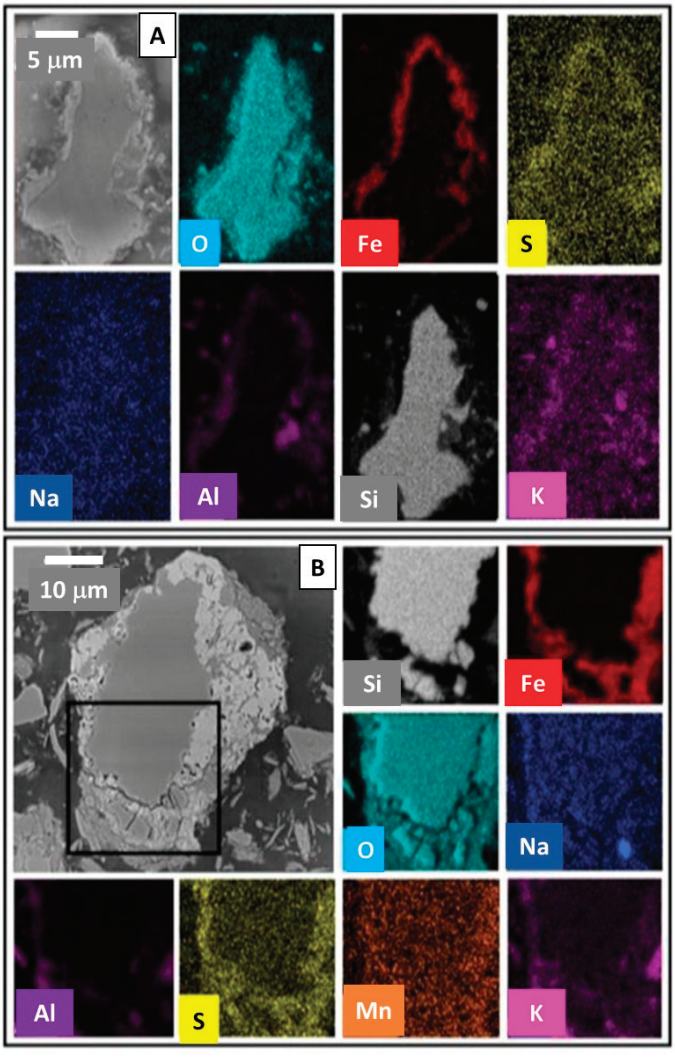

Figure 7. Representative SEM backscattered electron images and EDS elemental maps of S-bearing Fe oxide surface coatings on quartz (top panel (**A**), site 1), and a mix of Fe oxide and clay minerals on quartz (bottom panel (**B**), site 2). The black box in (**B**) indicates where EDS element maps were collected.

The μ-XRF analyses yielded similar results to the SEM–EDS analyses; thinner coatings were dominated by Fe(III) and were S poor, and thicker coatings were dominated by Fe(III) and Sox (Figure 8). The trace metal content in the Fe(III)–O-dominated surface coatings was the next highest of the four Fe-bearing phases in soils from sites 1 and 2 for Cr (Figure 4A,B), Mn (Figure 4C,D), and Ni (Figure 4E,F). The concentration of Cu was only higher compared to the other two Fe-bearing phases in the soil from site 2 (Figure 4H). At the grain scale, metal content was correlated with coating thickness, where thicker coatings (10–25 μm) contained higher concentrations of Cr, Mn, Ni, and Cu, whereas thinner coatings (less than 2 μm) exhibited a more limited trace metal content (Figure 8).

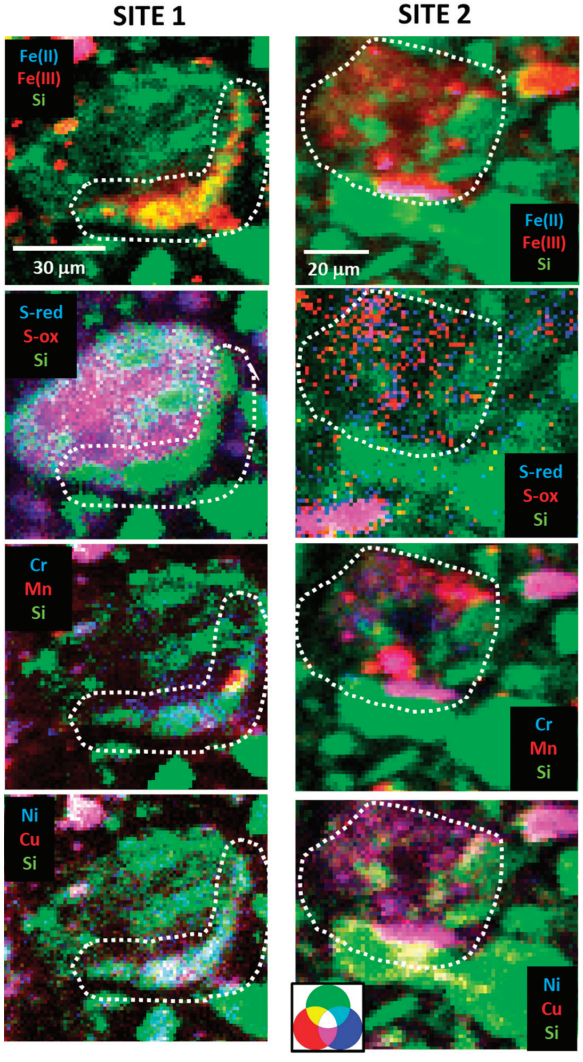

Figure 8. Representative μ-XRF images for Fe oxide surface coatings (regions in white-dashed lines), including redox maps (for Fe and S) and elemental maps (for Si, Cr, Mn, Ni, and Cu) for the samples from site 1 (**left column**) and site 2 (**right column**). The Fe and S maps are shown as two-component images (Fe(II) and Fe(III); S_{red} and S_{ox}) plus Si for orientation relative to the other maps. The color key is shown at the bottom right.

3.4. Discrete Secondary Fe-Bearing Phases

Discrete Fe-bearing grains, ranging in size from 10 μm to 20 μm to over 200 μm, were observed that were typically irregularly shaped with compositions dominated by Fe-O-S and were likely Fe(III)-(oxy)hydroxides-sulfates. Some of these discrete grains contained Si-rich inclusions (Figure 9A) and were likely clay grains incorporated during precipitation, whereas other discrete grains appeared to be relatively homogeneous single crystals (Figure 9B,C). The inclusion-bearing grains tended to have slightly lower S concentrations compared to the inclusion-free grains. Some of the larger discrete Fe grains were covered in fine-grained Si–O–Al–K-rich phases that are likely clay minerals and were up to 20 μm in thickness (Figure 9C).

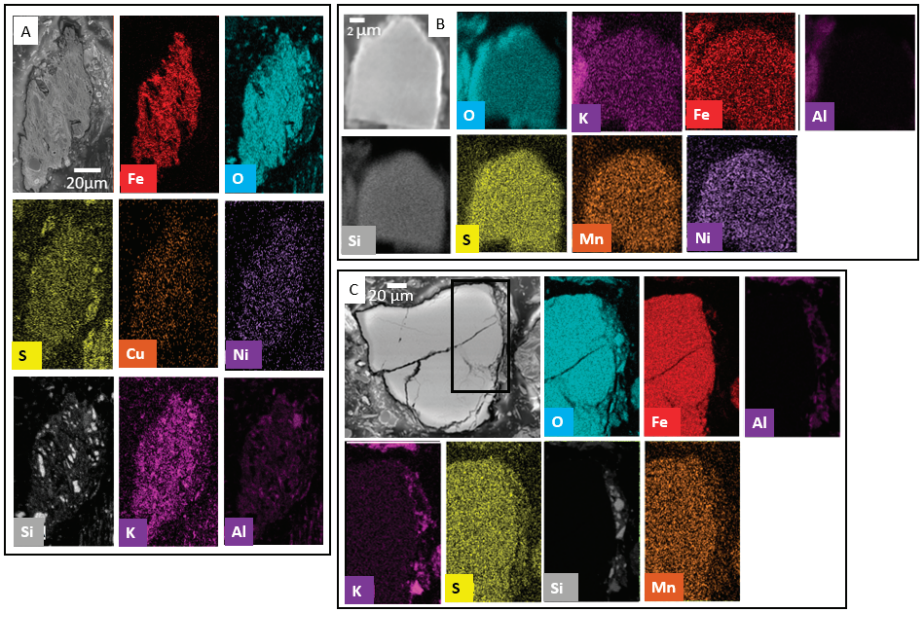

Figure 9. Representative SEM backscattered electron images and EDS elemental maps of a grain consistent with an Fe sulfate grain in an aggregate with clay particles ((**A**), site 1), and discrete particles of Fe sulfate ((**B**,**C**), site 2). The black box in (**C**) indicates where EDS element maps were collected.

The μ-XRF analyses were deemed to be consistent with the SEM–EDS analyses; smaller Fe-rich discrete grains (less than 5 μm) were Fe(III) rich and S poor, whereas larger grains were rich in both Fe(III) and S_{ox} (Figure 10). The larger grains were observed in the aggregates with Si-rich grains, although no Si-rich surface coatings were observed. However, the coatings observed via SEM–EDS were likely below the spatial detection limit of the μ-XRF analyses. Among the four Fe-bearing phases, the discrete Fe oxide grains exhibited significantly higher concentrations of Cr, Mn, Ni, and Cu compared to the other Fe-bearing phases in soils from both sites 1 and 2 (Figure 4), consistent with the SEM–EDS analyses. At the grain scale, trace metal content was correlated with the composition of the larger Fe-bearing grains, where Cu was associated with Fe(III)–O-rich phases (Figure 10), whereas Ni was associated with Fe(III)–O–S_{ox}-rich grains (Figure 6), and Mn and Cr were observed in pool types of large Fe(III) phases (Figure 10).

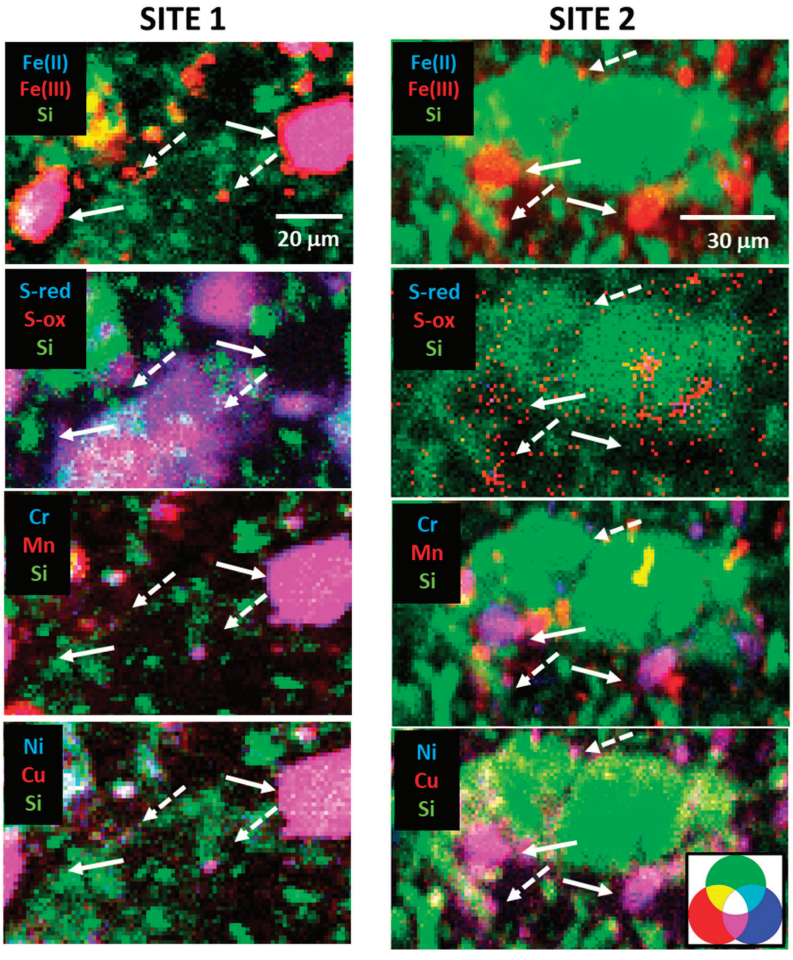

Figure 10. Representative µ-XRF images for discrete Fe oxide particles ranging from larger grains (solid white arrows) to smaller grains (white-dashed arrows), including redox maps (for Fe and S) and element maps (for Si, Cr, Mn, Ni, and Cu) for the samples from site 1 (**left column**) and site 2 (**right column**). The Fe and S maps are shown as two-component images (Fe(II) and Fe(III); S_{red} and S_{ox}) plus Si for orientation relative to the other maps. The color key is shown at the bottom right.

4. Discussion

4.1. Factors That Control Pyrite Weathering, Potential Fe Transport, and Re-Precipitation

The formation of secondary Fe oxides observed in the mine soils is controlled by factors from a combination of processes: (1) the oxidative dissolution of primary pyrite or other metal sulfide grains; (2) whether or not Fe is transported away from the pyrite surface before secondary precipitation; and (3) local hydrogeochemical conditions that may favor a specific secondary Fe oxide and grain texture. With respect to pyrite weathering, although other metal sulfides have been observed in the coal shale deposits within this watershed, pyrite is the dominant metal-bearing sulfide [36]. Broadly, sulfide mineral composition, morphology, particle size, reactive surface area, and texture control the oxidative dissolution-driven transformations and are typically dominated by the weathering of large (mm scale) crystals on surfaces within cracks in the grains [37]. It has been shown that for the oxidative dissolution of pyrite, a surface charge transfer to absorbed O_2 has been demonstrated to be

the rate-limiting step in the overall reaction [38]. Further, the oxygen in the sulfate reaction product has been shown to originate from water as a direct consequence of electrochemical mechanisms [39]. The combined effect of these processes provides support for the lack of complete pyrite weathering in shallow soils that are O_2-rich environments when the diffusion of H_2O may be limited, including relatively thin (<5 μm) surface coatings over pyrite (Figure 2A,B). Further, larger pyrite grains can remain unoxidized due the presence of thicker (10–20 μm) coatings that would limit both O_2 and H_2O diffusion (Figure 2C). The slower weathering of these grains within the coal shale matrix can persist decades after the bulk of the pyrite has been lost [40,41]. The pseudomorphic replacement of pyrite with Fe oxides has been shown to be the result of the limited diffusion of O_2 and subsequent transport of byproducts [42] and/or under a more buffered system (circumneutral to slightly alkaline) [43], even where aqueous Fe(III) concentrations are very low [44].

When pyrite oxidative dissolution coupled with Fe transport away from the pyrite surface does occur, the formation of secondary Fe oxides is controlled by local hydrogeochemical conditions, including pH and other pore water composition variables and flow parameters that range from the pore scale to the pedon scale [19]. With respect to pore water composition, higher sulfate concentrations (up to 3 g L^{-1}) and lower pH (2.5 to 4) values can result in the precipitation of schwertmannite and jarosite [45–47], and the formation of these phases can be strongly microbially mediated [48]. Following the precipitation of these metastable Fe(III)-bearing sulfates, jarosite and schwertmannite may either dissolve or transform into more ordered phases at higher pH values, particularly as pore water sulfate decreases over time as pyrite oxidation progresses. Sulfate-poor phases, such as ferrihydrite forming between pH 2 and pH 5, can form from direct Fe(III) precipitation and/or reprocessing of Fe(III) sulfates and typically go through further transformations into goethite at higher pH values (~5) and hematite at higher pH values (~7) [17]. The presence of both sulfate-rich and sulfate-poor Fe oxides in the current work (Figures 7 and 9) highlight the heterogeneous nature of the mine soils and complex precipitation pathways that could potentially be simultaneously present at the sub-mm scale.

With respect to the formation of secondary Fe oxide coatings versus discrete particles, it is possible that the discrete particles formed from the re-precipitation of the Fe downgradient from where it was originally released whereas coatings formed on or in closer proximity to the original pyrite grain [49]. This process may be coupled with transport through tight pore spaces that may favor Fe precipitation and aggregation in clay-rich regions [50,51]. More rapid precipitation due to the mixing of pore water with different compositions [52], rather than slower changes in an isolated pore water system, may also favor the precipitation of smaller grains either as discrete grains and/or within coatings. Further, the acid generated via the oxidation of pyrite can drive changes in its physical properties (e.g., porosity, permeability, and grain size distribution), which can affect solute transport [53], resulting in a continually changing landscape for Fe transport and re-precipitation. In the current work, both thicker secondary coatings (Figure 7) and larger particles (Figure 9) were sulfate rich, whereas smaller grains and thinner coatings were sulfate poor. It is possible that the sulfate-rich Fe oxides reflect an early post-pyrite weathering stage (when pore water sulfate concentrations are higher), and the sulfate-poor Fe oxides reflect later reworking of the Fe oxides.

4.2. Fate of Trace Metals

The re-sequestration of trace metals following their release from pyrite weathering results in the enrichment of these metals in secondary Fe oxides [54–56]. The relative enrichment of trace metals here (Mn > Cr > Ni > Cu) was also consistent with trace element concentrations in mine soils at the same site [25], indicating that grain- and sub-grain-scale reactions can control trace metal distribution at the pedon scale and is consistent with previous work [57–59]. In the current work, the discrete particles were observed to enrich these metals to a greater degree than the other secondary phases (Figure 4). Conversely, previous work has shown that trace metals are preferentially associated with

smaller grains with higher surface areas [60,61]. Further, metal uptake was also dependent on Fe oxide composition and size, with Cu associated with sulfate-poor grains, Ni with sulfate-rich grains, and Mn and Cr associated with larger grains (Figure 10). With respect to composition, a range of observations have been reported; for example, Fe(III) sulfates such as schwertmannite have been shown to have a limited divalent metal uptake ability during precipitation, but their subsequent transformation into goethite can result in metal uptake and retention [62]. In contrast, Cu has been shown to be preferentially sequestered by goethite and jarosite, while Ni and Zn accumulate in poorly crystalline schwertmannite [63]. With respect to particle size, we could not resolve as to whether Mn is present as separate Mn-bearing phases (e.g., Mn oxides) or present as Mn-bearing Fe oxides, although both have been previously identified in similar mine spoils [64]. It has also been shown that Cr uptake by Mn-bearing Fe oxides can exceed that of non-doped Fe oxides [65], which may explain the preferential accumulation of Cr by the larger, discrete Mn-bearing Fe oxides observed here (Figure 10). The summation of these results and comparison to previous work highlight the heterogeneous nature of mine soils and the complex relationship between hydrogeochemical factors that can drive mineral precipitation and metal uptake.

Comparisons of the concentrations of trace metals in the parent coal shale and the mine soils can also provide insights into the long-term dynamics that control metal transport versus retention. The concentrations of Cr, Mn, Ni, and Cu in the parent coal shale material are 2183 ppm, 768 ppm, 1500 ppm, and 90 ppm, respectively [35], and the concentrations in the bulk mine soils, and reflected in the grain- and sub-grain-scale analyses presented here, are 400 ppm, 2 wt.%, 75 ppm, and 50 ppm, respectively [25]. These results indicate that in the decades since waste emplacement, Mn has become enriched in the mine soils, whereas Cr, Ni, and Cu are slowly being leached. Similar results were observed in mine wastes, in which trace metals slowly continued to leach out after three decades since emplacement [66]. This is in contrast with previous work that has shown that Ni and Zn can accumulate in coal mine soils while Cu is leached [67]. These results highlight the need to integrate mine soil mineralogy and hydrogeochemistry to properly assess the long-term risk of metal leaching.

5. Conclusions

Analyses of near-surface mine spoils indicated the presence of pyrite as well as secondary Fe oxides that range in their grain size, texture, and morphology. The presence of a range of metal-bearing Fe(II) and Fe(III) phases highlights the chemically and physically complex heterogeneity in coal mine soils. Further, the presence of pyrite also indicates that the oxidative exhaustion of pyrite has yet to occur, despite nearly seven decades since the emplacement of the waste material, which is likely a direct result of the grain-scale complexity observed in the soils. Our results also underscore the potential importance of vegetation in driving weathering; for example, a previous study on forested sulfide mine waste showed little sulfide remaining after 40 years since emplacement [68], whereas a relatively unvegetated mine spoil site retained primary sulfides after more than 100 years since emplacement [69]. Increased organic matter content and plant activity can also lead to the long-term stabilization of metals within mine soils [70]. We have shown here that re-sequestration was dependent on grain size and morphology, and that the large, discrete Fe oxides were the most enriched in trace metals that originated from the pyrite. However, trace metals in the smaller particles and finer-grained secondary mineral coatings likely represent a more labile pool of trace metals that could be re-mobilized if local (bio)geochemical conditions were to shift. For example, during prolonged periods of saturation and reducing conditions, the fine-grained materials would be more likely to experience reductive dissolution [71,72]. Trends in metal enrichment (Mn) and depletion (Cr, Ni, and Cu) highlight the need for understanding metal speciation and distribution across scales in order to predict future metal transport.

Author Contributions: Conceptualization, M.A.R.C. and D.M.S.; methodology, M.A.R.C. and D.M.S.; validation, M.A.R.C. and D.M.S.; formal analysis, M.A.R.C. and D.M.S.; investigation, M.A.R.C. and

D.M.S.; resources, D.M.S.; data curation, D.M.S.; writing—original draft preparation, M.A.R.C. and D.M.S.; writing—review and editing, M.A.R.C. and D.M.S.; visualization, M.A.R.C. and D.M.S.; supervision, D.M.S.; project administration, D.M.S.; funding acquisition, D.M.S. All authors have read and agreed to the published version of the manuscript.

Funding: This research received no external funding.

Institutional Review Board Statement: Not applicable.

Informed Consent Statement: Not applicable.

Data Availability Statement: The data presented in this study are available on request from the corresponding author. The data are not publicly available due to the file size of the XMP data.

Acknowledgments: We would like to thank Matthew Newville, Tony Lanzirotti, and the APS GeoSoilEnviroCARS (GSE-CARS) staff for their beamline support. GSE-CARS is supported by the National Science Foundation-Earth Sciences (EAR-1634415) and the Department of Energy-GeoSciences (DE-FG02-94ER14466). This study used resources from the Advanced Photon Source; a U.S. Department of Energy (DOE) Office of Science User Facility operated for the DOE Office of Science by Argonne National Laboratory under the contract no. DE-AC02-06CH11357. We thank the following KSU graduate students for their support in soil sample collection and μ-XRF analyses: Max Barczok, Daniel Wood, Kortney Cole, and Lindsey Yazbek. We also thank Marissa Lautzenheiser (Huff Run Watershed Restoration Partnership) for her logistical support at the study site.

Conflicts of Interest: The authors declare no conflict of interest.

References

1. Rouhani, A.; Skousen, J.; Tack, F.M.G. An Overview of Soil Pollution and Remediation Strategies in Coal Mining Regions. *Minerals* **2023**, *13*, 1064. [CrossRef]
2. Skousen, J.; Daniels, W.L.; Zipper, C.E. Soils on Appalachian coal-mined lands. In *Appalachia's Coal-Mined Landscapes: Resources and Communities in a New Energy Era*; Springer: Cham, Germany, 2021; pp. 85–109.
3. Clark, E.V.; Daniels, W.L.; Zipper, C.E.; Eriksson, K. Mineralogical influences on water quality from weathering of surface coal mine spoils. *Appl. Geochem.* **2018**, *91*, 97–106. [CrossRef]
4. Feng, Y.; Wang, J.; Bai, Z.; Reading, L. Effects of surface coal mining and land reclamation on soil properties: A review. *Earth-Sci. Rev.* **2019**, *191*, 12–25. [CrossRef]
5. Singer, D.M.; Herndon, E.; Cole, K.; Koval, J.; Perdrial, N. Formation of secondary mineral coatings and the persistence of reduced metal-bearing phases in soils developing on historic coal mine spoil. *Appl. Geochem.* **2020**, *121*, 104711. [CrossRef]
6. Maiti, S.K. *Ecorestoration of the Coalmine Degraded Lands*; Springer Science & Business Media: New York, NY, USA, 2013.
7. Kirby, B.; Vengadajellum, C.; Burton, S.; Cowan, D. Coal, coal mines and spoil heaps. In *Handbook of Hydrocarbon and Lipid Microbiology*; Springer: Berlin/Heidelberg, Germany, 2010.
8. Shrestha, R.K.; Lal, R. Ecosystem carbon budgeting and soil carbon sequestration in reclaimed mine soil. *Environ. Int.* **2006**, *32*, 781–796. [CrossRef]
9. Large, R.R.; Halpin, J.A.; Danyushevsky, L.V.; Maslennikov, V.V.; Bull, S.W.; Long, J.A.; Gregory, D.D.; Lounejeva, E.; Lyons, T.W.; Sack, P.J.; et al. Trace element content of sedimentary pyrite as a new proxy for deep-time ocean–atmosphere evolution. *Earth Planet. Sci. Lett.* **2014**, *389*, 209–220. [CrossRef]
10. Dang, Z.; Liu, C.; Haigh, M.J. Mobility of heavy metals associated with the natural weathering of coal mine spoils. *Environ. Pollut.* **2002**, *118*, 419–426. [CrossRef]
11. Mishra, S.; Bharagava, R.N.; More, N.; Yadav, A.; Zainith, S.; Mani, S.; Chowdhary, P. Heavy Metal Contamination: An Alarming Threat to Environment and Human Health. In *Environmental Biotechnology: For Sustainable Future*; Springer: Singapore, 2019; pp. 103–125. [CrossRef]
12. Neculita, C.M.; Rosa, E. A review of the implications and challenges of manganese removal from mine drainage. *Chemosphere* **2019**, *214*, 491–510. [CrossRef]
13. Lindsay, M.B.; Condon, P.D.; Jambor, J.L.; Lear, K.G.; Blowes, D.W.; Ptacek, C.J. Mineralogical, geochemical, and microbial investigation of a sulfide-rich tailings deposit characterized by neutral drainage. *Appl. Geochem.* **2009**, *24*, 2212–2221. [CrossRef]
14. Cravotta, C.A., III. Abandoned Mine Drainage in the Swatara Creek Basin, Southern Anthracite Coalfield, Pennsylvania, USA: 2. Performance of Treatment Systems. *Mine Water Environ.* **2010**, *29*, 200–216. [CrossRef]
15. Ross, M.R.V.; Nippgen, F.; Hassett, B.A.; McGlynn, B.L.; Bernhardt, E.S. Pyrite Oxidation Drives Exceptionally High Weathering Rates and Geologic CO_2 Release in Mountaintop-Mined Landscapes. *Glob. Biogeochem. Cycles* **2018**, *32*, 1182–1194. [CrossRef]
16. Cravotta, C.A. Dissolved metals and associated constituents in abandoned coal-mine discharges, Pennsylvania, USA. Part 1: Constituent quantities and correlations. *Appl. Geochem.* **2008**, *23*, 166–202. [CrossRef]
17. Cudennec, Y.; Lecerf, A. The transformation of ferrihydrite into goethite or hematite, revisited. *J. Solid State Chem.* **2006**, *179*, 716–722. [CrossRef]

18. Nicholson, R.V.; Gillham, R.; Reardon, E. Pyrite oxidation in carbonate-buffered solution: 2. Rate control by oxide coatings. *Geochim. et Cosmochim. Acta* **1990**, *54*, 395–402. [CrossRef]
19. Gu, X.; Heaney, P.J.; Reis, F.D.A.A.; Brantley, S.L. Deep abiotic weathering of pyrite. *Science* **2020**, *370*, eabb8092. [CrossRef]
20. Von der Heyden, B.P.; Roychoudhury, A.N. Application, chemical interaction and fate of iron minerals in polluted sediment and soils. *Curr. Pollut. Rep.* **2015**, *1*, 265–279. [CrossRef]
21. Ruiz-Agudo, C.; Putnis, C.V.; Ruiz-Agudo, E.; Putnis, A. The influence of pH on barite nucleation and growth. *Chem. Geol.* **2015**, *391*, 7–18. [CrossRef]
22. Buerge-Weirich, D.; Hari, R.; Xue, H.; Behra, P.; Sigg, L. Adsorption of Cu, Cd, and Ni on Goethite in the Presence of Natural Groundwater Ligands. *Environ. Sci. Technol.* **2002**, *36*, 328–336. [CrossRef]
23. Karapınar, N. Removal of Heavy Metal Ions by Ferrihydrite: An Opportunity to the Treatment of Acid Mine Drainage. *Water Air Soil Pollut.* **2016**, *227*, 1–8. [CrossRef]
24. Marescotti, P.; Carbone, C.; Comodi, P.; Frondini, F.; Lucchetti, G. Mineralogical and chemical evolution of ochreous precipitates from the Libiola Fe–Cu-sulfide mine (Eastern Liguria, Italy). *Appl. Geochem.* **2012**, *27*, 577–589. [CrossRef]
25. Wise, M. *Huff Run Watershed Plan*; Huff Run Watershed Restoration Partnership, Inc.: Mineral City, OH, USA, 2005.
26. Wood, D.L.; Cole, K.A.; Herndon, E.M.; Singer, D.M. Lime slurry treatment of soils developing on abandoned coal mine spoil: Linking contaminant transport from the micrometer to pedon-scale. *Appl. Geochem.* **2023**, *151*, 105617. [CrossRef]
27. Smart, K.E.; Singer, D.M. Surface Coal Mine Soils: Evidence for Chronosequence Development. *Soil Syst.* **2023**, *7*, 59. [CrossRef]
28. Singer, D.; Herndon, E.; Zemanek, L.; Cole, K.; Sanda, T.; Senko, J.; Perdrial, N. Biogeochemical Controls on the Potential for Long-Term Contaminant Leaching from Soils Developing on Historic Coal Mine Spoil. *Soil Syst.* **2021**, *5*, 3. [CrossRef]
29. Chowdhury, A.R.; Singer, D.M.; Herndon, E. Colloidal metal transport in soils developing on historic coal mine spoil. *Appl. Geochem.* **2021**, *128*, 104933. [CrossRef]
30. Chowdhury, M.A.R.; Singer, D.M. Trace Metal Enrichment in the Colloidal Fraction in Soils Developing on Abandoned Mine Spoils. *Minerals* **2022**, *12*, 1290. [CrossRef]
31. ODNR. Economic Impact Analysis of the Ohio Abandoned Mine Land Program. In *Ohio Department of Natural Resources Division of Mineral Resources Management*; Ohio University's Voinovich School of Leadership and Public Affairs: Athens, OH, USA, 2014.
32. ODNR. Huff Run Watershed Acid Mine Drainage Abatement and Treatment Plan; Prepared for Ohio DNR by Gannett Fleming. Available online: watersheddata.com (accessed on 7 December 2014).
33. Newville, M.; Sutton, S.R.; Rivers, M.L.; Eng, P. Micro-beam X-ray absorption and fluorescence spectroscopies at GSECARS: APS beamline 13ID. *J. Synchrotron Radiat.* **1999**, *6*, 353–355. [CrossRef]
34. Newville, M. Larch: An Analysis Package for XAFS and Related Spectroscopies. *J. Phys. Conf. Ser.* **2013**, *430*, 012007. [CrossRef]
35. Yazbek, L.D.; Cole, K.A.; Shedleski, A.; Singer, D.; Herndon, E.M. Hydrogeochemical Processes Limiting Aqueous and Colloidal Fe Export in a Headwater Stream Impaired by Acid Mine Drainage. *ACS ES&T Water* **2020**, *1*, 68–78. [CrossRef]
36. Singer, D.M.; Herndon, E.; Cole, K.; Burkey, M.; Morisson, S.; Cahill, M.; Bartucci, M.A. Micron-scale distribution controls metal(loid) release during simulated weathering of a Pennsylvanian coal shale. *Geochim. Cosmochim. Acta* **2020**, *269*, 117–135. [CrossRef]
37. Deditius, A.P.; Utsunomiya, S.; Reich, M.; Kesler, S.E.; Ewing, R.C.; Hough, R.; Walshe, J. Trace metal nanoparticles in pyrite. *Ore Geol. Rev.* **2011**, *42*, 32–46. [CrossRef]
38. Chiriță, P.; Schlegel, M.L. Pyrite oxidation in air-equilibrated solutions: An electrochemical study. *Chem. Geol.* **2017**, *470*, 67–74. [CrossRef]
39. Holmes, P.R.; Crundwell, F.K. The kinetics of the oxidation of pyrite by ferric ions and dissolved oxygen: An electrochemical study. *Geochim. et Cosmochim. Acta* **2000**, *64*, 263–274. [CrossRef]
40. Ruppert, L.F.; Hower, J.C.; Eble, C.F. Arsenic-bearing pyrite and marcasite in the Fire Clay coal bed, Middle Pennsylvanian Breathitt Formation, eastern Kentucky. *Int. J. Coal Geol.* **2005**, *63*, 27–35. [CrossRef]
41. Diehl, S.; Goldhaber, M.; Koenig, A.; Lowers, H.; Ruppert, L. Distribution of arsenic, selenium, and other trace elements in high pyrite Appalachian coals: Evidence for multiple episodes of pyrite formation. *Int. J. Coal Geol.* **2012**, *94*, 238–249. [CrossRef]
42. Gu, X.; Rempe, D.M.; Dietrich, W.E.; West, A.J.; Lin, T.-C.; Jin, L.; Brantley, S.L. Chemical reactions, porosity, and microfracturing in shale during weathering: The effect of erosion rate. *Geochim. Cosmochim. Acta* **2020**, *269*, 63–100. [CrossRef]
43. Huminicki, D.M.; Rimstidt, J.D. Iron oxyhydroxide coating of pyrite for acid mine drainage control. *Appl. Geochem.* **2009**, *24*, 1626–1634. [CrossRef]
44. Rusch, B.; Hanna, K.; Humbert, B. Coating of quartz silica with iron oxides: Characterization and surface reactivity of iron coating phases. *Colloids Surf. A Physicochem. Eng. Asp.* **2010**, *353*, 172–180. [CrossRef]
45. Kim, H.-J.; Kim, Y. Schwertmannite transformation to goethite and the related mobility of trace metals in acid mine drainage. *Chemosphere* **2021**, *269*, 128720. [CrossRef]
46. Fitzpatrick, R.; Mosley, L.; Raven; Shand, P. Schwertmannite formation and properties in acidic drain environments following exposure and oxidation of acid sulfate soils in irrigation areas during extreme drought. *Geoderma* **2017**, *308*, 235–251. [CrossRef]
47. Chen, Q.; Cohen, D.R.; Andersen, M.S.; Robertson, A.M.; Jones, D.R. Stability and trace element composition of natural schwertmannite precipitated from acid mine drainage. *Appl. Geochem.* **2022**, *143*, 105370. [CrossRef]
48. Bigham, J.; Schwertmann, U.; Traina, S.; Winland, R.; Wolf, M. Schwertmannite and the chemical modeling of iron in acid sulfate waters. *Geochim. Cosmochim. Acta* **1996**, *60*, 2111–2121. [CrossRef]

49. Uzarowicz, Ł.; Skiba, S. Technogenic soils developed on mine spoils containing iron sulphides: Mineral transformations as an indicator of pedogenesis. *Geoderma* **2011**, *163*, 95–108. [CrossRef]
50. Duiker, S.W.; Rhoton, F.E.; Torrent, J.; Smeck, N.E.; Lal, R. Iron (hydr) oxide crystallinity effects on soil aggregation. *Soil Sci. Soc. Am. J.* **2003**, *67*, 606–611. [CrossRef]
51. Zhang, W.; Tang, X.-Y.; Xian, Q.-S.; Weisbrod, N.; Yang, J.E.; Wang, H.-L. A field study of colloid transport in surface and subsurface flows. *J. Hydrol.* **2016**, *542*, 101–114. [CrossRef]
52. Akcil, A.; Koldas, S. Acid Mine Drainage (AMD): Causes, treatment and case studies. *J. Clean. Prod.* **2006**, *14*, 1139–1145. [CrossRef]
53. Navarre-Sitchler, A.; Steefel, C.I.; Yang, L.; Tomutsa, L.; Brantley, S.L. Evolution of porosity and diffusivity associated with chemical weathering of a basalt clast. *J. Geophys. Res.* **2009**, *114*, 100. [CrossRef]
54. Bigham, J.M.; Nordstrom, D.K. Iron and Aluminum Hydroxysulfates from Acid Sulfate Waters. *Rev. Miner. Geochem.* **2000**, *40*, 351–403. [CrossRef]
55. Filipek, L.H.; Nordstrom, D.K.; Ficklin, W.H. Interaction of acid mine drainage with waters and sediments of West Squaw Creek in the West Shasta Mining District, California. *Environ. Sci. Technol.* **1987**, *21*, 388–396. [CrossRef]
56. Jambor, J.L.; Nordstrom, D.K.; Alpers, C.N. Metal-sulfate salts from sulfide mineral oxidation. *Rev. Mineral. Geochem.* **2000**, *40*, 303–350. [CrossRef]
57. Li, H.; Ji, H.; Shi, C.; Gao, Y.; Zhang, Y.; Xu, X.; Ding, H.; Tang, L.; Xing, Y. Distribution of heavy metals and metalloids in bulk and particle size fractions of soils from coal-mine brownfield and implications on human health. *Chemosphere* **2017**, *172*, 505–515. [CrossRef]
58. Strawn, D.G.; Hickey, P.J.; McDaniel, P.A.; Baker, L.L. Distribution of As, Cd, Pb, and Zn in redox features of mine-waste impacted wetland soils. *J. Soils Sediments* **2012**, *12*, 1100–1110. [CrossRef]
59. Lanzirotti, A.; Tappero, R.; Schulze, D.G. Chapter 2-Practical Application of Synchrotron-Based Hard X-Ray Microprobes in Soil Sciences. In *Developments in Soil Science*; Singh, B., Gräfe, M., Eds.; Elsevier: Amsterdam, The Netherlands, 2010; pp. 27–72.
60. Horowitz, A.J.; Elrick, K.A. The relation of stream sediment surface area, grain size and composition to trace element chemistry. *Appl. Geochem.* **1987**, *2*, 437–451. [CrossRef]
61. Luoma, S.N. Processes affecting metal concentrations in estuarine and coastal marine sediments. In *Heavy Metals in the Marine Environment*; CRC Press: Boca Raton, FL, USA, 2018; pp. 51–66.
62. Acero, P.; Ayora, C.; Torrentó, C.; Nieto, J.-M. The behavior of trace elements during schwertmannite precipitation and subsequent transformation into goethite and jarosite. *Geochim. Cosmochim. Acta* **2006**, *70*, 4130–4139. [CrossRef]
63. Sidenko, N.V.; Sherriff, B.L. The attenuation of Ni, Zn and Cu, by secondary Fe phases of different crystallinity from surface and ground water of two sulfide mine tailings in Manitoba, Canada. *Appl. Geochem.* **2005**, *20*, 1180–1194. [CrossRef]
64. Herndon, E.; Yarger, B.; Frederick, H.; Singer, D. Iron and Manganese Biogeochemistry in Forested Coal Mine Spoil. *Soil Syst.* **2019**, *3*, 13. [CrossRef]
65. Ghosh, A.; Pal, M.; Biswas, K.; Ghosh, U.C.; Manna, B. Manganese oxide incorporated ferric oxide nanocomposites (MIFN): A novel adsorbent for effective removal of Cr(VI) from contaminated water. *J. Water Process. Eng.* **2015**, *7*, 176–186. [CrossRef]
66. Clark, E.V.; Zipper, C.E.; Daniels, W.L.; Keefe, M.J. Appalachian coal mine spoil elemental release patterns and depletion. *Appl. Geochem.* **2018**, *98*, 109–120. [CrossRef]
67. Gao, X.; Xu, M.; Hu, Q.; Wang, Y. Leaching behavior of trace elements in coal spoils from Yangquan coal mine, Northern China. *J. Earth Sci.* **2016**, *27*, 891–900. [CrossRef]
68. Beauchemin, S.; Langley, S.; MacKinnon, T. Geochemical properties of 40-year old forested pyrrhotite tailings and impact of organic acids on metal cycling. *Appl. Geochem.* **2019**, *110*, 104437. [CrossRef]
69. Adams, R.; Ahlfeld, D.; Sengupta, A. Investigating the Potential for Ongoing Pollution from an Abandoned Pyrite Mine. *Mine Water Environ.* **2007**, *26*, 2–13. [CrossRef]
70. Hammond, C.M.; Root, R.A.; Maier, R.M.; Chorover, J. Metal Lability and Mass Transfer Response to Direct-Planting Phytostabilization of Pyritic Mine Tailings. *Minerals* **2022**, *12*, 757. [CrossRef]
71. Larsen, O.; Postma, D. Kinetics of reductive bulk dissolution of lepidocrocite, ferrihydrite, and goethite. *Geochim. et Cosmochim. Acta* **2001**, *65*, 1367–1379. [CrossRef]
72. Anschutz, A.J.; Penn, R.L. Reduction of crystalline iron(III) oxyhydroxides using hydroquinone: Influence of phase and particle size. *Geochem. Trans.* **2005**, *6*, 60. [CrossRef]

Disclaimer/Publisher's Note: The statements, opinions and data contained in all publications are solely those of the individual author(s) and contributor(s) and not of MDPI and/or the editor(s). MDPI and/or the editor(s) disclaim responsibility for any injury to people or property resulting from any ideas, methods, instructions or products referred to in the content.

soil systems

MDPI

Article

Use of *Cannabis sativa* L. for Improving Cadmium-Contaminated Mediterranean Soils—Effect of Mycorrhizal Colonization on Phytoremediation Capacity

Maria Androudi [1,2], Vasiliki Liava [1], Eleni Tsaliki [2], Ioannis Ipsilantis [1] and Evangelia E. Golia [1,*]

[1] Laboratory of Soil Science, School of Agriculture, Aristotle University of Thessaloniki, 541 24 Thessaloniki, Greece
[2] Hellenic Agricultural Organization DIMITRA (ELGO Dimitra), Institute of Plant Breeding and Genetic Resources, 570 01 Thessaloniki, Greece
* Correspondence: egolia@auth.gr; Tel.: +30-231-099-8809

Abstract: Although the phytoremediation strategy has been studied worldwide, little research data are available regarding the influence of mycorrhizae on the phytoremediation capacity of various plants grown in Cd-contaminated soils in Mediterranean environments. Therefore, a pot experiment was carried out to study the possible effectiveness of hemp plant (*Cannabis sativa* L.) in the remediation of moderately and heavily Cd-contaminated soils and additionally to quantify the effect of Cd on Arbuscular Mycorrhizal Fungi (AMFs). For this purpose, an alkaline clay soil collected from the Farm of Institute of Plant Breeding and Genetic Resources (North Greece) was contaminated with two levels of Cd (3 and 30 mg Cd kg^{-1}, corresponding to Levels A and B, respectively—first factor) at two incubation times (10 and 30 days—second factor) and six treatments (Control_30d, Control_10d, CdA_30d, CdB_30d, CdA_10d, CdB_10d) were created. Soil Cd concentrations, both pseudo-total and available to plants, were determined after extraction with Aqua Regia mixture and DTPA solution, respectively, before and after the cultivation of hemp plants and after the harvesting. Cd concentrations in the aboveground and underground plant parts were also estimated after digestion with Aqua Regia, while root colonization by AMFs was determined with a microscope. The highest plant's Cd concentration, more than 50%, was observed in its underground part, at all Cd-contaminated treatments, indicating a strong capacity for cadmium to gather up in the roots. Among different Cd levels and incubation days, significant differences were recorded in the rates of root colonization by AMFs. Among different Cd levels and incubation days, 3 mg Cd Kg^{-1} soil promoted AMF root colonization, particularly at 10-day incubation, while 30 mg Cd Kg^{-1} soil diminished it. Colonization was lower with longer incubation times at both levels of Cd. Hemp appears to be a viable option for phytostabilization in Cd-contaminated soils, enabling further utilization of AMFs to assist the phytoremediation process.

Keywords: arbuscular mycorrhizal fungi; phytostabilization; hemp; Cd; *Cannabis sativa*

Citation: Androudi, M.; Liava, V.; Tsaliki, E.; Ipsilantis, I.; Golia, E.E. Use of *Cannabis sativa* L. for Improving Cadmium-Contaminated Mediterranean Soils—Effect of Mycorrhizal Colonization on Phytoremediation Capacity. *Soil Syst.* **2024**, *8*, 100. https://doi.org/10.3390/soilsystems8030100

Academic Editor: Manfred Sager

Received: 22 July 2024
Revised: 10 September 2024
Accepted: 14 September 2024
Published: 16 September 2024

Copyright: © 2024 by the authors. Licensee MDPI, Basel, Switzerland. This article is an open access article distributed under the terms and conditions of the Creative Commons Attribution (CC BY) license (https://creativecommons.org/licenses/by/4.0/).

1. Introduction

Consistent with the rapid advancements of today's society, the volume of waste being generated worldwide is steadily growing [1], leading to the incremental contamination of natural habitats with a wide array of both organic compounds and inorganic elements that typically do not occur in nature [2]. Heavy metal (HM) presence in soil is becoming more and more prevalent at elevated levels, creating considerable environmental and public health hazards [3]. This is mainly attributed to the fact that HMs are not subjected to biodegradation; thus, they can persist in the environment for extended periods, and they tend to build up in various segments of the food chain [4,5]. Khan et al. [6] reported that HMs might cause long-lasting detrimental effects on the vitality of soil ecosystems and

negatively affect soil biological functions. At high levels, HMs can negatively impact microorganisms' growth, structure, and metabolic functions, reducing the functional diversity within soil ecosystems [7].

Cadmium (Cd) stands out as a significant hazardous heavy metal in the environment and has detrimental impacts on all kinds of organisms [8,9], arising from diverse industrial and agricultural activities such as mining, metallurgy, pigment production, plastic stabilization, sewage sludge, manure, straw, fertilizer application, and nickel–cadmium battery manufacturing [9–13]. Its prolonged biological persistence renders it a cumulative toxin, causing adverse effects on soil microbial communities and susceptible plants (something that mainly depends on the factors affecting their bioavailability), thus ultimately affecting human health [14,15]. Cd, when discovered in soils, due to metal aging and soil characteristics may cause a change in the geochemical dispersion pattern [16]. In terms of weathering, it has been established that metals deposited slowly in soils over a long time tend to be least bioavailable [17]; the main reason behind this is that the metals move over time to inaccessible residual soil reservoirs (e.g., enclosed in Fe and Al oxides or in poorly exchangeable interstitial nodules of phyllosilicate clays) [18]. Regarding the properties of soils, the most important ones that affect metal uptake in plants are soil pH, percentage of $CaCO_3$, redox potential, clay content, cation exchange capacity, organic matter, and mineral composition [19–21].

Arbuscular Mycorrhizal Fungi (AMFs) are some of the most widely known beneficial soil microorganisms, the key component of the rhizosphere. They form symbiotic relationships with most higher plants [22]. The mycorrhizal association has a crucial part in natural ecosystems by intracellular colonization of plant roots [23–25]. This interaction improves land assets, contributing to the effective management of environmental constraints [26–29]. Fungi strengthen the host plant's ability to assimilate both nutritional elements and water, and in exchange the host plants supply fungal carbohydrates for their own expansion [30,31]. AMFs also provide essential minerals to plants [32] and enhance soil chemical and physical characteristics, serving as barriers to prevent the entry of harmful xenobiotics through their fungal networks [33]. Consequently, mycorrhizae function as a protective layer, forming a shield around the plant roots they inhabit [34]. Furthermore, it has been demonstrated that AMFs significantly increase plant resilience against both biotic and abiotic stresses, including the presence of heavy metals [35]. Given their crucial role as an intermediary between the earth and plant roots, they play an essential part in managing the presence and impact of heavy metals on plants [36]. AMFs have been reported to minimize the hazardous impacts of HMs, improving the plants' resistance through different regulatory systems [37], like changing the chemical synthesis of the rhizosphere heavy metal-contaminated soil, enhancing plant nutritional status, and having a direct effect on the absorption and buildup of HMs [32,38,39].

In the last decades, the main and most suitable control technique used to eliminate HMs from the soil environment is phytoremediation [40]. This is an eco-friendly, economically efficient method, producing few side pollutants [41]. Phytoextraction and phytostabilization methods of phytoremediation seem to be well studied worldwide [42]. During phytoextraction, the plants used can build up the toxic elements in their overground parts by extracting metals from the soil [43,44]. Conversely, the second method involves immobilizing the HMs within the plant roots [42]. These mechanisms are used alone or in association between plants, as appropriate to the pollutant nature [38].

Industrial hemp (*Cannabis sativa* L.) is primarily cultivated for its fiber [45], seed production [46], medicinal purposes [47], and biomass for energy generation [48]; it presents highly favorable prospects as a phytoremediator. It exhibits rapid biomass growth and outperforms typical hyperaccumulators in heavy metal absorption, making it a valuable resource for environmental restoration [49]. *C. sativa* L. has a long radical system, keeps out of the trophic chain, provides easy cultivation and management, and has numerous other exceptional features [50]. It has been shown that mycorrhizal hemp may accumulate more Cd in the roots and may tolerate higher Cd concentrations [51], particularly with

AMF inoculum with origins from a Cd contaminated area [52]; research has found that mycorrhization enhanced translocation of Cd from hemp root to shoot [53]. Inoculation with AMF combined with protein hydrolysate increased shoot Cd uptake [54]. Additionally, unlike most bioenergy plants, hemp provides the opportunity for contributing to a circular economy pattern [2]. These findings are therefore encouraging, yet little research data are currently available concerning the impacts of mycorrhiza on the phytoremediation capacity of various plants grown in Cd-contaminated soils in a Mediterranean environment with distinct climatic characteristics.

Considering these issues, this study aimed to investigate the cultivation of *C. sativa*, a plant species that could be utilized after phytoremediation, in Cd-contaminated soil.

Moreover, the aim was to study the impact of Cd stress on hemp's root colonization by AMFs and additionally the influence of AMFs on the plant's ability to tolerate and accumulate Cd. Thus, the objectives of this work were to evaluate (a) the effect of different Cd levels and incubation periods on the colonization of hemp (*C. sativa* L.) roots by AMFs, (b) the correlation between AMF colonization and the growth and resistance of hemp plants, and (c) the survey of the potential relations or interactions between Cd distributed in plant parts and Cd impact on AMF colonization using the proper statistical tools.

2. Materials and Methods

2.1. Sampling and Experimental Design

The soil sample (depth 0–20 cm) used for the experiment was collected from the Farm of the Institute of Plant Breeding and Genetic Resources (ELGO-DIMITRA) located at Thermi, Thessaloniki, in North Greece. Specifically, for the examined sample, six subsamples with the help of a wooden spade were taken from a roughly 150 cm radius area [55]. Composite surface soils were specifically developed to reduce the amount of analyses meant to provide a representative sample, which is necessary for replicates to be conducted [56]. The sample was then transported to the Soil Laboratory at the Aristotle University of Thessaloniki, where it was air-dried and put through a sieve with <2 mm pores in order to be subjected to various physicochemical analyses (pH, EC, $CaCO_3$, particle size distribution, organic carbon content, available and pseudo-total Cd concentrations) [57,58].

The experimental design included one control (0 mg Cd kg^{-1}) and two levels of Cd—first factor (3 and 30 mg Cd kg^{-1}) at two incubation times—second factor (10 and 30 days). Six treatments with ten replicates per treatment were created. The treatment coding was outlined as shown in Table 1. The European Union's Directive 86/278/EEC was the base on which the Cd concentrations were chosen. As a result, Level A represents moderately contaminated soils, while Level B is analogous to heavily contaminated soils [59].

Table 1. The coding of the five treatments of the experiment.

Coding	mg Cd kg^{-1}	Incubation Days	Replicates
Control_10d	0	10	10
CdA_10d	3	10	10
CdB_10d	30	10	10
Control_30d	0	30	10
CdA_30d	3	30	10
CdB_30d	30	30	10

2.2. Artificial (Laboratory) Contamination of Soil Sample and Pot Experiment

The soil sample was chosen to have an undetectable Cd concentration so that contamination could be carried out in a laboratory. To achieve this objective, appropriate calculated volumes of solutions of cadmium nitrate were evaluated and incorporated into the soil samples of each treatment at two levels (A and B), respectively, contaminated with 3 and 30 mg Cd kg^{-1}. The Cd solutions were applied to the soils by spraying, and afterwards the mixture was manually stirred for 10 min. After mixing, the bags remained closed throughout the two periods of incubation time (for 10 and 30 days), during which the

moisture content was kept around 70% with occasional aeration and dehumidification. Following the proper incubation period, the soil samples were placed into the pots, and seeding was carried out with the Felina 32 variety. Felina 32 is a monoecious variety of French origin well adapted to the Mediterranean climate, usually cultivated for seeds or fiber production. Furthermore, Fellina 32 is registered in the European Catalogue with Δ-9 tetrahydrocannabinol content <0.3% as required by the European legislation. The main factor for the choice of this variety was its height (around one meter) that can be considered ideal for an experiment in pots [60]. In total, 30 pots with a capacity of 7 L each were used for the experiment, in each of which 10 seeds of the variety were placed around the perimeter, early in May 2023 (on 2 May 2023). One month after sowing (on 1 June 2023), thinning was carried out to allow 3–4 female plants of similar size in each pot to grow without competition. The harvest was carried out during Stage 2305 of plant growth according to the UPOV protocol [61], early in August 2023 (on 8 August 2023) while flowering was completed and seed ripening began. From May to August, the pots were kept outdoors and automatically watered. The experiment was conducted without fertilization. Meteorological data from the growing season (April to August) are presented in Table 2 and are typical for Mediterranean climates [3,56].

Table 2. Monthly and mean air temperature and precipitation during the growing period, *C. sativa*.

	2023					
	April	**May**	**June**	**July**	**August**	**Total**
Mean Temperature (°C)	14.0	18	23.3	28.8	27.8	-
Precipitation (mm)	75.6	70.0	85.8	9.0	40.0	280.4

2.3. Soil Chemical and Physical Analysis

After harvesting, soil samples from the pot experiments were subjected to physical and chemical analysis, as previously mentioned, according to Dimirkou et al. [58] and Golia [57]. Both electrical conductivity (EC) and soil reaction (pH) were calculated with the use of a 1:1 mixture of soil and water. For particle size distribution, the Bouyoukos method was used, while for the soil organic matter (OM) content appraisal, the modified Walkley–Black method was utilized, as described in Page [62]. With the use of a Bernard–Scheibler calcimeter, the appraisal of $CaCO_3$% was performed. Soil cadmium concentrations, pseudo-total and available to plants, were determined both before the cultivation of hemp plants and after harvesting. Available concentration of Cd was determined with DTPA solution (1:2 diethylene-triamine-pentaacetic acid pH 7.3) [57], while the pseudo-total concentration of Cd was determined with Aqua Regia ($HCl:HNO_3$ 3:1 digested at 180 °C for 2 h [63]. All reagents used did not contain impurities (Merck, Darmstadt, Germany).

Atomic absorption spectrophotometry (AAS) was used to measure the Cd concentrations, utilizing either the flame (F-AAS) or graphite furnace (GF) technique. The analytical recovery was validated using Standard Reference soil material 2710 (National Institute of Standards and Technology, Gaithersburg, MD). The recovery ratio of standards ranged from 89.3% to 104.4% and 88.1% to 103.7% for Cd in soil and plant, respectively.

2.4. Plant Analysis

After harvesting, both the belowground and the stem and leaf parts of *C. sativa* were gathered to carry out the plant's analyses. For this purpose, first, the aboveground parts were deposited in numbered bags made of paper, and the weight with water content of each plant part was measured. The roots were previously cleaned 2 to 3 times with the help of deionized water to remove the soil attached to them. A small weighted portion of the root (~0.5) was taken for the determination of AMF root length colonization. The specimens were subsequently heated at 60 °C for 48 h and weighed again when they reached the water concentration that could not be extracted with this method. Then, they were pulverized

with the use of an electric grinder and/or porcelain mortar, and the pulverized samples (aboveground and roots) were stored for chemical analyses. A 3:1 mixture of concentrated acids of HCl and HNO_3 was used for the Aqua Regia solution extraction method [63], which was conducted for Cd evaluation in the plant aboveground and underground parts.

2.5. Quantification of AMF Colonization in Roots: Clearing and Staining Roots

The following procedure was followed to quantify the root colonization by AMF [64]. Washed clean roots were placed in 10% KOH and remained there for 40 min at 80 °C. Then, after rinsing the KOH about 5 times with deionized water and acidifying the solution, the roots were stained with a 0.05% *w/v* trypan blue solution (1:1:1 *v*/*v*/*v* H_2O: glycerin: lactic acid). Then, in order to observe and measure the colonization, slides were prepared by placing roots in PVLG (Polyvinyl-Lacto-Glycerol) on the slide. The percentage of AMF root length colonization was appraised under a microscope following the method described by McGonigle et al. [65] at ×100 magnification (400× for details).

2.6. Statistical Processing of Data

The data were recorded and subsequently analyzed statistically using appropriate statistical packages (Sigmaplot12 and Microsoft Office Excel, SigmaPlot 12 (Systat Software, San Jose, CA, USA) and Excel (Microsoft 365 Version 2408)). Prior to analysis, the normality test (Shapiro–Wilk) and the equal variance test were conducted to ensure normal distribution and homogeneity of variance. Then, a two-way analysis of variance (ANOVA) was conducted to evaluate the effect of Cd levels on contaminated soil (Factor A), the incubation times (Factor B) and their interaction effect (A × B) on Cd accumulation in plant parts, the dry weight of aboveground and underground parts, and the AMF colonization in roots. The differences between means were distinguished by Fisher's least significant difference (LSD) test at $p = 0.05$.

3. Results and Discussion

3.1. Soil Characterization

Table 3 shows the physicochemical properties of the soil sample used in this study. These values are the averages of ten replicates. The studied soil was alkaline (pH > 7) and calcareous ($CaCO_3$ = 13.24%) with low organic matter (2.9%) which is typical of Mediterranean climates [66]. Soil had high clay content (56% clay) and high electrical conductivity (1082 µS/cm). Thus, the soil sample had a clay–clay texture based on the categorization of soils after the determination of the percentages of sand, silt, and clay by the Bouyoukos method [62].

Table 3. Values of soil physicochemical properties (average of replicates, n = 10).

Physicochemical Properties	Min	Max	Average	SD
pH (1:1)	7.6	9.1	8.3	±0.6
EC (µS/cm)	1082.0	1090	1086	±3.3
OM (%)	2.3	3.5	2.9	±0.5
$CaCO_3$ (%)	12.1	14.4	13.2	±1.0
Clay (%)	53	59	56	±2.4
Sand (%)	41	46	44	±2.0

Alloway et al. [20] noted and illustrated in their experiments that soil reaction and soil texture are determinant factors in the physicochemical properties of the soil environment. Indeed, reports indicate that some soil types can significantly diminish metal availability to plants; these soils usually have a higher pH, which makes metal cations less soluble [18], causes higher content of $CaCO_3$ [67] and clay minerals [60,68]. In this study, the $CaCO_3$ rates are completely linked to soil pH values.

Plant uptake and bioavailability of Cd is negatively correlated with pH [67,69]. In addition, the presence of divalent cations in the soil solution, such as Ca^{2+} and Zn^{2+}, may

increase Cd bioavailability due to competition for absorption sites and competing ion activities [70,71]. Napoletano et al. [72] and Papadimou et al. [56] confirmed their observations and experimental results on soils with elevated electrical conductivity, primarily due to human activities. In this study, the soil samples exhibited high electrical conductivity values, indicating a significant presence of salts in the soil solution [20,73]. The percentage of organic matter suggests that the soil samples are representative of typical agricultural soils from the area of Thessaloniki. Golia and Diakoloukas [74] examined a large number of soils from agricultural regions spanning four soil orders and found that organic matter values typically fall below 3%, a pattern also observed in the current study.

3.2. Pseudo-Total and Available Concentration of Cd in Soil Samples

In Figures 1 and 2, the pseudo-total and available Cd concentrations in soil samples are presented for 10 and 30 days of incubation, respectively, before (Initial) and after (Final) hemp cultivation in each treatment. It is evident from both figures that the control treatment, where no Cd was applied, exhibited undetectable levels of Cd concentrations. Conversely, in Cd treatments, measurable concentrations of Cd were observed across all treatments (CdA_30d, CdB_30d, CdA_10d, and CdB_10d). Comparing treatments with Cd at Level A (3 mg kg^{-1}) to those at Level B (30 mg kg^{-1}), considerably higher values were noted in the latter, indicating the pronounced impact of escalating Cd concentrations on extracted metal levels. Additionally, the influence of different incubation durations (10 and 30 days) on the Cd pseudo-total concentrations is noteworthy. Specifically, a shorter 10-day incubation period in the treatments with Cd at Level B resulted in lower pseudo-total Cd concentrations compared to the 30-day incubation period.

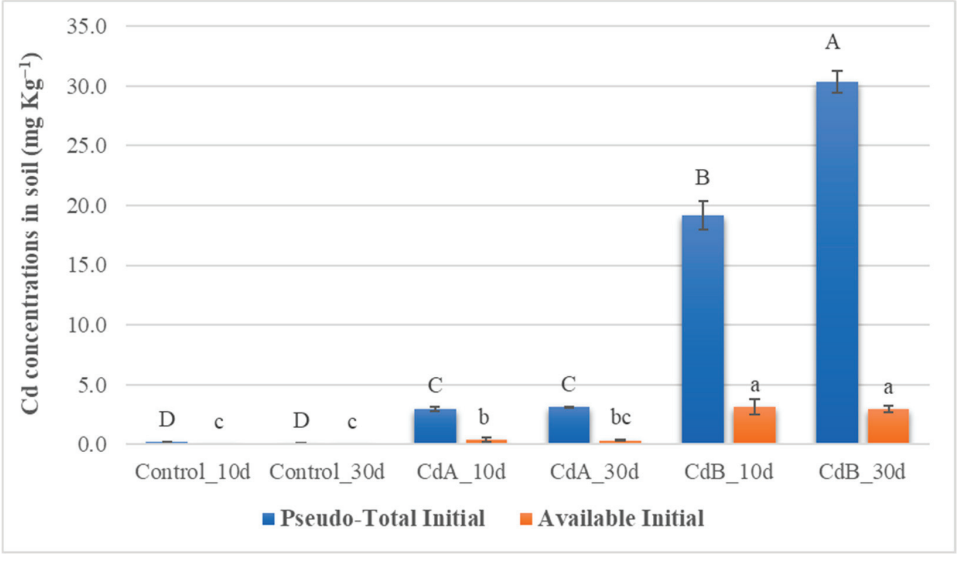

Figure 1. Pseudo-total and available Cd concentrations in soil (10 and 30 days of incubation time) before (Initial) hemp cultivation in each treatment (lowercase letters show the significant differences between the treatments for available Cd concentrations, while capital letters show the significant differences for pseudo-total Cd concentrations. Error bars indicate standard deviation. $LSD_{5\%}$ values for pseudo-total and available Cd concentrations: 0.8102 and 0.3845, respectively).

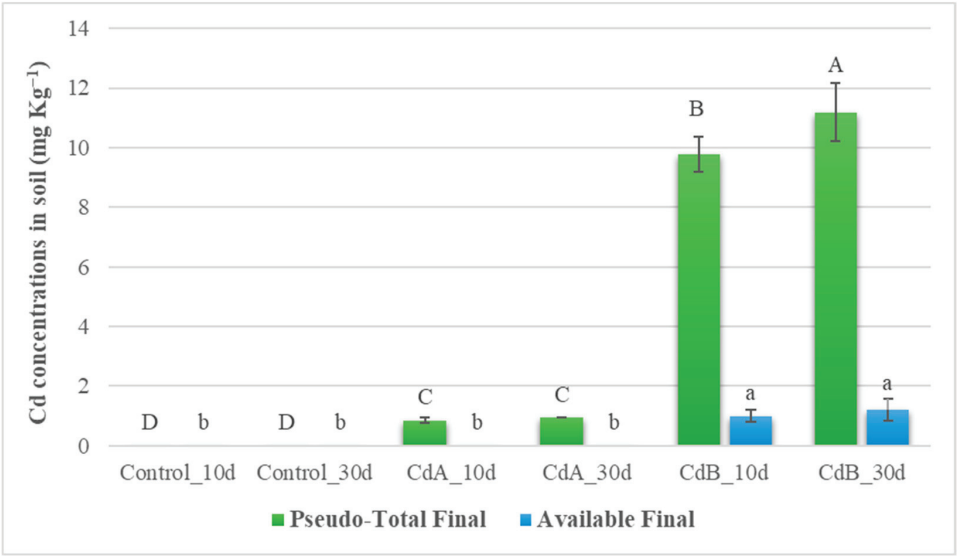

Figure 2. Pseudo-total and available Cd concentrations in soil (10 and 30 days of incubation time) after (Final) hemp cultivation in each treatment (lowercase letters show the significant differences between the treatments for available Cd concentrations, while capital letters show the significant differences for pseudo-total Cd concentrations. Error bars indicate standard deviation. $LSD_{5\%}$ values for pseudo-total and available Cd concentrations: 0.6117 and 0.2326, respectively).

As expected, the minimum concentration of Cd extracted from the soil was found in the control where no Cd was applied, while in the other treatments, higher values were recorded in the following order: Level B > Level A > Control. Moreover, as presented in Figure 3, there was a significant positive correlation between the pseudo-total and available Cd concentrations, as well as between the initial and the final Cd concentrations in the soil. This finding is in agreement with the experimental results of Marković et al. [75], who reported that with increasing soil Cd concentration, the concentrations of Cd in all soil fractions increased. After harvesting the plants, however, it was observed that both pseudo-total and available Cd concentrations extracted from the soil of each treatment were lower. This result indicates that a part of the added Cd concentration was probably taken up by the hemp plants so that the concentrations that remained in the soil after harvesting the plants were lower than those extracted before plant cultivation [58]. From the Cd available concentrations, however, it was indicated that the concentration of Cd, which became available to the plants, was not influenced significantly by the incubation time. In contrast to our results, Marković et al. [75] reported in their study that prolonged incubation time (2 months) was an important factor in Cd stabilization in the investigated soils. Our different results may be attributed to the fact that in our study, the longer incubation period was only 1 month. Lu et al. [76] similarly reported that as incubation time increased (>30 days), Cd was barely transformed from its exchangeable condition to other types. Based on the present work, it is possible to conclude that even with a short-day exposure to Cd pollution, the available concentration, i.e., that which can be taken up by plants and cause potential risks to the health and functionality of organisms, appears to be the same as that corresponding to a threefold action time. Therefore, the aging or senescence of contamination is a way of limiting the possible risks, leading to appropriate decisions for the proper management of contaminated soil systems [17].

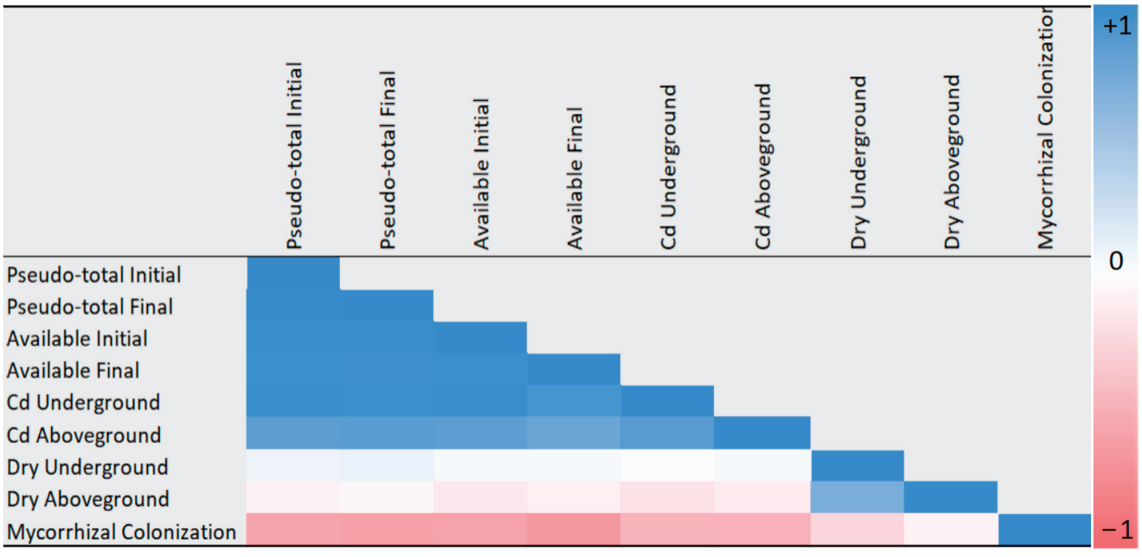

Figure 3. Heatmap of Pearson correlation coefficient.

3.3. Cd Levels in C. sativa Cultivated in the Contaminated Soil Samples

When the experiment was completed, Cd concentrations were measured across cannabis plant parts to assess Cd uptake. Figure 4 presents the Cd concentration absorbed by cannabis roots and the aboveground plant part. As expected, in the control treatment, Cd concentration was undetectable in both plant parts. Conversely, a clear dose-dependent response was evident in the soils contaminated with Cd. Comparing treatments with Cd Levels A (3 mg Cd kg^{-1}) and B (30 mg Cd kg^{-1}), it is evident that the latter exhibited markedly higher Cd concentrations in each plant part as there is a positive correlation between the Cd concentrations in soil and plant parts (Figure 3). This observation aligns with similar studies conducted on various industrial hemp varieties, suggesting that as Cd concentrations in the growth medium increase, so does Cd accumulation in plant tissues [77,78]. Interestingly, varying incubation durations between treatments did not appear to significantly affect this parameter, as Cd uptake levels remained relatively consistent, with a slight upward trend noted for a 10-day incubation period. Considering the fact that at the shorter incubation time, an increasing trend was observed in the available Cd concentration in the soil, i.e., in the concentration extracted with the DTPA solution, it is understandable that the direct availability of water-soluble Cd artificially added to the soil samples of the experiment is directly taken up by the hemp plant. The low but increased concentration noted in both the roots and overground plant parts indicates the tendency for the metal to move towards soil fractions that make it less available as time progresses [56].

Among the different plant tissues, the roots accumulated the highest concentration of Cd, while significantly lower values were recorded in the aboveground parts of the plant.

In the following Table 4, the values of the Bio Concentration Factor (BFC), the ratio of Cd concentrations in hemp parts to Cd soil levels, are presented. The values of the calculated BFCs are significantly higher in the underground than in the aboveground part of hemp. Moreover, the greatest values were recorded in the lower level of Cd, especially after 10-day incubation.

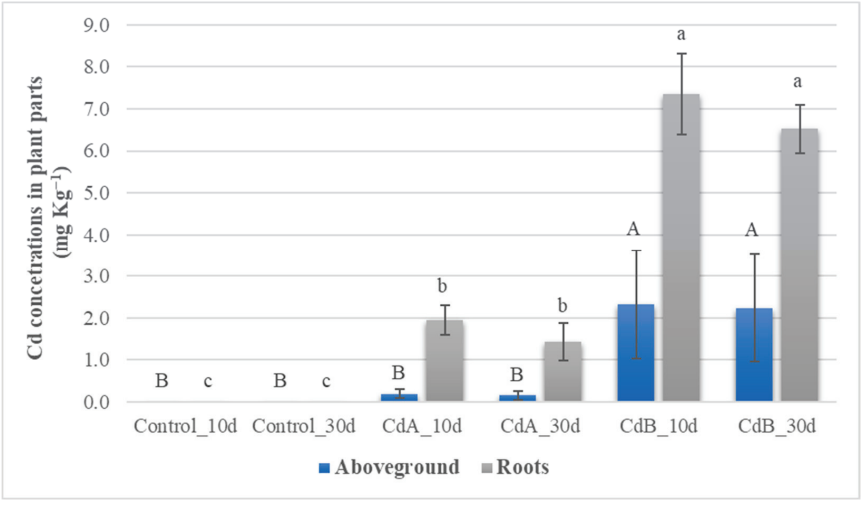

Figure 4. Cd concentrations in the aboveground part and the roots of hemp in the six treatments of the experiment (lowercase letters show the significant differences between the treatments of roots, while capital letters show the significant differences for aboveground parts. Error bars indicate standard deviation. $LSD_{5\%}$ values for aboveground and roots: 0.6772 and 0.6908, respectively).

Table 4. Values of Bio Concentration Factor (BFC) in hemp parts.

Treatements	Underground		Aboveground	
	$C_{plant}/C_{pseudo\text{-}total}$	$C_{plant}/C_{available}$	$C_{plant}/C_{pseudo\text{-}total}$	$C_{plant}/C_{available}$
Control_10d	0.00	0.00	0.00	0.00
Control_30d	0.00	0.00	0.00	0.00
CdA_10d	0.65	5.06	0.06	0.49
CdA_30d	0.45	4.51	0.05	0.49
CdB_10d	0.25	2.36	0.08	0.75
CdB_30d	0.22	2.21	0.07	1.01

This outcome is consistent with prior research on Cd bioaccumulation in cannabis plants, which reported that the highest metal concentrations were typically found in the underground part [53,60,79]. However, Shi et al. [80], in their investigation of the cumulative capacity of 18 different industrial hemp varieties in soil contaminated with 25 mg kg^{-1} of Cd, found that metal bioaccumulation varied among the different varieties. These findings are particularly encouraging, as they indicate that hemp, specifically the Felina 32 variety, tends to accumulate Cd in its roots. This characteristic allows for the utilization of its aboveground biomass, which holds significant economic importance for industrial purposes. Vasilou and colleagues [60] established that cultivating industrial hemp in Mediterranean soils suffering from anthropogenic cadmium pollution is an outstanding way of highlighting the important properties of the plant, as it can retain the pollutant in the soil, immobilizing it in the root, without allowing it to move to the upper parts of the plant from which cannabinoids (CBDs) are produced. Thus, hemp, it turns out, is an excellent plant that can successfully scavenge the soil, can produce the precious CBD, and can also provide its almost cadmium-free stems in order to produce ropes or other kinds of industrial products. Similarly, in *Silybum marianum* L., researchers Papadimou et al. [56,59] observed that there is potential for the exploitation of thistle weed for two important reasons: first, it can be directly used to recover soils contaminated not only with Cd, but also with Zn and Cu, yet simultaneously it can produce, unhindered, the human

health valuable substance silymarin which is found in the seeds of the plant, even though it is grown in extremely contaminated soils, without deteriorating its quality.

3.4. Roots and Aboveground Plant Biomass

In Figures 5 and 6, the dry biomass of the roots and aboveground parts, respectively, of C. sativa cultivated in soils with two different Cd levels and incubation periods are presented. A notable increase in plant biomass when the incubation period extended to 30 days was observed compared to the control at both Cd levels (A: 3 mg kg^{-1} and B: 30 mg kg^{-1}). Conversely, for treatments with a 10-day incubation period, a slight downward trend in plant dry weight was determined after comparison to the control, but it was not statistically significant.

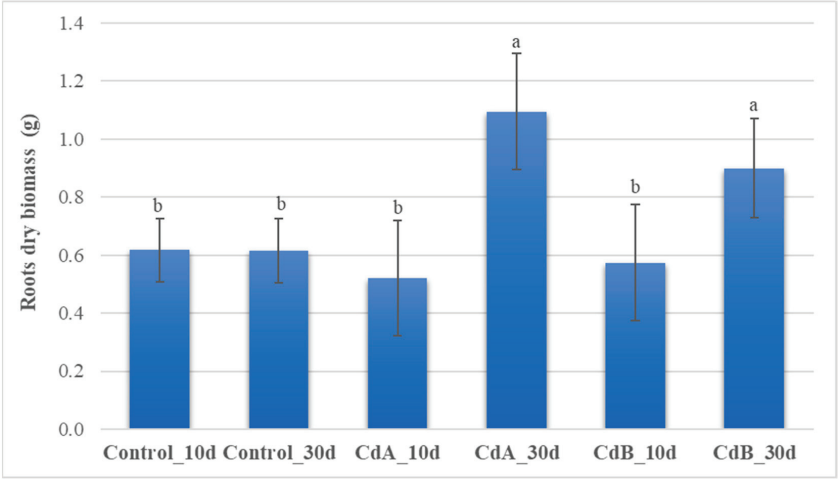

Figure 5. Dry biomass (g) of the roots of hemp in the six treatments of the experiment (The different letters show the significant differences between the treatments. Error bars indicate standard deviation. $LSD_{5\%}$ = 0.2343).

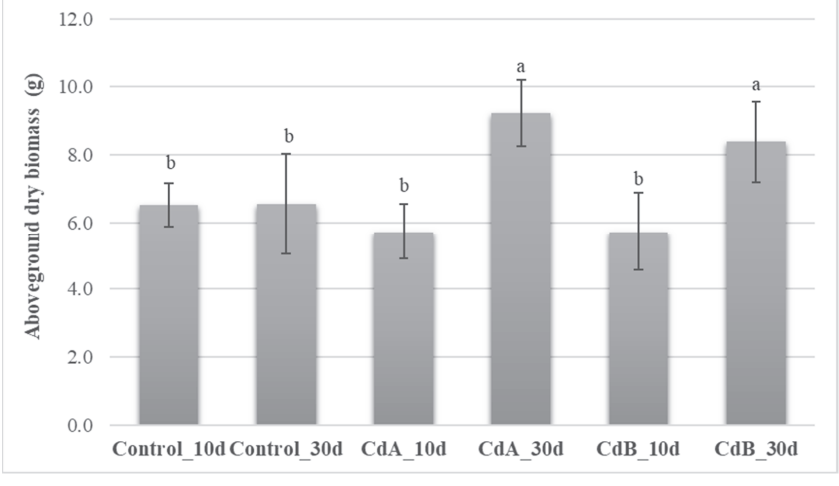

Figure 6. Dry biomass (g) of the aboveground part of the hemp in the six treatments of the experiment (The different letters show the significant differences between the treatments. Error bars indicate standard deviation. $LSD_{5\%}$ = 1.421).

These findings suggest that Cd incorporation in soil at both levels did not adversely affect the produced plant biomass. Moreover, as presented in Figure 3, there are no correlations between the Cd concentration in soil and the dry weight of aboveground or underground parts. Thus, hemp can thrive under these Cd concentrations without experiencing degradation in biomass. This outcome aligns with the findings of Linger et al. [81], who noted no significant differences in hemp root dry weight when plants were exposed to Cd concentrations, even at notably high levels (up to 100 mg Cd kg^{-1}). However, they did observe a significantly negative impact on leaf and shoot biomass when Cd concentrations exceeded 50 mg kg^{-1} in the soil. Similarly, Shi and Cai [82] conducted pot experiments investigating hemp growth at Cd concentrations ranging from 50 to 200 mg kg^{-1}. They found that root growth was only suppressed in the treatment with 200 mg Cd kg^{-1}. It is worth noting that previous studies have demonstrated a reduction in biomass for other plant species as Cd concentrations increased [83]. Different plants react variably to heavy metal stress, with their resilience and tolerance contingent upon the species' ability to activate molecular mechanisms [84]. Plant development parameters are being used as appropriate biomarkers of trace element toxicity. In particular, within the context of phytoremediation, when high levels of biomass are needed, substantial decreases in plant growth determine the plant tolerance limits and thereby the perspectives of the potential candidate crop species. Thus, several plants have displayed a unique ability to develop defense mechanisms for withstanding the stress of heavy metals. These mechanisms include metal removal, scavenging, refining, sequestration, and accumulation to reduce the effects of metal toxicity. Proteomics has become quite a strong tool in biotechnological research to determine how plants respond or react to heavy metal pollution. A deeper investigation of the molecular mechanisms in plants involved in metal removal and pressure reaction could be a subject of future research [85,86].

3.5. Effect of Different Levels of Cd Concentration on AMF Colonization Rates (%) at Different Incubation Times

Figure 7 presents the colonization rates (%) of cannabis roots by AMF across the six treatments of the experiment. The addition of 3 mg kg^{-1} of Cd (CdA_30d and CdA_10d treatments) exhibited significantly higher colonization rates, within the 60–70% range, compared to the control treatments. Conversely, in the treatments where a higher concentration of Cd (30 mg kg^{-1}) was added (CdB_30d and CdB_10d treatments), lower colonization rates were observed than with 3 mg kg^{-1} Cd, ranging from 35 to 55%. According to Figure 3, there was a negative relationship between the AMF colonization and the Cd concentration in the soil, owing to the values recorded at the higher level of Cd, although the correlation was not statistically significant. Also, notably, a comparison between the 30-day incubation treatments and the 10-day ones revealed that in the former case, the colonization of the roots was significantly lower.

To better describe the colonization of cannabis roots by AMFs, in Figure 8, observations from the microscope of cannabis blue-stained roots are presented. Specifically, in Figure 8a, the hyphae are illustrated, extending within the root and showing branching, while in Figure 8b,c, the intraradical vesicles and the arbuscules within the roots produced by AMF are presented, respectively.

These results indicate that the rate of colonization depends on the level of Cd added to the soil. This observation is consistent with the findings of Liu et al. [32], who demonstrated that the colonization rate of corn roots (*Zea mays* L.) varied between 30.3% and 72.3% across different Cd levels in the soil. Specifically, in our study, the addition of Cd at Level B (30 mg kg^{-1}) led to a decrease in root colonization rates, contrasting with the significant positive effect observed when Cd was added at Level A (3 mg kg^{-1}). According to Sun et al. [51], the increased colonization of cannabis roots by AMFs could be attributed to Cd presence in the rhizosphere, which may stimulate endoderm and root epidermis growth and promote secretion release, enhancing symbiosis between plants and fungi. Their study indicated that Cd presence in the soil enhanced the colonization of cannabis

roots by fungus Rhizophagus irregularis. Therefore, an increase in the mycorrhizal population induced an increase in the ability of industrial hemp to accumulate soil cadmium, contributing to the remediation of mainly moderate soils. In the case of heavily contaminated soil, Molina et al. [87] found that applying 0.7–1.2 mg of available Cd kg^{-1} to soil did not adversely affect the colonization of soybean roots by Arbuscular Mycorrhizal Fungi. However, the findings of Kanwal et al. [88] suggested a negative impact of Cd addition on the colonization of alfalfa mycorrhizal roots (*Medicago sativa* L.), with a downward trend observed as Cd concentration in the soil increased. Citterio et al. [53], working with cannabis and high Cd soil levels, showed a decrease in mycorrhizal colonization. Sun et al. [51], who worked with cannabis, AMFs, and a range of Cd soil concentrations, did not report colonization but did show positive effects of AMFs on hemp growth and Cd stress alleviation.

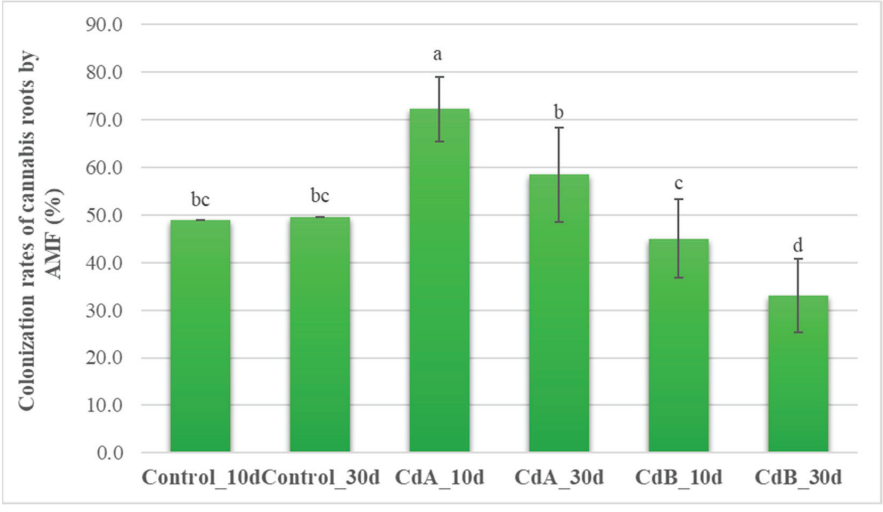

Figure 7. Colonization rates (%) of cannabis roots by AMFs across the six treatments of the experiment (The different letters show the significant differences between the treatments. Error bars indicate standard deviation. $LSD_{5\%}$ = 11.602).

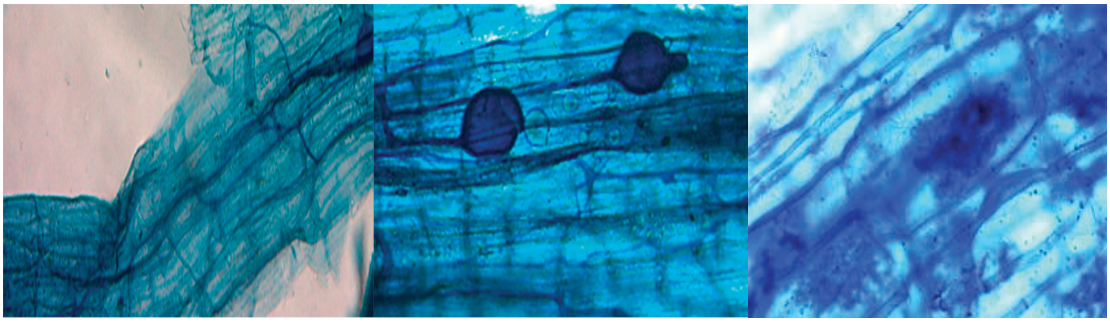

(**a**) (**b**) (**c**)

Figure 8. Observations from the microscope of cannabis blue-stained roots: (**a**) hyphae, extending within the root, (**b**) intraradical vesicles, and (**c**) arbuscules within the roots produced by AMFs.

In addition to the varying cadmium levels, different incubation periods were also found to have a notable effect on root colonization, with significantly higher values observed for the 10-day duration, indicating lower Cd toxicity relative to the respective 30-day

incubation at both Cd levels. This result is in line with the findings of Hassan et al. [7], who examined the impact of cadmium (ranging from 0 to 200 mg kg^{-1}) on microbial biomass over 10-, 20-, and 30-day incubation following soil contamination with Cd. They noted a direct correlation between Cd sensitivity and hatching time, indicating that Cd toxicity increased with prolonged incubation periods. Furthermore, Vig [89] estimated that Cd toxicity to soil biota varies depending on factors such as time, soil type, speciation, ageing, Cd source, organisms, and environmental conditions. Additionally, Sardar et al. [90] explored the breadth of the revocation, which significantly expanded with higher levels of heavy metals and varied across different incubation periods. Therefore, it was revealed in the present study that the growth and colonization of Arbuscular Mycorrhizal Fungi is significantly affected by the presence of toxic cadmium in the soil, but also by the residence time of this aqueous solution in the soil. Soil AMF microorganisms growing in the root appeared to proliferate normally when the Cd concentration was equal to the maximum permissible concentration as defined by the European Union. When the concentration is increased tenfold, then the microorganisms decrease, but still provide protection to the plant to cope with the toxic conditions of its immediate soil environment. The fact that the biomass of the plant both underground and aboveground increases when the Cd concentration is at the A level is therefore probably linked to the fact that there is an increase in the microroot population which helps the plant to cope and increase its mass and shoot, leaf, and root mass. Furthermore, at the A level of soil contamination, the highest rate of Cd transfer from soil to plant was observed, both above and underground, i.e., at the root. The respective Cd uptake rates for the aboveground and underground parts of the plant are 5% and 47.99% for 30-day incubation and 6.38% and 65.43% for 10-day incubation. At the B level of cadmium contamination of soils, a lower percentage movement of Cd from soil to plant was observed. The corresponding percentages of Cd movement were 7.39% and 21.54% for the above- and belowground part of the plant when the incubation lasted 30 days and 7.98% and 25.18% for the corresponding parts of the plant and 10-day incubation of Cd in the soil. Therefore, an increase in the mycorrhizal population induced an increase in the ability of industrial hemp to accumulate soil cadmium, contributing to the remediation of mainly moderate soils. In the case of heavily contaminated soils, which are not observed except in abandoned mine sites, the contribution of mycorrhizal AMFs to the remediation capacity of hemp appears to be significant but low.

4. Conclusions

In the current study, an approach was taken to find the possible relationship between the ability of industrial hemp to remediate cadmium-contaminated soils and the colonization of Arbuscular Mycorrhizal Fungi (AMFs). To this end, a pot experiment was conducted in which laboratory contamination of soils with two levels of cadmium corresponding to moderately and heavily contaminated soils was carried out, and in addition, two different incubation periods of the soils with cadmium-containing aqueous solutions added to the soil samples were studied. The ability of hemp to grow without problems in both levels of contaminated soils was observed, as no toxicity or inhibition of hemp growth was observed. The plant tended to accumulate most of the cadmium underground rather than aboveground. Therefore, the mechanism of phytoremediation that seems to prevail is phytostabilization. Cd accumulation from the soil to the cannabis root also appeared to be influenced by the aging of the pollution, as the plant accumulated greater amounts of metal when the pollution was fresh. A greater increase in plant mass was observed when the soil had the maximum concentration of cadmium allowed by the European Union, while at higher Cd concentrations, the mass increase was less significant. Under the same level of cadmium concentration, the highest rate of phytosuspension, i.e., a higher rate of uptake of Cd from the soil to the plant, as well as a higher rate of AMF colonization was observed. Therefore, the ability of industrial hemp to remediate Cd-impacted soils seems to have been significantly enhanced by the presence of AMFs, which contributed to the emergence

of a valuable plant for Mediterranean soils while yielding quality aboveground plant tissue suitable for industrial use.

Author Contributions: Conceptualization, M.A., E.T. and E.E.G.; methodology, M.A., V.L., E.T., I.I. and E.E.G.; software, M.A. and V.L.; validation, M.A., V.L., I.I. and E.E.G.; formal analysis, M.A. and V.L.; investigation, M.A., V.L., E.T., I.I. and E.E.G.; resources, E.T. and E.E.G.; data curation, M.A., V.L. and E.E.G.; writing—original draft preparation, M.A. and E.E.G.; writing—review and editing, M.A, V.L., I.I. and E.E.G.; visualization, M.A., V.L. and E.E.G.; supervision, E.E.G.; project administration, E.E.G. All authors have read and agreed to the published version of the manuscript.

Funding: This research received no external funding.

Institutional Review Board Statement: Not applicable.

Informed Consent Statement: Not applicable.

Data Availability Statement: Data supporting the findings of this study are available from the corresponding author upon reasonable request.

Conflicts of Interest: The authors declare no conflicts of interest.

References

1. Quagliata, G.; Celletti, S.; Coppa, E.; Mimmo, T.; Cesco, S.; Astolfi, S. Potential use of copper-contaminated soils for hemp (*Cannabis sativa* L.) cultivation. *Environments* **2021**, *8*, 111. [CrossRef]
2. Golia, E.E.; Bethanis, J.; Ntinopoulos, N.; Kaffe, G.G.; Komnou, A.A.; Vasilou, C. Investigating the potential of heavy metal accumulation from hemp. The use of industrial hemp (*Cannabis sativa* L.) for phytoremediation of heavily and moderated polluted soils. *Sustain. Chem. Pharm.* **2023**, *31*, 100961. [CrossRef]
3. Golia, E.E.; Angelaki, A.; Giannoulis, K.D.; Skoufogianni, E.; Bartzialis, D.; Cavalaris, C.; Vleioras, S. Evaluation of soil properties, irrigation and solid waste application levels on Cu and Zn uptake by industrial hemp. *Agron. Res.* **2021**, *19*, 92–99. [CrossRef]
4. Huang, X.; Wang, L.; Zhu, S.; Ho, S.H.; Wu, J.; Kalita, P.K.; Ma, F. Unraveling the effects of arbuscular mycorrhizal fungus on uptake, translocation, and distribution of cadmium in *Phragmites australis* (Cav.) Trin. ex Steud. *Ecotoxicol. Environ. Saf.* **2018**, *149*, 43–50. [CrossRef] [PubMed]
5. Gong, X.; Tian, D.Q. Study on the effect mechanism of Arbuscular Mycorrhiza on the absorption of heavy metal elements in soil by plants. *IOP Conf. Ser. Earth Environ. Sci.* **2019**, *267*, 052064. [CrossRef]
6. Khan, S.; Hesham, A.; Qiao, M.; Rehman, S.; He, J.Z. Effects of Cd and Pb on soil microbial community structure and activities. *Environ. Sci. Pollut. Res.* **2010**, *17*, 288–296. [CrossRef]
7. Hassan, W.; Akmal, M.; Muhammad, I.; Younas, M.; Zahaid, K.R.; Ali, F. Response of soil microbial biomass and enzymes activity to cadmium (Cd) toxicity under different soil textures and incubation times. *Aust. J. Crop Sci.* **2013**, *7*, 674–680.
8. Turner, A. Cadmium pigments in consumer products and their health risks. *Sci. Total Environ.* **2019**, *657*, 1409–1418. [CrossRef]
9. Yi, Y.; Liu, H.; Chen, G.; Wu, X.; Zeng, F. Cadmium Accumulation in Plants: Insights from Phylogenetic Variation into the Evolution and Functions of Membrane Transporters. *Sustainability* **2023**, *15*, 12158. [CrossRef]
10. Elinder, C.G. Cadmium: Uses, Occurrence, and Intake. In *Cadmium and Health*; CRC Press: Boca Raton, FL, USA, 2019.
11. Sharma, H.; Rawal, N.; Mathew, B.B. The characteristics, toxicity and effects of cadmium. *Int. J. Nanotechnol. Nanosci.* **2015**, *3*, 1–9.
12. Hu, Y.; Cheng, H.; Tao, S. The Challenges and Solutions for Cadmium-contaminated Rice in China: A Critical Review. *Environ. Int.* **2016**, *92–93*, 515–532. [CrossRef] [PubMed]
13. Zhao, X.; Li, L.; Xue, L.; Hu, Y.; Han, J. The Effect of Fertilizers on Soil Total and Available Cadmium in China: A Meta-Analysis. *Agronomy* **2024**, *14*, 978. [CrossRef]
14. Zhou, F.; Guo, M.; Zhao, N.; Xu, Q.; Zhao, T.; Zhang, W.; Qiu, R. The effect of thermal treatment on the transformation and transportation of arsenic and cadmium in soil. *J. Environ. Sci.* **2024**, *145*, 205–215. [CrossRef] [PubMed]
15. Wu, J.; Wu, Z.; Agathokleous, E.; Zhu, Y.; Fan, D.; Han, J. Unveiling a New Perspective on Cadmium-Induced Hormesis in Soil Enzyme Activity: The Relative Importance of Enzymatic Reaction Kinetics and Microbial Communities. *Agriculture* **2024**, *14*, 904. [CrossRef]
16. Khaliq, M.A.; James, B.; Chen, Y.H.; Ahmed Saqib, H.S.; Li, H.H.; Jayasuriya, P.; Guo, W. Uptake, translocation, and accumulation of Cd and its interaction with mineral nutrients (Fe, Zn, Ni, Ca, Mg) in upland rice. *Chemosphere* **2019**, *215*, 916–924. [CrossRef]
17. Papadimou, S.G.; Golia, E.E. Green and sustainable practices for an energy plant cultivation on naturally contaminated versus spiked soils. The impact of ageing soil pollution in the circular economy framework. *Environ. Res.* **2024**, *6*, 118130. [CrossRef]
18. Antoniadis, V.; Levizou, E.; Shaheen, S.M.; Ok, Y.S.; Sebastian, A.; Baum, C.; Prasad, M.N.V.; Wenzel, W.W.; Rinklebe, J. Trace elements in the soil-plant interface: Phytoavailability, translocation, and phytoremediation—A review. *Earth-Sci. Rev.* **2017**, *171*, 621–645. [CrossRef]
19. Adriano, D.C.; Wenzel, W.W.; Vangronsveld, J.; Bolan, N.S. Role of assisted natural remediation in environmental cleanup. *Geoderma* **2004**, *122*, 121–142. [CrossRef]

20. Alloway, B.J. Sources of heavy metals and metalloids in Soils. In *Heavy Metals in Soils, Environmental Pollution*; Alloway, B., Ed.; Springer: Dordrecht, The Netherlands, 2013; Volume 22, pp. 11–50. [CrossRef]
21. Zhang, X.; Hu, W.; Xie, X.; Wu, Y.; Liang, F.; Tang, M. Arbuscular mycorrhizal fungi promote lead immobilization by increasing the polysaccharide content within pectin and inducing cell wall peroxidase activity. *Chemosphere* **2020**, *267*, 128924. [CrossRef]
22. Ortas, I. The effect of mycorrhizal fungal inoculation on plant yield, nutrient uptake and inoculation effectiveness under long-term field conditions. *Field Crop. Res.* **2012**, *125*, 35–48. [CrossRef]
23. Smith, S.E.; Read, D.J. *Mycorrhizal Symbiosis*, 3rd ed.; Academic Press: New York, NY, USA, 2010. [CrossRef]
24. Brundrett, M. Diversity and classification of mycorrhizal associations. *Biol. Rev. Camb. Philos. Soc.* **2004**, *79*, 473–495. [CrossRef] [PubMed]
25. Brundrett, M.C. Mycorrhizal associations and other means of nutrition of vascular plants: Understanding the global diversity of host plants by resolving conflicting information and developing reliable means of diagnosis. *Plant Soil* **2009**, *320*, 37–77. [CrossRef]
26. Lenoir, I.; Fontaine, J.; Sahraoui, A.L.-H. Arbuscular mycorrhizal fungal responses to abiotic stresses: A review. *Phytochemistry* **2016**, *123*, 4–15. [CrossRef] [PubMed]
27. Torres, N.; Antolín, M.C.; Goicoechea, N. Arbuscular mycorrhizal symbiosis as a promising resource for improving berry quality in grapevines under changing environments. *Front. Plant Sci.* **2018**, *9*, 897. [CrossRef]
28. Balestrini, R.; Chitarra, W.; Antoniou, C.; Ruocco, M.; Fotopoulos, V. Improvement of plant performance under water deficit with the employment of biological and chemical priming agents. *J. Agric. Sci.* **2018**, *156*, 680–688. [CrossRef]
29. Shi, W.; Zhang, Y.; Chen, S.; Polle, A.; Rennenberg, H.; Bin Luo, Z. Physiological and molecular mechanisms of heavy metal accumulation in nonmycorrhizal versus mycorrhizal plants. *Plant Cell Environ.* **2019**, *42*, 1087–1103. [CrossRef]
30. Millar, N.S.; Bennett, A.E. Stressed out symbiotes: Hypotheses for the influence of abiotic stress on arbuscular mycorrhizal fungi. *Oecologia* **2016**, *182*, 625–641. [CrossRef]
31. Wang, W.; Shi, J.; Xie, Q.; Jiang, Y.; Yu, N.; Wang, E. Nutrient Exchange and Regulation in Arbuscular Mycorrhizal Symbiosis. *Mol. Plant* **2017**, *10*, 1147–1158. [CrossRef]
32. Liu, L.; Gong, Z.; Zhang, Y.; Li, P. Growth, cadmium uptake and accumulation of maize (*Zea mays* L.) under the effects of arbuscular mycorrhizal fungi. *Ecotoxicology* **2014**, *23*, 1979–1986. [CrossRef]
33. Wu, S.; Zhang, X.; Huang, L.; Chen, B. Arbuscular mycorrhiza and plant chromium tolerance. *Soil Ecol. Lett.* **2019**, *1*, 94–104. [CrossRef]
34. Ma, Y.; Rajkumar, M.; Oliveira, R.S.; Zhang, C.; Freitas, H. Potential of plant beneficial bacteria and arbuscular mycorrhizal fungi in phytoremediation of metal contaminated saline soils. *J. Hazard. Mater.* **2019**, *379*, 120813. [CrossRef] [PubMed]
35. Li, C.; Zhou, K.; Qin, W.; Tian, C.; Qi, M.; Yan, X.; Han, W. A Review on Heavy Metals Contamination in Soil: Effects, Sources, and Remediation Techniques. *Soil Sediment Contam. Int. J.* **2019**, *28*, 380–394. [CrossRef]
36. Boorboori, M.R.; Zhang, H.Y. Arbuscular Mycorrhizal Fungi Are an Influential Factor in Improving the Phytoremediation of Arsenic, Cadmium, Lead, and Chromium. *J. Fungi* **2022**, *8*, 176. [CrossRef]
37. Xie, X.; Huang, W.; Liu, F.; Tang, N.; Liu, Y.; Lin, H.; Zhao, B. Functional analysis of the novel mycorrhiza-specific phosphate transporter $AsPT_1$ and PHT_1 family from *Astragalus sinicus* during the arbuscular mycorrhizal symbiosis. *New Phytol.* **2013**, *198*, 836–852. [CrossRef] [PubMed]
38. Riaz, M.; Kamran, M.; Fang, Y.; Wang, Q.; Cao, H.; Yang, G.; Deng, L.; Wang, Y.; Zhou, Y.; Anastopoulos, I.; et al. Arbuscular mycorrhizal fungi-induced mitigation of heavy metal phytotoxicity in metal contaminated soils: A critical review. *J. Hazard. Mater.* **2021**, *402*, 123919. [CrossRef]
39. Zhang, Z.; Wu, X.; Tu, C.; Huang, X.; Zhang, J.; Fang, H.; Huo, H.; Lin, C. Relationships between soil properties and the accumulation of heavy metals in different *Brassica campestris* L. growth stages in a Karst mountainous area. *Ecotoxicol. Environ. Saf.* **2020**, *206*, 111150. [CrossRef]
40. Lebeau, T.; Braud, A.; J'ez´equel, K. Performance of bioaugmentation-assisted phytoextraction applied to metal contaminated soils: A review. *Environ. Pollut.* **2008**, *153*, 497–522. [CrossRef] [PubMed]
41. Morar, F.; Iantovics, L.B.; Gligor, A. Analysis of Phytoremediation Potential of Crop Plants in Industrial Heavy Metal Contaminated Soil in the Upper Mures River Basin. *J. Environ. Inform.* **2018**, *31*, 1–14. [CrossRef]
42. Muthusaravanan, S.; Sivarajasekar, N.; Vivek, J.S.; Paramasivan, T.; Naushad, M.; Prakashmaran, J.; Gayathri, V.; Al-Duaij, O.K. Phytoremediation of heavy metals: Mechanisms, methods and enhancements. *Environ. Chem. Lett.* **2018**, *16*, 1339–1359. [CrossRef]
43. Pajevic, S.; Borisev, M.; Nikolic, N.; Arsenov, D.D.; Orlovic, S.; Zupunski, M. Phytoextraction of heavy metals by fast-growing trees: A review. *Phytoremediation Manag. Environ. Contam.* **2016**, *3*, 29–64. [CrossRef]
44. Miransari, M. Hyperaccumulators, arbuscular mycorrhizal fungi and stress of heavy metals. *Biotechnol. Adv.* **2011**, *29*, 645–653. [CrossRef] [PubMed]
45. Bona, E.; Marsano, F.; Cavaletto, M.; Berta, G. Proteomic characterization of copper stress response in *Cannabis sativa* roots. *Proteomics* **2007**, *7*, 1121–1130. [CrossRef]
46. Campiglia, E.; Gobbi, L.; Marucci, A.; Rapa, M.; Ruggieri, R.; Vinci, G. Hemp Seed Production: Environmental Impacts of *Cannabis sativa* L. Agronomic Practices by Life Cycle Assessment (LCA) and Carbon Footprint Methodologies. *Sustainability* **2020**, *12*, 6570. [CrossRef]

47. Desaulniers Brousseau, V.; Goldstein, B.P.; Lachapelle, M.; Tazi, I.; Lefsrud, M. Greener green: The environmental impacts of the Canadian cannabis industry. *Resour. Conserv. Recycl.* **2024**, *208*, 107737. [CrossRef]
48. Todde, G.; Carboni, G.; Marras, S.; Caria, M.; Sirca, C. Industrial hemp (*Cannabis sativa* L.) for phytoremediation: Energy and environmental life cycle assessment of using contaminated biomass as an energy resource. *Sustain. Energy Technol. Assess.* **2022**, *52*, 102081. [CrossRef]
49. Mahmood, A.; Rashid, S.; Malik, R.N. Determination of toxic heavy metals in indigenous medicinal plants used in Rawalpindi and Islamabad cities, Pakistan. *J. Ethnopharmacol.* **2013**, *148*, 158–164. [CrossRef] [PubMed]
50. Tsaliki, E.; Kalivas, A.; Jankauskiene, Z.; Irakli, M.; Cook, C.; Grigoriadis, I.; Panoras, I.; Vasilakoglou, I.; Dhima, K. Fibre and Seed Productivity of Industrial Hemp (*Cannabis sativa* L.) Varieties under Mediterranean Conditions. *Agronomy* **2021**, *11*, 171. [CrossRef]
51. Sun, S.; Feng, Y.; Huang, G.; Zhao, X.; Song, F. Rhizophagus irregularis enhances tolerance to cadmium stress by altering host plant hemp (*Cannabis sativa* L.) photosynthetic properties. *Environ. Pollut.* **2022**, *314*, 120309. [CrossRef]
52. El Faiz, A.; Duponnois, R.; Winterton, P.; Ouhammou, A.; Meddich, A.; Boularbah, A.; Hafidi, M. Effect of Different Amendments on Growing of *Canna indica* L. Inoculated with AMF on Mining Substrate. *Int. J. Phytoremediation* **2014**, *17*, 503–513. [CrossRef]
53. Citterio, S.; Santagostino, A.; Fumagalli, P.; Prato, N.; Ranalli, P.; Sgorbati, S. Heavy metal tolerance and accumulation of Cd, Cr and Ni by *Cannabis sativa* L. *Plant Soil* **2003**, *256*, 243–252. [CrossRef]
54. Ofori-Agyemang, F.; Waterlot, C.; Manu, J.; Laloge, R.; Francin, R.; Papazoglou, E.G.; Alexopoulou, E.; Lounès-Hadj Sahraoui, A.; Tisserant, B.; Mench, M.; et al. Plant testing with hemp and miscanthus to assess phytomanagement options including biostimulants and mycorrhizae on a metal contaminated soil to provide biomass for sustainable biofuel production. *Sci. Total Environ.* **2024**, *912*, 169527. [CrossRef] [PubMed]
55. *ISO/ISO 10390*; Soil Quality, Determination of pH. International Standards Organization. ISO: Geneve, Switzerland, 2005.
56. Papadimou, S.G.; Barbayiannis, N.; Golia, E.E. Preliminary investigation of the use of *Silybum marianum* (L.) Gaertn. as a Cd accumulator in contaminated Mediterranean soils: The relationships among cadmium (Cd) soil fractions and plant Cd content. *Euro-Mediterr. J. Environ. Integr.* **2024**, *9*, 405–417. [CrossRef]
57. Golia, E.E. The impact of heavy metal contamination on soil quality and plant nutrition. Sustainable management of moderate contaminated agricultural and urban soils, using low cost materials and promoting circular economy. *Sustain. Chem. Pharm.* **2023**, *33*, 101046. [CrossRef]
58. Dimirkou, A.; Ioannou, Z.; Golia, E.E.; Danalatos, N.; Mitsios, I.K. Sorption of cadmium and arsenic by goethite and clinoptilolite. *Commun. Soil Sci. Plant Anal.* **2009**, *40*, 259–272. [CrossRef]
59. Papadimou, S.G.; Golia, E.E.; Barbayiannis, N.; Tsiropoulos, N.G. Dual role of the hyperaccumulator *Silybum marianum* (L.) Gaertn. in circular economy: Production of silymarin, a valuable secondary metabolite, and remediation of heavy metal contaminated soils. *Sustain. Chem. Pharm.* **2024**, *38*, 101454. [CrossRef]
60. Vasilou, C.; Tsiropoulos, N.G.; Golia, E.E. Phytoremediation & Valorization of Cu-contaminated Soils Through *Cannabis sativa* (L.) Cultivation: A Smart Way to Produce Cannabidiol (CBD) in Mediterranean Soils. *Waste Biomass Valorization* **2024**, *15*, 1711–1724. [CrossRef]
61. UPOV. International union for the protection of new varieties of plants. Guidelines for the conduct of tests for distinctness, uniformity and stability, *Cannabis sativa* L. Hemp, Cannabis. UPOV Code: CANNB_SAT. 2023. Available online: https://www.upov.int/edocs/mdocs/upov/en/twa_52/tg_276_2_proj_2.pdf (accessed on 13 September 2024).
62. Page, A.L. *Methods of Soil Analysis-Part 2: Chemical and Microbiological Properties*, 2nd ed.; American Society of Agronomy, Inc. Publisher: Madison, WI, USA, 1982; Volume 9, pp. 421–422.
63. *ISO/DIS 11466*; Environment Soil Quality. ISO Standards Compendium: Geneva, Switzerland, 1994.
64. Sylvia, D.M. Vesicular-Arbuscular Mycorrhizal Fungi. In *Methods of Soil Analysis: Part. 2. Microbiological and Biochemical Properties*, 3rd ed.; Peter, J., Bootomley, P.J., Scott Angle, J., Weaver, R.W., Eds.; Soil Science Society of America: Madison, WI, USA, 2020; pp. 351–360.
65. McGonigle, T.P.; Miller, M.H.; Evans, D.G.; Fairchild, G.L.; Swan, J.A. A new method which gives an objective measure of colonization of roots by vesicular—Arbuscular mycorrhizal fungi. *New Phytol.* **1990**, *115*, 495–501. [CrossRef]
66. Golia, E.E.; Dimirkou, A.; Floras, S.A. Spatial monitoring of arsenic and heavy metals in the Almyros area, Central Greece. Statistical approach for assessing the sources of contamination. *Environ. Monit. Assess.* **2015**, *187*, 399. [CrossRef]
67. Baldantoni, D.; Morra, L.; Zaccardelli, M.; Alfani, A. Cadmium accumulation in leaves of leafy vegetables. *Ecotoxicol. Environ. Saf.* **2016**, *123*, 89–94. [CrossRef]
68. Kwiatkowska-Malina, J. Functions of organic matter in polluted soils: The effect of organic amendments on phytoavailability of heavy metals. *Appl. Soil Ecol.* **2018**, *123*, 542–545. [CrossRef]
69. Wielgusz, K.; Praczyk, M.; Irzykowska, L.; Świerk, D. Fertilization and soil pH affect seed and biomass yield, plant morphology, and cadmium uptake in hemp (*Cannabis sativa* L.). *Ind. Crops Prod.* **2022**, *175*, 114245. [CrossRef]
70. Abedi, T.; Mojiri, A. Cadmium Uptake by Wheat (*Triticum aestivum* L.): An Overview. *Plants* **2020**, *9*, 500. [CrossRef] [PubMed]
71. O'Connor, G.A.; O'Connor, C.; Cline, G.R. Sorption of cadmium by calcareous soils: Influence of solution composition. *Soil Sci. Soc. Am. J.* **1984**, *48*, 12441247. [CrossRef]
72. Napoletano, P.; Guezgouz, N.; Di Iorio, E.; Colombo, C.; Guerriero, G.; De Marco, A. Anthropic impact on soil heavy metal contamination in riparian ecosystems of Northern Algeria. *Chemosphere* **2023**, *313*, 137522. [CrossRef]

73. Kabata-Pendias, A. Trace elements. In *Soils and Plants*, 4th ed.; CRC Press: Boca Raton, FL, USA, 2010.
74. Golia, E.E.; Diakoloukas, V. Soil parameters affecting the levels of potentially harmful metals in Thessaly area, Greece: A robust quadratic regression approach of soil pollution prediction. *Environ. Sci. Pollut. Res.* **2022**, *29*, 29544–29561. [CrossRef]
75. Marković, J.; Jović, M.; Smičiklas, I.; Šljivić-Ivanović, M.; Onjia, A.; Trivunac, K.; Popović, A. Cadmium retention and distribution in contaminated soil: Effects and interactions of soil properties, contamination level, aging time and in situ immobilization agents. *Ecotoxicol. Environ. Saf.* **2019**, *174*, 305–314. [CrossRef]
76. Lu, N.; Wei, Y.; Zhang, Z.; Li, Y.; Li, G.; Han, J. The Response of Cd Chemical Fractions to Moisture Conditions and Incubation Time in Arable Land Soil. *Sustainability* **2022**, *14*, 6270. [CrossRef]
77. Huang, L.; Wang, Q.; Zhou, Q.; Ma, L.; Wu, Y.; Liu, Q.; Wang, S.; Feng, Y. Cadmium uptake from soil and transport by leafy vegetables: A meta-analysis. *Environ. Pollut.* **2020**, *264*, 114677. [CrossRef]
78. Huang, R.; Dong, M.; Mao, P.; Zhuang, P.; Paz-Ferreiro, J.; Li, Y.; Li, Y.; Hu, X.; Netherway, P.; Li, Z. Evaluation of phytoremediation potential of five Cd (hyper)accumulators in two Cd contaminated soils. *Sci. Total Environ.* **2020**, *721*, 137581. [CrossRef]
79. Marabesi, A.O. Influence of Cadmium Exposure on Industrial Hemp Grown for Cannabinoid Production (*Cannabis sativa* L.). Doctoral Dissertation, University of Georgia, Athens, GA, USA, 2023.
80. Shi, J.; Qian, W.; Jin, Z.; Zhou, Z.; Wang, X.; Yang, X. Evaluation of soil heavy metals pollution and the phytoremediation potential of copper-nickel mine tailings ponds. *PLoS ONE* **2023**, *18*, e0277159. [CrossRef]
81. Linger, P.; Ostwald, A.; Haensler, J. *Cannabis sativa* L. growing on heavy metal contaminated soil: Growth, cadmium uptake and photosynthesis. *Biol. Plant.* **2005**, *49*, 567–576. [CrossRef]
82. Shi, G.; Cai, Q. Cadmium tolerance and accumulation in eight potential energy crops. *Biotechnol. Adv.* **2009**, *27*, 555–561. [CrossRef] [PubMed]
83. Rizwan, M.; Ali, S.; Adrees, M.; Ibrahim, M.; Tsang, D.C.W.; Zia-ur-Rehman, M.; Zahir, Z.A.; Rinklebe, J.; Tack, F.M.G.; Ok, Y.S. A critical review on effects, tolerance mechanisms and management of cadmium in vegetables. *Chemosphere* **2017**, *182*, 90–105. [CrossRef] [PubMed]
84. Chaney, R.L.; Malik, M.; Li, Y.M.; Brown, S.L.; Brewer, E.P.; Angle, J.S.; Baker, A.J. Phytoremediation of soil metals. *Curr. Opin. Biotechnol.* **1997**, *8*, 279–284. [CrossRef] [PubMed]
85. Alsafran, M.; Usman, K.; Ahmed, B.; Rizwan, M.; Saleem, M.H.; Al Jabri, H. Understanding the Phytoremediation Mechanisms of Potentially Toxic Elements: A Proteomic Overview of Recent Advances. *Front. Plant Sci.* **2022**, *6*, 881242. [CrossRef]
86. Al-Obaidi, J.R.; Jamaludin, A.A.; Rahman, N.A.; Ahmad-Kamil, E.I. How plants respond to heavy metal contamination: A narrative review of proteomic studies and phytoremediation applications. *Planta* **2024**, *259*, 103. [CrossRef]
87. Molina, A.S.; Lugo, M.A.; Pérez Chaca, M.V.; Vargas-Gil, S.; Zirulnik, F.; Leporati, J.; Ferrol, N.; Azcón-Aguilar, C. Effect of Arbuscular Mycorrhizal Colonization on Cadmium 57 Mediated Oxidative Stress in *Glycine max* (L.) Merr. *Plants* **2020**, *9*, 108. [CrossRef]
88. Kanwal, S.; Bano, A.; Malik, R.N. Effects of arbuscular mycorrhizal fungi on wheat growth, physiology, nutrition and cadmium uptake under increasing cadmium stress. *Int. J. Agron. Agric. Res.* **2015**, *7*, 30–42.
89. Vig, K. Bioavailability and toxicity of cadmium to microorganisms and their activities in soil: A review. *Adv. Environ. Res.* **2003**, *8*, 121–135. [CrossRef]
90. Sardar, K.; Qing, C.; El-Latif, H.A.; Yue, X.; He, J.Z. Soil enzymatic activities and microbial community structure with different application rates of Cd and Pb. *J. Environ. Sci.* **2007**, *19*, 834–840.

Disclaimer/Publisher's Note: The statements, opinions and data contained in all publications are solely those of the individual author(s) and contributor(s) and not of MDPI and/or the editor(s). MDPI and/or the editor(s) disclaim responsibility for any injury to people or property resulting from any ideas, methods, instructions or products referred to in the content.

soil systems

MDPI

Article

Adsorption of Arsenic and Cadmium on Biodegradable and Non-Biodegradable Microplastics in Soil: Comparison Based on Batch Experiment

Zaw Min Han [1], Sartaj Ahmad Bhat [2], Shiamita Kusuma Dewi [3], Yongfen Wei [2,3] and Fusheng Li [1,2,*]

[1] Graduate School of Engineering, Gifu University, 1-1 Yanagido, Gifu 501-1193, Japan; dm.98j.0952@s.thers.ac.jp
[2] River Basin Research Center, Gifu University, 1-1 Yanagido, Gifu 501-1193, Japan; sartajbhat88@gmail.com (S.A.B.); wei.yongfen.j3@f.gifu-u.ac.jp (Y.W.)
[3] The United Graduate School of Agricultural Science, Gifu University, 1-1 Yanagido, Gifu 501-1193, Japan; shiamitakd@gmail.com
* Correspondence: li.fusheng.i4@f.gifu-u.ac.jp; Tel.: +81-58-293-2453

Abstract: In the present study, the adsorption of arsenic(V) and cadmium(II) onto microplastics from poly(butylene succinate-co-butylene adipate) (PBSA) and low-density polyethylene (LDPE) plastic mulch films was investigated through batch experiment. The surface morphology and elemental composition of soil and microplastics were analyzed with scanning electron microscopy equipped with energy-dispersive X-ray spectroscopy (SEM-EDX) and Fourier-transform infrared (FTIR) spectroscopy. The results show that the adsorption of As(V) and Cd(II) on microplastics led to surfaces with coarseness and more cracks, and many small particles. Under the conditions added with 100 pieces of microplastic, PBSA enhanced the adsorption capacity of As(V) (from 0.43 to 0.49 mg/g), and LDPE increased the adsorption of Cd(II) (from 0.174 to 0.176 mg/g) due to the "superimposed effect" caused by hydrogen bonds. Conversely, LDPE reduced the adsorption of As(V) (from 0.44 to 0.40 mg/g) due to a "dilution effect" of PE. Particularly, PBSA exhibited an insignificant effect on the adsorption of Cd(II) in soil during the present study. Overall, our findings provide new insights into the impacts of microplastics on the fate and behavior of heavy metals in the soil system.

Keywords: microplastics; heavy metals; soil; adsorption; contamination

Citation: Han, Z.M.; Bhat, S.A.; Dewi, S.K.; Wei, Y.; Li, F. Adsorption of Arsenic and Cadmium on Biodegradable and Non-Biodegradable Microplastics in Soil: Comparison Based on Batch Experiment. *Soil Syst.* **2024**, *8*, 116. https://doi.org/10.3390/soilsystems8040116

Academic Editor: Manfred Sager

Received: 21 August 2024
Revised: 10 October 2024
Accepted: 8 November 2024
Published: 12 November 2024

Copyright: © 2024 by the authors. Licensee MDPI, Basel, Switzerland. This article is an open access article distributed under the terms and conditions of the Creative Commons Attribution (CC BY) license (https://creativecommons.org/licenses/by/4.0/).

1. Introduction

The growing problem of plastic pollution has become increasingly evident through the widespread presence of plastic waste across both terrestrial and aquatic ecosystems [1]. Extensive scientific research has focused on developing sophisticated analytical methodologies to better understand the source, prevalence, fate, and degradation mechanism of plastics in the environment. These studies have also critically examined the potential risks posed by plastic pollution to the natural ecosystem, wildlife, and human health [2]. Such investigations are vital for informing mitigation strategies and advancing our understanding of the long-term environmental and biological impacts of plastic waste. Microplastics, defined as plastic particles less than 5 mm in size, have become ubiquitous in terrestrial ecosystems, including agricultural soils [3,4]. These tiny plastic fragments, often originating from the breakdown of larger plastic items, have been found in various environmental matrices, including marine, freshwater, and terrestrial ecosystems [5]. Microplastics can originate from various sources, such as the breakdown of larger plastic items, the shedding of synthetic textiles, and the application of contaminated agricultural products [4]. These small plastic particles can adsorb and accumulate a wide range of pollutants, including heavy metals, on their surface, which can then potentially be transferred through

the food chain or can directly impact organisms. Microplastics can act as "carriers" for heavy metals, adsorbing them on their surfaces and potentially increasing their mobility and bioavailability in the soil [6,7]. This can lead to the accumulation of heavy metals in soil organisms—including plants, invertebrates, and microorganisms—which can then be transferred through the food chain and will ultimately reach humans. The presence of microplastics and heavy metals in soil can also disrupt the delicate balance of critical soil processes, including nutrient cycling, carbon sequestration, and the composition and function of the soil biota. This can ultimately lead to a decline in soil fertility and the overall productivity and resilience of terrestrial ecosystems [8–10]. One potential source of microplastics is the use of plastic mulch films in agriculture [11]. Plastic mulch films are widely used in horticulture and agriculture to enhance crop productivity, conserve soil moisture, and suppress weed growth [12], but they can break down over time, leading to the accumulation of microplastics in the soil [4,13,14]. Developing biodegradable alternatives to plastic mulch films, such as those made from renewable materials, can help mitigate the environmental concerns associated with microplastic pollution [15–17].

Biodegradable and non-biodegradable polymers, including poly(butylene succinate-co-butylene adipate) (PBSA) and low-density polyethylene (LDPE) microplastics, have been the subject of extensive research in the context of their behavior and effects in the soil environment and their interaction with heavy metals, potentially increasing their mobility and bioavailability [8]. Low-density polyethylene (LDPE) is a commonly encountered plastic in the environment, and its prevalence in agricultural soils is particularly concerning [7]. Researchers have found that the addition of low-molecular-weight polyethylene to soil can lead to alterations in soil properties, such as water-holding capacity, infiltration, and absorption, which can ultimately impact carbon cycling and storage [9]. The interactions between microplastics and heavy metals in the soil environment can have profound implications for soil health, ecosystem function, and human health [18].

Heavy metals, such as arsenic and cadmium, can also be introduced into the soil through anthropogenic activities like industrial processes, mining, and the application of pesticides and fertilizers. The co-occurrence of microplastics and heavy metals in soil is of particular interest, as their interactions can have profound consequences on the soil quality, ecosystem functions, and human health [19,20]. Prevailing research has demonstrated that the presence of microplastics in soil can alter the mobility, bioavailability, and toxicity of heavy metals, thereby posing a threat to the overall health and sustainability of terrestrial ecosystems [6,7]. Recent studies have significantly contributed to our understanding of the complex interactions between microplastics and heavy metals in soil [21]. Researchers have identified the adsorption of heavy metals onto microplastic surfaces as a key mechanism of their interaction, leading to increased mobility and bioavailability of these contaminants [22]. The novelty of this research lies in its comparative investigation of the adsorption characteristics of heavy metals (arsenic and cadmium) in soil with two distinct types of microplastics: non-biodegradable low-density polyethylene (LDPE), and biodegradable poly(butylene succinate-co-butylene adipate) (PBSA). Despite a growing body of literature on microplastic pollution, there is limited research on the comparative behavior of biodegradable and non-biodegradable microplastics in the soil environment, particularly in the context of heavy metal adsorption. While previous studies have established the basic mechanisms of microplastic–heavy metal interactions, there remains a gap in understanding how different types of microplastics (biodegradable vs. non-biodegradable) affect heavy metal mobility, adsorption capacity, and potential environmental risks. This study addresses this gap by focusing on two distinct microplastics—LDPE and PBSA—and their role in the behavior of arsenic and cadmium in agricultural soil. The main aims of this study were (1) to investigate the adsorption characteristics of As(V) and Cd(II) in soil in the presence of LDPE and PBSA microplastics, and (2) to characterize the surface properties of LDPE and PBSA microplastics by SEM-EDX and FTIR techniques.

2. Materials and Methods

2.1. Microplastics and Reagents

LDPE and PBSA commercial-grade agricultural plastic mulch films were purchased from Iwatani Materials Corporation (Osaka, Japan) and Takii Seed Co., Ltd. (Kyoto, Japan), respectively. Both films are used for applying mulch to crops. LDPE is a non-biodegradable plastic, while PBSA is a biodegradable plastic. Both film types were cut manually using scissors into square shapes of 3 mm × 3 mm. The two microplastics were first soaked in 0.1 M hydrochloric acid solution to remove the potential heavy metals from the surface, followed by washing with tap water and Milli-Q water, and then dried overnight at 40 °C in a drying oven.

Arsenic standard solution (H_3AsO_4 in HNO_3, 0.5 mol/L) and cadmium standard solution ($Cd(NO_3)_2$ in HNO_3, 0.5 mol/L) were purchased from Merck Japan. Nitric acid (HNO_3, 65% v/v) was purchased from Wako Pure Chemical Co., Ltd. (Osaka, Japan). All chemicals used in this study were of pure analytical grade. All of the equipment (digestion bottles, conical flasks, etc.) was soaked in 10% (v/v) HNO_3 for 24 h to remove any potential residual heavy metals or other impurities on the surface of the experimental apparatus, rinsed thoroughly with tap water and Milli-Q water, and then dried in an oven.

2.2. Soil

For this study, the soil was randomly collected from the top layer, which was 0–15 cm in depth, in an agricultural field located at Gifu University in Gifu, Japan. Following the removal of the plant materials, stones, and other debris, the soil was air-dried naturally, ground, and then passed through a 2 mm sieve and stored at room temperature to conduct further experiments. Soil is commonly used for agricultural practices all around the world, and this soil was typical of Japan and other places.

2.3. Characterization

The samples were suspended in Milli-Q water (solid to liquid = 1:2.5 w/v), shaken at 25 °C for 30 min, and settled for 15 min, before being measured using a pH and EC meter (GST-5731C and CT-57101B, DKK-TOA Corporation, Tokyo, Japan). The point of zero charge (pH_{pzc}) of the soil and microplastics was measured by the salt addition method [23]. Organic matter (OM) content was analyzed using weight loss as LOI (loss on ignition) [24]. Cation-exchange capacity (CEC) was determined by the ammonium acetate method at pH 7.0 [25]. DOC was extracted in Milli-Q water (solid to liquid, 1:5 w/v) by shaking at 120 rpm for an hour, followed by centrifugation at 2000× g for 10 min, and then filtered through a 0.2 μm cellulose acetate membrane filter. The DOC content in the solution was measured using a TOC analyzer (Shimadzu Co., Ltd., Tokyo, Japan). The total carbon (TC) and total nitrogen (TN) were analyzed by using the combustion method (CN Coder, Shimadzu). The surface morphology and elemental composition of the soil and microplastics were analyzed using SEM-EDX (scanning electron microscopy coupled with energy-dispersive X-ray spectroscopy) (SU3500, Hitachi Co., Ltd., Tokyo, Japan). Samples were placed and pressed onto conductive adhesive tape before being mounted on specimen stubs, and were then preconditioned prior to analysis using a platinum coater by coating for a few minutes. The functional groups of the soil and microplastics before and after the adsorption of heavy metals were analyzed by using attenuated total reflectance–Fourier-transform infrared (ATR-FTIR) spectroscopy (Agilent Cary 630 FTIR, Santa Clara, CA, USA). First, the diamond ART attachment was placed in the optical path of the spectrometer, and the background signal was recorded. Then, the sample was closely attached to the surface of the ATR attachment, and the IR spectrum was collected in the range of 4000–400 cm^{-1}. The specific surface area of the soil was analyzed by using the 3Flex Surface Characterization Analyzer (Micromeritics Instrument Corporation, Norcross, GA, USA). The sorbents were weighed into the sample tube and degassed at 200 °C, and then they were analyzed under N_2 flow. The total heavy metal contents of the soil and microplastics were determined according to the digestion method reported by [26]. The heavy metal concentrations were analyzed by an inductively coupled plasma spectrometer (ICP-MS) (Agilent 7500 series, Agilent, Santa Clara, CA, USA).

The elemental composition of the soil analyzed by SEM-EDX showed C (14.5%), N (0.21%), O (49.84%), Mg (0.73%), Al (8.84%), Si (17.36%), K (3.31%), Ca (1.27%), and Fe (3.10%). The general physicochemical properties of the soil (including TC and TN analyzed by the CN coder) are shown in Table 1. The nitrogen content shown in Table 1 is higher than that from the SEM-EDX analysis. This was probably caused by the non-uniform distribution of nitrogen in the small soil sample used in the SEM-EDX analysis—a quantification problem requiring confirmation and improvement in future studies.

Table 1. Physicochemical properties of soil.

	pH	EC (mS/m)	Organic Matter (%)	CEC (cmol/kg)	DOC (g/kg)	TC (g/kg)	TN (g/kg)	pH_{PZC}	SSA (m^2/g)	As (mg/kg)	Cd (mg/kg)
Soil	7.34	19.46	6.08	20.34	0.11	37.52	17.54	7.50	7.61	9.34	2.14

EC—electric conductivity, CEC—cation-exchange capacity, DOC—dissolved organic matter, TN—total nitrogen, TC—total carbon, pH_{PZC}—point of zero charge, SSA—specific surface area.

2.4. Adsorption Experiments

Batch adsorption studies were conducted to investigate the heavy metal adsorption capacity of the soil and microplastics. The working solutions of the desired concentrations—5 mg/L Cd(II) and 30 mg/L As(V)—were prepared by diluting the stock solutions Cd(II) and As(V) (1000 mg/L). Two grams of soil or of mixtures of soil and different dosages of microplastics (10, 50, and 100 pieces) was placed in the conical flasks, followed by adding 70 mL of the Cd(II) and As(V) solutions. All conical flasks were shaken at 220 rpm and 25 ± 1 °C for 48 h. Then, the samples were taken from all flasks at 1, 2, 8, 12, 24, and 48 h. The solutions were filtered through 0.2 µm cellulose acetate membrane filter paper to analyze their heavy metal concentrations. All of the experiments were conducted in triplicate, including the blank treatments. Table 2 presents the treatment descriptions and corresponding abbreviations.

Table 2. Treatments of batch experiments.

Description of Treatments	Abbreviations
Soil + As (V)	S_As
Soil + Cd (II)	S_Cd
100 LDPE + As (V)	100 LDPE_As
100 PBSA + As (V)	100 PBSA_As
100 LDPE + Cd (V)	100 LDPE_Cd
100 PBSA + Cd (V)	100 PBSA_Cd
Soil + 10 LDPE + As (V)	S_10 LDPE_As
Soil + 50 LDPE + As (V)	S_50 LDPE_As
Soil + 100 LDPE + As (V)	S_100 LDPE_As
Soil + 10 LDPE + Cd (II)	S_10 LDPE_Cd
Soil + 50 LDPE + Cd (II)	S_50 LDPE_Cd
Soil + 100 LDPE + Cd (II)	S_100 LDPE_Cd
Soil + 10 PBSA + As (V)	S_10 PBSA_As
Soil + 50 PBSA + As (V)	S_50 PBSA_As
Soil + 100 PBSA + As (V)	S_100 PBSA_As
Soil + 10 PBSA + Cd (II)	S_10 PBSA_Cd
Soil + 50 PBSA + Cd (II)	S_50 PBSA_Cd
Soil + 100 PBSA + Cd (II)	S_100 PBSA_Cd

The adsorption capacity (q) of soil with and without microplastics at equilibrium was calculated based on the following equation:

$$q = \frac{(C_0 - C_e) \cdot V}{W} \quad (1)$$

where q (mg/g) is the adsorption capacity, C_0 and C_e (mg/L) are the initial and equilibrium concentrations, respectively, V (L) is the volume of the water, and W (g) is the weight of the sample.

3. Results

3.1. Surface Characteristics of Microplastics and Soil

The morphological characteristics of the LDPE, PBSA, and soil samples, both prior to and following the adsorption of arsenic As(V) and cadmium Cd(II) ions, were analyzed using scanning electron microscopy (SEM). SEM micrographs provide a direct means of observing modifications in the surface microstructure of these materials, allowing for a detailed comparison between their pre- and post-adsorption states. As illustrated in Figure 1, the SEM images of the LDPE, PBSA, and soil samples revealed distinct surface alterations attributable to the adsorption processes of As(V) and Cd(II) ions. Before exposure to the metal ions, the surface of the soil exhibited a rough and irregular morphology, characterized by uneven topography and apparent open pores. These pores, as shown in Figure 1a, likely serve as potential sites for the transport and adsorption of metal ions, a characteristic that may facilitate the adsorptive interactions observed during the experimental process [27]. After the adsorption of As(V) and Cd(II), the surface of the soil was more disaggregated, with increased roughness (Figure 1b,c). Before the adsorption of As(V) and Cd(II), the surface of the LDPE and PBSA mulch films was smooth and virtually free of cracks and porosity (Figure 1d,g) [28]. After the adsorption of As(V) and Cd(II), the surface of the LDPE and PBSA mulch films became coarser and more cracked, with many small particles (Figure 1e,f,h,i) [29]. The surface alterations in the SEM images of the soil, LDPE, and PBSA may be associated with the effects of adsorption that occurred on the surface of LDPE and PBSA.

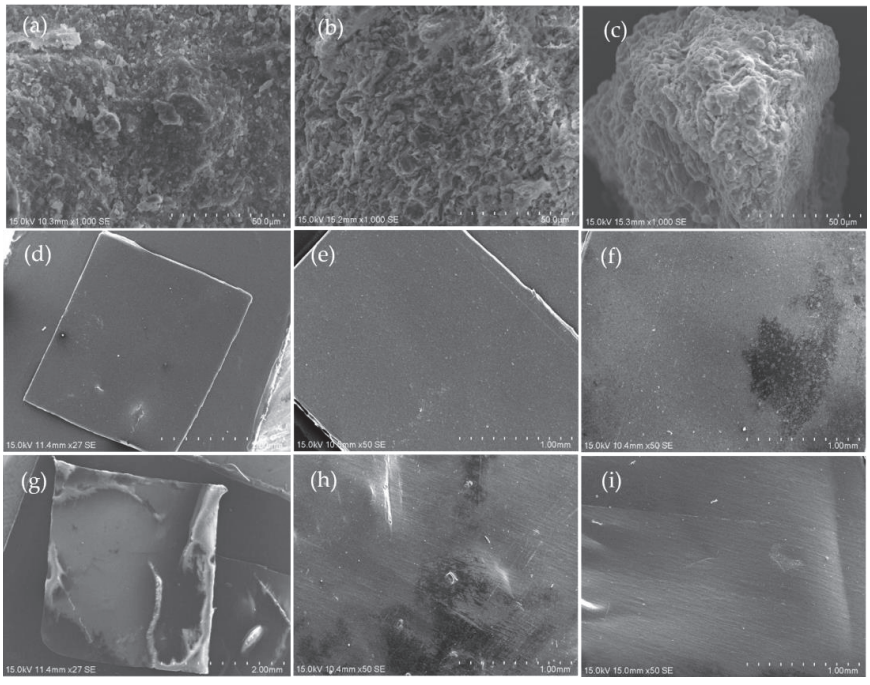

Figure 1. SEM micrographs of soil, LDPE, and PBSA before and after the sorption of As and Cd, where (**a**) represents soil, (**b**) soil after As adsorption, (**c**) soil after Cd adsorption, (**d**) LDPE, (**e**) LDPE after As adsorption, (**f**) LDPE after Cd adsorption, (**g**) PBSA, (**h**) PBSA after As adsorption and (**i**) PBSA after Cd adsorption.

The EDX elemental analysis of the soil samples, as illustrated in Figure 2a,b, confirmed the occurrence of As (0.11%) and Cd (0.34%) after the adsorption of As(V) and Cd(II). The elemental composition of the soil, LDPE, and PBSA before and after adsorption is shown in Table 3. In soil, after the adsorption of As(V) and Cd(II), oxygen was the most abundant chemical element, followed by carbon. The EDX spectra of LDPE, as shown in Figure 2c,d, prove that As(V) and Cd(II) ions were adsorbed on the surface of LDPE (0.11% and 0.02%, respectively). LDPE typically consists of approximately 90% carbon. The EDX spectra of PBSA, as depicted in Figure 2e,f, provide evidence that As(V) and Cd(II) ions were adsorbed onto the surface of the PBSA, with concentrations of As at 0.14% and Cd at 0.19%. PBSA is composed of roughly 60% carbon and 30% oxygen. Based on the EDX results, it was found that the surface of the microplastics had a higher affinity for the adsorption of heavy metals. Specifically, the adsorption of As(V) and Cd(II) by PBSA was more pronounced compared to LDPE.

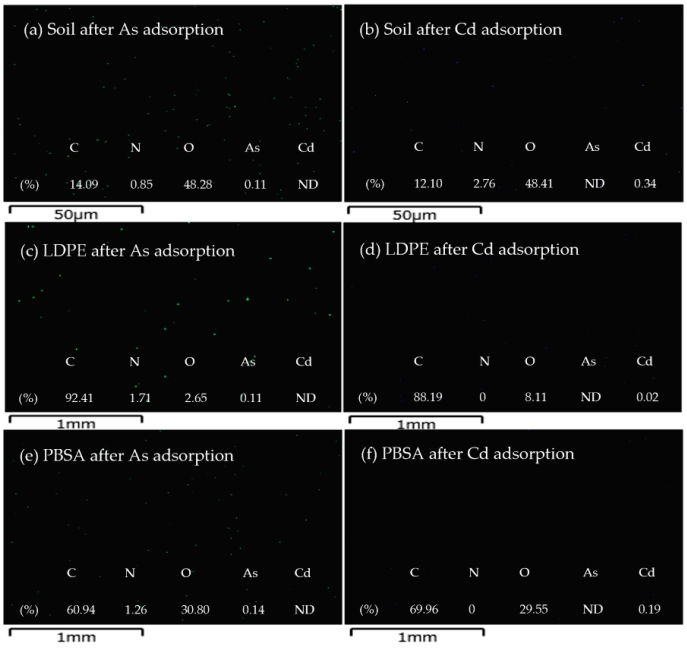

Figure 2. EDX spectra of soil, LDPE, and PBSA after (**a**,**c**,**e**) As adsorption and (**b**,**d**,**f**) Cd adsorption.

Table 3. Elemental composition of soil, LDPE, and PBSA before and after adsorption.

	Mass Concentration (%)				
Elemental Composition	**C**	**N**	**O**	**As**	**Cd**
Soil	14.50	0.21	48.28	ND	ND
Soil after As adsorption	14.09	0.85	48.28	0.11	ND
Soil after Cd adsorption	12.10	2.76	48.41	ND	0.34
LDPE	97.66	0	1.24	ND	ND
LDPE after As adsorption	92.41	1.71	2.65	0.11	ND
LDPE after Cd adsorption	88.19	0	8.11	ND	0.02
PBSA	72.73	0.25	26.79	ND	ND
PBSA after As adsorption	60.94	1.26	30.80	0.14	ND
PBSA after Cd adsorption	69.96	0	29.55	ND	0.19

ND: not detected.

Attenuated total reflectance–Fourier-transform infrared spectroscopy (ATR-FTIR) can be used to analyze the surface functional groups of microplastics. The FTIR spectra of LDPE,

PBSA, and soil are shown in Figure 3. The soil's characteristic peaks were identified as Si-O vibration at 797 and 987 cm^{-1}, Al-O vibration at 909 and 3619 cm^{-1}, -CH_2 oscillation (693 cm^{-1}), and -OH bending vibration at 3373 and 3697 cm^{-1} [30,31]. The characteristic adsorption peaks in LDPE and PBSA were evident, with no new peaks emerging after the adsorption of As(V) and Cd(II) ions. This observation suggests that no new functional groups were formed because of the adsorption process. However, the intensity of the existing peaks became more pronounced with the increased dosage of microplastics, indicating an enhanced interaction between the materials and the metal ions [32,33]. In the case of LDPE, four primary adsorption peaks were detected at 2914, 2847, 1451, and 719 cm^{-1} following the adsorption of As(V) and Cd(II). The peaks at 2914 cm^{-1} and 2847 cm^{-1} can be attributed to the symmetric stretching vibrations of the methylene (CH_2) groups. The peak observed at 1451 cm^{-1} corresponds to the bending deformation of CH_2, while the peak at 719 cm^{-1} is associated with the rocking deformation of the methylene group [34,35]. These findings suggest that, while the chemical structure of LDPE remains unaltered, there is a notable increase in peak intensity correlating with the adsorption process. These peaks were consistent when the amount of LDPE was increased (10, 50, and 100 pieces), indicating that the dosage did not affect the functional groups of the microplastics [36]. The FTIR spectra of PBSA for both As(V) and Cd(II) adsorption have several peaks. The peak at 3693 cm^{-1} was assigned to hydroxyl (O-H) stretching vibration of -COOH and -OH end groups [37]. Hydroxyl groups are strong polar groups that can form ionic or covalent bonds with metals and adsorb As(V) and Cd(II) ions. The prominent peak at 1710 cm^{-1} in the spectrum represented the carbonyl (C=O) stretching in the ester functional group in the chemical structure of PBSA [38]. The peaks at 1155 and 1267 cm^{-1} represented asymmetric C-O along with carbonyl carbon, indicating the synthesis of the ester groups through the structure [39]. The peaks of alcohol (-OH) appeared at 1386 and 1330 cm^{-1}. The vibrations of C-H stretching of methylene carbons (-CH_2-) are represented by the peak at 2944 cm^{-1}. The peak at 726 cm^{-1} was assigned to CH_2/CH_3 stretching, rocking, or bending vibrations. The above observations suggest that more active oxygen functional groups can be responsible for the differences in Cd(II) and As(V) adsorption capacity between microplastics and soil.

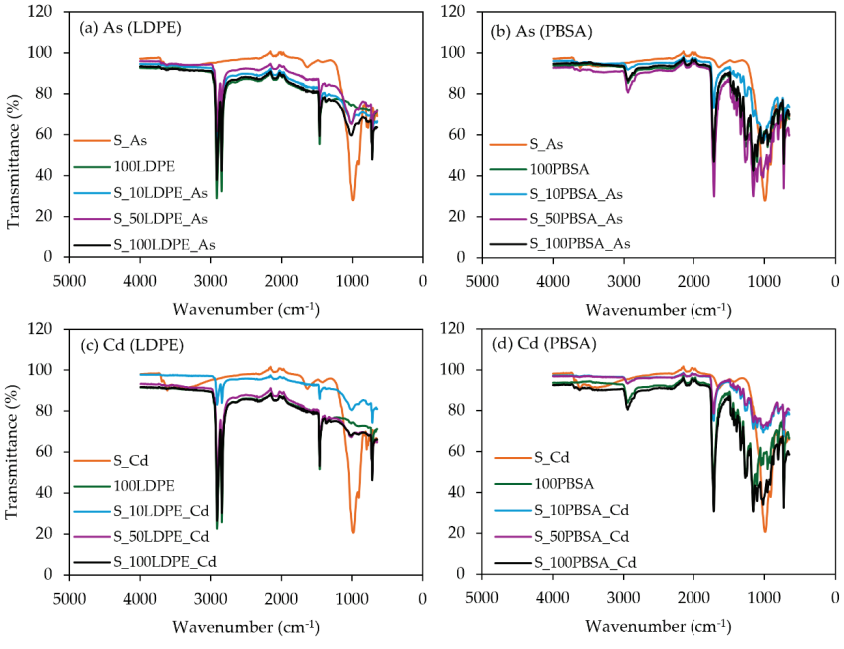

Figure 3. ATR-FTIR spectra of soil, LDPE, and PBSA before and after adsorption of (**a**,**b**) As and (**c**,**d**) Cd.

3.2. Adsorption of As(V) and Cd(II)

Microplastics have been detected in surface soil at concentrations ranging from 0.03% to 6.7% (*w*/*w*) [28,40]. To demonstrate the significant impact of microplastic concentrations in soil, the adsorption of As(V) and Cd(II) in soil was examined at different microplastic dosages (10, 50, and 100 pieces). At 100 pieces of microplastic, PBSA increased the adsorption of As(V) (from 0.43 to 0.49 mg/g). The occurrence of microplastics in soil enhanced the adsorption capacity for heavy metals, which was attributed to the "superimposed effect" caused by H bonding between heavy metals and microplastics. However, LDPE showed an inhibitory effect on the adsorption of As(V) (from 0.44 to 0.40 mg/g). This phenomenon was similar to the results presented in [10,35], where the authors expressed that the adsorption of Cd ions in soil was decreased by the addition of PE microplastics due to a "dilution effect" of PE and direct interaction of Cd with PE microplastics. Mostly, PBSA exhibited an insignificant effect on the adsorption of Cd(II) in soil in the present study. Therefore, the "microplastics effect" of inorganic arsenic transport in soil will be happening in agroecosystems.

To better understand the contact-time-dependent process of As(V) and Cd(II) adsorption by LDPE and PBSA, with and without soil, we performed batch adsorption experiments. Figure 4a–d represent the amounts of As(V) and Cd(II) adsorbed on LDPE, PBSA, and soil in milligrams of adsorbed metals per gram of adsorbent. The highest adsorption capacity for As(V) was observed in pure LDPE (100 pieces), and the lowest adsorption capacity was observed in soil with 100 pieces of LDPE (Figure 4a). In Figure 4b, the highest adsorption capacity for As(V) was observed in pure PBSA (100 pieces), and the lowest adsorption capacity was observed in soil with 10 pieces of PBSA. For cadmium, the highest adsorption capacity was found in pure LDPE (100 pieces), and the lowest adsorption capacity was observed in soil with 50 pieces of LDPE (Figure 4c). In Figure 4d, the highest Cd adsorption capacity was observed in pure PBSA (100 pieces), and the lowest adsorption capacity was observed in soil with 10 pieces of PBSA.

Figure 5 displays the amounts of As(V) and Cd(II) adsorbed on LDPE, PBSA, and soil in milligrams of adsorbed metals per square meter of adsorbent. The highest adsorption capacity for As(V) was observed in pure LDPE (100 pieces), and the lowest adsorption capacity was observed in soil with 100 pieces of LDPE (Figure 5a). In Figure 5b, the highest adsorption capacity for As(V) was observed in pure PBSA (100 pieces), and the lowest adsorption capacity was observed in soil with 10 pieces of PBSA. For cadmium, the highest adsorption capacity was found in pure LDPE (100 pieces), and the lowest adsorption capacity was observed in soil with 50 pieces of LDPE (Figure 5c). In Figure 5d, the highest adsorption capacity was observed in pure PBSA (100 pieces), and the lowest adsorption capacity was observed in soil with 10 pieces of PBSA. With increasing contact time, the adsorption capacity also increased until it reached equilibrium at 24 h (Figure 4a,c,d). In Figure 4b, there were no stable stages, and the adsorption capacities were fluctuating. The authors of [31] reported that the presence of microplastics had a substantial influence on the adsorption behavior of heavy metals in the soil. The adsorption process of heavy metals in soils, when coexisting with varying concentrations of microplastics, can be characterized by three distinct stages: (1) an initial rapid adsorption phase occurring within the first 12 h, (2) a subsequent slower adsorption phase between 12 and 24 h, and (3) the attainment of adsorption equilibrium after 24 h. During the early phase of adsorption, the soil and microplastics provided abundant adsorption sites, facilitating rapid uptake of heavy metals. However, as the contact time increased, the available adsorption sites were progressively occupied, resulting in a decline in the concentration of free sites, which, in turn, led to the deceleration of the adsorption process. This gradual reduction in adsorption rate reflects the transition to a slower phase, culminating in equilibrium as the system approaches saturation. These findings highlight the complex interactions between soil, microplastics, and heavy metals in the adsorption process.

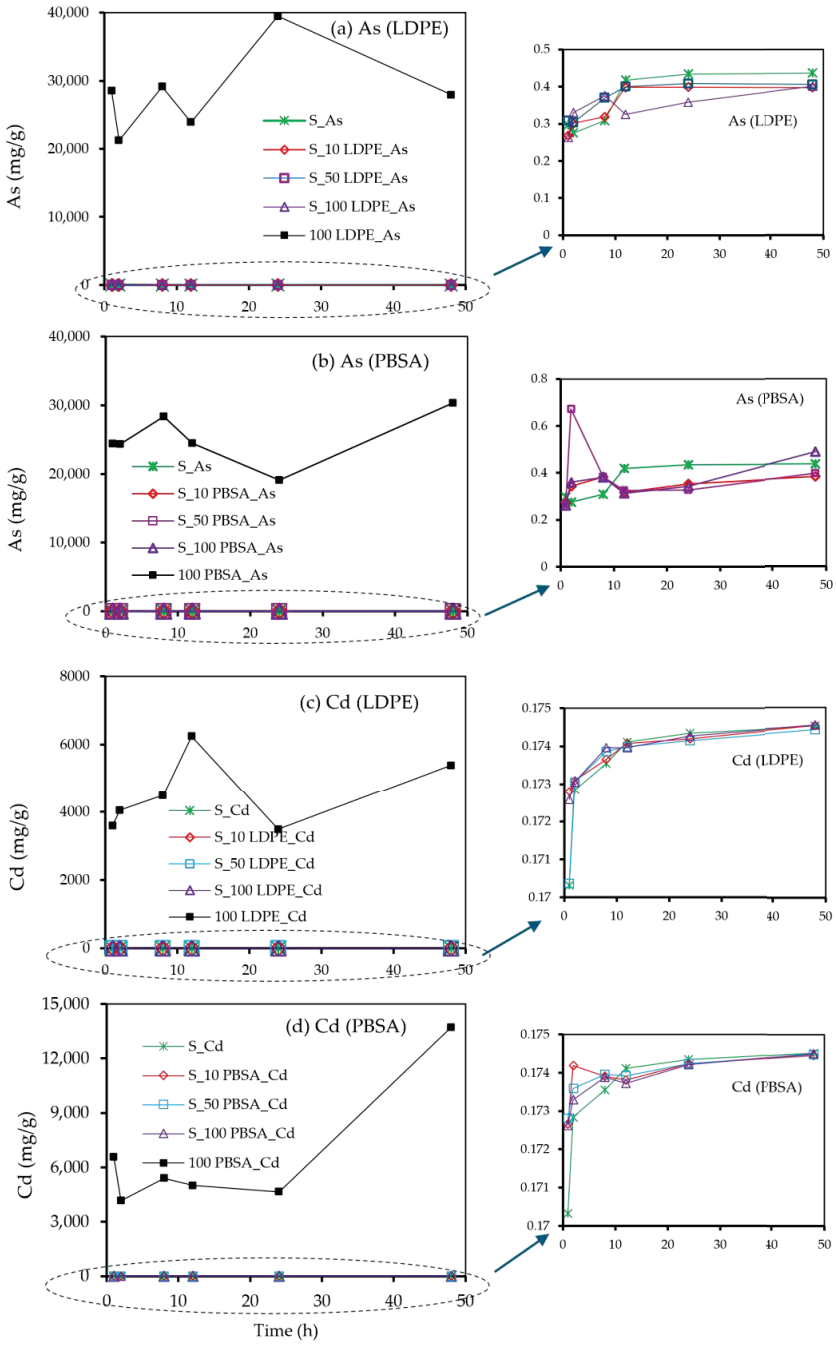

Figure 4. Adsorption capacity of (**a**) As on soil, LDPE, and soil with different contents of LDPE; (**b**) As on soil, PBSA, and soil with different contents of PBSA; (**c**) Cd on soil, LDPE, and soil with different contents of LDPE; and (**d**) Cd on soil, PBSA, and soil with different contents of PBSA.

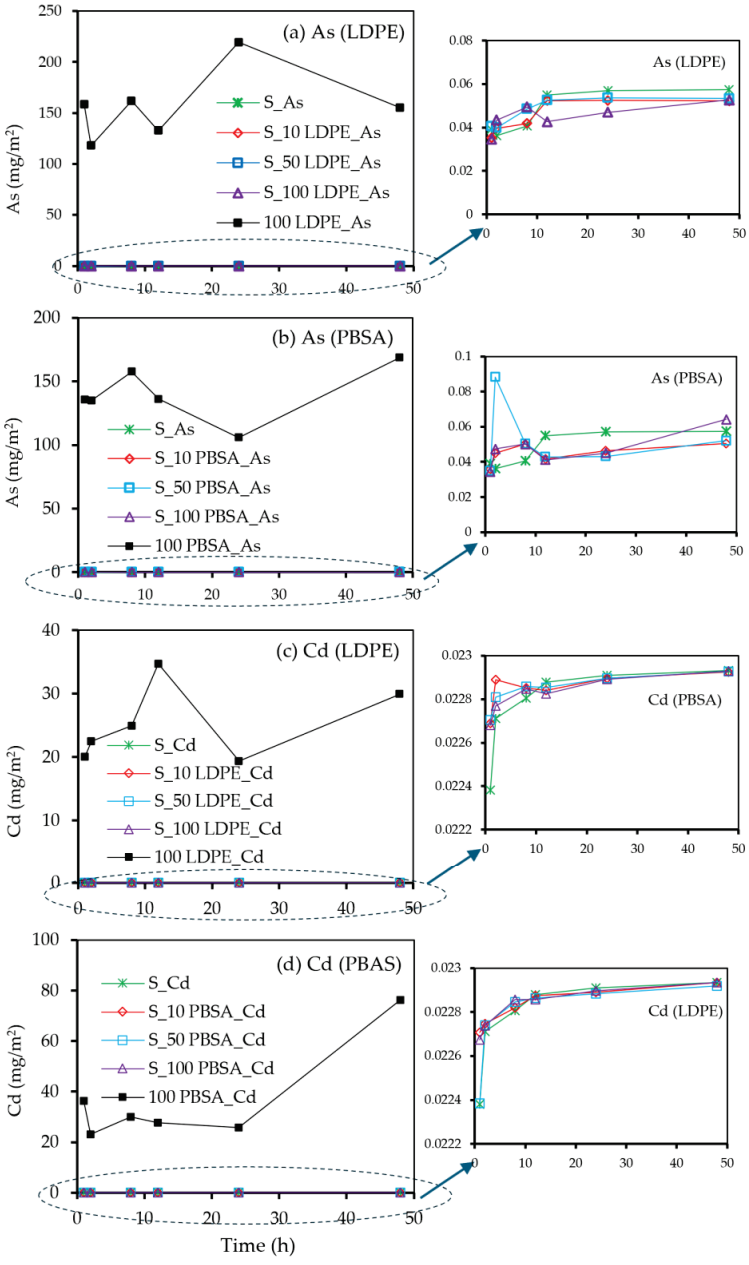

Figure 5. Adsorption capacity of (**a**) As on soil, LDPE, and soil with different contents of LDPE; (**b**) As on soil, PBSA, and soil with different contents of PBSA; (**c**) Cd on soil, LDPE, and soil with different contents of LDPE; and (**d**) Cd on soil, PBSA, and soil with different contents of PBSA.

Figure 6 presents the amounts of As(V) and Cd(II) adsorbed on LDPE, PBSA, and soil in milligrams of heavy metals per liter of adsorbent. As shown in Figure 6a,b, the highest adsorption capacity for As(V) was observed in soil, and the lowest adsorption capacity was observed in 100 pieces of pure LDPE, while the highest adsorption capacity for As(V) on PBSA was observed in soil with 100 pieces of PBSA, and the lowest adsorption capacity

was observed in 100 pieces of pure PBSA. In Figure 6c,d, the lowest adsorption capacity for Cd was observed in 10 pieces of pure LDPE and PBSA, and the highest adsorption capacity for Cd(II) was observed in soil with LDPE and PBSA (100 pieces). Moreover, among the 10-, 50-, and 100-piece microplastic samples, there were no significant differences in adsorption capacity. The authors of [34] revealed that polyvinyl chloride microplastic reduces the Cd(II) adsorption capacity.

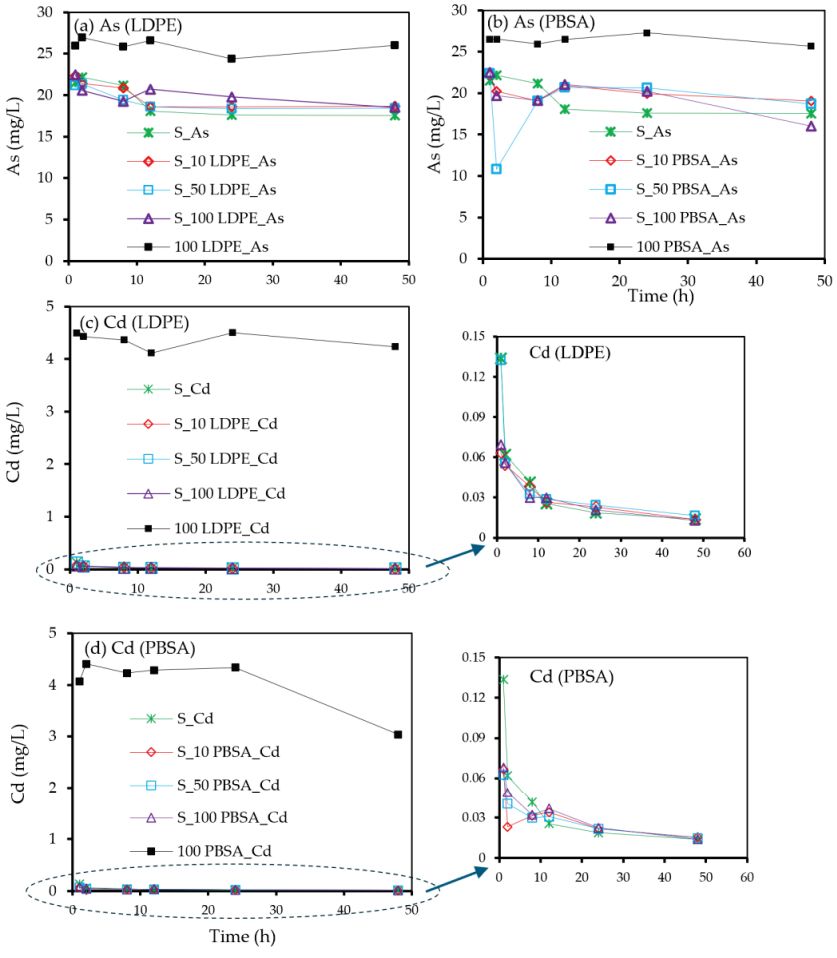

Figure 6. Concentration changes of arsenic and cadmium in water over time with the addition of soil, microplastics, and soil with different contents of microplastics: (**a**) As (LDPE), (**b**) As (PBSA), (**c**) Cd (LDPE), and (**d**) Cd (PBSA).

3.3. Adsorption Mechanisms

The adsorption of heavy metals onto microplastics is a complex process that is influenced by a variety of soil characteristics and physicochemical interactions. The exploration of adsorption mechanisms has shown that ion exchange, surface complexation, and hydrophobic interactions are the mechanisms for the adsorption of heavy metals by microplastics, indicating significant potential for the remediation of these hazardous metals [41].

As noted in Section 3.1, SEM analysis indicated that the LDPE and PBSA mulch surfaces became coarser and more cracked in the presence of Cd(II) and As(V). The authors

of [42,43] showed that the surface of microplastics was coarser with more pronounced cracks after the adsorption of heavy metals, which is consistent with our results. Furthermore, the ATR-FTIR and EDX analyses demonstrated that PBSA contains many oxygen-containing functional groups on the microplastic surface, such as hydroxyl (-OH, the peak at 3693 cm^{-1}), carbonyl groups (C-O peaks at 1155 and 1267 cm^{-1}, and C=O peak at 1710 cm^{-1}), and alcohol (-OH peaks at 1386 and 1330 cm^{-1}), with which the heavy metal cations interacted. This interaction is driven by the hydrophobic nature of microplastics, which can attract and bind cationic metal species [44]. This interaction can be influenced by the surface morphology and orientation of the microplastics, as well as by the presence of organic and inorganic molecules in the soil solution. On the other hand, LDPE does not have these oxygen-containing functional groups, which can reduce the heavy metal adsorption capacity of LDPE. The adsorption capacity of pure soil was generally higher than that in the soils with microplastics, implying that microplastics could reduce the adsorption of heavy metals to the soils through a dilution effect [30]. Microplastics with a higher surface area and more accessible adsorption sites may have a greater capacity to bind heavy metal ions, while the orientation of the microplastics can also affect the spatial distribution and accessibility of the adsorption sites [45].

In order to demonstrate the mechanisms of As(V) and Cd(II) adsorption on the soil, the SEM and ATR-FTIR spectra of the soil before and after the adsorption were compared. As shown in Figure 1, before the adsorption of As(V) and Cd(II), the surface of the soil was rough, with open pores and an irregular shape, while afterwards the surface of the soil was more disaggregated, with increased roughness. It was suggested that physical adsorption might be the main adsorption type [33]. As shown in Figure 3, As(V) and Cd(II) ions can exchange with metal cations such as K^+, Na^+, Ca^{2+}, and Mg^{2+} from the soil. Such ion exchange drives surface complexation of As(V) and Cd(II) with oxygen-containing functional groups such as the Si-O peaks at 797 and 987 cm^{-1}, Al-O peaks at 909 and 3619 cm^{-1} (inorganic groups). and -OH peaks at 3373 and 3697 cm^{-1} (organic group) [46]. The peaks of the -OH organic oxygen-containing functional groups after the introduction of microplastics into the soil may disappear due to the following reasons:

(1) The presence of microplastics may alter the composition of soil organic matter, leading to a reduction in the relative abundance of organic compounds containing hydroxyl groups [47].
(2) The adsorption of organic compounds, including those with OH groups, onto the surface of microplastics may effectively "mask" these functional groups, making them undetectable in spectroscopic analyses [48].
(3) Dilution effect: Microplastics can physically disperse within the soil, leading to a redistribution of organic matter. The dilution of OH-containing compounds might make them less concentrated or detectable in the sampled area [30].

The effects of coexistence with microplastics on the adsorption of heavy metals by soil are shown in Figure 6. Both microplastics and soil can adsorb heavy metals; however, when coexisting with microplastics, soil's heavy metal adsorption capabilities slightly decreased when compared to the soil alone. When heavy metal ions, soil, and microplastics coexisted, the microplastics acted as a "heavy metal adsorbent" and a "pollutant adsorbed by soil" at the same time [49,50]. Microplastics exhibit strong hydrophobicity, high surface area, and more exposed reactive functional groups on their surfaces that can aggregate heavy metals in soil [51,52]. We observed that the exposed hydroxyl (-OH) and carbonyl (C = O) groups on the PBSA surfaces adsorbed and complexed with As(V) and Cd(II) in soil, and the stabilization of As(V) by PBSA was more potent.

4. Conclusions

The present study investigated the adsorption characteristics of As(V) and Cd(II) in soil in the presence of LDPE and PBSA microplastics. The characterization of microplastics in soil by SEM-EDS indicated that, before the adsorption of As(V) and Cd(II), the surfaces of the MPs were smooth and virtually free of cracks and porosity. After the adsorption

of As(V) and Cd(II), the surfaces of the microplastics became coarser and more cracked, with many small particles. These surface alterations may be associated with the effects of adsorption processes that can occur on the surface of LDPE and PBSA. The adsorption of As(V) and Cd(II) by PBSA was more pronounced compared to LDPE. The FTIR results suggested that more active oxygen functional groups may be responsible for the differences in Cd(II) and As(V) adsorption capacity between microplastics and soil. With the addition of 100 pieces of microplastic, PBSA increased the adsorption of As(V), and a particularly insignificant effect on the adsorption of Cd(II) in soil was observed in the present study. LDPE increased the adsorption of Cd(II) and exerted an inhibitory effect on the adsorption of As(V). These findings prove that biodegradable microplastics are more effective for the adsorption of As(V) compared to non-biodegradable microplastics.

Author Contributions: Conceptualization, Z.M.H. and F.L.; methodology, Z.M.H. and F.L.; software, Z.M.H.; validation, Z.M.H. and F.L.; formal analysis, Z.M.H.; investigation, Z.M.H. and S.K.D.; resources, F.L.; data curation, Z.M.H. and F.L.; writing—original draft preparation, Z.M.H. and S.A.B.; writing—review and editing, S.A.B., S.K.D., Y.W. and F.L.; visualization, Z.M.H. and F.L.; supervision, F.L.; project administration, F.L.; funding acquisition, F.L. All authors have read and agreed to the published version of the manuscript.

Funding: This research received no external funding.

Institutional Review Board Statement: Not applicable.

Informed Consent Statement: Not applicable.

Data Availability Statement: Data are contained within the article.

Conflicts of Interest: The authors declare no conflicts of interest.

References

1. Amoakwah, E.; Ahsan, S.; Rahman, M.A.; Asamoah, E.; Essumang, D.K.; Ali, M.K.; Islam, K.R. Assessment of Heavy Metal Pollution of Soil-water-vegetative Ecosystems Associated with Artisanal Gold Mining. *Soil Sediment Contam. Int. J.* **2020**, *29*, 88–803. [CrossRef]
2. Bagai, A. Beating the Plastic Pollution: A Policy Perspective on India and UNEP Partnership. *Environ. Policy Law* **2021**, *51*, 265–269. [CrossRef]
3. O'Kelly, B.C.; El-Zein, A.; Liu, X.; Patel, A.; Fei, X.; Sharma, S.; Mohammad, A.; Goli, V.S.N.S.; Wang, J.J.; Li, D.; et al. Microplastics in soils: An environmental geotechnics perspective. *Environ. Geotech.* **2021**, *8*, 586–618. [CrossRef]
4. He, D.; Bristow, K.L.; Filipović, V.; Lv, J.; He, H. Microplastics in Terrestrial Ecosystems: A Scientometric Analysis. *Sustainability* **2020**, *12*, 8739. [CrossRef]
5. Horton, A.A.; Dixon, S. Microplastics: An introduction to environmental transport processes. *Wiley Interdiscip. Rev. Water* **2017**, *5*, e1268. [CrossRef]
6. Rai, M.; Pant, G.; Pant, K.; Aloo, B.N.; Kumar, G.; Singh, H.B.; Tripathi, V. Microplastic Pollution in Terrestrial Ecosystems and Its Interaction with Other Soil Pollutants: A Potential Threat to Soil Ecosystem Sustainability. *Resources* **2023**, *12*, 67. [CrossRef]
7. Lwanga, E.H.; Bériot, N.; Corradini, F.; Silva, V.; Yang, X.; Baartman, J.; Rezaei, M.; Schaik, L.V.; Riksen, M.; Geissen, V. Review of microplastic sources, transport pathways and correlations with other soil stressors: A journey from agricultural sites into the environment. *Chem. Biol. Technol. Agric.* **2022**, *9*, 20. [CrossRef]
8. Šerá, J.; Huynh, F.; Ly, F.; Vinter, Š.; Kadlečková, M.; Krátká, V.; Máčalová, D.; Koutný, M.; Wallis, C.J. Biodegradable Polyesters and Low Molecular Weight Polyethylene in Soil: Interrelations of Material Properties, Soil Organic Matter Substances, and Microbial Community. *Int. J. Mol. Sci.* **2022**, *23*, 15976. [CrossRef]
9. Wang, F.; Zhang, X.; Zhang, S.; Zhang, S.; Adams, C.A.; Sun, Y. Effects of Co-Contamination of Microplastics and Cd on Plant Growth and Cd Accumulation. *Toxics* **2020**, *8*, 36. [CrossRef]
10. Zhang, B.; Yang, X.; Chen, L.; Chao, J.; Jiang, T.; Wang, Q. Microplastics in soils: A review of possible sources, analytical methods and ecological impacts. *J. Chem. Technol. Biotechnol.* **2020**, *95*, 2052–2068. [CrossRef]
11. Li, C.; Sun, M.; Xu, X.; Zhang, L. Characteristics and influencing factors of mulch film use for pollution control in China: Microcosmic evidence from smallholder farmers. *Resour. Conserv. Recycl.* **2021**, *164*, 105222. [CrossRef]
12. Zhang, M.; Xue, Y.; Jin, T.; Zhang, K.; Li, Z.; Sun, C.; Mi, Q.; Li, Q. Effect of Long-Term Biodegradable Film Mulch on Soil Physicochemical and Microbial Properties. *Toxics* **2022**, *10*, 129. [CrossRef] [PubMed]
13. Kumari, A.; Rajput, V.D.; Mandzhieva, S.; Rajput, S.; Minkina, T.; Kaur, R.; Sushkova, S.; Kumari, P.; Ranjan, A.; Kalinitchenko, V.; et al. Microplastic Pollution: An Emerging Threat to Terrestrial Plants and Insights into Its Remediation Strategies. *Plants* **2022**, *11*, 340. [CrossRef] [PubMed]

14. Yang, N.; Sun, Z.; Liu, F.; Zheng, M.; Chi, D.; Meng, W.; Hou, Z.; Bai, W.; Li, K. Plastic Film Mulching for Water-Efficient Agricultural Applications and Degradable Films Materials Development Research. *Mater. Manuf. Process.* **2014**, *30*, 143–154. [CrossRef]
15. Ning, R.; Liang, J.; Sun, Z.; Liu, X.; Sun, W. Preparation and characterization of black biodegradable mulch films from multiple biomass materials. *Polym. Degrad. Stab.* **2021**, *183*, 109411. [CrossRef]
16. Borrowman, C.K.; Johnston, P.; Adhikari, R.; Saito, K.; Patti, A.F. Environmental degradation and efficacy of a sprayable, biodegradable polymeric mulch. *Polym. Degrad. Stab.* **2020**, *175*, 109126. [CrossRef]
17. Shah, F.; Wu, W. Use of plastic mulch in agriculture and strategies to mitigate the associated environmental concerns. *Adv. Agron.* **2020**, *164*, 231–287. [CrossRef]
18. Monkul, M.M.; Özhan, H.O. Microplastic Contamination in Soils: A Review from Geotechnical Engineering View. *Polymers* **2021**, *13*, 4129. [CrossRef]
19. Kumar, R.; Sharma, P. Recent Developments in Extraction, Identification, and Quantification of Microplastics from Agricultural Soil and Groundwater. *Fate Transp. Subsurf. Pollut.* **2020**, *24*, 125–143. [CrossRef]
20. Kaur, P.; Singh, K.; Singh, B. Microplastics in soil: Impacts and microbial diversity and degradation. *Pedosphere* **2022**, *32*, 49–60. [CrossRef]
21. Miao, J.; Huang, W.; Pan, R.; Zhou, K. Research progress and hotspot analysis of soil microplastics: A bibliometrics-based review. *Front. Environ. Sci.* **2023**, *11*, 1297646. [CrossRef]
22. Liu, R.; Wang, Z.; Han-chun, Y.; Li, W.; Zong, R.; Tian, X. Effects of Different Plastic Mulching Film on Soil Hydrothermal Status and Water Utilization by Spring Maize in Northwest China. *Front. Mater.* **2021**, *8*, 74833. [CrossRef]
23. Mustafa, S.; Dilara, B.; Nargis, K.; Naeem, A.; Shahida, P. Surface properties of the mixed oxides of iron and silica. *Colloids Surf. A Physicochem. Eng. Asp.* **2002**, *205*, 273–282. [CrossRef]
24. Högberg, M.N.; Bååth, E.; Nordgren, A.; Arnebrant, K.; Högberg, P. Contrasting effects of nitrogen availability on plant carbon supply to mycorrhizal fungi and saprotrophs—A hypothesis based on field observations in boreal forest. *New Phytol.* **2003**, *160*, 225–238. [CrossRef]
25. Chapman, H.D. Cation-exchange capacity. In *Methods of Soil Analysis: Part 2 Chemical and Microbiological Properties*; American Society of Agronomy: Madison, WI, USA, 1965; Volume 9, pp. 891–901.
26. Navarrete-López, M.; Jonathan, M.P.; Rodríguez-Espinosa, P.F.; Salgado-Galeana, J.A. Autoclave decomposition method for metals in soils and sediments. *Environ. Monit. Assess.* **2012**, *184*, 2285–2293. [CrossRef]
27. Asuquo, E.; Martin, A.; Nzerem, P.; Siperstein, F.; Fan, X. Adsorption of Cd (II) and Pb (II) ions from aqueous solutions using mesoporous activated carbon adsorbent: Equilibrium, kinetics and characterisation studies. *J. Environ. Chem. Eng.* **2017**, *5*, 679–698. [CrossRef]
28. Tang, S.; Sun, P.; Ma, S.; Jin, W.; Zhao, Y. The interfacial behaviors of different arsenic species on polyethylene mulching film microplastics: Roles of the plastic additives. *J. Hazard. Mater.* **2023**, *442*, 130037. [CrossRef]
29. Tang, S.; Lin, L.; Wang, X.; Feng, A.; Yu, A. Pb (II) uptake onto nylon microplastics: Interaction mechanism and adsorption performance. *J. Hazard. Mater.* **2020**, *386*, 121960. [CrossRef]
30. Guo, J.-J.; Li, F.; Xiao, H.-C.; Liu, B.-L.; Feng, L.-N.; Yu, P.-F.; Meng, C.; Zhao, H.-M.; Feng, N.-X.; Li, Y.-W.; et al. Polyethylene and polypropylene microplastics reduce chemisorption of cadmium in paddy soil and increase its bioaccessibility and bioavailability. *J. Hazard. Mater.* **2023**, *449*, 130994. [CrossRef]
31. Peng, H.; Lin, Z.; Lu, D.; Yu, B.; Li, H.; Yao, J. How do polystyrene microplastics affect the adsorption of copper in soil? *Sci. Total Environ.* **2024**, *924*, 171545. [CrossRef]
32. Xiong, W.; Hu, M.; He, S.; Ye, Y.; Xiang, Y.; Peng, H.; Chen, Z.; Xu, Z.; Zhang, H.; Li, W.; et al. Microplastics enhance the adsorption capacity of zinc oxide nanoparticles: Interactive mechanisms and influence factors. *J. Environ. Sci.* **2025**, *147*, 665–676. [CrossRef] [PubMed]
33. Deng, S.; Liu, Y.; Guo, C.; Zhou, X.; Lu, Q.; Fan, Z.; Gao, Z.; Xiang, Q.; Jin, Z.; Chen, X. Polyvinyl chloride microplastics reduce Cd (II) adsorption and enhance desorption with soil-dependent mechanisms. *Environ. Technol. Innov.* **2024**, *34*, 103607. [CrossRef]
34. Atugoda, T.; Wijesekara, H.; Werellagama, D.R.I.B.; Jinadasa, K.B.S.N.; Bolan, N.S.; Vithanage, M. Adsorptive interaction of antibiotic ciprofloxacin on polyethylene microplastics: Implications for vector transport in water. *Environ. Technol. Innov.* **2020**, *19*, 100971. [CrossRef]
35. Tang, S.; Sun, P.; Qu, G.; Tian, Y.; Liu, J.; Pervez, M.N.; Li, X.; Cao, C.; Zhao, Y. Photo-aged non-biodegradable and biodegradable mulching film microplastics alter the interfacial behaviors between agricultural soil and inorganic arsenic. *J. Hazard. Mater.* **2023**, *455*, 131552. [CrossRef]
36. Lv, M.; Zhang, T.; Ya, H.; Xing, Y.; Wang, X.; Jiang, B. Effects of heavy metals on the adsorption of ciprofloxacin on polyethylene microplastics: Mechanism and toxicity evaluation. *Chemosphere* **2023**, *315*, 137745. [CrossRef]
37. Wu, C.S. Utilization of peanut husks as a filler in aliphatic–aromatic polyesters: Preparation, characterization, and biodegradability. *Polym. Degrad. Stab.* **2012**, *97*, 2388–2395. [CrossRef]
38. Cao, Y.; Ma, X.; Chen, N.; Chen, T.; Zhao, M.; Li, H.; Song, Y.; Zhou, J.; Yang, J. Polypropylene microplastics affect the distribution and bioavailability of cadmium by changing soil components during soil aging. *J. Hazard. Mater.* **2023**, *443*, 130079. [CrossRef]
39. Debuissy, T.; Pollet, E.; Avérous, L. Synthesis and characterization of biobased poly (butylene succinate-ran-butylene adipate). Analysis of the composition-dependent physicochemical properties. *Eur. Polym. J.* **2017**, *87*, 84–98. [CrossRef]

40. Fuller, S.; Gautam, A. A procedure for measuring microplastics using pressurized fluid extraction. *Environ. Sci. Technol.* **2016**, *50*, 5774–5780. [CrossRef]
41. Guo, K.; Han, F.X.; Kingery, W.L.; Sun, H.; Zhang, J. Development of novel nanomaterials for remediation of heavy metals and radionuclides in contaminated water. *Nanotechnol. Environ. Eng.* **2016**, *1*, 7. [CrossRef]
42. Zhao, H.; Li, P.; Su, F.; He, X.; Elumalai, V. Adsorption behavior of aged polybutylene terephthalate microplastics coexisting with Cd(II)-tetracycline. *Chemosphere* **2022**, *301*, 134789. [CrossRef] [PubMed]
43. Wang, H.; Qiu, C.; Song, Y.; Bian, S.; Wang, Q.; Chen, Y.; Fang, C. Adsorption of tetracycline and Cd(II) on polystyrene and polyethylene terephthalate microplastics with ultraviolet and hydrogen peroxide aging treatment. *Sci. Total Environ.* **2022**, *845*, 157109. [CrossRef] [PubMed]
44. Muthu, M.; Wu, H.; Gopal, J.; Sivanesan, I.; Chun, S. Exploiting Microbial Polysaccharides for Biosorption of Trace Elements in Aqueous Environments—Scope for Expansion via Nanomaterial Intervention. *Polymers* **2017**, *9*, 721. [CrossRef] [PubMed]
45. Mbachu, O.; Jenkins, G.A.; Kaparaju, P.; Pratt, C. The rise of artificial soil carbon inputs: Reviewing microplastic pollution effects in the soil environment. *Sci. Total Environ.* **2021**, *780*, 146569. [CrossRef]
46. Zhang, F.; Wang, X.; Yin, D.; Peng, B.; Tan, C.; Liu, Y.; Tan, X.; Wu, S. Efficiency and mechanisms of Cd removal from aqueous solution by biochar derived from water hyacinth (Eichornia crassipes). *J. Environ. Manag.* **2015**, *153*, 68–73. [CrossRef]
47. Prata, J.C.; Costa, J.P.D.; Lopes, I.; Andrady, A.L.; Duarte, A.C.; Rocha-Santos, T. A One Health perspective of the impacts of microplastics on animal, human and environmental health. *Sci. Total Environ.* **2021**, *777*, 146094. [CrossRef]
48. Solomon, O.O.; Thavamani, P. Microplastics in the Marine Environment: Current Status, Assessment Methodologies, Impacts and Solutions. *J. Pollut. Eff. Control.* **2016**, *4*, 1000161. [CrossRef]
49. Kumar, R.; Verma, A.; Rakib, M.R.J.; Gupta, P.K.; Sharma, P.; Garg, A.; Girard, P.; Aminabhavi, T.M. Adsorptive behavior of micro(nano)plastics through biochar: Co-existence, consequences, and challenges in contaminated ecosystems. *Sci. Total Environ.* **2023**, *856*, 159097. [CrossRef]
50. Tang, S.; Yang, X.; Zhang, T.; Qin, Y.; Cao, C.; Shi, H.; Zhao, Y. Adsorption mechanisms of metal ions (Pb, Cd, Cu) onto polyamide 6 microplastics: New insight into environmental risks in comparison with natural media in different water matrices. *Gondwana Res.* **2022**, *110*, 214–225. [CrossRef]
51. Liu, S.; Huang, J.; Zhang, W.; Shi, L.; Yi, K.; Yu, H.; Zhang, C.; Li, S.; Li, J. Microplastics as a vehicle of heavy metals in aquatic environments: A review of adsorption factors, mechanisms, and biological effects. *J. Env. Manag.* **2022**, *302*, 113995. [CrossRef]
52. Vedolin, M.C.; Teophilo, C.Y.S.; Turra, A.; Figueira, R.C.L. Spatial variability in the concentrations of metals in beached microplastics. *Mar. Pollut. Bull.* **2018**, *129*, 487–493. [CrossRef]

Disclaimer/Publisher's Note: The statements, opinions and data contained in all publications are solely those of the individual author(s) and contributor(s) and not of MDPI and/or the editor(s). MDPI and/or the editor(s) disclaim responsibility for any injury to people or property resulting from any ideas, methods, instructions or products referred to in the content.

soil systems

MDPI

Article

Spatial Variability in the Speciation of Lead (Pb) and Other Metals Across Urban Lawns Is Linked to Post-Deposition Weathering Reactions

Chukwudi E. Nwoko, David M. Singer *, Allyson C. Tessin, Rachel Izworski and Chloe Heestand

Department of Earth Sciences, Kent State University, Kent, OH 44242, USA; cnwoko@kent.edu (C.E.N.)
* Correspondence: dsinger4@kent.edu

Abstract: The historical use of lead (Pb) poses ongoing health risks via exposure to contaminated urban soils. However, there is limited information about heterogeneity in Pb speciation and distribution at the house lot scale. This study determined highly spatially resolved Pb and other metal speciation along horizontal transects and vertical soil cores from three homes in the Akron, Ohio (USA) municipal. Solid phase characterization was coupled with a sequential extraction protocol to determine operationally defined speciation (exchangeable (M_{EX}), reducible (M_{RED}), oxidizable (M_{OX}), and residual (M_{RES})). Lead and Zn were strongly correlated across all fractions (R^2 = 0.92). Total extractable Pb and Zn were found in low weight percent concentrations nearest to the homes, and speciation was dominated by M_{EX} and M_{RED}. High Pb in the M_{EX} fraction was correlated with the presence of Pb-bearing paint chips in the soil. Lead in the M_{EX} fraction in soils near the homes decreased with increasing time due to exterior renovations coupled with increases in Pb and Zn in the M_{RED} fraction. These results suggest that homes are the dominant source of Pb and Zn due to the weathering of exterior surfaces and highlight the acute risk of exposure to more labile Pb immediately following exterior renovations and damage to home exteriors in areas of older housing stock.

Keywords: lead; urban soils; zinc; sequential extraction; paint; housing stock age

Citation: Nwoko, C.E.; Singer, D.M.; Tessin, A.C.; Izworski, R.; Heestand, C. Spatial Variability in the Speciation of Lead (Pb) and Other Metals Across Urban Lawns Is Linked to Post-Deposition Weathering Reactions. *Soil Syst.* **2024**, *8*, 113. https://doi.org/10.3390/soilsystems8040113

Academic Editors: Manfred Sager and Girish Choppala

Received: 15 July 2024
Revised: 15 October 2024
Accepted: 1 November 2024
Published: 6 November 2024

Copyright: © 2024 by the authors. Licensee MDPI, Basel, Switzerland. This article is an open access article distributed under the terms and conditions of the Creative Commons Attribution (CC BY) license (https://creativecommons.org/licenses/by/4.0/).

1. Introduction

The industrial adoption of lead (Pb) in the United States was primarily driven by its inherent properties, particularly for use in paint production, where it was valued for its ability to enhance the brightness and durability of paints, and for use as an anti-knocking additive in automobile gasoline to improve engine performance [1]. The extensive use of Pb in the United States from 1921 to the beginning of the Pb phase-out in 1973 resulted in widespread environmental Pb exposure [2]. Exposure to Pb has been linked to significant health concerns, such as neurological abnormalities, kidney and cardiovascular damage, and anemia [3,4], with adverse health effects being pronounced in children (through age five). Although there is no established safe blood lead level (BLL) [5], the Center for Disease Control and Prevention (CDCP) uses a BLL reference value of 3.5 µg/dL to identify children with elevated BLLs. Although BLL values in children have decreased from historical highs in the late 1970s (as high as 15 ug/dL) [6] as a result of the phasing out and banning of Pb-based paint and gasoline (from the 1970s to 1990s), over half a million children in the United States were reported to have BLL values above 3.5 µg/dL in 2012 [7], and more than half of all children in the country had a BLL above 1 µg/dL between 2018 and 2020 [8]. However, the risk of exposure is not equally distributed among the population, with black children making up more than 50% of children with a BLL greater than 1 ug/dL [9], underscoring the use of high Pb levels as a socioeconomic indicator of inequality.

The use of Pb-based products, particularly in urban environments, resulted in the wide-scale contamination of soils, a primary source of Pb exposure to children, with weight percent soil concentrations well over the U.S. Environmental Protection Agency's (EPA) actional level of 200 ppm being reported across older urban cores [10–13]. Although the Pb concentrations in soils have declined over time, there is leftover Pb in the environment due to previously deposited Pb in the soil and newer inputs from the degradation of Pb-based paint chips that continue to be added into soils. Although previous studies have typically examined the distribution of total Pb in urban soils, there has not been a comprehensive examination of speciation (i.e., the chemical and physical form(s) in which Pb is present in the environment) [14], which is crucial to establishing exposure risks [15].

Current Pb speciation and distribution in soils likely reflect a complex relationship between the input of primary sources and post-deposition transformations [16]. With respect to Pb speciation in primary sources, Pb in paint and gasoline exists in inorganic and organic forms, respectively. Lead-based paint can include Pb oxides, Pb sulfates, and carbonates [17], and as the paint weathers and breaks down on the exterior of homes, Pb(II) ions are released into the soil [18]. Despite Pb paint being banned, much of the older housing stock in urban areas is still covered with Pb paint, with at least 34.6 million homes (30% of US homes) having Pb-based paint and 18.2 million homes (15% of US homes) having deteriorated Pb-based paint. These homes were built primarily before 1978 in the US Northeast and Midwest regions. The paint can chip off through the weathering of exterior surfaces and/or renovations [15,19], releasing Pb(II) into soils. In terms of leaded gasoline, the combustion of the organo-lead compound tetraethyllead results in the release of Pb(II) into soil [20,21]. The Pb(II) released from the breakdown of paint and gasoline can then react with and form a range of labile to recalcitrant pools of soil Pb with different chemical and/or physical properties [17,22–25]. The resulting differences in reactivity impact potential exposure, with ingestion and inhalation being the primary exposure pathways, especially for children who engage in hand-to-mouth behavior [26,27]. Although the phasing out and ban of Pb-based gasoline, pipes, and paints resulted in a direct decrease in the BLL of children aged 1–5 years [8], a large pool of labile Pb still exists in urban soils. Furthermore, the risk of exposure to Pb depends on Pb speciation and its concentrations in soil, which can change over time.

The Pb(II) ions released following the deposition of primary phases are typically retained in soils [11,28] and sequestered by metal oxides, clays, and organic matter [29]. However, as weathering progresses, the chemical form of Pb(II) is expected to change due to its increasing degree of transformation. It is unclear how this transformation impacts its chemical form with respect to an increasing distance from the site of deposition. An increase in Pb solubility can lead to a rise in its potential bioavailability, which can vary spatially and temporally depending on the nature of transformation it undergoes. After Pb(II) compounds are introduced into the soil, the resultant particles undergo translocation across both horizontal and vertical distances from their initial point of deposition. Furthermore, these particles are subject to a range of soil formation processes that facilitate their physicochemical transformation [11] and association with different minerals in the soil. Identifying the current speciation of Pb along the vertical and horizontal transects can provide valuable insights into the spatial changes in soil Pb speciation after deposition. Indirect methods to determine metal speciation, such as sequential extractions, can be more cost-effective and efficient compared to direct methods, such as synchrotron-based X-ray Absorption Spectroscopy, in determining the distribution of metals with operationally defined fractions including exchangeable, reducible, oxidizable, and residual fractions [30–35].

Current metal speciation and the fraction of potentially bioavailable Pb and other metals are therefore the result of a complex set of interactions, including (1) the type of source(s) and rate and timing of input; (2) local mineralogical and (bio)geochemical conditions which control which metal-bearing species can be formed; and (3) the rate of

metal loss through soil loss and erosion, which might result in the preferential transport of certain metal-bearing phases over others. The summation of these interactions can potentially result in heterogeneous metal speciation across an urban landscape that can change in space and time. Previous studies of Pb speciation, typically based on acid-extractable metal concentrations, provide a coarse picture of Pb speciation at the city scale. This work aimed to determine the spatial distribution of soil Pb species and other metals along vertical and horizontal transects adjacent to homes with known historical Pb paint use and to determine potential changes in speciation over time following deposition. Furthermore, the sampling density used here provided a higher resolution of changes in metal speciation across urban lawns compared to previous studies that typically take one sample per lot, allowing for the observation of previously unknown local-scale heterogeneity. This work was based in Akron, OH (USA), using a sequential extraction method combined with solid phase characterization of the soils for bulk properties and electron microscopy for targeted phase identification. This approach aimed to provide valuable insights into the environmental processes that affect the mobility and fate of Pb in the soil and identify an approach to be used for constraining the scope of targeted remediation.

2. Materials and Methods

2.1. Site Description and Sample Collection and Processing

Soil samples were collected in proximity to three residential homes in and around Akron, OH (USA) (Figures 1 and S1), a metropolitan area with a population of approximately 190,000 [36]. Akron rapidly increased in population and industrial growth (dominated by the rubber and tire industries), and its population peaked at 290,000 in the 1960s. Soil samples were collected in areas dominated by older (pre-1978) housing stock [37]. Although BLL data are limited for Akron and Summit County, data from 2012 through 2014 indicate that 4.1% of tested children had elevated BLLs in comparison to the national average of approximately 2.5% around the same period [26]. The homeowners of all three homes confirmed that Pb-based paints had been used on the exterior of the houses; however, the paint was removed as part of renovations at the three Sites 2, 11, and 25 years before soil sampling occurred, respectively. From each house, three sets of samples were collected in June 2021 as follows (and summarized in Table S1): (1) along a horizontal transect collected at 1 m intervals from areas immediately adjacent to the house to the road verge, excluding areas inaccessible due to existing road pavement and sidewalks (n = 16, 10, and 13 for Sites 1, 2, and 3, respectively); (2) a horizontal transect from an area immediately next to the back of the house toward the end of the property (n = 13, 3, and 2 for Sites 1, 2, and 3, respectively); and (3) a vertical core collected from an area immediately adjacent to the front of the house at 10 cm internals (n = 5 and 4 for Sites 1 and 3; no core was collected at Site 2). For surface samples, a 2 cm deep soil sample was collected after clearing any surface vegetation that may have been present. Each sample was sieved (2 mm) to remove any debris and large rocks. Samples were dried at 40 °C for 12 h using a Binder ED-115 Oven (Binder Inc., Bohemia, NY, USA). Approximately 25 g of each sieved sample was milled using a SPEX ball mill 8000 M (Cole Palmer, Metuchen, NJ, USA) with tungsten carbide balls for 10 min to produce a homogenous powder. The milling canister was cleaned using isopropyl alcohol between runs to prevent cross-contamination. Milled soil samples were used for bulk mineralogical characterization and sequential extractions (described below), and sieved-only samples were analyzed by electron microscopy. The pH of the topsoil closest to the three homes was measured using 1 g of soil in 11 mL of DDI-H_2O (Table S2); the average soil pH values for the three sites were 5.98 $\pm$ 0.03, 5.60 $\pm$ 0.14, and 5.82 $\pm$ 0.06, respectively (Table S2).

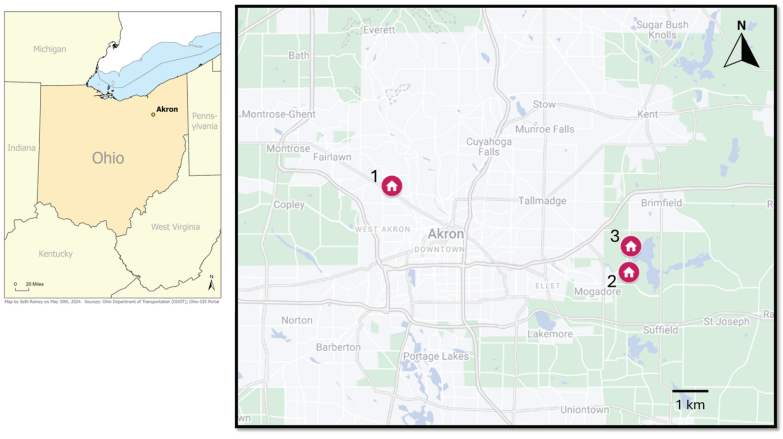

Figure 1. An overview map of the Akron metropolitan area (with the location of Akron in Ohio shown in the insert map) indicating the general positions of the three houses from which the soil samples were collected. Precise coordinates of the houses are not shown in this map to maintain homeowner privacy.

2.2. Sequential Extraction of Pb and Other Metals from Soils

A four-step sequential extraction method based on the BCR method [38] and modified to target a range of potentially bioavailable metals and trace elements in urban soils [31] was used to determine metal speciation for the following fractions and steps using 1 g of milled soil: (1) exchangeable: 20 mL of 0.11 mol/L acetic acid at 22 °C for eight hours; (2) reducible: 20 mL of 0.11 mol/L hydroxylammonium chloride at 22 °C, followed by centrifugation and acidification with 2 mol/L nitric acid; (3) oxidizable: 10 mL of 8.8 mol/L hydrogen peroxide added twice at 85 °C, followed by extraction with 50 mL of 1 mol/L ammonium acetate, and (4) residual: aqua regia solution containing 7.0 mL of concentrated nitric acid and 2.3 mL of concentrated hydrogen chloride (HCl). The resulting solution was extracted for 1.5 h at 85 °C. After each step, the samples were centrifuged at 3000 rpm for 20 min. The decanted solutions underwent ×10 dilution for fractions 1 and 2 and ×20 dilution for fractions 3 and 4 prior to a Thermo Scientific iCAP PRO XP inductively coupled plasma optical emission spectroscopy (ICP-OES, Thermo Fisher Scientific, Waltham, MA, USA) analysis for the following elements, with their detection limits noted in parenthesis: Al (0.1 µg/L), S (0.5 µg/L), K (0.5 µg/L), Ca (0.3 µg/L), Ti (0.3 µg/L), Cr (0.3 µg/L), Mn (0.3 µg/L), Fe (0.2 µg/L), Co (0.3 µg/L), Cu (0.2 µg/L), Zn (0.1 µg/L), Cd (0.3 µg/L), and Pb (0.3 µg/L). A total of six standards, including a blank solution, were prepared to calibrate the concentrations. An internal Y standard was used to correct for plasma instability. The ICP-OES standards prepared for the analysis of fractions 1 and 2 had concentrations of 0.01 ppm, 0.1 ppm, 1 ppm, 10 ppm, and 30 ppm, respectively. For each site, five to ten randomly selected samples were treated as duplicates; the differences between duplicate sub-samples and repeated standards were lower than 5% for all elements. All reagents used were analytical grade, and solutions were prepared with distilled deionized water (DDI-H_2O) (18.2 MΩ; Milli-Q Direct-Q 3UV-R, Millipore Sigma, Burlington, MA, USA). A Pearson correlation analysis was performed (see Excel file in the electronic annex) to investigate the correlation between extracted metals and other soil properties as described below.

2.3. Solid Phase Characterization

Mineral identification and abundance were determined by X-ray diffraction using a Rigaku Miniflex 6G (Rigaku, The Woodlands, TX, USA) X-ray diffractometer (3–90°, 0.02° step size; 2° min^{-1}) of milled powders. Phase identification was performed using Rigaku's PDXL software v.2.9, with the Whole Pattern Powder Fitting (WPPF) method connected to

the ICDD PDF-2 database. Loss on ignition (LOI) was used as a proxy for organic matter content [39,40] following a previously established procedure [41]. A weighed mass of subsample with a target mass of 2.5 g was placed in ceramic crucibles with lids and brought to 550 °C using a Thermo Fisher Thermolyne muffle furnace (Thermo Fisher Scientific, Waltham, MA, USA) for one hour and then allowed to cool before being re-weighed. Scanning Electron Microscopy with Energy Dispersive Spectroscopy (SEM-EDS) was used to determine the composition and morphology of Pb-bearing particles in the soils sampled near the homes using a Hitachi Benchtop Scanning Electron Microscope TM3030 equipped with Quantax70 Energy Dispersive X-ray Spectrometry using dry powders deposited on carbon sticky tape (Hitachi USA, Santa Clara, CA, USA). A MalvernTM Mastersizer 2000 laser diffraction particle size analyzer equipped with a Hydro 2000MU manual inlet system (Malvern Panalytical Inc., Westborough, MA, USA) was used to conduct a particle size analysis using sieved (<2 mm) but not milled samples. The particle size distribution was binned to determine the contribution of sand- (63 μm–2 mm), silt- (2 μm–63 μm), and clay-sized (<2 μm) particles.

3. Results

3.1. Metal Speciation in Soils in Horizontal Transects and Depth Cores

Metal speciation and distribution are discussed below for metals with the highest levels of contamination (Pb and Zn) and other industrial metals potentially related to anthropogenic activities (first-row transition metals plus Cd); changes in the speciation and distribution of elements less likely to be anthropogenically impacted (Al, S, K, Ca, and Ti) are reported in the Supporting Information document (Figures S2–S6). Metal speciation is reported in terms of the total extractable concentration ($[M]_{T\text{-}EX}$), which is the sum of metal concentrations in the exchangeable ($[M]_{EX}$), reducible ($[M]_{RED}$), oxidizable ($[M]_{OX}$), and residual ($[M]_{RES}$) fractions.

3.1.1. Pb and Zn

The distribution of Pb in topsoil along horizontal transects in front of each home exhibited similar overall trends at all three homes, with a maximum $[Pb]_{T\text{-}EX}$ closest to the homes, which rapidly decreased within two to three meters (Figure 2a). The maximum $[Pb]_{T\text{-}EX}$ values for the three homes were 21,720 mg/kg, 11,115 mg/kg, and 1854 mg/kg, respectively. At Site 1, the maximum $[Pb]_{T\text{-}EX}$ value was located at a 1 m distance, whereas the maximum $[Pb]_{T\text{-}EX}$ value at Sites 2 and 3 were located immediately adjacent to the homes (i.e., at 0 m). At all three sites, the $[Pb]_{T\text{-}EX}$ values remained relatively constant beyond two to three meters from the houses, with average values of 166 ± 68 mg/kg, 1422 ± 781 mg/kg, and 243 ± 198 mg/kg, respectively. A noticeable deviation to the flat trend across the lawn was observed at Site 1, where a spike in $[Pb]_{T\text{-}EX}$ of 548 mg/kg was observed at the end of the transect near the street curb. Although fewer topsoil samples were collected along the horizontal transect from the back of each home, it is clear that these soils exhibited a similar overall trend compared to the front, with the highest $[Pb]_{T\text{-}EX}$ values being found immediately adjacent to the homes, which decreased quickly within 2–3 m. The maximum $[Pb]_{T\text{-}EX}$ values for the three homes were 381 mg/kg, 6620 mg/kg, and 1368 mg/kg, respectively (Figure 2b). The average values for $[Pb]_{T\text{-}EX}$ further from the homes were 215 ± 69 mg/kg, 129.51 mg/kg at the only remaining point, and 174 ± 119 mg/kg, respectively. Within the vertical soil core (Figure 2c) at Site 1, the highest $[Pb]_{T\text{-}EX}$ value (2826 mg/kg) was observed in the shallow sample (0–10 cm) and decreased steadily with depth to 454 mg/kg. At site 3, $[Pb]_{T\text{-}EX}$ did not exhibit a trend with depth, and the average value was 2186 ± 225 mg/kg. Lead speciation in topsoil from the horizontal transect in the front of each house was dominated by the reducible fraction (Pb_{RED}) closest to the home and the residual fraction (Pb_{RES}) further from the homes (Figure 2d–f) with a relatively linear change in each fraction across the transect. The maximum percentages of Pb_{RED} were found closest to each house, with values of 74%, 69%, and 75%, respectively, which decreased to 40%, 32%, and 29%, respectively, closest to the

street. The minimum percentages of Pb_{RES} closest to each house were 5%, 13%, and 9%, respectively, and increased to 48%, 44%, and 55%, respectively, closest to the street. Lead in the exchangeable fraction was the highest nearest the houses, with maximum percentage Pb_{EX} values of 25%, 14%, and 4%, respectively. No apparent trend in the contribution of Pb in the oxidizable fraction (Pb_{OX}) was observed, with average Pb_{OX} contributions of 13 ± 9%, 9 ± 3%, and 12 ± 7% being found on each respective site. Lead speciation in topsoil from the transect at the back of the houses (Figure 2g–i) did not exhibit the same clear trends compared to the front of the houses, although Pb_{RED} was the dominant fraction at the back of the houses. The speciation of Pb in the vertical cores from Sites 1 and 3 did not exhibit a significant trend with depth (Figure 2j,k), with average percentage values for Pb_{EX}, Pb_{RED}, Pb_{OX}, and Pb_{RES} of 8 ± 3%, 61 ± 8%, 13 ± 8%, and 18 ± 9%, respectively, for Site 1, and 17 ± 5%, 64 ± 4%, 6 ± 1%, and 14 ± 2%, respectively, for Site 3.

The distribution pattern of Zn in the soil along the horizontal transects in front of each home displayed similar trends across all three homes. Maximum $[Zn]_{T\text{-}EX}$ values were observed immediately adjacent to the homes, followed by a rapid decline within two to three meters (Figure 3a). The maximum $[Zn]_{T\text{-}EX}$ values for the three homes were 2525 mg/kg, 1120 mg/kg, and 609 mg/kg, respectively. At Site 1, the maximum $[Zn]_{T\text{-}EX}$ value was located at a 1 m distance, whereas the maximum $[Zn]_{T\text{-}EX}$ values at Sites 2 and 3 were located immediately adjacent to the homes (i.e., at 0 m). At all three sites, the $[Zn]_{T\text{-}EX}$ values remained relatively constant beyond two to three meters from the houses, with average values of 624 ± 596 mg/kg, 399 ± 256 mg/kg, and 268 ± 118 mg/kg, respectively. A noticeable deviation to the uniform trend across the lawn was observed at Site 1, where a spike of 568 mg/kg in the $[Zn]_{T\text{-}EX}$ value was observed at the end of the transect near the street curb. In the horizontal transects collected from the rear of each house, the highest $[Zn]_{T\text{-}EX}$ values were observed immediately adjacent to the homes, which decreased quickly within 2–3 m. The maximum $[Zn]_{T\text{-}EX}$ values for the three homes were 669 mg/kg, 779 mg/kg, and 1268 mg/kg, respectively (Figure 3b). The average values for $[Zn]_{T\text{-}EX}$ further from the homes were 408 ± 107 mg/kg, 345 mg/kg at the only remaining point, and 645 ± 540 mg/kg, respectively. Along the vertical transect (Figure 3c), the $[Zn]_{T\text{-}EX}$ values at Sites 1 and 2 did not exhibit apparent trends and averages at 654 ± 178 mg/kg and 534 ± 14 mg/kg, respectively. Along the front horizontal transect, Zn speciation in the topsoil was dominated by the exchangeable fraction closest to the houses, but once the Zn concentration dropped off within 2–3 m, the residual fraction dominated (Figure 3d–f). The minimum percentages of Zn_{RES} closest to each house were 20%, 56%, and 62%, respectively, and they increased to 93%, 96%, and 93%, respectively, closest to the street. Zinc in the exchangeable fraction was the highest nearest the houses, with maximum percentages of Zn_{EX} values of 43%, 27%, and 12%, at the three homes, respectively. The contribution of Zn_{RED} decreased with an increasing distance from the homes, averaging 12 ± 14%, 6 ± 3%, and 3 ± 3% at Sites 1, 2, and 3, respectively. No apparent trend in the distribution of Zn in the oxidizable fraction was observed, with average percentages of Zn_{OX} values of 7 ± 7%, 6 ± 5%, and 6 ± 4%. Zinc speciation in topsoil from the transect in the back of the houses (Figure 3g–i) did not exhibit the same clear trends compared to the front of the house, although Zn_{RED} was the dominant fraction in the back of the houses. Along the vertical core at site 1, from 0–10 cm to 40–50 cm, the percentage contribution of Zn_{EX} decreased from 18% to 3% with depth as the percentage contribution of Zn_{RES} increased from 34% to 72%, respectively. At Site 3, from 0 cm to 10 cm, 30 cm, and 40 cm, the Zn_{EX} value increased from 9% to 12% as the Zn_{RES} value decreased from 77% to 71% with depth, respectively. The percentage contributions of Zn_{RED} and Zn_{OX} do not exhibit significant variations with the depth and have averages of 15 ± 11% and 14 ± 7% in site 1 and averages of 6 ± 1% and 10 ± 2% in Site 3, respectively.

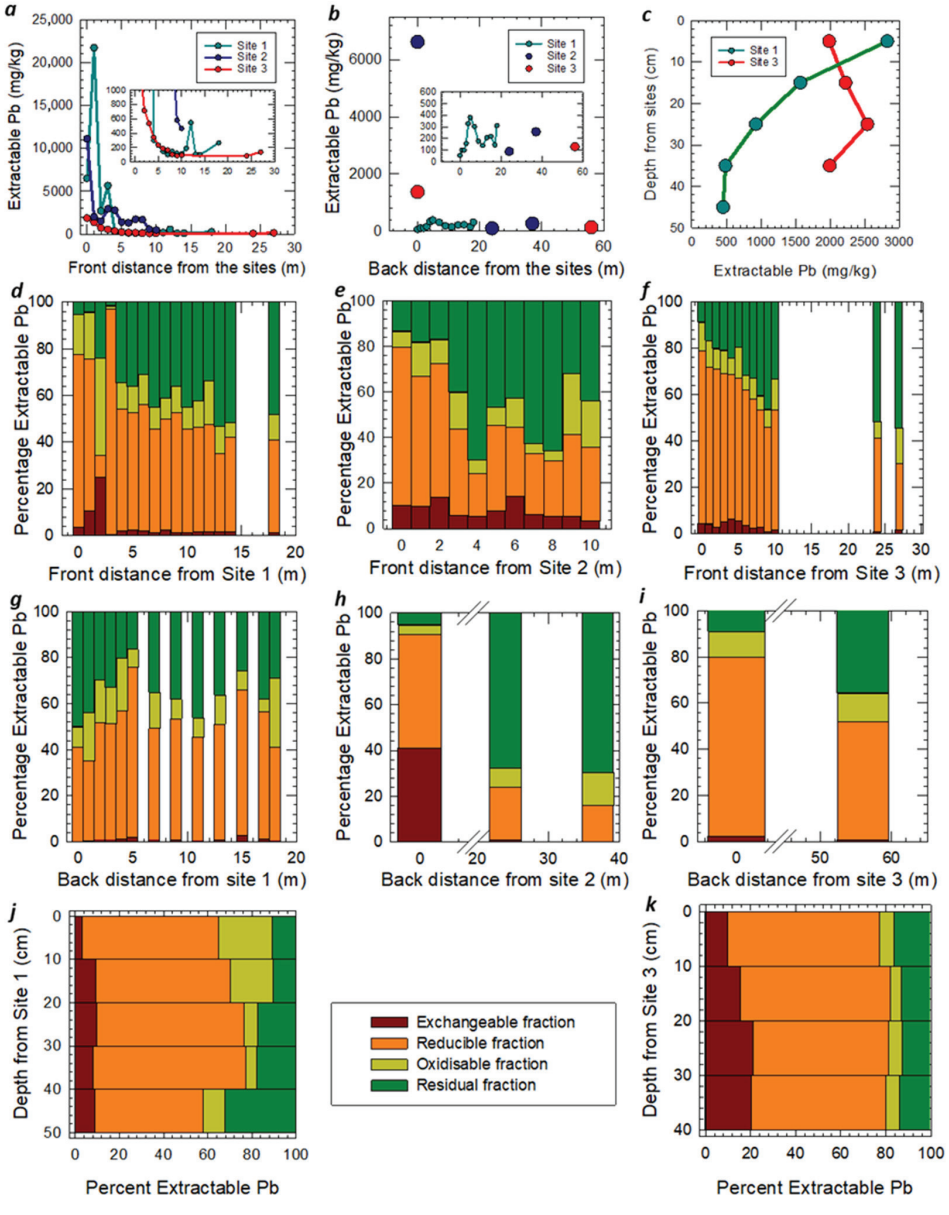

Figure 2. (**a**–**c**) The total extractable Pb from the three houses along the front, back, and vertical transects; (**d**–**f**) the proportional distribution of the four fractions across the front transect of each house; (**g**–**i**) the proportional distribution of the four fractions across the back transect of each house; and (**j**,**k**) the proportional distribution of the four fractions along the vertical transect of each house. Note that a core was not collected at Site 2.

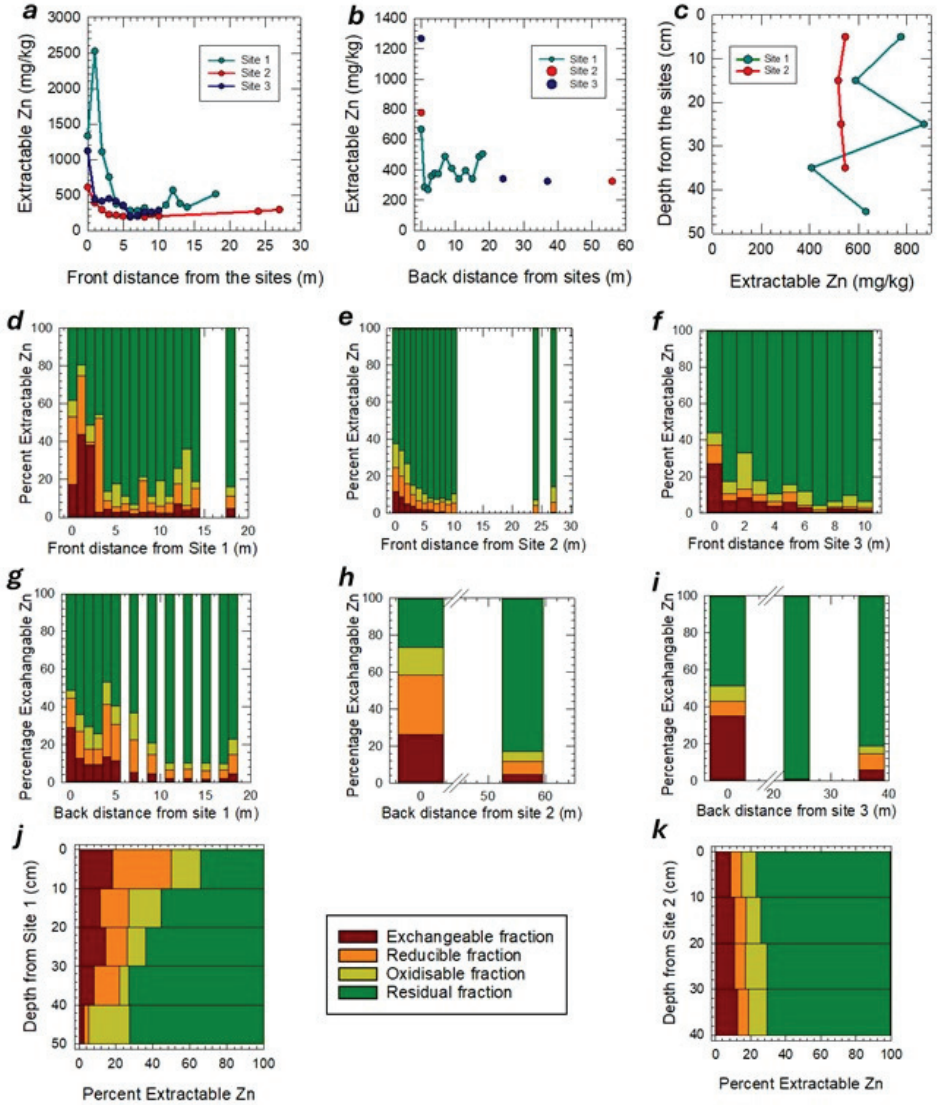

Figure 3. (**a**–**c**) The total extractable Zn from the three houses along the front, back, and vertical transects; (**d**–**f**) the proportional distribution of the four fractions across the front transect of each house; (**g**–**i**) the proportional distribution of the four fractions across the back transect of each house; and (**j**,**k**) the proportional distribution of the four fractions along the vertical transect of each house.

3.1.2. Cr, Mn, Fe, Co, Cu, and Cd

In the horizontal transects from all three sites, [$Cr_{T\text{-}EX}$] did not present conspicuous trends over horizontal and vertical transects (Figure 4). Across all the transects on the sites, the [$Cr_{T\text{-}EX}$] values averaged at 54 ± 12 mg/kg, 36 ± 7 mg/kg, and 35 ± 5 mg/kg. Across all the transects, Cr_{RES} dominated the speciation, increasing from a 78% contribution at 0 m to 92% at 18 m, while Cr_{OX} followed with a decrease from 20% at 0 m to 8% at 18 m at Site 1. In contrast, Cr_{EX} and Cr_{RED} contributed less than averages of 0.26 ± 1% and 0.05 ± 1% to $Cr_{T\text{-}EX}$. This trend was maintained in Sites 2 and 3 (Figure 4d–k). The average speciation

contributions in Site 2 were 0%, 2.8 ± 3%, 15.5 ± 8%, and 82 ± 9%, while in Site 3, they were 0%, 1.6 ± 1%, 14 ± 8%, and 85 ± 8%, respectively.

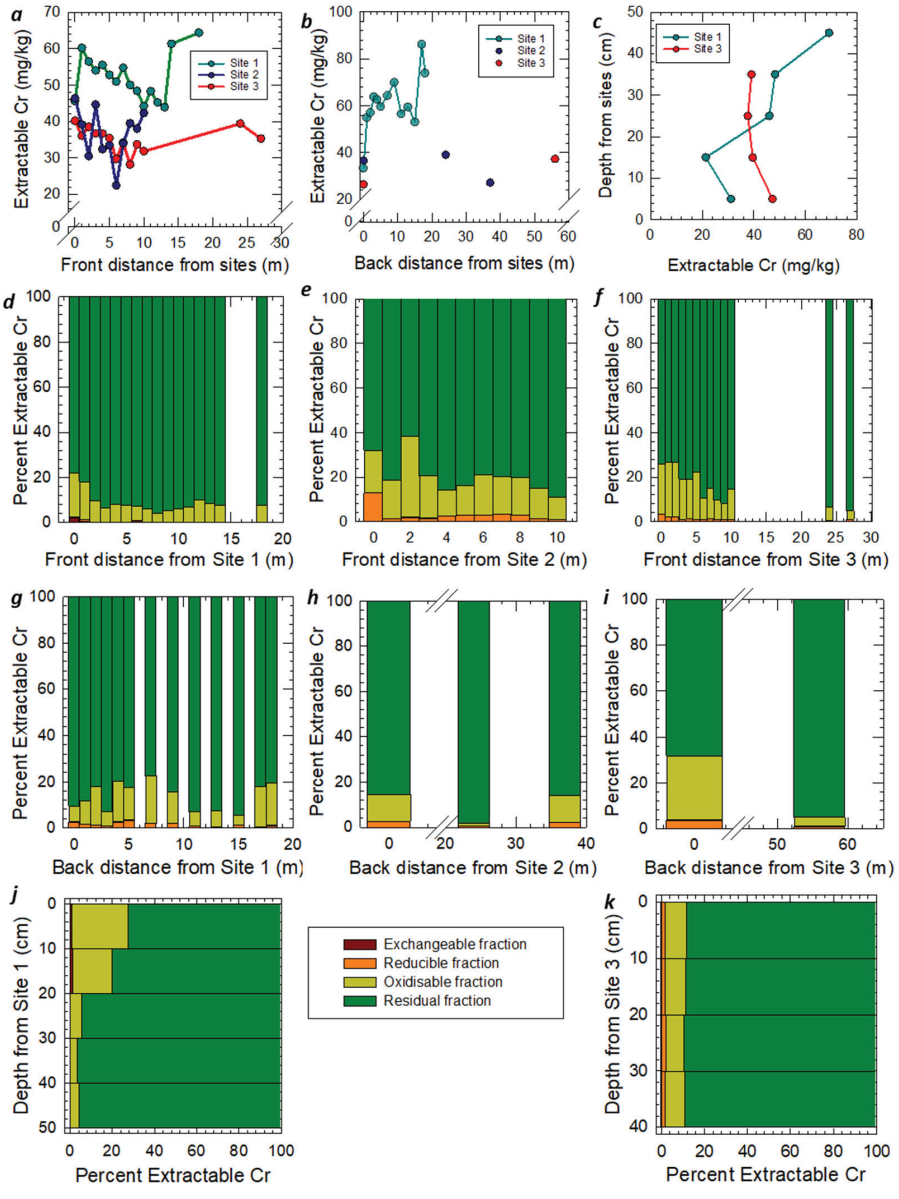

Figure 4. (**a**–**c**) The total extractable Cr from the three houses along the front, back, and vertical transects; (**d**–**f**) the proportional distribution of the four fractions across the front transect of each house; (**g**–**i**) the proportional distribution of the four fractions across the back transect of each house; and (**j**,**k**) the proportional distribution of the four fractions along the vertical transect of each house.

The total extractable Mn in the front horizontal transects in Site 1 was the lowest near the home and relatively constant beyond 5 cm, whereas the $[Mn]_{T\text{-}EX}$ values at Sites 2 and 3 were the highest near the homes and decreased with distance, with higher values

for Site 3 being found near the end of the transect. The values of $[Mn]_{T\text{-}EX}$ in the rear horizontal and vertical cores did not exhibit significant trends with distance or depth. The average $[Mn]_{T\text{-}EX}$ values from all samples for the three sites were 1457 ± 315 mg/kg, 910 ± 414 mg/kg, and 1087 ± 319 mg/kg (Figure 5a–c). Along the front transect at Sites 1, 2, and 3 (Figure 5d–f), the Mn_{EX} proportion decreased with an increasing distance from the homes. The percentage contribution of $[Mn]_{EX}$ varied from 36% to 19%, from 18% to 6%, and from 27% to 18%, respectively. In contrast, the Mn_{RES} and Mn_{OX} proportions remained relatively stable as the distance from the homes increased, with average percentage contributions of 33 ± 7% and 4 ± 1% in Site 1, 18 ± 9% and 3 ± 1% in Site 2, and 10 ± 7% and 3 ± 2% in Site 3, respectively. Across the horizontal back transect of the three sites, Mn_{RES} saw a slight increase in proportion with an increasing distance from the homes, with average concentrations shifting from 33% to 50%, from 55% to 57%, and from 63 to 85%, respectively. Along the back transect, no apparent trend was observed in Mn speciation (Figure 5g–i). The average percentage contribution of $[Mn]_{EX}$ across Sites 1, 2, and 3 were 23 ± 7%, 13 ± 5%, and 21 ± 1%, respectively. Mn_{RED} contributes average percentages of 45 ± 10%, 55 ± 25%, and 47 ± 18% to the $Mn_{T\text{-}EX}$ in Sites 1, 2, and 3, respectively. Along the vertical transect at Site 1, the percentage contribution of $[Mn]_{EX}$ decreased from 56% at 0 cm to 8% at 50 cm, while $[Mn]_{RES}$ increased from a 17% contribution at 0 cm to 66% at 50 cm with little change in the contributions of $[Mn]_{RED}$ and $[Mn]_{OX}$ with depth. The average percentage contributions of $[Mn]_{T\text{-}EX}$ were 34 ± 12% and 3 ± 1%, respectively. In contrast, in Site 3, the speciation of Mn with depth remained relatively constant. The average concentrations of Mn_{EX}, Mn_{RED}, Mn_{OX}, and Mn_{RES} were 17 ± 4%, 31 ± 3%, 1.5 ± 1%, and 51 ± 3%, respectively (Figure 5h–j).

The average weight percentages of $Fe_{T\text{-}EX}$ across the horizontal distance for the three homes were 8.9 ± 2%, 8.8 ± 2%, and 7.9 ± 2% at Sites 1, 2, and 3, respectively. In the vertical transect, the $Fe_{T\text{-}EX}$ content increased with depth, ranging from 3.93% at 0–10 cm to 12.9% at 40–50 cm at Site 1 and from 9.7% at 0–10 cm to 10% at 30–40 cm at Site 3 (Figure 6a–c). The speciation of Fe did not significantly change with distance or depth. The contribution of Al_{EX} across all transects was generally below the detection limit, while Al_{RED}, AL_{OX}, and Al_{RES} averaged at 2 ± 1%, 1.5 ± 2%, and 96 ± 3% (Site 1); 2 ± 1%, 1.6 ± 2%, and 96 ± 2% (Site 2); and 1.6 ± 1%, 1 ± 1%, and 97 ± 1% (Site 3), respectively (Figure 6d–k). In the vertical profile at Site 1, $Fe_{T\text{-}EX}$ increased with depth from the topsoil, concurrent with the decrease in both Fe_{OX} and Fe_{RED} with depth.

The concentration of Co did not exhibit noticeable trends over horizontal and vertical transects. Across the transects on the sites, the $Co_{T\text{-}EX}$ concentration averaged at 37 ± 21 mg/kg, 20 ± 4 mg/kg, and 18 ± 5 mg/kg in Sites 1, 2, and 3, respectively (Figure 7). Cobalt speciation across the front and back transects in the three homes remained relatively constant with an increasing distance from the homes. The average percentage contributions of the exchangeable, reducible, oxidizable, and residual fractions were 11 ± 8%, 15 ± 8%, 9 ± 6%, and 65 ± 16% in Site 1; 9 ± 4%, 7 ± 8%, 8.6 ± 2%, and 75.6 ± 9% in Site 2; and 15 ± 7%, 11 ± 4%, 10 ± 3%, 64 ± 9% in Site 3, respectively.

The concentration of total extractable Cu was the highest near the homes, measuring 186 mg/kg, 93 mg/kg, and 95 mg/kg in Sites 1, 2, and 3, respectively (Figure 8). The trend generally flattened at about 5 cm from the homes, contributing an average of 61 ± 23 mg/kg, 43 ± 3 mg/kg, and 42 ± 5 mg/kg, respectively, between 5 m and the end of the front horizontal transects. Along the back transect, $[Cu]_{T\text{-}EX}$ increased from 60 mg/kg to 99 mg/kg for Site 1 and remained relatively constant for Sites 2 and 3, with average values of 56 ± 12 mg/kg and 66 ± 1 mg/kg, respectively. Compared to Sites 2 and 3, Site 1 showed more variability along the horizontal transects. In contrast, the depth profile does not reveal a substantial change in concentration with depth at Site 1, averaging 54 ± 24 mg/kg, while Site 3 increased with depth from 268 mg/kg at 0–10 cm to 1636 mg/kg at 40–50 cm (Figure 8a–c). Although Cu speciation was dominated by the residual fraction, a significant fraction of Cu was in the oxidizable fraction (Figure 8) in contrast to the other metals. The values of $[Cu]_{OX}$ were typically the highest near the

homes and decreased with horizontal distance ranging from 37% to 10% (Site 1), 11% to 5% (Site 2), and 44% to 9% (Site 3) along the front transect (Figure 8d–f). The contribution of Cu_{EX} across the front transect of the sites was also the highest within three meters from the homes, with their highest proportions measuring 4.8% (Site 1), 4.6% (Site 2), and 3.7% (Site 3). The contribution of Cu_{RED} decreased with horizontal distance along the front transect from 7.6% to 2.5% at Site 1, from 8.4% to 1.6% at Site 2, and from 11% to 4.5% at Site 3. The concentration of Cu_{EX} at the back transect was below the instrument's detection limit across all homes. However, unlike the front transect, Cu_{OX} did not show a conspicuous trend, with average contributions of 13 ± 7%, 6 ± 6%, and 18 ± 6% at Sites 1, 2, and 3, respectively. The contributions of Cu_{RES} along the back transect also averaged at 4± 2%, 4 ± 4%, and 6.7 ± 1%, respectively. Along the vertical transect (Figure 8j,k), the percentage contribution of Cu_{RES} at Site 1 dominated the speciation and increased from 51% at 0–10 cm to 97% at 40–50 cm, while Cu_{OX} presented the inverse, decreasing from 47% at 0–10 cm to 2% at 40–50 cm. The reducible fraction contributed an average of 2.5 ± 2%. Conversely, at Site 3, the contribution of Cu_{EX} to $Cu_{T\text{-}EX}$ increased from 7% at 0–10 cm to 44% at 30–40 cm, while that of Cu_{RES} decreased from 51% at 0–10 cm to 17% at 30–40 cm. The average contributions of Cu_{EX} and Cu_{OX} were 24.8 ± 4% and 15.7 ± 5%.

The average $Cd_{T\text{-}EX}$ across the horizontal and vertical transects was higher in Site 1 (2 ± 2 mg/kg), followed by Site 2 (1.2 ± 1 mg/kg) and Site 3 (0.96 ± 1 mg/kg). Along the front transects, $Cd_{T\text{-}EX}$ was higher between one to three meters from the three homes, gradually decreasing with an increasing horizontal distance from them (Figure 9). Specifically, the $Cd_{T\text{-}EX}$ concentration decreased from 8 mg/kg, 2 mg/kg, and 2 mg/kg to 2 mg/kg, 0.9 mg/kg, and 0.9 mg/kg at Sites 1, 2, and 3, respectively. The residual fraction dominated Cd speciation across all the transects in the homes, while the Cd associated with the exchangeable fraction was only present in Site 1 and concentrated close to the home. The average percentage contributions of the exchangeable, reducible, oxidizable, and residual fractions in the soil were 15.6 ± 16%, 17 ± 19%, 0.4 ± 2%, and 66.7 ± 27% in Site 1; 0%, 3.7 ± 7%, 6.2 ± 13%, and 90 ± 13% in Site 2; and 6.5 ± 14%, 0%, and 93.5 ± 14% in Site 3. In Site 1, Cd speciation along the vertical transect decreased with depth from a 34% percentage contribution between 0 and 10 cm to 11% between 40 and 50 cm in the Cd_{EX} fraction, while the Cd_{RED} fraction decreased from an 81% percentage contribution between 0 and 10 cm to 0% between 40 and 50 cm. In contrast, the percentage contribution of the Cd_{RES} fraction increased from 15% between 0 and 10 cm to 89% between 40 and 50 cm. The residual fraction dominated the speciation of Cd in Site 3 and did not present any change in speciation.

3.1.3. Element Correlation Relationships

Strong significant positive correlations were observed between Pb and Zn (for $M_{T\text{-}EX}$ and across all fractions) and with other metals (Cr, Fe, Co, Cu, and Cd) (electronic annex and Table S2). In contrast, these metals exhibited a strong negative correlation with Mn. Other notable observed correlations included the following: (1) the soil organic content had a strong positive correlation with a range of elements (Mg, S, Ti, Mn, Fe, Co, Cu, Zn, Cd, and Pb) and sand-sized particles and (2) the total extractable sulfur in soils correlated strongly with the oxidizable fraction of a range of metals (Cr, Mn, Fe, Co, Cu, Zn, Cd, and Pb).

3.1.4. Changes in Speciation in Soils as a Function of Time Since Exterior Renovations

The sequential extraction results reveal that in soils immediately adjacent to the homes, the total extractable Pb and Zn (and the percentages of Pb and Zn in the exchangeable fraction) decreased as a function of time since exterior renovations occurred (i.e., when exterior Pb-based paints were removed) (Figure 10a,b). With an increasing time since renovation, $Pb_{T\text{-}EX}$ was 21,700 mg/kg at Site 1, 11,115 mg/kg at Site 2, and 1865 mg/kg at Site 3, and $Zn_{T\text{-}EX}$ was 2525 mg/kg at Site 1, 1120 mg/kg at Site 2, and 608 mg/kg at Site 3. The percentage of Pb_{EX} was 25% at Site 1, 14% at Site 2, and 6% at Site 3, and the

percentage of Zn_{EX} was 44% at Site 1, 27% at Site 2, and 12% at Site 3. This trend was not observed for other metals, for example, Mn and Cr (Figure 10c,d).

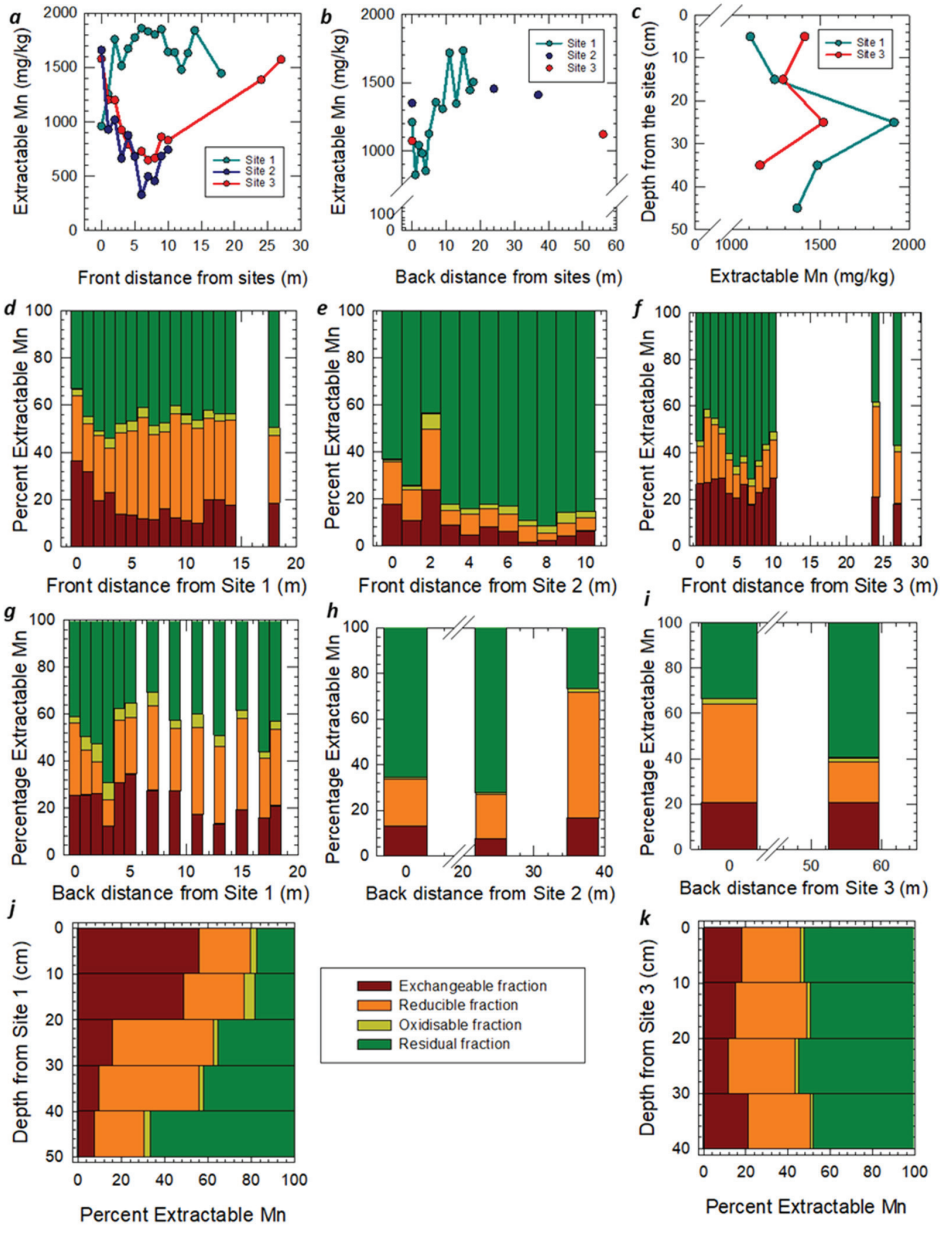

Figure 5. (**a**–**c**) The total extractable Mn from the three houses along the front, back, and vertical transects; (**d**–**f**) the proportional distribution of the four fractions across the front transect of each house; (**g**–**i**) the proportional distribution of the four fractions across the back transect of each house; and (**j**,**k**) the proportional distribution of the four fractions along the vertical transect of each house.

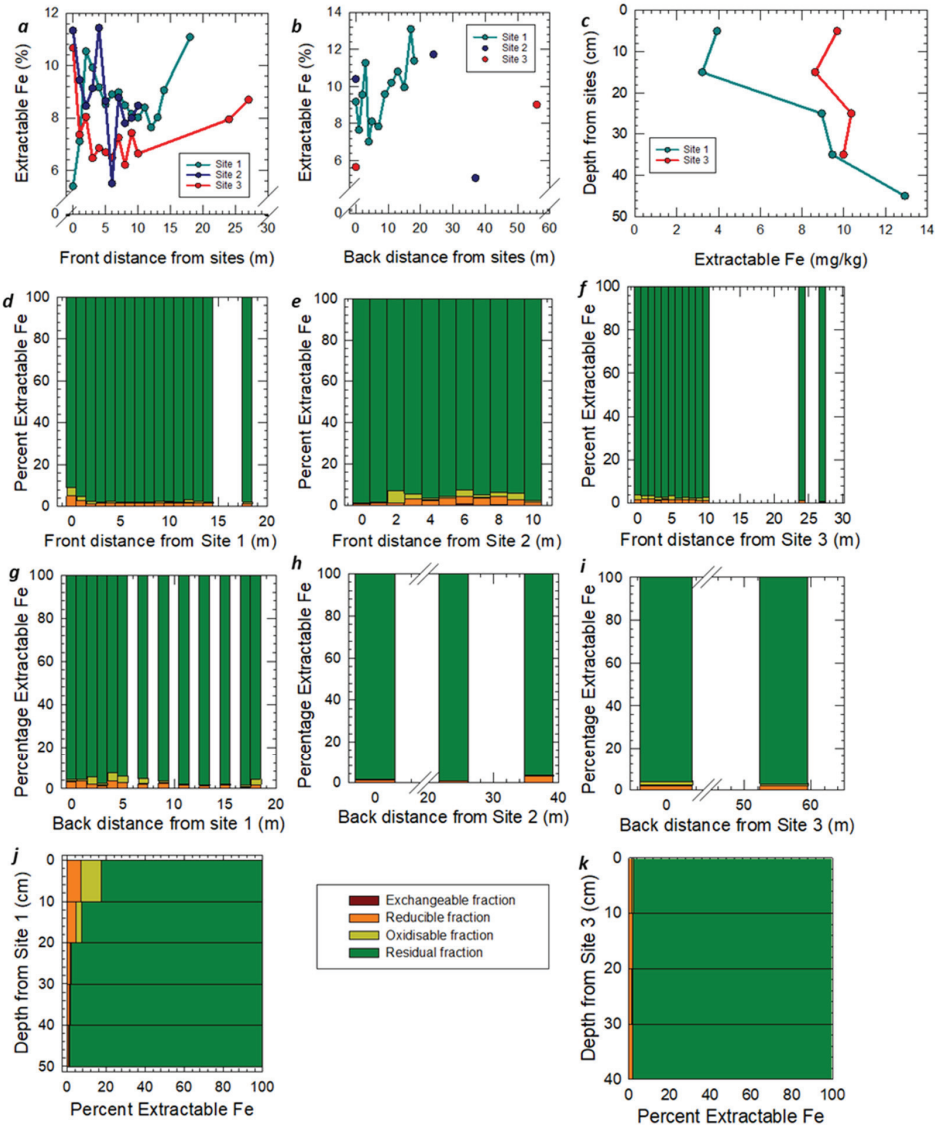

Figure 6. (**a**–**c**) The total extractable Fe from the three houses along the front, back, and vertical transects; (**d**–**f**) the proportional distribution of the four fractions across the front transect of each house; (**g**–**i**) the proportional distribution of the four fractions across the back transect of each house; and (**j**,**k**) the proportional distribution of the four fractions along the vertical transect of each house.

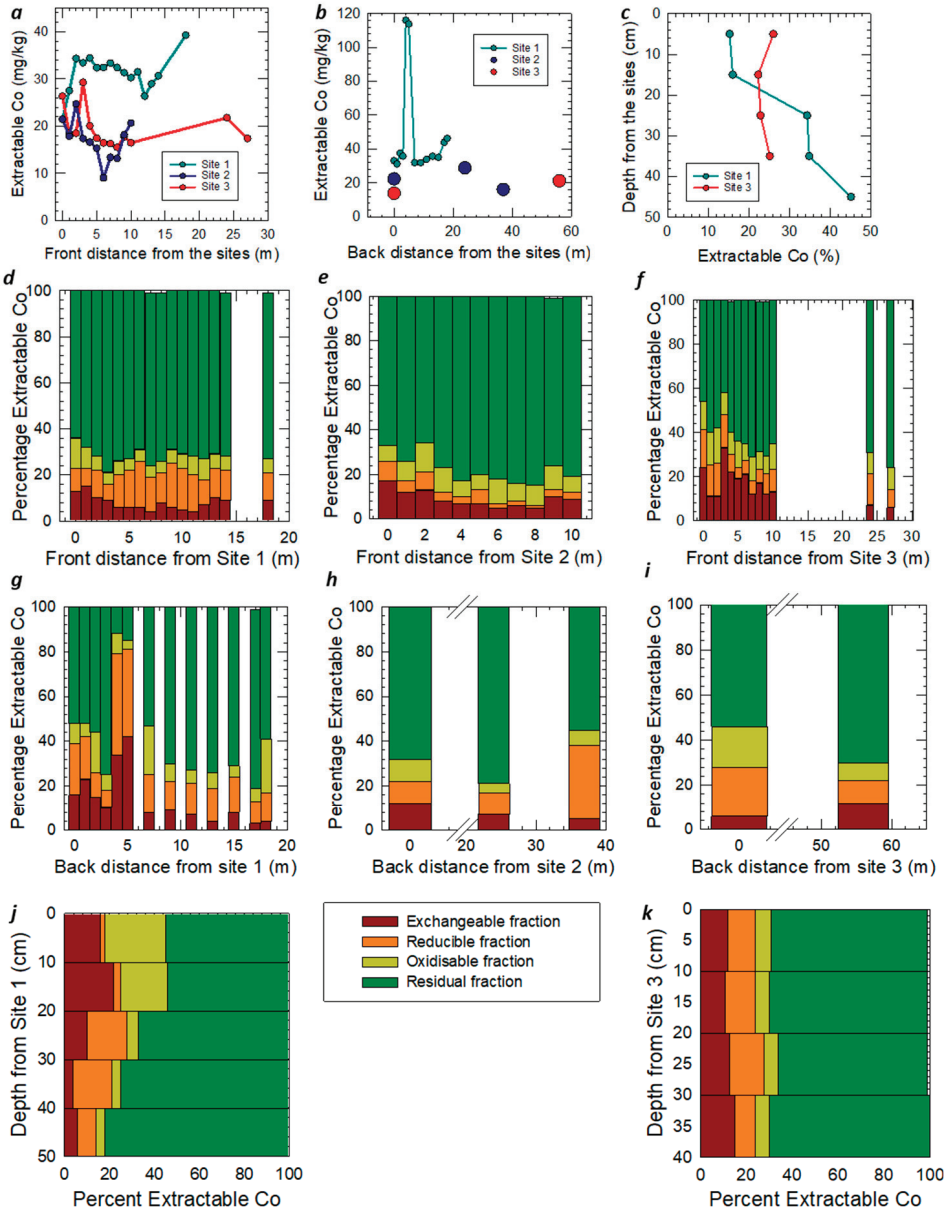

Figure 7. (**a**–**c**) The total extractable Co from the three houses along the front, back, and vertical transects; (**d**–**f**) the proportional distribution of the four fractions across the front transect of each house; (**g**–**i**) the proportional distribution of the four fractions across the back transect of each house; and (**j**,**k**) the proportional distribution of the four fractions along the vertical transect of each house.

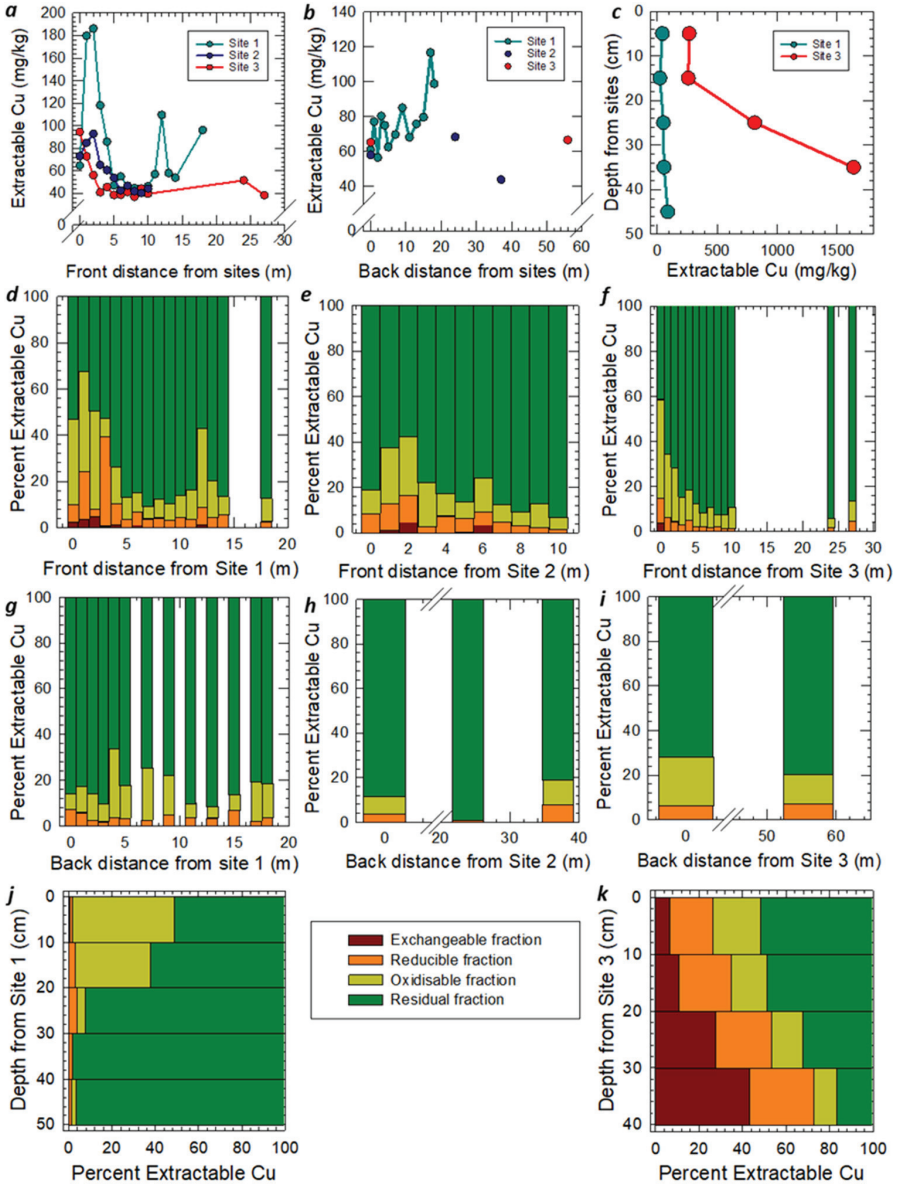

Figure 8. (**a**–**c**) The total extractable Cu from the three houses along the front, back, and vertical transects; (**d**–**f**) the proportional distribution of the four fractions across the front transect of each house; (**g**–**i**) the proportional distribution of the four fractions across the back transect of each house; and (**j**,**k**) the proportional distribution of the four fractions along the vertical transect of each house.

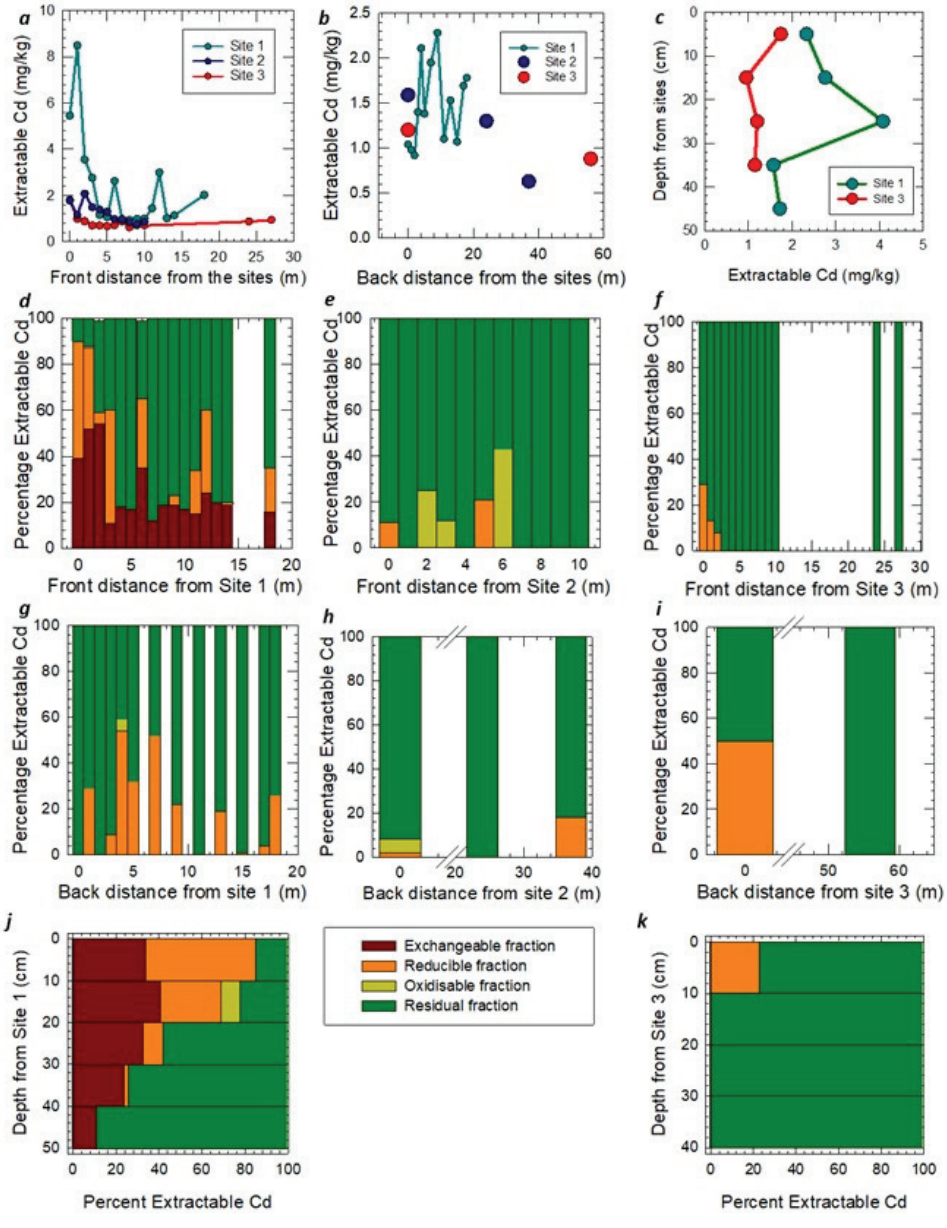

Figure 9. (**a**–**c**) The total extractable Cd from the three houses along the front, back, and vertical transects; (**d**–**f**) the proportional distribution of the four fractions across the front transect of each house; (**g**–**i**) the proportional distribution of the four fractions across the back transect of each house; and (**j**,**k**) the proportional distribution of the four fractions along the vertical transect of each house.

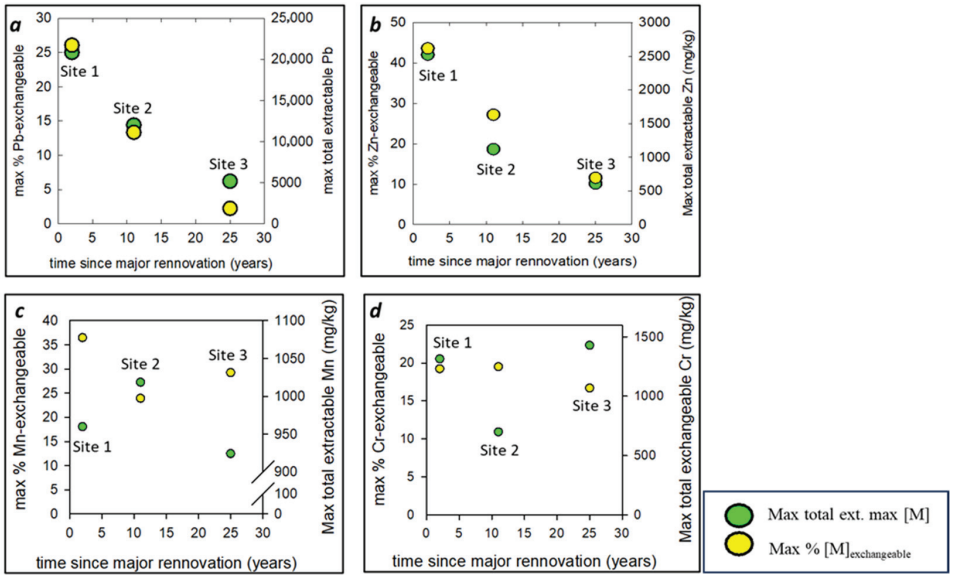

Figure 10. The maximum total extractable metals ($[M]_{T\text{-}EX}$) and maximum percentage exchangeable metals ($[M]_{EX}$) versus time since major renovation on the homes. (**a**) Pb, (**b**) Zn, (**c**) Mn, and (**d**) Cr for the soils collected immediately adjacent to the three homes.

3.2. Soil Solid Properties

3.2.1. Soil Organic Content

At Sites 1 and 3, the LOI values were the highest near the homes and decreased with distance. Their organic content decreased from 29% and 21% closest to the homes to 11% and 6% at the end of the transect, respectively (Figure 11a,c). In contrast, LOI at Site 2 was lower near the home and at the end of the transect, with a spike in LOI to 40% at 6 cm. The LOI values across the transect averaged at 16 ± 10% (Figure 11b). In the back transect, at Site 1, the organic content demonstrated a similar spatial variation. Starting at 4.5% at 0 m, LOI peaked at 5 cm (28%) and decreased with distance to 6% at 15 m. Further away, at 18 m from the home, the organic content measured 12% (Figure 11d). For both Site 2 and Site 3, which had fewer samples, the average LOI measurements were 5.5 ± 2% and 11 ± 2%, respectively (Figure 11e,f). Along the vertical transect, the LOI value was the highest at the topsoil at 43% and 7.2% at Sites 1 and 3, and it decreased with depth to 4.5% and 5%, respectively (Figure 11g,h). In general, higher LOI values correlated with higher concentrations and percentage contributions of Pb_{OX} (Figure S7).

3.2.2. Particle Size Distribution and Soil Mineralogy

Across the horizontal transects, the percentage contribution was invariant. Soils from the three sites were dominated by the silt fraction across all the transects, followed by the sand fraction and the clay fraction (Figure 12). The particle size distribution in the front and back transects were similar. The average amounts of sand, silt, and clay in the front and back transects were 42 ± 9%, 54 ± 8%, and 4 ± 1%, for Site 1; 52 ± 5%, 45 ± 5%, and 2.6 ± 1%, for Site 2; and 45 ± 7%, 52 ± 7%, and 3 ± 1%, for Site 3. The only profile that showed a change in distribution was the vertical profile in Site 1, where the sand percentage decreased from 58% (0–10 cm) to 40% (40–50 cm) along the vertical transect, while the clay fraction increased from 2% in topsoil to 6% (40–50 cm). Despite the fact that the sites were in three different parts of Akron, their bulk mineralogy contents were very similar (Figure 13). The soils across the transects in the sites were composed of quartz, feldspars (albite, orthoclase, and anorthite), micas (muscovite, biotite, and paragonite),

and clays (illite, kaolinite, montmorillonite, and chlorite). Across the sites, the average compositions of the soils were 57 ± 9% of quartz, 19 ± 10% of feldspars, 14 ± 6% of micas, and 9 ± 9% of clays at Site 1; 69 ± 9% of quartz, 16 ± 10% of feldspar, 16 ± 10% of mica, and 8 ± 3% of clays at Site 2; and 69 ± 7% of quartz, 18 ± 6% of feldspar, 9 ± 5% of mica, and 4 ± 3% of clays at Site 3 (Figure 13). In the topsoil near the Site 1 house, sub-mm white flakes were visually observed. These particles were found to be aggregates that contained irregularly shaped Pb-O-rich grains ranging from 1 to 25 μm (Figure 14). Notably, these particles were absent in deeper soils near the Site 1 house and along the horizontal transect. These grains are compositionally similar to Pb-bearing paint chips collected from the Site 1 house (Figure S8). Furthermore, no such particles were observed at Sites 2 or 3. The Pb-bearing aggregates were observed in a Ti-bearing background. Other Si-Al-O-rich particles, characteristic of common soil (alumino)silicate minerals, were observed forming aggregates with the Pb-bearing phases as well.

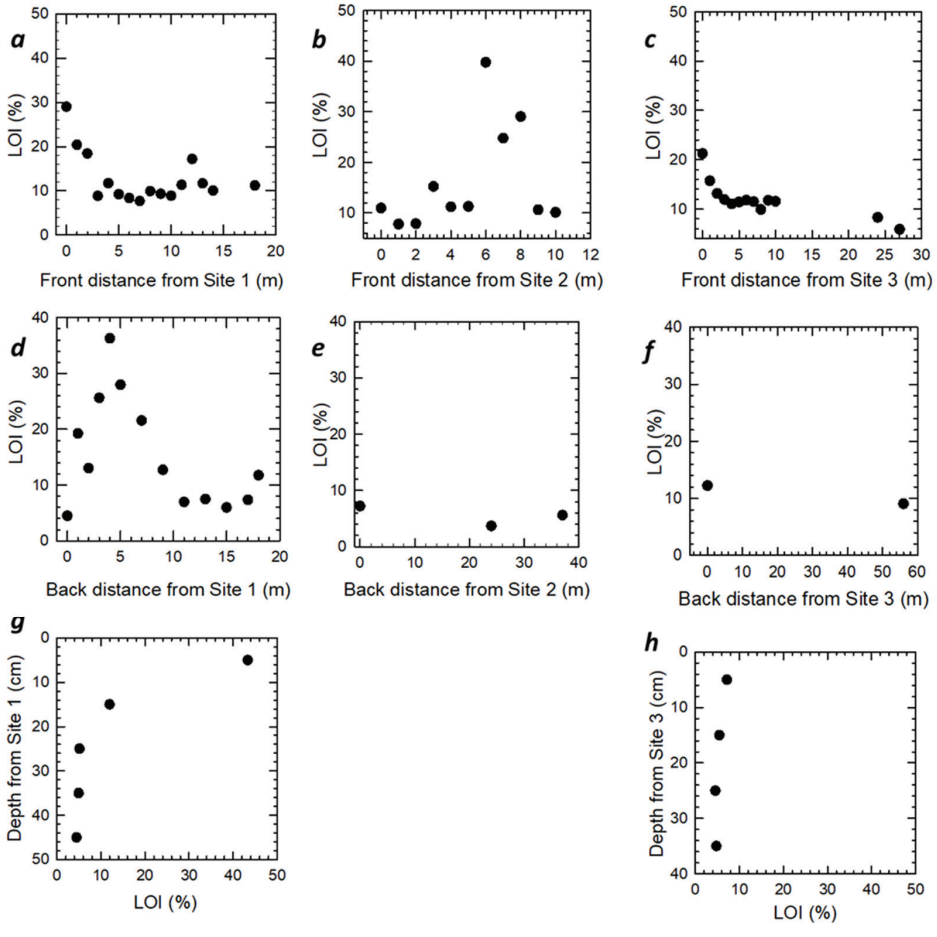

Figure 11. (**a**–**c**) Variability of loss on ignition (LOI) with horizontal distance along front transect of sites. (**d**–**f**) Variability of LOI with horizontal distance at back transect of sites. (**g**,**h**) Variability of LOI with vertical depth from sites.

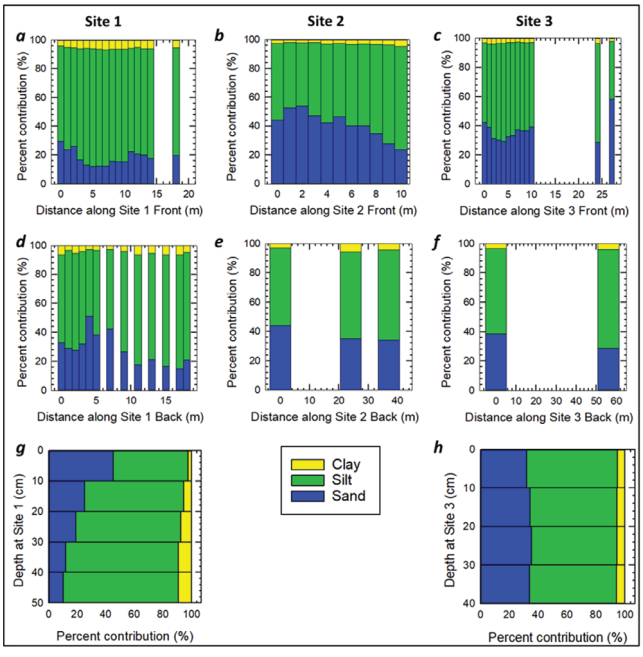

Figure 12. The percentage contributions of clay-, silt-, and sand-sized soils at the three sites (**a**–**c**) distributed across the front transects; (**d**–**f**) distributed across the back transects; and (**g**,**h**) distributed across the vertical transects.

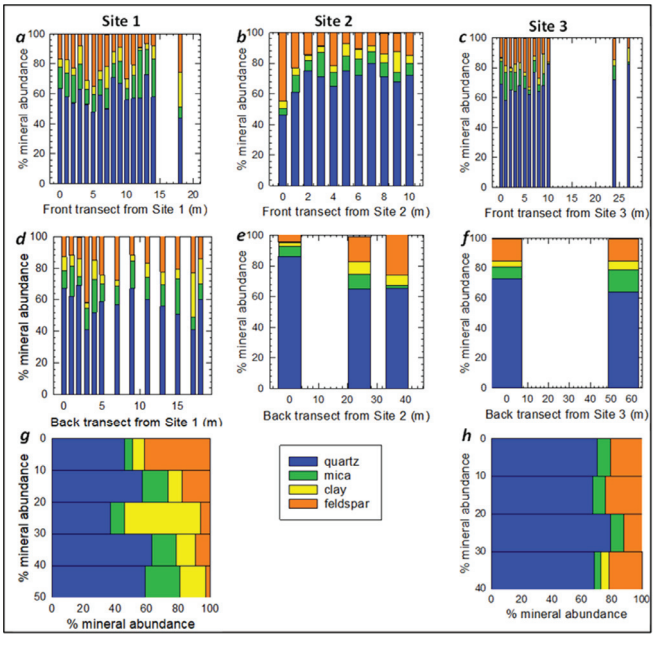

Figure 13. The percentage abundances of quartz, feldspars (albite, orthoclase, and anorthite), micas (muscovite, biotite, and paragonite), and clays (illite, kaolinite, montmorillonite, and chlorite) at the three sites (**a**–**c**) distributed across the front transects; (**d**–**f**) distributed across the back transects; and (**g**,**h**) distributed across the vertical transects.

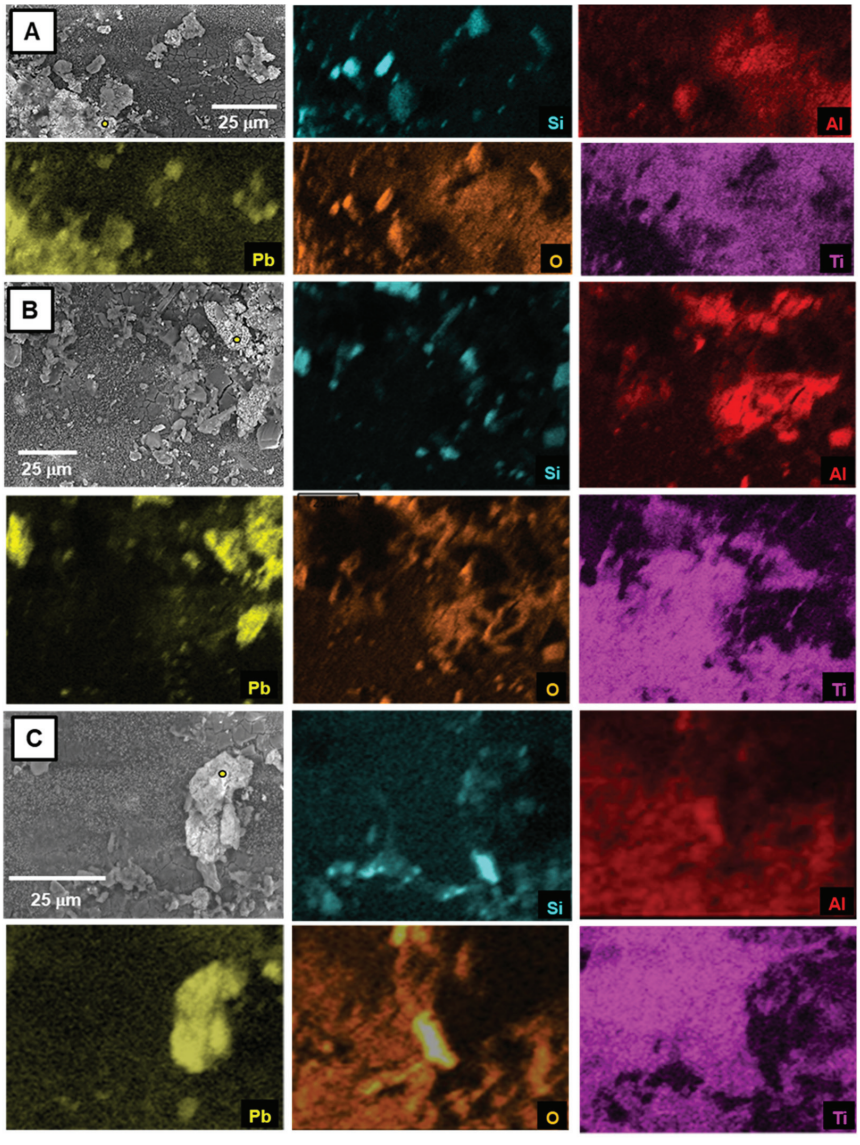

Figure 14. Representative SEM images (**A**–**C**) and EDS element maps (Si, Al, Pb, O, and Ti) for each image of Pb-bearing particles observed as white flakes present in shallow soils collected from areas immediately adjacent to the Site 1 house. The yellow spots in the SEM images indicate the positions of EDS spot analyses (see Table S4).

4. Discussion

4.1. Dominant Controls on Pb and Zn Speciation and Distribution Around Urban Homes

Lead and Zn were above local background concentrations (52 mg/kg and 91 mg/kg, respectively) [42] in all samples based on the total extractable Pb and Zn concentrations, indicating that Pb and Zn are more impacted by anthropogenic activities compared to other trace metals. With respect to current metal speciation present in the soils (when the soils were sampled in 2021), Pb and Zn were detected in all three labile fractions (exchangeable, reducible, and oxidizable) of the soil samples (Figures 2 and 3), indicating

that Pb and Zn have undergone complex (bio)geochemical reactions subsequent to the initial deposition given that typical Pb and Zn sources would not be dominated by the same fractions and/or be in the same proportions within those fractions. With respect to current speciation, the exchangeable fractions of Pb and Zn were shown to be dominated by metals weakly bound to clay minerals and other soil solids and soluble metal-bearing phases [43]. Clay minerals are effective sinks from metals such as Pb and Zn over a wide range of soil conditions [44,45] via the formation of Pb- and Zn-bearing surface sorption complexes [46]. Lead and Zn in the reducible fraction are commonly dominated by Fe-(oxy)hydroxides [47], consistent with our observation of Pb and Zn correlated with Fe (electronic annex). Lead and Zn sorption to Fe-(oxy) hydroxides has commonly been observed in contaminated soils [16]. Manganese oxides are also known to effectively sequester Pb and Zn [48,49]; however, in Akron soils, there is no evidence that the Mn oxides are sequestering Pb and Zn. Manganese was negatively correlated with Pb and Zn (electronic annex), indicating that Mn-bearing phases are likely not a dominant sink for Pb and Zn. Although Mn oxides are recognized as effective sorbents of Pb [48], the results suggest that Fe oxides are the dominant sink for Pb and Zn in this fraction and are outcompeting Mn oxides. It is likely that the sorption of Pb was dominated by Fe oxides in these soils given their higher abundance based on the higher total extractable concentration of Fe compared to Mn oxides based on the average values of 0.1 wt% for $Mn_{T\text{-}EX}$ and 0.9 wt% for $Fe_{T\text{-}EX}$ across all the sites (Figures 5 and 6). Lead and Zn in the oxidizable fraction are typically dominated by solid organic matter [50]. The proportions of Pb and Zn associated with organic matter remained relatively constant throughout the horizontal transect. Flower beds near homes and trees along the horizontal transects correlate with the higher LOI (Figure 7), supporting the observations that increased organic input in the soil offers more binding sites for Pb in the oxidizable fraction [51]. Lastly, Pb and Zn in the residual fraction are likely bound within phosphates and other recalcitrant phases [43,52].

The total extractable Pb and Zn also varied with distance and depth, and the $Pb_{T\text{-}EX}$ and $Zn_{T\text{-}EX}$ concentration distributions align with previous findings showing that the concentrations of Pb and Zn in the soil decreases with an increasing distance from the homes due to the deposition of exterior Pb-based paint from homes into the soils [53]. Furthermore, at Site 1, soil particles consistent with paint chips observed near the home (Figure 14) suggested that the homes are the primary source of Pb. Similarly, zinc roofing sheets, identified as a prominent source of Zn deposition in residential areas [54,55], were used to finish the Akron homes, likely serving as the main source of Zn in the soils as the roofing sheets weather. In contrast, higher concentrations of Pb and Zn near structures have been attributed to the role structures play in trapping fine metal particles during wind transportation from more distant sources [10,56]. However, the presence of paint chips in the soil close to the Site 1 home suggests that the homes are more likely the dominant metal source. Increases in Pb and Zn near the road at Site 1 suggests the potential trapping of Pb from legacy automobile emissions in the roadside soils. The deposition of Pb and Zn here is more likely the result of historic leaded gasoline use and the wearing of Zn-bearing brake pads [57]. The higher Pb and Zn concentrations near the road at Site 1 and not at Sites 2 and 3 are also consistent with the higher traffic density at Site 1, which is closer to Akron's urban core. With respect to vertical speciation and distribution, the concentrations of $Pb_{T\text{-}EX}$ and $Zn_{T\text{-}EX}$ decreased with depth. This decline is likely due to metal leaching, where a small fraction of the Pb and Zn migrate from the topsoil [28]. Physical processes, such as erosion and metal translocation, along depth profiles, have also been proposed to account for variations in metal concentration with depth [11].

In addition to changes in concentration, Pb and Zn exhibited changes in speciation, most notably that the percentages of Pb and Zn in the exchangeable and reducible fractions were the highest near the homes and decreased with distance, with greater percentages of Pb and Zn being found in the residual fraction furthest from the homes. These results are consistent with a more labile source of Pb and Zn sourced from the homes and less labile Pb and Zn further from the homes that would be more consistent with background

concentrations and speciation [58]. The percentages of Pb and Zn associated with the oxidizable fraction varied much less than the other fractions, and in general, higher LOI values corresponded to slightly higher percentages of Pb and Zn in the oxidizable fraction (Figures 2 and 3), which is consistent with a high affinity of soil organic matter for Pb and Zn [59]. Ultimately, the current speciation and distribution of Pb and Zn in the soils is likely controlled by Pb and Zn being sourced primarily from the homes, although speciation changes with the time since deposition.

4.2. Factors That Control Changes in Pb and Zn Speciation over Time

The three Akron homes underwent major external renovations at 2, 11, and 25 years prior to the collection of soil samples (for Sites 1, 2, and 3, respectively). These renovations included the removal of Pb-based paint from the exteriors and alterations to the home siding and roofs. Such actions are known to result in the rapid addition of high concentrations of Pb and Zn to adjacent soils, particularly in labile forms [60–62]. The impact of renovations was observed as a high proportion of Pb and Zn in the exchangeable fraction close in the soils immediately adjacent to the homes (Figures 2 and 3). Furthermore, the speciation and total extractable amounts of Pb and Zn exhibited a linear change with time since renovation, with a decrease in $M_{T\text{-}EX}$ and a shift in speciation from the exchangeable to the reducible fraction (Figure 10a,b). Given that the ongoing addition of Pb and Zn to the soils from the homes was likely minimal compared to the period during renovations, the decrease in total Pb and Zn likely reflects the leaching and erosion of metals as aqueous and/or colloidal species [11,63]. The continual leaching of Pb and Zn without the additional introduction of new high concentrations would result in Site 3 having the lowest $M_{T\text{-}EX}$ concentrations and Site 1 having the highest concentrations based on the time since renovation and independent of the age of the house. Concurrent with decreases in the total extractable Pb and Zn, the proportions of exchangeable Pb and Zn in the soil decreased with corresponding increases in Pb and Zn in the reducible fraction (Figures 2 and 3). This change in speciation from more labile phases (i.e., dominated by the exchangeable fraction) to less labile and slightly more recalcitrant phases (i.e., dominated by the reducible fraction) over time is consistent with previous observations of the weathering of Pb- and Zn-bearing phases in soil [64]. The primary source of Pb from the exterior of the homes would have been Pb-bearing paint, which can include Pb oxides, Pb carbonates, and Pb sulfates [17,65]. The weathering of deposited Pb-bearing paint chips results in the formation of $Pb(OH)_2$ and, ultimately, the release of aqueous Pb(II) [66]. The primary source of Zn from galvanized roofs is metallic zinc [67]. Similarly to Pb, the weathering of the Zn coating from roofing sheets produces Zn carbonates and oxides, which further liberate aqueous Zn(II) during weathering [68]. Over time, as labile Pb- and Zn-bearing proceed through weathering, a fraction of the Pb and Zn would be lost to leaching and mobilization, while some would be re-sequestered by Fe-(oxy)hydroxides, resulting in the observed decrease in $[M_{T\text{-}EX}]$ and increase in percentage of M_{EX} over time. Furthermore, given the similar soil pH values of the three sites (Table S2), it is unlikely that changes in soil porewater dominate the observed changes in Pb and Zn speciation between the three homes.

The rapid addition of a pulse of Pb and Zn to soil at a known time provides a unique opportunity to calculate the subsequent loss rate of Pb and Zn for the broader region based on similar soil properties. The observed changes in total extractable Pb and Zn and changes in speciation exhibited linear changes over time, although it is possible that these trends will be non-linear over long time periods. The rates of Pb and Zn loss in the soils were 845 mg/kg/year ($R^2 = 0.97$) and 79 mg/kg/year ($R^2 = 0.86$), respectively, over a two-decade period. A related study conducted within an urban metropolis reported lower rates within a 15-year time period, with soil Pb loss at 2.4 mg/kg/year [28]. It is noteworthy that the soil Pb concentrations in that study ranged from 54 to 99 mg/kg, which are significantly lower than those observed in the Akron homes, indicating potential non-linearity in Pb loss over time when lower Pb concentrations are reached. Similarly, Zn has been reported to have a faster loss rate (up to 58%) in soils compared to other potentially toxic elements,

such as Cd, Cu, and Pb [69,70]. It was also possible to determine the rate of change in Pb and Zn from the exchangeable to reducible form, which was 0.79%/year for Pb (R^2 = 0.96) and 1.37%/year for Zn (R^2 = 0.98). Ultimately, the relative proportions of Pb and Zn in the exchangeable and reducible fractions at the three homes suggest that speciation is changing over the decadal time scale. Further work is warranted to find homes with a broader time range of renovations and metal speciation to determine the relationship in metal loss and potential non-linear behavior over longer time periods and/or a broader range of soil Pb and Zn concentrations.

4.3. Anthropogenic Impacts on Other Trace Metals in Urban Soils

Other metals, such as Cu, Mn, Co, Cr, and Cd, are also prone to anthropogenic impact in soils. The maximum total extractable concentrations of these metals in the Akron topsoil were 186 ppm for Cu; 1862 ppm for Mn; 116 ppm for Co; 86 ppm for Cr; and 8 ppm for Cd (with the highest values being observed at Site 1) (Figures 4, 5 and 7–9). All of these values exceeded their background concentrations in soils from this metropolitan area, namely Cu (37 ppm), Mn (30 ppm), Co (20 ppm), Cr (19 ppm), and Cd (0.8 ppm) [71], which is consistent with evidence of anthropogenic impact at varying degrees. The elevated concentrations of $Cu_{T\text{-}EX}$ and $Cr_{T\text{-}EX}$ above the background have been linked to metal release during the wear and tear of the braking system in automobiles [72,73]. The elevated Mn concentrations could be the result of a complex mix of anthropogenic and natural sources, including electronic wastes, pesticides, plant organic matter, and Mn-rich fertilizers for gardening [74]. The speciation of Cu, Cr, and Mn also varied in the soils. Compared to other metals, large fractions of Cr and Cu were observed in the oxidizable fraction of the Akron soils (Figures 4 and 8), which is consistent with findings from similar studies which observed the high affinity these metals have with organic matter [75,76]. The large pools of Cu and Cr in the residual fraction are also consistent with previous studies of urban soils [69,77–79]. The labile fractions of Cu and Cr positively correlated with Pb and Zn, which seem to be driven by combustion emissions and vehicle wear-off. The concentration of Mn in the Akron soils dominated the labile fractions, aligning with another study which investigated the fractionation of heavy metals in urban soils [69]. Conversely, another study found Mn in the soil predominantly in the reducible fraction [80]. Manganese may have become labile upon release into the Akron soil, subsequently being associated with both exchangeable and reducible fractions (Figure 5). The exchangeable fraction of Mn positively correlates with LOI (electronic annex), suggesting that Mn is associated with the organic content around the homes and is readily released into the soils. The reactive portion of Cd in the soils is dominated by the reducible fraction (Figure 9), which seems to include contributions from anthropogenic sources such nickel–cadmium batteries and landfill leachates [81,82]. Cadmium in urban soils has also been linked to its historical use in producing glass and paint pigments [83,84]. The positive correlation among Cd, Zn, and Pb, coupled with the elevated concentration of labile Cd near the homes, indicates that there is a common source, which is likely to be the homes. Ultimately, in comparison to Pb and Zn, the Akron soils are less anthropogenically influenced by Cu, Mn, Co, Cr, and Cd, as shown by their total extractable concentrations and distribution profiles.

5. Conclusions

This study revealed that the distribution and chemical speciation of Pb and Zn at the house lot scale vary both spatially and temporally. With respect to space, the Pb and Zn concentrations are the highest closest to the homes, with speciation being dominated by more labile fractions in soils immediately adjacent to the homes, and more recalcitrant fractions are dominant towards the edge of the home properties. These results suggest that the homes are the dominant source of Pb and Zn leaching into soils as a result of exterior renovations and the flaking off of Pb-based paint and Zn-bearing materials. With respect to temporal variation, longer times since renovations resulted in lower Pb and Zn concentrations as well as smaller fractions of labile Pb and Zn. These results are

consistent with previous studies that have shown the importance of the release of Pb from the exterior of older homes as an important source of Pb to soils; however, the current results bring to focus the acute risk of exposure to more labile Pb immediately following exterior renovations and damage to home exteriors in areas of older housing stock. These results suggest that screening soils as part of a hazard assessment should not be a one-time occurrence but rather be conducted in response to changes in housing development. Furthermore, screening should take into account speciation and the fraction of total Pb that is labile. For example, the U.S. Environmental Protection Agency's nationwide screening level for Pb in residential properties is 200 mg/kg, and for properties with multiple Pb sources (e.g., lead water service lines and lead-based paint), it is 100 mg/kg [85]. However, these standards refer to the total Pb concentration and do not account for the potentially bioaccessible fractions. Assuming that the total extractable amount of Pb is approximately one third of the total Pb [16], then approximately half of all the soil samples in the current study (and all of the samples within 4 m of the homes) would exceed the screening level. However, given that speciation changes over time, it would be most critical to assess the potential risk of exposure immediately after performing renovations.

The results presented here also highlight the value of using sequential extraction methods as a cost-effective method for determining metal speciation, which can inform remediation efforts. For example, based on the 'bullseye' pattern of Pb speciation and distribution surrounding the homes, targeted remediation would only need to treat or cover soils closest to the homes within approximately 5 m, where Pb concentrations are the highest (i.e., above the EPA action limit of 200 mg/kg), which accounts for a fraction of the total property (approximately 30% for Site 1 and approximately 10% for Sites 2 and 3) rather than needing to treat soil across the entire property. These results also highlight the need for a balanced sampling density plan across an urban landscape, where low-density sampling could result in the risk of Pb exposure being underestimated (if the samples are only taken near the edges of properties) or overestimated (if the samples are only taken from areas immediately adjacent to homes). In areas of older housing stock with a high proportion of homes that have recently undergone renovation or have been damaged, it would be critical to balance broad soil sampling across a neighborhood with a more targeted sampling effort at some homes to determine if the bullseye patterns of Pb speciation and distribution are observed to better constrain the risk of exposure. Finally, given the high fraction of labile Pb in the soils, a more thorough assessment of physical speciation (i.e., discrete grains of Pb-bearing phases versus aggregates of Pb-bearing grains coating larger grains) is warranted to determine the risk of exposure through the remobilization of Pb into wind-blown dust and aerosols.

Supplementary Materials: The following supporting information can be downloaded at https://www.mdpi.com/article/10.3390/soilsystems8040113/s1, Figure S1: Site photos; Figure S2: Al speciation and distribution; Figure S3: S speciation and distribution; Figure S4: K speciation and distribution; Figure S5: Ca speciation and distribution; Figure S6: Ti speciation and distribution; Figure S7: Comparison of LOI and $Pb_{OX'}$; Figure S8: SEM-EDS analysis of Pb-bearing paint chip; Table S1: Number of soil samples collected along the front, back, and vertical transects of each house (represented as site) within the study area. Horizonal samples were primarily collected in 1 m increments; the cores were collected in 10 cm increments. Table S2: pH measurement of the soil locations closest to the homes. Table S3: Calculated *p*-values for the correlations between $[M]_{T\text{-}EX}$ across the front transect of Site 1, with an alpha level set at 0.05. Table S4: Energy Dispersive X-ray Spectrometry spot analyses of grains A, B, and C. The SI document also includes ICP-OES data and a correlation matrix of all experimental variables.

Author Contributions: The contributions of each author to this project are as follows: Conceptualization, C.E.N. and D.M.S.; Methodology, C.E.N. and D.M.S.; Validation, D.M.S. and A.C.T.; Formal Analysis, C.E.N., A.C.T., R.I. and C.H.; Investigation, C.E.N., D.M.S., A.C.T., R.I. and C.H.; Resources, D.M.S.; Data Curation, D.M.S.; Writing—Original Draft, C.E.N. and D.M.S.; Writing—Review and Editing, C.E.N. and D.M.S.; Visualization, C.E.N. and D.M.S.; Supervision, D.M.S.; Project Adminis-

tration, D.M.S.; and Funding Acquisition, C.E.N. and D.M.S. All authors have read and agreed to the published version of the manuscript.

Funding: This research received no external funding.

Institutional Review Board Statement: Not applicable.

Informed Consent Statement: Not applicable.

Data Availability Statement: All data are contained within the article or Supplementary Materials.

Acknowledgments: We are grateful to the three Akron-area homeowners for providing access to their properties. The authors also thank Madison Wood for helping with sample collection and Timothy Gallagher for providing assistance with the ICP-OES data analysis. We thank the three anonymous reviewers for providing constructive comments.

Conflicts of Interest: The authors declare no conflicts of interest.

References

1. Ali, E.; Sheet, E. New Anti-knock Additives to Improve Gasoline Octane Number. *J. Pet. Res. Stud.* **2011**, *3*, 1–14.
2. EESI. A Brief History of Octane in Gasoline: From Lead to Ethanol [Internet]. Environmental and Energy Study Institute. 2016. Available online: https://www.eesi.org (accessed on 10 September 2023).
3. Collin, M.S.; Venkatraman, S.K.; Vijayakumar, N.; Kanimozhi, V.; Arbaaz, S.M.; Stacey, R.G.S.; Anusha, J.; Choudhary, R.; Lvov, V.; Tovar, G.I.; et al. Bioaccumulation of lead (Pb) and its effects on human: A review. *J. Hazard. Mater. Adv.* **2022**, *7*, 100094. [CrossRef]
4. Rooney, A.A.; Boyles, A.L.; Taylor, K. *NTP Monograph: Health Effects of Low Level Lead*; National Toxicology Program: US Department of Health and Human Services: Washington, DC, USA, 2012.
5. Gilbert, S.G.; Weiss, B. A rationale for lowering the blood lead action level from 10 to 2 µg/dL. *NeuroToxicology* **2006**, *27*, 693–701. [CrossRef]
6. Egan, K.B.; Cornwell, C.R.; Courtney, J.G.; Ettinger, A.S. Blood lead levels in U.S. children ages 1–11 years, 1976–2016. *Environ. Health Perspect.* **2021**, *129*, 037003. [CrossRef]
7. Brown, M.J.; Margolis, S. Lead in Drinking Water and Human Blood Lead Levels in the United States. *Morbidity Mortality Wkly. Rep.* **2012**, *61*, 1–9.
8. Hauptman, M.; Niles, J.K.; Gudin, J.; Kaufman, H.W. Individual- and Community-Level Factors Associated with Detectable and Elevated Blood Lead Levels in US Children: Results from a National Clinical Laboratory. *JAMA Pediatr.* **2021**, *175*, 1252–1260. [CrossRef]
9. Yeter, D.; Banks, E.C.; Aschner, M. Disparity in risk factor severity for early childhood blood lead among predominantly Afri-can-American black children: The 1999 to 2010 US NHANES. *Int. J. Environ. Res. Public Health* **2020**, *17*, 1552. [CrossRef]
10. Mielke, H.W.; Anderson, J.C.; Berry, K.J.; Mielke, P.W.; Chaney, R.L.; Leech, M. Lead Concentrations in Inner-City Soils as a Factor in the Child Lead Problem. *Am. J. Public Health* **1983**, *73*, 1366–1369. [CrossRef] [PubMed]
11. Wade, A.M.; Richter, D.D.; Craft, C.B.; Bao, N.Y.; Heine, P.R.; Osteen, M.C.; Tan, K.G. Urban-soil pedogenesis drives contrasting legacies of lead from paint and gasoline in city soil. *Environ. Sci. Technol.* **2021**, *55*, 7981–7989. [CrossRef]
12. Brinkmann, R. Lead pollution in soils in Milwaukee county, Wisconsin. *J. Environ. Sci. Health Part A Environ. Sci. Eng. Toxicol.* **1994**, *29*, 909–919. [CrossRef]
13. Mielke, H.W. Nature and extent of metal-contaminated soils in urban environments (keynote talk). *Environ. Geochem. Health* **2016**, *38*, 987–999. [CrossRef] [PubMed]
14. Wilken, R.D. Metal Species. In *Environmental Analysis*, 3rd ed.; Kleibohmer, W., Ed.; Elsevier Science: Amsterdam, The Netherlands, 2021; pp. 263–275.
15. Sowers, T.D.; Blackmon, M.D.; Wilkin, R.T.; Rovero, M.; Bone, S.E.; Jerden, M.L.; Nelson, C.M.; Bradham, K.D. Lead Speciation, Bioaccessibility, and Sources for a Contaminated Subset of House Dust and Soils Collected from Similar United States Residences. *Environ. Sci. Technol.* **2024**, *58*, 9339–9349. [CrossRef] [PubMed]
16. Santoro, N.; Singer, D.M.; Mulvey, B.K.; Halasa, K.; Teutsch, N.; Shedleski, A.; Wood, M. Neighborhood-scale lead (Pb) speciation in Akron, Ohio (USA) soils: Primary sources, post-deposition diagenesis, and high concentrations of labile Pb. *Environ. Geochem. Health* **2024**, *46*, 164. [CrossRef] [PubMed]
17. Beauchemin, S.; MacLean, L.C.W.; Rasmussen, P.E. Lead speciation in indoor dust: A case study to assess old paint contribution in a Canadian urban house. *Environ. Geochem. Health.* **2011**, *33*, 343–352. [CrossRef]
18. Chaney, R.L.; Mielke, H.W. Speciation, Mobility and Bioavailability of Soil Lead. *Environ. Geochem. Health* **1989**, *11*, 105–129. Available online: https://www.researchgate.net/publication/284048911 (accessed on 31 January 2020).
19. Mielke, H.W.; Powell, E.T.; Shah, A.; Gonzales, C.R.; Mielke, P.W. Environmental Health Perspectives • VOLUME [Internet]. Volume 109. 2001. Available online: http://ehpnet1.niehs.nih.gov/docs/2001/109p973-978mielke/abstract.html (accessed on 31 January 2020).
20. Seyferth, D. The Rise and Fall of Tetraethyllead. *Organometallics* **2003**, *22*, 5154–5178. [CrossRef]

21. Wuana, R.A.; Okieimen, F.E. Heavy Metals in Contaminated Soils: A Review of Sources, Chemistry, Risks and Best Available Strategies for Remediation. *ISRN Ecol.* **2011**, *2011*, 402647. [CrossRef]
22. Plumlee, G.S.; Morman, S.A.; Ziegler, T.L. The toxicological geochemistry of earth materials: An overview of processes and the interdisciplinary methods used to understand them. *Rev. Miner. Geochem.* **2006**, *64*, 5–57. [CrossRef]
23. Casteel, S.W.; Weis, C.P.; Henningsen, G.M.; Brattin, W.J. Estimation of relative bioavailability of lead in soil and soil-like materials using young swine. *Environ. Health Perspect.* **2006**, *114*, 1162–1171. [CrossRef]
24. Davis, A.; Drexler, J.W.; Ruby, M.V.; Nicholson, A. Micromineralogy of Mine Wastes in Relation to Lead Bioavailability, Butte, Montana. *Environ. Sci. Technol.* **1993**, *27*, 1415–1425. [CrossRef]
25. Yan, K.; Dong, Z.; Naidu, R.; Liu, Y.; Li, Y.; Wijayawardena, A.; Sanderson, P.; Li, H.; Ma, L.Q. Comparison of in vitro models in a mice model and investigation of the changes in Pb speciation during Pb bioavailability assessments. *J. Hazard. Mater.* **2020**, *388*, 121744. [CrossRef] [PubMed]
26. Hauptman, M.; Bruccoleri, R.; Woolf, A.D. An Update on Childhood Lead Poisoning. *Clin. Pediatr. Emerg. Med.* **2017**, *18*, 181–192. [CrossRef] [PubMed]
27. Mielke, H.W.; Reagan, P.L. Soil Is an Important Pathway of Human Lead Exposure. *Environ. Health Perspect.* **1998**, *106*, 217. [CrossRef]
28. Mielke, H.W.; Gonzales, C.R.; Powell, E.T.; Laidlaw, M.A.S.; Berry, K.J.; Mielke, P.W., Jr.; Egendorf, S.P. The concurrent decline of soil lead and children's blood lead in New Orleans. *Proc. Natl. Acad. Sci. USA* **2019**, *116*, 22058–22064. [CrossRef]
29. Kabata-Pendias, H.A.; Mukherjee, A.B. *Trace Elements from Soil to Human*; Springer: Berlin/Heidelberg, Germany, 2007; ISBN 978-3-540-32714-1. [CrossRef]
30. Sanchez, F.; Garrabrants, A.C.; Kosson, T.T.; Méhu, J.; Kosson, D.S. Evaluation of contaminant release mechanisms for stabilized/solidified wastes. In *Studies in Environmental Science*; Elsevier: Amsterdam, The Netherlands, 1997; pp. 787–802.
31. Pueyo, M.; Mateu, J.; Rigol, A.; Vidal, M.; López-Sánchez, J.F.; Rauret, G. Use of the modified BCR three-step sequential extraction procedure for the study of trace element dynamics in contaminated soils. *Environ. Pollut.* **2008**, *152*, 330–341. [CrossRef]
32. Cambier, P.; Philippe, C.; Charlatchka, R.; Bourgeois, S. Influence of Reducing Conditions on the Solubility of Divalent Trace Metals in Polluted Soils. 2014. Available online: https://www.researchgate.net/publication/240628173 (accessed on 1 December 2020).
33. Shao, Y.; Lu, Y.; Luo, M.; Yang, K.; Zhou, G.; Zhao, C.; Cheng, H.; Xu, D.; Ma, L. Speciation Study on Pb in Different Particle Size Fractions by Sequential Extraction and XAFS Spectroscopy. *Water Air Soil Pollut.* **2021**, *232*, 1–11. [CrossRef]
34. Peng, L.; Liu, P.; Feng, X.; Wang, Z.; Cheng, T.; Liang, Y.; Lin, Z.; Shi, Z. Kinetics of heavy metal adsorption and desorption in soil: Developing a unified model based on chemical speciation. *Geochim. Cosmochim. Acta* **2018**, *224*, 282–300. [CrossRef]
35. Scheckel, K.G.; Ryan, J.A.; Allen, D.; Lescano, N.V. Determining speciation of Pb in phosphate-amended soils: Method limitations. *Sci. Total Environ.* **2005**, *350*, 261–272. [CrossRef]
36. U.S. Census Bureau. United States Census Bureau. 2020. Available online: https://www.census.gov/ (accessed on 15 March 2023).
37. Schuch, L.; Curtis, A.; Davidson, J. Reducing Lead Exposure Risk to Vulnerable Populations: A Proactive Geographic Solution. *Ann. Assoc. Am. Geogr.* **2017**, *107*, 606–624. [CrossRef]
38. Muntau, H.; Quevauviller, P.; Griepink, B. Speciation of heavy metals in soils and sediments an account of the improvement and harmonization of extraction techniques undertaken under the auspices of the bcr of the commission of the european communities. *Int. J. Environ. Anal. Chem.* **1993**, *51*, 135–151.
39. Dean, W.E. Determination of carbonate and organic matter in calcareous sediments and sedimentary rocks by loss on ignition; comparison with other methods. *J. Sediment. Res.* **1974**, *44*, 242–248.
40. Konen, M.; Jacobs, P.; Burras, L.; Talaga, B.; Mason, J. Equations for Predicting Soil Organic Carbon Using Loss-on-Ignition for North Central, U.S. Soils. *Soil Sci. Soc. Am. J. SSSAJ* **2002**, *66*, 1878–1881. [CrossRef]
41. Williams, J.C.; Basu, A.R.; Bhargava, O.N.; Ahluwalia, A.D.; Hannigan, R.E. Resolving original signatures from a sea of overprint—The geochemistry of the Gungri Shale (Upper Permian, Spiti Valley, India). *Chem. Geol.* **2012**, *324*, 59–72. [CrossRef]
42. Christman, T.; Martin, J.; Myers, F.; Rasik, C.; Sainey, E.; Steigerwald-Dick, V. *Evaluation of Background Metal Soil Concentrations in Cuyahoga County—Cleveland Area, OH-EPA Summary Report*; Ohio EPA: Columbus, OH, USA, 2013. Available online: https://dam.assets.ohio.gov/image/upload/epa.ohio.gov/Portals/30/vap/docs/Evaluation%20of%20Background%20Metal%20Soil%20Concentrations.pdf (accessed on 29 October 2021).
43. Filgueiras, A.V.; Lavilla, I.; Bendicho, C. Chemical sequential extraction for metal partitioning in environmental solid samples. *J. Environ. Monit.* **2002**, *4*, 823–857. [CrossRef]
44. Ugwu, M.I.; Igbokwe, A.O. Sorption of Heavy Metals on Clay Minerals and Oxides: A Review. In *Advanced Sorption Process Applications*; IntechOpen: London, UK, 2019.
45. Uddin, M.K. A review on the adsorption of heavy metals by clay minerals, with special focus on the past decade. *Chem. Eng. J.* **2017**, *308*, 438–462. [CrossRef]
46. Fan, T.-T.; Cui, P.-X.; Sun, Q.; Zhou, D.-M.; Alves, M.E.; Wang, Y.-J. Combining Path Analysis and X-Ray Absorption Spectroscopy to Unravel the Zn Sorption Mechanism on Soils. *Soil Sci. Soc. Am. J.* **2018**, *82*, 796–802. [CrossRef]
47. Kotoky, P.; Bora, B.J.; Baruah, N.K.; Baruah, J.; Baruah, P.; Borah, G.C. Chemical fractionation of heavy metals in soils around oil installations, Assam. *Chem. Speciat. Bioavailab.* **2003**, *15*, 115–126. [CrossRef]
48. O'Reilly, S.; Hochella, M.F. Lead sorption efficiencies of natural and synthetic Mn and Fe-oxides. *Geochim. Cosmochim. Acta* **2003**, *67*, 4471–4487. [CrossRef]

49. Peli, M.; Bostick, B.C.; Barontini, S.; Lucchini, R.G.; Ranzi, R. Profiles and species of Mn, Fe and trace metals in soils near a ferromanganese plant in Bagnolo Mella (Brescia, IT). *Sci. Total Environ.* **2021**, *755*, 143123. [CrossRef]
50. Kaste, J.M.; Friedland, A.J.; Miller, E.K. Potentially mobile lead fractions in montane organic-rich soil horizons. *Water Air Soil Pollut.* **2005**, *167*, 139–154. [CrossRef]
51. Lu, A.; Zhang, S.; Shan, X.-Q. Time effect on the fractionation of heavy metals in soils. *Geoderma* **2005**, *125*, 225–234. [CrossRef]
52. Ma, L.Q.; Rao, G.N. Effects of Phosphate Rock on Sequential Chemical Extraction of Lead in Contaminated Soils. *J. Environ. Qual.* **1997**, *26*, 788–794. [CrossRef]
53. Clark, J.J.; Knudsen, A.C. Extent, Characterization, and Sources of Soil Lead Contamination in Small-Urban Residential Neighborhoods. *J. Environ. Qual.* **2013**, *42*, 1498–1506. [CrossRef] [PubMed]
54. McIntyre, J.; Winters, N.; Rozmyn, L.; Haskins, T.; Stark, J. Metals leaching from common residential and commercial roofing materials across four years of weathering and implications for environmental loading. *Environ. Pollut.* **2019**, *255*, 113262. [CrossRef]
55. Galster, S.; Helmreich, B. Copper and Zinc as Roofing Materials—A Review on the Occurrence and Mitigation Measures of Runoff Pollution. *Water* **2022**, *14*, 291. [CrossRef]
56. Laidlaw, M.A.; Filippelli, G.M. Resuspension of urban soils as a persistent source of lead poisoning in children: A review and new directions. *Appl. Geochem.* **2008**, *23*, 2021–2039. [CrossRef]
57. Whiley, A.J. Copper and Zinc Loading Associated with Automotive Brake-Pad and Tire Wear: Puget Sound Basin [Internet]. Olympia, Washington; December 2011. Available online: www.ecy.wa.gov/biblio/1110087.html (accessed on 8 November 2020).
58. Li, Q.; Wang, Y.; Li, Y.; Li, L.; Tang, M.; Hu, W.; Chen, L.; Ai, S. Speciation of heavy metals in soils and their immobilization at micro-scale interfaces among diverse soil components. In *Science of the Total Environment*; Elsevier B.V.: Amsterdam, The Netherlands, 2022; Volume 825.
59. Stone, M.; Marsalek, J. Trace metal composition and speciation in street sediment: Sault Ste. Marie, Canada. *Water Air Soil Pollut.* **1996**, *87*, 149–169. [CrossRef]
60. EPA NWS. *Managing Lead Contamination in Home Maintenance, Renovation and Demolition Practices: A Guide for Councils*; NSW Environment Protection Authority: Sydney, Australia, 2003.
61. Spanier, A.J.; Wilson, S.; Ho, M.; Hornung, R.; Lanphear, B.P. The contribution of housing renovation to children's blood lead levels: A cohort study. *Environ. Health* **2013**, *12*, 72. [CrossRef]
62. Farfel, M.R.; Chisolm, J.J. Health and Environmental Outcomes of Traditional and Modified Practices for Abatement of Residential Lead-Based Paint. *Am. J. Public Health* **1990**, *80*, 1240–1245. [CrossRef]
63. Yin, X.; Gao, B.; Ma, L.Q.; Saha, U.K.; Sun, H.; Wang, G. Colloid-facilitated Pb transport in two shooting-range soils in Florida. *J. Hazard. Mater.* **2010**, *177*, 620–625. [CrossRef]
64. Caporale, A.G.; Violante, A. Chemical Processes Affecting the Mobility of Heavy Metals and Metalloids in Soil Environments. *Curr. Pollut. Rep.* **2016**, *2*, 15–27. [CrossRef]
65. Hunt, A. Relative bioaccessibility of Pb-based paint in soil. *Environ. Geochem. Health* **2016**, *38*, 1037–1050. [CrossRef]
66. Haque, E.; Thorne, P.S.; Nghiem, A.A.; Yip, C.S.; Bostick, B.C. Lead (Pb) concentrations and speciation in residential soils from an urban community impacted by multiple legacy sources. *J. Hazard. Mater.* **2021**, *416*, 125886. [CrossRef] [PubMed]
67. Coni, N.; Gipiela, M.L.; Oliveira, A.S.; Marcondes, P.V.P. Study of the Mechanical Properties of the Hot Dip Galvanized Steel and Galvalume®. *J. Braz. Soc. Mech. Sci. Eng.* **2009**, *31*, 319–326. [CrossRef]
68. Zheng, R.; Carmeliet, J.; Hens, H.; Janssens, A.; Bogaerts, W. A hot box-cold box investigation of the corrosion behavior of highly insulated zinc roofing systems. *J. Therm. Envel. Build. Sci.* **2004**, *28*, 27–44. [CrossRef]
69. Tack, F.; Singh, S.; Verloo, M. Leaching behaviour of Cd, Cu, Pb and Zn in surface soils derived from dredged sediments. *Environ. Pollut.* **1999**, *106*, 107–114. [CrossRef] [PubMed]
70. Tyler, G. Leaching rates of heavy metal ions in forest soil. *Water Air Soil Pollut.* **1978**, *9*, 137–148. [CrossRef]
71. Kasich, J.; Taylor, M. Evaluation of Background Metal Soil Concentrations in Summit County-Akron Area Developed in Support of the Ohio Voluntary Action Program Summary Report *Generalized Soil Map for the State of Ohio Department of Natural Resources Evaluation of Background Metal Concentrations in Akron-Area Urban Soils Summary Report for Ohio EPA's Voluntary Action Program. 2015. Available online: https://dam.assets.ohio.gov/image/upload/epa.ohio.gov/Portals/30/vap/docs/Toledo%20Background%20Summary%20Report_FINAL.pdf (accessed on 7 December 2021).
72. Adamiec, E.; Jarosz-Krzemińska, E.; Wieszała, R. Heavy metals from non-exhaust vehicle emissions in urban and motorway road dusts. *Environ. Monit. Assess.* **2016**, *188*, 1–11. [CrossRef]
73. Anasiei, I.; Mitrica, D.; Badea, I.-C.; Șerban, B.-A.; Trapp, J.; Storz, A.; Carcea, I.; Olaru, M.T.; Burada, M.; Constantin, N.; et al. Characterization of Complex Concentrated Alloys and Their Potential in Car Brake Manufacturing. *Materials* **2023**, *16*, 5067. [CrossRef]
74. Reboredo, F.; Simões, M.; Jorge, C.; Mancuso, M.; Martinez, J.; Guerra, M.; Ramalho, J.C.; Pessoa, M.F.; Lidon, F. Metal content in edible crops and agricultural soils due to intensive use of fertilizers and pesticides in Terras da Costa de Caparica (Portugal). *Environ. Sci. Pollut. Res.* **2019**, *26*, 2512–2522. [CrossRef]
75. Imperato, M.; Adamo, P.; Naimo, D.; Arienzo, M.; Stanzione, D.; Violante, P. Spatial distribution of heavy metals in urban soils of Naples city (Italy). *Environ. Pollut.* **2003**, *124*, 247–256. [CrossRef] [PubMed]

76. Mahanta, M.J.; Bhattacharyya, K.G. Total concentrations, fractionation and mobility of heavy metals in soils of urban area of Guwahati, India. *Environ. Monit. Assess.* **2011**, *173*, 221–240. [CrossRef] [PubMed]
77. Lu, Y.; Zhu, F.; Chen, J.; Gan, H.; Guo, Y. Chemical fractionation of heavy metals in urban soils of Guangzhou, China. *Environ. Monit. Assess.* **2007**, *134*, 429–439. [CrossRef] [PubMed]
78. Wu, Y.; Liu, C.; Tu, C. Distribution and sequential extraction of some heavy metals in urban soils of Guiyang City, China. *Chin. J. Geochem.* **2008**, *27*, 401–406. [CrossRef]
79. Pavlović, D.; Pavlović, M.; Čakmak, D.; Kostić, O.; Jarić, S.; Sakan, S.; Đorđević, D.; Mitrović, M.; Gržetić, I.; Pavlović, P. Fractionation, Mobility, and Contamination Assessment of Potentially Toxic Metals in Urban Soils in Four Industrial Serbian Cities. *Arch. Environ. Contam. Toxicol.* **2018**, *75*, 335–350. [CrossRef]
80. Davidson, C.M.; Urquhart, G.J.; Ajmone-Marsan, F.; Biasioli, M.; da Costa Duarte, A.; Díaz-Barrientos, E.; Grčman, H.; Hossack, I.; Hursthouse, A.S.; Madrid, L.; et al. Fractionation of potentially toxic elements in urban soils from five European cities by means of a harmonised sequential extraction procedure. *Anal. Chim. Acta* **2006**, *565*, 63–72. [CrossRef]
81. Kubier, A.; Wilkin, R.T.; Pichler, T. Cadmium in soils and groundwater: A review. *Appl. Geochem.* **2019**, *108*, 104388. [CrossRef]
82. Abdu, N.; Agbenin, J.O.; Buerkert, A. Fractionation and mobility of cadmium and zinc in urban vegetable gardens of Kano, Northern Nigeria. *Environ. Monit. Assess.* **2012**, *184*, 2057–2066. [CrossRef]
83. Burgio, L. Pigments, dyes and inks: Their analysis on manuscripts, scrolls and papyri. *Archaeol. Anthr. Sci.* **2021**, *13*, 194. [CrossRef]
84. Hayat, M.T.; Nauman, M.; Nazir, N.; Ali, S.; Bangash, N. Environmental Hazards of Cadmium: Past, Present, and Future. In *Cadmium Toxicity and Tolerance in Plants: From Physiology to Remediation*; Elsevier: Amsterdam, The Netherlands, 2018; pp. 163–183.
85. U.S. Environmental Protection Agency. EPA Strengthens Safeguards to Protect Families and Children from Lead in Contaminated Soil at Residential Sites in Region 7. 2024. Available online: https://www.epa.gov/newsreleases/epa-strengthens-safeguards-protect-families-and-children-lead-contaminated-soil (accessed on 1 September 2024).

Disclaimer/Publisher's Note: The statements, opinions and data contained in all publications are solely those of the individual author(s) and contributor(s) and not of MDPI and/or the editor(s). MDPI and/or the editor(s) disclaim responsibility for any injury to people or property resulting from any ideas, methods, instructions or products referred to in the content.

soil systems

MDPI

Article

Distribution and In Vitro Bioaccessibility of Potentially Toxic Metals in Soils at Select Urban Parks at Eastern Canadian Cities

Matt Dodd *, Abdurrazzaq Durojaiye and Julia Dupuis

School of Environment and Sustainability, Royal Roads University, 2005 Sooke Rd, Victoria, BC V8T 2L1, Canada; abdurrazzaqd@yahoo.ca (A.D.)
* Correspondence: matt.dodd@royalroads.ca

Abstract: This study investigated the human health risks associated with exposure to potentially toxic metals, including arsenic, barium, cadmium, chromium, cobalt, copper, lead, nickel, and zinc, at select parks in Eastern Canadian cities. Except for arsenic in Halifax, the mean metal concentrations in the cities, including Saint John, Fredericton, Ottawa, Toronto, London, Windsor, Woodstock, Kitchener, Guelph, Chatham, and Montreal, were below the Canadian Council of Ministers of Environment soil quality guideline for parkland use. Metal distribution reflected either the regional natural-occurring concentrations or anthropogenic sources such as industrial activities, historical land use, and heavy traffic corridors. In vitro bioaccessibility values were variable and in the order chromium < nickel < cobalt < arsenic < zinc < copper < lead < cadmium. The risk associated with incidental soil ingestion for children, incorporating bioaccessibility, indicated unacceptable levels of non-carcinogenic effects for 6 out of the 101 samples analyzed. For adults, unacceptable non-carcinogenic effects were noted for only one sample. Lead was the leading contributor to the non-carcinogenic risk. Carcinogenic risk for arsenic was limited to two samples. The overall risks associated with exposure to metals in soils in most of the parks studied were deemed low except for arsenic and lead at a few parks.

Keywords: urban parks; playgrounds; metals; in vitro bioaccessibility

Citation: Dodd, M.; Durojaiye, A.; Dupuis, J. Distribution and In Vitro Bioaccessibility of Potentially Toxic Metals in Soils at Select Urban Parks at Eastern Canadian Cities. *Soil Syst.* **2024**, *8*, 123. https://doi.org/10.3390/soilsystems8040123

Academic Editor: Girish Choppala

Received: 9 August 2024
Revised: 1 November 2024
Accepted: 25 November 2024
Published: 27 November 2024

Copyright: © 2024 by the authors. Licensee MDPI, Basel, Switzerland. This article is an open access article distributed under the terms and conditions of the Creative Commons Attribution (CC BY) license (https://creativecommons.org/licenses/by/4.0/).

1. Introduction

Core ideas:

- Potentially toxic metals distribution in surface soils at select parks and playgrounds in 12 Canadian cities reflect natural and anthropogenic sources.
- In vitro bioaccessibility values are variable due to different soil physicochemical properties.
- The risk which is associated with incidental ingestion of potentially toxic metals in soils incorporating bioaccessibility is low except for arsenic and lead at a few parks.

Urban green spaces, including playgrounds and sports fields, often have bare patches that can serve as potential deposition points for contaminants. The world's population is increasingly becoming urbanized, and according to the United Nations World Urbanization Prospects 2018, 81.4% of Canadians live in urban areas [1]. This rise in urbanization likely leads to the increasing use of outdoor green spaces by urban residents with the corresponding potential increase in exposure to soils through dermal contact, incidental ingestion, and inhalation of suspended particles. Incidental soil ingestion is typically an exposure pathway, especially for young children during recreational activities at these parks and playgrounds, due to their playing on the ground and frequent mouthing of hands, toys, and other objects [2]. Characterization and mapping of potentially toxic metals and metalloids in soils at urban parks and playgrounds is thus an important first step in the evaluation of ecological and human health risks toward the overall achievement of the United Nations Sustainable Development Goal 3: Good Health and Well-Being.

Surrounding land use affects metal and metalloid (collectively referred to as metals) distribution in urban surface soils, and, in general, samples collected from locations close

to roads with heavy traffic have higher metal concentrations compared to soils farther from roads [3]. Vehicular traffic has been shown to contribute to the environmental loading of arsenic (As), cadmium (Cd), chromium (Cr), copper (Cu), nickel (Ni), lead (Pb) and zinc (Zn) [4–6]. Studies in urban parks and playgrounds have also identified elemental contamination from treated wood structures in addition to natural sources, industry, and traffic [7]. Five out of twenty-four sites that were surveyed in Istanbul, Turkey, had systematically higher As, Cu, Cr, or Zn concentrations, compared to the backgrounds that were attributed to leaching from wooden structures [7]. Data from European and American cities surveyed indicated moderate to heavy contamination with Cd, Cu, Pb, and Zn, which were attributed to anthropogenic sources [8]. Geostatistical and multivariate statistical analyses indicated that the two principal sources of trace elements, especially Cu, Pb, and Zn, in the urban soils in China were industrial discharges and traffic emissions, while As and mercury (Hg) primarily originated from coal combustion, partly for home-heating activities [8]. Other activities identified as potential sources of metals include incineration of municipal, medical, and other wastes (As, Cd, Cr, Pb, Ni, and Zn), metal works (Cd, Cr, Cu, Ni, Pb, and Zn), oil refining (As, Co, Cr, Cu, Ni, Pb, and V), glassworks (As, Cd, Co, Cu, Ni, Pb, and Zn), battery production (As, Cd, Cr, Cu, Hg, Ni, Pb, and Zn) and pesticide production and use (As, Cd, Cu, Hg, Pb, and Zn) [3,8].

Various studies have incorporated bioaccessibility data in human health risk assessment of metals in urban environments [7–10]. The inclusion of the bioaccessibility data resulted in a more realistic estimation of the human health risk associated with incidental soil ingestion. These studies have shown that bioaccessibility varies widely among different metals and soils from different cities and that metals of natural origin generally have lower solubility and bioaccessibility than those from anthropogenic sources.

In light of the potential toxicity of metals, especially to children through inadvertent soil ingestion, it is pertinent to identify and quantify the concentration of contaminants in soils at parks and playgrounds while utilizing urban green spaces. Due to the lack of data on the distribution of metals in Canadian urban parks, this study was conducted as an initial scoping survey; it provides the first regional overview of the metal distribution and potential health risks associated with incidental exposure to soils at select parks in Eastern Canada. It involves the meta-analysis of metal concentrations in surface soil samples collected from select parks and playgrounds at 12 urban centers in Eastern Canada. Eight potentially toxic metals, including As, Cd, Co, Cr, Cu, Ni, Pb, and Zn, were selected for the meta-analysis based on their potential to be introduced into the urban environment from various anthropogenic sources. The relationships between soil metal concentrations and traffic, surrounding land use, and site history were explored. The influence of soil pH and total organic carbon on bioaccessibility was also investigated and the potential risk associated with exposure to the metal contaminants was estimated.

2. Methodology

2.1. Soil Sampling and Preparation

Sampling was conducted at select parks in eight cities, including Halifax (10), Ottawa (8), London (4), Windsor (4), Woodstock (4), Kitchener (4), Guelph (4), and Chatham (4) (Figure 1). Data for samples collected from previous investigations, including Toronto (15) [11], Saint John (10) [12], Fredericton (10) [12], and Montreal (16) [13], were included in the meta-analysis. The geographical coordinates of the sampling locations are given in Table S1 in the Supplemental Material. The parks were selected to reflect different surroundings, such as residential, industrial, educational institutes, and commercial. Travel volumes in the vicinities as well as historical land use of adjacent areas were also considered. One composite soil sample was collected from the top 0–5 cm layer from visibly disturbed patches due to human activities in easily accessible areas in each park, including picnic areas and near play structures. Samples were placed into Ziploc bags and transported to the laboratory. Each sample was air-dried in a paper sandwich bag at ambient temperatures (~20 °C) in a fume hood in the laboratory. The dried sample was sieved to <250 μm [14].

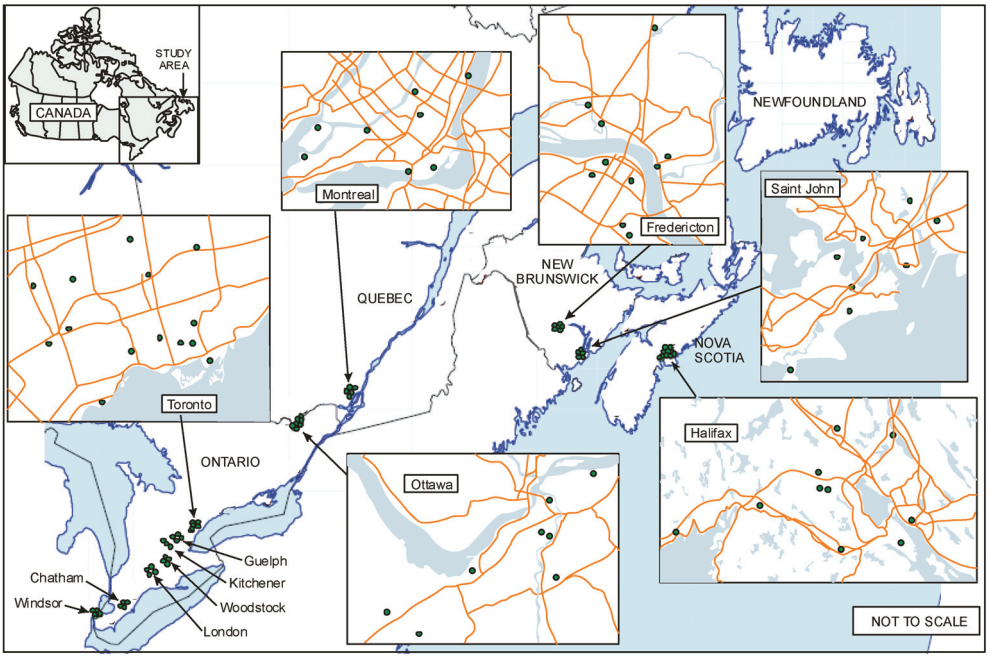

Figure 1. Sampling locations. Green dots represent sampling locations at each city.

2.2. Soil pH, Carbon Content and Total Metal Content

Soil pH was measured using a soil-to-deionized water ratio of 1:2 (*w*/*v*). Approximately 10 g of sieved soil sample was measured into a 50 mL beaker, and 20 mL of water was added. The suspension was allowed to settle for 1 h, following which the pH of the supernatant was measured using a standardized pH meter. Total carbon was determined using the loss-on-ignition (LOI) method in two sequential phases to estimate the organic matter (OM) and carbonate content of the soils [13]. Samples were analyzed in triplicate for this procedure. Total metal concentrations in the soils were determined by ICP-MS using the USEPA 3050B aqua regia variant [15].

2.3. In Vitro Extraction Assay (IVBA)

The IVBA methodology was based on the United States Environmental Protection Agency (USEPA) Method 1340 [16]. One gram of the sieved soil was extracted by end-to-end rotation for 1 h in 100 mL of 30 g/L glycine, adjusted to a pH of 1.5 with concentrated HCl. The extract was filtered through a 0.45 µm cellulose acetate syringe filter and analyzed for total metals by ICP-MS. Percent metal bioaccessibility was calculated for each sample by dividing the concentration in the IVBA extract by the total metal concentration as determined by aqua regia variant digestion and ICP-MS analysis. The QA/QC program included procedure blanks, certified reference materials (NIST 2711a). and duplicates. Concentrations obtained for the procedure blanks indicated minimal interferences from the extraction solution and equipment. The IVBA values for the reference materials were within the control limits while the relative percent difference for the duplicates were generally less than 30%, suggesting good reproducibility.

2.4. Statistical Analysis and Data Evaluation

Total metal concentrations were evaluated using the Canadian Council of Ministers of Environment (CCME) soil quality guidelines for residential/parkland use. The guidelines provide concentrations of contaminants in soil, at or below which no appreciable human

health risk is expected [17]). The potential impact of anthropogenic sources on metal concentrations was evaluated using enrichment factor (EF) while the geoaccumulation index (Igeo) was used to assess the level of pollution [18]. Enrichment factor (EF) was calculated as follows:

$$EF = \left(\frac{Ms}{Fes}\right) / \left(\frac{Mb}{Feb}\right) \quad (1)$$

where Ms and Fes are the concentrations of metal and Fe in the soil sample while Mb and Feb are the relevant background concentrations of the metal and Fe. Regional elemental background concentrations reported by Dodd et al. [5] were used in this study. An EF < 2 indicates deficiency to minimal enrichment; 2–5 moderate enrichment; 5–20 implies significant enrichment; 20–40 implies very high enrichment, and >40 extremely high enrichment [18].

The geoaccumulation index (Igeo) was calculated using Equation (2):

$$Igeo = \log_2 \left[\frac{Ms}{I.5Mb}\right] \quad (2)$$

The Igeo data were evaluated using the following descriptive classes: ≤ 0 = unpolluted; 0–1 = unpolluted to moderately polluted; 1–2 = moderately polluted; 2–3 = moderately to highly polluted; 3–4 = highly polluted; 4–5 = highly to extremely high polluted; and 5–6 extremely high polluted [18].

2.5. Human Health Exposure Assessment

Although exposure to contaminants in soil at the urban parks and playgrounds can occur through ingestion, dermal contact, and inhalation, the human health exposure assessment was conducted for the oral ingestion route, since this was deemed the most important risk pathway relative to the others [19,20]. The risk estimate was based on equations described by Health Canada [14].

The chemical daily intake (CDI) due to incidental ingestion of contaminated soil was calculated using Equation (3):

$$CDI = \frac{Cs \times IRs \times RAForal \times ET}{BW \times LE} \quad (3)$$

where CDI = chemical daily intake (mg kg^{-1} day^{-1}); Cs = concentration of metal in soil (mg kg^{-1}); IRs = ingestion rate of soil (0.00002 kg day^{-1}); RAForal = relative absorption factor from the gastrointestinal tract (unitless); ET = exposure term (unitless) = days/week x weeks/year (x years for carcinogens); BW = body weight (32.9 kg for a child and 70.7 kg for an adult) and LE = life expectancy for assessment of carcinogens (75 years) [21]). The metal bioaccessibility value was used as a surrogate for the absorption factor from the gastrointestinal tract, incorporating RBA/IVBA regression equations where available [22]. The CDI was divided by the tolerable daily intake (TDI) (mg kg^{-1} d^{-1}) to obtain the hazard quotient (HQ) for non-cancer risk (Equation (4)).

$$\text{Hazard Quotient HQ} = \frac{CDImetal}{TDI} \quad (4)$$

The TDI values used were As: 0.0003 mg kg^{-1} d^{-1}; Cd: 0.0008 mg kg^{-1} d^{-1}; Co: 0.03 mg/kg-day; Cr: 0.001 mg kg^{-1} d^{-1}; Cu: 0.426 mg kg^{-1} d^{-1}; Ni; 0.011 mg kg^{-1} d^{-1}; Pb: 0.0005 mg kg^{-1} d^{-1}; and Zn: 0.48, 0.48, and 0.57 mg kg^{-1} d^{-1} [23,24]. The HQ for the individual metals (As, Cd, Co, Cr, Cu, Ni, Pb, and Zn) were summed to obtain the overall hazard index (HI) (Equation (5)).

$$HI = \sum HQi \quad (5)$$

Carcinogenic risk (CR) was determined for As, since it was the only carcinogenic substance that exceeded the CCME guideline using Equation (6):

$$CR = CDI \times SF \quad (6)$$

where SF = oral slope factor $(mg/kg\ d)^{-1}$. The oral slope factor used for As was 1.80 $(mg/kg\ d)^{-1}$ (Health Canada, 2021).

Statistical analyses were performed using Minitab® 19 Statistical Software and ProUCL version 5.1 [25]. Summary statistics, including the mean, median, standard deviation, and 95 percentiles were compiled to allow for a comparison of the data among the cities. Pearson correlation analysis was used to determine the relationship between soil pH, OM, metal concentrations and IVBA while principal component analysis (PCA) was conducted to explore the sources of elemental concentration after the data were transformed using varimax rotation.

3. Results and Discussion

3.1. Summary Statistics

Descriptive statistics of soil pH, organic matter (OM), and metal concentrations, including median, mean, standard deviation, 95 percentiles, and maximum for the urban centers, are given in Table 1. The entire dataset is shown in Table S2 in the Supplemental Material.

Table 1. Descriptive statistics of total metal concentrations (mg/kg), pH, and organic matter (OM%).

City		As	Cd	Co	Cr	Cu	Ni	Pb	Zn	pH	OM
CCME R/P		**12**	**10**	**50**	**64**	**63**	**50**	**140**	**200**		
Halifax (n = 10)	Mean	***36***	0.21	6.7	16	25	15	53	85	4.59	9.8
	Median	9.9	0.21	7.4	16	23	16	17	48	4.51	8.5
	Std Dev	68	0.12	2.2	3.3	13	4.9	71	65	0.68	5.1
	95% tile	***154***	0.35	8.9	21	47	21	174	187	5.50	16.8
	Maximum	***218***	0.37	9.0	21	49	22	***234***	***204***	5.59	17.6
Saint John (n = 10)	Mean	8.9	0.27	9.3	21	32	19	46	96	6.99	12.5
	Median	7.6	0.17	9.2	22	29	19	22	84	6.80	8.3
	Std Dev	3.7	0.21	2.5	4.2	14	6.6	53	53	0.71	10.1
	95% tile	***15***	0.65	13.0	28	54	30	148	196	8.13	29.8
	Maximum	***17***	0.78	13.3	29	63	33	175	199	8.38	38.0
Fredericton (n = 10)	Mean	10	0.19	10.8	31	23	32	35	79	6.54	7.1
	Median	11	0.16	9.3	29	19	29	28	80	6.37	7.6
	Std Dev	3.9	0.10	3.3	6.6	9	13	22	25	1.13	3.2
	95% tile	***16***	0.35	16.3	41	38	54	69	115	7.96	11.0
	Maximum	***17***	0.42	19.3	44	48	***67***	74	138	8.15	11.0
Montreal (n = 16)	Mean	5.1	0.33	8.7	24	35	22	35	88	7.68	8.9
	Median	3.7	0.34	8.7	22	36	22	28	88	7.85	8.8
	Std Dev	2.6	0.19	3.7	11	15	10	22	32	0.43	4.3
	95% tile	10	0.60	14.6	48	60	36	73	146	8.16	14.1
	Maximum	11	0.63	16.6	48	68	49	78	162	8.53	18.2
Ottawa (n = 8)	Mean	2.7	0.26	6.9	30	19	17	29	74	6.49	12.0
	Median	1.6	0.22	6.5	29	18	15	11	59	6.43	11.0
	Std Dev	2.3	0.14	3.3	17	8	9.2	33	38	0.43	4.5
	95% tile	6.5	0.48	11.9	56	30	32	84	129	7.08	18.9
	Maximum	6.9	0.57	13.1	69	31	37	89	134	7.11	20.4
Toronto (n = 15)	Mean	3.5	0.59	4.7	19	28	12	107	97	7.63	10.7
	Median	3.3	0.29	4.2	13	21	10	41	72	7.65	10.1
	Std Dev	1.5	1.06	1.8	21	23	7.1	165	77	0.50	4.2
	95% tile	6.6	1.80	7.1	40	***79***	26	***354***	198	8.25	16.8
	Maximum	6.7	4.60	9.3	***98***	***88***	33	***690***	***350***	8.85	21.7

Table 1. *Cont.*

City		As	Cd	Co	Cr	Cu	Ni	Pb	Zn	pH	OM
CCME R/P		**12**	**10**	**50**	**64**	**63**	**50**	**140**	**200**		
Windsor (n = 4)	Mean	4.7	0.54	4.4	17	24	15	39	112	6.28	13.5
	Median	4.7	0.47	4.7	16	20	16	38	80	6.30	12.1
	Std Dev	1.1	0.24	1.5	3.0	11	5.0	17	74	0.51	5.1
	95% tile	5.7	0.82	5.8	20	37	20	57	***201***	6.79	19.6
	Maximum	5.7	0.88	5.9	21	40	21	59	***222***	6.84	20.7
Guelph (n = 4)	Mean	4.8	0.44	4.1	11	14	8.4	40	122	7.01	10.7
	Median	3.4	0.42	4.1	11	14	8.2	43	123	7.09	10.8
	Std Dev	3.4	0.15	0.3	0.6	2	1.1	15	39	0.21	1.0
	95% tile	8.9	0.59	4.4	11	16	10	53	161	7.14	11.7
	Maximum	9.8	0.61	4.4	11	17	10	53	164	7.15	11.8
Kitchener (n = 4)	Mean	2.3	0.27	3.2	10	13	7.7	27	67	7.29	7.8
	Median	2.2	0.30	3.6	12	12	8.4	29	71	7.29	6.9
	Std Dev	1.1	0.06	1.1	3.6	5	2.0	14	14	0.09	3.3
	95% tile	3.3	0.31	3.9	13	17	9.1	39	77	7.38	11.7
	Maximum	3.3	0.31	3.9	13	18	9.1	40	78	7.39	12.5
Woodstock (n = 4)	Mean	3.4	0.24	4.0	12	24	8.5	27	55	6.91	10.2
	Median	3.0	0.24	3.8	12	20	8.1	26	58	6.93	9.5
	Std Dev	1.5	0.08	0.9	2.1	12	1.5	14	12	0.17	1.7
	95% tile	5.2	0.32	5.0	14	39	10	42	64	7.07	12.3
	Maximum	5.5	0.33	5.2	14	42	11	45	64	7.09	12.7
London (n = 4)	Mean	2.8	0.23	3.4	11	14	8.2	15	46	6.84	10.6
	Median	2.2	0.23	3.4	11	12	8.2	12	46	7.12	9.7
	Std Dev	1.5	0.04	0.6	2.4	8	1.7	9	10	0.63	4.8
	95% tile	4.6	0.28	4.0	13	24	10	26	56	7.21	16.0
	Maximum	5.0	0.28	4.1	13	26	10	28	56	7.22	16.8
Chatham (n = 4)	Mean	3.3	0.20	5.1	13	14	13	15	48	7.21	9.4
	Median	3.0	0.19	5.0	14	15	13	13	46	7.25	9.3
	Std Dev	1.0	0.03	1.5	3.2	4	4.4	6	19	0.09	2.3
	95% tile	4.5	0.24	6.5	16	18	17	22	68	7.27	11.8
	Maximum	4.8	0.25	6.6	16	18	17	23	71	7.27	11.9

Values in bold italics exceed the CCME soil quality guideline for residential/parkland use (CCME R/P). Std Dev = standard deviation.

Soil pH and OM were variable among the cities in Halifax showing more acidic pH (mean of 4.59) compared to the other cities. The lower pH in Halifax is consistent with previous observations of low pH in the region [15]. The maximum concentrations of select metals exceeded the CCME guideline, including: As, Pb, and Zn in Halifax; As in Saint John; As and Ni in Fredericton; Cr, Cu, Ni, Pb, and Zn in Toronto; and Zn in Windsor. Metal concentrations in samples collected from Montreal, Ottawa, Guelph, Kitchener, Woodstock, London, and Chatham were all below the CCME guidelines. Out of the 101 samples analyzed, the percentages of samples that exceeded the guidelines were 7% for As, 2% for Cr, 4% for Cu, 1% for Ni, 6% for Pb, and 3% for Zn.

The mean concentrations for the metals for the cities were below the CCME guideline except for As in Halifax. Arsenic was elevated in Halifax, Saint John, and Fredericton compared to the other cities while Pb was relatively higher in Toronto. The mean concentrations of As, Cr, Cu, and Pb were higher in the urban park and playground samples compared to regional background surface soil samples as reported by Dodd et al. [15].

3.2. Enrichment Factor and Geoaccumulation Index

Enrichment factors are summarized as individual value plots in Figure 2. One park, each from Halifax and Toronto, showed significant enrichment for As and Pb, respectively.

Moderate enrichment was shown for a few samples for As (Halifax), Pb (Halifax, Saint John, and Toronto), and Cu (Halifax, Fredericton, Saint John, and Toronto).

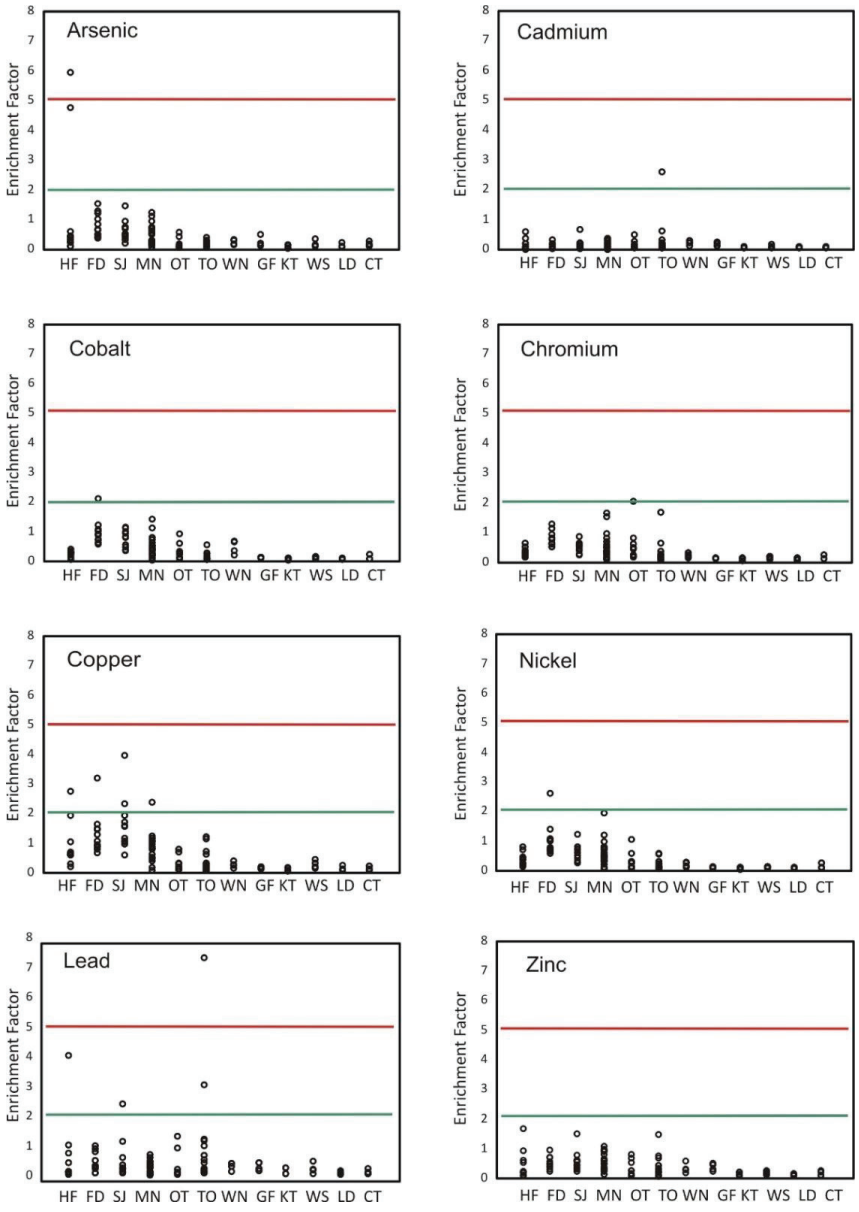

Figure 2. Metal enrichment factor for HF–Halifax, FD—Fredericton, SJ—Saint John, MN—Montreal, OT—Ottawa, TO—Toronto, WN—Windsor, GF—Guelph, KT—Kitchener, WS—Woodstock, LD—London, and CT—Chatham; Green line—minimal enrichment; Red line—moderate enrichment.

The Igeo values (Figure 3) indicated that most of the samples were unpolluted with specific metals based on the classification by Kowalska et al. [18]. However, one sample from Halifax and Toronto was moderately to highly polluted with As or Pb. This observation corroborated the enrichment factor data. Samples from a few parks from various cities

were moderately polluted with Cd and Cu while no pollution was associated with the Co, Cr, Ni and Zn.

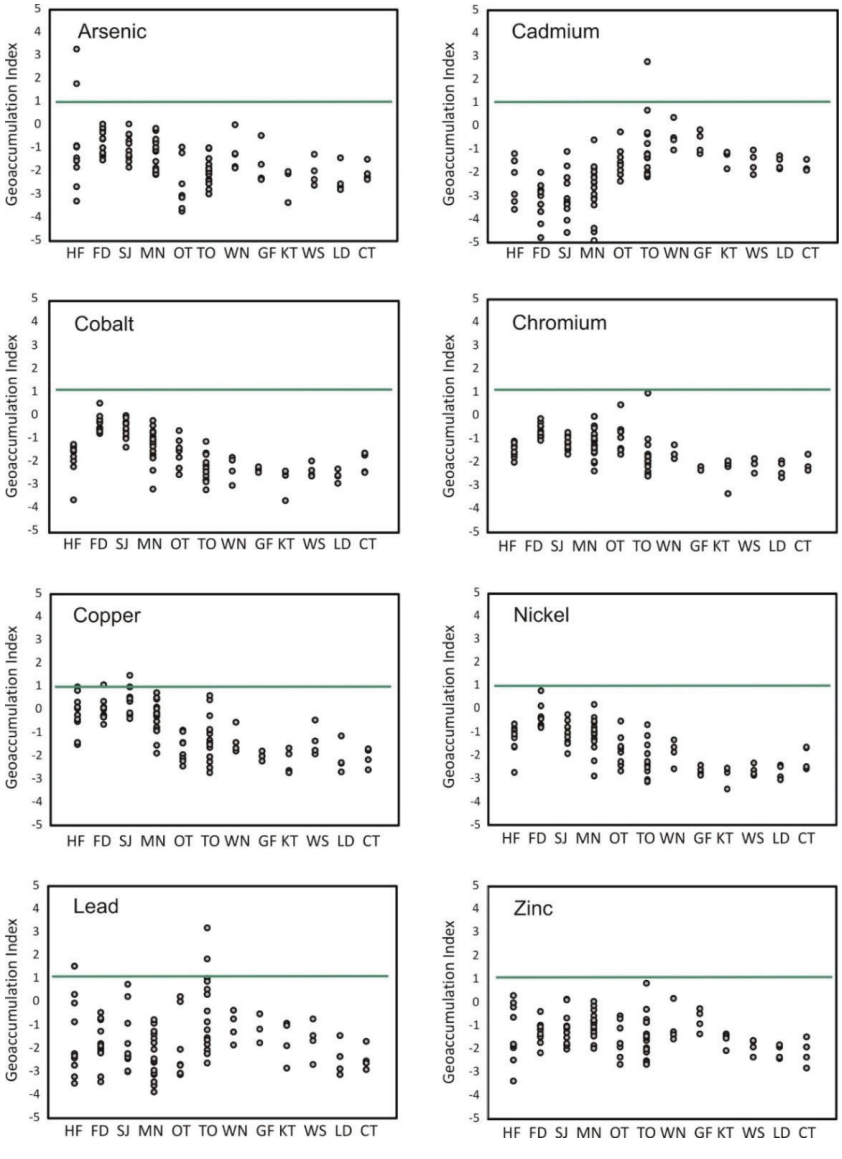

Figure 3. Geoaccumulation index for HF–Halifax, FD—Fredericton, SJ—Saint John, MN—Montreal, OT—Ottawa, TO—Toronto, WN—Windsor, GF—Guelph, KT—Kitchener, WS—Woodstock, LD—London, and CT—Chatham; Green line—moderate pollution.

3.3. Metal Distribution

3.3.1. Arsenic

The mean As concentrations in the cities were below the guideline of 12 mg/kg except for Halifax (mean 36 mg/kg). Elevated As concentrations that exceeded the guidelines were found in three samples, each collected from Halifax and Fredericton and two samples from Saint Johns. The highest concentration of As (218 mg/kg) was detected in a sample

obtained from a park in the Waverly Gold District, a region known to have elevated As levels from historical gold mining activities [26]. This sample had very high EF (5.9) and Igeo (3.3), indicating metal enrichment and moderate pollution. The second Halifax sample that exceeded the guideline was from a park in the city center; it had an EF (4.7) and Igeo (1.8) that suggested moderate enrichment and pollution. This sample also had elevated concentrations of Pb and Zn, and the pollution may be attributed to leaching from galvanic fences close to the sampling area [4,6]. All the samples from Fredericton and Saint Johns that exceeded the As guideline also had EF and Igeo values that suggested minimal enrichment and pollution. The elevated levels may be attributed to natural sources in line with previously reported high As in background samples collected from the region [15]. Arsenic concentrations in the samples from the remaining cities were all below the guideline, with the EF and Igeo values (Figures 2 and 3) indicating minimal enrichment and pollution.

3.3.2. Cadmium

Cadmium concentrations were all below the CCME guideline with comparable levels among the cities, except for one location in Toronto. The elevated concentration (4.6 mg/kg) was detected in a sample collected from a park near the airport and a busy transportation corridor. This sample showed moderate Cd enrichment and moderate pollution based on EF (2.6) and Igeo (2.8), respectively. The sample also contained elevated levels of Cr, Cu, Pb, and Zn, which could be associated with aircraft and automobile sources, as suggested by Ajmone-Marsan and Biasioli [4] and Wong et al. [6].

3.3.3. Cobalt

Cobalt concentrations in all the samples were below the CCME guideline with even distribution amongst the cities. Although the mean concentrations were higher than the corresponding regional background [15], the EF (Figure 2) and Igeo (Figure 3) indicated minimal Co enrichment and pollution.

3.3.4. Chromium

Anthropogenic sources of Cr in the urban environment include the burning of fossil fuels, use of wood preservatives, metallurgy, and incineration, leading to their ubiquitous presence in all the samples which were collected in this study. Chromium concentrations ranged from 5.0 to 98 mg/kg, with two samples exceeding the CCME guideline of 64 mg/kg. These included a park in Toronto near the airport and a transportation corridor which also contained elevated levels of Cd, Cu, Pb, and Zn, as discussed above. Miscellaneous refuse was noted at the second location, which could account for the elevated concentrations of Cr and other metals, such as Zn. The levels of enrichment and pollution at both locations were considered minimal based on the EF and Igeo (Figures 2 and 3).

3.3.5. Copper

Copper concentrations in two parks in Toronto and one park each in Saint John and Montreal exceeded the CCME guidelines. The first park in Toronto was near the airport and a busy transportation corridor (discussed above), whereas the second park was situated on former industrial port lands. The park in Montreal is used for road salt deposits and snow dumps in the winter, while the park in Saint John is situated in an industrial area, including a pulp and paper mill, a rock quarry, and a railway yard. The EF and Igeo values indicated moderate enrichment and pollution at these locations, suggesting the elevated levels may be due to the anthropogenic activities associated with the sources indicated above.

3.3.6. Nickel

Except for one sample collected from Fredericton, Ni concentrations were all below the CCME guideline. The sample which exceeded the guideline was retrieved from an amphitheater in the park, and there was no direct evidence to explain the elevated concen-

tration. Based on the EF, this sample showed moderated enrichment (Figure 2), while the Igeo samples (Figure 3) indicated minimal Ni pollution.

3.3.7. Lead

Lead concentrations were relatively higher in Toronto parks (mean 107 mg/kg) compared to the other cities; four out of the fifteen samples collected from Toronto contained lead in excess of the CCME guideline. The Toronto parks with the elevated Pb levels were situated in an industrial area (including metal recycling) and former industrial port lands. One sample, each taken from parks in Saint John and Halifax, which previously had buildings that were demolished, also contained elevated Pb levels, suggesting the contamination may have originated from the former facilities or other associated anthropogenic activities. The EF and Igeo values (Figures 2 and 3) showed moderate pollution and enrichment for the samples that exceeded the CCME guidelines.

3.3.8. Zinc

The concentrations of Zn in most of the soil samples were below the CCME guideline, except for one sample each from Halifax (park situated on a demolished building site), Windsor (a former city dump turned into a park), and Toronto (park located on former port lands), which had zinc at levels that exceeded the guidelines. The EF and Igeo values indicated minimal pollution and enrichment.

3.4. Principal Component Analysis

Principal component analysis was used to explore the inter-relationship between the metals. The result presented in Table 2 indicated Co, Cr, Fe, and Ni were strongly associated with one another within the first component; these metals showed minimal pollution and enrichment and may occur together because of their common origin from natural weathering and atmospheric deposition [3]. Elements such as Cd, Cu, Pb, and Zn, which may be impacted by anthropogenic sources, as discussed in the sections above, were grouped together in the second component, while As, which may be attributed to arsenic-bearing rocks, was unique. Elevated concentrations of As were found in the samples collected in areas where geological investigations have identified gold-bearing metasedimentary rocks (i.e., Meguma Supergroup) with As a major contaminant of concern [26].

Table 2. Component loadings for the principal component analysis of select metals in urban park soils, along with eigenvalues and the percentage of variance accounted for.

	PC1	PC2	Uniqueness
As			0.930
Cd		0.667	0.544
Co	0.944		0.108
Cr	0.757		0.320
Cu		0.746	0.296
Fe	0.875		0.221
Ni	0.941		0.091
Pb		0.783	0.377
Zn		0.783	0.373
Eigenvalue	3.844	1.895	
Proportion variance	0.427	0.211	
Cumulative	0.427	0.638	

Note. Applied rotation method is varimax.

3.5. In Vitro Bioaccessibility

In vitro bioaccessibility values varied among the metals, as depicted in the boxplots in Figure 4 (see Supplementary Material Table S3 for the entire data). Cadmium had the highest bioaccessibility (mean of 74.1%), followed by Pb (60.9% $\pm$ 19.0%), Cu (46.3 $\pm$ 18.1%), Zn (30.0 $\pm$ 13.2%), As (24.4 $\pm$ 13.2%), Cr (24.3 $\pm$ 10.5%), Ni (13.5 $\pm$ 6.8%),

and Co (5.1 ± 3.9%). The relatively high bioaccessibility of Cd is consistent with previous observations [27,28] and may be attributed to its occurrence as the highly soluble oxides in the surface soils analyzed. The mean in vitro bioaccessibility values were higher in the urban samples compared to Canadian background samples for As (7 ± 6%), Cu (20 ± 16%), and Pb (63 ± 19%) [15].

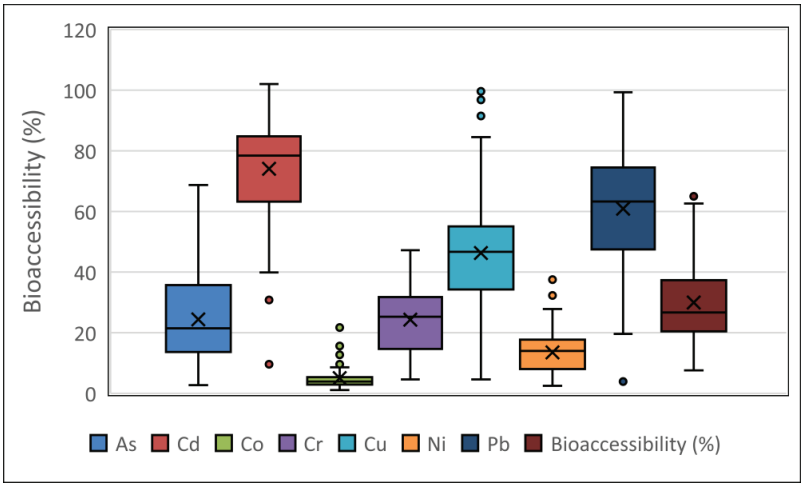

Figure 4. Boxplots of metal bioaccessibility in urban park soils.

Variable metal bioaccessibility among the samples may be due to metal speciation and physicochemical properties. Soil physicochemical properties that affect bioaccessibility include total metal concentration, iron content, pH, and soil organic matter [2,20,29]. The relationships between metal bioaccessibility and pH, LOI, iron, and total metal content were, therefore, explored through ordinary least square regression analyses. The outputs obtained are summarized in Table 3. Soil pH increased As and Zn bioaccessibility, while pH had no significant effect on the bioaccessibility of the other metals. Soil organic carbon had negligible effects on bioaccessibility, whereas increasing Fe concentration decreased bioaccessibility for all the metals except Cd. These observations are consistent with previous observations [2,15,29].

3.6. Human Health Risk Assessment

The non-carcinogenic hazard indices incorporating bioaccessibility for children and adult receptors for all the samples are summarized in Figures 5 and 6, respectively. For adults, unacceptable levels of non-carcinogenic effects (HI > 1) were noted for only 1 out of the 101 sampling locations. Lead was the leading contributor to the elevated human health risk via oral ingestion for this sample, which was collected from a park situated near an industrial area. The number of samples with non-carcinogenic risk for children was much higher, with six sites having HI > 1. As with the risk to adult receptors, Pb was the leading contributor to the non-carcinogenic risk.

The cancer risk for As for adults was greater than 1×10^{-5} at two sites. This represented an unacceptable risk based on the Canadian guidelines, which state that the acceptable risk is one excess cancer death per 100,000 people exposed [14]). The two sites were in Halifax, including a park in the Waverly Gold District, a region known to have elevated As levels from historical gold mining activities [26]. This sample had very high EF (5.9) and Igeo (3.3), indicating metal enrichment and moderate pollution. The second sample was from a park in the city center and had an EF (4.7) and Igeo (1.8), which suggested moderate enrichment and pollution.

Table 3. Correlation coefficients for regression analysis between metal bioaccessibility versus pH, organic matter (OM), iron (FeT), and metal concentration (metal).

		pH	OM	FeT	Metal
As	R	**0.4462**	0.0013	**−0.5986**	−0.1999
	p-value	<0.0001	0.7292	<0.0001	0.052
Cd	R	0.0389	0.1087	**0.3831**	0.0982
	p-value	0.0837	0.3670	0.001	0.4150
Co	R	0.0389	−0.0315	**−0.4706**	**−0.2789**
	p-value	0.7025	0.7659	<0.0001	0.0071
Cr	R	0.1932	0.0007	0.0319	0.1641
	p-value	0.1091	0.9995	0.1390	0.1747
Cu	R	0.0415	0.0802	**−0.2449**	0.0380
	p-value	0.6836	0.4299	0.0127	0.7091
Ni	R	0.0500	0.2629	**−0.3522**	**−0.2591**
	p-value	0.6230	0.0118	0.0006	0.0131
Pb	R	0.1934	0.0427	**−0.5738**	0.1898
	p-value	0.0564	0.6766	0.0000	0.0618
Zn	R	**0.3666**	0.1062	**−0.3466**	**0.3839**
	p-value	0.0003	0.3085	0.0006	0.0001

Note: Values in bold refer to relationships dimmed significant with $p < 0.05$.

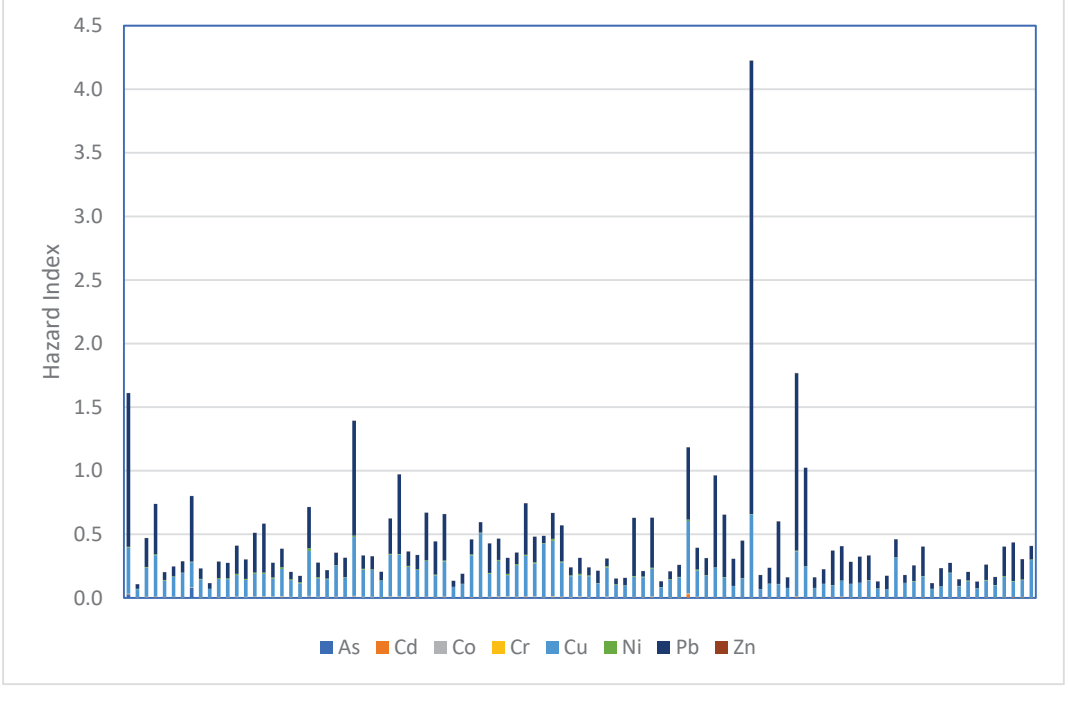

Figure 5. Hazard indices for children.

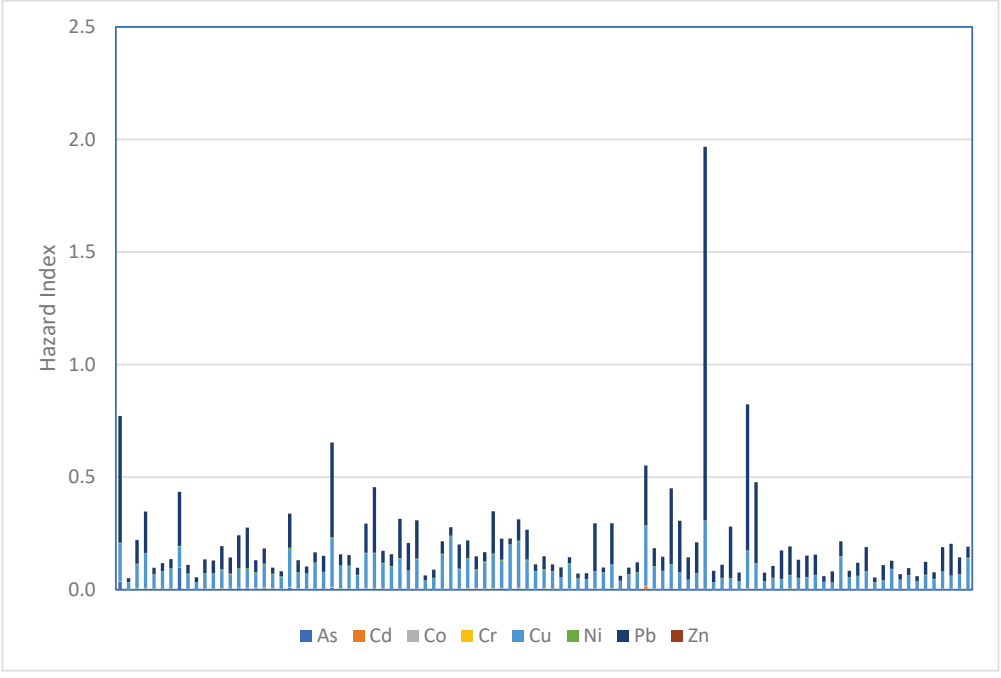

Figure 6. Hazard indices for adults.

4. Conclusions

Metal distribution in surface soils in the parks and playgrounds at the 12 Canadian cities studied reflected the regional natural-occurring differences in metal concentrations and anthropogenic sources, such as proximity to industrial areas (e.g., metal fabrication and recycling facilities), heavy traffic corridors (airport, highways and railway yard) and historical land use (e.g., industrial port land and demolished buildings). Cobalt, Cr, Fe, and Ni showed minimal pollution and enrichment and co-occurred because of their common origin from natural weathering and atmospheric deposition, whereas Cd, Cu, Pb, and Zn concentrations were impacted by anthropogenic sources. Arsenic was unique in that the elevated levels may have been attributed to arsenical-bearing rocks. Metals bioaccessibility values were variable and in the order Cr < Ni < Co < As < Zn < Cu < Pb < Cd. The human health risk associated with incidental soil ingestion for children, incorporating bioaccessibility, indicated unacceptable levels of non-carcinogenic effects for 6 out of the 101 samples analyzed. Lead was the leading contributor to the non-carcinogenic risk. Carcinogenic risk for As was limited to two samples. The importance of personal hygiene in limiting hand-to-mouth contact for children during playtime at these parks and playgrounds is warranted. Additional sampling to delineate the extent of contamination at parks and playgrounds with potential health risks is recommended along with notification of local health authorities.

Supplementary Materials: The following supporting information can be downloaded at: https://www.mdpi.com/article/10.3390/soilsystems8040123/s1. The dataset used in this paper are included as follows: Table S1 provides the coordinates for all the sampling locations; Table S2 shows total metal concentrations; and Table S3 gives the in vitro bioaccessibility data.

Author Contributions: M.D.: Conceptualization; funding acquisition; field investigation; laboratory analysis; data curation; supervision; writing—initial draft. A.D.: Methodology, field investigation; analysis; data analysis; writing—review and editing. J.D.: Methodology, field investigation; laboratory analysis; data analysis; writing—review and editing. All authors have read and agreed to the published version of the manuscript.

Funding: This research was supported by Canada Foundation for Innovation (instrumentation), Health Canada and Royal Roads University internal research grants. We are grateful to the Canadian Foundation for Innovation, Health Canada and Royal Roads University, Victoria, Canada, for funding.

Institutional Review Board Statement: Not applicable for studies not involving humans or animals.

Data Availability Statement: Data provided as Supplementary Materials.

Conflicts of Interest: The authors declare no conflicts of interest.

References

1. United Nations, Department of Economic and Social Affairs, Population Division. World Urbanization Prospects: The 2018 Revision, Online Edition. 2018. Available online: https://population.un.org/wup/Download/ (accessed on 31 October 2024).
2. Cave, M.R.; Wragg, J.; Denys, S.; Jondreville, C.; Feidt, C. Oral bioavailability. In *Dealing with Contaminated Sites*; Swartjes, F.A., Ed.; Springer Science Business Media B.V.: Berlin/Heidelberg, Germany, 2011. [CrossRef]
3. Meuser, H. *Contaminated Urban Soils*; Springer: Dordrecht, The Netherlands, 2010. [CrossRef]
4. Ajmone-Marsan, F.; Biasioli, M. Trace Elements in Soils of Urban Areas. *Water Air Soil Pollut.* **2010**, *213*, 121–143. [CrossRef]
5. Binner, H.; Sullivan, T.; Jansen, M.A.K.; McNamara, M.E. Metals in urban soils of Europe: A systematic review. *Sci. Total Environ.* **2023**, *854*, 158734. [CrossRef] [PubMed]
6. Wong, C.S.C.; Li, X.; Thornton, I. Urban environmental geochemistry of trace metals. *Environ. Pollut.* **2006**, *142*, 1–16. [CrossRef] [PubMed]
7. Guney, M.; Zagurya, G.J.; Dogan, N.; Onay, T.T. Exposure assessment and risk characterization from trace elements following soil ingestion by children exposed to playgrounds, parks and picnic areas. *J. Hazard. Mater.* **2010**, *182*, 656–664. [CrossRef] [PubMed]
8. Luo, X.; Ding, J.; Xu, B.; Wang, Y.; Li, H.; Yu, S. Incorporating bioaccessibility into human health risk assessments of heavy metals in urban park soils. *Sci. Total Environ.* **2012**, *424*, 88. [CrossRef] [PubMed]
9. Cocerva, T.; Robb, M.; Wong, A.; Doherty, R.; Newell, J.; Ofterdinger, U.; Carey, M.; Cave, M.; Cox, S.F. Using oral bioaccessibility measurements to refine risk assessment of potentially toxic elements in topsoils across an urban area. *Ecotoxicol. Environ. Saf.* **2024**, *276*, 116293. [CrossRef] [PubMed]
10. Han, Q.; Wang, M.; Cao, J.; Gui, C.; Liu, Y.; He, X.; He, Y.; Liu, Y. Health risk assessment and bioaccessibilities of heavy metals for children in soil and dust from urban parks and schools of Jiaozuo, China. *Ecotoxicol. Environ. Saf.* **2020**, *191*, 110157. [CrossRef] [PubMed]
11. Dakane, A. Bioaccessibility of Metals in Toronto City Parks. Master's Thesis, Royal Roads University, Victoria, BC, Canada, 2012. Available online: https://www.viurrspace.ca/items/35ee9ff5-7853-4737-b4d0-0a216f578dca (accessed on 31 October 2024).
12. Dupuis, J. Metals Bioaccessibility of Soils in Urban Parks in Fredericton and Saint John, New Brunswick. Master's Thesis, Royal Roads University, Victoria, BC, Canada, 2013. Available online: https://www.viurrspace.ca/items/990a9856-7c37-43ff-b8e4-c02be975b255 (accessed on 31 October 2024).
13. Durojaiye, A.O. Bioaccessibility of Metals in Soils of Selected Playgrounds in Montreal. Master's Thesis, Royal Roads University, Victoria, BC, Canada, 2014. Available online: https://www.viurrspace.ca/items/936d12c0-efb0-4b1a-81ee-2c9e404c20de (accessed on 31 October 2024).
14. Health Canada. *Federal Contaminated Site Risk Assessment in Canada. Supplemental Guidance on Human Health Risk Assessment for Oral Bioavailability of Substances in Soil and Soil-Like Media*; Health Canada: Ottawa, ON, Canada, 2017.
15. Dodd, M.; Richardson, G.M.; Wilson, R.; Rencz, A.; Friske, P. Elemental Concentrations and In Vitro Bioaccessibility in Canadian Background Soils. *Environ. Geochem. Health* **2017**, *39*, 759–777. [CrossRef] [PubMed]
16. USEPA. SW-846 Test Method 1340: In Vitro Bioaccessibility Assay for Lead in Soil. 2017. Available online: https://www.epa.gov/hw-sw846/sw-846-test-method-1340-vitro-bioaccessibility-assay-lead-soil (accessed on 31 October 2024).
17. Canadian Council of Ministers of the Environment (CCME). *A Protocol for the Derivation of Environmental and Human Health Soil Quality Guidelines*; Canadian Council of Ministers of the Environment: Winnipeg, MB, Canada, 2006.
18. Kowalska, J.B.; Mazurek, R.; Gasiorek, M.; Zaleski, T. Pollution indices as useful tools for the comprehensive evaluation of the degree of soil contamination–A review. *Environ. Geochem. Health* **2018**, *40*, 2395–2420. [CrossRef] [PubMed]
19. Ng, J.C.; Juhasz, A.; Smith, E.; Naidu, R. Assessing the bioavailability and bioaccessibility of metals and metalloids. *Environ. Sci. Pollut. Res.* **2015**, *22*, 8802–8825. [CrossRef] [PubMed]
20. Basta, N.T.; Juhasz, A. Using In Vivo Bioavailability and/or In Vitro Gastrointestinal Bioaccessibility Testing to Adjust Human Exposure to Arsenic from Soil Ingestion. *Rev. Mineral. Geochem.* **2014**, *79*, 451–472. [CrossRef]
21. Health Canada. *Federal Contaminated Site Risk Assessment in Canada, Part I: Guidance on Human Health Preliminary Quantitative Risk Assessment (PQRA)*; Version 2.0; Health Canada: Ottawa, ON, Canada, 2004.

22. Amponsah, L.O.; Dodd, M.; Darko, G. Gastric bioaccessibility and human health risks associated with soil metal exposure via ingestion at an e-waste recycling site in Kumasi, Ghana. *Environ. Geochem. Health* **2020**, *44*, 497–509. [CrossRef]
23. Health Canada. *Federal Contaminated Site Risk Assessment in Canada: Toxicological Reference Values (TRVs)*; Version 3.0; Health Canada: Ottawa, ON, Canada, 2021.
24. USEPA. Integrated Risk Information System. 2022. Available online: https://www.epa.gov/iris (accessed on 31 October 2024).
25. United States Environmental Protection Agency (USEPA). Statistical Software ProUCL 5.1 for Environmental Applications for Data Sets with and without Nondetect Observations. 2016. Available online: https://www.epa.gov/land-research/proucl-software (accessed on 31 October 2024).
26. Drage, J. Review of the Environmental Impacts of Historic Gold Mine Tailings in Nova Scotia, Nova Scotia Department of Natural Resources, Open File Report ME 2015-004. 2015. Available online: https://www.novascotia.ca/natr/meb/hazard-assessment/docs/7_-_ofr_me_2015-004.pdf (accessed on 31 October 2024).
27. Li, H.-B.; Li, M.-Y.; Zhao, D.; Li, J.; Li, S.-W.; Xiang, P.; Juhasz, A.L.; Ma, L.Q. Arsenic, lead, and cadmium bioaccessibility in contaminated soils: Measurements and validations. *Crit. Rev. Environ. Sci. Technol.* **2020**, *50*, 1303–1338. [CrossRef]
28. Khan, M.A.; Nawab, J.; Khan, A.; Brusseau, M.L.; Khan, S.N.; Ali, N.; Bahadur, S.; Khan, S.; Huang, Q. Human health and ecological risks associated with total and bioaccessible concentrations of cadmium and lead in urban park soils. *Bull. Environ. Contam. Toxicol.* **2023**, *110*, 61. [CrossRef]
29. Ruby, M.V. Bioavailability of soil-borne chemicals: Abiotic assessment tools. *Hum. Ecol. Risk Assess.* **2004**, *10*, 647–656. [CrossRef]

Disclaimer/Publisher's Note: The statements, opinions and data contained in all publications are solely those of the individual author(s) and contributor(s) and not of MDPI and/or the editor(s). MDPI and/or the editor(s) disclaim responsibility for any injury to people or property resulting from any ideas, methods, instructions or products referred to in the content.

soil systems

MDPI

Article

Nickel Effects on Growth and Phytolith Yield of Grasses in Contaminated Soils

Enilson de Barros Silva [1,*], Múcio Mágno de Melo Farnezi [2], Lauana Lopes dos Santos [1], Alexandre Chistofaro Silva [2], Paulo Henrique Grazziotti [2], Luís Reynaldo Ferracciú Alleoni [3], Ingrid Horák-Terra [4], Sandra Antunes do Nascimento [5] and Bento Gil Uane [6]

[1] Department of Agronomy, Federal University of the Jequitinhonha and Mucuri Valley (UFVJM), Campus JK, Diamantina 39100-000, MG, Brazil; lauana.santos@ufvjm.edu.br
[2] Department of Forestry, Federal University of the Jequitinhonha and Mucuri Valley (UFVJM), Campus JK, Diamantina 39100-000, MG, Brazil; mucio.farnezi@ufvjm.edu.br (M.M.d.M.F.); alexandre.christo@ufvjm.edu.br (A.C.S.); paulo.grazziotti@ufvjm.edu.br (P.H.G.)
[3] Department of Soil Science, Luiz de Queiroz College of Agriculture (ESALQ), University of São Paulo, Av. Pádua Dias, 11, Piracicaba 13418-900, SP, Brazil; alleoni@usp.br
[4] Institute of Agrarian Sciences, Federal University of the Jequitinhonha and Mucuri Valley (UFVJM), Campus Unaí, Unaí 38610-000, MG, Brazil; ingrid.horak@ufvjm.edu.br
[5] Institute of the Environment and Water Resources, Av. Luís Viana Filho, 600, Salvador 41745-900, BA, Brazil; atendimento.seia@inema.ba.gov.br
[6] Department of Agro-processing and Veterinary, Pungue University, P.O. Box 333, Chimoio 2200, Mozambique; bentogiluane@gmail.com
* Correspondence: ebsilva@ufvjm.edu.br

Abstract: Nickel (Ni) is extremely toxic to plants at high concentrations. Phytoliths have the potential to sequester the heavy metals absorbed by plants and act as a detoxification mechanism for the plant. The authors of the present study aimed to evaluate the effects of Ni on the growth and phytolith yield of grasses in two artificially contaminated soils. Two experiments separated by soil types (Typic Quartzipsamment and Rhodic Hapludox) were conducted in a completely randomized design in a 2 × 4 factorial scheme with three replications. The factors were two species of grass (*Urochloa decumbens* and *Megathyrsus maximus*) and three concentrations of Ni (20, 40, and 120 mg kg^{-1}) and control treatment. The grasses were influenced by the increase in Ni rates in the soils. Ni exerted a micronutrient function with the addition of 30 mg kg^{-1} of Ni in soils, but this concentration caused toxicity in grasses. Such a level is lower than the limits imposed by the Brazilian environmental legislation. Higher Ni availability in Typic Quartzipsamment promoted Ni toxicity, with reduced growth and increased phytolith yield in the shoot, increased Ni in the shoot, and Ni occlusion in phytoliths by grasses, in comparison with Rhodic Hapludox. The yield and Ni capture in phytoliths by grasses in Ni-contaminated soils are related to the genetic and physiological differences between grasses and Ni availability in soils. Ni capture by phytoliths indicates that it may be one of the detoxification mechanisms of *Urochloa decumbens* to Ni contamination, providing additional tolerance. *Megathyrsus maximus* may be a future grass for the phytoremediation technique in Ni-contaminated soils.

Keywords: heavy metal; *Urochloa*; *Megathyrsus maximus*; entisol; oxisol; phytolith

Citation: Silva, E.d.B.; Farnezi, M.M.d.M.; Santos, L.L.d.; Silva, A.C.; Grazziotti, P.H.; Alleoni, L.R.F.; Horák-Terra, I.; Nascimento, S.A.d.; Uane, B.G. Nickel Effects on Growth and Phytolith Yield of Grasses in Contaminated Soils. *Soil Syst.* **2024**, *8*, 17. https://doi.org/10.3390/soilsystems8010017

Academic Editor: Manfred Sager

Received: 27 November 2023
Revised: 23 January 2024
Accepted: 24 January 2024
Published: 26 January 2024

Copyright: © 2024 by the authors. Licensee MDPI, Basel, Switzerland. This article is an open access article distributed under the terms and conditions of the Creative Commons Attribution (CC BY) license (https://creativecommons.org/licenses/by/4.0/).

1. Introduction

Nickel (Ni) is a micronutrient for normal plant growth and development [1,2] and is required in very small concentrations for optimum plant growth [2]. It is extremely toxic in high concentrations and is among the most common heavy metals in soils [1,2].

The phytoremediation technique uses the potential of some plants to tolerate heavy metals for the restoration of contaminated soils [3]. Therefore, tolerant species can be characterized according to their ability to uptake, translocate, and concentrate metals in the plant [3,4]. Depending on the criteria, a plant may or may not be considered a

phytoextractor of metal [3,4]. In general, critical toxicity levels of Ni are 10 mg kg^{-1} dry matter in sensitive species, 50 mg kg^{-1} dry matter in moderately tolerant species, and 100 mg kg^{-1} dry matter in tolerant species [5].

Phytoliths represent biomineralizations comprising either silica or calcium, which undergo precipitation within cellular structures or intercellular spaces of plant tissues [6–9]. The deposition of phytoliths confers upon plants the capacity to ensnare and neutralize deleterious metal ions, which is particularly evident in certain plant species belonging to the Cyperaceae and Poaceae families [6,9]. Certain members of the Poaceae family demonstrate resilience to an accumulation of toxic metals [3,4], characterized by elevated rates of growth and substantial biomass yield capabilities, coupled with heightened phytolith production [6–9].

The grasses scrutinized in this investigation encompass species such as *Megathyrsus maximus* and *Urochloa decumbens*, exhibiting noteworthy biomass generation and swift growth rates [1]. Grasses are categorized based on their handling and soil fertility prerequisites [10]. *Megathyrsus maximus* has attained global recognition for its elevated productivity and adeptness in adapting to various soil and climatic contexts [10], whereas *Urochloa decumbens* grasses distinguish themselves for their ruggedness and commendable adaptability across diverse environments [11]. However, the phytolith production capacity of these grasses remains undetermined.

The Brazilian National Environmental Council recently established investigation values for metals in agricultural soils, including Ni [12], without specifically mentioned soil type. However, soil type plays a key role in controlling the heavy-metal availability for plant uptake [7,13,14]. Phytolith yield in plants is not yet fully understood; however, yield is related to climatic conditions, plant age and taxonomy, evapotranspiration rate, soil type, and heavy-metal availability [7,15]. Therefore, the relationship between Ni availability and phytolith yield in grass to select grasses with phytoremediation potential in Ni-contaminated soils has not been studied yet. Given the above, we aimed to evaluate the effects of Ni on the growth and phytolith yield of grasses in two artificially contaminated soils.

2. Material and Methods

2.1. Soil and Experimental Design

Two greenhouse experiments were carried out in Diamantina (18°15′ S, 43°36′ W, 1250 m a.s.l.), located in the state of Minas Gerais, Brazil. The soils under investigation were identified as Typic Quartzipsamment (TQ) and Rhodic Hapludox (RH) following Soil Taxonomy [16], displaying distinct chemical and textural attributes. These soils were sourced from their native "Cerrado" (savanna) state to guarantee the absence of metal contamination in the superficial soil layer (0–0.2 m depth). A subsample was procured, subjected to air-drying, and sieved at 2.0 mm for subsequent chemical analysis and determination of soil texture [17] (Table 1). The total Ni concentration was evaluated by the USEPA 3052 method using microwaves with a digestion solution of H_2O_2 + HNO_3 + HF and H_3BO_3 [18] (Table 1).

Liming was addressed using dolomitic limestone with 38.0% CaO, 12.5% MgO, and 90% total neutralizing power. The liming calculation was executed employing the base saturation method, utilizing the subsequent formula: Liming requirements (Mg ha^{-1}) = ((Vg − Va) × CEC)/100, where Vg signifies the recommended base saturation for grasses (45%), Va denotes the base saturation determined in soil analysis, and CEC represents the cation exchange capacity (Table 1). Application of limestone to the soils occurred, allowing for a 30-day reaction period under soil moisture conditions at field capacity. Monitoring of soil moisture levels was conducted through daily weighing of the pots.

Table 1. Chemical attributes and soil texture before applying treatments.

Attribute	Unit	Soil	
		Typic Quartzipsamment (TQ)	Rhodic Hapludox (RH)
pH [a] $_{water}$	-	5.1	5.2
P [b]	mg kg^{-1}	0.2	0.2
K [b]	$mmol_c$ kg^{-1}	0.4	0.2
Ca [c]	$mmol_c$ kg^{-1}	6.7	4.5
Mg [c]	$mmol_c$ kg^{-1}	3.5	1.8
Al [c]	$mmol_c$ kg^{-1}	7.8	4.2
Cation-exchange capacity (CEC)	$mmol_c$ kg^{-1}	40.6	71.5
Base saturation	%	26.0	9.0
Organic carbon [d]	g kg^{-1}	3.5	5.8
Ni [e]	mg kg^{-1}	<0.1	<0.1
Maximum P adsorption capacity	mg kg^{-1}	100	250
Fe_2O_3 [f]	g kg^{-1}	7	298
Al_2O_3 [f]	g kg^{-1}	33	166
Clay [g]	g kg^{-1}	60	510

[a] Soil/water 1:2.5. [b] Mehlich-1 extractor. [c] KCl 1 mol L^{-1} extractor. [d] Walkley–Black method. [e] USEPA 3052 method. [f] Sulfuric acid digestion. [g] Pipette method.

The basal fertilization rates adhered to recommended guidelines [1], except phosphate fertilization, where the fertilization rate was determined based on the maximum phosphorus adsorption capacity of each soil (Table 1), extrapolated from Langmuir isotherm second region data [19]. Consequently, the applied phosphorus rates were 200 mg for Typic Quartzipsamment (TQ) and 450 mg for Rhodic Hapludox (RH) per kg of soil, utilizing NaH_2PO_4 as the phosphorus source. Nutrients were administered in the form of pure analytical-grade reagents, thoroughly mixed, and allowed to incubate for 15 days in each soil. Nickel concentrations, post-liming and basic fertilization, were introduced as nickel chloride with analytical-grade chemical reagent standards. The concentrations were meticulously incorporated into the soil within a 5 kg plastic bag and subsequently transferred to pots for a 15-day reaction in the soil.

Two distinct experiments, segregated by soil type (TQ and RH), were established employing a completely randomized design, distributed in a 3 × 4 factorial arrangement with three replications in polyvinyl chloride pots weighing 4 kg and filled with 3 kg of soil. The experimental treatments comprised the combination of two grass species (Urochloa decumbens (Stapf) R.D. Webster cv. Basilisk and Megathyrsus maximus (Jacq.) B.K. Simon and S.W.L. Jacobs cv. Mombaça) and three nickel (Ni) concentrations (20, 40, and 120 mg kg^{-1} of soil), along with a control treatment involving no addition of Ni. These concentrations correspond to 0.3, 0.6, and 1.8 times the investigated values in the soils [12].

Soil samples were taken from each pot one day before sowing. Sampling was carried out with a polyvinyl chloride pipe of a half inch 0.40 m in length, with four holes throughout the length of the pot with soil. Subsequently, the soil samples were air-dried and sieved through sieves of <2 mm in diameter. The available Ni concentration in soil was extracted with Mehlich-1 [14].

Five seeds from each grass species were sown in pots. Seedlings were thinned to one plant per pot within 14 days after emergence and the four top-dressing fertilizations of 50 mg N (urea) per kg soil every 15 days, after the thinning of grasses. The pots were irrigated daily with distilled water to maintain soil moisture at field capacity with daily checks by weighing the pots throughout the experimental period.

2.2. Measurements and Analytical Determinations

After 120 days of thinning of grasses, the plants were harvested from the shoot. Shoot samples were washed three times in deionized water and dried in a forced ventilation oven

at 65 °C until constant weight, with subsequent weighing to obtain shoot dry weight. A microwave oven (CEM MarsTM 6) with nitric acid (65% v/v—Merck, Rahway, NJ, USA) was used to extract Ni from the shoots of the grasses. Graphite furnace atomic absorption spectrometry (Perkin–Elmer Analyst 800) was used to determine the Ni concentration in the aerial part of grasses. Quality control of Ni analysis used certified reference material (NIST SRM 1573a Tomato leaves) with a recovery rate of 98 ± 2.

The extraction of phytoliths from the shoot of grasses as prepared and separated was performed using the process adapted from [20]. The concentration of phytoliths was determined by weighing 10 g of dry mass from the crushed aerial part in a porcelain crucible which was subsequently subjected to calcination at 600 °C in a muffle furnace for six hours. The resulting ashes were transferred to Falcon tubes, where carbonates were removed by the application of 2.5 mL of 1 mol L^{-1} HCl. The ashes were then purified using 2.5 mL of hydrogen peroxide (H_2O_2) of 30 volume. The residue underwent consecutive washes with distilled water, followed by centrifugation at 300 rad s^{-1} for five minutes, with the supernatant being discarded. This procedure was repeated in five cycles. The resulting residue (silica phytolith) was dried at 105 °C in a drying oven until a constant weight was achieved. Quantification was conducted through classical gravimetry, employing a precision analytical balance with an accuracy of 0.00001 g. The phytolith concentration results were expressed in g kg^{-1} of the initially crushed dry mass.

Nickel was extracted from phytoliths using the USEPA 3052 method, with digestion in a microwave oven (CEM MarsTM 6) with H_2O_2 + HNO_3 + HF and the addition of H_3BO_3 [18]. Atomic Absorption Spectrometry using a graphite furnace (AAnalyst 800, Perkin-Elmer, Waltham, MA, USA) was used to determine the Ni concentration in the filtered solutions of phytoliths extracted from the shoots of grasses.

2.3. Statistics

The normality and homoscedasticity of the variables evaluated were assessed before the analysis of variance. The data were subjected to an analysis of variance, which consisted of the study of Ni concentrations and the control and the grasses in each soil type. This means that the grasses were compared by Tukey's test at 5%. The regression equations were adjusted for the variables depending on the Ni concentrations added to the soil. Statistical analyses were performed using Sisvar v. 5.6 [21] and the graphs were plotted in SigmaPlot v. 10.0 (Systat Software Inc., Chicago, IL, USA).

3. Results

3.1. Soil Characteristics

The soils exhibited highly contrasting chemical and textural characteristics (Table 1). The TQ soil exhibited much lower clay, Fe and Al concentrations, yielding a lower CEC than the RH soil. Both soils exhibited no Ni contamination in natural conditions. Despite the different chemical attributes between the two soils, the available concentration of Ni increased linearly with the applied concentrations in both soils (Figure 1). The Ni availability, based on the regression coefficients of the adjusted equations (Figure 1), indicates that in each kg of soil available, there was 0.68 mg of Ni in the TQ soil and 0.48 mg in the RH soil, with the Ni availability in the TQ being 42% higher than in the RH soil.

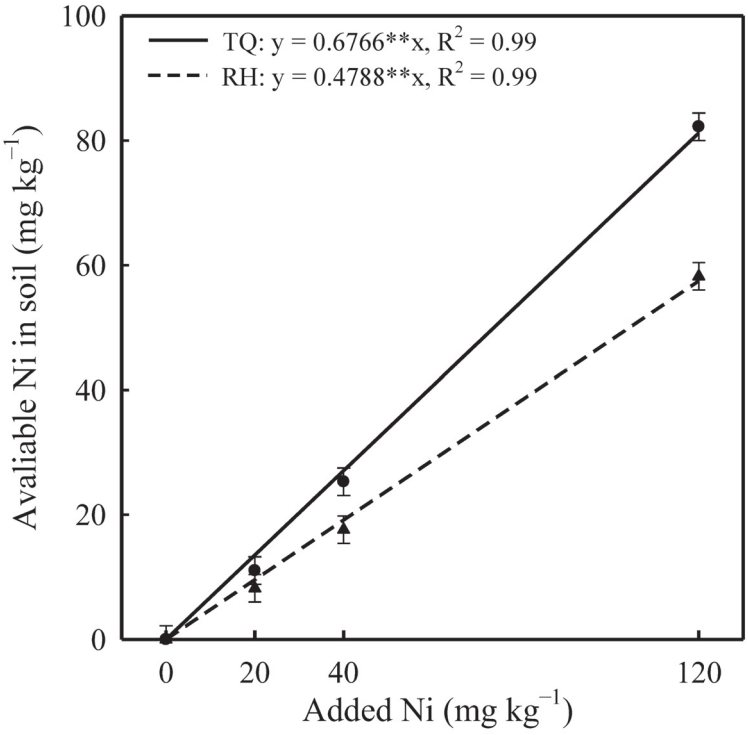

Figure 1. Availability of Ni as extracted with Mehlich-1 after 15-day incubation of soils (TQ: Typic Quartzipsamment and RH: Rhodic Hapludox) with increasing concentrations of Ni. ** Significant coefficient of the equation at 1% by *t*-test.

3.2. Nickel Effects on Shoot and Phytolith Yield in Grasses

The shoot dry matter yield of the grasses was affected by the Ni addition in both soils ($p < 0.01$). The square root model better explains the variation in the shoot dry matter of the grasses as a function of the Ni addition for each soil. The maximum dry matter yield of grasses was achieved with the maximum concentration (MC) of Ni added to the soils (Figure 2a,b), with an average MC of 30 mg kg^{-1} of Ni.

The grasses showed positive responses with increasing Ni concentrations added to the soil until reaching MC (Figure 2a,b), reflecting the essentiality of Ni as a micronutrient for plants. The positive response of grasses grown in the TQ soil was twice as high as when grown in the RH soil, with Ni concentrations added to the soil increasing from control (no Ni added) to reach MC (Table 2), due to greater Ni availability in the TQ soil (Figure 1). *M. maximus* had a response to Ni addition in the soil 2.4 times greater than *U. decumbens* when cultivated in the soils (TQ and RH) with increasing Ni concentrations from the control (without Ni addition) until reaching MC (Table 2). Therefore, the higher shoot dry matter yield of *M. maximus* compared to *U. decumbes* is due to its greater adaptability to different cultivation conditions.

The dry matter yield of grasses decreased after reaching the MC with increased Ni concentrations in the soils (Figure 2a,b), causing Ni toxicity due to increased Ni availability in soils (Figure 1). The Ni toxicity effect was 1.8 times higher in grasses grown in the TQ soil than in the RH soil (Table 2) due to higher Ni availability in the TQ soil (Figure 1). The comparison of grasses revealed that *M. maximus* had a shoot dry matter yield of 1.3 times greater compared to *U. decumbens*, with increasing concentrations of Ni added in the MC soil until the maximum concentration of added Ni (120 mg kg^{-1}) was reached. The greater

tolerance potential of *M. maximus* to Ni can be attributed to the greater biomass production and its adaptability to the high availability of Ni in soils (Figure 1).

Phytolith yield by grasses was influenced by the increase in Ni concentrations ($p < 0.01$) only when grown in the TQ soil (Figure 2c,d). There was a reduction in phytoliths until MC for dry matter yield and a subsequent increase when the Ni concentrations increased, adjusting to the square root model (Figure 2c). The phytolith reduction is due to the dilution effect in the positive response of grasses to Ni, while the increase is due to the toxic effect of Ni in the shoots of grasses (Figure 2a). The dilution effect did not cause a difference in phytolith yield between the two grasses (Figure 2c). The effect of Ni toxicity caused a greater increase in the phytoliths in *U. decumbens* than in *M. maximus*, with a higher yield with the application of maximum concentration added (120 mg kg^{-1}) (Figure 2c), reflecting the genetic and physiological differences between grasses in the phytolith yield.

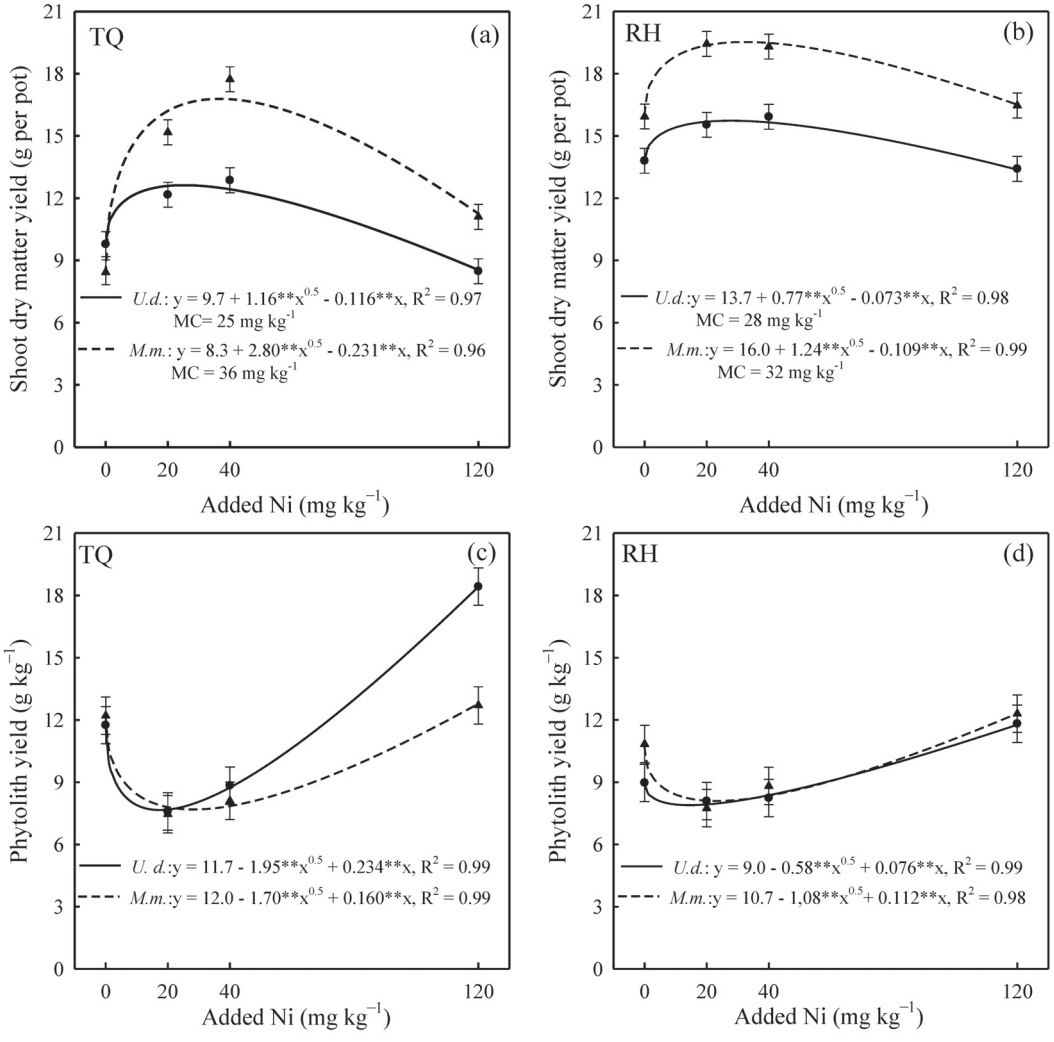

Figure 2. Shoot dry weight (**a**,**b**) and phytolith yield (**c**,**d**) of grasses (*Ud*: *Urochloa decumbens* and *M.m.*: *Megathyrsus maximus*) with increasing concentrations of Ni and maximum concentration (MC) within 120 days of thinning in two soils (TQ: Typic Quartzipsamment and RH: Rhodic Hapludox). ** Significant coefficient of the equation at 1% by *t*-test.

Table 2. Shoot dry matter yield corresponding to the control, maximum concentration (MC) for maximum shoot dry matter yield of two species of grasses, and maximum concentration added (MCA) to the soil within 120 days of thinning in two soils [(a)].

Grasses	Typic Qurtzipsmment (TQ)			Rhodic Hpludox (RH)		
	Control	MC	MCA	Control	MC	MCA
Urochlo decumens	9.7	12.6	8.5	13.7	15.7	13.4
Megthyrsus mximus	8.3	16.8	11.3	16.0	19.5	16.5
Average	9.0	14.7	9.9	14.9	17.6	15.0

[(a)] Shoot dry matter yield was estimated by replacing the control (no Ni addition), maximum concentration (MC) of shoot dry weight of two grasses, and maximum concentration added (MCA) to soils in the equations relating to the Ni concentrations (Figure 2a,b).

3.3. Nickel in Shoots and Phytoliths

Nickel concentrations in the shoot and phytoliths were assessed to examine Ni uptake and Ni sequestration within phytoliths by the grasses, respectively. The nickel concentrations in both shoots and phytoliths of grasses were significantly influenced by the Ni additions to the soils ($p < 0.01$). The addition of Ni into the soils exhibited a positive and linear correlation with the Ni concentrations in both the shoots and phytoliths of the grasses (Figure 3). Disparities in Ni uptake were observed among the grass species (Figure 3a,b), and Ni occlusion in phytoliths (Figure 3c,d) was evident only when cultivated in the TQ soil.

Elevated Ni concentrations in the shoots of grasses were observed when cultivated in the TQ soil compared to the RH soil (Figure 3a,b). This discrepancy is attributed to the greater Ni availability in the TQ soil (Figure 1), manifesting as an augmented positive response and a toxic impact of Ni on the dry matter yield of grasses (Figure 2a). Specifically, the Ni concentration in the shoot was higher in *Megathyrsus maximus* compared to *Urochloa decumbens* when cultivated in the TQ soil (Figure 3a).

The Ni occlusion within phytoliths exhibited a higher magnitude when grasses were grown in the TQ soil compared to the RH soil (Figure 3c,d). This response is attributed to the heightened toxic impact of Ni, stemming from its increased availability in the TQ soil (Figure 1). When the grasses reached their maximum shoot growth phase (Figure 2a), there was no discernible disparity in Ni occlusion (Figure 3c). This uniformity can be attributed to the adequacy of Ni concentration in the shoots to attain maximal growth, thereby affirming the essentiality of Ni as a micronutrient. Notably, *Urochloa decumbens* demonstrated a greater Ni occlusion in phytoliths than *Megathyrsus maximus* when cultivated in TQ soil at the highest applied concentration (120 mg kg^{-1}) (Figure 3c). This observation may be associated with the tolerance mechanism of *U. decumbens* to Ni toxicity.

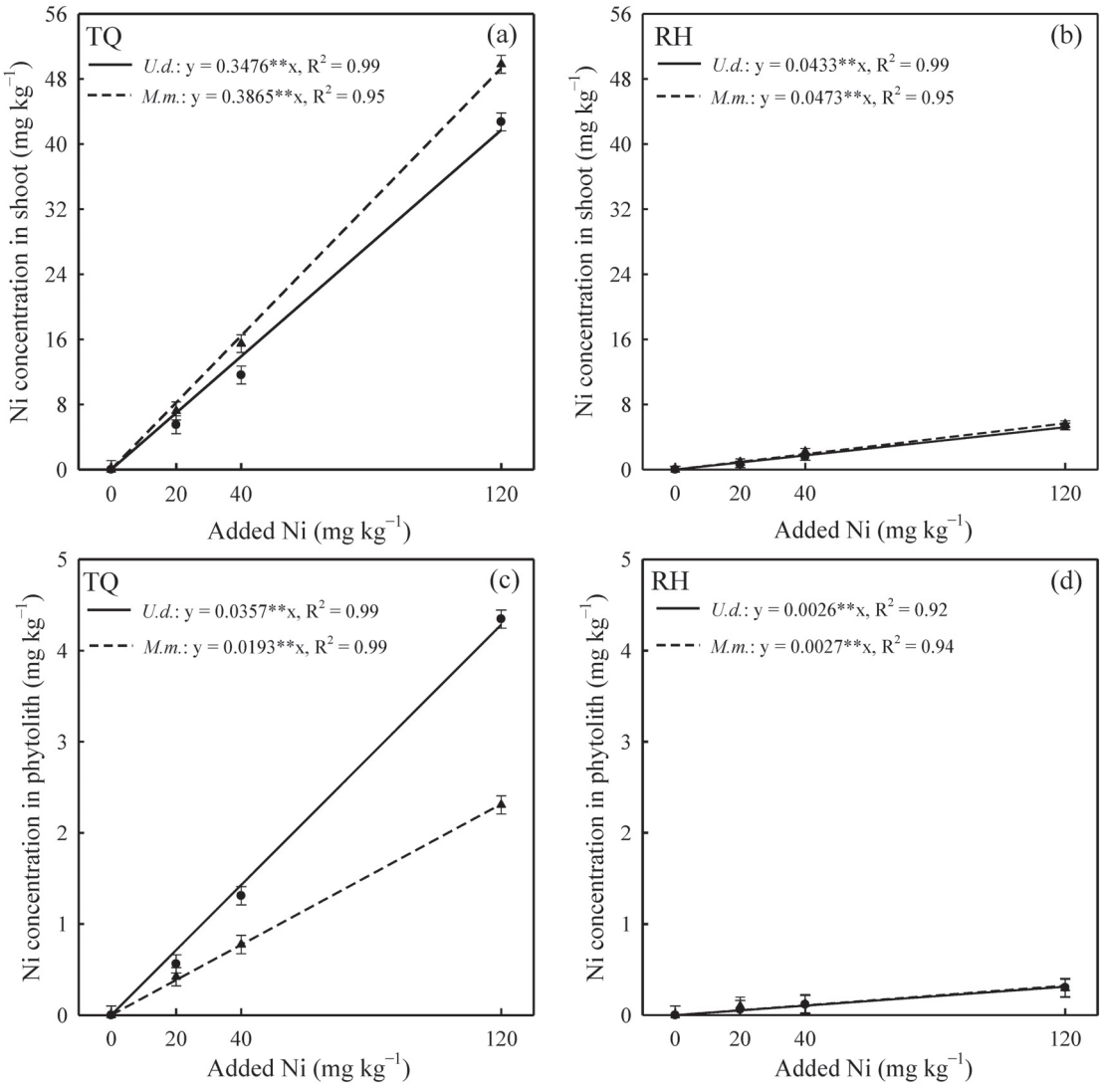

Figure 3. Concentration of Ni in the shoot (**a**,**b**) and phytolith (**c**,**d**) of grasses (*Ud*: *Urochloa decumbens* and *M.m.*: *Megathyrsus maximus*) with increasing concentrations of Ni within 120 days of thinning in two soils (TQ: Typic Quartzipsamment and RH: Rhodic Hapludox). ** Significant coefficient of the equation at 1% by *t*-test.

4. Discussion

The main differences between the evaluated soils that influenced the Ni availability for grasses were the concentrations of iron and aluminum oxides, carbon organic, and clay (Table 1). Such differences in soil characteristics resulted in a lower CEC for the TQ soil when compared to the RH soil (Table 1). Consequently, Ni became more available in the TQ soil (Figure 1), providing increased Ni uptake and Ni occlusion in the phytoliths by the grasses (Figure 3a,c) and causing an increase when reaching the MC of Ni and, subsequently, a reduction in the biomass yield (Figure 2a) and, inversely, in the phytolith yield (Figure 2c). Ni retention occurs, for the most part, through the electrostatic forces of the negatively charged particles, which makes it highly dependent on soil CEC [5,7,13,14].

The interaction between chemical forms of metals present in the soil solution and the surface of clay minerals and organic colloids in the soil, called adsorption, is the chemical process that most alters the metal availability in the soil [13,14].

The yield of plants grown in contaminated soil acts as a bioindicator of a plant's response to elements added to the soil. The maximum concentrations (MC) of Ni (Figure 2) can be considered as recommended concentrations of Ni for the growth of grasses in soils. The recommended average concentration of 30 mg kg^{-1} of Ni is in the range commonly found in agricultural soils [13] and reinforces the essentiality of Ni for plants [1,2]. On the other hand, the MC of Ni (Figure 2) was below the investigation value (70 mg kg^{-1} of Ni) established by Brazilian legislation for agricultural soils [12]. Therefore, unacceptable Ni concentrations for agricultural soils were toxic to grasses even in pot experiments, showing grass sensitivity to excess Ni in soils [1,2].

The grasses responded differently to Ni application (Figure 2a,b), proving Ni's essentiality as a micronutrient, i.e., low concentrations of Ni have a significant effect on plant growth and development. When the MC was reached, it reduced the shoot dry matter of the grasses, reflecting the toxicity effect on the plants. The supply of Ni in low concentrations increased the shoot dry matter yield of the grasses up to the MC, while higher concentrations added to the soil above the MC reduced the dry matter of the grasses in both soils (Figure 2a,b). The results prove the essentiality of Ni as a micronutrient [1,2]; that is, in small concentrations Ni has a positive effect, increasing the growth of grasses, but it has a toxic effect on plants in high concentrations above the MC, resulting in lower grass growth [1,14]. The decline in grass growth following exposure to Ni after reaching the MC also corresponds to the inhibition of active enzymes, mineral nutrition, and chlorophyll biosynthesis in plants [5].

M. maximus responded most and tolerated to soil Ni, i.e., it presented higher growth and less reduction in the shoot when compared to *U. decumbens* (Figure 2a,b). The *Megathyrsus maximus* species has a high productive potential in relation to the genus *Urochloa*, being more responsive to soil fertilization and adaptation to different soil conditions [1,10]. The species *M. maximus* was more responsive when grown in the TQ soil than in the RH soil compared to *U. decumbens* (Figure 2a,b). This suggests that in addition to the species, the texture and mineralogy of the soil influence the availability of Ni and, consequently, the absorption of Ni by the plant. Ni absorption by plants depends on the metabolism and plant species [1,10], the form of Ni and concentration in the soil [1,2,5], the presence of other nutrients [5], and the physical and chemical attributes of the soil [7,13,14].

The phytolith yield of grasses and Ni toxicity in the shoot in response to Ni application in soils (Figure 2a,b) provide the potential of grasses as producers of phytoliths (Figure 2c,d). The reduction in phytolith yield from grasses (Figure 2c,d) in response to the Ni application from the shoot (Figure 2a,b) is caused by the phytolith's dilution effect on the plant. The effect can be characterized when the relative growth rate of the shoot is higher than the relative yield rate of the phytolith. The superior growth of the shoot of grasses in response to Ni application demonstrates the essentiality of Ni for plants [1,2]. However, under conditions of stress caused by excess Ni, the grasses showed an increase in phytolith yield when cultivated in TQ soil (Figure 2c). The greater formation of phytoliths in conditions of excess Ni suggests the presence of a detoxification mechanism of grasses to Ni. The role of phytoliths as a plant detoxification mechanism for various heavy metals has been reported in some studies [6,8,9].

The grasses had different capacities for producing phytoliths in conditions of Ni toxicity in soil with greater availability of Ni, such as TQ soil (Figure 2c). The phytolith concentrations in plants are correlated with the Ni availability in the soil [7,15], which can directly reflect the phytolith yield of grasses [6–9]. The greatest increase in phytolith yield occurred with *U. decumbens,* rather than *M. maximus,* in response to the toxic effect of Ni (Figure 2c), where the greater rusticity of the genus *Urochloa* [11] possibly provided greater phytolith yield to tolerate Ni toxicity. However, the reasons for the phytolith yield of plants are still unknown, but phytoliths can be produced in adverse conditions and can

increase the resistance of many terrestrial plants against biotic and abiotic stress, especially species of the Cyperaceae and Poaceae families [6,9], which are the families of the grasses evaluated [11].

The Ni concentration in the shoot and phytoliths was inverse between the grasses *U. decumbens* and *M. maximus* when cultivated in TQ soil (Figure 3a). This result is contrary to that observed in rice, where it was observed that the higher the elemental concentration of the plant, the higher the metal concentration in the phytoliths [7], demonstrating that *U. decumbens* develops a mechanism that allows the capture and stabilization of Ni in phytoliths. This capture is possibly due to the higher rusticity and ability to grow in adverse soil conditions in relation to *Megathyrsus maximus* [11]. The phytolith yield is a mechanism of tolerance to the metal developed by the plant, which immobilizes and makes the metal unavailable, giving phytoliths the characteristic of sequestering the metal and preventing its return to the soil in cases of senescence of the plant or ingestion by fauna, making the metal unavailable to the food chain [8]. The correlation between the concentration of phytoliths in plants and the elemental concentration of phytoliths, that is, the greater the availability of the element in the soil, the greater its absorption, significantly affecting the production of phytoliths in plant organs [7]. However, the reasons for phytoliths' yield by plants are still poorly understood, but it is known that phytoliths can be produced under adverse conditions and increase resistance against biotic and abiotic stress in many land plants, especially species from the Cyperaceae family and Poaceae [6,9]. Several factors can influence these phytoliths' yield by plants, such as taxonomic character, environmental conditions, availability of water in the soil, availability of monosilic acid in the soil solution, and evapotranspiration rate [6,8,9]. Furthermore, the morphology and chemical composition of phytoliths and environmental conditions can affect the sequestration of elements in phytoliths [6,8,9]. This explains why the elemental composition in organs is related to the elemental composition in phytoliths [7].

The toxicity level of Ni patterns in plant species is classified into sensitive, moderately tolerant, and non-tolerant [5]. *U. decumbens* is classified as a sensitive species because it has Ni toxicity when the concentration in the shoot is less than 10 mg kg^{-1} e. *M. maximus* is moderately tolerant because it has a Ni concentration between 10 and 50 mg kg^{-1} (Figure 3a). Therefore, the increased yield (Figure 2c) and Ni occlusion (Figure 3c) in phytoliths by *U. decumbens* did not confer greater tolerance to Ni toxicity compared to *M. maximus*. In contrast, *M. maximus* presented desirable characteristics such as a higher dry matter yield (Figure 2a) and shoot Ni concentration (Figure 3a), indicating that this species is more tolerant to excess Ni. Grasses with phytoremediation potential should have desirable phytoextraction characteristics, such as high growth rate, biomass yield, root growth, and the ability to tolerate and accumulate toxic metals [3,4].

The *M. maximus* grass had the highest growth response, accumulation of Ni in the shoot, and less yield and Ni occlusion in phytoliths to *U. decumbens* (Figure 3), demonstrating that the yield and Ni sequestration by phytoliths is not a possible mechanism of tolerance to Ni toxicity but has desirable characteristics of grasses with phytoremediation potential [3,4]. Some researchers claim that it is possible to improve the rate of metal sequestration in phytoliths through the selection of high-production species and the sequestration of elements in the phytolith [15]. However, species cannot be selected solely based on yield and metal sequestration by the phytolith but must be considered in combination with other desirable characteristics, such as biomass production and productivity [15]. In addition, other limiting factors, such as differences in location, climatic conditions [15], and species characteristics, need to be considered, as well as other mechanisms involved in plants' tolerance to heavy metals [3].

5. Conclusions

Nickel was phytotoxic to grasses at an added concentration of about 30 mg kg^{-1} below the investigation value (70 mg kg^{-1}) for agricultural soils established by Brazilian Environmental Legislation.

The yield and Ni occlusion in phytoliths by grasses in Ni-contaminated soils is related to the genetic and physiological differences between grasses and the Ni availability in soils.

Ni capture by phytoliths indicates that it may be one of the detoxification mechanisms of *Urochloa decumbens* to Ni-contaminated soils, providing additional evidence that *Megathyrsus maximus* may be a future grass for the phytoremediation technique for Ni-contaminated soils.

Author Contributions: Conceptualization, E.d.B.S.; Methodology, E.d.B.S., M.M.d.M.F., L.L.d.S., A.C.S., I.H.-T., S.A.d.N. and B.G.U.; Formal analysis, E.d.B.S., M.M.d.M.F., S.A.d.N. and B.G.U.; Investigation, E.d.B.S., M.M.d.M.F. and L.L.d.S.; Resources, E.d.B.S., M.M.d.M.F., A.C.S., P.H.G., L.R.F.A., I.H.-T., S.A.d.N. and B.G.U.; Writing—original draft, E.d.B.S., M.M.d.M.F., L.L.d.S., A.C.S., P.H.G., L.R.F.A., I.H.-T., S.A.d.N. and B.G.U.; Writing—review and editing, E.d.B.S., M.M.d.M.F., L.L.d.S., A.C.S., P.H.G., L.R.F.A., I.H.-T., S.A.d.N. and B.G.U.; Visualization, E.d.B.S. and M.M.d.M.F.; Supervision, E.d.B.S.; Project administration, E.d.B.S.; Funding acquisition, E.d.B.S. and L.R.F.A. All authors have read and agreed to the published version of the manuscript.

Funding: This research was funded by the National Council for Scientific and Technological Development (CNPq) grant number 303599/2015-4 and the Research Supporting Foundation for the State of Minas Gerais (Fapemig) grant number CAG-PPM-00480-16.

Institutional Review Board Statement: Not applicable.

Informed Consent Statement: Not applicable.

Data Availability Statement: Data are contained within the article.

Acknowledgments: We acknowledge The Coordination for the Improvement of Higher Level Personnel (Capes) who provided a graduate student stipend. The Department of Soil Science, ESALQ, University of São Paulo, provided the laboratory analysis of soil samples. The Federal University of the Jequitinhonha and Mucuri Valley (UFVJM) provided the infrastructure needed to conduct this study.

Conflicts of Interest: The authors declare no conflicts of interest.

References

1. Silva, E.B.; Souza, F.V.P.; Grazziotti, P.H.; Alleoni, L.R.F.; Nardis, B.O.; Ferreira, E.A. Growth of tropical grasses in Oxisol contaminated by nickel. *Chil. J. Agric. Res.* **2017**, *77*, 273–280. [CrossRef]
2. Shahzad, B.; Tanveer, M.; Rehman, A.; Cheema, S.A.; Fahad, S.; Rehman, S.; Sharma, A. Nickel; whether toxic or essential for plants and environment—A review. *Plant Physiol. Biochem.* **2018**, *132*, 641–651. [CrossRef] [PubMed]
3. Bhargava, A.; Carmona, F.F.; Bhargava, M.; Srivastava, S. Approaches for enhanced phytoextraction of heavy metals. *J. Environ. Manag.* **2012**, *105*, 103–120. [CrossRef] [PubMed]
4. Fernandes-Horn, H.M.; Sampaio, R.A.; Horn, A.H.; Oliveira, E.S.A.; Lepsch, I.F.; Bilal, E. Use of Si-Phytoliths in depollution of mining areas in the Cerrado-Caatinga region, MG, Brazil. *Int. J. Geomate* **2016**, *11*, 2216–2221.
5. Yusuf, M.; Fariduddin, Q.; Hayat, S.; Ahmad, A. Nickel: An overview of uptake, essentiality and toxicity in plants. *Bull. Environ. Contam. Toxicol.* **2011**, *86*, 1–17. [CrossRef] [PubMed]
6. Buján, E. Elemental composition of phytoliths in modern plants (Ericaceae). *Quat. Int.* **2013**, *287*, 114–120. [CrossRef]
7. Li, Z.; Song, Z.; Cornelis, J.T. Impact of rice cultivar and organ on elemental composition of phytoliths and the release of bio-available silicon. *Front. Plant Sci.* **2014**, *5*, 529. [CrossRef] [PubMed]
8. Pan, W.; Song, Z.; Liu, H.; Müeller, K.; Yang, X.; Zhang, X.; Li, Z.; Liu, X.; Qiu, S.; Hao, Q.; et al. Impact of grassland degradation on soil phytolith carbon sequestration in Inner Mongolian steppe of China. *Geoderma* **2017**, *308*, 86–92. [CrossRef]
9. Yang, X.; Song, Z.; Liu, H.; Van Zwieten, L.; Song, A.; Li, Z.; Hao, Q.; Zhang, X.; Wang, H. Phytolith accumulation in broadleaf and conifer forests of northern China: Implications for phytolith carbon sequestration. *Geoderma* **2018**, *312*, 36–44. [CrossRef]
10. Pezzopane, J.R.M.; Santos, P.M.; Mendonça, F.M.; Araujo, L.C.; Cruz, P.G. Dry matter production of Tanzania grass as a function of agrometeorological variables. *Pesqui. Agropecuária Bras.* **2012**, *47*, 471–477. [CrossRef]
11. Pivello, V.R.; Shida, C.N.; Meirelles, S.T. Alien grasses in Brazilian savannas: A threat to the biodiversity. *Biodivers. Conserv.* **1999**, *8*, 1281–1294. [CrossRef]
12. Conama. *National Environmental Council of Brazil. Resolução no 420/2009. It Provides Criteria and Guiding Values of Soil Quality for the Presence of Chemical Substances and Establishes Guidelines for the Environmental Management of Areas Contaminated by These Substances as a Result of Anthropic Activities*; Ministry of the Environment: Belo Horizonte, Brazil, 2009.
13. Kim, R.Y.; Yoon, J.K.; Kim, T.S.; Yang, J.E.; Owens, G.; Kim, K.R. Bioavailability of heavy metals in soils: Definitions and practical implementation-a critical review. *Environ. Geochem. Health* **2015**, *37*, 1041–1061. [CrossRef] [PubMed]

14. Silva, E.B.; Alves, I.S.; Alleoni, L.R.F.; Grazziotti, P.H.; Farnezi, M.M.M.; Santos, L.L.; Prochnow, J.T.; Fontan, I.C.I. Availability and toxic level of cadmium, lead and nickel in contaminated soils. *Commun. Soil Sci. Plant Anal.* **2020**, *51*, 1341–1356. [CrossRef]
15. Parr, J.F.; Sullivan, L.A. Phytolith occluded carbon and silica variability in wheat cultivars. *Plant Soil* **2011**, *342*, 165–171. [CrossRef]
16. Soil Survey Staff. *Soil Taxonomy: Keys to Soil Taxonomy*, 11th ed.; Department of Agriculture, Natural Resources and Conservation Services: Washington, DC, USA, 2010.
17. Teixeira, P.C.; Donagemma, G.K.; Fontana, A.; Teixeira, W.G. *Manual for Methods of Soil Analysis*, 3rd ed.; Embrapa: Brasília, Brazil, 2017.
18. USEPA. *United States Environmental Protection Agency. Microwave Assisted Acid Digestion of Sediments, Sludges, Soils and Oils-Method 3052-SW-846*; EPA: Washington, DC, USA, 2007.
19. Santos, S.R.; Silva, E.B.; Alleoni, L.R.F.; Grazziotti, P.H. Citric acid influence on soil phosphorus availability. *J. Plant Nutr.* **2017**, *40*, 2138–2145. [CrossRef]
20. Parr, J.F.; Lentfer, C.J.; Boyd, W.E. A comparative analysis of wet and dry ashing techniques for the extraction of phytoliths from plant material. *J. Archaeol. Sci.* **2001**, *28*, 875–886. [CrossRef]
21. Ferreira, D.F. Sisvar: A computer statistical analysis system. *Ciência e Agrotecnologia* **2011**, *35*, 1039–1042. [CrossRef]

Disclaimer/Publisher's Note: The statements, opinions and data contained in all publications are solely those of the individual author(s) and contributor(s) and not of MDPI and/or the editor(s). MDPI and/or the editor(s) disclaim responsibility for any injury to people or property resulting from any ideas, methods, instructions or products referred to in the content.

soil systems

MDPI

Communication

Sediments as Sentinels of Pollution Episodes in the Middle Estuary of the Tinto River (SW Spain)

Luis Miguel Cáceres [1], Francisco Ruiz [1,*], Javier Bermejo [2], Lucía Fernández [2], María Luz González-Regalado [1], Joaquín Rodríguez Vidal [1], Manuel Abad [3], Tatiana Izquierdo [3], Antonio Toscano [1], Paula Gómez [1] and Verónica Romero [1]

[1] Departamento de Ciencias de la Tierra, Universidad de Huelva, 21071 Huelva, Spain; mcaceres@uhu.es (L.M.C.); jrvidal@uhu.es (J.R.V.)
[2] Departamento de Historia, Geografía y Antropología, Universidad de Huelva, 21071 Huelva, Spain; javier.bermejo@dhis1.uhu.es (J.B.); lucia.fernandez@dhga.uhu.es (L.F.)
[3] Departamento de Biología y Geología, Física y Química Inorgánica, Universidad Rey Juan Carlos, 28933 Móstoles, Spain; tatiana.izquierdo@urjc.es
* Correspondence: ruizmu@uhu.es

Abstract: Estuaries are excellent environments for identifying pollution episodes that have affected river basins, as their sediments are the final destination of some of the pollutants. This paper studies the geochemical evolution of five elements (As, Co, Cu, Pb, Zn) in a core extracted from the middle estuary of the Tinto River (SW Spain). The results are based on facies interpretation, ICP atomic emission spectrometry analysis, the application of a regional background to obtain the geoaccumulation index and dating. The main objective of this communication is the detection of natural or anthropogenic pollution episodes in the middle estuary of the Tinto River (SW Spain). Four pollution episodes have been detected: (1) ~5.8 cal. kyr BP, probably caused by natural acid rock drainage processes derived from the oxidation of the Iberian Pyritic Belt deposits found in its drainage basin; (2) 4.7–4.5 kyr BP, coming from the first mining activities and characterized by a significant increase in the concentrations of the five elements analyzed; (3) 1850–1960 interval, coinciding with intensive mining and characterized by increasing values of As and, to a lesser extent, Pb (intensive mining); and (4) the second half of the 20th century, with high element concentrations from mining and industrial effluents. All episodes show an increase in their geochemical classes deduced from the geoaccumulation index. This communication can serve as an example for assessing the impact of different types of pollution in estuarine environments.

Keywords: sediment; pollution; core; geoaccumulation index; estuary; SW Spain

Citation: Cáceres, L.M.; Ruiz, F.; Bermejo, J.; Fernández, L.; González-Regalado, M.L.; Vidal, J.R.; Abad, M.; Izquierdo, T.; Toscano, A.; Gómez, P.; et al. Sediments as Sentinels of Pollution Episodes in the Middle Estuary of the Tinto River (SW Spain). *Soil Syst.* **2023**, *7*, 95. https://doi.org/10.3390/soilsystems7040095

Academic Editor: Manfred Sager

Received: 14 September 2023
Revised: 20 October 2023
Accepted: 21 October 2023
Published: 24 October 2023

Copyright: © 2023 by the authors. Licensee MDPI, Basel, Switzerland. This article is an open access article distributed under the terms and conditions of the Creative Commons Attribution (CC BY) license (https://creativecommons.org/licenses/by/4.0/).

1. Introduction

Numerous anthropogenic activities (e.g., industrial effluents, mining waste, agricultural residues, urban inputs), the natural erosion of geological formations or even high-energy events (river floods, storms, tsunamis, etc.) leave their mark on the geochemical levels of sediments and soils [1–7]. One of the most common effects is the increase in concentrations of certain elements, among which heavy metals are commonly used as a reference to measure the level of pollution [8–11]. To determine the heavy metal contamination in a soil or sediment, various indices are often used, such as the enrichment factor (EF) or the geoaccumulation index (I_{geo}) [12–14]. The latter index requires a regional background in order to calculate the degree of contamination, which may be unique for each metal regardless of grain size (e.g., [15–17]), or may include a differentiation between sandy and muddy sediments [18].

Estuaries are often the final repositories of many of these natural processes or human actions, as they often contain the inputs of heavy metals produced in their river basins at present or in the past [19–21]. In the last few years, numerous investigations have focused on

the historical heavy metal pollution of these environments, based on geochemical studies of continuous sediment cores [22–24]. Some of them have applied the geoaccumulation index to detect pollution episodes and, in conjunction with radiocarbon dating and historical data, to pinpoint the time interval in which they occurred [25,26].

The main objective of this short communication is the detection of natural or anthropogenic pollution episodes in a continuous sediment core extracted from the middle estuary of the Tinto River (SW Spain), based on the vertical geochemical variations and the application of the regional geoaccumulation index to five elements. The results obtained will be compared with previous paleoenvironmental reconstructions and historical mining data to identify the age of these episodes and their importance according to the degree of contamination deduced. Furthermore, it is intended that these results can be used to compare the importance of these episodes or be extrapolated in the future to analyses of recent sediments from this estuary.

2. Materials and Methods

2.1. Study Area

The Tinto River is a small stream that flows through the southwest of Spain and forms a large estuary together with the Odiel River at its mouth in the Atlantic Ocean, surrounded by Neogene–Pleistocene formations (Figure 1A,B). The hydrodynamics of this estuary are tidally dominated, as river discharges are very rare and vary from minimum flows during very dry years to about 350 Hm^3 in rainy years [27]. The tidal regime is mesotidal (2.1 m), with a low diurnal inequality [28].

This estuary can be divided into three sectors, depending on the interaction between the river and tidal inputs [29]: (i) fluvial estuary, composed of numerous braided channels; (ii) middle estuary, with numerous marshes that come to form small islands (e.g., Figure 1B: Bacuta Island); and (iii) marine estuary, with a central island (Figure 1B: Saltés Island), two main channels (Padre Santo channel, Punta Umbría channel) and two sandy spits (Punta Arenillas, Punta Umbría) that partially protect it. In the marine estuary, wave energy is medium, and 75% of the waves do not exceed 0.5 m in height [30]. The coastal drift currents are oriented towards the east, with a high annual transport of sediment ($1.8 - 3 \times 10^5$ m^3) [31,32], and have historically favored the development of the two spits and the progressive closure of the innermost parts of the estuary.

2.2. Historical Pollution

Southwest Spain is part of the Iberian Pyritic Belt, one of the most important metallogenic provinces in Europe, which includes some of the largest massive sulfide deposits in the world. These giant deposits have been exploited for 5000 years within the Tinto River drainage basin [27], with important mining activity during the Roman period (2100–1700 yr BP) and especially in the last 150 years, with an intensive extraction of pyrite and minor quantities of gold and silver. Currently, the waters of the Tinto River suffer from acid mine drainage, due to this age-old mining activity and to the heavy-metal-rich inputs from the washing of the waste dumps generated [33].

In addition, this estuary has been affected by discharges from two industrial concentrations located on its banks since the 1960s (Figure 1B), made up of copper producers, fertilizer factories and refineries, among others. As a final result of these mining–industrial pollutant inputs, the surface sediments of the Tinto–Odiel estuary are among the most polluted in the world, with very high concentrations of As (up to 3000 mg kg^{-1}), Cu (up to 4415 mg kg^{-1}), Pb (up to 10,400 mg kg^{-1}) and Zn (up to 5280 mg kg^{-1}) in its surface sediments [18,34]. Since 1985, this zone has come under a corrective plan for the control of industrial waste disposal.

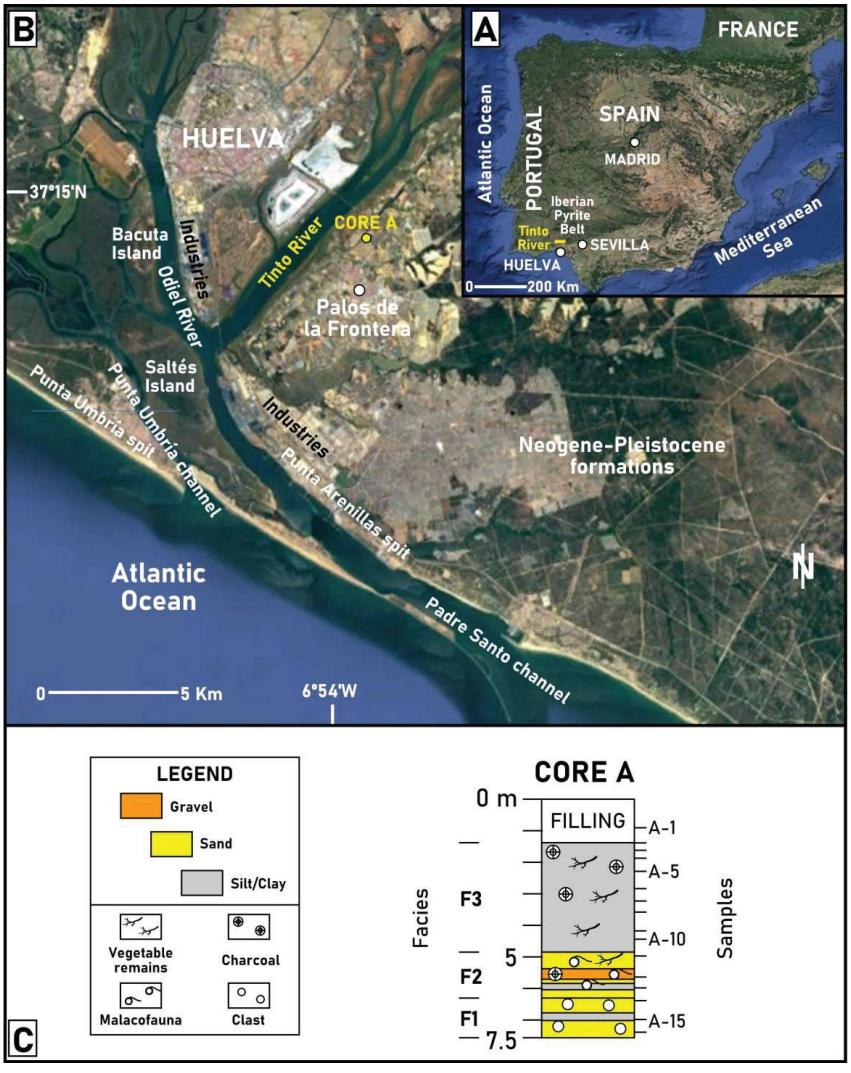

Figure 1. (**A**) Location of the Tinto–Odiel estuary. (**B**) Synthetic geomorphological map of the Tinto–Odiel estuary, with location of core A. (**C**) Log of core A, including sedimentary facies and sampling. (**A**,**B**) Courtesy Google Earth.

2.3. Coring, Sampling and Holocene Paleoenvironmental Evolution

Core A (Figure 1B,C; 7.5 m depth; 37°14′06″ N; 6°53′54″ W) was extracted in the middle estuary of the Tinto River by usual rotary drilling techniques, with an almost continuous recovery of sediment and a barrel diameter of 11.6 cm. Its location was selected in an area away from the main channel of the Tinto River, only flooded during high tides and not subject to the erosive action of the occasional large flows that characterize this highly seasonal river. Sixteen samples (2 cm thickness) were obtained, with a distribution of samples linked to (a) the presence of different sedimentary facies, (b) the definition of its limits and (c) the visual distribution of bioclasts in the core. The Holocene paleoenvironmental reconstruction of this core was inferred by [35], with basal alluvial sands (Figure 1C: facies F1), bioclastic sands and gravels from the marine flood of this area during the MIS-1 transgression (F2) and upper muddy marsh deposits (F3).

2.4. Chemical Analysis

The chemical analysis of sixteen sediment samples was performed and certified by MS Analytical (Langley, BC, Canada). Samples were collected manually by hand picking. They were individually crushed and subsequently ground into powder using an agate mortar. The concentrations of five elements (As, Co, Cu, Pb, Zn) were determined by ICP atomic emission spectrometry (total digestion with concentrated acids), with less than 5% variation between different replicate samples and quality control based on more than 30 references (e.g., OREAS 904). In these samples, detection limits varied between 0.01 mg kg^{-1} (e.g., Co) and 2 mg kg^{-1} (e.g., Zn).

2.5. Background and Geoaccumulation Index

A regional background of this estuary was obtained by [36] for both unpolluted sandy and muddy sediments of the Tinto–Odiel estuary. This background was applied to obtain the geoaccumulation index of the extracted sediments, according to the following formula:

$$I_{geo} = \log_2 C_n/1.5 \times B_n,$$

where C_n is the concentration of an element in a given sample and B_n is the background of that element for the grain size of that sample (e.g., sand or mud). This background differentiates sandy (S) and muddy (M) sediments: As (S: 6.8 mg kg^{-1}; M: 7.3 mg kg^{-1}), Co (S: 4.2 mg kg^{-1}; M: 6.8 mg kg^{-1}), Cu (S: 13.1 mg kg^{-1}; M: 13 mg kg^{-1}), Pb (S: 4.3 mg kg^{-1}; M: 15.4 mg kg^{-1}) and Zn (S: 15.9 mg kg^{-1}; M: 39 mg kg^{-1}).

The pollution classes originally proposed by [37] were slightly modified as follows: unpolluted (UP; $I_{geo} < 0$), very low pollution (VLP; $0 < I_{geo} < 1$), low pollution (LP; $1 < I_{geo} < 2$), moderately polluted (MP; $2 < I_{geo} < 3$), highly polluted (HP; $3 < I_{geo} < 4$), very highly polluted (VHP; $4 < I_{geo} < 5$) and strongly polluted (SP; $I_{geo} > 5$).

2.6. Dating

Two dates of core A were produced at the National Center of Accelerators (Sevilla, Spain). These dates were calibrated using CALIB version 8.2, and the final results correspond to calibrated ages using 2σ intervals.

3. Results and Discussion

3.1. Facies, Geochemistry and Dating

The basal alluvial sandy–muddy deposits of this core (F1; 7.5–6.3 m depth; samples A-16 to A-14) have very low concentrations of most of the elements studied, even lower than the regional background (Table 1). They were deposited during the Middle Holocene, according to the dating obtained near the boundary between F1 and F2 (Figure 1C and Table 2; sample A-13; ~5.8 cal. kyr BP). The bioclastic sediments of this last facies (6.3–4.9 m depth; samples A-13 to A-11; ~5.8–5 cal. kyr BP) were deposited during the flooding of this area due to the MIS-1 transgression. A first pollution level was detected near the base of this facies (sample A-13: ~5.8 cal. kyr BP), with a noticeable increase in the concentrations of Cu (from 9.5 mg kg^{-1} to 39 mg kg^{-1}), Pb (from 11.1 mg kg^{-1} to 74.1 mg kg^{-1}) and Zn (from 25 mg kg^{-1} to 93 mg kg^{-1}). The age of this level would indicate early natural pollution, as mining did not begin in this area until some thousand years later [27,38]. The origin of this first contamination is unknown, although it could come from the natural oxidation of the sulfides and formation of the gossans of the Iberian Pyritic Belt by acid rock drainage processes, which started more than 24 million years ago in this area [39]. Metals from the washing of these deposits would have been transported to the Tinto estuary and deposited in core A when its environment was flooded during the Holocene transgression. This episode has been detected in other cores of the Tinto estuary [40], and this research confirms this first natural pollution.

Table 1. Geochemistry of core A (in mg kg^{-1}). Bold: three highest values of each element.

Sample	Depth (m)	Sediment	Facies	Interpretation	As	Co	Cu	Pb	Zn
A-1	0.9	Sand	Filling	Recent filling	7	3.7	21	14.7	30
A-2	1.4	Mud	F4	Marsh	**43.8**	**13.1**	**284.4**	**98**	**539**
A-3	1.6	Mud	F4	Marsh	**39.3**	**12.7**	27.5	37.9	88
A-4	1.9	Mud	F4	Marsh	**36.7**	**14.1**	23.8	23.2	85
A-5	2.3	Mud	F4	Marsh	18.3	12	20.3	22.1	87
A-6	2.8	Mud	F4	Marsh	19.2	12.1	22.7	27.9	89
A-7	3.3	Mud	F4	Marsh	17.2	10.3	15.7	40.6	68
A-8	3.6	Mud	F4	Marsh	22.2	11.5	22.8	18.6	87
A-9	4.2	Mud	F4	Marsh	30.1	12.4	**51.8**	**46.9**	**107**
A-10	4.5	Mud	F4	Marsh	18.2	9.7	18.5	17.8	69
A-11	5	Sand	F2	MIS-1 transgression	12.3	5.9	11.7	12.4	44
A-12	5.7	Gravel	F2	MIS-1 transgression	8.5	3.9	8.4	10	28
A-13	6	Mud	F2	MIS-1 transgression	27.3	10.6	**39**	**74.1**	**93**
A-14	6.4	Sand	F1	Alluvial	4.8	4.4	9.5	11.1	25
A-15	7	Mud	F1	Alluvial	6.7	6.4	10.9	14.9	33
A-16	7.4	Sand	F1	Alluvial	7.2	5.8	21.3	10.6	34

Table 2. Radiocarbon database.

Sample	Laboratory Number	Material	$\delta^{13}C$ (%)	Uncalibrated Age BP	Calibrated Age BP	Mean Calibrated Age (kyr BP)
A-12	CNA-4272	Organic matter	−22.6	6467 ± 32	5483–5368	5.4
A-13	CNA-4274	Shell	−1.3	5428 ± 33	5892–5711	5.8

The second pollution level was detected in the marshy muds collected near the base of F3 (Table 1: sample A-9), with some of the highest values of Cu (51.8 mg kg^{-1}), Pb (46.9 mg kg^{-1}) and Zn (107 mg kg^{-1}) of core A and increasing concentrations of As and Co. According to the average sedimentation rates (1.7–2 mm yr^{-1}) calculated by [41] in this estuary around 5000–4000 yr BP and the aforementioned dating, this new episode would have taken place approximately between ~4.7 kyr BP and ~4.5 kyr BP, coinciding with the development of the first mining and metallurgical works in this area [38]. This first episode of anthropogenic contamination has been detected in numerous cores in the Tinto River estuary e.g., [35,40].

The concentrations of the five elements decrease between 4.2 m depth and 2.3 m depth, with a further increase in As (from 18.3 mg kg^{-1} to 36.9–39.3 mg kg^{-1}) and, to a lesser extent, Pb (up to 37.9 mg kg^{-1}) observed between 1.9 and 1.6 m depth. This third pollution episode is associated with the start of intensive mining in the Tinto River basin from the second half of the 19th century to 1960. This increasing trend is confirmed at 1.4 m depth (e.g., the surface of core A before the recent anthropogenic filling), with the maximum values of all five elements, especially Cu (284.4 mg kg^{-1}), Pb (98 mg kg^{-1}) and Zn (539 mg kg^{-1}). This fourth episode would correspond to the conjunction of this intensive mining and inputs from nearby industrial complexes during the second half of the 20th century, which have caused strong pollution in the recent sediments of the Tinto–Odiel estuary [42,43]. These high values confirm this last episode as the most important in the geochemical history of the middle estuary of the Tinto River. Transit to the overlying artificial filling is evidenced by the presence of unpolluted fine sands in the upper 1.3 m of this core (Table 1: sample A-1).

3.2. Geoaccumulation Index and Pollution Episodes

These four episodes are also detected when I_{geo} is applied to the concentrations of the five elements (Figure 2). The first episode (~5.8 cal. kyr BP) is characterized by the transition from UP (As, Co, Cu) or VLP (Pb) sediments to VLP (Co) or LP (As, Cu, Pb)

sediments. These four elements also show similar variations in their pollution class during the second episode (~4.7–4.5 kyr BP), most marked for Pb (from UP to LP) and to a lesser extent for As (from VLP to LP).

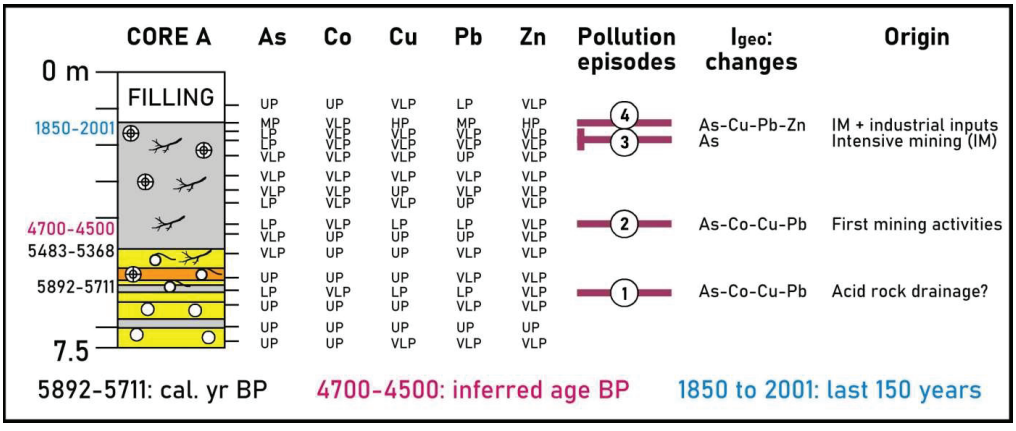

Figure 2. Application of I_{geo} to core A. For legend, see Figure 1.

The third episode (~1850–1960) is mainly defined by As (from VLP to LP), although an increase in the concentration of most of the other elements is observed (see previous subsection). The fourth episode (~1960–2000) is clearly the most important, with the presence of MP (As, Pb) to HP (Cu, Zn) sediments. Consequently, this last polluting episode is the most important in the geochemical history of the Tinto–Odiel estuary, as evidenced by the analysis of other sediment cores extracted in this area [35,44,45].

A final thought is needed on the calculation of the geoaccumulation index. It is a simple method to define the degree of contamination of a soil or sediment, but its formula includes a factor (1.5; see Section 2.5) because of possible variations in the background data due to different lithologies. Since heavy metals tend to concentrate in finer sediments, it would be advisable to use a background for each lithology (sand, silt, clay), if possible. On the other hand, the use of this multiplying factor in the denominator of the Igeo should be considered in the future, depending on the degree of lithification of sediment in estuaries, as it significantly increases the concentration of an element above which sediments are considered as contaminated.

4. Conclusions

The joint application of geochemical analysis and the geoaccumulation index has proved to be an effective tool for detecting pollution episodes in the middle estuary of the Tinto River (SW Spain), in conjunction with historical data on mining activities in this area. Four episodes have been distinguished, characterized by an increase in the concentration of the elements studied and their geochemical classes based on I_{geo}. The first recorded pollution was of natural origin and coincided with the flooding of this estuary during the Holocene transgression. The next three episodes are linked to the start of mining activities, a period of intensive mining, and the coincidence of intensive mining and the discharge of highly polluted industrial effluents into the estuary. The application of this background can be useful for determining the degree of contamination of the sediments of this estuary in relation to possible new sources of pollution, and the concentrations obtained can be used as a reference for assessing their importance in relation to the historical episodes referred to in this communication.

Author Contributions: All authors have participated in all stages of the paper. All authors have read and agreed to the published version of the manuscript.

Funding: This study was mainly financed by the Palos de la Frontera Council. It was also carried out through the following projects: (a) DGYCIT project CTM2006-06722/MAR; (b) DGYCIT project CGL2006-01412; (c) Roman cities of the Baetica, CORPVS VRBIVM BAETICARVM (I) (CUB) (Andalusian Government); (d) From the Atlantic to the Tyrrhenian, the Hispanic ports and their commercial relations with Ostia Antica, DEATLANTIR II—HAR2017-89154-P (Plan Nacional de I + D + i); and (e) FEDER 2014–2020 project UHU-1260298. Other funds have come from the Andalusian Government (groups HUM-132, RNM-238, and RNM-293). It is a contribution to the Research Center in Historical, Cultural and Natural Heritage (CIPHCN) of the University of Huelva.

Institutional Review Board Statement: Not applicable.

Informed Consent Statement: Not applicable.

Data Availability Statement: Data are available upon request to the corresponding author.

Conflicts of Interest: The authors declare no conflict of interest.

References

1. Chagué-Goff, C.; Szczucinski, W.; Shinozaki, T. Applications of geochemistry in tsunami research: A review. *Earth-Sci. Rev.* **2017**, *165*, 203–244. [CrossRef]
2. Silva, H.F.; Silva, N.F.; Oliveira, C.M.; Matos, M.J. Heavy Metals Contamination of Urban Soils—A Decade Study in the City of Lisbon, Portugal. *Soil Syst.* **2021**, *5*, 27. [CrossRef]
3. Chebykina, E.; Abakumov, E.; Shamilishvilly, G.; Kouzov, S. Soil Diversity of the Island of Gogland in the Gulf of Finland: History of Land Development and Current Status. *Soil Syst.* **2022**, *6*, 85. [CrossRef]
4. Mangas-Suarez, M.; Garcia-Ordiales, E.; Pérez, J.A.; Álvarez, R.; Villa, A.; Ordoñez, A.; Roqueñí, N. Enrichment of Metals in the Sediments of an Industrially Impacted Estuary: Geochemistry, Dispersion and Environmental Considerations. *Appl. Sci.* **2022**, *12*, 10998. [CrossRef]
5. Papadimou, S.G.; Kantzou, O.-D.; Chartodiplomenou, M.-A.; Golia, E.E. Urban Soil Pollution by Heavy Metals: Effect of the Lockdown during the Period of COVID-19 on Pollutant Levels over a Five-Year Study. *Soil Syst.* **2023**, *7*, 28. [CrossRef]
6. Nassiri, O.; Rhoujjati, A.; Moreno-Jimenez, E.; Hachimi, M.L.E.L. Environmental and Geochemical Characteristics of Heavy Metals in Soils Around the Former Mining Area of Zeïda (High Moulouya, Morocco). *Water Air Soil Pollut.* **2023**, *234*, 110. [CrossRef]
7. Pereira, J.G.; Raikar, S.S.; Bhatti, A.G.; Fatarpekar, P.G.; Nasnodkar, M.R. Metal bioavailability, bioaccumulation, and toxicity assessment through sediment and edible biota from intertidal regions of the Aghanashini Estuary, India. *Mar. Environ. Res.* **2023**, *191*, 106172. [CrossRef]
8. Niu, S.; Xia, Y.; Yang, C.; Liu, C. Impacts of the steel industry on sediment pollution by heavy metals in urban water system. *Environ. Pollut.* **2023**, *335*, 122364. [CrossRef]
9. Hossain, M.B.; Sultana, J.; Pingki, F.H.; Nur, A.; Mia, M.S.; Bakar, M.A.; Yu, J.; Paray, B.A.; Arai, T. Accumulation and contamination assessment of heavy metals in sediments of commercial aquaculture farms from a coastal area along the northern Bay of Bengal. *Front. Environ. Sci.* **2023**, *11*, 1148360. [CrossRef]
10. Hamarashid, R.A.; Fiket, Ž.; Mohialdeen, I.M.J. Environmental Impact of Sulaimani Steel Plant (Kurdistan Region, Iraq) on Soil Geochemistry. *Soil Syst.* **2022**, *6*, 86. [CrossRef]
11. Rashid, A.; Schutte, B.J.; Ulery, A.; Deyholos, M.K.; Sanogo, S.; Lehnhoff, E.A.; Beck, L. Heavy Metal Contamination in Agricultural Soil: Environmental Pollutants Affecting Crop Health. *Agronomy* **2023**, *13*, 1521. [CrossRef]
12. Kroeksakul, P.; Ngamniyom, A.; Silprasit, K.; Singhaboot, P. Relationship between Potential Trace Elements Contamination in Sediment and Macrofauna in the Upper Gulf of Thailand. *J. Environ. Public Health* **2023**, *2023*, 4231930. [CrossRef]
13. Kumar, V.; Bhatti, R.C.; Kaur, R.; Singh, S.; Nirmala, C.; Singh, A.N. Comparative Geo-Accumulation Index of Heavy Metal Concentration in the Urban Soils of Chandigarh and Baddi Areas under Industrial Activities in A Lower Shiwalik Region, India. *Eur. Chem. Bull.* **2023**, *12*, 937–953. [CrossRef]
14. Fadlillah, L.N.; Utami, S.; Rachmawati, A.A.; Jayanto, G.D.; Widyastuti, M. Ecological risk and source identifications of heavy metals contamination in the water and surface sediments from anthropogenic impacts of urban river, Indonesia. *Heliyon* **2023**, *9*, e15485. [CrossRef]
15. Parvez, M.S.; Nawshin, S.; Sultana, S.; Hossain, M.S.; Rashid Khan, M.H.; Habib, M.A.; Nijhum, Z.T.; Khan, R. Evaluation of Heavy Metal Contamination in Soil Samples around Rampal, Bangladesh. *ACS Omega* **2023**, *8*, 15990–15999. [CrossRef] [PubMed]
16. Zaakour, F.; Kholaiq, M.; Khouchlaa, A.; El Mjiri, I.; Rahimi, A.; Saber, N. Assessment of Heavy Metal Contamination Using Pollution Index, Geo-Accumulation Index, and Potential Ecological Risk Index in Agricultural Soil—A Case Study in the Coastal Area of Doukkala (Morocco). *Ecol. Eng. Environ. Technol.* **2023**, *24*, 38–44. [CrossRef] [PubMed]
17. Kahangwa, C.A. Application of Principal Component Analysis, Cluster Analysis, Pollution Index and Geoaccumulation Index in Pollution Assessment with Heavy Metals from Gold Mining Operations, Tanzania. *J. Geosc. Environ. Protect.* **2022**, *10*, 303–317. [CrossRef]

18. Ruiz, F. Trace metals in estuarine sedirnents from the southwestern Spanish coast. *Mar. Pollut. Bull.* **2001**, *42*, 481–489. [CrossRef]
19. Li, H.; Gu, Y.; Liang, R.; Wang, Y.; Jordan, R.W.; Wang, L.; Jiang, S. Heavy metals in riverine/estuarine sediments from an aquaculture wetland in metropolitan areas, China: Characterization, bioavailability and probabilistic ecological risk. *Environ. Pollut.* **2023**, *324*, 121370. [CrossRef]
20. Chahouri, A.; Lamine, I.; Ouchene, H.; Yacoubi, B.; Moukrim, A.; Banaoui, A. Assessment of heavy metal contamination and ecological risk in Morocco's marine and estuarine ecosystems through a combined analysis of surface sediment and bioindicator species: *Donax trunculus* and *Scrobicularia plana*. *Mar. Pollut. Bull.* **2023**, *192*, 115076. [CrossRef]
21. Wang, Q.; Huang, X.; Zhang, Y. Heavy Metals and Their Ecological Risk Assessment in Surface Sediments of the Changjiang River Estuary and Contiguous East China Sea. *Sustainability* **2023**, *15*, 4323. [CrossRef]
22. Babasaheb, R.; Thorat, P.; Prasad, A.R. Heavy metal accumulation in a moderately polluted Ulhas estuary, Western India. *Reg. Stud. Mar. Sci.* **2023**, *60*, 102818. [CrossRef]
23. Fan, J.; Fan, D.; Wu, Y. Spatiotemporal variations of heavy metal historical accumulation records and their influencing mechanisms in the Yangtze River Estuary. *Sci. Total Environ.* **2023**, *854*, 158733. [CrossRef] [PubMed]
24. Filippi, G.; Dassenakis, M.; Paraskevopoulou, V.; Lazogiannis, K. Sediment quality assessment in an industrialized Greek coastal marine area (western Saronikos Gulf). *Biosgeosciences* **2023**, *20*, 163–189. [CrossRef]
25. Ubonyaem, T.; Bureekul, S.; Charoenpong, C.; Luadnakrob, P.; Sompongchaiyakul, P. Preindustrial levels and temporal enrichment trends of mercury in sediment cores from the Gulf of Thailand. *Environ. Geochem. Health* **2023**, *45*, 4243–4256. [CrossRef] [PubMed]
26. Nishitha, D.; Amrish, V.N.; Arun, K.; Warrier, A.K.; Udayashankar, H.N.; Balakrishn, K. Study of trace metal contamination and ecological risk assessment in the sediments of a tropical river estuary, Southwestern India. *Environ. Monit. Assess.* **2022**, *194*, 94. [CrossRef] [PubMed]
27. Davis, R., Jr.; Welty, A.; Borrego, J.; Morales, J.A.; Pendon, J.G.; Ryan, J.G. Rio Tinto estuary (Spain): 5000 years of pollution. *Environ. Geol.* **2000**, *39*, 1107–1116. [CrossRef]
28. Borrego, J.; Morales, J.A.; Pendón, J.G. Holocene filling of an estuarine lagoon along the mesotidal coast of Huelva: The Piedras River mouth, southwestern Spain. *J. Coast. Res.* **1993**, *9*, 242–254.
29. Borrego, J. Sedimentología del estuario del río Odiel (Huelva, S.O. España). Ph.D. Thesis, Universidad de Huelva, Huelva, Spain, 1992.
30. CEDEX (Centro de estudios y experimentación de Obras Públicas). *Dinámica litoral de la flecha de El Rompido (Huelva)*; Ministerio de Obras Públicas: Madrid, Spain, 1991; p. 100.
31. CEEPYC (Centro de Estudios y Experimentacion de Puertos y Costas 'Ramon Iribarren'). *Plan de Estudio de la Dinámica Litoral de la Provincia de Huelva*; Informe Direccion General de Puertos y Costas: Madrid, Spain, 1979; p. 37.
32. Cuena, G.J. *Proyecto de Regeneración de Las Playas de Isla Cristina. Informe del Servicio de Costas*; Ministerio de Obras Publicas y Turismo: Madrid, Spain, 1991; p. 100.
33. Olías, M.; Cánovas, C.R.; Macías, F.; Basallote, M.D.; Nieto, J.M. The evolution of pollutant concentrations in a river severely affected by acid mine drainage: Río Tinto (SW Spain). *Minerals* **2020**, *10*, 598. [CrossRef]
34. Nelson, C.H.; Lamothe, P.J. Heavy metal anomalies in the Tinto and Odiel River and estuary system, Spain. *Estuaries* **1993**, *16*, 496–511. [CrossRef]
35. Arroyo, M.; Ruiz, F.; González-Regalado, M.L.; Rodríguez Vidal, J.; Cáceres, L.M.; Olías, M.; Campos, J.M.; Fernández, L.; Abad, M.; Izquierdo, T.; et al. Natural and anthropic pollution episodes during the Late Holocene evolution of the Tinto River estuary (SW Spain). *Sci. Mar.* **2021**, *85*, 113–123. [CrossRef]
36. Ruiz, F.; González-Regalado, M.; Borrego, J.; Morales, J.A.; Pendón, J.G.; Muñoz, J.M. Stratigraphic sequence, elemental concentrations and heavy metal pollution in Holocene sediments from the Tinto-Odiel Estuary, southwestern Spain. *Environ. Geol.* **1998**, *34*, 270–278. [CrossRef]
37. Muller, G. Index of Geoaccumulation in Sediments of the Rhine River. *J. Geol.* **1979**, *2*, 108–118.
38. Nocete, F. The first specialised copper industry in the Iberian peninsula: Cabezo Juré (2900-2200 BC). *Antiquity* **2006**, *80*, 646–657. [CrossRef]
39. Essalhi, M.; Sizaret, S.; Barbanson, L.; Chen, Y.; Lagroix, F.; Demory, F.; Nieto, J.M.; Sáez, R.; Capitán, M.A. A case study of the internal structures of gossans and weathering processes in the Iberian Pyrite Belt using magnetic fabrics and paleomagnetic dating. *Miner. Depos.* **2011**, *46*, 981–999. [CrossRef]
40. Arroyo, M.; Ruiz, F.; Campos, J.M.; Bermejo, J.; González-Regalado, M.L.; Rodríguez Vidal, J.; Cáceres, L.M.; Olías, M.; Abad, M.; Izquierdo, T.; et al. Where did Christopher Columbus start?: The estuarine scenario of a historical date. *Estuar. Coast. Shelf Sci.* **2021**, *250*, 107162. [CrossRef]
41. Lario, J.; Zazo, C.; Goy, J.L.; Dabrio, C.J.; Borja, F.; Silva, P.G.; Sierro, F.; González, A.; Soler, V.; Yll, E. Changes in sedimentation trends in SW Iberia Holocene estuaries (Spain). *Quat. Int.* **2002**, *93–94*, 171–176. [CrossRef]
42. Cabrera, F.; Conde, B.; Flores, V. Heavy metals in the surface sediments of the tidal river Tinto (SW Spain). *Fresen. Environ. Bull.* **1992**, *1*, 400–405. Available online: https://hdl.handle.net/11441/134478 (accessed on 5 September 2023).
43. López-González, N.; Borrego, J.; Carro, B.; Soria-Lozano, O. Biodisponibilidad de Fe y metales pesados en los sedimentos de la ría de Huelva. *Geogaceta* **2005**, *37*, 219–222.

44. Ruiz, F.; Borrego, J.; González-Regalado, M.L.; López González, N.; Carro, B.; Abad, M. Impact of millennial mining activities on sediments and microfauna of the Tinto River estuary (SW Spain). *Mar. Pollut. Bull.* **2008**, *56*, 1258–1264. [CrossRef]
45. Abad, M.; Arroyo, M.; Ruiz, F.; González-Regalado, M.L.; Rodríguez Vidal, J.; Cáceres, L.M.; Toscano, A.; Gómez, P.; Gomez, G.; Romero, V. Miocene-Holocene paleoenvironmental changes in the Tinto River estuary (SW Spain) evidenced by sedimentology, geochemistry and fauna. *Carnets Geol.* **2022**, *22*, 825–845. Available online: https://hdl.handle.net/10.2110/carnets.2022.2219 (accessed on 5 September 2023). [CrossRef]

Disclaimer/Publisher's Note: The statements, opinions and data contained in all publications are solely those of the individual author(s) and contributor(s) and not of MDPI and/or the editor(s). MDPI and/or the editor(s) disclaim responsibility for any injury to people or property resulting from any ideas, methods, instructions or products referred to in the content.

soil systems

MDPI

Article

Heavy Metals in Wetland Ecosystem: Investigating Metal Contamination in Waterbirds via Primary Feathers and Its Effect on Population and Diversity

Jeganathan Pandiyan [1], Radjassegarin Arumugam [2], Khalid A. Al-Ghanim [3], Nadezhda Sachivkina [4,*], Marcello Nicoletti [5] and Marimuthu Govindarajan [6,7]

[1] Department of Zoology and Wildlife Biology, A.V.C. College, Mannampandal, Mayiladuthurai 609305, Tamil Nadu, India; jpandiyan@avccollege.net
[2] Department of Botany, A.V.C. College, Mannampandal, Mayiladuthurai 609305, Tamil Nadu, India; rmugam@gmail.com
[3] Department of Zoology, College of Science, King Saud University, Riyadh 11451, Saudi Arabia; kghanim@ksu.edu.sa
[4] Department of Microbiology V.S. Kiktenko, Institute of Medicine, Peoples Friendship University of Russia Named after Patrice Lumumba (RUDN University), Moscow 117198, Russia
[5] Department of Environmental Biology, Sapienza University of Rome, 00185 Rome, Italy; marcello.nicoletti@uniroma1.it
[6] Unit of Mycology and Parasitology, Department of Zoology, Annamalai University, Annamalainagar 608002, Tamil Nadu, India; dr.m.govindarajan@gcwk.ac.in
[7] Unit of Natural Products and Nanotechnology, Department of Zoology, Government College for Women (Autonomous), Kumbakonam 612001, Tamil Nadu, India
* Correspondence: sachivkina@yandex.ru

Abstract: Wetlands are dynamic ecosystems that provide feeding and nesting grounds for diverse species of waterbirds. The quality of wetland habitat may have an impact on the density, diversity, and species richness of waterbirds. Toxic metal contamination is one of the most significant threats to wetland habitats. Feathers are a key indicator of heavy metal contamination in avian communities as a non-invasive method. We examined the levels of Arsenic (As), Cadmium (Cd), Cobalt (Co), Chromium (Cr), Copper (Cu), Lead (Pb), Nickel (Ni), and Zinc (Zn) using ICP-AAS and standards of digestion procedure from the primary feathers of 10 distinct species of waterbirds. The study was conducted at four wetlands, viz., Point Calimere Wildlife Sanctuary (Ramsar site); Pallikaranai Marshland (Ramsar site); Perunthottam freshwater lake (unprotected wetland), Tamil Nadu and the Pulicat Lake, Andhra Pradesh, (Ramsar site), India. The Large crested tern had higher concentrations of As, Co, Cr, and Ni. Cu was greater in the Indian pond heron, and Zn was higher in the Grey heron. The accumulation of metals differed among the waterbirds ($p < 0.05$), and the inter-correlation of metals found positive influences between the tested metals, i.e., Co was positively associated with As, Cr had a positive correlation with As and Co, and Ni was positively correlated with As, Co, Cr, and Cu. In contrast, Pb had a positive association with Cu and Ni. The Zn was associated with Co, Cr and Cu. The level of metals in waterbirds was Zn > Cu > Cr > Ni > Pb > Co > Cd > As. The results showed that metal levels in the primary feathers of waterbirds were greater than the other species of waterbirds examined across the world. Thus, the study emphasizes that managing wetlands and controlling pollution is crucial to saving waterbirds; otherwise, the population and diversity of waterbirds will decline and become a significant threat to waterbird communities.

Keywords: pollution; wetlands; heavy metals; feathers; waterbirds; impact and management

Citation: Pandiyan, J.; Arumugam, R.; Al-Ghanim, K.A.; Sachivkina, N.; Nicoletti, M.; Govindarajan, M. Heavy Metals in Wetland Ecosystem: Investigating Metal Contamination in Waterbirds via Primary Feathers and Its Effect on Population and Diversity. *Soil Syst.* **2023**, *7*, 104. https://doi.org/10.3390/soilsystems7040104

Academic Editor: Manfred Sager

Received: 9 October 2023
Revised: 10 November 2023
Accepted: 11 November 2023
Published: 16 November 2023

Copyright: © 2023 by the authors. Licensee MDPI, Basel, Switzerland. This article is an open access article distributed under the terms and conditions of the Creative Commons Attribution (CC BY) license (https://creativecommons.org/licenses/by/4.0/).

1. Introduction

The abundance, distribution, and diversity of waterbirds are determined by the quality of their wetland habitat [1,2]. Indeed, wetlands support numerous species of waterbirds

as feeding and breeding grounds [3]. However, globally, the diversity of waterbirds is declining due to various factors, and pollution is one of the major factors [4]. The water and soil quality parameters influence waterbirds' density, diversity, and species richness in a wetland habitat [5,6]. Studies reported that many vertebrates might be lost in the future due to anthropogenic pressures, especially due to heavy metals [7,8].

Heavy metals severely contaminate the environment, which poses intensive problems to humans and free-ranging animals [9,10]. Metal accumulation may affect the physiology and behaviour of waterbirds, for instance, their foraging behaviour, development (ontogeny), metabolic processes, breeding rates, moulting, memory, migration, and population size [11]. In the aquatic ecosystem, the soil sediments, water, crustaceans, mud-dwelling organisms, and fishes, as well as waterbirds' various organs (such as the liver, kidney, muscles, and feathers) and the embryonic development of their eggs, are severely damaged by the toxic metals [12,13]. Several studies have shown that heavy metals have intensive, serious physiological impacts on waterbirds, resulting in the deformation of several organs and metabolic disorders [14–16].

Evaluating metal contamination using free-ranging animals is a very contentious issue; the bioethical commission's standards forbid the slaughter of such species for biomonitoring or other scientific purposes [17]. Therefore, we aimed to use the primary feathers of waterbirds that were found dead in diverse aquatic environments in India to evaluate the metal levels in the birds' bodies. Several studies have concluded that examining feathers is simple and non-destructive biomonitoring technique for evaluating metals [18–21]. A study has explained the presence of metals in bird feathers through different mechanisms, i.e., digestion, forming of feathers, and releasing salt and oils from preen gland in waterbirds [22]. Furthermore, several investigations demonstrated that internal metal deposition occurred in feathers throughout their growth and development [18]. The present study focused on eight metals, As, Cd, Co, Cr, Cu, Pb, Ni, and Zn, because these metals are deeply involved in the food chain of aquatic organisms [23,24] and are severely damaging the physiology of plants and animals [25]. Numerous studies have revealed that these eight metals globally threaten the reproductive behaviour of several waterbirds [15,24].

Moreover, studies reported that As, Cd, Co, Cr, Cu, Pb, Ni and Zn have remarkable impacts on avian communities; for example, an excessive level of As can damage the DNA in birds [26]. A higher level of Cd in birds can damage their flying mechanisms and lead to poor development of bones [27]. Co is considered a significant element necessary for metabolism but can negatively affect birds in excessive concentrations [28]. The toxicity of Cr had several impacts on birds, including on embryo development and egg-hatching success in Mallard [29]. Cu is one of the major toxic elements that causes severe kidney issues in waterbirds when its concentration is beyond the threshold level [30]. Higher content of Pb could destroy birds' thermoregulation, growth of nestlings, and recognition of siblings [31]. Even in lower concentrations, Ni can affect the pigment colouring of feathers during feather moulting [32]. Severe reproductive failure and increased kidney toxicity have been reported in birds due to Zn poisoning [33].

The level of metals in birds is severely affecting their physiology and behaviour by causing severe ailments. The current research aimed to evaluate the metal content of the primary feathers of 10 distinct waterbird species' dead carcasses from four wetland habitats in India, including the Point Calimere Wildlife Sanctuary, Pallikaranai Marshland, and Pulicat Lakes and Perunthottam Freshwater lake. These wetlands are Ramsar sites, except Perunthottam Freshwater lake and they support a greater diversity of waterbird species annually as feeding and breeding habitats [34–36]. However, studies revealed that waterbirds' density, diversity, and species richness drastically declined in the three wetland habitats (Ramsar sites) due to pollution, especially heavy metals. In order to understand the level of metals, this study also compared the concentration of metals in waterbirds with the results of metals examined from the birds investigated in other parts of the globe.

2. Materials and Methods

2.1. Study Area

The study was carried out at four wetlands, viz., (i) Point Calimere Wildlife Sanctuary, Kodikkarai, (ii) Perunthottam aquatic freshwater lake, (iii) Pallikaranai Marshland, Tamil Nadu, and (iv) Pulicat Lake, Andhra Pradesh, India, during 2019–2023 (Figure 1 and Table 1).

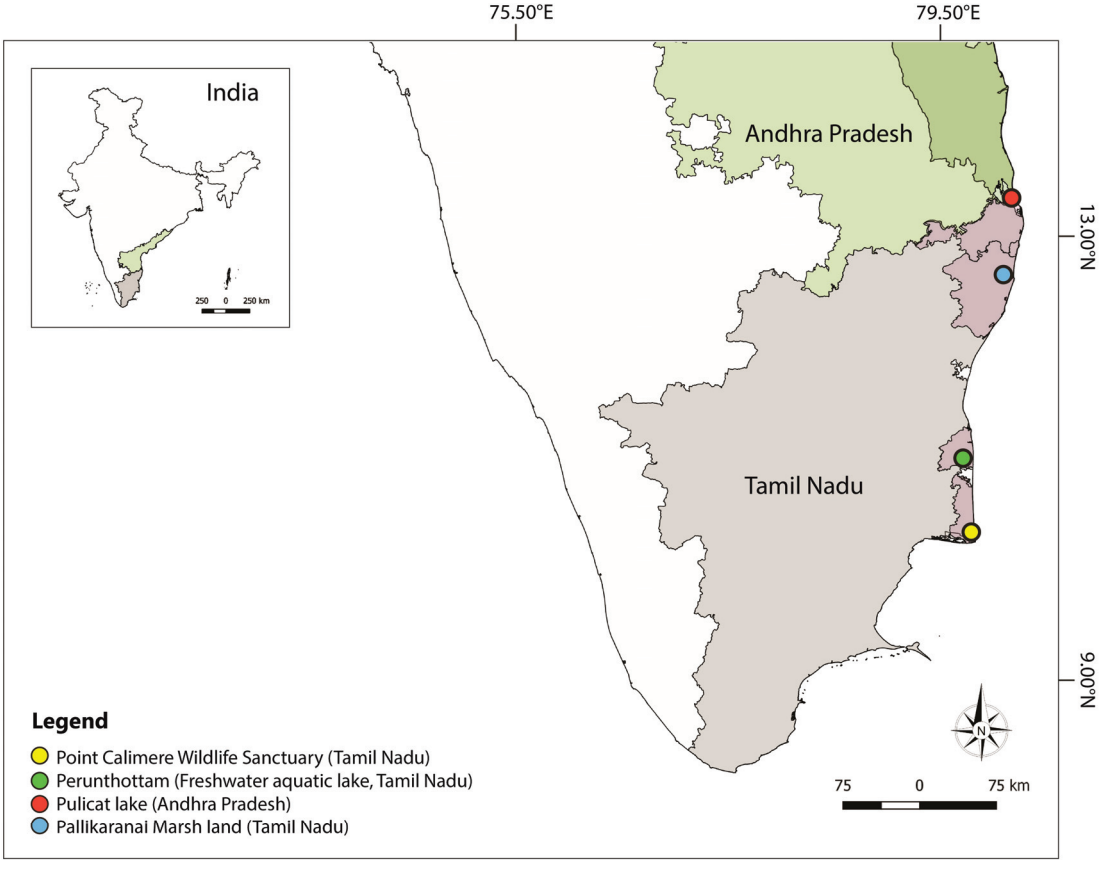

Figure 1. Map showing the locations of the four different wetlands, Tamil Nadu, and Andhra Pradesh, India.

Table 1. The details of waterbirds collected from the four different wetlands, Andhra Pradesh, and Tamil Nadu, India, during 2019–2023.

S.No.	Name of the Waterbirds	Name of the Wetlands
1.	Purple heron (*Ardea purpurea*)	Point Calimere Wildlife Sanctuary, Tamil Nadu (Ramsar site)
2.	Northern Shoveler (*Spatula clypeata*)	
3.	Large egret (*Ardea alba*)	Perunthottam (Freshwater aquatic lake) Tamil Nadu (Unprotected wetland)
4.	Pond heron (*Ardeola grayii*)	
5.	Grey heron (*Ardea cinerea*)	

Table 1. *Cont.*

S.No.	Name of the Waterbirds	Name of the Wetlands
6.	Striated heron (*Butorides striata*)	Pulicat Lake, Andhra Pradesh (Ramsar site)
7.	Spot-billed pelican (*Pelecanus philippensis*)	
8.	Heuglin's gull (*Larus heuglini*)	Pallikaranai Marshland, Tamil Nadu (Ramsar site)
9.	Brown headed-gull (*Chroicocephalus brunnicephalus*)	
10.	Large crested tern (*Thalasseus bergii*)	

The Point Calimere Wildlife Sanctuary (PCWLS), Kodikkarai, is located on the east coast of southern India, Tamil Nadu. The PCWLS was declared a Ramsar site in India in August 2002 since it is a globally significant wetland that supports and provides suitable habitats for migratory, resident migratory, and resident species of waterbirds annually [34–36]. The PCWLS receives water from the Bay of Bengal and rainwater during the monsoon season [35]. The Chemplast and small-scale saltpans are functioning in and around the PCWLS.

The Perunthottam Lake is a unprotected fresher-water wetlands, and the lake supports numerous species of waterbirds seasonally, including common and near-threatened species of waterbirds. Heronries are the lake's largest population, and the birds use this lake as a suitable feeding and breeding habitat (Unpublished data). Water from the Cauvery River fills the Perunthottam lake and irrigates the fields that run beside the river's bundh.

The Pallikaranai wetland is a globally important marshlands and has recently been declared Ramsar site. The wetland covers 700 acres, and it is located in the metropolitan city of greater Chennai Corporation of Tamil Nadu, India. According to research, several species of waterbirds use the Pallikaranai as a breeding and roosting site [37]. The Pulicat Lake is the second greatest saline waterbody lagoon and one of the Ramsar sites on the east coast of southern India. The lake provides critical support to various species of migratory and resident migratory waterbirds, functioning as feeding and breeding grounds during their migration. The lake receives water through various river systems, including the Araani and Kalangi rivers, which pass through various agricultural and industrial areas.

The Pulicat lake has a larger population and richer diversity of species over each season [38]. Moreover, numerous small, medium, and large-scale factories, industries, refineries, distilleries, battery companies, fertilizer companies, and national highways are located adjacent to the wetlands, and oil spills (through fishing vessels), discharges of effluents, and sewage water are the major sources of pollution in the wetlands.

2.2. Collection of Bird Feathers

Feathers were collected from four select wetland habitats; the details of the feathers are presented in Table 1. Primary feathers were collected from each species of waterbird (dead carcasses), such as the Purple heron, Northern Shoveler, Large egret, Pond heron, Grey heron, Striated heron, Spot-billed pelican, Heuglin's gull, Brown headed-gull, and Large crested tern, to assess them for metals. The Spot-billed pelican is in the Near Threatened Category (NT), and the other nine species of waterbirds are in the Least Concern (LC) category (IUCN, 2023). Though we collected more than three specimens for each species, we used only three specimens for the metal analysis to meet the statistical exploration. The primary feathers of birds are extensively used for assessing metal pollution [14,39]. The primary feathers of birds are the outermost wing feathers, which are protected by minute bones. There are generally ten primary feathers present in every species of bird. Additional inner primary feathers are also found in birds, but the outer primary feathers or flight feathers were employed for the current study [21].

2.3. Digestion of Bird Feather Samples

The feathers were washed in distilled water to remove any accumulated contaminants (external) on their surface. Washed feathers dried for 24 h using a hot air oven at 60 °C until constantly dehydrated (dry mass), and the feathers were weighed to the nearest 0.001 g [14]. The feathers were digested using a microwave digestion process using 10 mL of HNO_3 (69%) for five minutes, 1 mL of $HClO_4$ (70%) for five minutes, and 5 mL of H_2O_2 (30%) for ten minutes at 250 W magnetron power settings. Filter paper was used to filter the digested samples, which were made into 25 mL by using (MP) H_2O. The samples were kept in polythene tubes in the deep freezer until metal analysis [14].

2.4. Quality Control and Analytical Procedure

A quality control (QC) sample was injected for every six samples to assess the instrument's stability. In addition, for better accuracy, blank and standard samples were run in a set of three (triplicate) for each analytical course [14]. Regarding the accuracy of the systematic procedure in the metal analysis, the relative standard deviation (RSD) was obtained at the 5–10% range, and the RSD was calculated from the STD/mean values. For each metal, separate calibration curves were prepared at 0.5, 1.0, 2.0, 5.0, and 10 ppm. The working solution was also prepared every day to analyse the different metals by making a stock solution with the mixture of 65% (v/v) HNO_3, 30% (v/v) H_2O_2, and H_2O ($v/v/v$ = 1:1:3) ratios [40]. The instrument was set to zero concentration for every sample set using a blank solution. The results of each metal were determined using (triplicate) samples. All glassware was rinsed with distilled water before use, soaked in nitric acid (30%) overnight, and air-dried before being used to analyse metals. Analyses were performed using ICP-MS. The results are expressed as ppm [14,40,41].

2.5. Data Analysis

The descriptive statistics were completed for each metal that was assessed from the various waterbird species collected from the four wetlands. The values are given as a mean of ±SE (ppm). Shapiro–Wilk has also been tested to ascertain the normality of the data for further analysis. One-way variance analysis (ANOVA) has explored the variations of metal load among the waterbird species collected at different wetlands. We completed inter-correlation analysis to understand the sources and relationships among the metals examined to the different wetlands based on the feathers of various species of waterbirds. The analysis was conducted by using SPSS 25.0 software (South Asia Private Limited, Bangalore, India), and the outcomes are represented using the interpretations described by Sokal and Rohl [42].

3. Results

Metals were assessed from the primary feathers of 10 distinct species of waterbirds from four different wetlands (Figures 2–9). Arsenic (As) was higher in Large crested tern (0.1 ± 0.002 ppm) than the other metals examined. The cadmium (Cd) concentration was high in Purple heron (0.10 ± 0.030 ppm). The Cobalt (Co) and Chromium (Cr) concentrations were detected at higher levels (0.02 ± 0.053) and (1.29 ± 0.406 ppm), respectively, in the Large crested tern. Higher levels of Copper (Cu) (1.28 ± 0.012) and Lead (Pb) (1.10 ± 0.321 ppm) were found in the Indian Pond heron. Nickel (Ni) concentration was higher in the Large crested tern (3.511 ± 0.130 ppm). In the Grey heron, the Zinc (Zn) level was dominant, with 14.79 ± 0.408 (ppm) compared to the other species of waterbirds studied. The metals, viz., As, Cd, Co, Cr, Cu, Ni, Pb, and Zn showed differences among the various species of waterbirds examined in the wetlands (Figures 2–9). The concentrations of the eight different metals in the primary feathers of the 10 distinct species of waterbirds were Zn> Cu > Cr > Ni > Pb > Co > Cd > As.

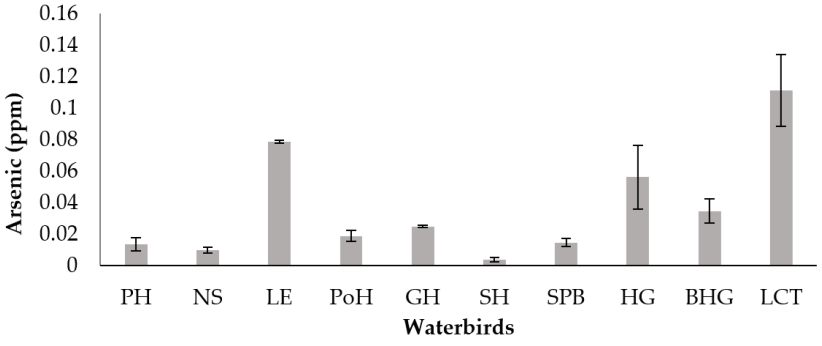

Figure 2. Level of Arsenic (As) accumulated in the feathers of the different waterbirds studied in various wetlands in India. [PH = Purple heron; NS = Northern Shoveler; LE = Large egret; PoH = Pond Heron; GH = Grey heron; SH = Striated heron; SPB = Spot-billed pelican; HG = Heuglin's gull; BHG = Brown-headed gull; LCT = Large-crested tern]. (Bar indicates the mean value and the line indicates the standard error values).

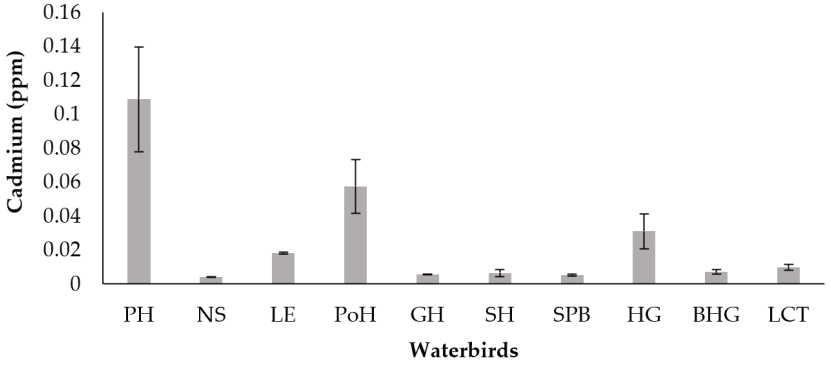

Figure 3. Level of Cadmium (Cd) accumulated in the feathers of the different waterbirds studied in diverse wetlands in India. (Bar indicates the mean value and the line indicates the standard error values).

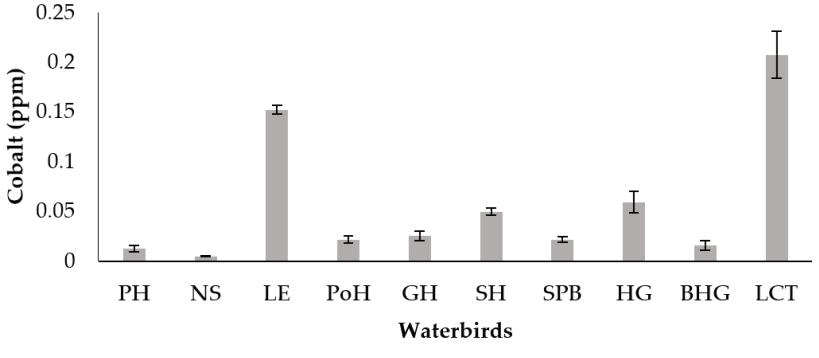

Figure 4. Level of Cobalt (Co) accumulated in the feathers of the different waterbirds studied in different wetlands in India. (Bar indicates the mean value and the line indicates the standard error values).

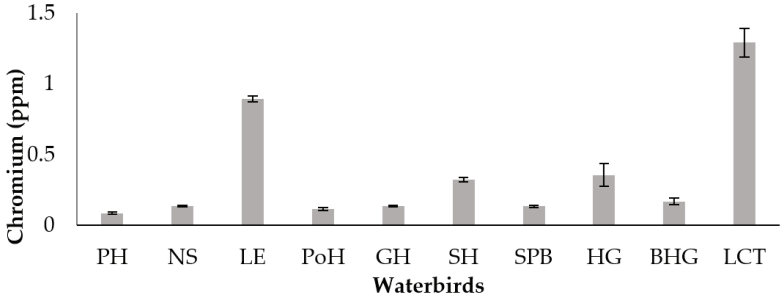

Figure 5. Level of Chromium (Cr) accumulated in the feathers of the different waterbirds studied in diverse wetlands in India. (Bar indicates the mean value and the line indicates the standard error values).

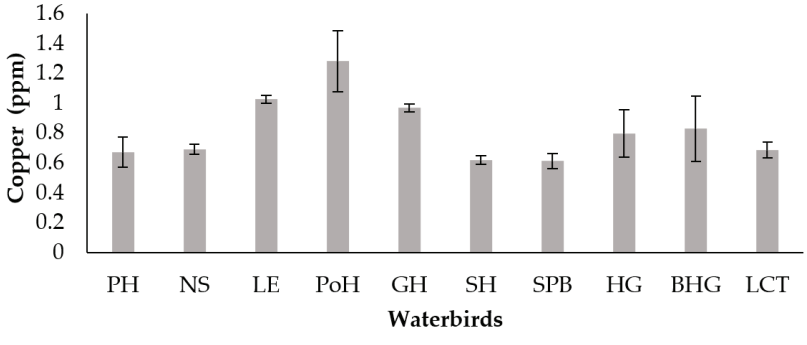

Figure 6. Level of Copper (Cu) accumulated in the feathers of the different waterbirds studied in diverse wetlands in India. (Bar indicates the mean value and the line indicates the standard error values).

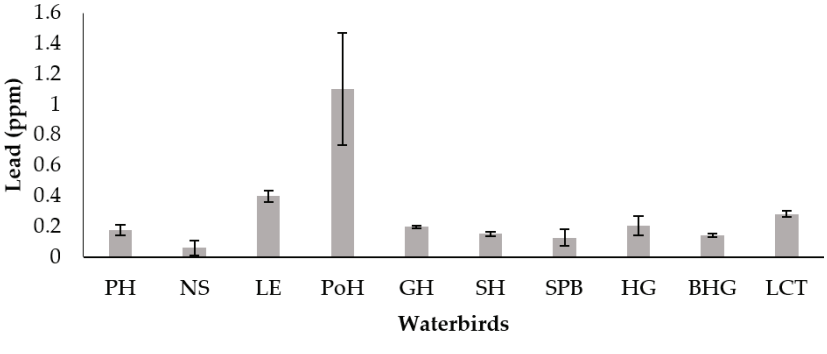

Figure 7. Level of Lead (Pb) accumulated in the feathers of the different waterbirds studied in diverse wetlands in India. (Bar indicates the mean value and the line indicates the standard error values).

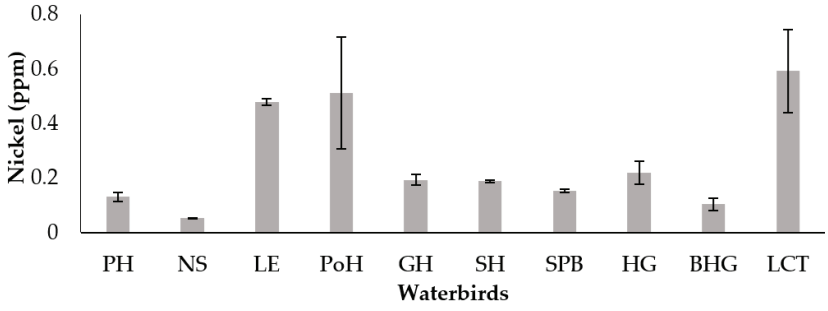

Figure 8. Level of Nickel (Ni) accumulated in the feathers of the different waterbirds studied in diverse wetlands in India. (Bar indicates the mean value and the line indicates the standard error values).

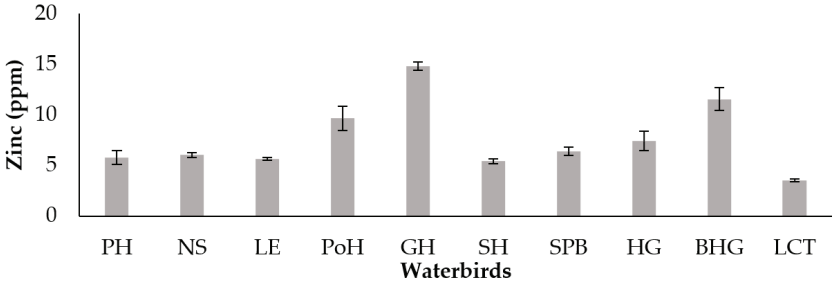

Figure 9. Level of Zinc (Zn) accumulated in the feathers of the different waterbirds studied in diverse wetlands in India. (Bar indicates the mean value and the line indicates the standard error values).

The inter-correlation of metals showed positive correlations among the metals examined in the 10 different species of waterbirds. A positive association was predicted between Co and As (r = 0.910; $p < 0.01$); Cr also showed similar results with As and Co (r = 0.901 and 0.991; $p < 0.01$). Ni exhibited absolute relationships with As (r = 0.680; $p < 0.01$), Co (r= 0.739; $p < 0.01$), Cr (r =0.711; $p < 0.01$), and Cu (r = 0.557; $p < 0.01$). Pb showed a positive correlation with Cu (r = 0.729; $p < 0.01$) and Ni (r = 0.686; $p < 0.01$). Zn was correlated with Co (r = 0.422; $p < 0.05$), Cr (r = 0.427; $p < 0.05$) and Cu (r = 0.532; $p < 0.01$) (Table 2).

Table 2. Inter-correlation of metals examined from the 10 different species of waterbirds studied from the four different wetlands, Andhra Pradesh, and Tamil Nadu, India, during 2019–2022.

Metals	As	Cd	Co	Cr	Cu	Ni	Pb	Zn
As	1							
Cd	0.083	1						
Co	0.910 **	0.158	1					
Cr	0.901 **	0.182	0.991 **	1				
Cu	0.205	0.163	0.077	0.043	1			
Ni	0.680 **	0.017	0.739 **	0.711 **	0.557 **	1		
Pb	0.073	0.220	0.070	0.026	0.729 **	0.686 **	1	
Zn	0.208	0.056	0.422 *	0.427 *	0.532 **	0.119	0.206	1

** Correlation is significant at the 0.01 level (2-tailed); * Correlation is significant at the 0.05 level (2-tailed).

4. Discussion

The presence of metal pollutants in aquatic environments has been found to have a negative impact on waterbird communities, resulting in reduced abundance, distribution, diversity, and species richness. This is due to the effects of the pollutants on the reproductive physiology and behaviour of these avian species. Numerous studies have indicated that the presence of diverse pollutants, particularly metals, can have an impact on the well-being and longevity of waterbird populations in terms of their fitness and sustainability [23]. The current study examined the metals that are directly associated with trophic structures [24]. The study revealed critical results on the concentration of metals in waterbirds examined. Zinc (Zn) was highest (14.79 $\pm$ 0.408 ppm) in the Grey heron and lowest in the Large crested tern (3.51 $\pm$ 0.130). The Pond heron had the highest Copper (Cu) and Lead (Pb) when compared to other waterbirds that were studied from the four wetlands (Figures 2–9). Zn was higher in the Grey heron; this may have occurred because this bird mainly feeds on fish species, but can also prefer to consume aquatic invertebrates when the distribution and abundance of fish species are low in their foraging grounds [14]. Numerous reports describe that Zn occurred at a higher level in fish [16,43,44]; since the Grey heron's preferred and principal diet is fishes, this may have influenced the level of Zn in their primary feathers, which was higher in the present study.

Cu and Pb were higher in the Pond heron. The Pond heron is a carnivorous bird that forges on various prey species in the aquatic habitat, such as fishes, molluscs, crustaceans, insects, and other mud-dwelling organisms (occasionally). The birds that feed on those prey species might have accumulated more Cu and Pb [15]. Youssef et al. [45] reported that crustaceans and fishes showed higher amounts of Cu and Pb. Similarly, another study described the extensive accumulation of Cu and Pb in fishes and crustaceans through their feeding preferences [46]. Battley et al. [47] reported that top predators in an aquatic ecosystem, including heronries, showed maximum Cu and Pb because waterbird species feed on fishes, amphibians, crustaceans, and molluscs. Consequently, it is verified that the quality of the ecosystem may affect the accumulation of metals in predators, such as waterbirds.

This study also found that the highest level of Zn was in Grey heron, and Cu and Pb were highest in Pond heron. The dead specimen of Grey heron and Pond heron were collected from the Perunthottam freshwater wetland, which is one of the unprotected wetlands. The lake gets water from the Cauvery River, which covers more than 600 km from its source in Talai-Cauveri, Kodagu District, Karnataka State, to its mouth at the east coast of Tamil Nadu, southern India. The Cauvery River not only loads fresh water from the natural sources of Western Ghats, it is also the outlet for various pollutants from agricultural farmlands, tanneries, as well as small, medium and large scale factories, municipal and corporation wastes, sewages of distilleries companies, oil leaks, etc., from locations all along the Cauvery basin. Therefore, the lake is loaded with various pollutants through the river water; this can affect the waterbirds since they are using the lake as feeding and breeding grounds. In addition, the current study witnessed that the level of Zn was higher in the feathers of Grey heron, and Cu and Pb were higher in the feathers of the Pond heron. In fact, Zn is a vital element for animals, but a surplus level of Zn will affect its the metabolic and vital physiological systems [10,48].

Moreover, the results of the present study revealed that most of the waterbird species showed 4–6 times higher concentrations of Zn compared to other species of waterbirds studied globally, such as Spotted Redshank (2.1 $\pm$ 0.20), Black-winged stilt (2.559 $\pm$ 0.35), Common redshank (2.041 $\pm$ 0.29), and Painted stork (1.5 $\pm$ 0.12) [48,49]. The highest mortality has been reported in terrestrial and wetland birds due to Zn poisoning; ducks and a few species of Columbiformes showed severe physiological effects with a higher level of Zn concentration [50,51]. Indeed, the high amount of Cu and Pb in avian communities has been linked to several health problems and tissue abnormalities [52,53], and problems with reproductive behaviour, thermoregulation, movement, poor growth and survival of nestlings, and kin recognition have been reported in birds with Pb poisoning [52]. In

addition, memory loss was also reported in migratory birds due to the heavy load of Cu and Pb [52–54]. In fact, a greater level of Cu was reported in the Red knot, Sanderling, and Semipalmated sandpiper [53] and Pb in the Red knot (484 ppm), Sanderling (367 ppm), and Semipalmated sandpiper (411 ppm), than in the current study [53].

Moreover, As, Co, Cr, and Ni were higher in Large-crested tern (Figures 2, 4, 5 and 8). The concentration level of As was lower in waterbirds studied than in the other species of birds examined, i.e., *Calidris canutus* (446 ± 42 ng/g), *Calidris alba* (311 ± 64 ng/g), and *Calidris pusilla* (842 ± 101 ng/g), which were discussed at Delaware Bay, USA [53]. In fact, a higher level of cobalt was reported in the *Alectoris chukar* (1.2 ppm), *Ammoperdix griseogularis* (5.4 ppm), and *Columba livia* (1.3 ppm) compared with those from the current study [55]. Co is important for various metabolic activities; however, higher cobalt accumulation in waterbirds influences enzymes that are essential for several physiological activities [30,54]. In addition, a higher concentration of Cr was reported from various species of birds than in the present study [29,52,56]. Above 1.8 ppm of Cr has shown adverse effects in birds, but the present study did not observe harmful levels of Cr [29,52,57]. Compared to other studies worldwide, the level of Ni in the waterbirds studied was lower [58,59]. Studies have reported that Ni could affect the pigmentation in feathers and moulting mechanisms when the Ni concentration is exceeded in birds [15–17].

The dead Large-crested tern examined in this study was found at Pallikaranai marshland, one of the largest marshland in the urban ecosystem of Tamil Nadu, India. One study described that the Pallikaranai lake supports numerous species of avian communities by providing necessary prey species, i.e., 46 fish species, five species of crustaceans, nine molluscs, and 10 species of amphibians [60]. However, research found higher concentrations of As, Co, Cr, and Ni in Pallikaranai lake water [61], and the results stressed that the contamination of the lake was largely due to the dumping of solid and liquid wastes from the Chennai metropolitan city and the emergence of a new building in and around the lake. This might be why the Large crested tern shows a higher level of As, Co, Cr and Ni in its feathers. The chief prey for the Large crested tern is fish and prawn species [62]. A study reported that reported that the accumulation of Co and Cr was greater in fishes and prawn species [16]. Terns mostly feed on fishes and prawn species, which could be a reason that Co and Cr are greater in the Large crested tern.

The Purple heron and Northern shoveler carcasses were collected from the Point Calimere Wildlife Sanctuary. The dead Striated heron and Spot-billed pelican were collected at Pulicat lake, Andhra Pradesh, India. These four species showed lower concentrations of metals in their feathers when compared to the other six species of waterbirds. However, if the number of samples was increased, we could shed more light on the concentration of metals from the feathers of these species of waterbirds. Studies have reported that the water, sediment, and prey species, as well as several species of waterbirds in the Point Calimere Wildlife Sanctuary and Pulicate lake are contaminated with metal load [12,63–65].

The inter-correlation of metals showed a positive correlation among the metals ($p < 0.01$ and $p < 0.05$). Co was positively correlated with As, Cr showed a positive correlation with As and Co, and Ni positively correlated with As, Co, Cr, and Cu. In contrast, Pb is positively associated with Cu and Ni. Zn was linked to Ni, which showed that the metals have a close association with each other, which is one of the driving forces behind the accumulation of metals in biological organisms, especially top predators. Similarly, several studies have shown the accumulation of metals in top predators through their prey or environment [15–17]. Indeed, the uptake of toxic metals in waterbirds may occur through their feeding behaviour, which involves water, soil, and prey species. A study reported that metals enter the waterbirds' bodies through water and soil while they are searching, pecking, probing, catching, swallowing, etc. [66]. The accumulation of metals in the waterbirds could also occur through their prey species [67,68].

The results of the present study showed that the waterbirds carry more significant levels of toxic metals in their body than other species of birds examined elsewhere. However, globally, several studies reported that waterbirds' abundance, composition, density,

diversity, and species richness has declined [14,16,34,35]. In fact, certain species of waterbirds are critically endangered, for example, the white-bellied heron, spoon-billed sandpiper, and social lapwing. Moreover, the white-headed duck, white-winged wood duck, great knot, greater adjutant, black-bellied heron, and black-bellied tern are endangered (IUCN 2023). These species of waterbirds have not been observed recently on the east coast of southern India. The reason for this is unknown, but it may be due to pollution of the wetlands [14]. Moreover, studies have also indicated that refuel sites have been degraded through pollution, and thus, migratory waterbirds are facing critical consequences during their migration [69]. Studies also state that heavy metals influence 19% of the physiological activities of bird communities, along with other pollutants, such as pesticides, oil, noise, light, plastic, air, and pharmaceutical and radioactive pollution [70–72]. Toxic metals threaten the wetlands habitats and various species of fauna and flora, depending on the wetlands [73].

5. Conclusions

The current study showed the variations of metal accumulation in waterbirds; these variations may occur because different species use different hunting techniques and consume different foods. Moreover, the age of the birds and their principal and preferred prey also could directly influence the accumulation of metals, but the study did not investigate the feeding and habitat selection for waterbirds used in the current study. In addition, the pollution in aquatic habitats in the study area comes from various sources, which could also influence the metal load in the waterbirds studied. The load of metals in the waterbirds come not only from the wetlands studied, but also where the birds are moving and using other wetlands as feedings grounds, which could also facilitate the accumulation of metals in the waterbirds. Overall, the study emphasises that the waterbirds accumulate toxic metals from their feeding and breeding habitats through different sources. Therefore, the study cautioned that we must monitor and manage the wetlands as pollution-free habitats because the metals not only affect the waterbird communities, they also influence the health of human society. Nutritious foods, such as fishes, molluscs and crustaceans, are collected from the wetlands and consumed by human society, which could damage human health.

Author Contributions: Conceptualization, J.P. and M.G.; methodology, J.P. and R.A.; software, J.P. validation, J.P.; formal analysis, J.P. and R.A.; investigation, J.P. and R.A.; resources, K.A.A.-G.; data curation, J.P., N.S., M.N. and M.G.; writing—original draft preparation, J.P. and M.G.; writing—review and editing, M.N., N.S., K.A.A.-G. and M.G.; supervision, J.P.; funding acquisition, K.A.A.-G. All authors have read and agreed to the published version of the manuscript.

Funding: Researchers Supporting Project Number (RSP2023R48) King Saud University, Riyadh, Saudi Arabia.

Institutional Review Board Statement: Not applicable.

Informed Consent Statement: Not applicable.

Data Availability Statement: On request, the data will be provided.

Acknowledgments: The authors express their sincere appreciation to the Researchers Supporting Project Number (RSP2023R48), King Saud University, Riyadh, Saudi Arabia. We sincerely thank the Department of Zoology and Wildlife Biology, AVC College (Autonomous), Mannampandal, Mayiladuthurai, Tamil Nadu, India, for providing the necessary facilities. This paper was also supported by the RUDN University Strategic Academic Leadership Program.

Conflicts of Interest: The authors declare no conflict of interest.

References

1. Goss-Custard, J.D.; Stillman, R.A.; West, A.D.; Caldow, R.W.G.; Triplet, P.; dit Durell, S.E.A.l.A.; McGrorty, S. When enough is not enough: Shorebirds and shellfishing. *Proc. R. Soc. Lond. Ser. B Biol. Sci.* **2004**, *271*, 233–237. [CrossRef]
2. Li, X.; Anderson, C.J.; Wang, Y.; Lei, G. Waterbird diversity and abundance in response to variations in climate in the Liaohe Estuary, China. *Ecol Indic.* **2021**, *132*, 108286. [CrossRef]

3. Yang, X.; Duan, Z.; Li, S.; Zhang, C.; Qu, M.; Hua, G.; Yu, D. Factors Driving the Abundance of Wintering Waterbirds in Coastal Areas of Guangdong Province, China. *Front. Ecol. Evol.* **2022**, *9*, 1040. [CrossRef]
4. Nagarajan, R.; Thiyagesan, K. Waterbirds and substrate quality of the Pichavaram wetlands, southern India. *Ibis* **1996**, *138*, 710–721. [CrossRef]
5. Manikannan, R.; Asokan, S.; Ali, A.M.S. Abundance and factors affecting population characteristics of waders (Charadriiformes) in great vedaranyam swamp of point calimere wildlife sanctuary, south-east coast of India. *Int. J. Ecosyst.* **2012**, *2*, 6–14. [CrossRef]
6. Hoffmann, M.; Hilton-Taylor, C.; Angulo, A.; Böhm, M.; Brooks, T.M.; Butchart, S.H.; Veloso, A. The impact of conservation on the status of the world's vertebrates. *Science* **2010**, *330*, 1503–1509. [CrossRef]
7. Sanderson, F.J.; Donald, P.F.; Pain, D.J.; Burfield, I.J.; Van Bommel, F.P. Long-term population declines in Afro-Palearctic migrant birds. *Biol. Conserv.* **2006**, *131*, 93–105. [CrossRef]
8. Eeva, T.; Belskii, E.; Kuranov, B. Environmental pollution affects genetic diversity in wild bird populations. *Mutat. Res. Genet. Toxicol. Environ. Mutagen.* **2006**, *608*, 8–15. [CrossRef]
9. Manjula, M.; Mohanraj, R.; Devi, M.P. Biomonitoring of heavy metals in feathers of eleven common bird species in urban and rural environments of Tiruchirappalli, India. *Environ. Monit. Assess.* **2015**, *187*, 267. [CrossRef]
10. Agoramoorthy, G.; Pandiyan, J. Toxic pollution threatens migratory shorebirds in India. *Environ Sci Pollut Res.* **2016**, *23*, 15771–15772. [CrossRef]
11. Malik, R.N.; Zeb, N. Assessment of environmental contamination using feathers of *Bubulcus ibis* L., as a biomonitor of heavy metal pollution, Pakistan. *Ecotoxicology* **2009**, *8*, 522–536. [CrossRef] [PubMed]
12. Zaccaroni, A.; Amorena, M.; Naso, B.; Castellani, G.; Lucisano, A.; Stracciari, G.L. Cadmium, chromium and lead contamination of Athene noctua, the little owl, of Bologna and Parma, Italy. *Chemosphere* **2003**, *52*, 1251–1258. [CrossRef]
13. Qadir, A.; Malik, R.N. Heavy metals in eight edible fish species from two polluted tributaries (Aik and Palkhu) of the River Chenab, Pakistan. *Biol. Trace Elem. Res.* **2011**, *143*, 1524–1540. [CrossRef]
14. Pandiyan, J.; Jagadheesan, R.; Karthikeyan, G.; Mahboob, S.; Al-Ghanim, K.A.; Al-Misned, F.; Ahmed, Z.; Krishnappa, K.; Elumalai, K.; Govindarajan, M. Probing of heavy metals in the feathers of shorebirds of Central Asian Flyway wintering grounds. *Sci. Rep.* **2020**, *10*, 22118. [CrossRef]
15. Kim, J.; Koo, T.H. The use of feathers to monitor heavy metal contamination in herons. Korea. Arch. Environ. *Contam. Toxicol.* **2007**, *53*, 435–441. [CrossRef]
16. Pandiyan, J.; Mahboob, S.; Jagadheesan, R.; Elumalai, K.; Krishnappa, K.; Al-Misned, F.; Govindarajan, M. A novel approach to assess the heavy metal content in the feathers of shorebirds: A perspective of environmental research. *J. King Saud. Univ. Sci.* **2020**, *32*, 3065–3071. [CrossRef]
17. Furness, R.W. Cadmium in birds. In *Environmental Contaminants in Wildlife: Interpreting Tissue Concentrations*; Lewis: Boca Raton, FL, USA, 1996; pp. 389–404.
18. Martínez, A.; Crespo, D.; Fernández, J.Á.; Aboal, J.R.; Carballeira, A. Selection of flight feathers from *Buteo buteo* and *Accipiter gentilis* for use in biomonitoring heavy metal contamination. *Sci. Total Environ.* **2012**, *425*, 254–261. [CrossRef] [PubMed]
19. Rutkowska, M.; Płotka-Wasylka, J.; Lubinska-Szczygeł, M.; Różańska, A.; Możejko-Ciesielska, J.; Namieśnik, J. Birds' feathers–suitable samples for determination of environmental pollutants. *Trend. Anal. Chem.* **2018**, *109*, 97–115. [CrossRef]
20. Khan, B.N.; Ashfaq, Y.; Hussain, N.; Atique, U.; Aziz, T.; Alharbi, M.; Albekairi, T.H.; Alasmari, A.F. Elucidating the effects of heavy metals contamination on vital organ of fish and migratory birds found at fresh water ecosystem. *Heliyon.* **2023**, *9*, e20968. [CrossRef]
21. Goede, A.A.; De Bruin, M. 1986. The use of bird feathers for indicating heavy metal pollution. *Environ. Monit. Assess.* **1986**, *7*, 249–256. [CrossRef]
22. Braune, B.W. Comparison of total mercury levels in relation to diet and molt for nine species of marine birds. *Arch. Environ. Contam. Toxicol.* **1987**, *16*, 217–224. [CrossRef]
23. Burger, J.; Gochfeld, M. Effects of lead and exercise on endurance and learning in young herring gulls. *Ecotoxicol. Environ. Safe* **2004**, *57*, 136–144. [CrossRef]
24. Bostan, N.; Ashrif, M.; Mumtaz, A.S.; Ahmad, I. Diagnosis of heavy metal contamination in agro-ecology of Gujranwala, Pakistan using cattle egret as bioindicator. *Ecotoxicology* **2007**, *6*, 247–251. [CrossRef]
25. Ullah, K.; Hashmi, M.Z.; Malik, R.N. Heavy-metal levels in feathers of cattle egret and their surrounding environment: A case of the Punjab province, Pakistan. *Arch. Environ. Contam.Toxicol.* **2014**, *66*, 139–153. [CrossRef] [PubMed]
26. Laine, V.N.; Verschuuren, M.; van Oers, K.; Espín, S.; Sánchez-Virosta, P.; Eeva, T.; Ruuskanen, S. Does arsenic contamination affect DNA methylation patterns in a wild bird population? *An experimental approach. Environ. Sci. Technol.* **2021**, *55*, 8947–8954. [CrossRef] [PubMed]
27. Spahn, S.A.; Sherry, T.W. Cadmium and lead exposure associated with reduced growth rates, poorer fledging success of little blue heron chicks (Egretta caerulea) in south Louisiana wetlands. *Arch. Environ. Contam. Toxicol.* **1999**, *37*, 377–384. [PubMed]
28. Roginski, E.E.; Mertz, W. A biphasic response of rats to cobalt. *J. Nutr.* **1997**, *107*, 1537–1542. [CrossRef]
29. Kertész, V.; Fáncsi, T. Adverse effects of (surface water pollutants) Cd, Cr and Pb on the embryogenesis of the mallard. *Aquat. Toxicol.* **2003**, *65*, 425–433. [CrossRef]
30. Burger, J.; Gochfeld, M. Metal levels in feathers of 12 species of seabirds from MidwayAtoll in the northern Pacific Ocean. *Sci. Total Environ.* **2000**, *257*, 37–52. [CrossRef]

31. Sato, H.; Ishii, C.; Nakayama, S.M.; Ichise, T.; Saito, K.; Watanabe, Y.; Ogasawara, K.; Torimoto, R.; Kobayashi, A.; Kimura, T.; et al. Behavior and toxic effects of Pb in a waterfowl model with oral exposure to Pb shots: Investigating Pb exposure in wild birds. *Environ. Pollut.* **2022**, *308*, 119580. [CrossRef]
32. Jayakumar, R.; Muralidharan, S. Metal contamination in select species of birds in Nilgiris District, Tamil Nadu, India. *Bull. Environ. Contam. Toxicol.* **2011**, *87*, 166–170. [CrossRef] [PubMed]
33. Carpenter, J.W.; Andrews, G.A.; Beyer, W.N. Zinc toxicosis in a free-flying trumpeter swan (*Cygnus buccinator*). *J. Wildl. Dis.* **2004**, *40*, 769–774. [CrossRef] [PubMed]
34. Ali, S. Point Calimere as a refuge for wintering shorebirds. *J. Bombay Nat. Hist. Soc.* **1963**, *60*, 458–460.
35. Balachandran, S. *The Decline in Wader Populations along the East Coast of India with Special Reference to Point Calimere, South-East India*; Boere, G.C., Galbraith, C.A., Stroud, D.A., Eds.; Waterbirds around the World; The Stationery Office: Edinburgh, UK, 2006; pp. 296–301.
36. Jagadheesan, R.; Pandiyan, J. Seasonal Variations of Small Wading Birds in the Pichavaram Mangrove Forest, India. *Curr. World Environ.* **2021**, *16*, 399. [CrossRef]
37. Raj, P.P.N.; Ranjini, J.; Dhanya, R.; Subramanian, J.; Azeez, P.A.; Bhupathy, S. Consolidated checklist of birds in the Pallikaranai Wetlands, Chennai, India. *J. Threat. Taxa.* **2010**, *2*, 1114–1118. [CrossRef]
38. Kannan, V.; Pandiyan, J. Shorebirds (Charadriidae) of Pulicat Lake, India with special reference to conservation. *World J. Zool.* **2012**, *7*, 178–191.
39. Burger, J.; Gochfeld, M. Metals in Laysan Albatrosses from Midway Atoll. *Arch. Environ. Contamin. Toxicol.* **2000**, *38*, 254–259. [CrossRef]
40. Muralidharan, S.; Jayakumar, R.; Vishnu, G. Heavy metals in feathers of six species of birds in the district Nilgiris, India. *Bull. Environ. Contam. Toxicol.* **2004**, *73*, 285–291. [CrossRef]
41. Chen, Z.; Khan, N.I.; Owens, G.; Naidu, R. Elimination of chloride interference on arsenic speciation in ion chromatography inductively coupled mass spectrometry using an octopole collision/reaction system. *Microchem. J.* **2007**, *87*, 87–90. [CrossRef]
42. Sokal, R.R.; Rohlf, F.I. *Biometry: The Principles and Practice of Statistics in Biological Research*; Freeman Company: New York, NY, USA, 2012; pp. 1–776.
43. Rajkowska, M.; Protasowicki, M. Distribution of metals (Fe, Mn, Zn, Cu) in fish tissues in two lakes of different trophy in Northwestern Poland. *Environ. Monit. Assess.* **2013**, *185*, 3493–3502. [CrossRef]
44. Sobhanardakani, S.; Tayebi, L.; Farmany, A.; Cheraghi, M. Analysis of trace elements (Cu, Cd, and Zn) in the muscle, gill, and liver tissues of some fish species using anodic stripping voltammetry. *Environ. Monit. Assess.* **2012**, *184*, 6607–6611. [CrossRef]
45. Youssef, M.; Madkour, H.; Mansour, A.; Alharbi, W.; El-Taher, A. Invertebrate shells (mollusca, foraminifera) as pollution indicators, Red Sea Coast, Egypt. *J. Afr. Earth Sci.* **2017**, *133*, 74–85. [CrossRef]
46. Jabeen, G.M.; Azmat, J.H. Assessment of heavy metals in the fish collected from the river Ravi, Pakistan. *Pak. Vet. J.* **2012**, *32*, 107–111.
47. Edwards, J.W.; Edyvane, K.S.; Boxall, V.A.; Hamann, M.; Soole, K.L. Metal levels in seston and marine fish flesh near industrial and metropolitan centres in South Australia. *Mar. Pollut. Bull.* **2001**, *42*, 389–396. [CrossRef]
48. Adegbe, E.A.; Babajide, O.O.; Maina, L.R.; Adeniji, S.E. Heavy metal levels in cattle egrets (*Bubulcus ibis*) foraging in some abattoirs in Lagos State metropolis. *Bull. Natl. Res. Cent.* **2021**, *45*, 71. [CrossRef]
49. Kim, J.; Oh, J.M. Monitoring of heavy metal contaminants using feathers of shorebirds. *Korean J. Environ. Monit.* **2012**, *14*, 651–656. [CrossRef]
50. Mado-Filho, G.M.; Salgado, L.T.; Rebelo, M.F.; Rezende, C.E.; Karez, C.S.; Pfeiffer, W.C. Heavy metals in benthic organisms from Todosos Santos Bay, Brazil. *Braz. J. Biol.* **2008**, *68*, 95–100. [CrossRef]
51. Vanderzee, J.; Zwart, P.; Schotman, A.J.H. Zinc poisoning in a Nicobar pigeon. *J. Zoo. Anim. Med.* **1985**, *16*, 68–69.
52. Kertész, V.; Bakonyi, G.; Farkas, B. Water pollution by Cu and Pb can adversely affect mallard embryonic development. *Ecotoxicol. Environ. Saf.* **2006**, *65*, 67–73. [CrossRef]
53. Burger, J.; Tsipoura, N.; Niles, J.; Gochfeld, M.; Dey, A.; Mizrahi, D. Mercury, Lead, Cadmium, Arsenic, Chromium and Selenium in Feathers of Shorebirds during Migrating through Delaware Bay, New Jersey: Comparing the 1990s and 2011/2012. *Toxics* **2015**, *3*, 63–74. [CrossRef]
54. Burger, J. Heavy metals in avian eggshells: Another excretion method. *J. Ecotoxicol. Environ. Health.* **1994**, *41*, 207–220. [CrossRef] [PubMed]
55. Burger, J. Metals in avian feathers: Bioindicators of environmental pollution. *Rev. Environ. Contam. Toxicol.* **1993**, *5*, 203–311.
56. Jayakumar, R.; Muralidharan, S.; Dhananjayan, V.; Sugitha, C. Monitoring of Metal Contamination in the Eggs of Two Bird Species in India. *Expert. Opin. Environ. Biol.* **2013**, *2*, 3.
57. Norouzi, M.; Mansouri, B.; Hamidian, A.H.; Ebrahimi, T.; Kardoni, F. Comparison of the Metal Concentrations in the Feathers of Three Bird Species from Southern Iran. *Bull. Environ. Contam. Toxicol.* **2012**, *89*, 1082–1086. [CrossRef]
58. Tsipoura, N.; Burger, J.; Newhouse, M.; Jeitner, C.; Gochfeld, M.; Mizrahi, D. Lead, mercury, cadmium, chromium, and arsenic levels in eggs, feathers, and tissues of Canada geese of the New Jersey Meadow lands. *Environ. Res.* **2011**, *111*, 775–784. [CrossRef]
59. Nazneen, S.; Jayakumar, S.; Albeshr, M.F.; Mahboob, S.; Manzoor, I.; Pandiyan, J.; Krishnappa, K.; Rajeswary, M.; Govindarajan, M. Analysis of Toxic Heavy Metals in the Pellets of Barn Owls: A Novel Approach for the Evaluation of Environmental Pollutants. *Toxics.* **2022**, *10*, 693. [CrossRef]

60. Vencatesan, J. Protecting wetlands. *Curr. Sci.* **2007**, *93*, 288–290.
61. Karpagavalli, M.S.; Malini, P.; Ramachandran, A. Analysis of heavy metals in dying wetland Pallikaranai, Tamil Nadu, India. *J. Environ. Biol.* **2012**, *33*, 757.
62. Jagadheesan, R.; Pandiyan, J. Temporal variations of large wading birds in the Point Calimere Wildlife Sanctuary, Tamil Nadu, India. *Ind. J. Sci. Technol.* **2021**, *14*, 1–7. [CrossRef]
63. Varagiya, D.; Jethva, B.; Pandya, D. Feather heavy metal contamination in various species of waterbirds from Asia: A review. *Environ. Monit. Assess.* **2022**, *194*, 26. [CrossRef]
64. Batvari, B.P.D.; Sivakumar, S.; Shanthi, K.; Lee, K.J.; Oh, B.T.; Krishnamoorthy, R.R.; Kamala-Kannan, S. Heavy metals accumulation in crab and shrimps from Pulicat lake, north Chennai coastal region, southeast coast of India. *Toxicol. Ind. Health* **2016**, *32*, 1–6. [CrossRef] [PubMed]
65. Prabhu, B.; Batvari, D.; Kamala-Kannan, S.; Shanthi, K.; Krishnamoorthy, R.; Lee, K.J.; Jayaprakash, M. Heavy metals in two fish species (*Carangoidel malabaricus* and *Belone stronglurus*) from Pulicat Lake, North of Chennai, Southeast Coast of India. *Environ. Monit. Assess.* **2008**, *145*, 167.
66. Morel, F.M.M.; Kraepiel, A.M.L.; Amyot, M. The chemical cycle and bioaccumulation of mercury. *Annu. Rev. Ecol. Syst.* **1998**, *29*, 543–566. [CrossRef]
67. Dange, S.; Manoj, K. Bioaccumulation of heavy metals in sediment, polychaetes (annelid) worms, mud skipper and mud crab at Purna River Estuary, Navsari, Gujarat, India. *Int. J. Curr. Microbiol. Appl. Sci.* **2015**, *4*, 571–575.
68. Abdullah, M.; Fasola, M.; Muhammad, A.; Malik, S.A.; Boston, N.; Bokhari, H. Avian feathers as a nondestructive bio-monitoring tool of trace metals signatures: A case study from severely contaminated areas. *Chemosphere* **2015**, *119*, 553–561. [CrossRef] [PubMed]
69. Richard, F.J.; Gigauri, M.; Bellini, G.; Rojas, O.; Runde, A. Warning on nine pollutants and their effects on avian communities. *Glob. Ecol. Conserv.* **2021**, *32*, e01898. [CrossRef]
70. Ceballos, G.; Ehrlich, P.R.; Dirzo, R. Biological annihilation via the ongoing sixth mass extinction signaled by vertebrate population losses and declines. *Proc. Natl. Acad. Sci. USA* **2017**, *114*, E6089–E6096. [CrossRef] [PubMed]
71. Garcıa-Fernández, A.J. Ecotoxicology, avian. *Encycl. Toxicol.* **2014**, *2*, 289–294.
72. Tartu, S.; Goutte, A.; Bustamante, P.; Angelier, F.; Moe, B.; Clément-Chastel, C.; Chastel, O. To breed or not to breed: Endocrine response to mercury contamination by an Arctic seabird. *Biol. Lett.* **2013**, *9*, 20130317. [CrossRef]
73. Sun, F.; Yu, G.; Han, X.; Chi, Z.; Lang, Y.; Liu, C. Risk assessment and binding mechanisms of potentially toxic metals in sediments from different water levels in a coastal wetland. *J. Environ. Sci.* **2023**, *129*, 202–212. [CrossRef]

Disclaimer/Publisher's Note: The statements, opinions and data contained in all publications are solely those of the individual author(s) and contributor(s) and not of MDPI and/or the editor(s). MDPI and/or the editor(s) disclaim responsibility for any injury to people or property resulting from any ideas, methods, instructions or products referred to in the content.

MDPI AG
Grosspeteranlage 5
4052 Basel
Switzerland
Tel.: +41 61 683 77 34

Soil Systems Editorial Office
E-mail: soilsystems@mdpi.com
www.mdpi.com/journal/soilsystems

Disclaimer/Publisher's Note: The title and front matter of this reprint are at the discretion of the Guest Editor. The publisher is not responsible for their content or any associated concerns. The statements, opinions and data contained in all individual articles are solely those of the individual Editor and contributors and not of MDPI. MDPI disclaims responsibility for any injury to people or property resulting from any ideas, methods, instructions or products referred to in the content.

Academic Open
Access Publishing

mdpi.com

ISBN 978-3-7258-3708-3